



Geological Fieldwork 2023

A Summary of Field Activities and Current Research



Ministry of
Energy, Mines and
Low Carbon Innovation

Paper 2024-01



Ministry of
Energy, Mines and
Low Carbon Innovation





Ministry of
Energy, Mines and
Low Carbon Innovation



Geological Fieldwork 2023

A Summary of Field Activities and Current Research

Ministry of Energy, Mines and Low Carbon Innovation
British Columbia Geological Survey

Paper 2024-01

Ministry of Energy, Mines and Low Carbon Innovation Responsible Mining and Competitiveness Division British Columbia Geological Survey

Recommended citation format for individual papers:

Hickin, A.S., Ootes, L., Orovan, E.A., Brzozowski, M.J., Northcote, B.K., Rukhlov, A.S., and Bain, W.M., 2024. Critical minerals and mineral systems in British Columbia. In: Geological Fieldwork 2023, British Columbia Ministry of Energy, Mines and Low Carbon Innovation, British Columbia Geological Survey Paper 2024-01, pp. 13-51.

Front Cover:

View south along Atlin Lake from Black Mountain, near the Yukon border. Marginal phases of the Fourth of July batholith (Middle Jurassic, in foreground) envelop screens of chert, basalt and mantle rocks of the Cache Creek terrane. See Mihalyuk, M.G., Zagorevski, A., Campbell, R., Hajiegeh, A., and Vaillancourt, A., 2024. Preliminary results from revision mapping of the Gladys Lake area, near Atlin, northwest British Columbia. In: Geological Fieldwork 2023, British Columbia Ministry of Energy, Mines and Low Carbon Innovation, British Columbia Geological Survey Paper 2024-01, this volume. **Photo by Nate Corcoran.**

Back Cover:

Liesegang rings in intermediate to felsic coherent volcanic rocks of the Hazelton Group (Lower-Middle Jurassic) approximately 2 km west-southwest of Mount Evindsen, Kitsault River area, northwestern British Columbia. See van Straaten, B.I., 2024. Upper Hazelton Group stratigraphy along the Stikine arch, northwestern British Columbia. In: Geological Fieldwork 2023, British Columbia Ministry of Energy, Mines and Low Carbon Innovation, British Columbia Geological Survey Paper 2024-01, this volume. **Photo by Bram van Straaten.**

This publication is available, free of charge, from the British Columbia Geological Survey website:

<https://www2.gov.bc.ca/gov/content/industry/mineral-exploration-mining/british-columbia-geological-survey/publications>

British Columbia Cataloguing in Publication Data

Main entry under title:

Geological Fieldwork: - 1974 -

Annual.

Issuing body varies

Vols. for 1978-1996 issued in series: Paper / British Columbia. Ministry of Energy, Mines and Petroleum Resources; vols. for 1997 - 1998, Paper / British Columbia. Ministry of Employment and Investment; vols. for 1999-2004, Paper / British Columbia. Ministry of Energy and Mines; vols. for 2005-2009, Paper / British Columbia. Ministry of Energy, Mines and Petroleum Resources; vols. for 2010, Paper / British Columbia. Ministry of Forests, Mines and Lands; vols. for 2011, Paper / British Columbia. Ministry of Energy and Mines; vols. for 2012- , Paper / British Columbia. Ministry of Energy, Mines and Natural Gas; vols. for 2014- , Paper / British Columbia. Ministry of Energy and Mines; vols. for 2018- , Paper / British Columbia. Ministry of Energy, Mines and Petroleum Resources; vols. for 2021- , Paper / British Columbia. Ministry of Energy, Mines and Low Carbon Innovation.

Includes Bibliographical references.

ISSN 0381-243X=Geological Fieldwork

1. Geology - British Columbia - Periodicals. 2. Mines and mineral resources - British Columbia - Periodicals. 3. Geology - Fieldwork - Periodicals. 4. Geology, Economic - British Columbia - Periodicals. 5. British Columbia. Geological Survey Branch - Periodicals. I. British Columbia. Geological Division. II. British Columbia. Geological Survey Branch. III. British Columbia. Geological Survey Branch. IV. British Columbia. Dept. of Mines and Petroleum Resources. V. British Columbia. Ministry of Energy, Mines and Petroleum Resources. VI. British Columbia. Ministry of Employment and Investment. VII. British Columbia Ministry of Energy and Mines. VIII. Series: Paper (British Columbia. Ministry of Energy, Mines and Petroleum Resources). IX. Series: Paper (British Columbia. Ministry of Employment and Investment). X. Series: Paper (British Columbia Ministry of Energy and Mines). XI. Series: Paper (British Columbia Ministry of Energy, Mines and Petroleum Resources). XII. Series: Paper (British Columbia Ministry of Forests, Mines and Lands). XIII. Series: Paper (British Columbia Ministry of Energy and Mines). XIV. Series: Paper (British Columbia Ministry of Energy, Mines and Natural Gas). XV. Series: Paper (British Columbia Ministry of Energy and Mines). XVI. Series: Paper (British Columbia Ministry of Energy, Mines and Petroleum Resources). XVII. Series: Paper (British Columbia Ministry of Energy, Mines and Low Carbon Innovation).

QE187.46 622.1'09711 C76-083084-3 (Rev.)

Victoria
British Columbia
Canada

January 2024

Preface

Geological Fieldwork 2023

Geological Fieldwork 2023 is the forty-ninth edition of the annual volume that presents peer-reviewed papers detailing the results of British Columbia Geological Survey (BCGS) geoscience activities. The Survey also publishes other reports, maps, and databases and contributes to peer-reviewed journals and partners publications throughout the year. This work can be accessed for free through the online BCGS Publication Catalogue. BCGS also publishes an annual companion volume, the Provincial Overview of Exploration and Mining in British Columbia.

As is tradition, the first paper in the volume, by Ootes et al., provides an overview of Survey activities in 2023. Critical minerals are a consistent theme in this edition of Fieldwork. Hickin et al. highlight some of the important critical mineral systems in British Columbia and the recent work that is revealing critical mineral opportunities and potential in the province. Orovan et al. describe characteristics of the past-producing Kitsault porphyry Mo-Ag deposit (Paleogene) and some of the rock textures in drill core from dikes that provide evidence for mineralizing fluid behaviour. Brzozowski et al. follow a similar approach, describing rock textures in core from the E&L magmatic Ni-Cu-PGE sulphide deposit with evidence about the source of S and the emplacement of metals. Building on the mineral systems approach and with the increased interest in land-use planning, Wearmouth et al. review past and present approaches to mineral potential modelling, comparing results from the 1990s to recent analysis in northern British Columbia. Developing a critical mineral exploration tool, Rukhlov et al. assess regional stream-sediment data from the eastern part of the province underlain by carbonatites and related rocks known to host rare earth elements, Ta, and Nb. Ootes et al. highlight the value of other BCGS geochemical data from geochronology and litho-geochemistry databases. Based on new geological mapping near the British Columbia-Yukon border, Mihalyuk et al. continue to define the ophiolitic Atlin terrain and provide evidence for its obduction onto the Cache Creek terrain. van Straaten presents a revised stratigraphy for the Hazelton Group (late Early to Middle Jurassic) of Stikine terrain, in and around the so-called ‘Golden Triangle’.

The Survey is continuing with its renewal phase, actively recruiting new staff and filling vacancies with expertise that is building for the future. The Survey developed and implemented an internal strategic plan in 2023, which is designed to position the Survey to optimize its growing resources for the benefit of British Columbia. I am particularly proud to have established an engagement geoscience position and programs that will bring British Columbia’s geology to Indigenous communities, the public, and other government colleagues. It is an exciting time at the BCGS as our work contributes foundational science for developing the British Columbia’s Critical Minerals Strategy, informing ongoing land-use planning initiatives, and supporting the economic opportunities exploration investment brings to rural communities.



Adrian S. Hickin
Chief Geologist and Executive Director
British Columbia Geological Survey

Table of Contents

Ootes, L., Cui, Y., Clarke, G., and Hickin, A.S.: British Columbia Geological Survey annual program review 2023-2024.	1
Hickin, A.S., Ootes, L., Orovan, E.A., Brzozowski, M.J., Northcote, B.K., Rukhlov, A.S., and Bain, W.M.: Critical minerals and mineral systems in British Columbia	13
Orovan, E.A., Zaborniak, K., and Hooker, K.: Textural evidence for ore fluid transport and the magmatic to hydrothermal transition at the past-producing Kitsault Mo-Ag mine	53
Brzozowski, M.J., and Zaborniak, K.: Sulphide mineralization at the E&L magmatic Ni-Cu-PGE deposit: Textural evidence for contamination, vapour saturation, fluid immiscibility, and metal remobilization	65
Wearmouth, C.D., Peters, K.J., Czertowicz, T.A., and Orovan, E.A.: Mineral potential modelling results for northwestern British Columbia, a comparison between past and current work at the British Columbia Geological Survey	79
Rukhlov, A.S., Cui, Y., Cunningham, Q., Fortin, G., and Anderson, C.: Geochemical signals of carbonatite-related critical metals in provincial stream sediments.....	97
Ootes, L., Rukhlov, A.S., and Han, T.: British Columbia Geological Survey rock geochemical and geochronological data products: Examples of utility	123
Mihalynuk, M.G., Zagorevski, A., Campbell, R., Hajiegeh, A., and Vaillancourt, A.: Preliminary results from revision mapping of the Gladys Lake area, near Atlin, northwest British Columbia.....	131
van Straaten, B.I.: Upper Hazelton Group stratigraphy along the Stikine arch, northwestern British Columbia.....	149
Appendix: British Columbia Geological Survey Publications 2023, including peer-reviewed external papers co-authored by BCGS staff.....	179

British Columbia Geological Survey annual program review 2023-2024



Luke Ootes¹, Yao Cui¹, Gordon Clarke², and Adrian S. Hickin^{1, a}

¹ British Columbia Geological Survey, Ministry of Energy, Mines and Low Carbon Innovation, Victoria, BC, V8W 9N3

² British Columbia Geological Survey, Ministry of Energy, Mines and Low Carbon Innovation, Vancouver, BC, V6Z 2G3

^a corresponding author: Adrian.Hickin@gov.bc.ca

Recommended citation: Ootes, L., Cui, Y., Clarke, G., and Hickin, A.S., 2024. British Columbia Geological Survey program review 2023-2024. In: Geological Fieldwork 2023, British Columbia Ministry of Energy, Mines and Low Carbon Innovation, British Columbia Geological Survey Paper 2024-01, pp. 1-11.

Abstract

This paper provides an overview of current British Columbia Geological Survey (BCGS) geoscience activities and highlights key findings from 2023 projects. Headquartered in Victoria, the Survey is part of the Responsible Mining and Competitiveness Division in the British Columbia Ministry of Energy, Mines and Low Carbon Innovation. The Survey generates geoscience knowledge and data to inform land use and resource management decisions, and to support the growth of British Columbia as a competitive jurisdiction for mineral exploration.

The Cordilleran Geoscience Section conducts field and office research including bedrock and surficial geology mapping programs, regional geochemical surveys, and targeted mineral deposit studies. Like most geological survey organizations around the world, critical minerals, which are essential for low-carbon technologies, are a major theme for the Survey. To inform the Critical Minerals Strategy being developed by the provincial government, the Survey compiled a critical minerals atlas as the initial step in evaluating the critical mineral endowment of the province and in building awareness of critical mineral opportunities for the exploration and mining industries. The Survey also began field projects directed at assessing opportunities through mineral system studies in regions known to contain critical minerals. Both to aid in the search for critical minerals and to inform land-use conversations between multiple parties having diverse interests, the Survey has revitalized the mineral potential modelling of the 1990s. This new modelling takes advantage of about 30 years of new data, knowledge, and advances in GIS applications and computer power to enable statistical analysis of spatial data. The past year has seen further progress of multi-year mapping projects such as detailed mapping in the northwest part of the province in the Kitsault area, along the Stikine arch, and near Atlin.

Responsible for maintaining and developing provincial geoscience and mineral resource databases, the Resource Information Section disseminates data online through web portals, MapPlace geospatial web services, and the BC Data Catalogue. Information managed by the team includes traditional geological maps and reports, geochemical, geophysical, and geological databases, in addition to mineral resource inventory and exploration assessment reports. The databases and webservices are designed to update data, facilitate data mining, and support applications for mineral exploration (particularly for critical minerals), and land-use planning. The team has started projects to modernize information systems and build a geoscience Spatial Data Infrastructure (SDI).

The Mineral Development Office (MDO) is the Vancouver base of the Survey. It provides investment intelligence to government and global business and publishes the annual Provincial Overview of Exploration and Mining in British Columbia volume. The MDO is staffed by a group of Regional Geologists who, stationed in exploration centres across the province, track minerals activities and provide geoscience expertise in their jurisdictions.

1. Introduction

The British Columbia Geological Survey (BCGS), headquartered in Victoria, is a public geoscience agency in the Responsible Mining and Competitiveness Division of the British Columbia Ministry of Energy Mines and Low Carbon Innovation. BCGS creates and disseminates public geoscience information that supports effective mineral exploration, sound land use management, and responsible governance and attracts investment. The Survey is the primary repository for provincial geoscience knowledge. Maps, reports, and databases are freely available online and are public resources for Indigenous peoples, local communities, the minerals industry, public safety agencies, environmental scientists, research organizations, and other government agencies. Current research programs and publications (Figs.1, 2) continue to define the geological evolution and mineral resources of the province, generating knowledge and data to support land use and resource

management decisions that balance economic, environmental, and community interests.

The BCGS consists of three sections: 1) Cordilleran Geoscience; 2) Resource Information; 3) the Mineral Development Office (Fig. 3). The Cordilleran Geoscience Section generates new knowledge through field, laboratory, and office-based research activities including geological mapping programs, regional geochemical surveys, and targeted geological and mineral deposit studies. The Section is also divided into two teams. The Framework Geoscience team is primarily focused on bedrock and surficial geological mapping and targeted foundational geological studies (e.g., magmatic, stratigraphic, structural, metallogenic). The Economic Geology and Geochemistry team conducts thematic studies on the origin of mineral deposits, the spatial and temporal distribution of commodities, mineral systems, exploration tools, and regional geochemistry. Team members also manage in-house laboratory

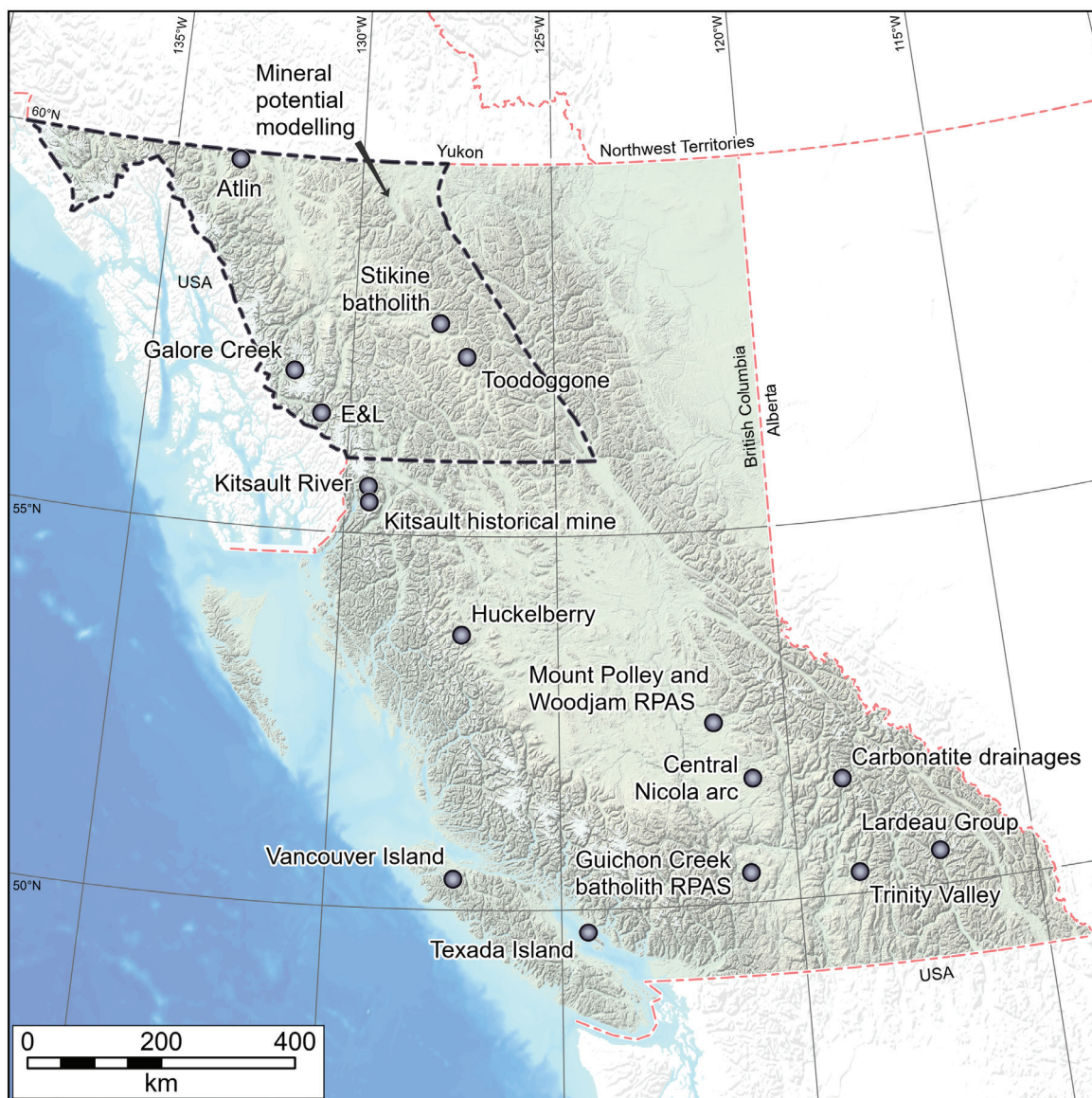
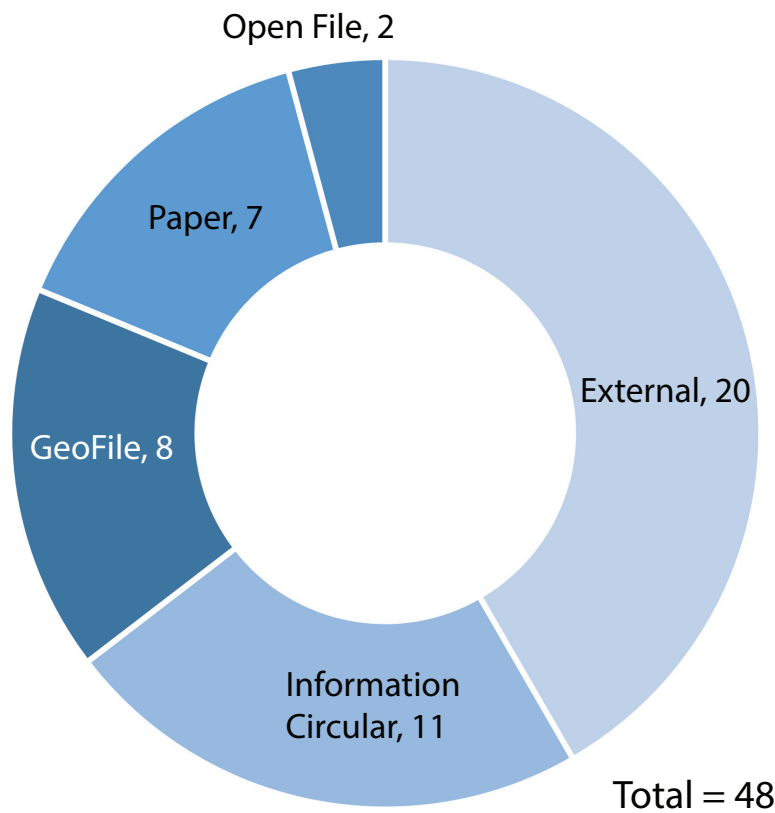


Fig. 1. British Columbia Geological Survey projects in 2023.

facilities and curate the provincial sample archive. The Resource Information Section is responsible for developing and updating provincial geoscience databases and disseminating data online through geospatial web services (MapPlace). The Section is divided into two teams. The Geomatics Information team is responsible for geoscience data and managing databases, publications, geoscience data products, interoperable data sharing, and geospatial web services. The Mineral Resource Information team is responsible for reviewing mineral assessment reports, compiling mineral occurrences, archiving exploration technical documents, and updating mineral resource inventory data. The Mineral Development Office (MDO) is the Vancouver base of the Survey and provides investment intelligence to government and global business. The MDO is staffed by a group of Regional Geologists who, stationed in exploration centres across the province, track minerals activities and provide geoscience expertise in their regions. The

MDO publishes the annual Provincial Overview of Exploration and Mining in British Columbia volume (Clarke et al., 2024).

Like most geological survey organizations around the world, critical minerals, which are essential for low-carbon technologies, are a major theme for the Survey. These minerals are required for electric vehicles, mobile phones, solar panels, wind turbines, electrical transmission lines, batteries, and medical devices, and to manufacture products for national defense. As society places more value on the transition to low-carbon energy, demand for minerals important for energy generation, storage, and transmission will increase. British Columbia is developing its own Critical Minerals Strategy and BCGS is contributing geoscience information that will be foundational for the strategy. The Survey has compiled a critical minerals atlas as the initial step in evaluating the critical mineral endowment of the province and in building awareness of critical mineral opportunities for the exploration and mining



Papers*: This series is reserved for reviews and final thematic or regional works. Geological Fieldwork, our annual review of field activities and current research, is released as the first Paper of each year.

Geoscience Maps: This series is the BCGS vehicle for publishing final maps.

Open Files: These maps and reports present the interim results of ongoing research, particularly mapping projects.

GeoFiles: These publications enable rapid release of extensive data tables from ongoing geochemical, geochronologic, and geophysical work. As such, they serve the same function as data repositories provided by many journals, providing immediate access to raw data from specific projects.

Information Circulars: These publications provide accessible geoscience information to a broad audience in government, industry, and the general public. Included in the Information Circular series is the annual Provincial Overview of Exploration and Mining in British Columbia.

Contributions to partner publications: This category includes reports, maps, and other products published by another agency such as the Geological Survey of Canada or Geoscience BC, but have received contributions from British Columbia Geological Survey staff.

External publications: These are contributions to the peer reviewed literature and published in a recognized national or international scientific journal.

*The count refers to the total number of articles authored by BCGS personnel in a volume.

Fig. 2. Types and numbers of publications produced by the British Columbia Geological Survey in 2023.

industries (Hickin et al., 2023). In addition, the Survey began field projects directed at assessing opportunities through mineral system studies in regions known to contain critical minerals. These studies are primarily focused on assessing potential critical mineral co- and by-products in the mineral systems that host major producing mines and will assess some of the more underexplored mineral systems in British Columbia such as carbonatites and iron skarns.

As overlapping and potentially competing interests in the provincial land base continue to grow, land use planning has received renewed emphasis in British Columbia. The approach is broad and aims to ensure that all aspects, such as wildlife, forestry, mineral interests, and cultural heritage are considered in land decisions. In 2019, the Province of British Columbia committed to Indigenous reconciliation with the passing of the Declaration on the Rights of Indigenous Peoples Act, which

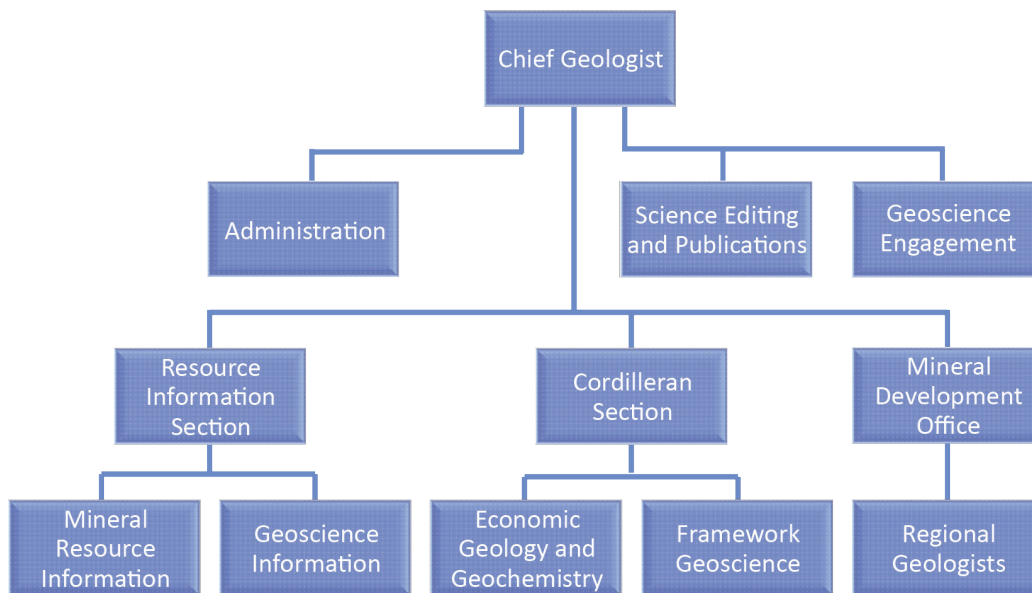


Fig. 3. British Columbia Geological Survey organizational chart.

has the objective of creating paths that respect the rights of Indigenous Peoples. This, combined with other initiatives like establishing Indigenous Protected and Conservation areas (IPCA) where Indigenous governments have the primary role in protecting and conserving ecosystems through Indigenous laws, governance, and knowledge systems, and the Tripartite Framework Agreement on Nature Conservation (Government of British Columbia, 2023), has elevated the need for robust mineral potential information. Building on work it conducted in the 1990s, BCGS has revitalized its mineral potential mapping efforts, taking advantage of about 30 years of new data, knowledge, and advances in GIS applications and computer power to enable statistical analysis of spatial data.

Recognizing the need to provide better outreach and to link geoscience with people and communities, BCGS hired its first Engagement Geoscientist. This position was created to connect Indigenous Peoples, local communities, governments, the minerals industry, and the public to the geology and mineral resources of the province. Developing meaningful relationships with Indigenous communities near where the BCGS conducts fieldwork is a contribution to reconciliation. The Engagement Geoscientist serves as the primary liaison between Survey geologists and communities, supports field programs, and translates technical outputs into consumable information for the public. This position builds geoscience outreach capacity and enhances geoscience literacy by developing materials, presentations, and working directly with non-technical stakeholders and rightsholders.

2. Partnerships

Partnerships continue to be an effective way for the Survey to lever its resources. Working with other geoscience professionals, agencies, and industry, these partnerships extend across a wide spectrum of collaboration, all with the aim of

enhancing public geoscience. In addition to inter-Ministry cooperation and working with external commercial service providers, BCGS has partnered with six university laboratories to acquire research-grade analyses for key initiatives such as our rock archive re-analysis. The Survey is working closely with laboratories at the University of British Columbia, University of Victoria, University of Alberta, University of Manitoba, Carleton University, Queens University, University of Windsor, and Memorial University. The Survey is also partnering directly with researchers from several Canadian universities. Since the early 2000s, BCGS has had a formal partnership with the University of Victoria. This partnership continued this year with one project using magnetite as an indicator mineral and another assessing the exhumation history of Hogen batholith. As part of a volcanogenic massive sulphide (VMS) project that will study deposits at several Canadian sites, the Survey is collaborating with Memorial University and other Canadian research institutions on provincial examples. BCGS is working with the Mineral Deposits Research Unit (MDRU) at the University of British Columbia to establish a joint project directed at sedimentary exhalative deposits in British Columbia.

The Survey continues to support training the next generation of geoscientists by its summer field assistant hiring program and by supporting graduate student projects. The Survey is co-funding and supervising a M.Sc. project at Simon Fraser University in which remotely piloted aircraft systems (RPAS; also known as unmanned aerial vehicles, UAV or ‘drones’) are used to collect geophysical data that will help assess mineral dispersion in till. Also, Survey staff are helping to supervise two M.Sc. projects at the University of British Columbia that address the context and structural evolution of the Galore Creek and Big Bulk deposits in northwestern British Columbia.

The Survey continues to partner with industry through formal

and informal collaborations and is working with Coast Copper Corp. at the Merry Widow deposit on Vancouver Island and with Galore Creek Mining Corporation at their Galore Creek copper deposit in northwestern British Columbia. The Survey has also initiated collaborations at the E&L property (Garibaldi Resources Corp.), the Huckleberry mine (Imperial Metals; on care and maintenance since 2016), the Kitsault Valley project (Dolly Varden Silver Corp), the historical Kitsault Mo-Ag mine (New Moly LLC), the Berg property (Surge Copper Corp), and skarn mineralization on Texada Island (Acrosa Specialty Metals and Lafarge Canada Inc.).

The BCGS and the Geological Survey of Canada (GSC) have a long history of partnering. Currently BCGS and GSC are collaborating on a Geomapping for Energy and Minerals (GEM-North) project focused on the tectonic assembly of the Intermontane region close to the Yukon-British Columbia border. This project will examine the relationships between tectono-stratigraphic units and determine magmatic, structural and exhumation histories to better understand terrane architecture in three dimensions, which will aid exploration decisions. To help interpret regional airborne geophysics and guide geophysical inversion models, the Survey has partnered with the GSC's Pacific Laboratory to establish the physical properties of rocks held in the BCGS archive. The Survey has also applied for partnership funding with the federal government for several multi-year projects through the Critical Minerals Geoscience and Data initiative.

Canada's Information and Data Management (IDM) Working Group is co-lead by the BCGS and is part of the Canadian National Geological Surveys Committee (NGSC). In support of the Pan-Canadian Geoscience Strategy and co-chaired by BCGS and GSC, the IDM has initiated a pilot project to create a distributed national mineral occurrence database and web service that includes data from nine provincial, territorial, and national geological surveys.

BCGS is committed to working with industry, government, academia, and communities and open to collaboration. Interested parties are encouraged to contact the Survey.

3. Staffing

The Survey remains an organization in transition. In the last year, the Survey has embarked on a hiring campaign to fill vacancies that resulted from retirements, departures, and growth. BCGS is currently staffed by 38 permanent staff (Fig. 4); five vacancies are at various stages of competition. In addition to its complement of permanent staff, the Survey hires 8-12 seasonal or term employees each year, usually university students or recent graduates, to aid safe fieldwork or to assist in targeted projects. These are excellent opportunities for early career geoscientists to gain experience as they develop skillsets that are valued by the sector.

Early in the year, the Survey restructured slightly, adding a layer of technical leadership to ease our expansion in personnel (Fig. 3). In the Resource Information section, Jessica Norris manages the Mineral Resource Information



Fig. 4. British Columbia Geological Survey staff.

team while Gabe Fortin manages the Geomatics Information team. Don Harrison and Ryan Grundy have accepted positions as Mineral Assessment Geologists responsible for reviewing and approving the assessment reports submitted by industry to retain mineral tenures in good standing. Bronwen Wallace is helping to resolve a backlog of assessment reports while taking on the new role of coordinating systems and website development. Kerri Shaw accepted the Mineral Inventory Geologist position responsible for the BCGS MINFILE database and its modernization.

In the Cordilleran Section, Luke Ootes has been acting Director since the departure of Neil Wildgust in late 2022. Luke has now accepted a permanent posting as the Manager of Economic Geology and Geochemistry team where Curran Wearmouth is the new Mineral Potential Geologist and Matthew Brzozowski is a new Economic Geologist. Bram van Stratten has become the Manager of the Framework Geoscience team and Roddy Campbell joined the team as a Minerals Geologist. The Mineral Development Office appointed Cary Pothorin as the Regional Geologist for the South Central Region, a position that had been vacant for many years. In the Chief Geologists Office, Branch Coordinator Cinthia Kong took leave this year and Jenny Boulet-Marshall filled in. Jenny subsequently accepted another position in government and her position is being filled by Madhur Upadhyay on a temporary assignment. He is being assisted by Di Tang to keep the Branch running smoothly. Also joining the Chief Geologist's Office is Rafael Bacha, the Survey's first Engagement Geoscientist.

4. Cordilleran Geoscience Section

Section geologists collect fundamental geoscience data through single and multi-year field-based programs complemented by laboratory and office studies. These programs include regional-scale mapping, mineral deposit studies, and new mineral exploration method development. Expertise encompasses tectonics, structural geology, stratigraphy, petrology, metallogeny, Quaternary and surficial geology, critical minerals, and geochemistry.

4.1. Critical minerals

Jurisdictions in Canada and around the world are developing strategies to ensure critical minerals supply chains are robust and resilient. As a contribution to British Columbia's CleanBC Roadmap to 2030, Hickin et al. (2023) prepared an atlas (Fig. 5) that inventories commodities in the province that appear on the Canadian critical minerals list or on those of key trading partners.

Part of province-wide studies directed at critical minerals, Hickin et al. (2024) provide an overview of six mineral systems that are important to British Columbia's critical minerals inventory, including: porphyry, volcanogenic massive sulphide, deep-water basin and platformal base metal, magmatic mafic to ultramafic, carbonatite, and iron skarn. Orovan et al. (2024) examined core at the past-producing Kitsault mine and recognized features (e.g., unidirectional solidification textures) that might record permeable structures that focused ore-bearing fluids. Brzozowski and Zaborniak (2024) examined core at the E&L magmatic Ni-Cu-PGE sulphide deposit that provided textural evidence indicating that sedimentary rock assimilation contributed to the sulphide saturation history of the E&L magma and shallow-level volatile exsolution, sulphide liquid transport through conduit plumbing, and subsequent metal remobilization. Using geochemical data collected as part of Regional Geochemical Survey (RGS)

programs, Rukhlov et al. (2024) define a multivariant 'critical mineral index' to assess prospectivity for carbonatite-hosted critical metals in the British Columbia alkaline province. Detailed data from carbonatites in the Blue River area, including the Upper Fir Nb-Ta deposit, served to develop this critical mineral index. Data from the Aley carbonatite complex were used to examine downstream dispersion from a known deposit. Ongoing field investigations were conducted at the past-producing Huckleberry Mine (Cu-Mo) and on Vancouver and Texada islands investigating Fe-skarns and their potential to host critical minerals.

Both to aid in the search for critical minerals and to support current land-use decisions the Survey has revitalized its mineral potential mapping work of the 1990s. This new work takes advantage of about 30 years of new data, knowledge, advances in GIS applications, and computer power to enable statistical analysis of spatial data using weights of evidence modelling (Fig. 6; British Columbia Geological Survey, 2023). A comparison of results between work done in the 1990s and the current work for an area that includes a large part of the northern British Columbia indicates that the new work largely corroborates the old and that both are of value for assisting mineral exploration and land-use decisions (Wearmouth et al., 2024).

4.2. Northern British Columbia

Based on the initial season of a two-year field-based project along the British Columbia-Yukon border, Mihalyuk et al. (2024) presented the initial results of mapping in the Gladys Lake area near Atlin, reassigning ophiolitic rocks previously considered part of Cache Creek terrane to Atlin terrane and describing what might be distal ultramafic-associated massive sulphide (UAMS) mineralization (Fig. 7). van Straaten et al. (2023) released GIS, structural, magnetic susceptibility, and other digital data to support the recently published map (van Straaten et al., 2022) of the Dease Lake area, and van Straaten (2024) synthesized stratigraphic and geochronologic work focused on the upper part the Hazelton Group along the Stikine arch in northern Stikinia with particular focus on the Stikine batholith, Mount Blair, Spatsizi (Fig. 8), and Yehiniko Lake areas, providing detailed maps, composite stratigraphic sections, lithological descriptions, contact relationships, and preliminary geochronological data. In the Kitsault area, an ongoing multi-year Survey program (Miller et al., 2023; Fig. 9) continues to expand regional bedrock mapping coverage to better understand the stratigraphic, magmatic, structural, metallogenic, and tectonic framework of this region. In the Toadoggone area, new mapping initiatives are underway (e.g., Ootes, 2023) to help compare the stratigraphy and intrusive history established in the more western parts of Stikinia (e.g., van Straaten, 2024). Jones et al. (2023) presented new igneous zircon Hf-O data from Hogem batholith (north-central Quesnel terrane) that indicate predominantly juvenile magmatic sources with minimal contribution by Ancestral North America crust. Milidragovic et al. (2023a) presented detrital

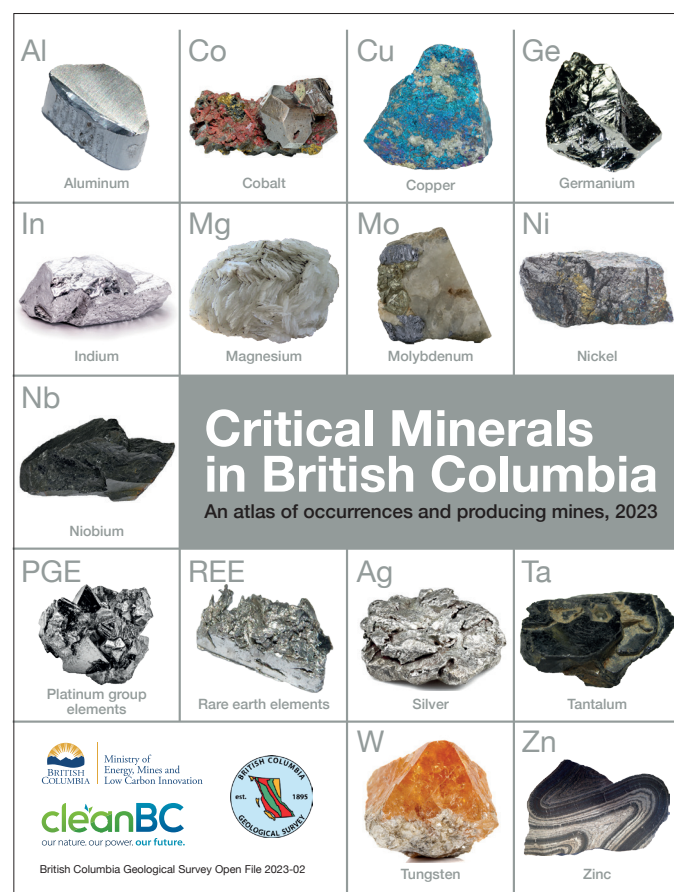


Fig. 5. British Columbia critical minerals atlas; see Hickin et al. (2023).

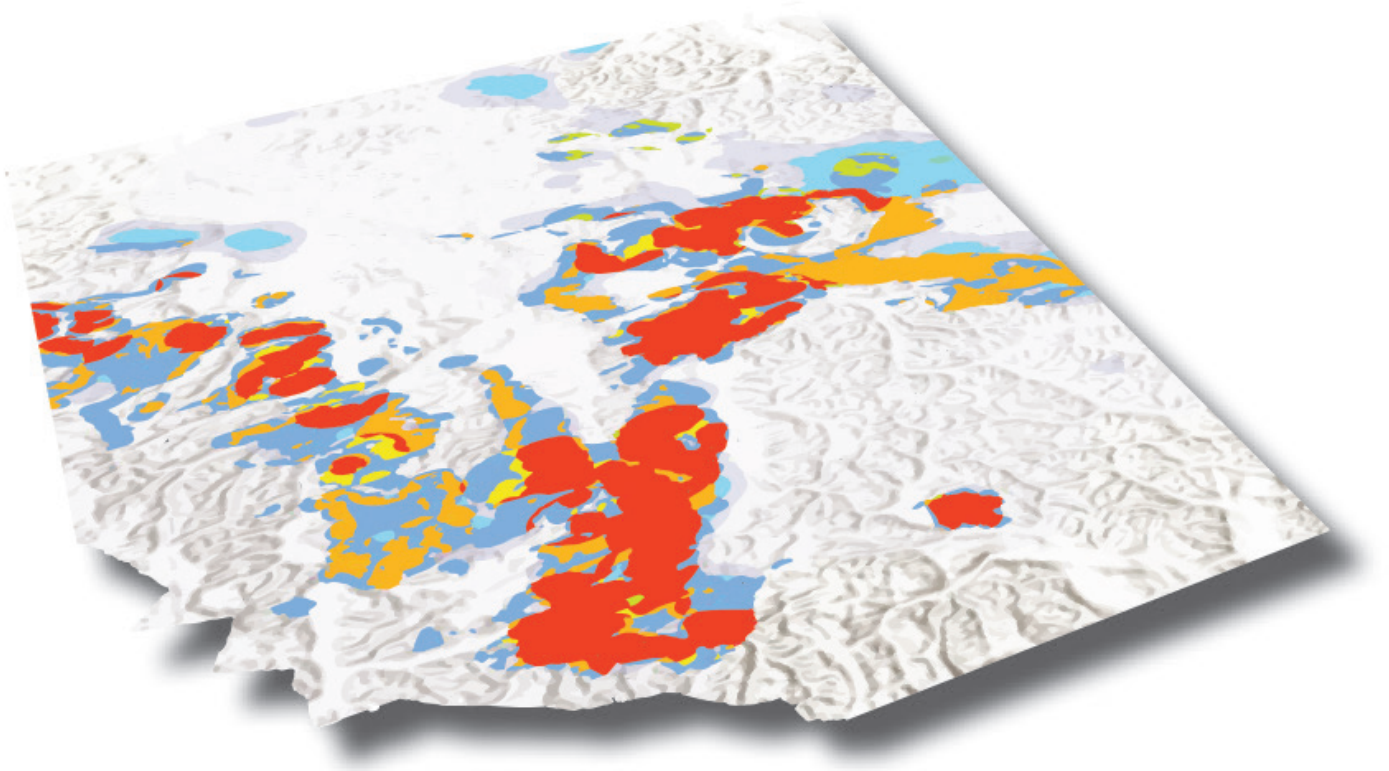


Fig. 6. Mineral potential model displaying relative prospectivity; greatest in red. See Wearmouth et al. (2024).

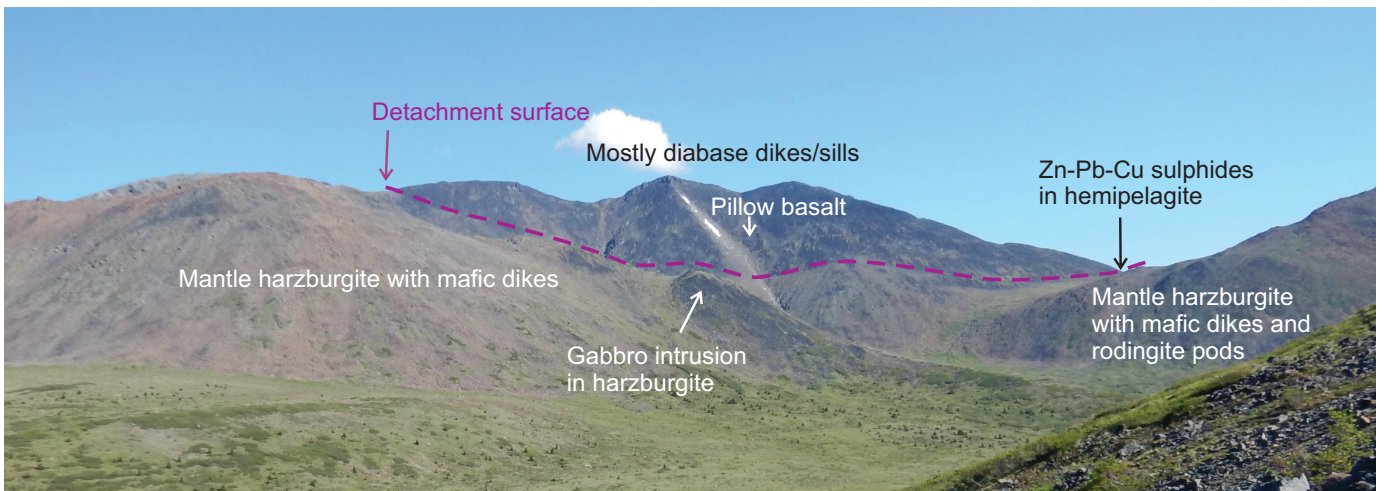


Fig. 7. View of intraoceanic detachment surface (dashed purple line) where mantle was exhumed to just below the sea floor. Hemipelagite samples with Zn-Pb-Cu sulphides, possible distal ultramafic-associated massive sulphide (UAMS) deposits, were collected from above the detachment (sample site beneath arrow). See Mihalynuk et al. (2024).

zircon U-Pb, Lu-Hf, and trace element data to document that the Cunningham formation in north-central British Columbia is a latest Triassic overlap succession linking Cache Creek terrane to Stikinia. Milidragovic et al. (2023b) examined the sulphur isotopic composition of primary sulphides at the Polaris Alaskan-type ultramafic-mafic intrusion, concluding that the sub-arc mantle contributed subducted sulphate.

4.3. Southern British Columbia

Elia et al. (2023) summarized the remotely piloted aircraft system (RPAS) platforms and sensors that were used to acquire spectrometer, magnetometer, and lidar data in the Mount Polley mine, Woodjam prospect, and Guichon Creek batholith areas and the methods for processing RPAS survey data, as an aid for mapping surficial geology and drift prospecting.



Fig. 8. At base, augite-plagioclase-phyric flow several m thick with highly vesicular flow overlain by 1 m-thick bed of volcanic breccia with common spatter clasts, overlain by 4 m-thick augite-plagioclase-phyric flow. Upper Hazelton Group, Horn Mountain Formation, Sister Mary mafic to intermediate volcanic unit in the Spatsizi area. See van Straaten (2024).

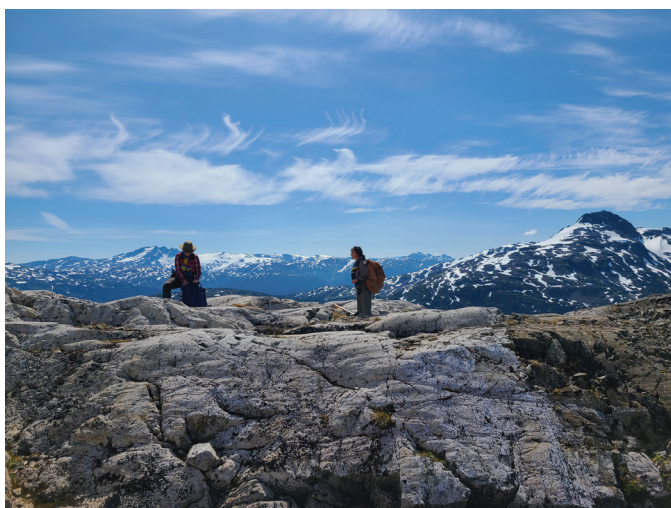


Fig. 9. Dark mafic volcanic rocks of the Stuhini Group (Late Triassic) on right cut by hornblende-phyric diorite dike of the Hyder plutonic suite (Eocene) near the eastern margin of the Coast Plutonic complex. Kitsault River area, near Mt. Camber, view to the northwest.

Elia et al. (2024) applied RPAS-acquired lidar data to map surficial sediments in the Interior Plateau, and Ferbey et al. (2024) applied RPAS-acquired radiometric data to quantify potassium concentrations in these sediments. Geological investigations and data compilation continues in the Cadwallader terrane near the Chilcotin River (Schiarizza and Friedman, 2023), the central Nicola arc north of Kamloops, the Lardeau Group north and west of Kootenay Lake (Mihalynuk et al., 2023), and the Trinity Valley area east of Vernon.

4.4. Sample archive

Rukhlov et al. (2023) reported on the inventory of the Survey's sample archive. In tandem with updates to rock

geochemical (Han and Rukhlov, 2024) and geochronological datasets (e.g., Ootes et al., 2024) the archive is being used to obtain and build a province-wide whole rock radiogenic isotope database (Sm-Nd, Rb-Sr, Lu-Hf, Pb-Pb). In partnership with the Geological Survey of Canada (Pacific), the Survey is continuing to advance the provincial rock petrophysical database by collecting magnetic, gravity, and porosity data from archived hand samples.

5. Resource Information Section

The BC Geological Survey collects, compiles, and disseminates provincial public geoscience that supports effective mineral exploration, sound land use management, and responsible governance. This public geoscience includes geological maps, reports, thematic studies, and the province-wide digital coverage of bedrock geology (BC Digital Geology). It also includes databases for mineral assessment reports (ARIS), mineral inventory (MINFILE), coal information (COALFILE), geochemical and geophysical surveys, and collections of previously unpublished private documents donated by government, universities, industry, and individuals (Property File). The Survey operates a few dozen information systems to update these databases and deliver them through web portals and MapPlace, the BCGS geospatial web service. As part of the Survey's digital transformation efforts, information systems are being re-engineered to build a geoscience spatial data infrastructure (gSDI) to improve efficiency in operating and updating databases, further digitalize analytical-ready geoscience information, and enable interoperable data sharing.

5.1. Geoscience spatial data infrastructure (gSDI)

Geoscience data need to be managed coherently because they are inherently related to each other. The Survey currently operates geoscience databases and applications built in the last two decades, mostly in discrete systems of varying legacy or obsolete technologies and, in most cases, the ability to link interpretations to raw data or observations are lacking. The Survey has been making efforts to build a gSDI to manage all geological and mineral resource data together as sub-systems in the same environment using common data and system components and well-defined interfaces across service boundaries. In 2022, ARIS was modernized as a first step towards a gSDI; in 2023 the Survey has been working on opportunities to modernize MINFILE and BC Digital Geology.

5.2. MapPlace

MapPlace is the BCGS geospatial web service to discover, visualize, search, and generate summary reports and maps from province-wide geoscience databases. Easy access to, and analysis of, geoscience maps and data are fundamental to inform decisions on mineral exploration, mining, environmental protection, and land-use management. MapPlace provides a platform to facilitate data mining and analysis of geoscience information in the context of all other relevant data such as mineral titles, assessment reports, land ownership, public

infrastructure, aquifers, and topographic base maps. Some of the data layers and applications are specifically developed to enable research and analytics for mineral exploration and prospecting.

5.3. ARIS assessment reports and database

Results of mineral exploration are submitted by industry as assessment reports to the government in compliance with the Mineral Tenure Act. After a one-year confidentiality period, the assessment reports become freely available to the public. The Survey manages these reports in the Assessment Report Indexing System (ARIS) database with metadata to search the locations, mineral occurrences, commodities, claims, and work types as documented in the reports. ARIS contains more than 40,300 reports dating from 1947. All the assessment reports are available online as PDF documents through the ARIS website, and more than 800 of them contain data (e.g., geochemical analyses and geophysical surveys) in common digital data formats that can be readily used. In addition to the search interface on the ARIS website and MapPlace, a copy of the ARIS metadata is available through the BC Data Catalogue.

The BCGS has set up an Assessment Report and Digital Data Submission portal, to encourage inclusion of digital files such as spreadsheets, databases, GIS maps, and grids in report submissions. Explorationists will benefit because digital data can be easily retrieved, integrated, and recast for specific needs. Digital submission will also enable the Survey to better maintain province-wide databases and create derivative products that use past results to guide future exploration. Both assessment reports and digital data can be uploaded through the ARIS data submission page. In addition, the Survey continues to digitally extract information for our assessment report-sourced surface sediment geochemical database (ARSSG), and has started digital extraction of drillhole collar and core geochemical data from assessment reports.

5.4. MINFILE mineral occurrence database

MINFILE is a database containing geological, location, and economic information for more than 16,100 mineral, coal, and industrial mineral mines, deposits, and occurrences in British Columbia. In 2023, more than 195 new occurrences and 900 updates were added to the database. In addition to spatial and non-spatial search and visualization on MapPlace, a dedicated web search interface is available to query the database and retrieve details such as geological setting, deposit type, mineralogy, age, commodity, host rock, production, and source of data. Query results are available to download as summary reports, spreadsheets, and KML. MINFILE/pc is a portable extract of the MINFILE database with a search interface and printable reports. The BCGS has transformed part of the MINFILE mineral occurrence data to the EarthResourceML Lite schema and mapped the contents using the vocabularies adopted by the IUGS Commission for the Management and Application of Geoscience Information (CGI). The EarthResourceML Lite-compliant mineral occurrence data

is accessible via the OneGeology portal and open standard-based interface such as Web Mapping Service (WMS) and Web Feature Service (WFS) specification. In 2023, the BCGS has been working with other participating Canadian provincial, territorial and the federal geological surveys to develop a national mineral occurrence database and web service that are compliant with a Canadian adoption of the EarthResourceML standard.

5.5. British Columbia Digital Geology

The BCGS offers province-wide digital coverage of bedrock geology including details from field mapping, with a typical regional compilation at a scale of 1:50,000 (Cui et al., 2017). A geospatial frame data (GFD) model is used to simplify the compilation and integration of new regional mapping into the BC Digital Geology database (Cui, 2021). Bedrock geology is standardized with consistent stratigraphic coding, ages, and rock types to enable computations, and is available for download in GeoPackage and Esri shapefile formats. Customized bedrock geological maps and legends can be explored, and data downloaded as KML by spatial and non-spatial queries via MapPlace. The BCGS has transformed the digital geology to the GeoSciML Lite schema and mapped the contents using the vocabularies adopted by the IUGS Commission for the Management and Application of Geoscience Information (CGI). The GeoSciML Lite-compliant digital geology is accessible via the OneGeology portal and open standard-based interface such as Web Mapping Service (WMS) and Web Feature Service (WFS) specification, to enable interoperable data sharing and analytics.

5.6. Other databases

The Survey also manages dozens of other databases. COALFILE includes a collection of assessment reports dating from 1900. Property File is a collection of spatially referenced archived reports, maps, photos, and technical notes documenting mineral exploration activities in British Columbia from the late 1800s. The provincial geochemical databases hold field and geochemical data from multi-media surveys by the Geological Survey of Canada, the BCGS, and Geoscience BC. The databases are updated regularly and contain results from the Regional Geochemical Survey program, till surveys, and lithochemical samples. Accompanying the physical relocation and rationalization of the BCGS Sample Archive in 2022, a modern digital inventory was created for integration with other provincial datasets (Rukhlov et al., 2023).

6. Mineral Development Office

The mining industry contributes greatly to the economy of British Columbia. Particularly important for northern communities and First Nations, the mineral exploration, mining, and related sectors employ more than 35,000 people. For 2023, the forecast value of mine production in British Columbia is \$15.9 billion (Clarke et al., 2024).

Mineral exploration is the backbone of mining and an

estimated \$643.5 million was spent on exploration in 2023. More than 200 companies have projects in British Columbia and these projects are monitored by the Mineral Development Office (MDO) and its Regional Geologists. The MDO is the Vancouver base of the British Columbia Geological Survey. It links the more than 1100 exploration and mining companies headquartered in Vancouver to provincial mineral and coal information. The MDO distributes Survey data and provides technical information and expertise about mineral opportunities to the domestic and international investment community. The MDO monitors the activities of the mining and exploration sectors and produces the Provincial Overview of Exploration and Mining in British Columbia, an annual volume that summarizes activities in the different regions of the province (see e.g., Clarke et al., 2024). The British Columbia Regional Geologists (Table 1) represent the provincial government on geological matters at a regional level, and capture information on industry activity in their jurisdictions. Within their communities, the Regional Geologists provide information on exploration trends, possible investment opportunities, land use processes, First Nation capacity building, and public outreach.

Table 1. British Columbia Regional Geologists.

Regional Geologist	Office	Region
Nate Corcoran	Smithers	Northwest
Hassan Heidarian	Prince George	Northeast and North Central
Cary Pothorin	Kamloops	South Central
	Cranbrook	Southeast
Bruce Northcote	Vancouver	Southwest

Acknowledgment

We thank George Owsiaci of Total Earth Science Services (Victoria) for desktop publishing of this volume.

References cited

- British Columbia Geological Survey, 2023. Mineral potential modelling at the British Columbia Geological Survey: The next generation. British Columbia Ministry of Energy, Mines and Low Carbon Innovation, British Columbia Geological Survey Information Circular 2023-07, 7 p. (brochure).
- Brzozowski, M.J., and Zaborniak, K., 2024. Petrology of sulphide mineralization at the E&L magmatic Ni-Cu-PGE deposit: Textural evidence for contamination, vapor saturation, fluid immiscibility, and metal remobilization. In: *Geological Fieldwork 2023*, British Columbia Ministry of Energy, Mines and Low Carbon Innovation, British Columbia Geological Survey Paper 2024-01, pp. 65-78.
- Clarke, G., Northcote, B.K., Corcoran, N.L., Pothorin, C., Heidarian, H., and Hancock, K., 2024. Exploration and Mining in British Columbia, 2023: A summary. In: *Provincial Overview of Exploration and Mining in British Columbia, 2023*. British Columbia Ministry of Energy, Mines and Low Carbon Innovation, British Columbia Geological Survey Information Circular 2024-01, pp. 1-53.
- Cui, Y., 2021. A geospatial frame data model to simplify digital map compilation and integration. British Columbia Ministry of Energy, Mines and Low Carbon Innovation, British Columbia Geological Survey Paper 2021-03, 20 p.
- Cui, Y., Miller, D., Schiarizza, P., and Diakow, L.J., 2017. British Columbia digital geology. British Columbia Ministry of Energy, Mines and Petroleum Resources, British Columbia Geological Survey, Open File 2017-8, 9p. Data version 2019-12-19. <<https://www2.gov.bc.ca/gov/content/industry/mineral-exploration-mining/british-columbia-geological-survey/geology/bcdigitalgeology>> (accessed December 2023).
- Elia, E.A., Ferbey, T., Ward, B.C., Shives, R.B.K., Best, M., and Martin-Burtart, N., 2023. Remotely piloted aircraft system (RPAS) for investigating surface sediments in the Interior Plateau of British Columbia: Methods, data, and products. British Columbia Ministry of Energy, Mines and Low Carbon Innovation, British Columbia Geological Survey GeoFile 2023-07, 22 p.
- Elia, E.A., Ferbey, T., and Ward, B.C., 2024. Mapping surficial sediments in the Interior Plateau using remotely piloted aircraft system lidar. British Columbia Ministry of Energy, Mines and Low Carbon Innovation, British Columbia Geological Survey Open File, in press.
- Ferbey, T., Elia, E.A., Shives, R.B.K., Martin-Burtart, N., Best, M., and Ward, B.C., 2024. Quantifying potassium concentrations in Interior Plateau surface sediments using remotely piloted aircraft system gamma-ray spectrometry. British Columbia Ministry of Energy, Mines and Low Carbon Innovation, British Columbia Geological Survey Open File, in press.
- Government of British Columbia, 2023. Government of Canada, British Columbia and the First Nations Leadership Council sign a historic tripartite nature conservation framework agreement. <<https://news.gov.bc.ca/stories/government-of-canada-british-columbia-and-the-first-nations-leadership-council-sign-a-historic-tripa>> (Accessed November 2023).
- Han, T., and Rukhlov, A.S., 2024. Update of rock geochemical database at the British Columbia Geological Survey. British Columbia Ministry of Energy, Mines and Low Carbon Innovation, British Columbia Geological Survey GeoFile, in press.
- Hickin, A.S., Orovan, E.A., Brzozowski, M.J., McLaren, K., Shaw, K.L., and Van der Vlugt, J., 2023. Critical minerals in British Columbia: An atlas of occurrences and producing mines, 2023. British Columbia Ministry of Energy, Mines and Low Carbon Innovation, British Columbia Geological Survey Open File 2023-02, 102 p.
- Hickin, A.S., Ootes, L., Orovan, E.A., Brzozowski, M.J., Northcote, B.K., Rukhlov, A.S., and Bain, W.M., 2024. Critical minerals and mineral systems in British Columbia. In: *Geological Fieldwork 2023*, British Columbia Ministry of Energy, Mines and Low Carbon Innovation, British Columbia Geological Survey Paper 2024-01, pp. 13-51.
- Jones, G., Ootes, L., Luo, Y.A., Vezinet, A., Stern, R., Milidragovic, D., and Pearson, D.G., 2023. The relative roles of ancient and juvenile crust in building accretionary orogens—Minimal ancient crust involved in the magmatic evolution of a North American Cordillera accreted terrane indicated by igneous zircon Hf-O. *Lithos*, article 107213. <<https://doi.org/10.1016/j.lithos.2023.107213>>
- Mihalynuk, M.G., Ootes, L., Drobe, J.R., Wall, C., and Friedman, R.M., 2023. Lardeau Group mapping update—implications for ultramafic-associated massive sulfide and critical metal exploration in southeast British Columbia. British Columbia Ministry of Energy, Mines and Low Carbon Innovation, British Columbia Geological Survey GeoFile 2023-06 (poster).
- Mihalynuk, M.G., Zagorevski, A., Campbell, R., Hajiegeh, A., and Vaillancourt, A., 2024. Preliminary results from revision mapping of the Gladys Lake area, near Atlin, northwest British Columbia. In: *Geological Fieldwork 2023*, British Columbia Ministry of Energy, Mines and Low Carbon Innovation, British Columbia Geological Survey Paper 2024-01, pp. 131-148.
- Milidragovic, D., Ootes, L., Zagorevski, A., Cleven, N., Wall, C.J., and Luo, Y., 2023a. Detrital geochronology of the Cunningham

- Lake formation: an overlap succession linking Cache Creek terrane to Stikinia at ~205 Ma. *Canadian Journal of Earth Sciences*, 60. <<https://doi.org/10.1139/cjes-2023-0018>>
- Mildragovic, D., Nott, J.A., Spence, D.W., Schumann, D., Scoates, J.S., Nixon, G.T., and Stern, R.A., 2023b. Sulfate recycling at subduction zones indicated by sulfur isotope systematics of Mesozoic ultramafic island arc cumulates in the North American Cordillera. *Earth and Planetary Science Letters*, 620, article 118337. <<https://doi.org/10.1016/j.epsl.2023.118337>>
- Miller, E.A., van Straaten, B.I., and Hunter, R.C., 2023. Update on bedrock mapping in the Kitsault River area, northwestern British Columbia. In: *Geological Fieldwork 2022*, British Columbia Ministry of Energy, Mines and Low Carbon Innovation, British Columbia Geological Survey Paper 2023-01, pp. 23-32.
- Ootes, L., 2023. Did epithermal mineralization in the northern Toadogone region develop synchronously with large scale folding? In: *Geological Fieldwork 2022*, British Columbia Ministry of Energy, Mines and Low Carbon Innovation, British Columbia Geological Survey Paper 2023-01, pp. 13-21.
- Ootes, L., Rukhlov, A.S., and Han, T., 2024. British Columbia Geological Survey rock geochemical and geochronological data products: Examples of utility. In: *Geological Fieldwork 2023*, British Columbia Ministry of Energy, Mines and Low Carbon Innovation, British Columbia Geological Survey Paper 2024-01, pp.123-129.
- Orovan, E.A., Zaborniak, K., and Hooker, K., 2024. Textural evidence for ore fluid transport and the magmatic to hydrothermal transition at the past-producing Kitsault Mo-Ag mine. In: *Geological Fieldwork 2023*, British Columbia Ministry of Energy, Mines and Low Carbon Innovation, British Columbia Geological Survey Paper 2024-01, pp. 53-64.
- Rukhlov, A.S., Coats, B., Van der Vlugt, J., Beaupre-Olsen, I.J., and Zaborniak, K., 2023. British Columbia Geological Survey Sample Archive: An emerging resource for public geoscience. In: *Geological Fieldwork 2022*, British Columbia Ministry of Energy, Mines and Low Carbon Innovation, British Columbia Geological Survey Paper 2023-1, pp. 85-90.
- Rukhlov, A.S., Cui, Y., Cunningham, Q., Fortin, G., and Anderson, C., 2024. Geochemical signals of carbonatite-related critical metals in provincial stream sediments. In: *Geological Fieldwork 2023*, British Columbia Ministry of Energy, Mines and Low Carbon Innovation, British Columbia Geological Survey Paper 2024-01, pp. 97-122.
- Schiarizza, P., and Friedman, R.M., 2023. U-Pb zircon dates for rhyolite and sandstone of Cadwallader terrane, lower Chilcotin River area, south-central British Columbia. In: *Geological Fieldwork 2022*, British Columbia Ministry of Energy, Mines and Low Carbon Innovation, British Columbia Geological Survey Paper 2023-01, pp. 65-84.
- van Straaten, B.I., 2024. Upper Hazelton Group stratigraphy along the Stikine arch, northwestern British Columbia. In: *Geological Fieldwork 2023*, British Columbia Ministry of Energy, Mines and Low Carbon Innovation, British Columbia Geological Survey Paper 2024-01, pp. 149-177.
- van Straaten, B.I., Logan, J.M., Nelson, J.L., Moynihan, D.P., Diakow, L.J., Gibson, R., Bichlmaier, S.J., Wearmouth, C.D., Friedman, R.M., Golding, M.L., Miller, E.A., and Poulton, T.P., 2022. Bedrock geology of the Dease Lake area. British Columbia Ministry of Energy, Mines and Low Carbon Innovation, British Columbia Geological Survey Geoscience Map 2022-01, 1:100,000 scale.
- van Straaten, B.I., Logan, J.M., Nelson, J.L., Moynihan, D.P., Diakow, L.J., Gibson, R., Bichlmaier, S.J., Wearmouth, C.D., Friedman, R.M., Golding, M.L., Miller, E.A., and Poulton, T.P., 2023. Bedrock geology of the Dease Lake area: Supporting GIS, structural, magnetic susceptibility, and other digital data, British Columbia Ministry of Energy, Mines and Low Carbon Innovation, British Columbia Geological Survey GeoFile 2023-08, 5 p.
- Wearmouth, C.D., Peters, K.J., Czertowicz, T.A., and Orovan, E.A., 2024. Mineral potential modelling results for northwestern British Columbia, a comparison between past and current work at the British Columbia Geological Survey. In: *Geological Fieldwork 2023*, British Columbia Ministry of Energy, Mines and Low Carbon Innovation, British Columbia Geological Survey Paper 2024-01, pp. 79-95.

Critical minerals and mineral systems in British Columbia



Adrian S. Hickin¹, Luke Ootes¹, Evan A. Orovan¹, Matthew J. Brzozowski¹,
Bruce K. Northcote¹, Alexei S. Rukhlov¹, and Wyatt M. Bain¹

¹ British Columbia Geological Survey, Ministry of Energy, Mines and Low Carbon Innovation, Victoria, BC, V8W 9N3

^a corresponding author: Adrian.hickin@gov.bc.ca

Recommended citation: Hickin, A.S., Ootes, L., Orovan, E.A., Brzozowski, M.J., Northcote, B.K., Rukhlov, A.S., and Bain, W.M., 2024. Critical minerals and mineral systems in British Columbia. In: *Geological Fieldwork 2023*, British Columbia Ministry of Energy, Mines and Low Carbon Innovation, British Columbia Geological Survey Paper 2024-01, pp. 13-51.

Abstract

Mining is essential to produce the commodities needed to combat climate change. Low-carbon technologies need critical minerals to produce electric vehicles, mobile phones, solar panels, wind turbines, electrical transmission lines, batteries, and medical devices, and to manufacture products for national defense. Because of global demands, many of these critical minerals are predicted to see shortages, and British Columbia is faced with a generational opportunity for mining that will not only contribute to a low-carbon future but generate significant economic and societal benefits. Already mining critical minerals, British Columbia is Canada's largest producer of Cu, only producer of Mo, mines Mg, and recovers Zn, Ag, and Pb. Adopting a mineral systems approach, the British Columbia Geological Survey is engaging in field, laboratory, and mineral potential modelling studies to evaluate the critical mineral endowment of the province, clarify by- and co-production possibilities of critical minerals not being recovered from current base and precious metal mines, and serve the provincial Critical Minerals Strategy. Six mineral systems are of particular importance: porphyry; volcanogenic massive sulphide; deep-water basin and platformal base-metal; magmatic mafic to ultramafic; carbonatite, and iron skarn. Providing foundational geoscience data and developing novel exploration techniques will encourage discoveries and enhance exploration for underexplored mineral systems. By increasing awareness of critical mineral opportunities for the exploration and mining industries, and by enhancing the critical mineral knowledge base, the province seeks to encourage investment that could lead to new discoveries, expand existing resources, and make British Columbia a significant supplier of the raw materials necessary to address the climate crisis.

Keywords: Critical minerals, critical minerals strategy, mineral criticality, mineral systems, mineral potential modelling, porphyry, volcanogenic massive sulphide, SEDEX, MVT, magmatic mafic to ultramafic, carbonatite, iron skarn

1. Introduction

Critical minerals are essential for low-carbon technologies. These minerals are required for electric vehicles, mobile phones, solar panels, wind turbines, electrical transmission lines, batteries, and medical devices, and to manufacture products for national defense. As society places more value on the transition to low-carbon-based energy, demand for minerals important for energy generation, storage, and transmission will increase. Consequently, jurisdictions around the world are developing strategies to ensure critical mineral supply chains are robust and resilient. In 2021, the Government of Canada released a national critical minerals list (Fig. 1) and the Canadian Critical Minerals Strategy (NRCan, 2022) to encourage investment in critical minerals and strengthen economies while combating climate change. British Columbia, the other provinces, and the territories are also pursuing strategies to take advantage of the global interest in stable and responsible mining jurisdictions.

Mining and mineral exploration contribute greatly to the economy of British Columbia. Employing more than 35,000 people, these industries are particularly important to rural communities. In the last five years, the total value of mining production was \$63.4 billion and the mineral exploration expenditure was \$2.8 billion (Clarke et al., 2020, 2021, 2022, 2023, 2024).

In this paper we first consider how critical minerals are defined, the jurisdictional dependence and transient nature of critical mineral lists and introduce British Columbia's critical minerals atlas. We then describe how the British Columbia Geological Survey has moved away from historical mineral deposit profiles to a more encompassing 'mineral systems' approach, how this approach is applied to modern mineral potential modelling and summarize six mineral systems of importance to critical minerals in British Columbia: porphyry, volcanogenic massive sulphide, deep-water basin and platformal base-metal, magmatic mafic to ultramafic, carbonatite, and iron skarn.

2. Critical minerals and criticality

Although some critical mineral lists do include a small number of minerals or groups of minerals, the term 'critical mineral' is a misnomer because it commonly refers to elements rather than actual minerals. The criticality of minerals is defined by different groups, for different purposes, in different ways, but two criteria are commonly used. First, a mineral may be deemed critical if it serves an essential purpose (e.g., national security or economic health) and second, if it is at risk of supply disruption (e.g., National Research Council, 2008; Graedel et al., 2012; Gunn, 2014; Hayes and McCullough, 2018). Critical mineral lists are neither universal nor static (e.g., Jowitt et al., 2018).

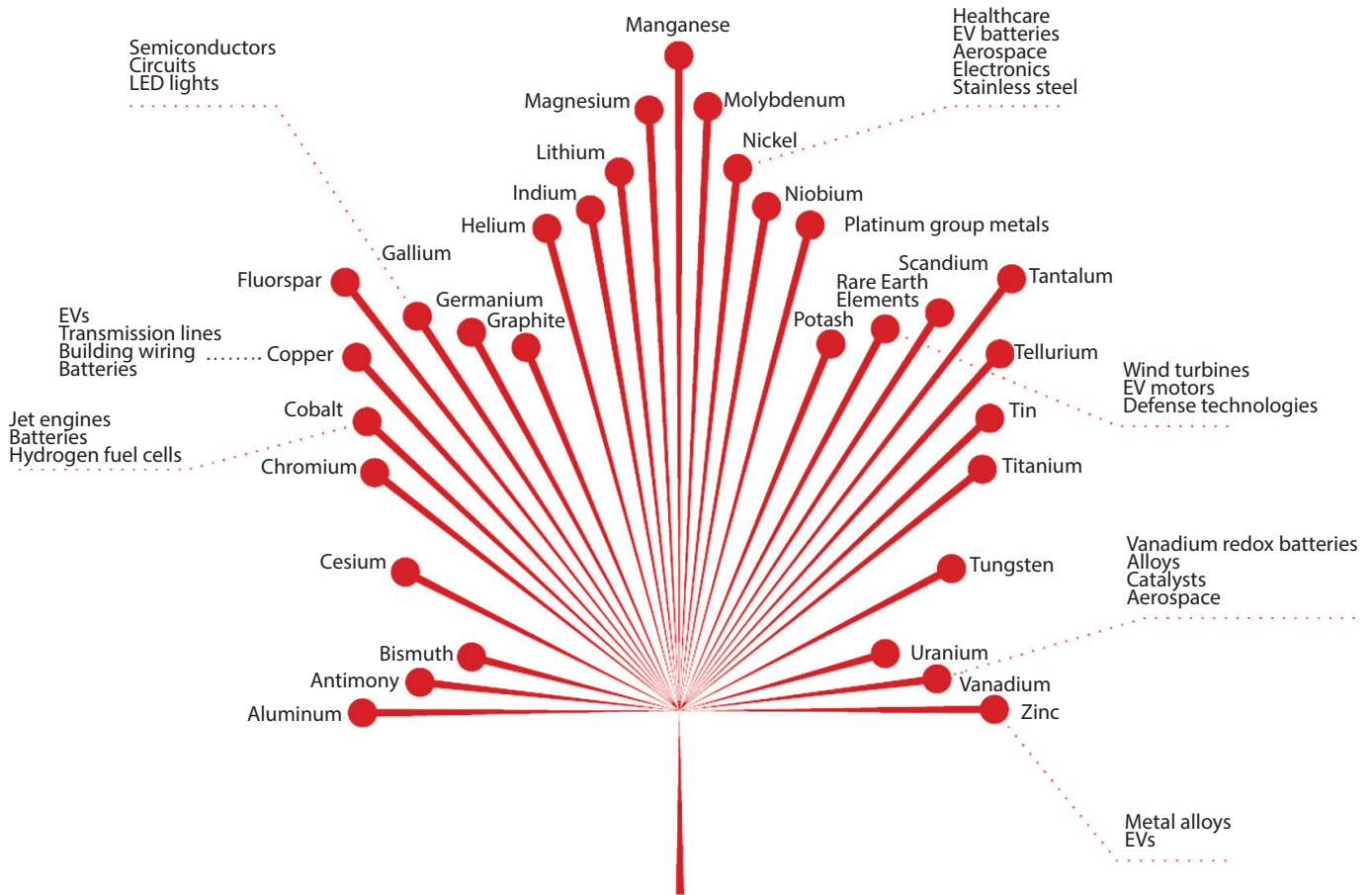


Fig. 1. The 31 critical minerals on the Canadian list and some of their uses. After NRCan (2022).

Based on specific demands and supply vulnerabilities, different countries have different critical minerals lists (e.g., Table 1). Each jurisdiction has variations reflecting supply chain access, geography, and geopolitical circumstance. Critical mineral lists also change with time as demand shifts and technology evolves (e.g., Fortier et al., 2022). Nonetheless, the lists from different jurisdictions have many items in common. From Table 1, more than ten lists include Sb, Bi, Cr, Co, Ga, graphite, In, Li, Mg, Mn, Ni, Nb, platinum group elements (PGE), rare earth elements (REE), Ta, Sn, Ti, W, and V. Five to ten jurisdictions list Al, barite, Be, Cs, Cu, fluorspar, Ge, Hf, He, Mo, P, potash, Rh, Sc, Si, Sr, Te, U, Zn, and Zr. Fewer jurisdictions (less than five) share As, B, Cd, metallurgical coal (coking coal), feldspar, Au, Fe, Pb, Rb, Se, and Ag.

In the last two decades, many organizations have adopted a variation of the United States National Research Council (2008) framework for evaluating the criticality of a material (e.g., Blengini et al., 2020). In general, the criticality framework has two dimensions, one quantifying supply risk, the other economic importance (Fig. 2). For each mineral, risk and economic importance are estimated using proxy indices for different parameters (e.g., Blengini et al., 2020; Nassar et al., 2020). A mineral is deemed critical only if it overcomes user-

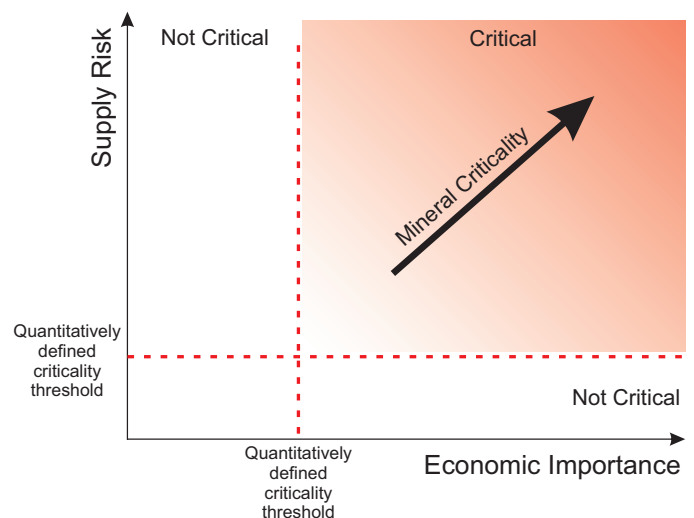


Fig. 2. Two-dimensional criticality framework. Jurisdictions calculate supply risk and economic importance for a mineral then define acceptable thresholds. Minerals with minimal supply risk will not be critical even if of great economic importance. Similarly, minerals of low economic importance will not be critical even if supply risk is high. A combination of both increasing supply risk and economic importance yields increasing criticality. From Hickin et al. (2023).

Table 1. Canadian and key global partner critical mineral lists. Coloured boxes indicate relevance to British Columbia: green are significant; yellow require further evaluation; red are unlikely to be produced. After Hickin et al. (2023).

Minerals	North America							Asia and Australia				Europe		South America	
	USA	CAN	AB	ON	QC	SK	YK	Japan	South Korea	India	AUS	EU	UK	Brazil	Chile
Aluminum/bauxite	x	x	x						x		x	x		x	
Antimony	x	x		x	x		x	x	x	x	x	x	x		
Arsenic	x		x								x	x			
Barite/barium	x		x	x				x				x			x
Beryllium	x			x				x		x	x	x			
Bismuth	x	x	x	x	x		x	x	x	x	x	x	x		
Borate/boron								x				x			
Cadmium					x					x					
Cesium	x	x		x	x			x							
Chromium/chromite	x	x	x	x		x	x	x	x		x				
Cobalt	x	x	x	x	x	x	x	x	x	x	x	x	x	x	x
Copper		x		x	x	x	x		x	x		x		x	x
Feldspar												x			
Fluorspar/fluorine	x	x		x		x	x	x			x	x			
Gallium	x	x	x	x	x	x	x	x	x	x	x	x	x		
Germanium	x	x	x	x			x	x		x	x	x			
Gold														x	
Graphite/carbon	x	x	x	x	x	x		x	x	x	x	x	x	x	x
Hafnium	x		x					x		x	x	x			
Helium		x	x			x						x			
Indium	x	x	x	x	x		x		x	x	x		x		
Iron														x	
Lead									x						
Lithium	x	x	x	x	x	x	x	x	x	x	x	x	x	x	x
Magnesium	x	x	x	x	x	x	x	x	x		x	x	x		
Manganese	x	x	x	x		x	x	x	x		x	x		x	x
Metallurgical coal												x			
Molybdenum		x		x		x	x	x	x	x	x			x	x
Nickel	x	x	x	x	x	x	x	x	x	x		x		x	
Niobium	x	x	x	x	x	x	x	x	x	x	x	x	x	x	
PGE	x	x	x	x	x	x	x	x	x	x	x	x	x	x	x
Phosphate/phosphorous	x			x						x		x		x	
Potash		x	x			x				x				x	
REE	x	x	x	x	x	x	x	x	x	x	x	x	x	x	x
Rhenium								x		x	x				x
Rubidium	x							x							
Scandium	x	x	x	x	x	x				x	x	x			
Selenium				x				x	x	x	x				
Silica/silicon								x	x	x	x	x	x	x	
Silver															
Strontium								x	x	x		x			
Tantalum	x	x	x	x	x	x	x	x	x	x	x	x	x	x	
Tellurium	x	x		x	x		x	x		x	x		x		
Tin	x	x	x	x	x	x	x		x	x			x	x	
Titanium	x	x	x	x	x	x	x	x	x	x	x	x		x	x
Tungsten	x	x		x		x	x	x	x	x	x	x	x	x	x
Uranium	x	x	x	x		x	x							x	
Vanadium	x	x	x	x	x		x	x	x	x	x	x	x	x	x
Zinc	x	x	x	x	x	x	x		x						x
Zirconium	x		x	x				x	x	x	x				

defined thresholds in supply risk and economic importance. The Government of Canada has taken a criteria-based approach in developing the national critical mineral list (Gadd et al., 2022a). The criteria, which were established in consultation with the provinces, territories, and industry representatives, specify that the critical mineral must be: 1) essential to Canada's economic security; 2) required for Canada's transition to a low-carbon economy; and/or 3) a sustainable source for partner nations. The current list (Fig. 1) consists of 31 critical minerals including 27 elements, two groups of elements (platinum group elements and rare earth elements), and two minerals (fluorspar, potash).

3. British Columbia's critical mineral atlas

British Columbia is developing its own Critical Minerals Strategy and BCGS has compiled a critical minerals atlas as the initial step in evaluating the critical mineral endowment of the province and in building awareness of critical mineral opportunities for the exploration and mining industries (Hickin et al., 2023). The atlas is not British Columbia's official critical mineral list. Instead, it represents an inventory of commodities in the province that appear on the Canadian list or on those of key trading partners (Table 1). Acknowledging that many are unlikely to appear on the final critical minerals list for British Columbia, 41 elements/minerals are detailed. Each is presented on a data sheet that provides descriptions, mineral properties, uses and importance, global production, modes of occurrence, and overviews of occurrences in British Columbia. A map is included with each data sheet depicting the distribution of known occurrences in British Columbia and shows the status of each occurrence (current producer, past producer, developed prospect, prospect, showing). Where available, current, past production, and mineral resource data are tabulated.

4. From mineral deposit profiles to mineral systems

The British Columbia Geological Survey has mapped and inventoried the mineral deposits of the province for more than 130 years (Sutherland Brown, 1998). More than 30 years ago, the Survey initiated a study to assess the mineral potential of the entire province. This pioneering work combined known mineral occurrences, what was then understood about which rocks favour mineral deposition, and the geology of a given area to develop a relative ranking of mineral potential (Kilby, 1995, 2004; Grunsky, 1997; MacIntyre and Kilby, 2009). Emphasizing the differences between deposit types, mineral potential assessments focused on deposit profiles that classified occurrences into about 120 deposit types based mainly on genetic models (e.g., Lefebvre and Jones, 2022). The profiles included descriptions of geological characteristics, mineral exploration techniques, resource data, age of mineralization, tectonic setting, and concepts about deposit origins. The approach used built on work by the United States Geological Survey (Brew, 1992; Singer, 1993) but modified for British Columbia (Kilby, 2004). Tracts of land of similar geological character were defined and experts from government, industry, and

academia assessed all available data to determine probabilistic estimates for the expected number of undiscovered deposits. The ranking of the land base for metallic deposits was based on the gross in-place value of the commodities for both known and estimated undiscovered deposits. The dollar value of each tract was determined using expert input, commodity prices, and a Monte Carlo simulation to determine probable tonnage and grade information for each deposit type. Importantly, the dollar scores were intended as a ranking tool and not intended to imply a particular dollar value to the ground being ranked. These mineral potential data remain a valuable contribution for land use assessment, but do not provide commodity-specific information.

To support current land-use decisions and evaluate critical mineral opportunities, the Survey is now reviving provincial mineral potential assessment (Wearmouth et al., 2024). In contrast to previous approaches, which emphasized the differences between deposits split into about 120 types, the current assessment adopts a mineral system approach, which emphasizes similarities between deposits and uses a large-scale view of all the factors that control generating and preserving deposits (e.g., Knox-Robinson and Wyborn, 1997; Hronsky and Groves, 2008; McCuaig et al., 2010; Ford et al., 2019; Groves et al., 2022). Originally proposed by Wyborn et al. (1994) and drawing on ideas from the petroleum industry (e.g., Magoon and Dow, 1994), each mineral system includes an ore source and driving force, a transport mechanism and pathway, and a physical or chemical trap (Knox-Robinson and Wyborn, 1997). The approach recognizes that the ore deposit, which is relatively small (<1 km in plan view), is the central feature of a larger system that may be detectable at a regional scale (>10 km in plan view). Being process-based, the mineral systems approach is neither restricted to a geological setting nor limited to a specific ore deposit type. The mineral systems approach focuses on processes that are common across mineral systems, which enables the simultaneous assessment of many deposit types at a variety of scales (McCuaig et al., 2010).

5. Six important mineral systems in British Columbia

Gadd et al. (2022a) highlighted important mineral systems in Canada of significance for precious and base metals and critical minerals. Following a similar approach, below we summarize selected mineral systems that are important to British Columbia and the ongoing Survey research directed at better understanding mineral potential and critical mineral opportunities.

The mineral endowment of British Columbia and the tectonic evolution of the Canadian Cordillera are intimately linked. The Canadian Cordillera records a history of supercontinent rifting and a succession of island arc volcanosedimentary and intrusive assemblages (terranes) developed outboard of Ancestral North America and accreted to each other and to the proto-continental margin with final amalgamation produced by collisions driven by the westward motion of the North American continental plate. The amalgamated Cordillera then

became the site of Cretaceous and Cenozoic arc and post-arc magmatism. Terrane evolution continues today as the Juan de Fuca plate slides beneath Vancouver Island (Fig. 3). As reviewed by Nelson et al. (2013a), Hickin et al. (2017) and Colpron and Nelson (2021), the diverse tectonic processes, from supercontinent breakup through development of long-lived arc terranes, to terrane accretion and post-accretion magmatism, metamorphism, deformation, and sedimentation, have generated diverse mineral systems across the province.

present-day Cascadia subduction zone and Queen Charlotte fault. Modern-day volcanic complexes related to Cascadia subduction are distributed along the length of the western Cordillera, and many of the terranes are partially covered by sedimentary rocks that were deposited during terrane accretion and collision, when older rocks were deformed, uplifted, eroded, and redeposited in newly created sedimentary basins. The variety of tectonic settings and paleogeographic environments recorded by these terranes and superterranes

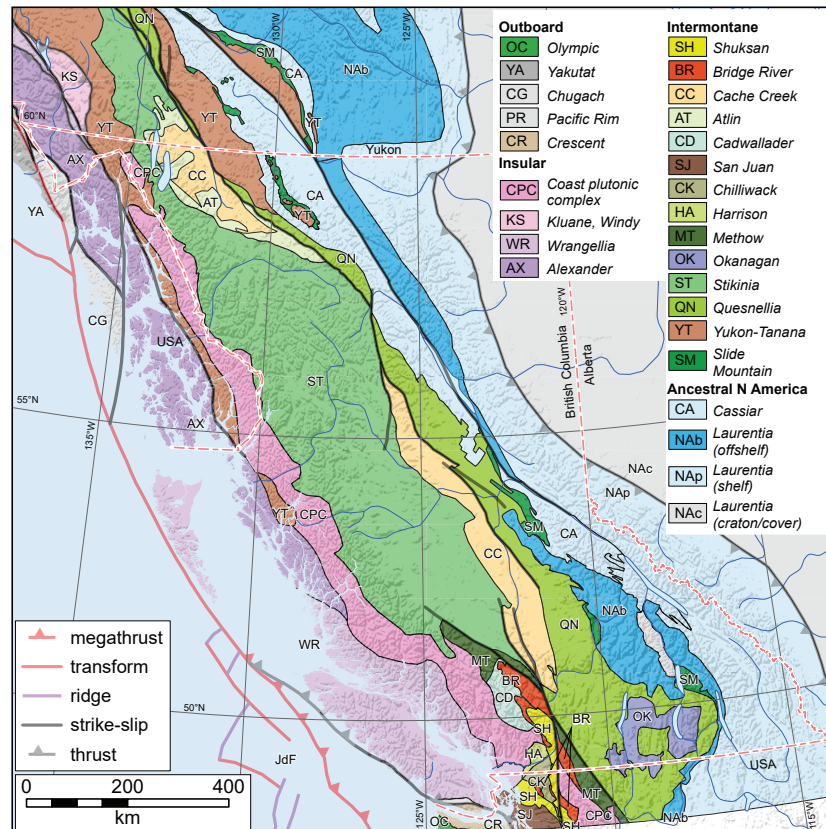


Fig. 3. Superterranes, terranes, and modern tectonic elements of the Canadian Cordillera in British Columbia. Modified after Colpron (2020).

West of Ancestral North America, Cordilleran terranes are commonly grouped into superterranes and terranes (Fig. 3). Ancestral North America consists of predominantly sedimentary rocks that were deposited on cratonic basement during the Paleoproterozoic and Mesoproterozoic and during and after the Neoproterozoic to Cambrian breakup of the supercontinent Rodinia, which created the western margin of Laurentia, the nucleus of what is now North America. The Intermontane superterrane consists of a diverse group of Late Paleozoic to Mesozoic volcano-sedimentary assemblages and kindred intrusive bodies that formed mainly in and adjacent to island arcs outboard of Ancestral North America in the proto-Pacific Ocean. The Insular superterrane consists of similar island arc terranes; the Intermontane-Insular terrane boundary lies within the syn- to post-accretionary Coast Plutonic complex, a linear arc-axial belt that extends the length of the Cordillera. The Outboard terranes are mostly late Mesozoic to Cenozoic forearc siliciclastic assemblages, bounded to the west by the

since the Mesoproterozoic generated conditions favourable for a variety of mineral systems.

5.1. Porphyry systems

Porphyry deposits are the world's largest source of Cu and Mo and individually can contain 100s of millions to billions of metric tons of ore. These deposits typically form above subduction zones at convergent plate margins associated with calc-alkaline volcano-plutonic arcs but can also form from alkaline magmas in post-subduction settings, such as has been inferred in British Columbia, particularly in Quesnel and Stikine terranes (Fig. 4; Nelson et al., 2013a; Logan and Mihalynuk, 2014; Hickin et al., 2017; Colpron and Nelson, 2021). Of the eleven mines that operated in British Columbia in 2023, seven are porphyry deposits. The province is the largest Canadian producer of copper (typically 40-50%) and only producer of molybdenum (Clarke et al., 2024), both of which are on the national critical minerals list (NRCan, 2022). Porphyry deposits have numerous

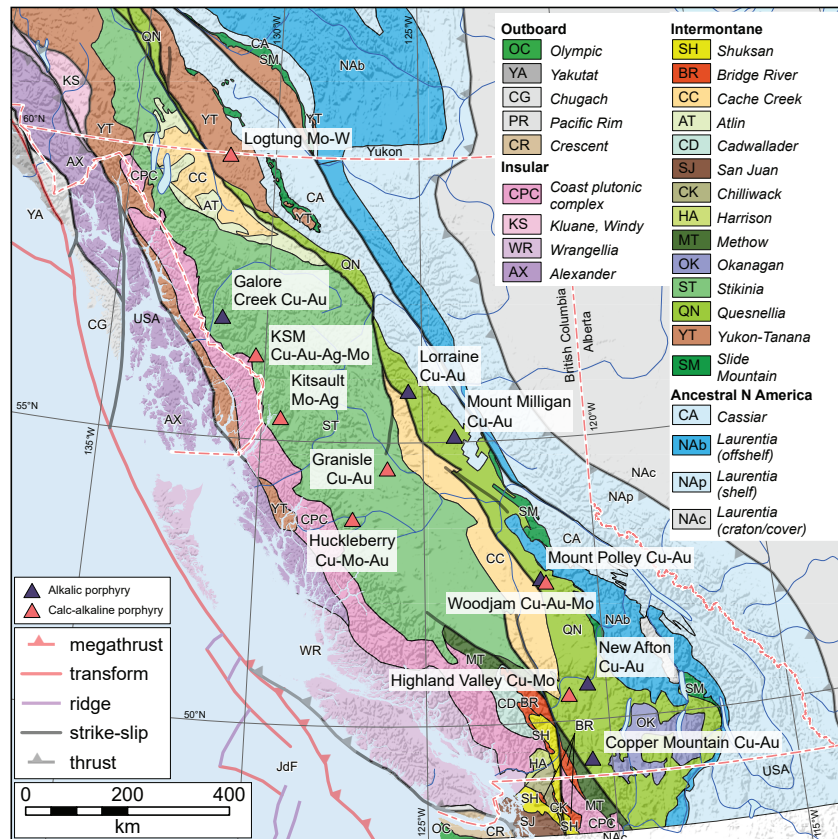


Fig. 4. Selected porphyry deposits in British Columbia. Terranes after Colpron (2020).

subtypes grouped under the broad class referred to as ‘porphyry (D)’ by Lefebvre and Jones (2022), and porphyry systems may also include other types such as skarn, carbonate replacement, and high- and intermediate-sulphidation epithermal deposits (Fig. 5; e.g., Sillitoe, 2010; Orovan and Hollings, 2020). In porphyry systems, hydrothermal fluids interact with surrounding rocks creating characteristic and predictable alteration assemblages (Fig. 5). In the green rock environment, an extensive and zoned alteration halo surrounds the potassic (K-feldspar-biotite-chalcopyrite) core centered on a porphyritic intrusive complex (Sillitoe, 2010; Orovan and Hollings, 2020). Immediately outwards from the potassic core is the inner propylitic subzone (or actinolite subzone), which is defined by the occurrence of actinolite. Other minerals in this assemblage may include combinations of albite, epidote, chlorite, calcite, hematite, magnetite, and pyrite. The medial propylitic zone is the epidote subzone; it has a similar mineral assemblage but lacks actinolite. The outermost propylitic zone is the chlorite subzone, which lacks actinolite, epidote, and commonly magnetite. This alteration zonation reflects the decreasing fluid temperature outward from a central heat source, providing a distinctive and observable guide to potential mineralization (Cooke et al., 2014; Orovan et al., 2018; Pacey et al., 2020; Orovan and Hollings, 2020). The green rock alteration domains may be subjacent to or overprinted by a lithocap, its feeder structures, or other late-stage upward-flaring alteration

features, which may include advanced argillic (quartz-alunite-clay), silicic (quartz), argillic (clay), phyllic/sericitic (quartz-sericite-pyrite), and intermediate argillic (sericite-clay-chlorite) alteration zones. High-sulphidation epithermal mineralization may be embedded in the lithocap environment, containing a combination of pyrite, enargite, covellite-digenite, chalcopyrite and tetrahedrite/tennantite. Sodic-calcic alteration (albite-epidote-chlorite-actinolite) may be present in a deep or medial position with respect to the mineralizing porphyritic intrusive complex, where it overprints potassic and/or propylitic alteration. Where reactive host-rock horizons are present, skarn alteration assemblages and mineralization may develop, consisting of Cu-rich minerals close to the intrusion, and more Zn-Pb-rich mineralization farther out. Within zones of high-angle normal faults or breccias that are medial to distal to the porphyritic intrusive complex, intermediate-sulphidation mineralization may form consisting of base metal sulphides, including silver-bearing tetrahedrite, electrum, chalcopyrite, barite, galena, and sphalerite. This mineralization typically occurs with quartz-adularia-illite-pyrite alteration.

The main commodity of economic interest in porphyry deposits is Cu, with Mo and Au common co-products and Ag the most common by-product. Porphyry Mo deposits typically lack co-products, although W or Ag have been reported (e.g., Kitsault Mo-Ag, Fig. 4; Steininger, 1985). The most noted by-products recovered from porphyry deposits include Ag, As,

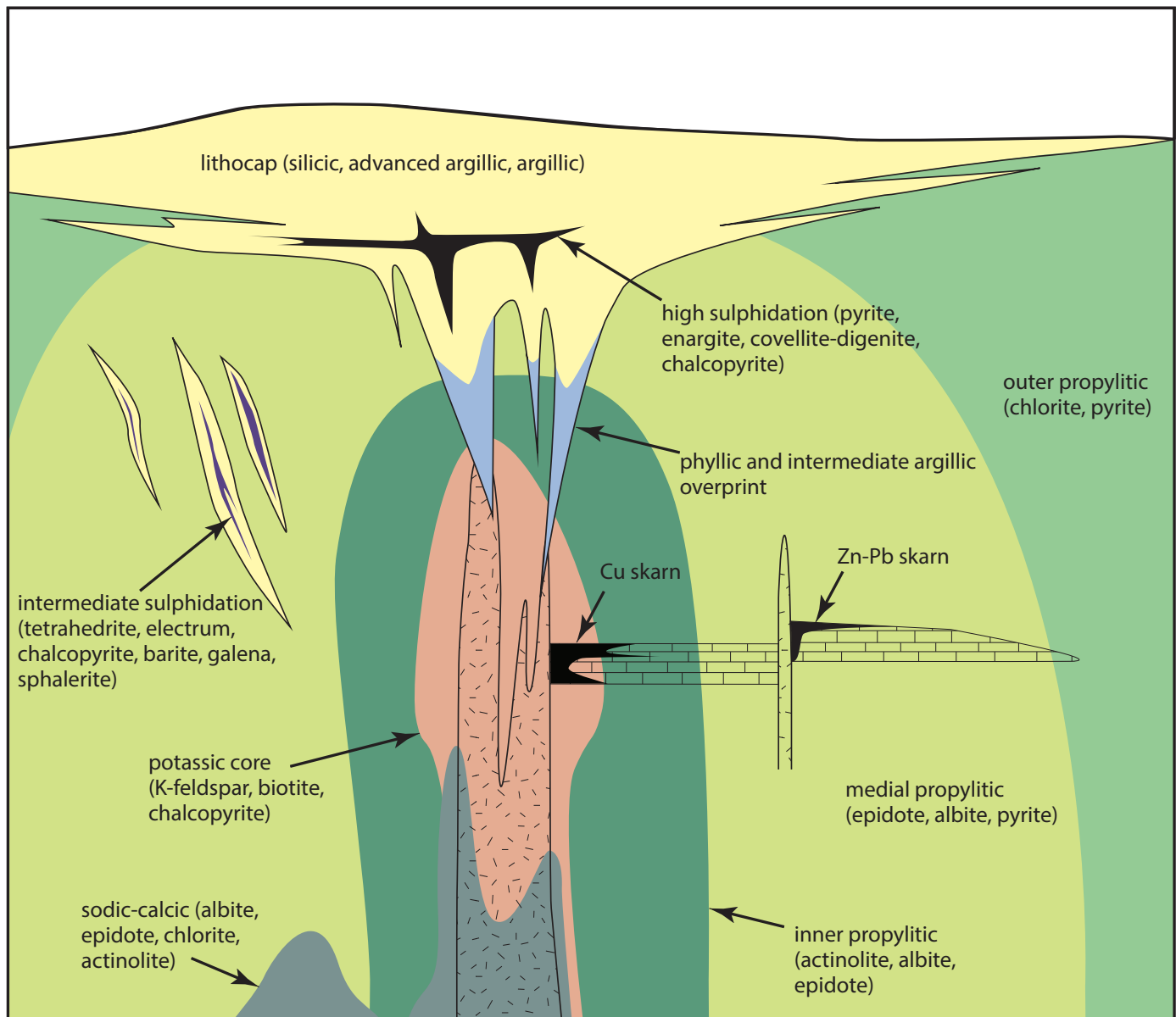


Fig. 5. Diagram of typical alteration zonation patterns and overprinting relationships in the porphyry environment. The green rock environment includes three subfacies of propylitic alteration that are zoned about an intrusive complex and proximal associated potassic alteration. The propylitic alteration passes outward from an inner high-temperature subzone characterized by the presence of actinolite to an intermediate-temperature subzone containing epidote to an outer low-temperature subzone with predominantly chlorite. Upward-flaring zones of phyllic (sericitic) and/or intermediate argillic (sericite-clay-chlorite) alteration may overprint the upper portions of the porphyry system and may transition into a lithocap (including silicic, advanced argillic, and argillic alteration) at shallow levels. The lithocap can host high-sulphidation epithermal mineralization. At deeper levels (or medial to the mineralizing intrusions) sodic-calcic alteration may overprint the potassic core and/or propylitic halo. Where reactive host-rock horizons are present, skarn alteration assemblages and mineralization may develop. Medial to distal fault intersections or breccia zones may host intermediate-sulphidation epithermal mineralization. Modified after Cooke et al. (2020).

PGE, Re, Se, Te, W, Sn, U, Zn, monazite, silica, and sulphuric acid (Sillitoe, 1983; John and Taylor, 2016). Additionally, Be and Bi can be enriched in porphyry Mo deposits (e.g., 1 cm-long beryl crystals and bismuthinite at the Logtung porphyry Mo-W deposit, (Fig. 4; Noble et al., 1995; Mihalyuk and Heaman, 2002). Other metals that may be enriched include Nb, In, Cs, F, Li, Rb, Ta, Co and REE but rarely in concentrations that are of economic interest (John and Taylor, 2016; Velasquez et al., 2020). Gold and Ag are the major commodities in porphyry-

related epithermal deposits; Pb, Zn and Hg are common co-products in intermediate-sulphidation deposits, whereas Cu is the most common co-product in high-sulphidation deposits.

Porphyry deposits are typically found in hydrous, oxidized, shallow-level intrusive rocks formed above subduction zones (Fig. 6), but can also occur in post-subduction and post-collision or extensional back-arc settings. Most magmatic rocks in these settings lack porphyry deposits, suggesting that a particular sequence of ore-forming conditions must be met (e.g., Park et

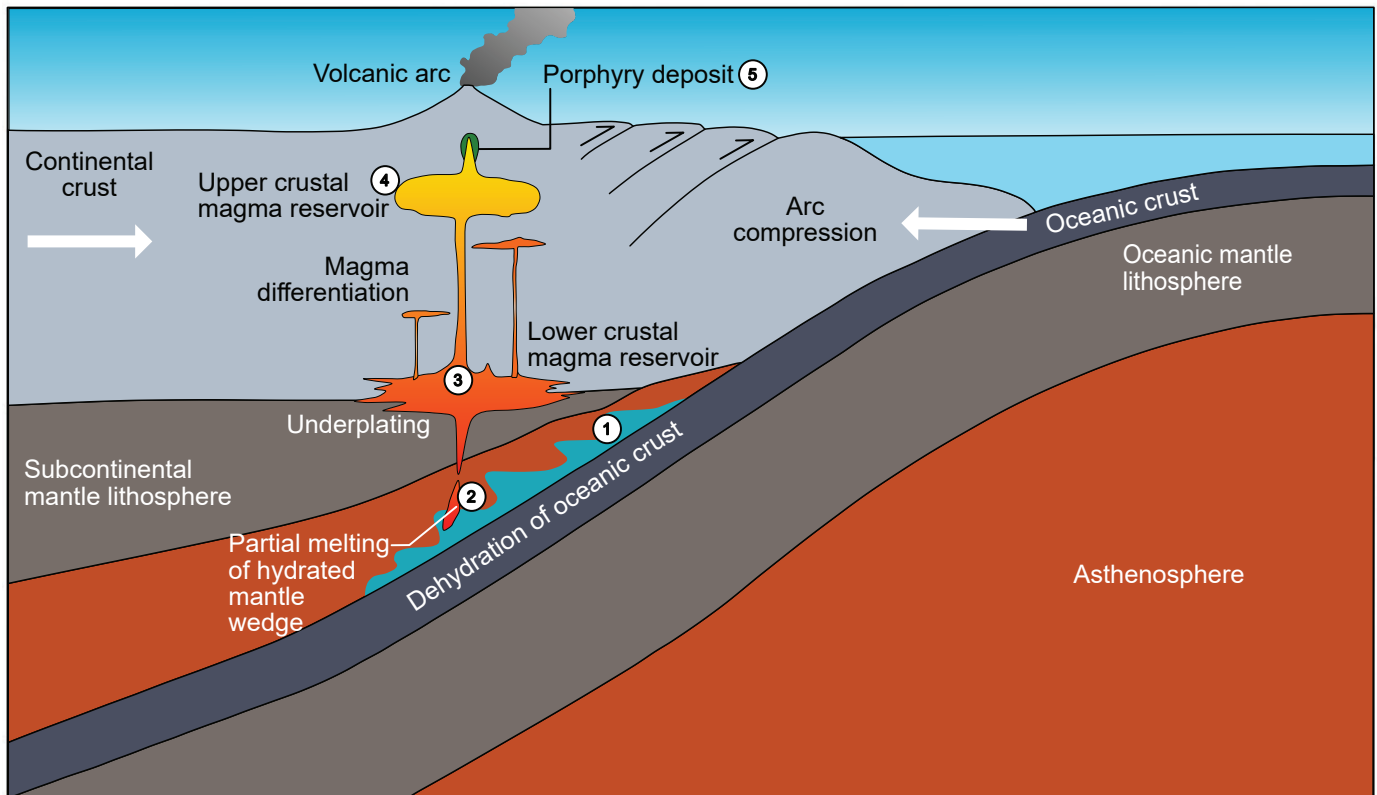


Fig. 6. Tectonic and magmatic conditions to form porphyry deposits. **1)** In a subduction zone, an oceanic plate consisting of hydrated sediments and altered oceanic crust is dragged downward toward the mantle. Fluids and hydrous melts are released from this subducting slab causing hydration of the overlying mantle wedge. **2)** Hydration of the mantle wedge results in flux melting of mantle peridotite, producing oxidized, hydrous basaltic arc magma reservoirs in the mid to lower crust (~30-70 km depth). **3)** The arc magma differentiates by fractional crystallization, crustal assimilation, recharge and mixing. **4)** The evolved magma rises to form an upper crustal magma chamber (~5-15 km depth). **5)** The melt intrudes into the shallow crust at depths of 1-7 km, forming porphyritic intrusions that exsolve Cu-rich ore fluids that form porphyry deposits. Modified after Park et al. (2021).

al., 2021). Several processes contribute to creating porphyry deposits, although workers may disagree on their relative importance (Fig. 6). First, fluids and hydrous melts are liberated from a subducting slab. Second, the mantle wedge is hydrated causing flux melting of mantle peridotite and the production of oxidized, hydrous basaltic arc magma, which ascends and pools in deep reservoirs in the mid to lower crust (~30-70 km depth; Richards, 2011). Magma in these deep reservoirs then differentiates by fractional crystallization, crustal assimilation, recharge, and mixing (Lee and Tang, 2020). This evolved magma then rises to the upper crust (~5-15 km depth) becoming fluid-saturated due to fractional crystallization and low H_2O solubility at low pressure (Chiaradia and Caricchi, 2017). Finally, the fluid-saturated melt intrudes into the shallow crust at depths of 1-7 km, forming pencil-shaped plugs, stocks, and dikes that exsolve fluids forming a hydrothermal circulation system precipitating metal-rich sulphide minerals (Sillitoe, 2010).

Although there are Late Neogene and Jurassic examples in Wrangell terrane on Vancouver Island (Nixon et al., 2020a), most porphyry deposits are in the interior of the province, in Triassic to Jurassic volcanoplutonic rocks of Quesnel and Stikine terranes (Fig. 4; e.g., Logan and Mihalynuk, 2014).

These deposits can be subdivided geochemically and by their metal endowment. Calc-alkaline porphyry deposits, the most common variety, include Cu, Mo, Cu-Mo, and Cu-Au systems (e.g., Highland Valley, KSM, Woodjam). Alkalic porphyry deposits are restricted to Cu-Au systems and are Late Triassic to Early Jurassic, and locally contain PGE (e.g., Copper Mountain, New Afton, Lorraine). The alkalic porphyry Cu-Au deposits can be associated with breccia complexes (e.g., Mt. Polley), silica-undersaturated alkalic intrusions (e.g., Galore Creek), or silica-saturated alkalic intrusions (e.g., Mount Milligan). The plutons that host Quesnel terrane deposits conform, in part, to a pattern defined by parallel belts of calc-alkaline and alkalic plutons that become progressively younger from west to east (Logan and Mihalynuk, 2014; Schiarizza, 2014). Logan and Mihalynuk (2014) emphasized that a narrow 15-m.y. time interval spanning the Jurassic-Triassic boundary, particularly a 6 m.y. pulse centred at 205 Ma, was a particularly prolific episode during which most of the mineralization took place. However, significant porphyry deposits also formed in Stikine terrane during the Cretaceous (e.g., Huckleberry) and Eocene (e.g., Granisle, Kitsault).

Because of their importance to the economy of British Columbia, porphyry deposits have been studied by Survey

geologists for many decades, a tradition that continues today. In the last ten years, integrated field and laboratory studies have been dedicated toward unravelling the tectonic and metallogenic evolution of the main porphyry-bearing terranes of Stikinia (e.g., Nelson and Kyba, 2014; Barresi et al., 2015; Mihalynuk et al., 2016; van Straaten and Nelson, 2016; van Straaten and Gibson, 2017; Febbo et al., 2019; Ootes et al., 2020; Stanley and Nelson, 2022; van der Vlugt, 2022; van Straaten et al., 2022, 2023; Jones et al., 2023; Norris et al., 2023; van Straaten, 2024) and Quesnellia (e.g., Logan and Mihalynuk, 2013, 2014; Mihalynuk and Logan, 2013a, b; Logan and Schiarizza, 2014; Schiarizza, 2015; Mihalynuk and Diakow, 2020; Schiarizza and Friedman, 2021). Recent publications by Logan et al. (2020), Nelson and van Straaten (2020), Colpron and Nelson (2021), and Nelson et al. (2022) synthesize some of this work, and recent dedicated volumes edited by Sharman et al. (2020) and Plouffe and Schetselaar (2021) provide additional province-wide and detailed studies. Particularly important has been the development of new tectonic models about the transition from the Stuhini arc to the Hazelton arc in Stikinia, a transition of arc reorganization with major metallogenic significance (Nelson et al., 2022) and the important role that long-lived, deep-level structural corridors have for generating porphyry deposits in Stikinia and perhaps elsewhere (Nelson and van Straaten, 2020).

Given the thick and extensive drift cover across many areas, considerable attention has also been devoted to examining the down-ice dispersal of material derived from hidden porphyry deposits using samples from subglacial tills, which typically represent the first derivative from bedrock. These studies include province-wide ice-flow compilations (Arnold and Ferbey, 2020), basal till potential maps (e.g. Ferbey, 2014), examinations of porphyry deposit indicator minerals (e.g., Ferbey et al., 2016, 2018; Canil et al., 2017; Lian and Hickin, 2017; Plouffe and Ferbey, 2017, 2019; Mao et al., 2017; Bustard et al., 2019; Lee et al., 2021; Plouffe et al., 2021), and using remotely piloted aircraft systems (drones) to collect lidar, radiometric, and magnetic data (e.g., Ferbey and Elia, 2021; Elia et al., 2023, 2024; Ferbey et al., 2024). Current work includes characterizing the petrogenesis and critical mineral deportment across alteration assemblages and delineating co- and by-products across the spectrum of porphyry deposit subtypes in the province, starting with the historical Kitsault Mo-Ag mine (Orovan et al., 2024).

5.2. Volcanogenic massive sulphide systems (VMS)

Volcanogenic massive sulphide (VMS) deposits are accumulations of sulphide minerals precipitated at sites of rift-related submarine volcanism on the floors of modern and ancient seas. The deposits form where hot metal-rich magmatic fluids rise, discharge, and mix with seawater (e.g., Lydon, 1984, 1988; Franklin et al., 2005; Galley et al., 2007; Cousens and Piercey, 2008; Hannington et al., 2011; Piercey, 2011; Ross and Mercier-Langevin, 2014). Based on volcanic rock type(s) typically related to tectonic setting, VMS deposits have been

subdivided into numerous categories named after type localities included in the “marine volcanic association” of Lefebvre and Jones (2022; see Northcote, 2022 for review). The primary metals in VMS systems are Cu and Zn, with secondary Pb. More rarely, VMS systems contain Co (e.g., Windy-Craggy, in British Columbia; Fig. 7; Peter and Scott, 1999; Leybourne et al., 2022), or are rich in Au and Ag (Eskay Creek in British Columbia; Sherlock et al., 1999; Mercier-Langevin et al., 2011). By-products from VMS production may include Au and Ag, and some deposits have a host of other critical metals (e.g., Bi, Co, Ga, Ge, In, Sb, Sn, Te, Tl; Paradis, 2015; Leybourne et al., 2022).

Volcanogenic massive sulphide deposits form in extensional tectonic settings where new sea floor is being created, such as at mid-oceanic ridges (MOR), rifting-arcs, and back-arc basins (Fig. 8; Lentz, 1998; Franklin et al., 2005; Galley et al., 2007; Cousens and Piercey, 2008; Piercey, 2011). Although many modern mid-ocean ridge examples have been documented, ancient examples are rare because thin, juvenile oceanic crust is easily subducted. Rifting arcs and back-arc basins have a higher preservation potential and are the tectonic settings most represented in the rock record.

Observations of modern seafloor processes have provided direct information on the origin of VMS, making this deposit class one of the best studied and understood mineralizing systems (Fig. 9; e.g., Lydon, 1984, 1988; Franklin et al., 2005; Galley et al., 2007). Driven by magmatic heat, oceanic water circulates through seafloor volcanic and sedimentary deposits as hydrothermal fluids. These fluids scavenge metals and are focused and discharged through hydrothermal vents called black smokers, precipitating the metals as sulphide complexes within vents and adjacent aprons (Franklin et al., 2005; Galley et al., 2007). In some deposits, syn-volcanic intrusions are the source of metals (e.g., Leybourne et al., 2022), and some deposits form during sub-seafloor replacement processes (Doyle and Allen, 2003; Piercey, 2015). Intervals of volcanic quiescence are required to establish significant massive sulphide accumulations undiluted by large volumes of volcanic rock. Ancient deposits are likely deformed and/or metamorphosed. Although the genetic model for VMS formation generally applies, the geometry of the mineralization, alteration envelope, and host-rocks may be significantly and unpredictably modified, and the search for potential VMS deposits in deformed terranes requires a combination of detailed structural and lithofacies mapping (e.g., Lafrance et al., 2020).

Key features of VMS deposits (Fig. 9) include: 1) occurrence in seafloor volcanic and sedimentary rocks; 2) spatial relationship to syn-volcanic caldera complexes, which are recognized by lateral facies changes, such as transitions away from plateau flows to escarpments to escarpment-related breccia aprons; 3) proximity to syn-volcanic intrusions, which act as heat pumps for circulating hydrothermal fluids; 4) textural preservation of primary volcanic rock-forming minerals albeit altered by interactions with hydrothermal fluids; 5) accumulations of sulphide minerals, typically

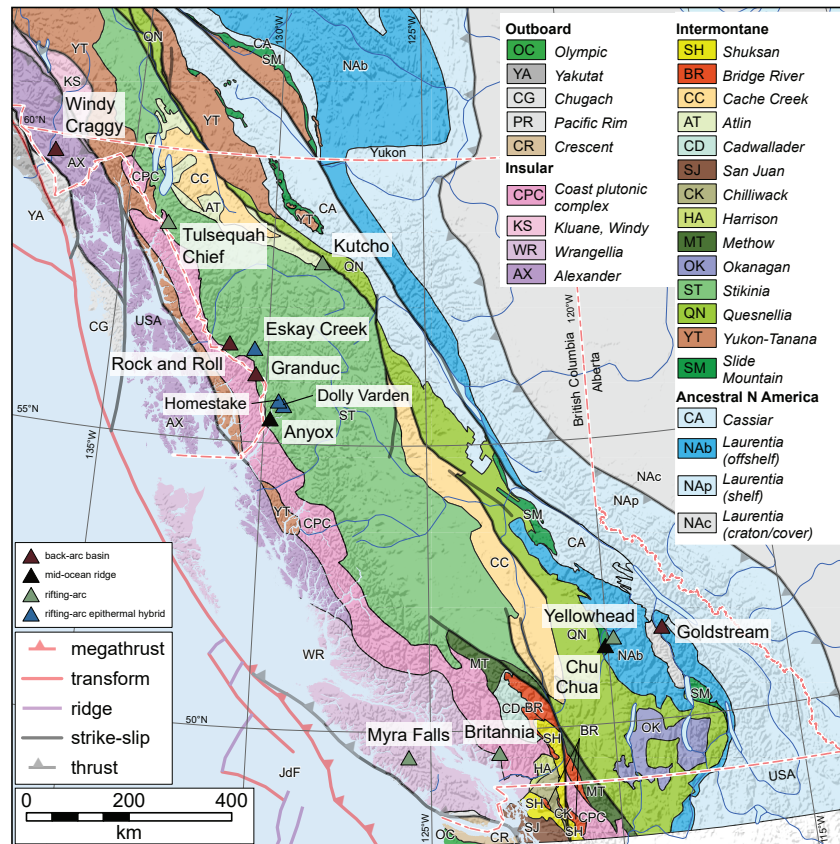


Fig. 7. Selected volcanogenic massive sulphide deposits in British Columbia (see Northcote, 2022 for review). Terranes after Colpron (2020).

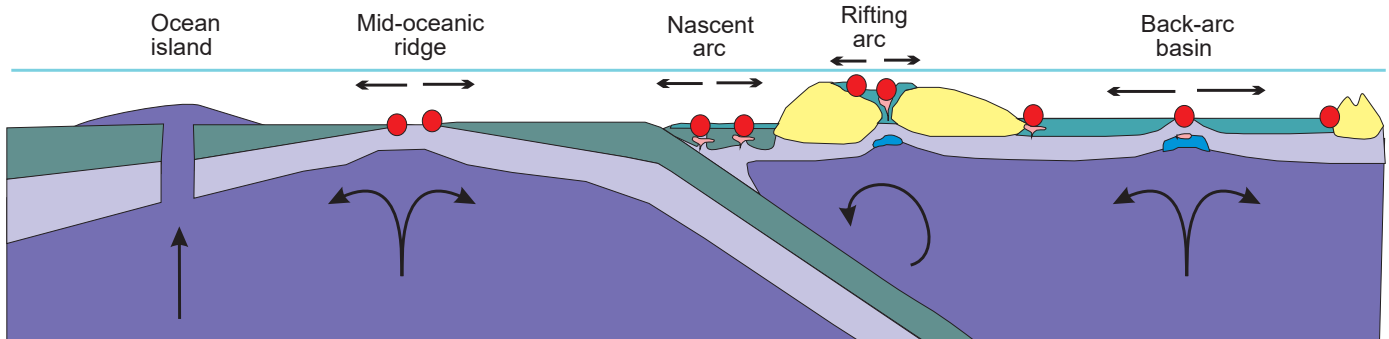


Fig. 8. Tectonic settings of volcanogenic massive sulphide (VMS) deposits (red circles).

chalcopyrite and sphalerite (\pm galena), pyrite, and pyrrhotite, in hydrothermal vent complexes; 6) additional replacement mineralization in vent and apron environments; and 7) lateral transitions to exhalative deposits such as those similar to banded iron formations that may have elevated Zn, Mn, or Ba. Key starting points for recognizing environments with potential for VMS mineralization include deep-water volcanic rocks with abrupt facies changes, alteration of primary compositions (e.g., bleaching, epidote-rich cores to pillowed basalts), and potential syn-volcanic intrusions (Campbell et al., 1981; Hannington et al., 2003; Franklin et al., 2005; Galley et al., 2007; Cousens and Piercey, 2008; Piercey, 2011).

VMS and vent-proximal SEDEX deposits (see section 5.3.) form in similar ways, but there are a few key differences. First, VMS deposits are mainly hosted by volcanic rocks, whereas SEDEX deposits are hosted by deep-water sedimentary rocks with only sparse volcanic rocks. Second, syn-volcanic intrusions are common in VMS deposits but not in SEDEX deposits. Third, alteration of host-rocks near VMS deposits is extensive and can be used as an exploration tool, whereas alteration in SEDEX host rocks is not significant. Fourth, VMS mineralization is predominantly Cu-Zn (\pm Pb, Au, Ag), whereas SEDEX deposits contain Zn-Pb (\pm Ba) with little to no Cu.

Most VMS occurrences in British Columbia are rifting arc-

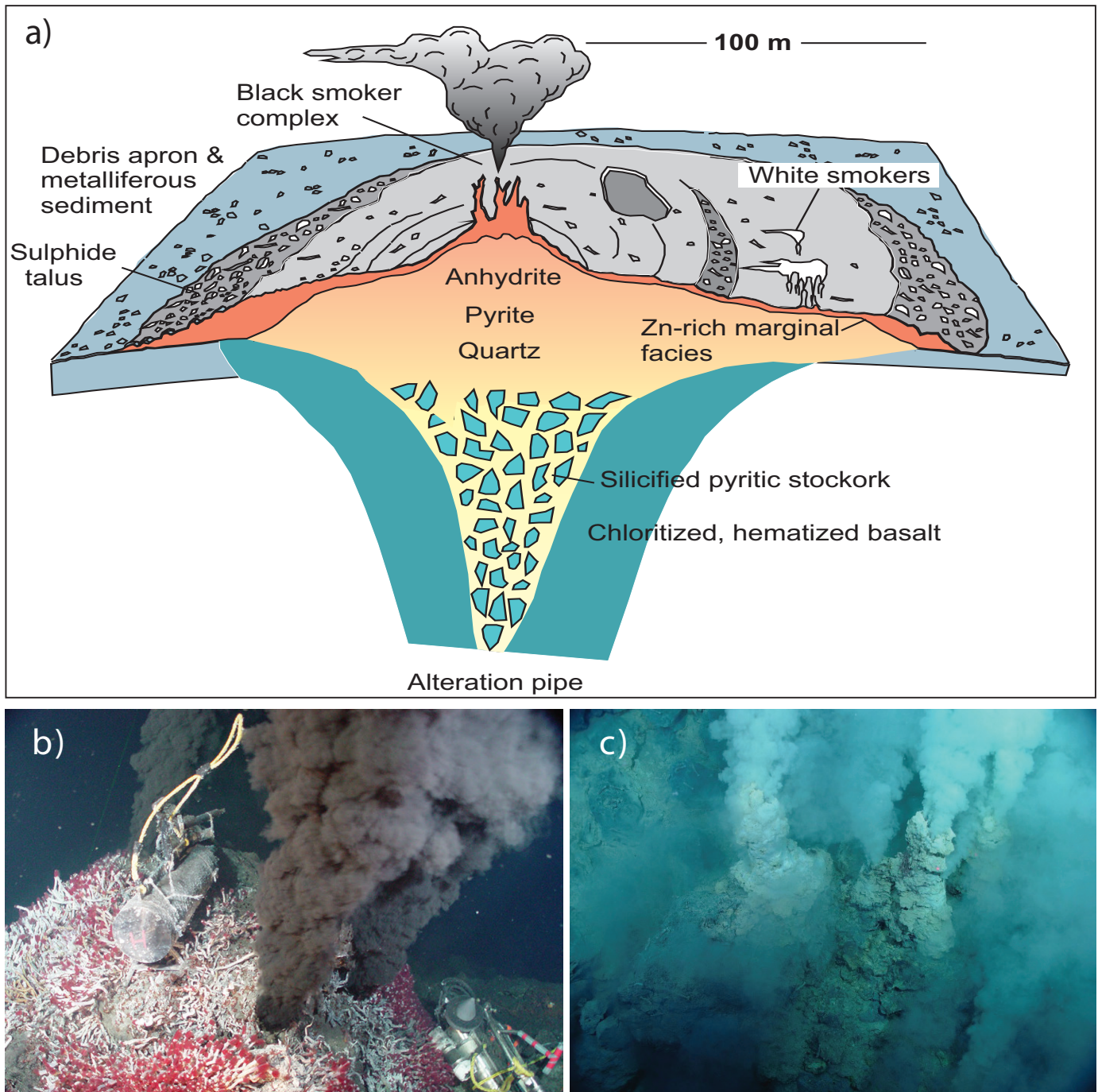


Fig. 9. a) Schematic diagram of a modern hydrothermal chimney complex discharging metal-rich hydrothermal fluids on the seafloor. Modified after Galley et al. (2007) and references therein. **b)** Black smoker venting metal-rich hydrothermal fluids and precipitating fine-grained sulphide minerals on the seafloor (United States National Oceanic and Atmospheric Administration). **c)** Lower temperature white smoker venting carbonate- and sulphate-rich minerals on the sea floor (United States National Oceanic and Atmospheric Administration).

related Zn-Pb-Cu-Ag-Au deposits including the currently producing Myra Falls mine and past-producing Britannia and Tulsequah Chief mines (Fig. 7). However, precious metals-enriched rifting-arc VMS and epithermal hybrid deposits are also high priority targets. The high-grade Eskay Creek deposit, in volcanic and sedimentary rocks filling the narrow north-trending, fault-bounded Eskay rift, exemplifies this

type. East of the Eskay rift but with a slightly older inferred time of deposition, mineralization at the Dolly Varden and Homestake deposits also has characteristics of both VMS and epithermal vein and open-space filling styles (Hunter et al., 2022; Turner and Hough, 2023). The combined Homestake and Dolly Varden deposits contain a 4.153 Mt Indicated resource of 34.731 Moz Ag, 166.0 koz Au, 2.87 Mlb Cu, and

1.25 Mlb Pb and an additional 6.831 Mt Inferred resource containing 29.3 Moz Ag and 817 koz Au (Turner and Hough, 2023). The Kutcho Creek rifting arc deposits are hosted by primitive arc volcanic and volcanoclastic rocks of the Kutcho assemblage (Permian-Triassic; Schiarizza, 2012). Orebodies are in a sequence of lapilli, crystal-lithic, and quartz-feldspar crystal tuffs. The feasibility stage project has a combined Measured and Indicated 22.8 Mt grading 1.52% Cu, 2.18% Zn, 28.1 g/t Ag, and 0.39 g/t Au. The Inferred resource is 12.9 Mt grading 1.10% Cu, 1.58% Zn, 20.0 g/t Ag, and 0.25 g/t Au (CSA Global Mining Industry Consultants Canada Limited, 2021). The feasibility-stage Yellowhead deposit is also a rifting arc VMS (Höy, 1997), hosted in metavolcanic and metasedimentary rocks of the Upper Eagle Bay assemblage (Devonian-Lower Mississippian). The deposit is remobilized but remains generally conformable with host rock stratigraphy. Total potentially bulk mineable resources are estimated at 1292 Mt grading 0.25% Cu, 0.028 g/t Au, and 1.2 g/t Ag Measured and Indicated and 109 Mt grading 0.21% Cu, 0.024 g/t Au, and 1.2 g/t Ag Inferred (Taseko Mines Limited, 2020). Back-arc basin and mid-oceanic ridge VMS (Besshi and Cyprus) types are less common although there are important examples of both (e.g., back-arc Windy Craggy, Granduc, and Goldstream; mid-ocean ridge in the Anyox camp). Chu Chua is an exploration-stage mid-oceanic ridge deposit in the Fennel Formation (Mississippian to Permian). An updated resource estimate has an Inferred 2.29 Mt resource grading 2.11% Cu, 0.30% Zn, 9.99 g/t Ag, and 0.50 g/t Au. Cobalt values of 310-475 ppm were noted historically in the ore zone (Raffle et al., 2021).

In the last decade, the stratigraphy, volcanology, sedimentology, structural geology, geochronology, and isotopic evolution of VMS-bearing rocks and allied intrusions in northwestern British Columbia have been intensively studied (e.g., Nelson and Kyba, 2014; Cutts et al., 2015; van Straaten and Nelson, 2016; Nelson, 2017; Nelson et al., 2013b, 2018) and recently synthesized (Nelson and van Straaten, 2020; Colpron and Nelson, 2021; Nelson et al., 2022; van Straaten et al., 2022). Recent mapping in the Kitsault River area (Hunter and van Straaten, 2020; Hunter et al., 2022; Miller et al., 2023) indicates that precious metals-enriched VMS mineralization is slightly older than in what is traditionally considered the bounds of the Eskay rift to the west. Mihalynuk et al. (2019) presented U-Pb zircon data consistent with VMS mineralization at the Granduc and Rock and Roll deposits being Late Triassic. In northern British Columbia, Mihalynuk et al. (2024) are examining ophiolitic rocks near Atlin for ultramafic-associated massive sulphide mineralization, and in southeastern British Columbia, the Survey is currently examining ultramafic-associated Ni- and Co-enriched VMS mineralization in the Lardeau Group.

5.3. Deep-water basin and platformal base-metal systems

Sedimentary exhalative (SEDEX) and Mississippi Valley-type (MVT) deposits are the most significant hosts of base-

metals genetically related to the deposition and diagenesis of sedimentary rocks in British Columbia. Potential exists for other types in which sedimentary processes play a predominant role. These two deposit types (SEDEX and MVT) are included in the broad class referred to as ‘sediment-hosted (D)’ by Lefebvre and Jones (2022).

SEDEX deposits, such as the historic Pb-Zn-Ag Sullivan mine (Fig. 10), typically form in deep-water, off-shelf settings coeval with background sedimentation of fine-grained argillaceous material (Fig. 11). In ‘vent-proximal’ deposits, sulphide minerals grow near hydrothermal seafloor vents surrounded by fine-grained sediments. ‘Vent-distal’ deposits lack an apparent relationship to hydrothermal vents entirely and display a stratiform geometry with alternating sulphide-rich and fine-grained interlayers (e.g., Goodfellow and Lydon, 2007; Sangster, 2018). Both represent the syndepositional accumulation of sulphide minerals derived from waters that have circulated through underlying basement rocks and the sedimentary pile and ascended to the sediment-water interface or close to it. The primary metals in SEDEX deposits are Pb and Zn (\pm Ag, Ge, In); some have a spatial association with stratiform barite deposits. Historical records indicate the Sullivan mine contained Sn, Cu, Au, Fe, Sb, Cd, Bi, In, and W.

In contrast to the typical deep-water setting of SEDEX deposits, Mississippi Valley-type (MVT) deposits are hosted by relatively shallow-water platformal carbonate successions (Fig. 11) in which both penecontemporaneous dolomitization of original calcium carbonate sediment and karst processes create void spaces for the precipitation of base-metal sulphides from low-temperature hydrothermal fluids to form stratabound epigenetic deposits (e.g., Sangster, 1990; Paradis et al., 2007). Lead and Zn are the primary metals, but MVT-like deposits have potential to contain Mg, Ga, Ge, In, REE, and F (e.g., Mt. Brussilof mine where Mg is now being produced, Fig. 10). Barite is a potential primary commodity, and at least one REE (F, Ba)-bearing deposit (Rock Canyon Creek) has similarities in tectonic and stratigraphic setting to Mississippi Valley-type Zn-Pb deposits in the same district (Simandl et al., 2019).

Other deep-water basin and platform-hosted mineralization types in the Cordillera include ‘hyper-enriched black shales’ and ‘sediment-hosted Cu’ (‘red-bed’, or Kupferschiefer-type). Hyper-enriched black shales deposited off-shelf of the Laurentian margin (Kechika trough) in the Middle Devonian (Gadd et al., 2020, 2022b), can contain concentrations of Zn, Ni, Cu, Mo, Se, U, V, Cr, Co, Ag, Au, Re, PGE and REE, and Gadd et al. (2022b) described an example below younger SEDEX mineralization at the Akie deposit. Redbed copper deposits in marginal marine evaporites and related rocks of the Coates Lake Group (Neoproterozoic, Mackenzie Mountains, NT) display both syngenetic and epigenetic styles (e.g., Ootes et al., 2013; Brown et al., 2014) and there may be potential for this type of mineralization in Neoproterozoic units in northern British Columbia. Sedimentary or volcanic-hosted Cu mineralization also occurs in the Takla and Hazelton groups (Late Triassic to Early Jurassic) in eastern Stikine terrane (e.g., Sustut copper

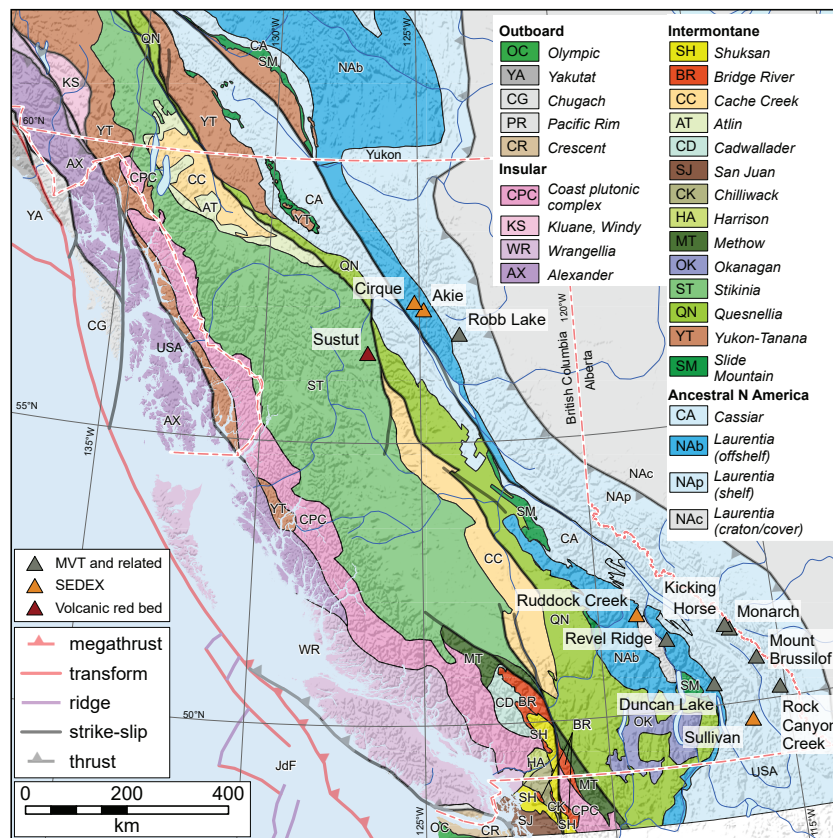


Fig. 10. Selected sedimentary exhalative (SEDEX) and Mississippi Valley Type (MVT) deposits in British Columbia. Terranes after Colpron (2020).

deposit; Church, 1975; Legun, 2001, Fig. 10), although the timing of mineralization remains unknown.

Consistent with the global distribution of such base metal deposits (Hoggard et al., 2020; Huston et al., 2023), SEDEX and MVT deposits in British Columbia formed in extensional tectonic settings, particularly related to the development of cratonic margins (e.g., Emsbo, 2009; Fig. 11). The famous Sullivan deposit (Figs. 10, 12) formed in the deeper parts of the Belt-Purcell basin in an intracratonic sag generated by stretching of the Laurentian continental nucleus about 1.45 billion years ago (e.g., Lydon et al., 2000; Lydon, 2007). Early Paleozoic SEDEX and MVT deposits formed contemporaneously on the western flank of Ancestral North America during the breakup of the supercontinent Rodinia, suggesting a broad genetic relationship with regional platform to off-shelf fluid flow (Fig. 2; e.g., Nelson et al., 2002, 2013a; Ootes et al., 2013).

Lead isotope studies suggest crustal sources of mineralization in MVT and SEDEX deposits (Godwin and Sinclair, 1982; Nelson et al., 2002; Leach et al., 2005; Ootes et al., 2013). Siliciclastic debris derived from continental basement and carbonate deposits are potential sources (Fig. 2b; Goodfellow and Lydon, 2007; Paradis et al., 2007; Emsbo et al., 2016; Leach et al., 2010). Leach et al. (2005) suggested that mineralization is related to the circulation of large volumes of saline brines, concentrated by the evaporation of seawater, or in the case of MVT, possibly evaporite dissolution (Fig. 11). SEDEX fluids

range from low to high temperature, 70-300°C, and salinities of 10-30 wt.% total dissolved solids, like oilfield brines (Emsbo, 2016 and references therein), whereas MVT are somewhat lower temperature, 75-200°C and up to 30 wt.% equivalent NaCl+CaCl (e.g., Paradis et al., 2007; Kontak et al., 2022). The mechanisms of heating and circulation remain conjectural and may reflect high regional geothermal gradients (with possible magmatic underplating), or deep circulation of brines (Fig. 11b). Proposed mechanisms driving fluid flow include sediment compaction and discharge, heat-driven buoyancy convection, topography-driven flow, and density-driven flow of evaporatively concentrated brines (Emsbo et al., 2016; Wilkinson, 2014; Sangster, 2020).

Syn depositional faults are the foci of mineralizing fluids in SEDEX models (Figs. 11 b, c). In the case of MVT, faults, fractures, breccias and karst features all may supply permissive permeability and porosity (Fig. 11 d). Confluences of physical and chemical conditions that focus and alter mineralizing fluids include changing lithology, changing pressure-temperature, and fluid mixing. In the Cordillera, long-lived basement structures transverse to the structural grain may have exerted controls (Lund, 2008; McMechan, 2012; Hayward and Paradis, 2021). Precipitation of sulphides requires reduced sulphur. A trap involves a change from limestone to dolomite, a permeable organic rich near-seafloor layer, exhalation into euxinic seafloor conditions, or other mixing of fluids with contrasting properties

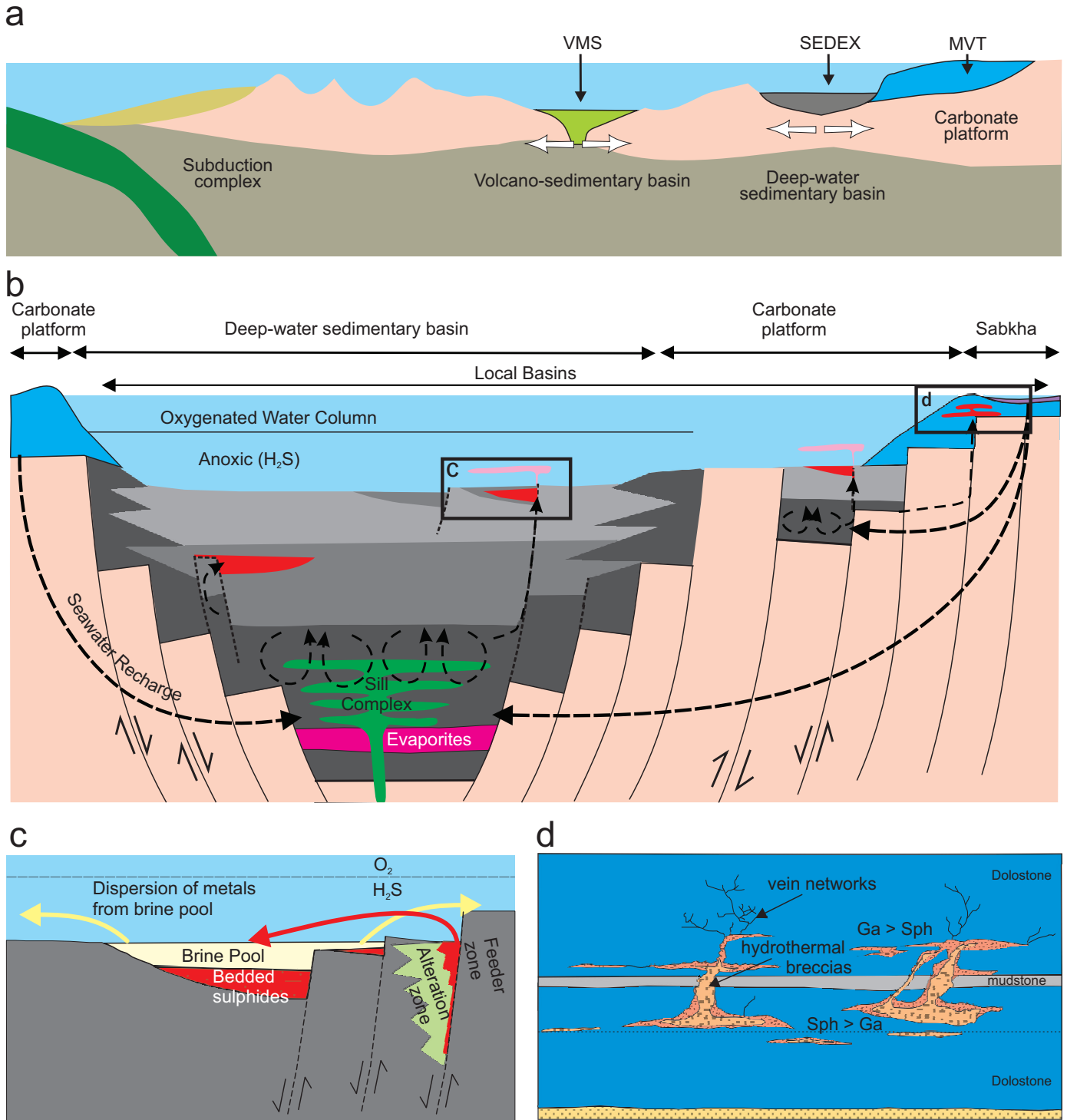


Fig. 11. a Tectonic model showing extensional environments where volcanogenic massive sulphide (VMS), sedimentary exhalative (SEDEX), and Mississippi Valley-type deposits occur. Simplified from Nelson et al. (2002). **b** Schematic diagram showing the relationship between a deep-water sedimentary basin and carbonate platform. Black arrows depict fluid flow through basement and sedimentary basins. Locations of mineralization are red. Black box outlines are for SEDEX and MVT mineralization depicted in c) and d). Simplified from Goodfellow and Lydon (2007). **c** Schematic diagram of vent-distal SEDEX mineralization related to extensional faults and dispersion of metal-rich hydrothermal fluids at the seafloor. Modified after Goodfellow and Lydon (2007). **d** Schematic depiction of MVT mineralization from Robb Lake. Simplified from Paradis et al. (2007).



Fig. 12. Folded bands of massive sulphides interlayered with fine-grained siliciclastic deposits from the historical Sullivan SEDEX mine, southeastern British Columbia.

(e.g., Goodfellow and Lydon, 2007; Leach et al., 2010; Magnall et al., 2020; Kontak et al., 2022).

British Columbia is home to numerous SEDEX deposits. The Ruddock Creek deposit is in isoclinally folded amphibolite facies metasedimentary rocks (Höy, 2001, 2002) in the hanging wall of a crustal-scale ductile shear (Monashee decollement). Based on sulphide lead isotope ages, mineralization formed between Neoproterozoic deposition (ca. 663 Ma) and ca. 535 ±30 Ma (Theny et al., 2015; Theny, 2016). The resource stands at 6.25 Mt grading 6.50% Zn, 1.33% Pb Measured and Indicated and 6.68 Mt grading 6.33% Zn, 1.20% Pb Inferred, based on a 2013 estimate (Imperial Metals Corporation, 2023) that does not include more recent drill results. SEDEX deposits in offshore rocks of the northern Rocky Mountain Laurentian margin are Late Devonian, hosted by carbonaceous shale of the Gunsteel Formation (Upper Devonian), Earn Group, and include vent-proximal and, more commonly, vent-distal types (Goodfellow, 2007). Cirque, a vent-distal deposit, currently has the largest (historical) resource estimate with 38 Mt of 8% Zn, 2.2% Pb, and 47.2 g/t Ag for the main Cirque, and 15.5 Mt of 6.9% Zn, 1.4% Pb, and 32 g/t Ag for the south Cirque (MacIntyre, 1992). The Akie project includes the Cardiac Creek vent-proximal deposit, which has an Indicated resource of 22.7 Mt of 8.32% Zn, 11.61% Pb, and 14.1 g/t Ag, and an Inferred resource of 7.5 Mt of 7.04% Zn, 1.24% Pb, and 12.0 g/t Ag (JDS Energy & Mining Inc., 2018).

Most MVT and related deposits in British Columbia are in early stages of modern exploration, (e.g., Robb Lake, Duncan Lake) or have been mined out (e.g., Monarch, Kicking Horse). However, the Revel Ridge project is a more advanced project with a zone of carbonate-hosted Ag-Zn-Pb mineralization variously described as metamorphic complex lead-zinc type (like Ruddock Creek) or MVT as favoured in a recent compilation by Stone et al. (2021). The total resource estimate

across all zones, including veins, is 6.7 Mt of 1.93% Pb, 3.68% Zn, 50 g/t Ag, and 3.69 g/t Au Measured and Indicated and 6 Mt of 1.19% Pb, 2.20% Zn, 39 g/t Ag, and 4.70 g/t Au Inferred. Although Late Devonian SEDEX mineralization in the Earn Group prompted exploration at the Silvertip deposit, the primary target is currently considered to be related to an enigmatic Cretaceous intrusion and represent a carbonate replacement manto (Nelson and Bradford, 1993; Cullen, 2010.)

Decades of foundational mapping and deposit studies in British Columbia that followed the pioneering work of Fyles and Eastwood (1962), Fyles (1964), Höy (1983), among others continues today with focus on comparing different carbonate-hosted deposits. Paradis et al. (2022) reviewed carbonate-hosted deposits of the southeastern Canadian Cordillera, including paragenetic and isotopic data and concluded that most formed in high-porosity dolostones at the margins of carbonate platform and that mineralization occurred predominantly in two main episodes: Middle to Late Cambrian and Late Devonian to Middle Carboniferous. Simandl et al. (2020, 2022) compared the REE contents of carbonate minerals in Pb-Zn deposits, finding general evidence of re-equilibration with diagenetic, hydrothermal, or metamorphic fluids. Kontak et al. (2022) compared petrographic, fluid inclusion, and stable isotope data of MVT deposits in British Columbia and Alberta suggesting that mixing of sulphur-poor metalliferous and sulphide bearing metal-poor fluids generally plays a role in mineralization. Paradis and Simandl (2017, 2018) considered genetic links between MVT and SEDEX types and between carbonate hosted barite-Zn and magnesite. Green et al. (2017) and Simandl et al. (2019) noted the similar setting of the Rock Canyon Creek deposit, which includes REE-bearing fluorocarbonates, phosphates, and fluorite (Hoshino et al., 2017), and MVT deposits of southeastern British Columbia.

5.4. Magmatic mafic to ultramafic systems

Magmatic sulphide deposits in mafic-ultramafic intrusions are the main hosts of Ni and platinum-group elements (PGE) globally and in British Columbia (Mudd and Jowitt, 2014; Mudd et al., 2018). These deposits form where sulphide liquid can segregate from a silicate magma, interact with this magma to become enriched in metals, and accumulate in small volumes of mafic-ultramafic rock in accessible portions of the crust (Naldrett, 1999; Barnes et al., 2015; Lawley et al., 2021). In the BCGS deposit profile classification (Lefebure and Jones, 2022), the general ‘mafic/ultramafic’ (M) category of this mineralizing system includes the ‘flood basalt-associated Ni-Cu’ (M01), ‘gabbroid stocks Ni-Cu’ (M02), ‘Alaskan-type Pt±Os±Rh±Ir’ (M05), and ‘Giant Mascot-type Ni-Cu±Co (M09)’ subcategories. The main metals of economic interest are Ni, Cu, Co, and the PGE (Pt and Pd > Os, Ir, Rh, and Ru; Mudd and Jowitt, 2014; Mudd et al., 2018). However, these deposits can also contain significant concentrations of V, Ti, and Cr, which are hosted primarily by chromitites and Fe-Ti-V oxide ores (Cawthorn et al., 2005; Mondal and Mathez, 2007; Pang et al., 2008) and Sc, which is concentrated

principally in clinopyroxene and amphibole (Wang et al., 2021b). Metalloids (e.g., Bi, As, Te, and Pb) that may be associated with platinum-group minerals (PGM) are rarely present in economic concentrations.

Magmatic Ni-Cu-PGE sulphide deposits can be hosted by layered mafic plutons, such as the Bushveld Complex in South Africa (e.g., Maier et al., 2023) and Duluth Complex in USA (e.g., Thériault et al., 2000), or volumetrically smaller conduit-type plutons, such as the Current (Brzozowski et al., 2023), E&L (Hancock, 1990; Brzozowski and Zaborniak, 2024), and Voisey's Bay (Lightfoot et al., 2012) deposits in Canada. It is generally agreed that most of these deposits formed from parental magmas generated by high degrees of partial melting of mantle plumes beneath craton boundaries (Fig. 13a; Begg et al., 2010), forming Large Igneous Provinces (Ernst and Jowitt, 2013). Subduction zones have not traditionally been considered prospective targets for magmatic sulphide deposits because of the paucity of mafic-ultramafic intrusions containing economic concentrations of Ni (Ripley, 2010). This view is rapidly changing as increasingly more Ni-Cu-PGE deposits are identified at convergent margins (Fig. 13b) around the world such as in Spain (e.g., Aguablanca, Piña et al., 2010) and China (e.g., Huangshandong, Huangshanxi, and Kalatongke, Song and Li, 2009; Mao et al., 2014; Wang et al., 2021a). In British Columbia (Fig. 14), such deposits include Giant Mascot (Manor et al., 2016), Turnagain (Scheel et al., 2005; Jackson-Brown et al., 2014; Nixon et al., 2019), E&L (Brzozowski and Zaborniak, 2024), Tulameen (Spence et al., 2022), and Polaris

(Nixon et al., 1990; Nott et al., 2020; Milidragovic et al., 2021, 2023).

Regardless of tectonic setting, the mechanisms by which magmatic sulphide deposits form are largely the same (Fig. 15). These include: 1) generation of a mafic-ultramafic magma by high degrees of mantle partial melting; 2) segregation of an immiscible sulphide liquid from the magma; 3) migration of this sulphide- and crystal-laden magma upwards through the crust; and 4) enrichment of the sulphide liquid in metals (Naldrett, 2010). A high degree of mantle partial melting is critical to generating these deposits because it allows for complete melting of sulphides in the mantle source, which releases metals to the resulting magma (Arndt et al., 2005; Naldrett, 2010). Despite the importance of generating an immiscible sulphide liquid, this process is challenged because most magmas arriving near the Earth's surface are undersaturated in sulphide; this is particularly true for the oxidized magmas that form at convergent margins (Mavrogenes and O'Neill, 1999; Jugo, 2009). Some additional mechanism is, therefore, required to cause a magma to become saturated in sulphide, the most common of which being addition of external S, although addition of Si, magma mixing, and crystal fractionation can also lead to sulphide saturation (Ripley and Li, 2013). Transport of the crystal- and sulphide-laden magma from the mantle to the upper portion of the crust is driven by buoyancy and dike propagation, with sulphide transport possibly being assisted by flotation on vapor bubbles (Barnes et al., 2015; Yao and Mungall, 2020). Craton boundaries serve as ideal structural

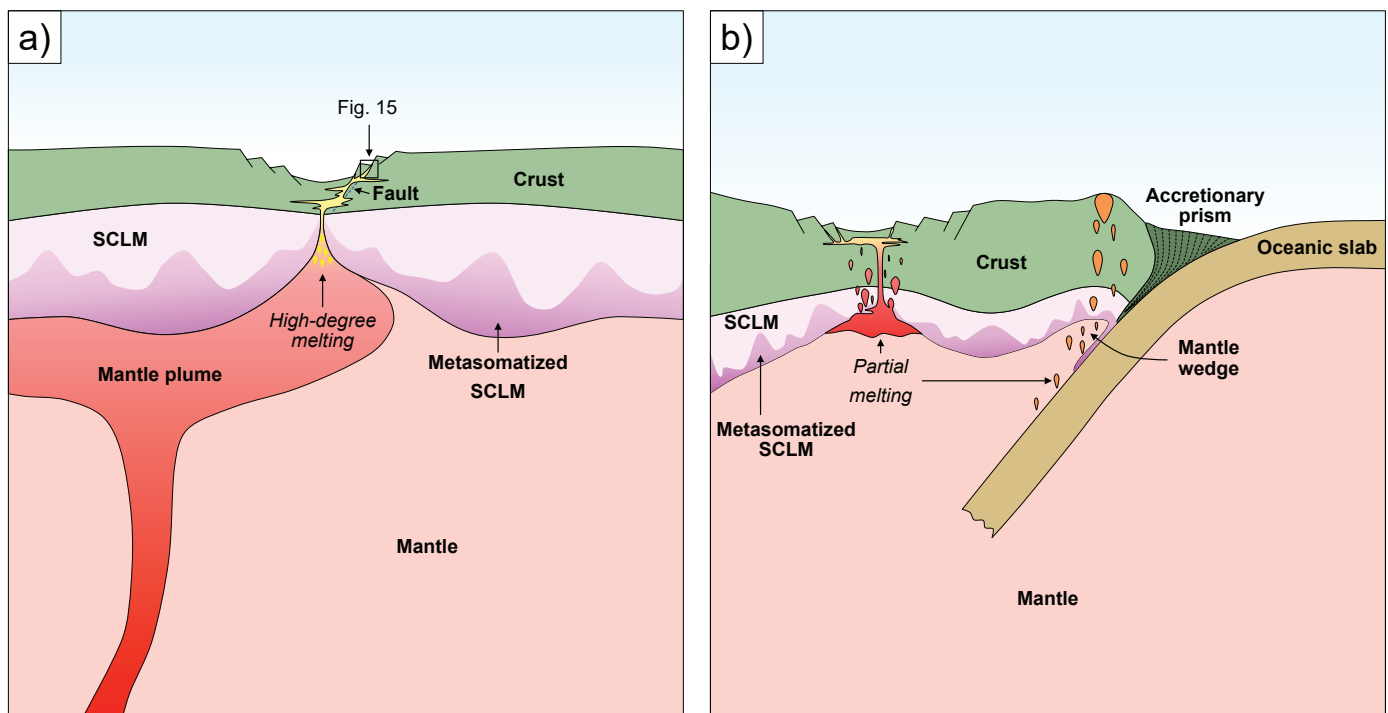


Fig. 13. Schematic diagrams illustrating the generation of magmas and associated mafic-ultramafic intrusions in **a)** an intracontinental setting associated with a mantle plume and **b)** a convergent margin (modified after Jiang et al., 2019). Most mafic-ultramafic plutons in British Columbia formed from arc-related magmas at convergent margins. Some mineralized Alaskan-type intrusions appear to have been emplaced coeval with (e.g., Polaris) or just preceding (e.g., Turnagain) the accretion of major arc terranes in the northern Cordillera (Nixon et al., 2019, 2020b).

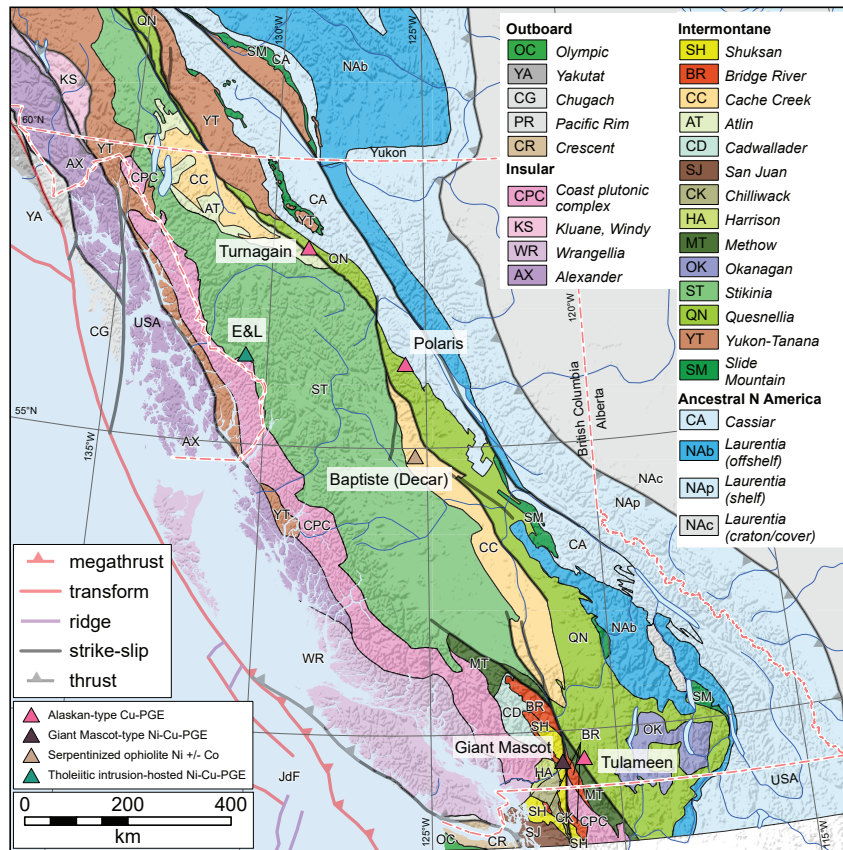


Fig. 14. Selected mafic-ultramafic Ni-Cu-PGE deposits in British Columbia. Modified after Nixon et al. (2020b). Terranes after Colpron (2020).

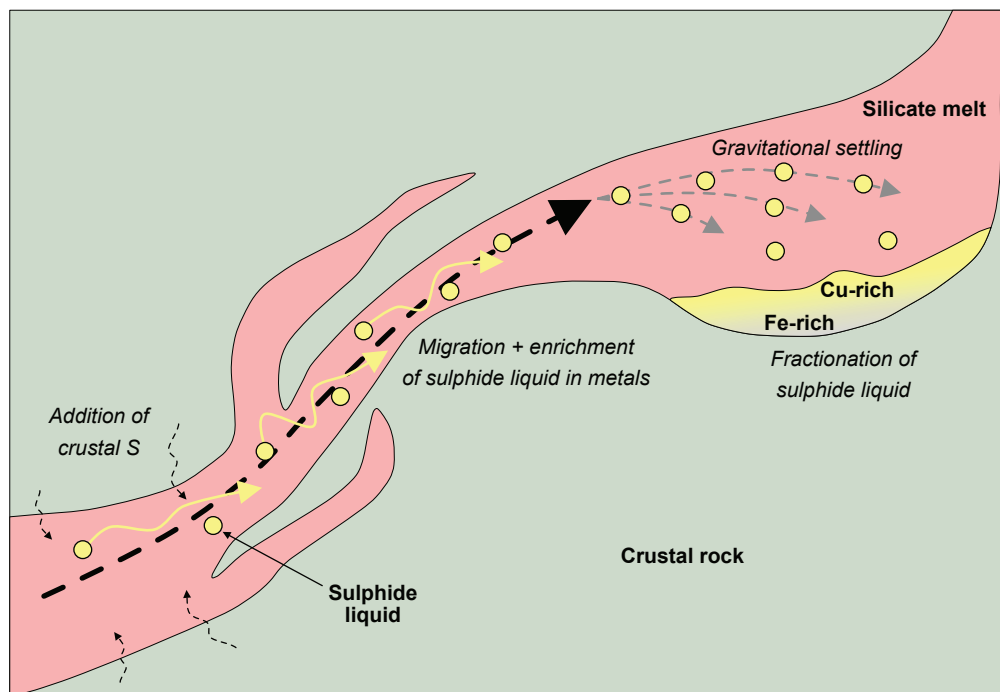


Fig. 15. Schematic diagram illustrating the range of intrusion-scale processes that operate to form base- and precious-metal-rich magmatic sulphide deposits. These processes include the: addition of externally derived S; generation of an immiscible sulphide liquid; enrichment of the sulphide liquid in metals via interaction with silicate melt; gravitational settling of the dense sulphide liquid; fractionation of the sulphide liquid and formation of Fe-rich monosulphide solid solution and Cu-rich intermediate solid solution; and exsolution of pyrrhotite-pentlandite from monosulphide solid solution and chalcopyrite from intermediate solid solution.

corridors for magma transport because Moho-penetrating faults can be reactivated, allowing magmatism to be concentrated (Barnes et al., 2015). Smaller-scale migration and emplacement occurs where these deep faults interact with local crustal anisotropies, such as faults, fractures, and foliation (Barnes et al., 2015). During magma transport and emplacement, the immiscible sulphide liquid becomes progressively enriched in metals by selectively concentrating dispersed metals in the magma via sulphide liquid-silicate melt interaction (Mungall et al., 2020). This metal enrichment process, which is quantified as 'R factor' (Campbell and Naldrett, 1979), operates most effectively in dynamic magma systems where small volumes of sulphide liquid can interact with large volumes of silicate melt (e.g., conduit-type intrusions, Barnes and Lightfoot, 2005). Finally, the metal-rich sulphide liquid needs to be concentrated in traps via mechanical processes related to silicate melt-sulphide liquid density differences and changes in magma flow regime (Barnes et al., 2015). These traps largely occur where the morphology of conduits change, causing a change in magma dynamics and, hence, sulphide carrying capacity (e.g., embayments, changes in conduit orientation; Evans-Lamswood et al., 2000; Barnes et al., 2015).

Nickel-Cu-PGE sulphide deposits in British Columbia (Fig. 14) are almost exclusively hosted by Alaskan-type and other mafic-ultramafic intrusions in Quesnel and Stikine terranes. The intrusion-hosted deposits are mineralogically and metallogenically distinct; some are endowed in PGE, but have limited sulphide (e.g., Tulameen, Polaris), whereas others are endowed in base metals and are sulphide rich (e.g., Giant Mascot, Turnagain, E&L). The Giant Mascot deposit, which is hosted by dunite, peridotite, and olivine-bearing pyroxenite that intruded the Settler schist and Spuzzum pluton (Coast Plutonic complex), is the only previously mined Ni-Cu-PGE deposit in British Columbia. It contains disseminated, net-textured, and (semi-) massive orebodies comprising chalcopyrite, pyrrhotite, and pentlandite (Nixon, 2003; Manor et al., 2016). At Turnagain, Ni-Cu-PGE mineralization in the form of disseminated to semi-massive pyrrhotite, pentlandite, and lesser chalcopyrite occurs predominantly in the dunite-wehrlite core of an otherwise typically zoned Alaskan-type pluton that intruded greenschist-facies volcano-sedimentary strata (Nixon, 1998; Scheel et al., 2005; Jackson-Brown et al., 2014; Nixon et al., 2020b). The Polaris Alaskan-type intrusion was emplaced into metasedimentary and metavolcanic rocks of the Lay Range assemblage in Quesnel terrane. It contains Ir-rich mineralization in chromite-bearing dunite and Cu-Pt-Pd-Au-rich magmatic sulphide in clinopyroxenite (Nixon et al., 1997; Nott et al., 2020; Milidragovic et al., 2021, 2023). The Tulameen intrusion, in the southern part of Quesnel terrane, is a zoned, sill-like Alaskan-type body emplaced into metavolcanic and metasedimentary rocks of the Nicola Group. It contains sulphide-poor, PGE-rich mineralization in chominites in the dunite core and sulphide-rich, Cu-PGE mineralization in clinopyroxenites in a peripheral zone. At the E&L deposit, which is hosted by a tholeiitic gabbro stock that cuts Lower

Jurassic Hazelton Group rocks in Stikine terrane, sulphide-rich Ni-Cu-PGE mineralization consists of chalcopyrite, pyrrhotite, and pentlandite mainly in varitextured gabbro and wehrlite (Vandenburg, 2020; Brzozowski and Zaborniak, 2024). Although not as common, Ni mineralization also occurs in serpentinized ophiolites. These deposits are genetically distinct from magmatic sulphide deposits and form, in part, by the release of Ni from olivine because of hydrothermal alteration. An example of such a deposit in British Columbia is Baptiste, in the Mount Sidney Williams ultramafic-ophiolite complex of Cache Creek terrane. Mineralization is in the peridotite as disseminated awaruite (Ni-Fe alloy) that resulted from serpentinization of Ni-rich olivine (Britten, 2017).

In the last several decades, British Columbia Geological Survey programs have undertaken research characterizing the petrogenesis of magmatic sulphide deposits and their host mafic-ultramafic plutons, particularly those in the accretionary terranes (e.g., Hancock, 1990; Nixon et al., 1990, 1997; Nixon, 1998, 2003). Recent work has built upon these foundational studies to continue expanding our understanding of these economically significant deposits. Manor et al. (2014) and Jackson-Brown et al. (2014) provided the first published details of the mineralogy of sulphides and platinum-group minerals in the Giant Mascot and Turnagain sulphide-rich deposits, respectively. Milidragovic et al. (2017) developed a magma mixing model to explain unusually Fe-rich rocks of the Mount Hickman intrusive system, contributing to our understanding of barren versus fertile Alaskan-type plutons. Nott et al. (2020) refined the lithological units of the Polaris pluton that were originally defined by Nixon et al. (1997), identified lithological characteristics indicating remobilization of ultramafic cumulates triggered by magma recharge, and described the spatial variability of sulphide-rich and sulphide-poor PGE mineralization. Milidragovic et al. (2023) presented sulphur isotopic data indicating that seawater sulphate was added to the sub-arc source of the Polaris magmas. Spence et al. (2022) mapped the textural relationships between ultramafic cumulates of the Tulameen pluton, and identified zones of intermingled ultramafic cumulates that were interpreted as evidence for magma recharge and remobilization of crystal mushes. Steinhorsdottir et al. (2020) described the alteration and protoliths of a dismembered ophiolite containing the Baptiste deposit and highlighted the potential importance of the degree of serpentinization to the distribution, abundance, and grain size of brucite and awaruite.

As part of the current critical minerals program at the Survey, ongoing research to further our understanding of the spectrum of magmatic sulphide deposits in the province was initiated at the E&L deposit (Brzozowski and Zaborniak, 2024).

5.5. Carbonatite and related systems

Carbonatites are rare igneous rocks that contain abundant primary carbonate minerals, at least 30% (Mitchell, 2005) or 50% (Le Maitre, 2002). As the exclusive source of critical metals such as Nb and REE, these rare rocks have become

important exploration targets. Most carbonatites are spatially and temporally associated with much larger volumes of silicate rocks such as ultramafic, melilitic, ijolite-series, and syenitic rocks, suggesting genetic relationships between the carbonate and the silica-undersaturated and alkaline silicate magmas (Woolley, 2003; Mitchell, 2005; Woolley and Kjarsgaard, 2008). The deposit profile scheme of Lefebure and Jones (2022) refers to carbonatite deposits as ‘carbonatite-associated deposits: magmatic, replacement, and residual (N01); and to related rock deposits as “nepheline syenites” (R13)’. Carbonatite- or related rock-hosted deposits also produce fluorapatite, phosphate, Fe, Al, Ti, Zr, V, Cu, Ni, Au, PGE, Ta, Mo, Ba, Sr, Th, U, lime, olivine, phlogopite, and vermiculite as the main commodities or bi/co-products (Mariano, 1989). Mitchell and Gittins (2022) distinguished the high-temperature magmatic carbonatites from the low-temperature, deuteric, residual ‘carbothermalites’ resulting from fluids enriched with CO₂ and/or carbonate anions. Both carbonatites and carbothermalites are important sources of critical metals such as Nb and REE, but carbothermalites can derive from different magmas found in a wider range of tectonic settings than carbonatites. Thus, identifying the hosts is important for critical mineral exploration. Major global examples of carbonatite-hosted deposits include REE producers such as Bayan Obo in China (Kynicky et al., 2012) and Mountain Pass in the USA (Castor, 2008) and Nb producers such as Araxá in Brazil (Biondi, 2005) and St. Honoré in Canada (Néron et al., 2018). Elsewhere, Mo production at Huanglongpu in central China is an example of an economic carbothermalite-hosted Nb-U-REE-Mo deposit within an orogenic belt (Xu et al., 2010; Song et al., 2016). Pegmatite-hosted rare-metal deposits include Nb-Y-F (e.g., Strange Lake, Québec) related to peralkaline granites or syenites and Li-Cs-Ta (e.g., Greenbushes, Australia) related to peraluminous S-type granites (e.g., Černý and Ercit, 2005; Goodenough et al., 2019).

Globally, carbonatites are typically restricted to intracratonic settings as part of crustal-scale doming and extensional systems (e.g., Bell, 1989). However, the origin and ultimate source of carbonatite-hosted critical metals on the one hand and peralkaline granite and syenite-hosted Nb, Ta, and REE on the other remains controversial. Both the lower mantle and recycled materials have been suggested as sources for carbonatite magmas (Rukhlov et al., 2015, 2018, 2019; Çimen et al., 2019), whereas peralkaline granitic and syenitic hosts might have formed by partial melting of a metasomatized lower crust (Martin, 2012). Carbonatite magmas can be the products of immiscible separation or fractional crystallization of parental carbonated silicate magmas, or the products of low-degree partial melting of a carbonate-bearing mantle (Bell, 1989; Bell and Rukhlov, 2004; Berkesi et al., 2023; Gittins and Mitchell, 2023). Ubiquitous fluoride and oxyfluoride complexes in the Nb-Y-F pegmatites suggest an important role of F for Nb transport and enrichment in these systems (Mitchell, 2015). The magmatic evolution of rare-metal pegmatites is characterized by progressive Ta enrichment and roughly

concentric zoning due mainly to in-situ differentiation (Černý et al., 1986). These systems derive from volatile-rich, highly evolved, felsic magmas (Černý and Ercit, 2005). Crustal-scale faults control pathways of both mantle- and crust-derived melts and fluids that concentrate, transport and precipitate Nb, Ta, and REE. Based on experimental evidence, Anenburg et al. (2020) concluded that complexing with alkalis, in addition to halogens and carbonate anions, are required for transport and trapping of economic-grade, carbonatite-hosted REE deposits (Trofanenko et al., 2016).

In the Canadian Cordillera, carbonatite and related igneous bodies (Fig. 16) were emplaced episodically at ca. 810-700 Ma (Mount Copeland, Perry River, Ren), 500-400 Ma (Blackfoot Creek, Bush River, Felix, HP, Kechika River, Little Chicago, Mons Creek, Swanson Peak), and 360-320 Ma (Aley, Howard Creek, Ice River, Lonnie, Mount Grace, Mud Lake, Ospika, Paradise Lake, Serpentine Creek, Three Valley Gap, Upper Fir, Trident Mountain, Vergil, Verity, Wicheeda); the Cross kimberlite is 245 Ma. Collectively, these rocks form part of the British Columbia alkaline province, which defines a long (at least 1000 km), narrow (ca. 200 km) orogen-parallel belt along the western flank of Ancestral North America (Scammell and Brown, 1990; Rukhlov and Bell, 2010; Millonig et al., 2012; Millonig and Groat, 2013; Chakhmouradian et al., 2015; Rukhlov et al., 2018). Similar to the intracratonic tectonic setting of carbonatites globally, the Neoproterozoic and Cambrian carbonatites were injected during the protracted breakup of the supercontinent Rodinia and subsequent passive margin development on the western flank of Laurentia (Figs. 17 a, b; Bond and Kominz, 1984; Ross, 1991; Colpron et al., 2002; Li et al., 2008). Both the Neoproterozoic and Cambrian pulses of carbonatite magmatism were accompanied by the emplacement of the large igneous provinces (LIP) such as Gunbarrel, Franklin-Thule, Gataga-Edwardsburg, Hamill-Gog, and Wichita (Ernst and Bleeker, 2010). In contrast, the more numerous late Paleozoic carbonatites, which host Nb-Ta deposits (e.g., Upper Fir in the Blue River area and Aley) and REE deposits (e.g., Wicheeda) are unusual relative to typical global occurrences (Bell, 1989) because they were emplaced near the continental margin while subduction was taking place to the west rather than in the cratonic interior during continental breakup (Fig. 17 c; Nelson et al., 2013a).

Hosted by the parautochthonous rocks of the Omineca and Foreland belts, carbonatites and related ultramafic, silica-undersaturated and alkaline silicate rocks in British Columbia range from intrusive complexes with a paucity of carbonatites (e.g., Trident Mountain, Mount Copeland) to carbonatite complexes with a paucity of silicate rocks (e.g., Aley, Blue River, Frenchman Cap). Both the carbonatites and host rocks experienced multiple episodes of deformation and metamorphism during Mesozoic and Cenozoic accretionary tectonics while outboard terranes welded to each other and to Laurentia (Scammell, 1987, 1993; Scammell and Brown, 1990; Pell, 1994; Millonig et al., 2013). Intrusive complexes made up of mainly silica-undersaturated and alkaline silicate rocks, such

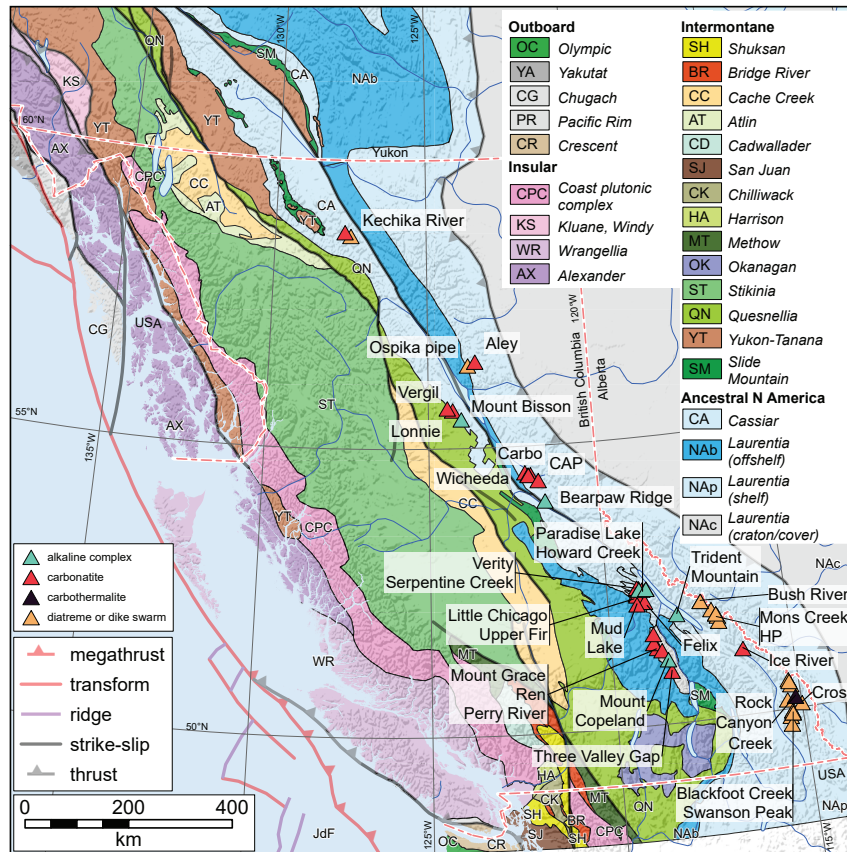


Fig. 16. Carbonatite and related rock occurrences along the British Columbia alkaline province (after Parrish and Scammell, 1988; Pell, 1994; Rukhlov and Bell, 2010; Millonig and Groat, 2013; Rukhlov et al., 2018). Terranes after Colpron (2020).

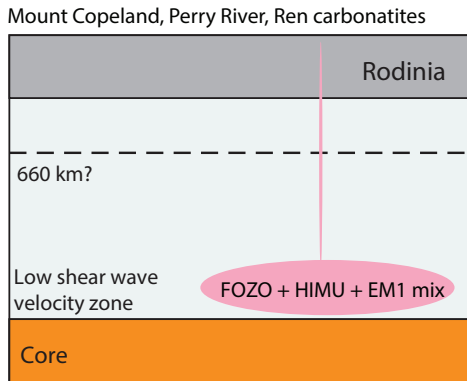
as the Ice River complex, form small (up to 29 km² at surface), compositionally zoned bodies that are circular to elongate to amoeboid in plan view (Dawson, 1886; Currie, 1975; Peterson and Currie, 1994). Associated REE-Sr-rich carbothermalite dikes, made up of Mn-calcite, barytocalcite, and zeolite with minor strontianite, Nb-ilmenite, and REE-F-carbonates, and ultramafic lamprophyres are common (Mumford, 2009; Brown, 2013). Carbonatites lacking associated contemporaneous silicate rocks typically form regional swarms of individual occurrences across areas of 1000 km² (e.g., Blue River; Pell, 1994; Mitchell et al., 2017; Rukhlov et al., 2018; Çimen et al., 2019). In the Blue River area (Fig. 16), at least 18 carbonatite and two alkaline, silica-undersaturated-rock bodies are exposed, including at the Upper Fir deposit, one of the largest and best studied Nb-Ta occurrences in the Canadian Cordillera (Chudy, 2013; Kulla and Hardy, 2015; Rukhlov et al., 2018). The carbonatites contain 5-10 vol.% amphiboles, 10-15 vol.% fluorapatite, and variable amounts of Ni-rich pyrrhotite, Nb-Zr-REE-Ti oxide phases, zircon, Fe²⁺-Na-rich phlogopite, Ti-rich magnetite, olivine, Fe³⁺-rich ilmenite, and monazite (Fig. 18). Coarse molybdenite (up to 1.7 cm long) occurs sporadically in both carbonatites and metasomatic glimmerites (carbonate-amphibole-phlogopite rocks) and fenites (calcite-clinopyroxene-amphibole rocks; Rukhlov et al., 2018) that mantle carbonatite sills. Molybdenite has been

observed in other carbonatite and related-rock occurrences in British Columbia, including Perry River, Mount Grace, Wicheeda, and the Mount Copeland past producer (Currie, 1976; White, 1982; Höy, 1988; Trofanenko et al., 2016).

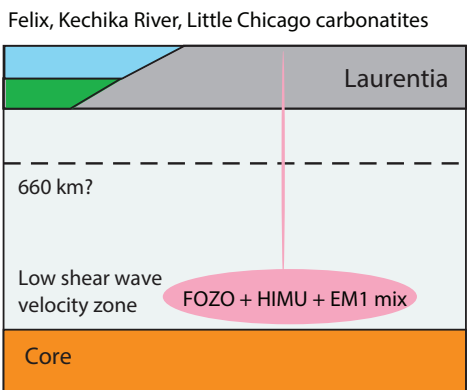
The Upper Fir carbonatite contains an NI 43-101-compliant resource of 48.4 Mt (Indicated) grading 1610 ppm Nb₂O₅ and 197 ppm Ta₂O₅ plus 5.4 Mt (Inferred) averaging 1760 ppm Nb₂O₅ and 191 ppm Ta₂O₅ (Kulla and Hardy, 2015). The main ore minerals include the Ta±U-rich pyrochlore supergroup and ferrocolumbite, with minor fersmite and nyoboaeschnite (Chudy, 2013; Rukhlov et al., 2018). Ferrocolumbite is the main Nb host in the ferriwinchite (transitional to actinolite)-dolomite carbonatite. In contrast, the ferrikatophorite (transitional to richterite and magnesio-arfvedsonite)-dolomite carbonatite contains predominantly U-Ta±Ti-rich pyrochlore.

Peralkaline granite- or syenite-related Nb-Y-F occurrences such as Mount Bisson and Coryell syenite contain Nb-Ta-Ti-REE minerals. In contrast, peraluminous S-type granite-related Li-Cs-Ta occurrences such as pegmatites in the Shuswap metamorphic complex in the Revelstoke area contain Sn-W-Ti-Ta minerals such as cassiterite, Nb-rutile, qitianlingite, bismutotantalite, hübnerite, and columbite-tantalite group (Dixon et al., 2014). Elsewhere, Li-Cs-Ta deposits are important sources of Li (e.g., Jiajika, China; Greenbushes, Australia; Tanco, Canada; e.g., Goodenough et al., 2019).

a) ca. 810-700 Ma, Rodinia breakup



b) ca. 500 Ma, passive margin



c) ca. 360 to 320 Ma, opening Slide Mountain ocean

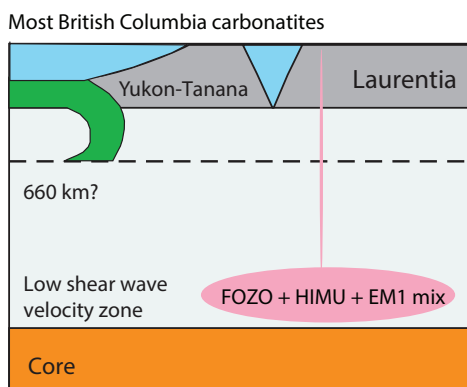


Fig. 17. Pulses of carbonatite magmatism in the Canadian Cordillera and origin of carbonatite-hosted critical metals (after Rukhlov et al., 2019). Parental magmas of Cordilleran carbonatites and related rocks were derived from an extensive, long-lived, deep-level equatorial mantle reservoir (low shear wave velocity zone) at the core-mantle boundary that was tapped episodically since the Neoproterozoic. **a)** ca. 810 to 700 Ma; protracted breakup of the supercontinent Rodinia. **b)** ca. 500 Ma; passive margin development on the western flank of Laurentia. **c)** ca. 360 to 320 Ma; subduction along the western flank of Laurentia and opening of the Slide Mountain ocean as a back-arc basin sourced by MORB magmas. Deep mantle components as follows: FOZO (FOCUS ZONE); HIMU (high- $^{238}\text{U}/^{204}\text{Pb}$ or μ); EM1 (enriched mantle 1).

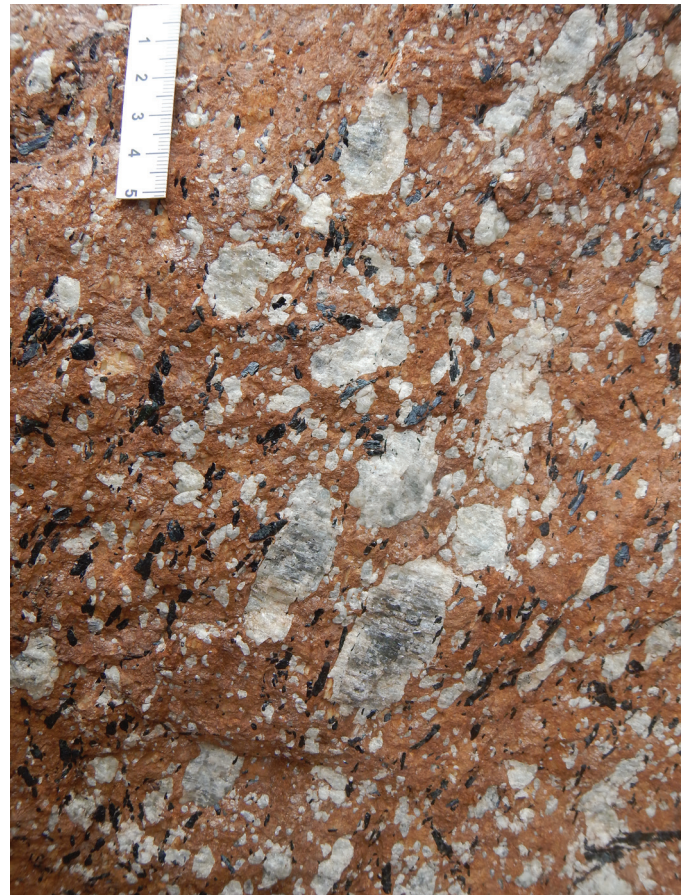


Fig. 18. Dolomite carbonatite with aligned light-toned fluorapatite megacrysts and dark-toned ferriakaphorite prisms set in a recrystallized ferroan dolomite matrix that readily oxidizes brown-red; Upper Fir deposit.

Rukhlov et al. (2018, 2019) examined the petrogenesis of the Blue River carbonatites and other examples from British Columbia using petrographic, whole-rock geochemistry, mineral chemistry, and both stable (C, O, and S) and radiogenic (Sr, Pb, and Nd) isotopic data. Isotopic systematics provide key constraints on magmatic evolution and source of the carbonatite-hosted critical metals. Despite metamorphism and deformation, most carbonatites in British Columbia, except the late Paleozoic Nb-Ta and REE carbothermal rocks, retain primary mantle carbon and oxygen isotopic signatures (Rukhlov et al., 2018, 2019; Çimen et al., 2019). The oxygen isotope equilibrium temperatures for dolomite, magnetite, ilmenite, zircon, and amphiboles coexisting with calcite in Blue River carbonatites yield values between 689-1079°C, which are much higher than the regional metamorphic temperatures (up to ~700°C) and hence reflect crystallization temperatures of relatively hot, oxidized (ΔQFM or quartz-fayalite-magnetite buffer = -0.5 to +5) magmas (Rukhlov et al., 2018). Furthermore, the Sr-Pb-Nd isotopic data indicate a heterogeneous, sub-lithospheric source of the British Columbia carbonatites involving mixing of isotopically distinct mantle end members such as FOZO (FOCUS ZONE), HIMU (high- $^{238}\text{U}/^{204}\text{Pb}$ or μ), and EM1 (enriched

mantle 1; Rukhlov et al., 2019). These mantle end members are found in the sources of ocean-island basalts or ‘hot spots’, young (<200 Ma) carbonatites worldwide, and the mantle plume-related Kola alkaline province (ca. 370 Ma; Rukhlov et al., 2015). The significance of high- $^3\text{He}/^4\text{He}$ FOZO component implies a relatively un-degassed deep-seated source (e.g., van Keken et al., 2002). Notably, the depleted, mid-ocean ridge mantle (DMM) end member, which represents the upper mantle, is excluded from the mixing trends defined by the carbonatite data from British Columbia and elsewhere (Rukhlov et al., 2015, 2018, 2019). Paleogeographic reconstructions place the western margin of Laurentia (Fig. 19; Li et al., 2008; Nelson et al., 2013a) and hence the 810-320 Ma British Columbia alkaline province, above the equatorial large low shear wave velocity province marked by a long-lived and extensive (continent-scale) reservoir at the core-mantle boundary (plume-generation zone; Burke, 2011) consisting of FOZO, HIMU, and EM1 components. Parental magmas of Cordilleran carbonatites and related silica-undersaturated and alkaline silicate rocks were likely derived from this reservoir that was tapped episodically as multiple plumes at different times since the Neoproterozoic (Fig. 17). Emplacement was probably aided by long-lived orogen parallel and orogen transverse lithospheric structures that were reactivated by regional tectonic processes during intracontinental rifting (Neoproterozoic, breakup of Rodinia), rifting of Ancestral North America (early Paleozoic, Cordilleran passive margin), and back-arc extension (late Paleozoic; during opening of Slide Mountain ocean as a back-arc basin west of the continental margin).

Simandl et al. (2017) used automated mineralogical analysis to evaluate carbonatite indicator minerals in stream sediments (Mackay and Simandl, 2015). To refine prospecting criteria for carbonatite-hosted critical metals and identify new potential targets, Rukhlov et al. (2024) are currently evaluating provincial drainage geochemistry collected as part of the Regional Geochemical Survey program.

5.6. Iron skarn, iron oxide-apatite (IOA), and iron oxide-copper-gold (IOCG) systems

British Columbia is not known for Fe skarn, iron oxide-apatite (IOA), and iron oxide-copper-gold (IOCG) deposits. Although these deposits have been explored for in the past, possible examples are not well understood, and the systems are underexplored in the modern context. The systems can host Co and In as well as Cu, REEs, Bi, Ni, and Zn but whether they represent a viable critical mineral opportunity in British Columbia remains largely untested.

Iron skarn, iron oxide-apatite (IOA), and iron oxide-copper-gold (IOCG) deposits typically share close spatial relationships with one another in regional mineral systems (e.g., Skirrow, 2022; Corriveau et al., 2022, and references therein) and commonly show spatial continuity with other deposit types such as copper skarns and alkalic porphyry Au deposits. Although with distinctive textural modes, these iron-rich deposits also share unusual characteristics including:

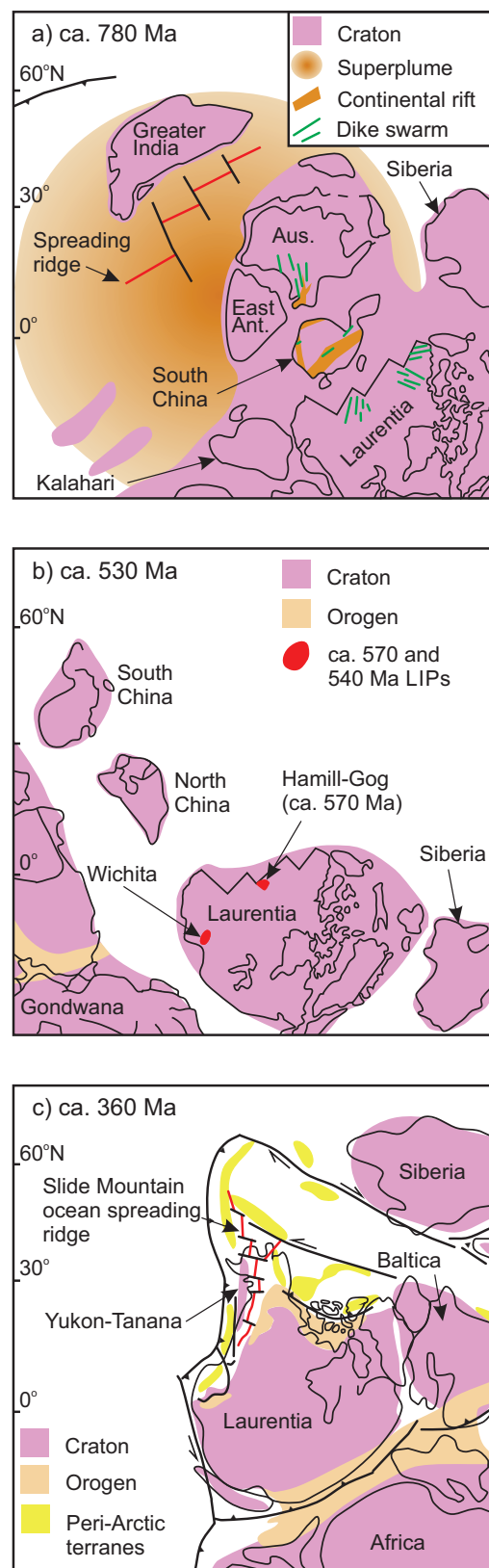


Fig. 19. Paleogeographic reconstructions of Neoproterozoic to Late Paleozoic continents at **a)** ca. 780 Ma; **b)** ca. 530 Ma, and **c)** ca. 360 Ma. The British Columbia alkaline province is in the equatorial and sub-equatorial region. Modified after Li et al. (2008) and Nelson et al. (2013a).

1) massive structurally controlled actinolite-rich magnetite ore bodies that are typically low in Ti and V (Hitzman et al., 1992); 2) regional-scale Na- and Na-Ca alteration and variable deposit-scale Fe-Ca-K alteration; 3) little to no hydrothermal quartz; 4) variable sulphide mineralization consisting mostly of pyrite-chalcopyrite-pyrrhotite (e.g., Sillitoe, 2003; Barton, 2013); and 5) enrichment in a similar spectrum of metals. These shared features make iron skarns, IOA, and IOCG deposits difficult to clearly classify and differentiate from one another and from other deposit types (Sillitoe, 2003; Skirrow, 2022). As a result, the deposit profiles identified by Lefebure and Jones (2022) classify examples of all three deposit types interchangeably in the 'Fe-Skarn (K03)' and 'iron oxide $\text{Cu}\pm\text{Au}\pm\text{P}\pm\text{REE}$ (D07)' groups.

All skarns have abundant garnet-rich calcsilicate alteration and typically develop along contacts between intrusions and carbonate strata (e.g., Meinert et al., 2005). However, iron skarns have distinctive features that set them apart including: 1) mineralization in the form of massive podiform magnetite orebodies (Ray, 2013); 2) abundant sodic-calcic and calcsilicate alteration that mainly replaces Si-rich igneous photoliths rather than carbonate sedimentary rocks (e.g., Golmohammadi et al., 2015; Cui et al., 2022; Mikaeili et al., 2023); and 3) a near complete lack of hydrothermal quartz (Meinert et al., 2005). Along with Fe, iron skarns produce notable quantities of Cu, Co, and Au from pyrrhotite, chalcopyrite, bornite, and arsenopyrite (Meinert et al., 2005) that occurs either as disseminated crystals in massive magnetite or as discrete massive sulphide pods. In addition, In and Ge mineralization have been identified in sphalerite-bearing iron skarns in the American southwest (e.g., the West Desert deposit, USA; Dyer et al., 2014) and elsewhere.

Iron oxide-apatite deposits commonly consist of tabular dike-like or, more rarely, massive orebodies with volcanic or plutonic textures. These orebodies commonly have sharp contacts with host rocks and resemble volcanic flows, layered tuff deposits, (e.g., Laco Norte, Chile, Tornos et al., 2016), podiform masses within silicate plutons (e.g., Great Bear Magmatic zone, Canada, Hildebrand, 1986), and pegmatite veins with well-developed epitaxial growth textures (e.g., Pasos Blancos, Chile, Tornos et al., 2016; Iron Springs, USA, Bain et al., 2020). These igneous textures and abundant euhedral magnetite, apatite, and actinolite are key distinguishing features (Sillitoe and Burrows, 2002; Tornos et al., 2023). Most IOA ore bodies are sulphide poor and primarily developed for Fe and minor amounts of chalcopyrite- and arsenopyrite-hosted Cu-Au-Co mineralization. However, recent discoveries of economic light REE mineralization derived from recrystallized primary apatite (e.g., Per Geijer, Sweden, Martinsson et al., 2016) highlight their potential for other critical minerals.

Relative to IOA systems, massive magnetite orebodies in IOCG deposits are more sulphide-rich and tend to consist of structurally controlled replacement zones suggestive of metasomatic processes (Groves, 2010). Alteration in IOCG systems consists primarily of broad regional-scale aureoles of

pervasive Na-Ca alteration (abltie-scapolite-actinolite±garnet; Barton, 2013) that are overprinted by K-Fe-Ca alteration in and around individual deposits. These deposits can form in any host rock and, although typically found in volcanic and sedimentary successions crosscut by a range of intrusive rocks, commonly lack a clear genetic relationship to magmatism of a particular composition (Skirrow, 2022). Most IOCG deposits are mined for Cu and Au in pyrrhotite, pyrite, chalcopyrite, and bornite disseminated in massive magnetite ores. However, these deposits can be enriched in a wide range of elements including Ag, Co, Ni, Bi, Se, Te, In, U, and Mo (Corriveau et al., 2022). Notably, several IOCG deposits feature enrichment in Co-Bi-Au (NICO deposit, NWT, Canada, Burgess et al., 2014; Acosta-Góngora et al., 2015) and U (Olympic Dam, Australia, Reeves et al., 1990; Ehrig et al., 2012).

Iron skarns tend to occur in broad metallogenetic belts along convergent margins (Fig. 20; e.g., Yangtze River metallogenic belt, China, Duan et al., 2021; Khaf-Kashmar-Bardaskan volcano-plutonic metallogenic belt, Iran, Golmohammadi et al., 2015) and form alongside gabbroic intrusions in oceanic island arc or back-arc settings (Meinert et al., 2005; Ray, 2013). Most genetic models for iron skarns mirror those of Cu-Au skarn systems. These models involve the exsolution of metal-rich saline fluids from crystallizing magmas at depth, the formation of calcsilicates in carbonate rocks via CO_3^{2-} - SiO_2 exchange, and the precipitation of base-metal mineralization via a decrease in temperature and a shift in fluid pH (Meinert et al., 2005). However, current research suggests that carbonic-sulphate fluids rather than aqueous chloride solutions might play a more important role in iron skarn formation by driving Fe mobility and controlling redox conditions on the deposit scale (e.g., Duan et al., 2021). Similar processes are also inferred in IOA and IOCG deposits.

Iron oxide-apatite deposits typically form in continental arc environments in extensional or transtensional settings (Skirrow, 2022). The characteristic magmatic textures of IOA ores provide clear evidence for an orthomagmatic genetic model in which mineralization represents crystallized Fe-P liquids formed via silicate melt immiscibility driven by the assimilation of sulphate-bearing carbonate rock (Tornos et al., 2023). Evidence for this model includes the common crosscutting relationship between mafic intrusions and evaporite-bearing carbonate strata in many IOA systems and abundant carbonate-sulphate melt inclusions in IOA ores (Bain et al., 2020, 2021). However, IOA systems commonly contain abundant Na-Ca and acid-sulphate alteration, dissolution-reprecipitation textures, and display a mixed sedimentary and magmatic-hydrothermal isotopic signature (e.g., Johnson et al., 2016). These features have led others to invoke contrasting metasomatic (Barton and Johnson, 1996) and magmatic-hydrothermal models (Sillitoe and Burrows, 2002; Reich et al., 2022).

Iron oxide-copper-gold deposits can form in diverse geodynamic contexts but are mainly found in: 1) orogenic settings in previously extended terrains with coeval felsic magmatism (Cloncurry Province, Australia, Williams and

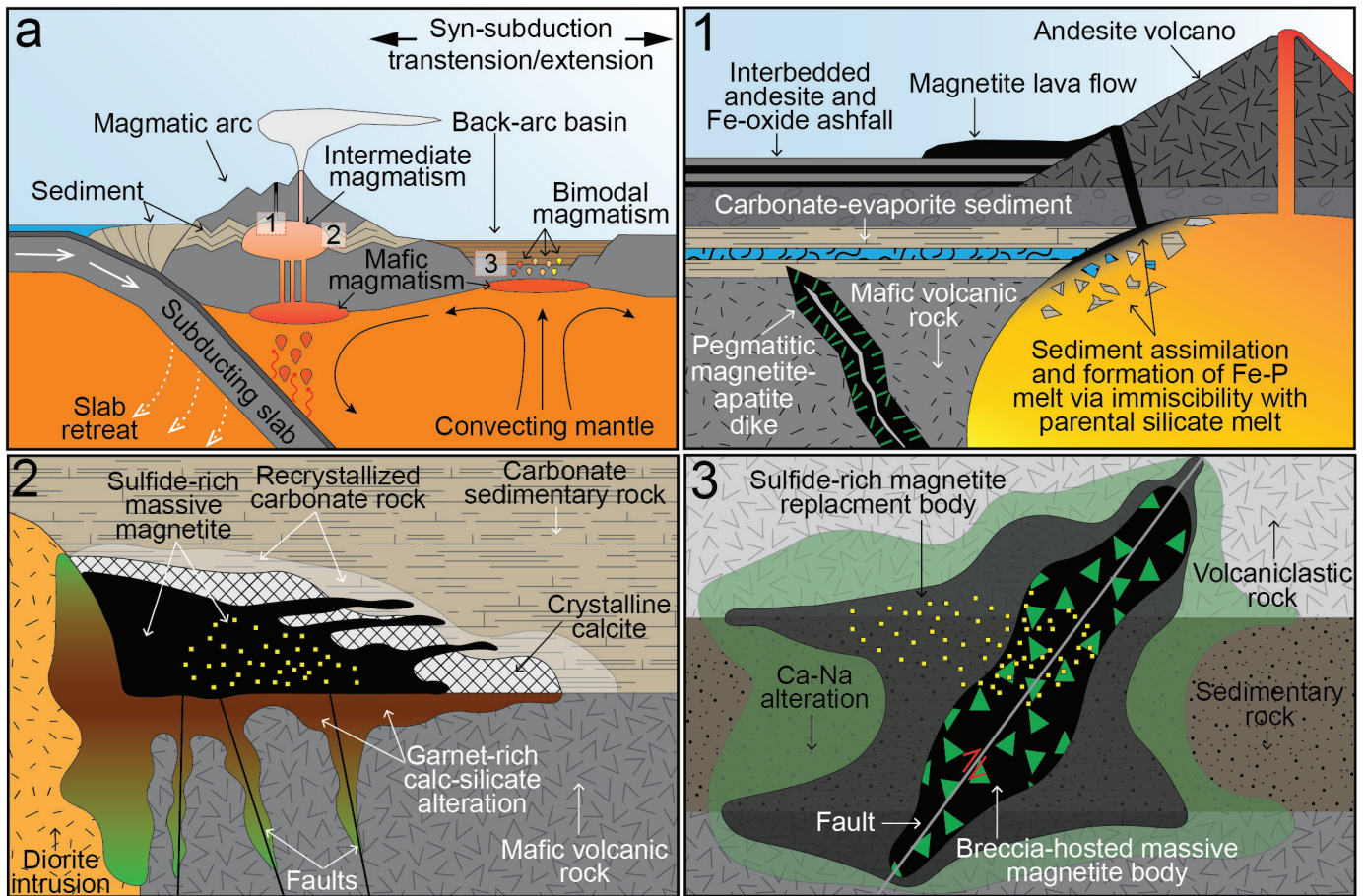


Fig. 20. a) Arc setting for iron skarns ('1'), IOA deposits ('2'), and IOCG deposits ('3'). **1)** Andesite volcanic complex hosting massive IOA ore bodies showing volcanic- and pegmatitic dike-like morphologies. Note the assimilation of evaporite-bearing carbonate sediments by silicate magma at depth and the formation of Fe-P melt via melt immiscibility. This is a representation of the orthomagmatic model for IOA deposits. Other models invoke metasomatic processes particularly when the ore bodies are more like that shown in panel '3'. **2)** Sulphide-rich iron skarn with calc-silicate alteration in the Si-rich volcanic and intrusive host rocks and an envelope of crystalline calcite and recrystallized carbonate rock surrounding the massive magnetite ore. Sulphides are denoted by yellow squares. **3)** Sulphide-rich breccia-hosted IOCG ore body surrounded by a replacement-style ore body and an aureole of Ca-Na alteration. Mineralization is focused along a fault and the distribution of the replacement ore and alteration follows lithologic contacts.

Pollard, 2001; Carajas Province, Brazil, Monteiro et al., 2008); 2) extended post-orogenic settings with bimodal, predominantly felsic, magmatism (Gawler Craton, Australia, Johnson and Cross, 1995), and 3) arc settings where a switch from compression to extension coincides with intermediate magmatism (Great Bear magmatic zone, Canada, Ootes et al., 2017; Andean Province, Chile and Peru, del Real et al., 2018). A range of genetic models exist for IOCG systems. Many recent studies invoke magmatic-hydrothermal processes as the key mechanisms and propose porphyry-like models involving the exsolution of saline, Fe-rich magmatic-hydrothermal fluids from magmas crystallizing at depth and magnetite precipitation via extensive fluid-rock reactions (e.g., del Real et al., 2020; Melfou et al., 2023). The analogy to porphyry-like hydrothermal processes goes further in some models invoking a continuum between IOCG and porphyry deposits, with IOCG mineralization representing the basal expression of regional hydrothermal systems (Mumin et al., 2010; Richards

and Mumin, 2013). These models are supported by the textures and the geochemical and stable isotope (S, O, C, Fe) signatures of ore and alteration mineralogy. However, these data sets also consistently reflect inputs from carbonate and evaporitic sedimentary sources. This has led others to attribute IOCG formation to the circulation of fluids of sedimentary or near-surface origin and extensive leaching of Fe from mafic host rocks by (e.g., Johnson and Barton, 1996).

Iron skarns are distributed in a northwest-trending belt extending from Vancouver Island and Texada Island to Haida Gwaii (Fig. 21; Ray, 2013) and are currently being investigated as part of the critical minerals program at the Survey (Fig. 22). Clear examples of IOA deposits in British Columbia are rare with two possibilities including the apatite-rich magnetite veins that crosscut the Heffley Creek Alaskan-type mafic-ultramafic pluton (Glen Iron and Magnet deposits, described by Ray and Webster, 2000) and the base of the New Afton porphyry Cu-Au deposit (described by Logan and Mihalynuk, 2005;

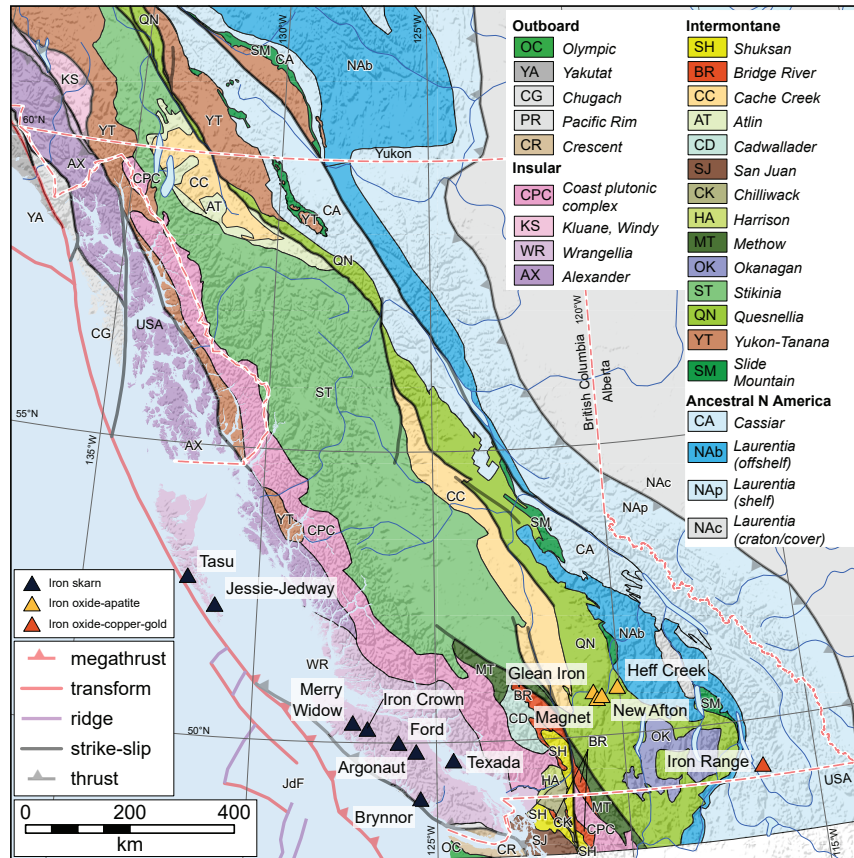


Fig. 21. Iron skarn, possible iron oxide-apatite (IOA), and possible iron oxide-copper-gold (IOCG) deposits in British Columbia. Terranes after Colpron (2020).

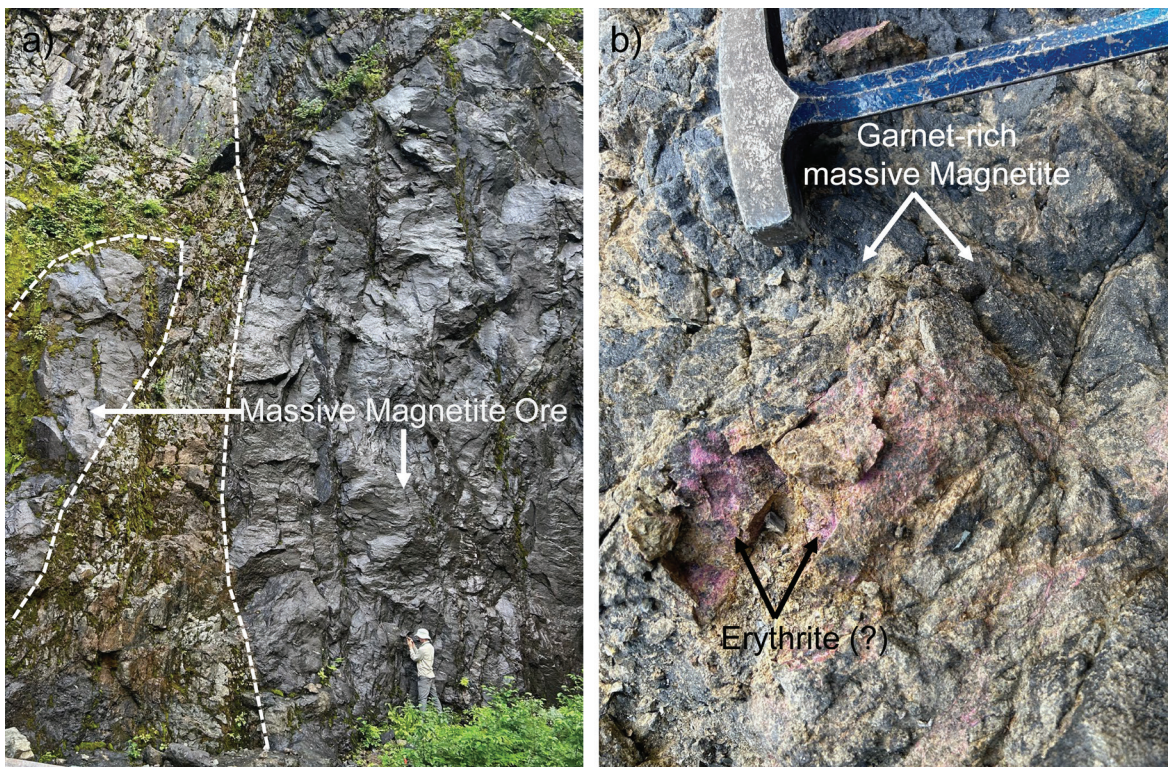


Fig. 22. a) Massive magnetite ore body along the southern wall of the Merry Widow mine, Vancouver Island. Not the sharp contacts between the ore and the host rocks. b) Erythrite-bearing (?), garnet-rich, podiform magnetite mineralization from northern Texada Island.

Hall and May, 2013; Thomas, 2021). The one possible IOCG example in the province would be replacement-style magnetite clusters along the Iron Range fault zone in Belt-Purcell basin (Mesoproterozoic) of south-central British Columbia (Stinson and Brown, 1995; Galicki et al., 2012). However, IOCG- and IOA-like mineralization commonly overprints or is spatially associated with the deep and peripheral areas of alkalic porphyries and base-metal skarns and could host additional Co-Bi- and REE-bearing mineralization, an idea that is currently being evaluated.

6. Discussion

British Columbia is already an important critical mineral producer. British Columbia is Canada's largest producer of Cu, only producer of Mo, mines Mg, and recovers Zn, Ag, and Pb. In addition to Pb and Zn, British Columbia smelters process metals not mined in the province: Al at the Rio Tinto smelter in Kitimat; and Ge, Cd, and In at the Teck Resources facility in Trail (Fig. 23). Several mine development and proposed mine projects in British Columbia could produce elements on Canada's critical minerals list as well as Ag, a metal that is typically classified as precious but with important applications in renewable energy such as for solar cells (Fig. 24). These proposed mines include Aley (Nb), Bull River (Cu, Ag), Galore Creek (Cu, Ag), Kemess Underground (Cu, Ag), Kemess East (Cu, Ag), Kitsault (Mo, Ag), KSM (Cu, Ag, Mo), Kutcho (Cu, Zn, Ag), Record Ridge (Mg), and Ruddock Creek (Zn).

The province also has many advanced projects with National Instrument 43-101 (NI 43-101)-compliant defined resources that include critical mineral elements (Fig. 24). Advanced projects include Akie (Zn, Pb, Ag), Berg (Cu, Mo, Ag), Chu Chua (Cu, Zn, Ag), Decar Nickel District (Ni, Co), Fox Tungsten (W), Yellowhead (Cu, Ag), Jersey-Emerald (W, Mo), Kitsault Valley-Dolly Varden (Ag), Kitsault Valley-Homestake Ridge (Ag, Cu), Kwanika (Cu, Ag), Lac La Hache (Cu, Ag), North Island (Cu, Mo, Re), Ootsa (Cu, Mo, Ag), Poplar (Cu, Ag, Mo), Revel Ridge (Zn, Ag), Ruby Creek (Mo), Schaft Creek (Cu, Mo), Silver Queen (Ag, Zn, Cu), Silvertip, (Ag, Zn, Pb), Stardust (Cu, Ag), Tatogga (Cu, Ag), Turnagain (Ni, Co), Wicheeda (REE), and Woodjam (Cu).

As British Columbia develops its Critical Mineral Strategy, new geoscience will be the foundation for establishing new opportunities. Ongoing geoscience research by the Survey is methodically assessing mineral systems to understand the spatial and temporal distribution of critical minerals at regional and deposit scales. In the short-term, clarifying by- and co-production possibilities of critical minerals not being recovered from current base and precious metal mines will likely be important. In the long-term, providing foundational geoscience data and developing novel exploration techniques will encourage discoveries and enhance exploration for underexplored mineral systems.

The digitization (direct analog-to-digital conversion of data and documents) and digitalization (enabling these data

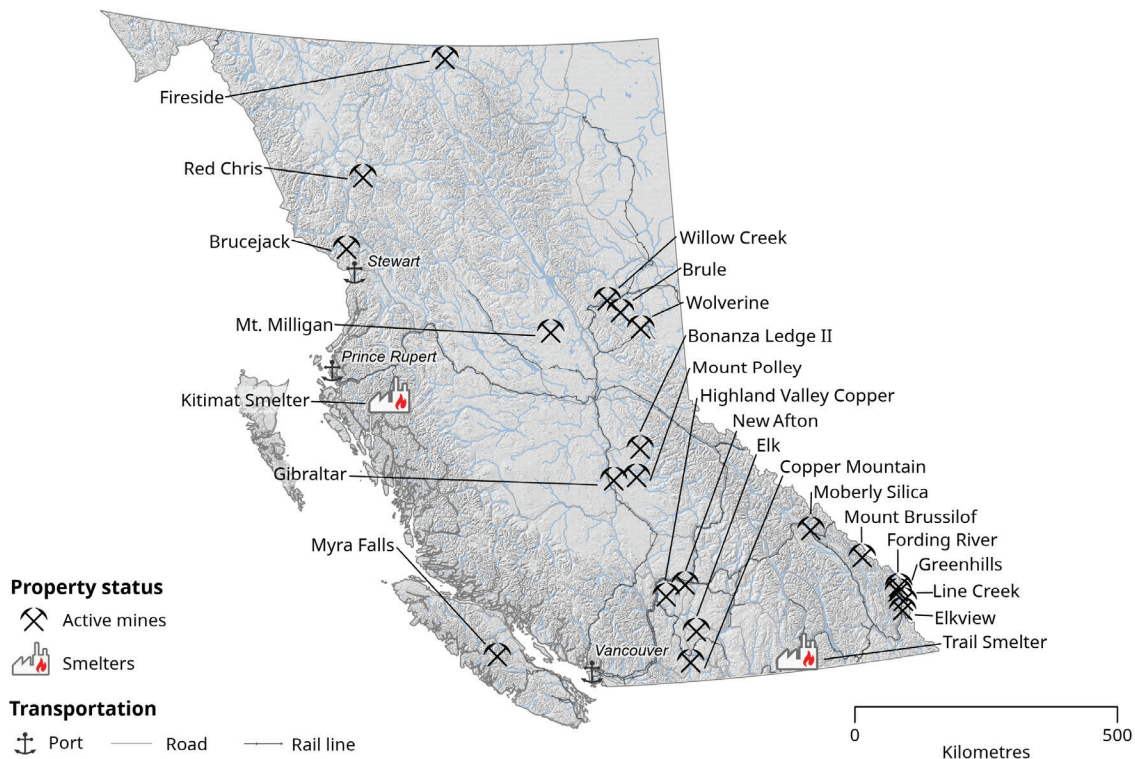


Fig. 23. Operating metal, coal, and industrial mineral (Fireside, Moberly, Mt. Brussilof) mines and smelters in British Columbia, 2022. From Hickin et al. (2023).

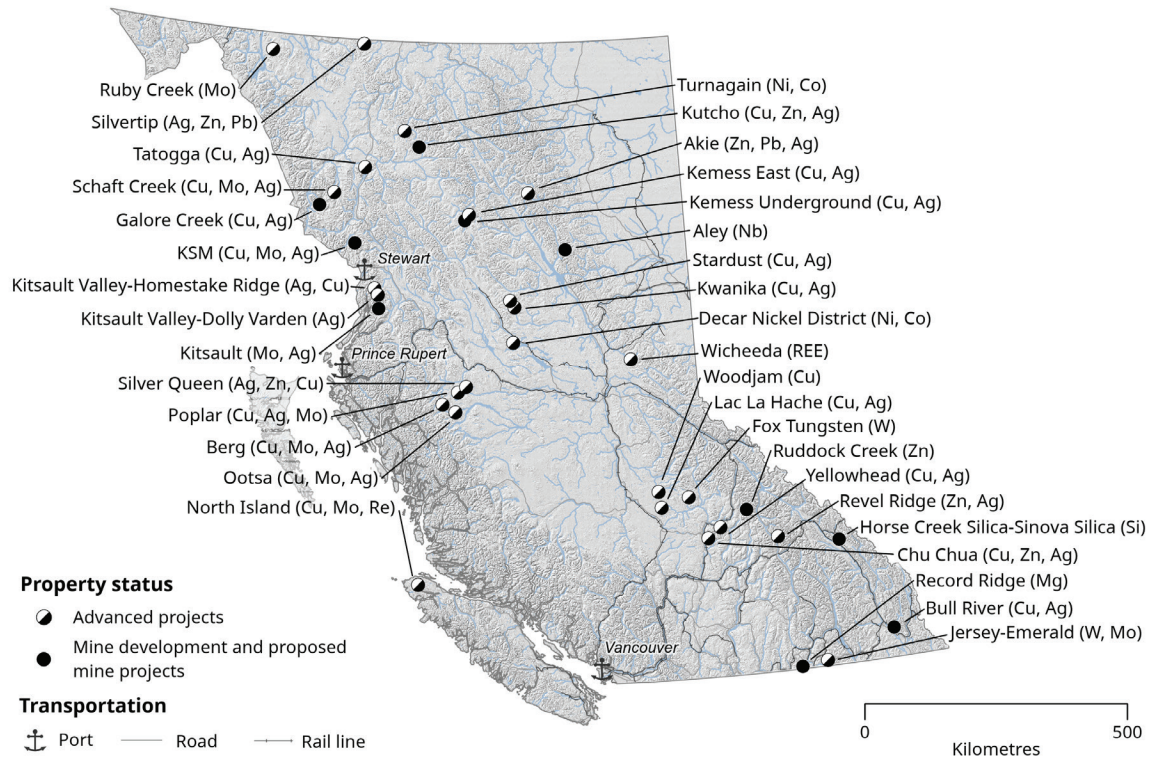


Fig. 24. Mine development and proposed mine projects and advanced projects in British Columbia, 2023, with critical minerals indicated in parentheses. From Hickin et al. (2023).

to be compatible and usable across information systems) of geoscience information is another essential activity for capitalizing on the global investment in critical minerals. Advances in computational power and sophistication have enabled innovative analysis of new and existing geochemical, geophysical, and geological data that has accelerated the recognition of patterns, trends, and the understanding of mineral systems. The expansion of digital data and the improvement of data-driven analytics is enabling the next generation of mineral potential modelling in British Columbia. Establishing the essential metal sources, transport pathways, and chemical and physical traps for a mineral deposit that can be mapped or detected, provides the foundation on which to evaluate British Columbia's mineral potential. The ability to digitally, statistically, spatially, and temporally interrogate provincial geoscience data allows probability models to be constructed that highlight potential mineral districts. These models are essential to ensure that decisions made by governments, rightsholders, stakeholders, and investors are appropriately informed so that the choices maximize the benefit to society.

7. Conclusion

A long and multifaceted tectonic history has endowed British Columbia with a host of mineral systems. Each of these systems form in different ways and have specific critical mineral endowments. Porphyry systems, an immediate consequence of magmatic arc evolution, provide the most significant

critical mineral resources in British Columbia. The principal commodity in most porphyry deposits is Cu, and porphyries are the only deposit type to contain significant Mo. Porphyry deposits in British Columbia may also contain appreciable Au and Ag and, to a lesser extent, the PGE, Re, Se, and Te. In the more Mo-rich porphyry deposits, Li, Nb, REE, Rb, Ta, and Sn may be present in recoverable quantities. Volcanogenic massive sulphide deposits represent another important system because they contain most of the Co and Zn in the province. Deep-water basin sedimentary exhalative systems are significant hosts to Pb, Zn, and Ag, could conceivably supply Bi, Ge, In, Sn, and W. Similarly, platformal Mississippi Valley systems supply Pb, Zn, and Mg, but have the potential to contain Ba, Ga, Ge, In, REE, and F. Magmatic sulphides represent a significant system that may host economic concentrations of Ni, PGE and Co. Carbonatites are also important because they are the only hosts to significant Nb and Ta in British Columbia and are the primary global source of REEs. IOA and related deposits may represent under-recognized potential in British Columbia for critical minerals, a hypothesis that continues to be tested.

Many greenhouse gas-reducing strategies require critical minerals that must be mined. British Columbia is presented with a generational opportunity to supply some mine products that can contribute to addressing the climate crisis while, at the same time, benefitting the provincial economy. With abundant hydroelectric power and the potential to use this power to produce critical minerals, British Columbia may be able to

provide materials with a substantially lower carbon footprint than jurisdictions that rely on fossil fuels.

The British Columbia Geological Survey is refining mineral systems models that may host critical minerals and developing exploration techniques that could lead to new discoveries and expand existing resources. By increasing awareness of critical mineral opportunities for the exploration and mining industries, and by enhancing the critical mineral knowledge base, the province seeks to encourage investment that could lead to British Columbia being a significant supplier of the raw materials necessary to support a low-carbon future.

Acknowledgments

We thank Kaitlyn McLaren for GIS support. JoAnne Nelson and Graham Nixon provided perceptive comments that improved the content and presentation of this paper.

References cited

- Acosta-Góngora, P., Gleeson, S., Samson, I., Corriveau, L., Ootes, L., Taylor, B.E., Creaser, R.A., and Muehlenbachs, K., 2015. Genesis of the Paleoproterozoic NICO iron-oxide-cobalt-gold-bismuth deposit, Northwest Territories, Canada: evidence from isotope geochemistry and fluid inclusions. *Precambrian Research*, 268, 168-193.
- Anenburg, M., Mavrogenes, J.A., Frigo, C., and Wall, F., 2020. Rare earth element mobility in and around carbonatites controlled by sodium, potassium, and silica. *Science Advances*, 6, article eabb6570. <<https://doi.org/10.1126/sciadv.abb6570>>
- Arndt, N., Leshner, C.M., and Czamanske, G.K., 2005. Mantle-derived magmas and magmatic Ni-Cu-(PGE) deposits. In: Hedenquist, J.W., Thompson, J.F.H., Goldfarb, R.J., Richards, J.P., (Eds.), *Economic Geology*, 100th Anniversary volume, 5-24.
- Arnold, H., and Ferbey, T., 2020. Ice-flow indicator database, British Columbia and Yukon. British Columbia Ministry of Energy, Mines and Petroleum Resources, British Columbia Geological Survey Open File 2020-03.
- Bain, W.M., Steele-MacInnis, M., Li, K., Li, L., Mazdab, F.K., Marsh, E.E., 2020. Carbonate-sulfate melts in iron oxide-apatite deposits. *Nature Geoscience*, 13, 751-757.
- Bain, W.M., Steele-MacInnis, M., Tornos, F., Hanchar, J.M., Creaser, E.C., and Pietruszka, D.K., 2021. Evidence for iron-rich sulfate melt during magnetite(-apatite) mineralization at El Laco, Chile. *Geology*, 49, 1044-1048.
- Barnes, S.J. and Lightfoot, P.C., 2005. Formation of magmatic nickel sulfide ore deposits and processes affecting their copper and platinum group element contents. In: Hedenquist, J.W., Thompson, J.F.H., Goldfarb, R.J., and Richards, J.P., (Eds.), *Economic Geology*, 100th Anniversary volume, pp. 179-213.
- Barnes, S.J., Cruden, A.R., Arndt, N., and Saumur, B.M., 2015. The mineral system approach applied to magmatic Ni-Cu-PGE sulphide deposits. *Ore Geology Reviews* 76, 296-316.
- Barresi, T., Nelson, J.L., and Friedman, R., 2015. Evolution of the Hazelton arc near Terrace, British Columbia: Stratigraphic, geochronological and geochemical constraints on a Late Triassic-Early Jurassic arc and Cu-Au porphyry belt. *Canadian Journal of Earth Sciences*, 52, 466-494.
- Barton, M.D., 2013. Iron oxide(-Cu-Au-REE-P-Ag-U-Co) systems. In: Turekian, K.K. and Holland, H.D., (Eds.), *Geochemistry of Mineral Deposits*, Treatise on Geochemistry, Elsevier, Amsterdam, 13, 515-541.
- Barton, M.D., and Johnson, D.A., 1996. Evaporitic-source model for igneous-related Fe oxide (REE-Cu-Au-U) mineralization. *Geology*, 24, 259-262.
- Begg, G.C., Hronsky, J.A.M., Arndt, N.T., Griffin, W.L., O'Reilly, S.Y., and Hayward, N., 2010. Lithospheric, cratonic, and geodynamic setting of Ni-Cu-PGE sulfide deposits. *Economic Geology*, 105, 1057-1070.
- Bell, K., (Ed.), 1989. *Carbonatites: Genesis and Evolution*. Unwin Hyman, London, 618 p.
- Bell, K., and Rukhlov, A.S., 2004. Carbonatites from the Kola Alkaline Province: origin, evolution and source characteristics. In: Wall, F., and Zaitsev, A.N., (Eds.), *Phoscorites and Carbonatites from Mantle to Mine: The Key Example of the Kola Alkaline Province*. Mineralogical Society Series, 10, The Mineralogical Society, London, United Kingdom, pp. 433-468.
- Berkesi, M., Myovela, J.L., Yaxley, G.M., and Guzmic, T., 2023. Carbonatite formation in continental settings via high pressure-high temperature liquid immiscibility. *Geochimica et Cosmochimica Acta*, 349, 41-54.
- Biondi, J.C., 2005. Brazilian mineral deposits associated with alkaline and alkaline-carbonate complexes. In: Comin-Chiaromonti, P., and Gomes, C.B., (Eds.), *Mesozoic to Cenozoic Alkaline Magmatism in the Brazilian Platform*. Editora da Universidade de São Paulo: Fapesp, São Paulo, 707-750.
- Blengini, G.A., El Latunussa, C., Eynard, U., Torres de Matos, C., Wittmer, D., Georgitzikis, K., Pavel, C., Carrara, S., Mancini, L., Unguru, M., Blagoeva, D., Mathieux, F., and Pennington, D., 2020. Study on the EU's list of critical raw materials, 2020. Executive summary. <<https://data.europa.eu/doi/10.2873/24089>>
- Bond, G.C., and Kominz, M.A., 1984. Construction of tectonic subsidence curves for the early Paleozoic miogeocline, Southern Canadian Rocky Mountains: Implications for subsidence mechanisms, age of breakup and crustal thinning. *Geological Society of America Bulletin*, 95, 155-173.
- Brew, D.A., 1992. Decision points and strategies in quantitative probabilistic assessment of undiscovered mineral resources. US Geological Survey, Open File 92-308, 23 p.
- Britten, R., 2017. Regional metallogeny and genesis of a new deposit type-Disseminated awaruite (Ni₃Fe) mineralization hosted in the Cache Creek Terrane. *Economic Geology*, 112, 517-550.
- Brown, A.C., 2014. Low-temperature sediment-hosted copper deposits. In: Turekian K.K., and Holland, H.D., (Eds.), *Geochemistry of Mineral Deposits*. Treatise on Geochemistry 13, Elsevier, Amsterdam, pp. 251-271.
- Brown, J.A., 2013. Waterloo Resources Ltd. 2012 field activities at the Ice River property, Waterloo Prospect area. British Columbia Ministry of Energy, Mines and Natural Gas, British Columbia Geological Survey, Assessment Report 33565, 39 p.
- Brzozowski, M.J., and Zaborniak, K., 2024. Petrology of sulphide mineralization at the E&L magmatic Ni-Cu-PGE deposit: Textural evidence for contamination, vapor saturation, fluid immiscibility, and metal remobilization. In: *Geological Fieldwork 2023*, British Columbia Ministry of Energy, Mines and Low Carbon Innovation, British Columbia Geological Survey Paper 2024-01, this volume.
- Brzozowski, M., Hollings, P., Heggie, G., MacTavish, A., Wilton, D., and Evans-Lamswood, D., 2023. Characterizing the supra- and subsolidus processes that generated the Current PGE-Cu-Ni deposit, Thunder Bay North Intrusive Complex, Canada: insights from trace elements and multiple S isotopes of sulfides. *Mineralium Deposita*, 58, 1559-1581. <<https://doi.org/10.1007/s00126-023-01193-9>>
- Burgess, H., Gowans, R.M., Hennessey, B.T., Lattanzi, C.R., and Puritch, E., 2014. Technical report on the feasibility study for the NICO gold-cobalt-bismuth-copper deposit, Northwest Territories, Canada. NI 43-101 Technical Report, Fortune Minerals Ltd., 385 p. <<https://www.sedarplus.ca/>>
- Burke, K., 2011. Plate tectonics, the Wilson cycle, and mantle plumes: Geodynamics from the top. *Annual Review of Earth and*

- Planetary Sciences, 39, 1-29.
<https://doi.org/10.1146/annurev-earth-040809-152521>>
- Bustard, A.L., Ferbey, T., and Arnold, H., 2019. Regional- to property-scale till geochemical and mineralogical surveys in British Columbia for base and precious metals. British Columbia Ministry of Energy, Mines and Petroleum Resources, British Columbia Geological Survey Open File 2019-04.
- Campbell, I.H., and Naldrett, A.J., 1979. The influence of silicate: sulfide ratios on the geochemistry of magnetic sulfides. *Economic Geology*, 74, 1503-1506.
- Campbell, I.H., Franklin, J.M., Gorton, M.P., Hart, T.R., and Scott, S.D., 1981. The role of subvolcanic sills in the generation of massive sulfide deposits. *Economic Geology*, 76, 2248-2253.
- Canil, D., Pisiak, L., Lacourse, T., Plouffe, A., Ferbey, T., and Grondahl, C., 2017. Magnetite as an indicator mineral in porphyry Cu±Au±Mo deposits of British Columbia, Canada. In: Ferbey, T., Plouffe, A., and Hickin, A.S., (Eds.), *Indicator Minerals in Till and Stream Sediments of the Canadian Cordillera*. Geological Association of Canada Special Paper volume 50, and Mineralogical Association of Canada Topics in Mineral Sciences volume 47, pp. 161-174.
- Castor, B., 2008. The Mountain Pass rare earth carbonatite and associated ultrapotassic rocks, California. *Canadian Mineralogist*, 46, 779-806.
- Cawthorn, R.G., Barnes, S.J., Ballhaus, C., and Malitch, K.N., 2005. Platinum-group element, chromium, and vanadium deposits in mafic and ultramafic rocks. *Economic Geology*, 100, 215-249.
- Černý P. and Ercit, T.S., 2005. The classification of granitic pegmatites revisited. *The Canadian Mineralogist*, 43, 2005-2026.
- Černý P., Goad, B.E., Hawthorne, F.C., and Chapman, R., 1986. Fractionation trends of the Nb- and Ta-bearing oxide minerals in the Greer Lake pegmatitic granite and its pegmatite aureole, southeastern Manitoba. *American Mineralogist*, 71, 501-517.
- Chakhmouradian, A.R., Reguir, E.P., Kressall, R.D., Crozier, J., Pisiak, L.K., Sidhu, R., and Yang, P., 2015. Carbonatite-hosted niobium deposit at Aley, northern British Columbia (Canada): Mineralogy, geochemistry and petrogenesis. *Ore Geology Reviews*, 64, 642-666.
- Chiaradia, M., and Caricchi, L., 2017. Stochastic modelling of deep magmatic controls on porphyry copper deposit endowment, *Scientific Reports*, 7, article 44523.
<https://doi.org/10.1038/srep44523>>
- Chudy, T.C., 2013. The petrogenesis of the Ta-bearing Fir carbonatite system, east-central British Columbia, Canada. Unpublished Ph.D. thesis, University of British Columbia, Canada, 316 p.
- Church, N.C., 1975. Geology of the Sustut area. British Columbia Ministry of Energy, Mines and Petroleum Resources, British Columbia Geological Survey Paper 1975-2, 5 p.
- Çimen, O., Kuebler, C., Simonetti, S.S., Corcoran, L., Mitchell, R.H., and Simonetti, A., 2019. Combined boron, radiogenic (Nd, Pb, Sr), stable (C, O) isotopic and geochemical investigations of carbonatites from the Blue River Region, British Columbia (Canada): Implications for mantle sources and recycling of crustal carbon. *Chemical Geology*, 529, 119240.
<https://doi.org/10.1016/j.chemgeo.2019.07.015>>
- Clarke, G., Northcote, B.K., Katay, F., and Tombe, S.P., 2020. Exploration and Mining in British Columbia, 2019: A summary. In: *Provincial Overview of Exploration and Mining in British Columbia, 2019*. British Columbia Ministry of Energy, Mines and Petroleum Resources, British Columbia Geological Survey, Information Circular 2020-01, pp.1-40.
- Clarke, G., Northcote, B.K., Katay, F., and Tombe, S.P., 2021. Exploration and Mining in British Columbia, 2020: A summary. In: *Provincial Overview of Exploration and Mining in British Columbia, 2020*, British Columbia Ministry of Energy, Mines and Low Carbon Innovation, British Columbia Geological Survey Information Circular 2021-01, pp. 1-45.
- Clarke, G., Northcote, B.K., Corcoran, N.L., and Hancock, K., 2022. Exploration and Mining in British Columbia, 2021: A summary. In: *Provincial Overview of Exploration and Mining in British Columbia, 2021*, British Columbia Ministry of Energy, Mines and Low Carbon Innovation, British Columbia Geological Survey Information Circular 2022-01, pp. 1-42.
- Clarke, G., Northcote, B.K., Corcoran, N.L., Heidarian, H., and Hancock, K., 2023. Exploration and Mining in British Columbia, 2022: A summary. In: *Provincial Overview of Exploration and Mining in British Columbia, 2022*, British Columbia Ministry of Energy, Mines and Low Carbon Innovation, British Columbia Geological Survey Information Circular 2023-01, pp. 1-48.
- Clarke, G., Northcote, B.K., Corcoran, N.L., Pothorin, C., Heidarian, H., and Hancock, K., 2024. Exploration and Mining in British Columbia, 2023: A summary. In: *Provincial Overview of Exploration and Mining in British Columbia, 2023*. British Columbia Ministry of Energy, Mines and Low Carbon Innovation, British Columbia Geological Survey Information Circular 2024-01, pp. 1-53.
- Colpron, M., 2020. Yukon terranes-A digital atlas of terranes for the northern Cordillera. Yukon Geological Survey.
<https://data.geology.gov.yk.ca/Compilation/2#InfoTab>>
- Colpron, M., and Nelson, J.L., 2021. Northern Cordillera: Canada and Alaska. In: Elias, S., and Alderton, D., (Eds.), *Encyclopedia of Geology*, Second Edition. Academic Press, pp. 93-106.
- Colpron, M., Logan, J., and Mortensen, J.K., 2002. U-Pb age constraint for late Neoproterozoic rifting and initiation of the lower Paleozoic passive margin of western Laurentia. *Canadian Journal of Earth Sciences*, 39, 133-143.
- Cooke, D.R., Baker, M., Hollings, P., Sweet, G., Chang, Z., Danyushevsky, L., Gilbert, S., Zhou, T., White, N.C., Gemmill, J.B., and Inglis, S., 2014. New advances in detecting the distal geochemical footprints of porphyry systems-epidote mineral chemistry as a tool for vectoring and fertility assessments: Society of Economic Geologists, Special Publication 18, pp. 127-152.
- Cooke, D.R., Agnew, P., Hollings, P., Baker, M., Chang, Z., Wilkinson, J.J., Ahmed, A., White, N.C., Zhang, L., Thompson, J., Gemmill, J.B., Danyushevsky, L., and Chen, H., 2020. Recent advances in the application of mineral chemistry to exploration for porphyry copper-gold-molybdenum deposits: detecting the geochemical fingerprints and footprints of hypogene mineralization and alteration. *Geochemistry: Exploration, Environment, Analysis*, 20, 176-188.
<https://doi.org/10.1144/geochem2019-039>>
- Corriveau, L., Montreuil, J.-F., Blein, O., Ehrig, K., Potter, E.G., Fabris, A., and Clark, J., 2022. Mineral systems with IOCG and affiliated deposits: part 2-geochemical footprints. In: Corriveau, L., Potter, E.G. and Mumin, A.H., (Eds.), *Mineral Systems With Iron Oxide Copper-Gold (IOCG) and Affiliated Deposits*. Geological Association of Canada Special Paper 52, pp. 159-204.
- Cousens, B., and Piercey, S.J., (Eds.), 2008. *Submarine Volcanism and Mineralization: Modern Through Ancient*, Geological Association of Canada Short Course Notes Volume 19, 178 p.
- CSA Global Mining Industry Consultants Canada Limited, 2021. Kutcho Copper Project British Columbia, Canada, Feasibility Study NI 43-101 Technical Report. Prepared for: Kutcho Copper Corp. Prepared by CSA Global Consultants Canada Limited. 468 p.
<https://www.sedarplus.ca/>>
- Cui, F.-H., Zhang, C., Jin, D.-T., Wang, L.-Y., Gao, J.-L., Ma, M., and Li, Y.-D., 2022. Mineral chemistry of the Lower Cretaceous Jinling iron skarn deposit, Western Shandong Province, North China Craton: Implications for the iron skarn mineralization process. *Minerals*, 12, 1152-1175.
- Cullen, R.D., 2010. NI 43-101 Technical Report Update on the Silvertip Property, Northern British Columbia, Canada for Silvercorp Metals Inc., a report prepared for Silvercorp Metals

- Inc., February 19, 2010, 100 p.
<<https://www.sedarplus.ca>>
- Currie, K.L. 1975. The geology and petrology of the Ice River Alkaline Complex, British Columbia. Geological Survey of Canada, Bulletin 245, 68 p.
- Currie, K.L., 1976. The alkaline rocks of Canada. Geological Survey of Canada, Bulletin 239, 228 p.
- Cutts, J.A., McNicoll, V.J., Zagorevski, A., Anderson, R.G., and Martin, K., 2015. U-Pb geochronology of the Hazelton Group in the McTagg anticlinorium, Iskut River area, northwest British Columbia. In: Geological Fieldwork 2014, British Columbia Ministry of Energy and Mines, British Columbia Geological Survey Paper 2015-1, pp. 87-101.
- Dawson, G.M. 1886. Geological and Natural History Survey of Canada, Annual Report 1, 122B-124B.
- del Real, I., Thompson, J.F.H., and Carriedo, J., 2018. Lithological and structural controls on the genesis of the Candelaria-Punta del Cobre iron oxide copper gold district, northern Chile. *Ore Geology Reviews*, 102, 106-153.
- del Real, I., Thompson, J.F.H., Simon, A.C., and Reich, M., 2020. Geochemical and isotopic signature of pyrite as a proxy for fluid source and evolution in the Candelaria-Punta del Cobre iron oxide copper-gold district, Chile. *Economic Geology*, 115, 1493-1517.
- Dixon, A., Cempirek, J., and Groat, L.A., 2014. Mineralogy and geochemistry of pegmatites on Mount Begbie, British Columbia. *The Canadian Mineralogist*, 52, 129-164.
- Doyle, M.G., and Allen, R.L., 2003. Subsea-floor replacement in volcanic-hosted massive sulfide deposits. *Ore Geology Reviews*, 23, 183-222.
- Duan, C., Li, Y., Mao, J., Zhu, Q., Xie, G., Wan, Q., Jian, W., and Hou, K., 2021. The role of evaporite layers in the ore-forming process of iron oxide-apatite and skarn Fe deposits: Examples from the middle-lower Yangze River metallogenic belt, East China. *Ore Geology Reviews*, 138, 104352.
- Dyer, T.L., Tietz, P.G., and Austin, J.B., 2014. Technical report on the West Desert zinc-copper indium-magnetite project, preliminary economic assessment, Juab County, Utah. NI 43-101 Technical Report, InZinc Mining Ltd., 188 p.
<<https://www.americanwestmetals.com/site/PDF/feef5f8c-6aca-42ce-8bf4-cc51e27611d5/TechnicalReport>>
- Ehrig, K.J., McPhie, J., and Kamenetsky, V.S., 2012. Geology and mineralogical zonation of the Olympic Dam iron oxide Cu-U-Au-Ag deposit, South Australia. In: Hedenquist, J. W., Harris, M., and Camus, F., (Eds.), *Geology and Genesis of Major Copper Deposits and Districts of the World: A Tribute to Richard H. Sillitoe*. Society of Economic Geologists Special Publication 16, pp. 237-267.
- Elia, E.A., Ferbey, T., Ward, B.C., Shives, R.B.K., Best, M., and Martin-Burtart, N., 2023. Remotely piloted aircraft system (RPAS) for investigating surface sediments in the Interior Plateau of British Columbia: Methods, data, and products. British Columbia Ministry of Energy, Mines and Low Carbon Innovation, British Columbia Geological Survey GeoFile 2023-07, 22 p.
- Elia, E.A., Ferbey, T., and Ward, B.C., 2024. Mapping surficial sediments in the Interior Plateau using remotely piloted aircraft system lidar. British Columbia Ministry of Energy, Mines and Low Carbon Innovation, British Columbia Geological Survey Open File, in press.
- Emsbo, P., 2009. Geologic criteria for the assessment of sedimentary exhalative (sedex) Zn-Pb-Ag deposits: U.S. Geological Survey Open-File Report 2009-1209, 21 p.
- Emsbo, P., Seal, R.R., Breit, G.N., Diehl, S.F., and Shah, A.K., 2016. Sedimentary exhalative (sedex) zinc-lead-silver deposit model: U.S. Geological Survey Scientific Investigations Report 2010-5070-N, 57 p.
<<http://dx.doi.org/10.3133/sir20105070N>>
- Ernst, R., and Bleeker, W., 2010. Large igneous provinces (LIPs), giant dyke swarms, and mantle plumes: significance for breakup events within Canada and adjacent regions from 2.5 Ga to the Present. *Canadian Journal of Earth Sciences*, 47, 695-739.
- Ernst, R.E., and Jowitt, S.M., 2013. Large igneous provinces (LIPs) and metallogeny. In: Colpron, M., Bissig, T., Rusk, B.G., and Thompson, J.F.H., (Eds.) *Tectonics, Metallogeny, and Discovery: The North American Cordillera and Similar Accretionary Settings*. Economic Geology Special Publication 17, pp. 17-51.
- Evans-Lamswood, D.M., Butt, D.P., Jackson, R.S., Lee, D.V., Muggridge, M.G., and Wheeler, R.I., 2000. Physical controls associated with the distribution of sulfides in the Voisey's Bay Ni-Cu-Co Deposit, Labrador. *Economic Geology*, 95, 749-769.
- Febbo, G.E., Kennedy, L.A., Nelson, J.L., Savell, M.J., Campbell, M.E., Creaser, R.A., Friedman, R.M., van Straaten, B.I., and Stein, H.J., 2019. The evolution and structural modification of the supergiant Mitchell Au-Cu porphyry, northwestern British Columbia. *Economic Geology*, 14, 303-324.
- Ferbey, T., 2014. Basal till potential of the Nadina River map area (NTS 093E/15), British Columbia. British Columbia Ministry of Energy, British Columbia Geological Survey Open File 2014-02, 1:50,000 scale.
- Ferbey, T., and Elia, E.A., 2021. Preliminary surficial geology of the northern Hogen batholith area, north-central British Columbia. In: *Geological Fieldwork 2020*, British Columbia Ministry of Energy, Mines and Low Carbon Innovation, British Columbia Geological Survey Paper 2021-01, pp. 57-64.
- Ferbey, T., Plouffe, A., and Bustard, A.L., 2016. Geochemical, mineralogical, and textural data from tills in the Highland Valley Copper mine area, south-central British Columbia. British Columbia Geological Survey GeoFile 2016-11, 15 p.
- Ferbey, T., Plouffe, A., and Hickin, A.S., 2018. Geochemistry and mineralogy of subsurface till samples recovered from diamond drill hole R17-01, Rateria property (porphyry Cu±Mo), south-central British Columbia, 15 p.
- Ferbey, T., Elia, E.A., Shives, R.B.K., Martin-Burtart, N., Best, M., and Ward, B.C., 2024. Quantifying potassium concentrations in Interior Plateau surface sediments using remotely piloted aircraft system gamma-ray spectrometry. British Columbia Ministry of Energy, Mines and Low Carbon Innovation, British Columbia Geological Survey Open File, in press.
- Ford, A., Peters, K.J., Partington, G.A., Blevin, P.L., Downes, P.M., Fitzherbert, J.A., and J.E. Greenfield, J.E., 2019. Translating expressions of intrusion-related mineral systems into mappable spatial proxies for mineral potential mapping: Case studies from the Southern New England Orogen, Australia. *Ore Geology Reviews*, 111, article 102943.
<<https://doi.org/10.1016/j.oregeorev.2019.102943>>
- Fortier, S.M., Nasser, N.T., Graham, G.E., Hammarstrom, J.M., Day, W.C., Mauk, J.L., and Seal, R.R., 2022. USGS critical mineral review. *Mining Engineering*, 74, pp. 34-48.
- Fyles, J.T., 1964. Geology of the Duncan Lake Area, Lardeau District, British Columbia. British Columbia Department of Mines and Petroleum Resources, British Columbia Geological Survey Bulletin 49, 100 p.
- Fyles, J.T., and Eastwood, G.E.P., 1962. Geology of the Ferguson Area, Lardeau district, British Columbia. British Columbia Department of Mines and Petroleum Resources, British Columbia Geological Survey Bulletin 45, 98 p.
- Franklin, J.M., Gibson, H.L., Jonasson, I.R., and Galley, A., 2005. Volcanogenic massive sulfide deposits. In: Hedenquist, J.W., Thompson, J.F.H., Goldfarb, R.J., and Richards, J.P., (Eds.), *Economic Geology, Economic Geology 100th Anniversary Volume*, pp. 523-560.
- Gadd, M.G., Peter, J.M., Hnatyshin, D., Creaser, R., Gouwy, S.A., and Fraser, T.A., 2020. A Middle Devonian basin-scale precious metal enrichment event across northern Yukon (Canada). *Geology*, 48, 242-246.

- Gadd, M.G., Lawley, C.J.M., Corriveau, L., Houlé, M., Pater, J.M., Plouffe, A., Potter, E., Sappin, A.-A., Pilote, J.-L., Marquis, G., and Label, D., 2022a. Public geoscience solutions for diversifying Canada's critical mineral production. In: Smelror, M., Hanghøj, K., and Schiellerup, H. (Eds). *The Green Stone Age: Exploration and Exploitation of Minerals for Green Technologies*. Special Publication of the Geological Society of London, 526, pp. 25-50. <<https://doi.org/10.1144/SP526-2021-190>>
- Gadd, M.G., Peter, J.M., and Layton-Matthews, D., 2022b. Genesis of hyper-enriched black shale Ni-Mo-Zn-Pt-Pd-Re mineralization in the northern Canadian Cordillera. In: Peter, J.M., and Gadd, M.G., (Eds.), *Targeted Geoscience Initiative 5: Volcanic- and Sediment-hosted Massive-sulfide Deposit Genesis and Exploration Methods*, Geological Survey of Canada Bulletin 617, pp. 15-38.
- Galicki, M., Marshall, D., Staples, R., Thorkelson, D., Downie, C., Gallagher, C., Enkin, R., and Davis, W., 2012, Iron oxide+Cu+Au deposits in the Iron Range, Purcell Basin, southeastern BC. *Economic Geology*, 107, 1293-1301.
- Galley, A.G., Hannington, M.D., and Jonasson, I.R., 2007. Volcanogenic massive sulphide deposits. In: Goodfellow, W.D., (Ed.), *Mineral Deposits of Canada: A Synthesis of Major Deposit-Types, District Metallogeny, the Evolution of Geological Provinces, and Exploration Methods*: Geological Association of Canada, Mineral Deposits Division, Special Publication 5, pp. 141-161.
- Godwin, C.J., and Sinclair, A.J., 1982. Average lead isotope growth curves for shale-hosted zinc-lead deposits, Canadian Cordillera. *Economic Geology*, 77, 675-690.
- Golmohammadi, A., Karimpour, M.H., Malekzadeh Shafaroudi, A., and Mazaheri, S.A., 2015. Alteration-mineralization, and radiometric ages of the source pluton at the Sangan iron skarn deposit, northeastern Iran. *Ore Geology Reviews*, 65, 545-563.
- Gittins, J., and Mitchell, R.H., 2023. The genesis of calcite and dolomite carbonatite-forming magma by liquid immiscibility: a critical appraisal. *Geological Magazine*. <<https://doi.org/10.1017/S001675682300050X>>
- Goodenough, K.M., Shaw, R.A., Smith, M., Estrade, G., Marqu, E., Bernard, C., and Nex, P., 2019. Economic mineralization in pegmatites: comparing and contrasting NYF and LCT examples. *The Canadian Mineralogist*, 57, 753-755.
- Goodfellow, W.D., 2007. Base metal metallogeny of the Selwyn Basin, Canada. In: Goodfellow, W.D., (Ed.), *Mineral Deposits of Canada: A Synthesis of Major Deposit-Types, District Metallogeny, the Evolution of Geological Provinces, and Exploration Methods*. Geological Association of Canada, Mineral Deposits Division, Special Publication 5, pp. 553-579.
- Goodfellow, W., and Lydon, J.W., 2007. Sedimentary exhalative (SEDEX) deposits. In: Goodfellow, W.D., (Ed.), *Mineral Deposits of Canada: A Synthesis of Major Deposit-Types, District Metallogeny, the Evolution of Geological Provinces, and Exploration Methods*. Geological Association of Canada, Mineral Deposits Division, Special Publication, pp. 163-184.
- Graedel, T., Barr, R., Chandler, C., Chase, T., Choi, J., Christoffersen, L., Freilander, E., Henly, C., Jun, C., Nassar, N.T., Schechner, D., Warren, S., Yang, M., and Zhu, C., 2012. Methodology of metal determination. *Environmental Science and Technology*, 46, 1063-1070.
- Green, C., Simandl, G.J., Paradis, S., Katay, F., Hoshino, M., Kon, Y., Kodama, S., and Graf, C., 2017. Geological setting of the Rock Canyon Creek REE-fluorite deposit, British Columbia, Canada. In: *Geological Fieldwork 2016*, British Columbia Ministry of Energy and Mines, British Columbia Geological Survey Paper 2017-01, pp. 195-203.
- Groves, D.L., Bierlein, F.P., Meinert, L.D., and Hitzman, M.W., 2010. Iron oxide copper-gold (IOCG) deposits through Earth history: Implications for origin, lithospheric setting, and distinction from other epigenetic iron oxide deposits. *Economic Geology*, 105, 641-654.
- Groves, D.L., Santosh, M., Müller, D., Zhang, L., Deng, J., Yang, L., and Wang, Q., 2022. Mineral systems: Their advantages in terms of developing holistic genetic models and for target generation in global mineral exploration. *Geosystems and Geoenvironment*, 1, article 100001. <<https://doi.org/10.1016/j.geogeo.2021.09.001>>
- Grunsky, E.C., 1997. Mineral resource estimation: the Mineral Potential Project: an evaluation of estimator responses for selected mineral deposit types for the province. In: *Geological Fieldwork 1996*, British Columbia Ministry of Employment and Investment, British Columbia Geological Survey, Paper 1997-01, pp. 267-282.
- Gunn, G., (Ed.), 2014. *Critical metals handbook*. John Wiley & Sons, Ltd., Oxford UK, 464 p.
- Hannington, M.D., Santaguida, F., Kjarsgaard, I.M., and Cathles, L.M., 2003. Regional-scale hydrothermal alteration in the Central Blake River Group, western Abitibi subprovince, Canada: Implications for VMS prospectivity. *Mineralium Deposita*, 38, 393-422.
- Hannington, M.D., Jamieson, J.W., Monecke, T., Petersen, S., and Beaulieu, S. 2011. The abundance of seafloor massive sulfide deposits. *Geology*, 39, 1155-1158.
- Hall, R.D., and May, B., 2013. Geology of the New Afton porphyry copper-gold deposit, Kamloops, British Columbia, Canada. In: Logan, J.M., and Schroeter, T.G., (Eds), *Porphyry Systems of Central and Southern BC: Prince George to Princeton*. Society of Economic Geologists Field Trip Guidebook 43, pp. 117-128.
- Hancock, K.D., 1990. Geology of Nickel Mountain and the E&L nickel-copper prospect (104B/10E). In: *Geological Fieldwork 1989*, British Columbia Ministry of Energy, Mines, and Petroleum Resources, British Columbia Geological Survey Paper 1990-01, pp. 337-341.
- Hayes, S.M., and McCullough, E.A., 2018. Critical minerals: A review of elemental trends in comprehensive criticality studies. *Resource Policy*, 59, pp. 192-199.
- Hayward, N., and Paradis, S., 2021. Geophysical reassessment of the role of ancient lineaments on the development of the western margin of Laurentia and its sediment-hosted Zn-Pb deposits, Yukon and Northwest Territories, Canada. *Canadian Journal of Earth Sciences*, 58.
- Hickin, A.S., Ward, B.C., Plouffe, A., and Nelson, J., 2017. Introduction to the geology, physiography, and glacial history of the Canadian Cordillera in British Columbia and Yukon. In: Ferbey, T., Plouffe, A., and Hickin, A.S., (Eds.), *Indicator Minerals in Till and Stream Sediments of the Canadian Cordillera*. Geological Association of Canada Special Paper Volume 50, and Mineralogical Association of Canada Topics in Mineral Sciences Volume 47, pp. 1-25.
- Hickin, A.S., Orovan, E.A., Brzozowski, M.J., McLaren, K., Shaw, K.L., and Van der Vlugt, J., 2023. *Critical minerals in British Columbia: An atlas of occurrences and producing mines, 2023*. British Columbia Ministry of Energy, Mines and Low Carbon Innovation, British Columbia Geological Survey Open File 2023-02, 102 p.
- Hildebrand, R.S., 1986. Kiruna-type deposits: their relationship to intermediate subvolcanic plutons in the Great Bear Magmatic zone, northwest Canada. *Economic Geology*, 81, 640-659.
- Hitzman, M.W., Oreskes, N., and Einaudi, M.T., 1992. Geological characteristics and tectonic setting of Proterozoic iron oxide (Cu-U-Au-REE) deposits. *Precambrian Research*, 58, 241-287.
- Hoggard, M.J., K. Czarnota, F.D. Richards, D.L. Huston, A.L. Jaques, and Ghelichkhan, S., 2020. Global distribution of sediment-hosted metals controlled by craton edge stability. *Nature Geoscience*, 13, 504-510. <<https://doi.org/10.1038/s41561-020-0593-2>>
- Hoshino, M., Kon, Y., Kodama, S., Simandl, G.J., Paradis, S., Green, C., Namatame, C., Matsunaga, I., and Takagi, T., 2017. Mineralogy of the Rock Canyon Creek REE-Fluorite Deposit,

- British Columbia, Canada. In: Geological Fieldwork 2016, British Columbia Ministry of Energy and Mines, British Columbia Geological Survey Paper 2017-1, pp. 205-213.
- Höy, T., 1997. Harper Creek: A volcanogenic sulphide deposit within the Eagle Bay Assemblage, Kootenay Terrane, Southern British Columbia. In Geological Fieldwork 1996, British Columbia Ministry of Employment and Investment, British Columbia Geological Survey Paper 1997-01, pp. 199-210.
- Höy, T., 1983. Geology in the Vicinity of the Sullivan Deposit, Kimberley, British Columbia. In: Geological Fieldwork 1982, British Columbia Ministry of Energy, Mines and Petroleum Resources, British Columbia Geological Survey Paper 1983-01, pp. 9-17.
- Höy, T., 1988. Geology of the Cottonbelt lead-zinc-magnetite layer, carbonatites and alkaline rocks in the Mount Grace area, Frenchman Cap dome, southeastern British Columbia. British Columbia Ministry of Energy, Mines and Petroleum Resources, British Columbia Geological Survey, Bulletin 80, 99 p.
- Höy, T., 2001. Sedex and Broken Hill-type deposits, Northern Monashee Mountains, southern B.C. In: Geological Fieldwork 2000, British Columbia Ministry of Energy and Mines, British Columbia Geological Survey Paper 2001-01, pp. 85-114.
- Höy, T., 2002. BHT and SEDEX Deposits of the Kootenay terrane. British Columbia Ministry of Energy and Mines, British Columbia Geological Survey Geofile 2002-4.
- Hronsky, J.M.A., and Groves, D.I., 2008. The science of targeting: definition, strategies, targeting and performance measurement. *Australian Journal of Earth Science*, 55, 3-12. <<https://doi.org/10.1080/08120090701581356>>
- Hunter, R.C., and van Straaten, B.I., 2020. Preliminary stratigraphy and geochronology of the Hazelton Group, Kitsault River area, Stikine terrane, northwest British Columbia. In: Geological Fieldwork 2019, British Columbia Ministry of Energy, Mines and Petroleum Resources, British Columbia Geological Survey Paper 2020-01, pp. 101-118.
- Hunter, R.C., Sebert, C.F.B., Friedman, R., and Wall, C., 2022. Revised stratigraphy and geochronology of the Hazelton Group, host rocks for volcanogenic mineralization in the Kitsault River area, northwest British Columbia. In: Geological Fieldwork 2021, British Columbia Ministry of Energy, Mines and Low Carbon Innovation, British Columbia Geological Survey Paper 2022-01, pp. 63-81.
- Huston, D.L., Champion, D.C., Czarnota, K., Duan, J., Hutchens, M., Paradis, S., Hoggard, M., Ware, B., Gibson, G.M., Doublier, M.P., Kelley, K., McCafferty, A., Hayward, N., Richards, F., Tessalina, S., and Carr, G., 2023. Zinc on the edge-isotopic and geophysical evidence that cratonic edges control world-class shale-hosted zinc-lead deposits. *Mineralium Deposita* 58, 707-729. <<https://doi.org/10.1007/s00126-022-01153-9>>
- Imperial Metals Corporation, 2023. Exploration, Ruddock Creek Project. <<https://imperialmetals.com/projects/ruddock-creek/reserve-and-resource/> (accessed September 28, 2023).
- Jackson-Brown, S., Scoates, J.S., Nixon, G.T., and Ames, D.E., 2014. Mineralogy of sulphide, arsenide, and platinum group minerals from the DJ/DB Zone of the Turnagain Alaskan-type ultramafic intrusion, north-central British Columbia. In: Geological Fieldwork 2013, British Columbia Ministry of Energy and Mines, British Columbia Geological Survey Paper 2014-01, pp. 157-168.
- JDS Energy & Mining Inc., 2018. NI 43-101 Technical Report, Akie project, British Columbia, Canada. Prepared for ZincX Resources Corporation, 304 p. <<https://www.sedarplus.ca/>>
- John, D.A., and Taylor, R.D., 2016. By-products of porphyry copper and molybdenum deposits. In: Verplanck, P.L., and Hitzman, M.W., (Eds.), *Rare Earth and Critical Elements in Ore Deposits*. *Reviews in Economic Geology* 18, pp. 137-164.
- Johnson, J.P., and Cross, K.C., 1995. U-Pb geochronological constraints on the genesis of the Olympic Dam Cu-U-Au-Ag deposit, South Australia. *Economic Geology*, 90, 1046-1063.
- Johnson, C.A., Day, W.C., and Rye, R.O., 2016. Oxygen, hydrogen, sulfur, and carbon isotopes in the Pea Ridge magnetite-apatite deposit, Southeast Missouri, and sulfur isotope comparisons to other iron deposits in the region. *Economic Geology*, 111, 2017-2032.
- Jiang, W., Yan, Q., Deng, L., Zhou, B., Xiang, Z., and Xia, W., 2019. Early Jurassic mafic intrusions in the Southern Youjiang Basin, SW China: Petrogenesis, tectonic and metallogenic implications. *Minerals* 9, 771. <<https://doi.org/10.3390/min9120771>>
- Jones, G., Ootes, L., Luo, Y., A. Vezinet, A., Stern, R., Milidragovic, D., and Pearson, D.G., 2023. The relative roles of ancient and juvenile crust in building accretionary orogens-Minimal ancient crust involved in the magmatic evolution of a North American Cordillera accreted terrane indicated by igneous zircon Hf-O. *Lithos*, 452-453, article 107213. <<https://doi.org/10.1016/j.lithos.2023.107213>>
- Jowitt, S.M., Mudd, G.M., Werner, T.T., Weng, Z., Barkoff, D.W., and McCaffrey, D., 2018. The critical metals: An overview and opportunities concept and concerns for the future. In: Arribas, A.M., and Mauk, J.L., (Eds.), *Metals, Minerals, and Society*. *Society of Economic Geologists Special Publication* 21, pp. 25-38.
- Jugo, P.J., 2009. Sulfur content at sulfide saturation in oxidized magmas. *Geology*, 37, 415-418.
- Kilby, W.E., 1995. Mineral Potential Project - overview. In: Geological Fieldwork 1994, Ministry of Energy, Mines and Petroleum Resources, British Columbia Geological Survey Paper 1995-01, pp. 411-416.
- Kilby, W.E., 2004. The British Columbia Mineral Potential Project 1992-1997 - methodology and results. Ministry of Energy and Mines, British Columbia Geological Survey, GeoFile 2004-2, 324 p.
- Knox-Robinson, C.M., and Wyborn, L.A.I., 1997. Towards a holistic exploration strategy: using geographic information systems as a tool to enhance exploration. *Australian Journal of Earth Sciences*, 44, 453-463.
- Kontak, D.J., Paradis, S., Waller, Z., and Fayek, M., 2022. Petrographic, fluid inclusion and ion mass spectrometry stable isotopic (O, S) study of Mississippi Valley-type mineralization in British Columbia and Alberta. In: Peter, J.M., and Gadd, M.G., (Eds.), *Targeted Geoscience Initiative 5: Volcanic- and sediment-hosted massive sulfide deposit genesis and exploration methods*, Geological Survey of Canada, Bulletin 617, pp. 203-245. <<https://doi.org/10.4095/327994>>
- Kulla, G., and Hardy, J., 2015. Commerce Resources Corp. Blue River tantalum-niobium project, British Columbia, Canada, project update report. NI 43-101 Technical Report, 138 p. <<https://www.sedarplus.ca/csaparty/records/document.html?id=77f946b8c242fc385f6d2b9dceeb25648a80c7bb0fb1f6b09dc8d9105a8f213>>
- Kynicky, J., Smith, M. P., and Xu, C., 2012. Diversity of rare earth deposits: The key example of China, *Elements*, 8, 361-367.
- Lafrance, B., Gibson, H.L., and Stewart, M.S., 2020. Chapter 4: Internal and external deformation and modification of volcanogenic massive sulfide deposits. In: Rowland, J.V., and Rhys, D.A., (Eds.), *Applied Structural Geology of Ore-Forming Hydrothermal Systems*. *Reviews in Economic Geology*, 21. <<https://doi.org/10.5382/rev.21>>
- Lawley, C.J.M., Tschirhart, V., Smith, J.W., Pehrsson, S.J., Schetselaar, E.M., Schaeffer, A.J., Houli, M.G., and Eglington, B.M., 2021. Prospectivity modelling of Canadian magmatic Ni (\pm Cu \pm Co \pm PGE) sulphide mineral systems. *Ore Geology Reviews*, 132, 103985. <<https://doi.org/10.1016/j.oregeorev.2021.103985>>

- Leach, D.L., Taylor, R.D., Fey, D.L., Diehl, S.F., and Saltus, R.W., 2010. A deposit model for Mississippi Valley-type lead-zinc ores, chapter A of Mineral deposit models for resource assessment. U.S. Geological Survey Scientific Investigations Report 2010-5070-A, 52 p.
- Leach, D.L., Sangster, D.F., Kelley, K.D., Large, R.R., Garven, G., Allen, C.R., Gutzmer, J., and Walters, S., 2005. Sediment-hosted lead-zinc deposits: a global perspective. In: Hedenquist, J.W., Thompson, J.F.H., Goldfarb, R.J., and Richards, J.P., (Eds.), *Economic Geology*, 100th Anniversary volume, pp. 561-607.
- Lee, C.T.A., and Tang, M., 2020. How to make porphyry copper deposits. *Earth and Planetary Science Letters*, 529, article 115868. <<https://doi.org/10.1016/j.epsl.2019.115868>>
- Lee, R.G., Plouffe, A., Ferbey, T., Hart, C.J.R., Hollings, P., and Gleeson, S.A., 2021. Recognizing porphyry copper potential from till zircon composition: A case study from the Highland Valley porphyry district, south-central British Columbia. *Economic Geology*, 116, 1035-1045.
- Lefebvre, D.V., and Jones, L.D., (compilers) 2022. British Columbia Geological Survey mineral deposit profiles, 1995 to 2012; updated with new profiles for VMS, porphyry, and mafic-ultramafic deposits. British Columbia Ministry of Energy, Mines and Low Carbon Innovation, British Columbia Geological Survey GeoFile 2020-11, 652 p.
- Legun, A.S., 2001. Geology of the area between the Sustut copper deposit and the Day porphyry copper prospect. In: Geological Fieldwork. British Columbia Ministry of Energy and Mines, British Columbia Geological Survey Paper 2001-01, 8 p.
- Le Maitre, R.W., compiler, 2002. *Igneous Rocks: a Classification and Glossary of Terms*, 2nd Edition. Cambridge University Press, Cambridge, United Kingdom, 236 p.
- Lentz, D.R., 1998. Petrogenetic evolution of felsic volcanic sequences associated with Phanerozoic volcanic-hosted massive sulfide systems: The role of extensional geodynamics. *Ore Geology Reviews*, 12, 289-327.
- Leybourne, M.I., Peter, J.M., Schmidt, M., Layton-Matthews, D., Voinot, A., and Mathieu, L., 2022. Sulfide trace element and bulk geochemical evidence for a magmatic contribution to the metal budget of the Windy Craggy Cu-Co-(±Zn) volcanogenic massive sulfide deposit, northwestern British Columbia, Canada. In: Peter, J.M., and Gadd, M.G., (Eds.), *Targeted Geoscience Initiative 5: Volcanic- and Sediment-Hosted Massive Sulfide Deposit Genesis and Exploration Methods*. Geological Survey of Canada Bulletin 617, pp. 287-312.
- Li, Z.-X., Bogdanova, S.V., Collins, A.S., Davidson, A., De Waele, B., Ernst, R.E., Fitzsimons, I.C.W., Fuck, R.A., Gladkochub, D.P., Jacobs, J., Karlstrom, K.E., Lu, S., Natapov, L.M., Pease, V., Pisarevsky, S.A., Thrane, K., and Vernikovskiy, V., 2008. Assembly, configuration, and break-up history of Rodinia: A synthesis. *Precambrian Research*, 160, 179-210.
- Lian, O.B., and Hickin, A.S., 2017. Origin and character of till and other diamictites and their applicability to mineral prospecting. In: Ferbey, T., Plouffe, A., and Hickin, A.S., (Eds.), *Indicator Minerals in Till and Stream Sediments of the Canadian Cordillera*. Geological Association of Canada Special Paper Volume 50, and Mineralogical Association of Canada Topics in Mineral Sciences Volume 47, pp. 109-127.
- Lightfoot, P.C., Keays, R.R., Evans-Lamswood, D., and Wheeler, R., 2012. S saturation history of Nain Plutonic Suite mafic intrusions: origin of the Voisey's Bay Ni-Cu-Co sulfide deposit, Labrador, Canada. *Mineralium Deposita*, 47, 23-50.
- Logan, J.M., and Mihalynuk, M.G., 2005. Regional geology and setting of the Cariboo, Bell, Springer and Northeast Porphyry Cu-Au zones at Mount Polley, south-central, British Columbia. In: Geological Fieldwork 2004, British Columbia Ministry of Energy, Mines and Petroleum Resources, British Columbia Geological Survey Paper 2005-01, pp. 249-270.
- Logan, J.M., and Mihalynuk, M.G., 2013. Bonaparte gold: another 195 Ma porphyry Au-Cu deposit in southern British Columbia? In: Geological Fieldwork 2012, British Columbia Ministry of Energy, Mines and Natural Gas, British Columbia Geological Survey Paper 2013-1, pp. 71-80.
- Logan, J.M., and Mihalynuk, M.G., 2014. Tectonic controls on Early Mesozoic paired alkaline porphyry deposit belts (Cu-Au+/-Ag-Pt-Pd-Mo) within the Canadian Cordillera. *Economic Geology*, 109, 827-858.
- Logan, J.M., and Schiarizza, P., 2014. The Rayfield River pluton, south-central British Columbia (NTS 92P/6): Geologic setting and copper mineralization. In: Geological Fieldwork 2013, British Columbia Ministry of Energy and Mines, British Columbia Geological Survey Paper 2014-01, pp. 15-28.
- Logan, J.M., Schiarizza, P., and Devine, F., 2020. Geology, structural setting, and porphyry deposits of the Hagem batholith, northeast British Columbia. In: Sharman, E.R., Lang, J.R., and Chapman, J.B., (Eds.), *Porphyry Deposits of the Northwestern Cordillera of North America: A 25-Year Update*. Canadian Institute of Mining and Metallurgy Special Volume 57, pp. 212-227.
- Lund, K., 2008. Geometry of the Neoproterozoic and Paleozoic rift margin of western Laurentia: Implications for mineral deposit settings. *Geosphere*, 4, 429-444. <<https://doi.org/10.1130/GES00121.1>>
- Lydon, J.W., 1984. Ore Deposit Models - 8. Volcanogenic massive sulphide deposits Part 2: Genetic models. *Geoscience Canada*, 11, 195-202.
- Lydon, J.W., 1988. Ore Deposit Models #14. Volcanogenic Massive Sulphide deposits Part 1: A descriptive model. *Geoscience Canada*, 15, 43-65.
- Lydon, J.W., 2007. Geology and metallogeny of the Belt-Purcell Basin. In: Goodfellow, W.D., (Ed.), *Mineral Deposits of Canada: A Synthesis of Major Deposit-Types, District Metallogeny, the Evolution of Geological Provinces, and Exploration Methods*. Geological Association of Canada, Mineral Deposits Division, Special Publication 5, pp. 581-607.
- Lydon, J.W., Höy, T., Slack, J.F., and Knapp, M.E., (Eds.), 2000. The geological environment of the Sullivan deposit, British Columbia. Geological Association of Canada, Mineral Deposits Division Special Publication 1, 834 p.
- MacIntyre, D.G., 1992. Geological setting and genesis of sedimentary exhalative barite and barite-sulfide deposits, Gataga district, northeastern British Columbia. *Exploration and Mining Geology*, volume I, pp. 1-20.
- MacIntyre, D.G., and Kilby, W.E., 2009. Atlin-Taku mineral resource assessment, northwestern British Columbia (Parts of NTS 104F, J, K, L, M, N): Methodology and results. In: Geological Fieldwork 2008, British Columbia Ministry of Energy Mines and Petroleum Resources, British Columbia Geological Survey Paper 2009-01, pp. 45-53.
- Mackay, D.A.R., and Simandl, G.J., 2015. Pyrochlore and columbite-tantalite as indicator minerals for specialty metal deposits. *Geochemistry: Exploration, Environment, Analysis*, 15, 167-178.
- Magnall, J.M., Gleeson, S.A., Creaser, R.A., Paradis, S., Glodny, J., and Kyle, J.R., 2020. The mineralogical evolution of the clastic dominant-type Zn-Pb ± Ba deposits at Macmillan Pass (Yukon, Canada)-tracing seafloor barite replacement in the layered mineralization. *Economic Geology* 115, 961-979. <<https://doi.org/10.5382/econgeo.4730>>
- Magoon, L.B., and Dow, W.G., 1994. The petroleum system. In: Magoon, L.B., and Dow, W.G., (Eds.), *The Petroleum System: From Source to Trap*. American Association of Petroleum Geologists Memoir, 60, pp. 2-24.
- Maier, W.D., Barnes, S.J., Godel, B.M., Grobler, D., and Smith, W.D., 2023. Petrogenesis of thick, high-grade PGE mineralisation in the Flatreef, northern Bushveld Complex. *Mineralium Deposita*, 58, 881-902.

- Mao, M., Rukhlov, A.S., Rowins, S.M., Hickin, A.S., Ferbey, T., Bustard, A., Spence, J., and Coogan, L.A., 2017. A novel approach using detrital apatite and till geochemistry to identify covered mineralization in the TREK area of the Nechako Plateau, British Columbia. In: Ferbey, T., Plouffe, A., and Hickin, A.S., (Eds.), Indicator Minerals in Till and Stream Sediments of the Canadian Cordillera. Geological Association of Canada Special Paper Volume 50, and Mineralogical Association of Canada Topics in Mineral Sciences Volume 47, pp. 191-243.
- Mao, Y., Qin, K., Li, C., Xue., and Ripley, E., 2014. Petrogenesis and ore genesis of the Permian Huangshanxi sulfide ore-bearing mafic-ultramafic intrusion in the Central Asian Orogenic Belt, western China. *Lithos*, 200-201, 111-125.
- Manor, M.J., Scoates, J.S., Nixon, G.T., and Ames, D.E., 2016. The Giant Mascot Ni-Cu-PGE Deposit, British Columbia: Mineralized conduits in a convergent margin tectonic setting. *Economic Geology*, 111, 57-87.
- Manor, M.J., Scoates, J.S., Nixon, G.T., and Ames, D.E., 2014. Platinum-group mineralogy of the Giant Mascot Ni-Cu-PGE deposit, Hope, B.C. In: Geological Fieldwork 2013, British Columbia Ministry of Energy and Mines, British Columbia Geological Survey Paper 2014-01, pp. 141-156.
- Mariano, A.N., 1989. Nature of economic mineralization in carbonatites and related rocks. In: Bell, K., (Ed.), Carbonatites: Genesis and Evolution. Unwin Hyman, London, United Kingdom, pp. 149-176.
- Martin, R.F., 2012. The petrogenesis of anorogenic felsic magmas and AMCG suites: insights on element mobility and mutual cryptic contamination from polythermal experiments. *Lithos*, 151, 35-45.
- Martinsson, O., Billström, K., Broman, C., Weihed, P., and Wanhainen, C., 2016. Metallogeny of the northern Norrbotten ore province, northern Fennoscandian shield with emphasis on IOCG and apatite-iron ore deposits. *Ore Geology Reviews*, 78, 447-492.
- Mavrogenes, J.A., and O'Neill, H.S.C., 1999. The relative effects of pressure, temperature and oxygen fugacity on the solubility of sulfide in mafic magmas. *Geochimica et Cosmochimica Acta*, 63, 1173-1180.
- McCuaig, T.C., Beresford, S., and Hronsky, J., 2010. Translating the mineral systems approach into an effective exploration targeting system. *Ore Geology Reviews*, 38, 128-138.
- McMechan, M.E., 2012. Deep transverse basement structural control of mineral systems in the southeastern Canadian Cordillera. *Canadian Journal of Earth Sciences*, 49, 693-708.
- Meinert, L.D., Dipple, G.M., and Nicolescu, S., 2005. World skarn deposits. In: Hedenquist, J.W., Thompson, J.F.H., Goldfarb, R.J., and Richards, J.P., (Eds.), Economic Geology 100th Anniversary Volume. Society of Economic Geologists Special Publication, pp. 299-336.
- Melfou, M., Richard, A., Tarantola, A., Villeneuve, J., Carr, P., Peiffert, C., Mercadier, J., Dean, B., and Drejning-Carroll, D., 2023. Tracking the origin of metasomatic and ore-forming fluids in IOCG deposits through apatite geochemistry (Nautanen North deposit, Norrbotten, Sweden). *Lithos*, 438-439, article 106995. <<https://doi.org/10.1016/j.lithos.2022.106995>>
- Mercier-Langevin, P., Hannington, M.D., Dubé, B., and Bécu, V., 2011. The gold content of volcanogenic massive sulfide deposits. *Mineralium Deposita*, 46, 509-539.
- Mihalynuk, M.G., and Diakow, L.J., 2020. Southern Nicola arc geology. British Columbia Ministry of Energy, Mines and Low Carbon Innovation, British Columbia Geological Survey Geoscience Map 2020-01, 1:50,000 scale.
- Mihalynuk, M.G., and Heaman, L.M., 2002. Age of mineralized porphyry at the Logtung deposit W-Mo-Bi-Be (beryl, aquamarine), northwest BC. British Columbia Geological Survey, Geological Fieldwork 2001, Paper 2002-01, pp. 35-40.
- Mihalynuk, M.G., and Logan, J.M., 2013a. Geological setting of Late Triassic porphyry Cu-Au mineralization at Miner Mountain, Princeton, southern British Columbia. In: Geological Fieldwork 2012, British Columbia Ministry of Energy, Mines and Natural Gas, British Columbia Geological Survey Paper 2013-01, pp. 81-96.
- Mihalynuk, M.G., and Logan, J.M., 2013b. Geological setting of Late Triassic porphyry Cu-Au mineralization at the Dillard Creek property near Merritt, southern British Columbia. In: Geological Fieldwork 2012, British Columbia Ministry of Energy, Mines and Natural Gas, British Columbia Geological Survey Paper 2013-01, pp. 97-113.
- Mihalynuk, M.G., Zagorevski, A., Joyce, N.L. and Creaser, R.A., 2016. Age of magmatism and mineralization at the Star (Sheslay, Copper Creek) copper porphyry prospect: Inception of the Late Triassic mineralized arc. In: Geological Fieldwork 2015, British Columbia Ministry of Energy and Mines, British Columbia Geological Survey Paper 2016-01, pp. 65-75.
- Mihalynuk, M.G., Zagorevski, A., Logan, J.M., Friedman, R.M., and Johnston, S.T., 2019. Age constraints for rocks hosting massive sulphide mineralization at Rock and Roll and Granduc deposits between Iskut and Stewart, British Columbia. In: Geological Fieldwork 2018, British Columbia Ministry of Energy, Mines and Petroleum Resources, British Columbia Geological Survey Paper 2019-01, pp. 97-111.
- Mihalynuk, M.G., Zagorevski, A., Campbell, R., Hajiegeh, A., and Vaillancourt, A., 2024. Preliminary results from revision mapping of the Gladys Lake area, near Atlin, northwest British Columbia. In: Geological Fieldwork 2023, Ministry of Energy, Mines and Low Carbon Innovation, British Columbia Geological Survey Paper 2024-01, this volume.
- Milidragovic D., Zagorevski, A., and Chapman, J.B., 2017. The Mount Hickman ultramafic complex: An Fe-rich Alaskan-type ultramafic intrusion. In: Geological Fieldwork 2016, British Columbia Ministry of Energy and Mines, British Columbia Geological Survey Paper 2017-01, pp. 117-132.
- Milidragovic, D., Nixon, G.T., Scoates, J.S., Nott, J.A., and Spence, D.W., 2021. Redox-controlled chalcophile element geochemistry of the Polaris Alaskan-type mafic-ultramafic complex, British Columbia, Canada. *The Canadian Mineralogist*, 59, 1627-1660.
- Milidragovic, D., Nott, J.A., Spence, D.W., Schumann, D., Scoates, J.S., Nixon, G.T., and Stern, R.A., 2023. Sulfate recycling at subduction zones indicated by sulfur isotope systematics of Mesozoic ultramafic island arc cumulates in the North American Cordillera. *Earth and Planetary Science Letters*, 620, article 118337. <<https://doi.org/10.1016/j.epsl.2023.118337>>
- Miller, E.A., van Straaten, B.I., and Hunter, R.C., 2023. Update on bedrock mapping in the Kitsault River area, northwestern British Columbia. In: Geological Fieldwork 2022, British Columbia Ministry of Energy, Mines and Low Carbon Innovation, British Columbia Geological Survey Paper 2023-01, pp. 23-32.
- Millonig, L.J., and Groat, L.A., 2013. Carbonatites in western North America-occurrences and metallogeny. In: Colpron, M., Bissig, T., Rusk, B.G., and Thompson, F.H., (Eds.), Tectonics, Metallogeny, and Discovery: The North American Cordillera and Similar Accretionary Settings. Society of Economic Geologists, Special Publication 17, pp. 245-264.
- Millonig, L.J., Gerdes, A., and Groat, L.A., 2012. U-Th-Pb geochronology of meta-carbonatites and meta-alkaline rocks in the southern Canadian Cordillera: a geodynamic perspective. *Lithos*, 152, 202-217.
- Millonig, L.J., Gerdes, A., and Groat, L.A., 2013. The effect of amphibolite facies metamorphism on the U-Th-Pb geochronology of accessory minerals from meta-carbonatites and associated meta-alkaline rocks. *Chemical Geology*, 353, 199-209.
- Mikaeili, K., Baghban, S., Hosseinzadeh, M.R., Lentz, D.R., and Moayyed, M., 2023. Genesis of the Brazin iron skarn deposit, NW Iran: Analysis of formation conditions of calc-silicates and

- the evolution of fluids responsible for the massive magnetite precipitation. *Journal of Geochemical Exploration*, 246, article 107162.
<<https://doi.org/10.1016/j.gexplo.2023.107162>>
- Mitchell, R.H., 2005. Carbonatites and carbonatites and carbonatites. *Canadian Mineralogist*, 43, 2049-2068.
- Mitchell, R.H., 2015. Primary and secondary niobium mineral deposits associated with carbonatites. *Ore Geology Reviews*, 64, 626-641.
- Mitchell, R.H., and Gittins, J., 2022. Carbonatites and carbothermalites: A revised classification. *Lithos*, 430-431, article 106861.
<<https://doi.org/10.1016/j.lithos.2022.106861>>
- Mitchell, R., Chudy, T., McFarlane, C.R.M., and Wu, F.-Y., 2017. Trace element and isotopic composition of apatite in carbonatites from the Blue River area (British Columbia, Canada) and mineralogy of associated silicate rocks. *Lithos*, 286-287, 75-91.
- Mondal, S.K., and Mathez, E.A., 2007. Origin of the UG2 chromitite layer, Bushveld Complex. *Journal of Petrology*, 48, 495-510.
- Monteiro, L.V.S., Xavier, R.P., de Carvalho, E.R., Hitzman, M.W., Johnson, C.A., de Souza Filho, C.R., and Torresi, I., 2008. Spatial and temporal zoning of hydrothermal alteration and mineralization in the Sossego iron oxide-copper-gold deposit, Carajás mineral province, Brazil: Paragenesis and stable isotope constraints. *Mineralium Deposita*, 43, 129-159.
- Mudd, G.M., and Jowitt, S.M., 2014. A detailed assessment of global nickel resource trends and endowments. *Economic Geology*, 109, 1813-1841.
- Mudd, G.M., Jowitt, S.M., and Werner, T.T., 2018. Global platinum group element resources, reserves and mining-A critical assessment. *Science of The Total Environment*, 622-623, 614-625.
<<https://doi.org/10.1016/j.scitotenv.2017.11.350>>
- Mumford, T., 2009. Dykes of the Moose Creek Valley, Ice River alkaline complex, southeastern BC. Unpublished M.Sc. thesis, The University of New Brunswick, Canada, 230 p.
- Mumin, H., Somarin, A., Jones, B., Corriveau, L., Ootes, L., and Camier, J., 2010. The IOCG porphyry-epithermal continuum in the Great Bear Magmatic Zone, Northwest Territories, Canada. *Geological Association of Canada, Short Course Notes* 20, pp. 57-75.
- Mungall, J.E., Jenkins, C.M., Robb, S.J., Yao, Z., and Brenan, J.M., 2020. Upgrading of magmatic sulfides, revisited. *Economic Geology*, 115, 1827-1833.
- Naldrett, A.J., 1999. World-class Ni-Cu-PGE deposits: key factors in their genesis. *Mineralium Deposita*, 34, 227-240.
- Naldrett, A.J., 2010. From the mantle to the bank: The life of a Ni-Cu-(PGE) sulfide deposit. *South African Journal of Geology*, 113, 1-32.
- Nassar, N.T., Brainard, J., Gulley, A., Manley, R., Matos, G., Lederer, G., Bird, I.R., Pineault, D., Alonso, E., Gambogi, J., and Fortier, S.M., 2020. Evaluating the mineral commodity supply risk of the U.S. manufacturing sector. *Science Advances* 6.
<<https://www.science.org/doi/10.1126/sciadv.aay8647>>
- National Research Council, 2008. Minerals, critical minerals, and the U.S. economy. National Academies Press, Washington, D.C., 262 p.
- Nelson, J., 2017. Composite pericratonic basement of west-central Stikinia and its influence on Jurassic magma conduits: Examples from the Terrace-Ecstall and Anyox areas. In: *Geological Fieldwork 2016*, British Columbia Ministry of Energy and Mines, British Columbia Geological Survey Paper 2017-01, pp. 61-82.
- Nelson, J.L., and Bradford, J.A., 1993. Geology of the Midway-Cassiar area northern British Columbia (1040, 104P). British Columbia Ministry of Energy, Mines and Petroleum Resources, British Columbia Geological Survey Bulletin 83, 100 p.
- Nelson, J., and Kyba, J., 2014. Structural and stratigraphic control of porphyry and related mineralization in the Treaty Glacier-KSM-Brucejack-Stewart trend of western Stikinia. In: *Geological Fieldwork 2013*, British Columbia Ministry of Energy and Mines, British Columbia Geological Survey Paper 2014-01, pp. 111-140.
- Nelson, J.L., and van Straaten, B., 2020. Recurrent syn- to postsubduction mineralization along deep crustal corridors in the Iskut-Stewart-Kitsault region of western Stikinia, northwestern British Columbia. In: Sharman, E.R., Lang, J.R., and Chapman, J.B., (Eds.), *Porphyry Deposits of the Northwestern Cordillera of North America: A 25-Year Update*. Canadian Institute of Mining and Metallurgy Special Volume 57, pp. 194-211.
- Nelson, J., Paradis, S., Christensen, J., and Gabites, J., 2002. Canadian Cordilleran Mississippi Valley-type deposits: A case for Devonian-Mississippian back-arc hydrothermal origin. *Economic Geology*, 97, 1013-1036.
- Nelson, J.L., Colpron, M., and Israel, S., 2013a. The Cordillera of British Columbia, Yukon and Alaska: tectonics and metallogeny. In: Colpron, M., Bissig, T., Rusk, B.G., and Thompson, F.H., (Eds.), *Tectonics, Metallogeny, and Discovery: The North American Cordillera and Similar Accretionary Settings*. Society of Economic Geologists Special Publication 17, pp. 53-109.
- Nelson, J., Diakow, L., van Staal, C. and Chipley, D., 2013b. Ordovician volcanogenic sulphides in the southern Alexander terrane, coastal NW British Columbia: Geology, Pb isotopic signature, and a case for correlation with Appalachian and Scandinavian deposits. In: *Geological Fieldwork 2012*, British Columbia Ministry of Energy, Mines and Natural Gas, British Columbia Geological Survey Paper 2013-01, pp. 13-33.
- Nelson, J., Waldron, J., van Straaten, B., Zagoresvski, A., and Rees, C., 2018. Revised stratigraphy of the Hazelton Group in the Iskut River region, northwestern British Columbia. In: *Geological Fieldwork 2017*, British Columbia Ministry of Energy, Mines and Petroleum Resources, British Columbia Geological Survey Paper 2018-01, pp. 15-38.
- Nelson, J.L., van Straaten, B., and Friedman, R., 2022. Latest Triassic-Early Jurassic Stikine-Yukon-Tanana terrane collision and the onset of accretion in the Canadian Cordillera: Insights from Hazelton Group detrital zircon provenance and arc-back-arc configuration. *Geosphere*, 18, 670-696.
<<https://doi.org/10.1130/GES02444.1>>
- Néron, A., Bédard, L.P., and Gaboury, D., 2018. The Saimt-Honoré carbonatite REE zone, Québec, Canada: Combined magmatic and hydrothermal processes. *Minerals*, 8.
<<https://doi.org/10.3390/min8090397>>
- Nixon, G.T., 1998. Ni-Cu sulphide mineralization in the Turnagain Alaskan-type complex: A unique magmatic environment. British Columbia Ministry of Employment and Investment, British Columbia Geological Survey Paper 1998-01, pp. 18-1-18-11.
- Nixon, G.T., 2003. Use of spinel in mineral exploration; the enigmatic Giant Mascot Ni-Cu-PGE deposit-possible ties to Wrangellia and Metallogenic significance. British Columbia Ministry of Energy and Mines, British Columbia Geological Survey Paper 2003-01, pp. 115-128.
- Nixon, G.T., Hammack, J.L., Connelly, J.N., and Case, G., 1990. Geology and noble metal geochemistry of the Polaris ultramafic complex, north-central British Columbia. British Columbia Ministry of Energy, Mines and Petroleum Resources, British Columbia Geological Survey Paper 1990-01, pp. 387-404.
- Nixon, G.T., Hammack, J.L., Ash, C.H., Cabri, L.J., Case, G., Connelly, J.N., Heaman, L.M., Laflamme, J.H.G., Nuttall, C., Paterson, W.P.E., and Wong, R.H., 1997. Geology and platinum-group-element mineralization of Alaskan-type ultramafic-mafic complexes in British Columbia. British Columbia Ministry of Employment and Investment, British Columbia Geological Survey Bulletin 93, 142 p.
- Nixon, G.T., Scheel, J.E., Scoates, J.S., Friedman, R.M., Wall, C.J., Gabites, J., and Jackson-Brown, S., 2019. Syn-accretionary multistage assembly of an Early Jurassic Alaskan-type intrusion

- in the Canadian Cordillera: U-Pb and $^{40}\text{Ar}/^{39}\text{Ar}$ geochronology of the Turnagain ultramafic-mafic intrusive complex, Yukon-Tanana terrane. *Canadian Journal of Earth Sciences*, 57, 575-600.
- Nixon, G.T., Friedman, R.M., and Creaser, R.A., 2020a. Late Neogene porphyry Cu-Mo(\pm Au-Ag) mineralization in British Columbia: the Klaskish Plutonic Suite, northern Vancouver Island. In: *Geological Fieldwork 2019*, British Columbia Ministry of Energy, Mines and Petroleum Resources, British Columbia Geological Survey Paper 2020-01, pp. 119-132.
- Nixon, G.T., Scoates, J.S., Milidragovic, D., Nott, J., Moerhuis, N., Ver Hoeve, T.J., Manor, M.J., and Kjarsgaard, I.M., 2020b. Convergent margin Ni-Cu-PGE-Cr ore systems: U-Pb petrochronology and environments of Cu-PGE vs. Cr-PGE mineralization in Alaskan-type intrusions. In: Bleeker, W., Houlé, M.G., (Eds.), *Targeted Geoscience Initiative 5: Advances in the understanding of Canadian Ni-Cu-PGE and Cr ore systems- Examples from the Midcontinent Rift, the Circum-Superior Belt, the Archean Superior Province, and Cordilleran Alaskan-type intrusions*. Geological Survey of Canada Open File 8722, pp. 197-218.
- Noble, S.R., Spooner, E.T.C., and Harris, F.R., 1995. Logtung-a porphyry W-Mo deposit in Southern Yukon. In: Schroeter, T.G., (Ed.), *Porphyry Deposits of the Northwestern Cordillera of North America*. Canadian Institute of Mining, Metallurgy, and Petroleum Special Volume 46, pp. 732-746.
- Norris, J.R., Tosdal, R.M., Lipske, J., and Wilson, A.J., 2023. Late-stage low-temperature hydrothermal alteration overprint at the East zone in the Red Chris porphyry Cu-Au deposit, northwestern British Columbia, Canada. *Economic Geology*, 118, 391-409.
- Northcote, B., 2022. Volcanogenic massive sulphide (VMS) deposits in British Columbia: A review. British Columbia Ministry of Energy, Mines and Low Carbon Innovation, British Columbia Geological Survey GeoFile 2022-11, 30 p.
- Nott, J., Milidragovic, D., Nixon, G.T., and Scoates, J.S., 2020. New geological investigations of the Early Jurassic Polaris ultramafic-mafic Alaskan-type intrusion, north-central British Columbia. In: *Geological Fieldwork 2019*, British Columbia Ministry of Energy, Mines and Petroleum Resources, British Columbia Geological Survey Paper 2020-01, pp. 59-76.
- NRCan, 2022. The Canadian critical minerals strategy. Natural Resources Canada, 52 p.
<<https://www.canada.ca/en/campaign/critical-minerals-in-canada/canadian-critical-minerals-strategy.html>>
- Ootes, L., Gleeson, S.A., Turner, E., Rasmussen, K., Gordey, S., Falck, H., Martel, E., and Pierce, K., 2013. Metallogenic evolution of the Mackenzie and eastern Selwyn mountains of Canada's northern Cordillera, Northwest Territories: A compilation and review. *Geoscience Canada*, 40, 40-69.
- Ootes, L., Snyder, D., Davis, W.J., Acosta-Góngora, P., Corriveau, L., Mumin, A.H., Gleeson, S.A., Samson, I.M., Montreuil, J.-F., Potter, E., and Jackson, V.A., 2017. A Paleoproterozoic Andean-type iron oxide copper-gold environment, the Great Bear magmatic zone, NW Canada. *Ore Geology Reviews*, 81, pp. 123-139.
- Ootes, L., Bergen, A.L., Milidragovic, D., Jones, G.O., Camacho, A., and Friedman, R., 2020. An update on the geology of northern Hogen batholith and its surroundings, north-central British Columbia. In: *Geological Fieldwork 2019*, British Columbia Ministry of Energy, Mines and Petroleum Resources, British Columbia Geological Survey Paper 2020-01, pp. 25-47.
- Orovan, E.A., and Hollings, P., 2020. Exploring the green rock environment: An introduction. *Economic Geology*, 115, 695-700.
- Orovan, E.A., Cooke, D.R., Harris, A.C., Ackerman, B., and Lawlis, E., 2018. Geology and isotope geochemistry of the Wainaulo Cu-Au porphyry deposit, Namosi district, Fiji. *Economic Geology*, 113, 133-161.
- Orovan, E.A., Zaborniak, K., and Hooker, K., 2024. Textural evidence for ore fluid transport and the magmatic to hydrothermal transition at the past-producing Kitsault Mo-Ag mine. In: *Geological Fieldwork 2023*, Ministry of Energy, Mines and Low Carbon Innovation, British Columbia Geological Survey Paper 2024-01, this volume.
- Pacey, A., Wilkinson, J.J., Boyce, A.J., and Millar, I.L., 2020. Magmatic fluids implicated in the formation of propylitic alteration: Oxygen, hydrogen, and strontium isotope constraints from the Northparkes porphyry copper-gold district, New South Wales, Australia. *Economic Geology*, 115, 729-748.
- Park, J-W., Campbell, I.H., Chiaradia, M., Hao, H., and Lee, C-T., 2021. Crustal magmatic controls on the formation of porphyry copper deposits. *Nature Reviews Earth and Environment*, 2, 542-557.
- Pang, K.-N., Zhou, M.-F., Lindsley, D., Zhao, D., and Malpas, J., 2008. Origin of Fe-Ti oxide ores in mafic intrusions: evidence from the Panzihua Intrusion, SW China. *Journal of Petrology*, 49, 295-313.
- Paradis, S., 2015. Indium, germanium and gallium in volcanic- and sediment-hosted base-metal sulphide deposits. In: Simandl, G.J., and Neetz, M., (Eds.), *Symposium on Strategic and Critical Materials Proceedings*, November 13-14, 2015, Victoria, British Columbia. British Columbia Ministry of Energy and Mines, British Columbia Geological Survey Paper 2015-03, pp. 23-29.
- Paradis, S., and Simandl, G.J., 2018. Are there genetic links between carbonate-hosted barite-zinc-lead sulphide deposits and magnetite mineralization in southeast British Columbia? In: Rogers, N., (Ed.), *Targeted Geoscience Initiative: 2017 Report of activities, Volume 1*. Geological Survey of Canada, Open File 8358, pp. 217-227.
<<http://doi.org/10.4095/306478>>
- Paradis, S., Hannigan, P., and Dewing, K., 2007. Mississippi Valley-type lead-zinc deposits. In: Goodfellow, W.D., (Ed.), *Mineral Deposits of Canada: A Synthesis of Major Deposit-Types, District Metallogeny, the Evolution of Geological Provinces, and Exploration Methods*. Geological Association of Canada, Mineral Deposits Division, Special Publication No. 5, pp. 185-203.
- Paradis, S., and Simandl, G.J., 2017. Is there a genetic link between the SEDEX and MVT deposits of the Canadian Cordillera? In: Roger, N., (Ed.), *Targeted Geoscience Initiative, 2016 report of activities*, Geological Survey of Canada, Open File 8199, pp. 107-113.
<<https://doi.org/10.4095/299623>>
- Paradis, S., Simandl, G.J., Drage, N., D'Souza, R.J., Kontak, D.J., and Waller, Z., 2022. Carbonate-hosted deposits (Mississippi Valley-type, magnetite, and REE-F-Ba) of the southeastern Canadian Cordillera: a review and isotopic data comparison. In: Peter, J.M., and Gadd, M.G., (Eds.), *Targeted Geoscience Initiative 5: Volcanic- and Sediment-hosted Massive-sulfide Deposit Genesis and Exploration Methods*, Geological Survey of Canada Bulletin 617, pp. 39-87.
- Pell, J., 1994. Carbonatites, nepheline syenites, kimberlites and related rocks in B.C. British Columbia Ministry of Energy, Mines and Petroleum Resources, British Columbia Geological Survey, Bulletin 88, 136 p.
- Peter, J., and Scott, S.D., 1999. Windy Craggy, northwest British Columbia: The world's largest Besshi-type deposit. In: Barrie, C.T., and Hannington, M.D., (Eds.), *Volcanic-Associated Massive Sulfide Deposits: Processes and Examples in Modern and Ancient Settings*. Reviews in Economic Geology, 8, pp. 261-295.
- Peterson, T.D., and Currie, K.L. 1994. The Ice River Complex, British Columbia. In: *Current Research, Part A*. Geological Survey of Canada, Paper 1994-A, pp. 185-192.
- Piercey, S.J., 2011. The setting, style, and role of magmatism in the formation of volcanogenic massive sulfide deposits. *Mineralium Deposita*, 46, 449-471.
- Piercey, S.J., 2015. A semipermeable interface model for the genesis of seafloor replacement-type volcanogenic massive sulfide (VMS) deposits. *Economic Geology*, 110, 1655-1660.

- Piña, R., Romeo, I., Ortega, L., Lunar, R., Capote, R., Gervilla, F., Tejero, R., and Quesada, C., 2010. Origin and emplacement of the Aguablanca magmatic Ni-Cu-(PGE) sulfide deposit, SW Iberia: A multidisciplinary approach. *Geological Society of America Bulletin*, 122, 915-925.
- Plouffe, A., and Ferbey, T., 2017. Porphyry Cu indicator minerals in till: A method to discover buried mineralization. In: Ferbey, T., Plouffe, A., and Hickin, A.S., (Eds.), *Indicator Minerals in Till and Stream Sediments of the Canadian Cordillera*. Geological Association of Canada Special Paper Volume 50, and Mineralogical Association of Canada Topics in Mineral Sciences Volume 47, pp. 129-159.
- Plouffe, A., and Ferbey, T., 2019. Indicator-mineral content of bedrock and till at the Gibraltar porphyry Cu-Mo deposit and the Woodjam porphyry Cu-Au-Mo prospect, south-central British Columbia. *British Columbia Ministry of Energy, Mines and Petroleum Resources, British Columbia Geological Survey Open File 2019-10*, 33 p.
- Plouffe, A., and Schetselaar, E., (Eds.), 2021. Targeted Geoscience Initiative 5: Contributions to the understanding and exploration of porphyry deposits. *Geological Survey of Canada, Bulletin*, 616, 223 p.
- Plouffe, A., Kjarsgaard, I. M., Ferbey, T., Wilton, D.H.C., Petts, D. C., Percival, J.B., Kobylinski, C.H., and McNeil, R., 2021. Detecting buried porphyry Cu mineralization in a glaciated landscape: a case study from the Gibraltar Cu-Mo Deposit, British Columbia, Canada. *Economic Geology*, 117, 777-799.
- Raffle, K.J., Nichols, S., and Rodriguez, A., 2021. Technical Report on the Chu Chua Property, Kamloops Mining Division, British Columbia. Prepared for Newport Exploration Ltd., by Apex Geoscience Ltd. 127 p.
<<https://www.sedarplus.ca>>
- Ray, G.E., 2013. A review of skarns in the Canadian Cordillera. *British Columbia Ministry of Energy and Mines, British Columbia Geological Survey Open File 2013-08*, 50 p.
- Ray, G.E., and Webster I.C.L., 2000. The Heff prospect at Heffley Lake, south-central B.C. (09ZINE096): An unusual example of a mafic-ultramafic-related Cu-Au-REE-bearing magnetite skarn. In: *Geological Fieldwork 1999*, British Columbia Ministry of Energy and Mines, *British Columbia Geological Survey Paper 2000-01*, pp. 273-286.
- Reeve, J.S., Cross, K.C., Smith, R.N., and Oreskes, N., 1990. Olympic Dam copper-uranium gold silver deposit. In: Hughes, F.E., (Ed.), *Geology of the Mineral Deposits of Australia and Papua New Guinea*. Australasian Institute of Mining and Metallurgy, Monograph 14, pp. 1009-1035.
- Reich, M., Simon, A.C., Barra, F., Palma, G., Hou, T., and Bilinker, L.D., 2022. Formation of iron oxide-apatite deposits. *Nature Reviews Earth & Environment*, 3, 758-775.
- Richards, J.P., 2011. Magmatic to hydrothermal metal fluxes in convergent and collided margins. *Ore Geology Reviews*, 40, 1-26.
- Richards, J.P., and Mumin, A.H., 2013. Magmatic-hydrothermal processes within an evolving Earth: Iron oxide-copper-gold and porphyry Cu±Mo±Au deposits. *Geology*, 41, 767-770.
- Ripley, E.M., 2010. A new perspective on exploration for magmatic sulfide-rich Ni-Cu-(PGE) deposits. In: Goldfarb, R.J., Marsh, E.E., and Monecke, T., (Eds.), *The Challenge of Finding New Mineral Resources: Global Metallogeny, Innovative Exploration, and New Discoveries Volume 1: Gold, Silver, and Copper-Molybdenum*. Society of Economic Geologists, Special Publication 15, pp. 437-450.
- Ripley, E.M., and Li, C., 2013. Sulfide saturation in mafic magmas: is external sulfur required for magmatic Ni-Cu-(PGE) ore genesis? *Economic Geology*, 108, 45-58.
- Ross, G.M., 1991. Tectonic setting of the Windermere Supergroup revisited. *Geology*, 19, 1125-1128.
- Ross, P.-S., and Mercier-Langevin, P., 2014. Igneous Rock Associations 14. The volcanic setting of VMS and SMS deposits: A review. *Geoscience Canada*, 41, 365-377.
- Rukhlov, A.S., and Bell, K., 2010. Geochronology of carbonatites from the Canadian and Baltic Shields, and the Canadian Cordillera: clues to mantle evolution. *Mineralogy and Petrology*, 98, 11-54.
- Rukhlov, A.S., Bell, K., and Amelin, Y., 2015. Carbonatites, isotopes and evolution of the subcontinental mantle: An overview. In: Simandl, G.J., and Neetz, M., (Eds.), *Symposium on Strategic and Critical Materials Proceedings*, November 13-14, 2015, Victoria, British Columbia, British Columbia Ministry of Energy and Mines, *British Columbia Geological Survey Paper 2015-3*, pp. 39-64.
- Rukhlov, A.S., Chudy, T.C., Arnold, H., and Miller, D., 2018. Field trip guidebook to the Upper Fir carbonatite-hosted Ta-Nb deposit, Blue River area, east-central British Columbia. *British Columbia Ministry of Energy, Mines and Petroleum Resources, Geological Survey GeoFile 2018-6*, 67 p.
- Rukhlov, A.S., Aspler, L.B., and Gabites, J., 2019. Are Cordilleran carbonatite hosts of Ta, Nb and REE from the deep mantle? *British Columbia Ministry of Energy, Mines and Petroleum Resources, British Columbia Geological Survey GeoFile 2019-08*.
- Rukhlov, A.S., Cui, Y., Cunningham, Q., Fortin, G., and Anderson, C., 2024. Geochemical signals of carbonatite-related critical metals in provincial stream sediments. In: *Geological Fieldwork 2023*, Ministry of Energy, Mines and Low Carbon Innovation, *British Columbia Geological Survey Paper 2024-01*, this volume.
- Sangster, D.F., 2018. Toward an integrated genetic model for vent-distal SEDEX deposits. *Mineralium Deposita*, 53, 509-527.
- Sangster, D.F., 1990. Mississippi Valley-type and sedex lead-zinc deposits: a comparative examination. *Transactions of the Institution of Mining and Metallurgy*, 99, 21-42.
- Sangster, D.F., 2020. Evidence that Broken Hill-type Pb-Zn deposits are metamorphosed SEDEX deposits. *Mineralium Deposita*, 55, 1263-1270.
- Scammell, R.J., 1987. Stratigraphy, structure and metamorphism of the north flank of the Monashee complex, southeastern British Columbia: a record of Proterozoic extension and Phanerozoic crustal thickening. Unpublished M.Sc. thesis, Carleton University, Ottawa, Canada, 205 p.
- Scammell, R.J., 1993. Mid-Cretaceous to Tertiary thermotectonic history of former mid-crustal rocks, southern Omineca belt, Canadian Cordillera. Unpublished Ph.D. thesis, Queens University, Kingston, Ontario, 576 p.
- Scammell, R.J., and Brown, R.L., 1990. Cover gneisses of the Monashee terrane: a record of synsedimentary rifting in the North American Cordillera. *Canadian Journal of Earth Sciences*, 27, 712-726.
- Scheel, E., Nixon, G.T., and Scoates, J.S., 2005. Geology of the Turnagain Alaskan-type Ultramafic Intrusive Suite and Associated Ni-Cu-PGE Mineralization, British Columbia. In: *Geological Fieldwork 2004*, British Columbia Ministry of Energy, Mines and Petroleum Resources, *British Columbia Geological Survey Paper 2005-01*, pp. 167-176.
- Schiarizza, P., 2012. Geology of the Kutcho Assemblage between the Kehlechoa and Tucho Rivers, Northern British Columbia (NTS 104I/01, 02). In: *Geological Fieldwork 2011*, British Columbia Ministry of Energy, Mines and Natural Gas, *British Columbia Geological Survey Paper 2012-01*, pp. 75-98.
- Schiarizza, P., 2014. Geological setting of the Granite Mountain batholith, host to the Gibraltar porphyry Cu-Mo deposit, southcentral British Columbia. In: *Geological Fieldwork 2013*, British Columbia Ministry of Energy, Mines and Petroleum Resources, *British Columbia Geological Survey Paper 2014-1*, pp. 95-110.

- Schiarizza, P., 2015. Geological setting of the Granite Mountain batholith, south-central British Columbia. In: Geological Fieldwork 2014, British Columbia Ministry of Energy and Mines, British Columbia Geological Survey Paper 2015-1, pp. 19-39.
- Schiarizza, P., and Friedman, R.M., 2021. U-Pb zircon dates for the Granite Mountain batholith, Burgess Creek stock, and Sheridan Creek stock, Gibraltar Mine area, south-central British Columbia. In: Geological Fieldwork 2020, British Columbia Ministry of Energy, Mines and Low Carbon Innovation, British Columbia Geological Survey Paper 2021-01, pp. 23-35.
- Simandl, G.J., Mackay, D.A.R., Ma, X., Luck, P., Gravel, J., and Akam, C., 2017. The direct indicator mineral concept and QEMSCAN® applied to exploration for carbonatite and carbonatite-related ore deposits. In: Ferbey, T., Plouffe, A. and Hickin, A.S., (Eds.), Indicator Minerals in Till and Stream Sediments of the Canadian Cordillera. Geological Association of Canada Special Paper Volume 50 and Mineralogical Association of Canada Topics in Mineral Sciences Volume 47, pp. 175-190.
- Simandl, G.J., Kon, Y., Paradis, S., Hoshino, M., Akam, C., Miller, D., Araoka, D., and Kodama, S., 2019. Geochemistry of the Rock Canyon Creek REE-F-Ba deposit, British Columbia, Canada. British Columbia Ministry of Energy, Mines and Petroleum Resources, British Columbia Geological Survey GeoFile 2019-07.
- Simandl, G.J., D'Souza, R.J., Paradis, S., Spence, J., and FitzGerald, W., 2020. REE in carbonates from sediment-hosted Pb-Zn deposits, southern Rocky Mountains, BC. British Columbia Ministry of Energy, Mines and Petroleum Resources, British Columbia Geological Survey GeoFile 2020-05.
- Simandl, G.J., D'Souza, R.J., Paradis, S., and Spence, J., 2022. Rare-earth element content of carbonate minerals in sediment-hosted Pb-Zn deposits, southern Canadian Rocky Mountains. In: Peter, J.M., and Gadd, M.G., (Eds.), Targeted Geoscience Initiative 5: volcanic and sediment-hosted massive sulphide deposit genesis and exploration methods. Geological Survey of Canada, Bulletin 617, 165-201.
- Sharman, E.R., Lang, J.R., and Chapman, J.B., (editors), 2020. Porphyry deposits of the northwestern Cordillera of North America: A 25-Year Update. Canadian Institute of Mining and Metallurgy Special Volume 57, 725 p.
- Sherlock, R.L., Roth, T., Spooner, E.T.C., and Bray, C.J., 1999. Origin of the Eskay Creek precious metal-rich volcanogenic massive sulfide deposit; fluid inclusion and stable isotope evidence. *Economic Geology*, 94, 803-824.
- Sillitoe, R.H., 1983. Unconventional metals in porphyry deposits. In: Shanks, W.C., (Ed.), Cameron Volume on Unconventional Mineral Deposits. Society of Mining Engineers of AIME, pp. 207-221.
- Sillitoe, R.H., 2010. Porphyry copper systems. *Economic Geology*, 105, 3-41.
- Sillitoe, R.H., 2003. Iron oxide-copper-gold deposits: An Andean view. *Mineralium Deposita*, 38, 787-812.
- Sillitoe, R.H., and Burrows, D.R., 2002. New field evidence bearing on the origin of the El Laco magnetite deposit northern Chile. *Economic Geology*, 97, 1101-1109.
- Singer, D.A., 1993. Basic concepts in three-part quantitative assessments of undiscovered mineral resources: Nonrenewable Resources, 2, 69-81.
- Skirrow, R.G., 2022. Iron oxide copper-gold (IOCG) deposits - A review (part 1): Settings, mineralogy, ore geochemistry and classification. *Ore Geology Reviews*, 140, article 104569. <<https://doi.org/10.1016/j.oregeorev.2021.104569>>
- Song, X., and Li, X., 2009. Geochemistry of the Kalatongke Ni-Cu-(PGE) sulfide deposit, NW China: implications for the formation of magmatic sulfide mineralization in a postcollisional environment. *Mineralium Deposita*, 44, 303-327.
- Song, W.L., Xu, C., Veksler, I.V., and Kynicky, J., 2016. Experimental study of REE, Ba, Sr, Mo and W partitioning between carbonatitic melt and aqueous fluid with implications for rare metal mineralization. *Contributions to Mineralogy and Petrology*, 171, 1-12.
- Spence, D.W., Crawford, H., Scoates, J.S., Nott, J.A., Nixon, G.T., and Milidragovic, D., 2022. Mapping ultramafic cumulates at the Tulameen ultramafic-mafic Alaskan-type intrusion, south-central British Columbia, aided by remotely piloted aircraft system photogrammetry. In: Geological Fieldwork 2021, British Columbia Ministry of Energy, Mines and Low Carbon Innovation, British Columbia Geological Survey Paper 2022-01, pp. 103-122.
- Stanley, B., and Nelson, J., 2022. Revised stratigraphy of the Stuhini and Hazelton groups and LA-ICP-MS zircon geochronology of the Scottie gold mine area, northwestern British Columbia. In: Geological Fieldwork 2021, British Columbia Ministry of Energy, Mines and Low Carbon Innovation, British Columbia Geological Survey Paper 2022-01, pp. 83-102.
- Steininger, R.C., 1985. Geology of the Kitsault molybdenum deposit, British Columbia. *Economic Geology*, 80, 57-71.
- Steinthorsdottir, K., Cutts, J., Dipple, G., Milidragovic, D., and Jones, F., 2020. Origin and serpentinization of ultramafic rocks in dismembered ophiolite north of Trembleur Lake, central British Columbia. In: Geological Fieldwork 2019, British Columbia Ministry of Energy, Mines and Petroleum Resources, British Columbia Geological Survey Paper 2020-01, pp. 49-58.
- Stinson, P., and Brown, D.A., 1995. Iron Range deposits, southern British Columbia (82F/1). British Columbia Ministry of Energy, Mines and Petroleum, British Columbia Geological Survey Paper 1995-01, pp. 127-134.
- Stone, W., Brown, F., Barry, J., Burga, D., Puritch, E., and Freudigmann, S., 2021. Technical Report and Updated Mineral Resource Estimate of the Revel Ridge Polymetallic property Revelstoke Mining Division, British Columbia Canada, for ROKMaster Resources Corp. by P&E Mining Consultants Inc. 263 p. <<https://www.sedarplus.ca/>>
- Sutherland Brown, A., 1998. British Columbia's Geological Surveys: A century of science and dedication. Pacific Section Geological Association of Canada, 157 p.
- Taseko Mines Limited, 2020. Technical Report on the Mineral Reserve Update at the Yellowhead Copper Project, British Columbia Canada. 372 p. <<https://www.sedarplus.ca/>>
- Thériault, R.D., Barnes, S.-J., and Severson, M.J., 2000. Origin of Cu-Ni-PGE sulfide mineralization in the Partridge River Intrusion, Duluth Complex, Minnesota. *Economic Geology*, 95, 929-943.
- Theny, L.M., 2016. Age, formation and tectonism of the Neoproterozoic Ruddock Creek zinc-lead deposit and host Windermere Supergroup, northern Monashee Mountains, southern Canadian Cordillera. Unpublished M.Sc. thesis, Simon Fraser University, 183 p.
- Theny, L.M., Gibson, H.D., and Crowley, J.L., 2015. Uranium-lead age constraints and structural analysis for the Ruddock Creek zinc-lead deposit: insight into the tectonic evolution of the Neoproterozoic metalliferous Windermere Supergroup, northern Monashee Mountains, southern British Columbia (NTS 082M); In: Geoscience BC Summary of Activities 2014, Geoscience BC Report 2015-1, pp. 151-164.
- Thomas, M.D., 2021. Spatial relationship between porphyritic Cu-Au mineral occurrences and magnetic signatures within the Iron Mask batholith, south-central Cordillera, British Columbia. In: Plouffe, A., and Schetselaar, E., (Eds.), Targeted Geoscience Initiative 5: Contributions to the Understanding and Exploration of Porphyry Deposits. Geological Survey of Canada, 616, pp. 65-90.
- Tornos, F., Velasco, F., and Hanchar, J.M., 2016. Iron-rich melts, magmatic magnetite, and superheated hydrothermal systems: The El Laco deposit, Chile. *Geology*, 44, 427-430.

- Tornos, F., Hanchar, J.M., Steele-MacInnis, M., Crespo, E., Kamenetsky, V.S., and Casquet, C., 2023. Formation of magnetite-(apatite) systems by crystallizing ultrabasic iron-rich melts and slag separation. *Mineralium Deposita*. <<https://doi.org/10.1007/s00126-023-01203-w>>
- Trofanenko, J., Williams-Jones, A.E., Simandl, G.J., and Migdisov, A.A., 2016. The nature and origin of the REE mineralization in the Wiccheeda carbonatite, British Columbia, Canada. *Economic Geology*, 111, 199-223.
- Turner, A.J., and Hough, R., 2023. Technical Report on the combined Kitsault Valley project, British Columbia Canada. Technical report prepared for Dolley Varden Silver Corporation by APEX Geoscience Ltd., 283 p. <<https://www.sedarplus.ca>>
- Vandenburg, E.D.J., 2020. The E&L magmatic Ni-Cu-(PGE) deposit, northwestern British Columbia: Preliminary sulfide petrology, platinum-group element mineralogy and lead isotope systematics. Unpublished B.Sc. thesis, The University of British Columbia, 194 p.
- Van der Vlugt, J., Rukhlov, A.S., and van Straaten, B.I., 2022. Lithochemical re-analysis of British Columbia Geological Survey archived rock samples from northwestern British Columbia. British Columbia Ministry of Energy, Mines and Low Carbon Innovation, British Columbia Geological Survey GeoFile 2022-14, 15 p.
- van Keken, P.E., Hauri, E.H., and Ballentine, C.J., 2002. Mantle mixing: the generation, preservation, and destruction of chemical heterogeneity. *Annual Review of Earth and Planetary Sciences*, 30, 493-525.
- van Straaten, B.I., 2024. Upper Hazelton Group stratigraphy along the Stikine arch, northwestern British Columbia. In: *Geological Fieldwork 2023*, Ministry of Energy, Mines and Low Carbon Innovation, British Columbia Geological Survey Paper 2024-01, this volume.
- van Straaten, B.I., and Gibson, R., 2017. Late Early to Middle Jurassic Hazelton Group volcanism and mineral occurrences in the McBride-Tanzilla area, northwest British Columbia. In: *Geological Fieldwork 2016*. British Columbia Ministry of Energy, Mines and Petroleum Resources, British Columbia Geological Survey Paper 2017-01, pp. 83-115.
- van Straaten, B.I., and Nelson, J., 2016. Syncollisional late Early to early Late Jurassic volcanism, plutonism, and porphyry style alteration on the northeastern margin of Stikinia. In: *Geological Fieldwork 2015*, British Columbia Ministry of Energy and Mines, British Columbia Geological Survey Paper 2016-01, pp. 113-143.
- van Straaten, B.I., Logan, J.M., Nelson, J.L., Moynihan, D.P., Diakow, L.J., Gibson, R., Bichlmaier, S.J., Wearmouth, C.D., Friedman, R.M., Golding, M.L., Miller, E.A., and Poulton, T.P., 2022. Bedrock geology of the Dease Lake area. British Columbia Ministry of Energy, Mines and Low Carbon Innovation, British Columbia Geological Survey Geoscience Map 2022-01, 1:100,000 scale.
- van Straaten, B.I., Friedman, R.M., and Camacho, A., 2023. Stratigraphy of the Stuhini Group (Upper Triassic) in the Galore Creek area, northwestern British Columbia. In: *Geological Fieldwork 2022*, British Columbia Ministry of Energy, Mines and Low Carbon Innovation, British Columbia Geological Survey Paper 2023-01, pp. 33-49.
- Velasquez, G., Carrizo, D., Salvi, S., Vela, I., Pablo, M. and Perez, A., 2020. Tracking cobalt, REE and gold from a porphyry-type deposit by LA-ICP-MS: a geological approach towards metal-selective mining in tailings. *Minerals*, 10. <https://doi.org/10.3390/min10_020109>
- Wearmouth, C.D., Peters, K.J., Czertowicz, T.A., and Orovan, E.A., 2024. Mineral potential modelling results for northwestern British Columbia, a comparison between past and current work at the British Columbia Geological Survey. In: *Geological Fieldwork 2023*. British Columbia Ministry of Energy, Mines and Low Carbon Innovation, British Columbia Geological Survey Paper 2024-01, this volume.
- Wang, S.-M., Wu, C.-Z., Muhtar, M.N., Lei, R.-X., and Brzozowski, M.J., 2021a. Mobilization of ore-forming metals during post-magmatic hydrothermal overprinting of the Huangshandong Ni-Cu sulfide deposit, Eastern Tianshan, NW China. *Ore Geology Reviews*, 137, article 104315. <<https://doi.org/10.1016/j.oregeorev.2021.104315>>
- Wang, Z., Li, M.Y.H., Liu, Z.-R.R., and Zhou, M.-F., 2021b. Scandium: Ore deposits, the pivotal role of magmatic enrichment and future exploration. *Ore Geology Reviews*, 128, article 103906. <<https://doi.org/10.1016/j.oregeorev.2020.103906>>
- Wyborn, L.A.I., Heinrich, C.A., and Jaques, A.L., 1994. Australian Proterozoic Mineral Systems: Essential Ingredients and Mappable Criteria. *Proceedings of the Australian Institute of Mining and Metallurgy Annual Conference*, Melbourne, 109-115.
- White, G.P.E., 1982. Notes on carbonatites in central British Columbia. In: *Geological Fieldwork 1981*. British Columbia Ministry of Energy, Mines and Petroleum Resources, British Columbia Geological Survey, Paper 1982-01, pp. 68-69.
- Wilkinson, J.J., 2014. Sediment-hosted zinc-lead mineralization. In: Holland, H.D., and Turekian, K.K., (Eds.) *Treatise on Geochemistry*, Second Edition, vol. 13, pp. 219-249.
- Williams, P.J., and Pollard, P.J., 2001. Australian Proterozoic iron oxide-Cu-Au deposits: an overview with new metallogenic and exploration data from the Cloncurry District, Northwest Queensland. *Exploration and Mining Geology*, 10, 191-213.
- Woolley, A.R., 2003. Igneous silicate rocks associated with carbonatites: Their diversity, relative abundances and implications for carbonatite genesis. *Periodico di Mineralogia*, 72, 9-17.
- Woolley, A.R., and Kjarsgaard, B.A., 2008. Paragenetic types of carbonatite as indicated by the diversity and relative abundances of associated silicate rocks: evidence from a global database. *The Canadian Mineralogist*, 46, 741-752.
- Xu, C., Kynicky, J., Chakhmouradian, A.R., Qi, L., and Song, W., 2010. A unique Mo deposit associated with carbonatites in the Qinling orogenic belt, central China. *Lithos*, 118, 50-60.
- Yao, Z., and Mungall, J.E., 2020. Flotation mechanism of sulphide melt on vapour bubbles in partially molten magmatic systems. *Earth and Planetary Science Letters*, 542, article 116298. <<https://doi.org/10.1016/j.epsl.2020.116298>>

Textural evidence for ore fluid transport and the magmatic to hydrothermal transition at the past-producing Kitsault Mo-Ag mine



Evan A. Orovan^{1, a}, Katya Zaborniak¹, and Kirsty Hooker¹

¹ British Columbia Geological Survey, Ministry of Energy, Mines and Low Carbon Innovation, Victoria, BC, V8W 9N3

^a corresponding author: Evan.Orovan@gov.bc.ca

Recommended citation: Orovan, E.A., Zaborniak, K., and Hooker, K., 2024. Textural evidence for ore fluid transport and the magmatic to hydrothermal transition at the past-producing Kitsault Mo-Ag mine. In: Geological Fieldwork 2023, British Columbia Ministry of Energy, Mines and Low Carbon Innovation, British Columbia Geological Survey Paper 2024-01, pp. 53-64.

Abstract

The Kitsault Mo-Ag mine is a low-F porphyry Mo-Ag deposit hosted in Paleogene rocks of the Lime Creek intrusive complex. This complex consists of multiple stocks and plugs of quartz diorite to quartz monzonite that are surrounded by a broad zone of biotite hornfels developed in argillite and greywacke of the Bowser Lake Group. Molybdenum mineralization defines a cylindrical mineralized body that is in part spatially coincident with a series of aplite dikes with disequilibrium textures (unidirectional solidification textures, pegmatites, miarolitic cavities). The Mo grade shell has been disrupted internally by a late phase of quartz monzonite porphyry (quartz monzonite porphyry II) that lacks aplite. A series of unmineralized biotite- and hornblende-phyric lamprophyre dikes crosscuts all phases of the Lime Creek intrusive complex and surrounding Bowser Lake Group sedimentary rocks. The disequilibrium textures observed in the aplite dikes are interpreted to represent a permeable structure that focused ore-bearing fluids along the aplitic crystal mush, which episodically released during pressure fluctuations. This mechanism is consistent with a spatial coincidence between aplite dikes and Mo mineralization, internal veins, and disequilibrium textures within the aplite dikes.

Keywords: Kitsault Mo-Ag deposit, low-F porphyry Mo, magmatic to hydrothermal transition, unidirectional solidification textures

1. Introduction

Molybdenum is considered a critical mineral in Canada (Natural Resources Canada, 2022). It is an essential element used in steel production and found in many components of wind turbines, and is, therefore, considered a valuable commodity for the transition to a low-carbon economy. Porphyry deposits are the main host of Mo worldwide (~95%), where it occurs as a co-product or by-product in porphyry Cu deposits, or as the principal commodity in porphyry Mo deposits (Sinclair, 2007; John and Taylor, 2016). British Columbia is the only province that produces Mo in Canada where it has been produced predominantly from porphyry Mo deposits (e.g., Endako, Kitsault, Boss Mountain) and, to a lesser extent, porphyry Cu deposits (e.g., Gibraltar, Highland Valley Copper; Clarke et al., 2024). Because porphyry Mo deposits are the most significant source of Mo in British Columbia, understanding their genesis and potential to host other critical minerals (e.g., Ag, W, Cu, and Zn), is important for the provincial economy.

In British Columbia, most porphyry Mo deposits are the arc-related, low-F variety. The largest, and type locality for this deposit class is the well-studied Endako deposit (Jurassic), which produced 253,228 t of Mo since 1965 (Carr, 1966; Bysouth and Wong, 1995; Selby et al., 2000; Selby and Creaser, 2001; Whalen et al., 2001; Villeneuve et al., 2001). Other low-F porphyry Mo deposits in British Columbia are less well studied, the most significant of which is the Kitsault Mo-Ag

deposit (Paleogene) with NI 43-101 compliant Measured and Indicated resources of 321,800,000 t at 0.071% Mo (228,478 t of contained Mo; Fulton, 2014). The Kitsault deposit was mined for Mo between 1967 and 1972, and stockpiled ore was processed on site during 1981 and 1982. The most recent study published on Kitsault summarized the geology, alteration and vein stages (Steininger, 1985), K-Ar ages were determined by Carter (1981), and incremental work that improves upon the geological map and geochemical character of the deposit has been presented in several assessment reports since (Barresi, 2011; Fulton, 2014).

Magmatic-hydrothermal disequilibrium textures are commonly found in porphyry Mo deposits (e.g., Shannon et al., 1982; Lowenstern and Sinclair, 1996). These textures can be used by exploration geologists as pathfinders to economic mineralization (e.g., Shannon et al., 1982; Lowenstern and Sinclair, 1996; Bain et al., 2022) and provide insight into deposit-forming processes (e.g., Carter et al., 2021). As part of fieldwork in 2023 at Kitsault, we observed many of these textures (e.g., unidirectional solidification textures, miarolitic cavities, pegmatites) that were not previously recognized. This paper forms a preliminary study based on field and hand sample observations to determine crosscutting relationships and identify magmatic and hydrothermal features that can be used to interpret the paragenesis and potential mechanisms of ore formation. This work was carried out in the Nass Area and Nass

Wildlife Area as described in the Nisga'a Final Agreement, and on the traditional territories of the Northern Tsimshian.

2. Regional geology

The Kitsault mine is in the Intermontane superterrane along its western boundary with the Coast Plutonic complex of the Insular superterrane (Figs. 1, 2). The Intermontane superterrane includes an assemblage of multi-phase volcanic island arc terranes (e.g., Stikinia and Quesnellia) that accreted onto the

western margin of Ancestral North America in the Middle Jurassic (Nelson and van Straaten, 2020; George et al., 2021; Nelson et al., 2022). The Coast Plutonic complex consists of a range of granitic rocks that were emplaced during the Jurassic to Paleogene (Gehrels et al., 2009; Brown, 2020). Overlying these belts are the eroded remnants of Recent plateau-lava flows. The Kitsault mine is within the so-called Golden Triangle (Fig. 1), a loosely defined metal-rich area delineating a region in west central Stikinia that contains significant copper-gold-silver-molybdenum resources.

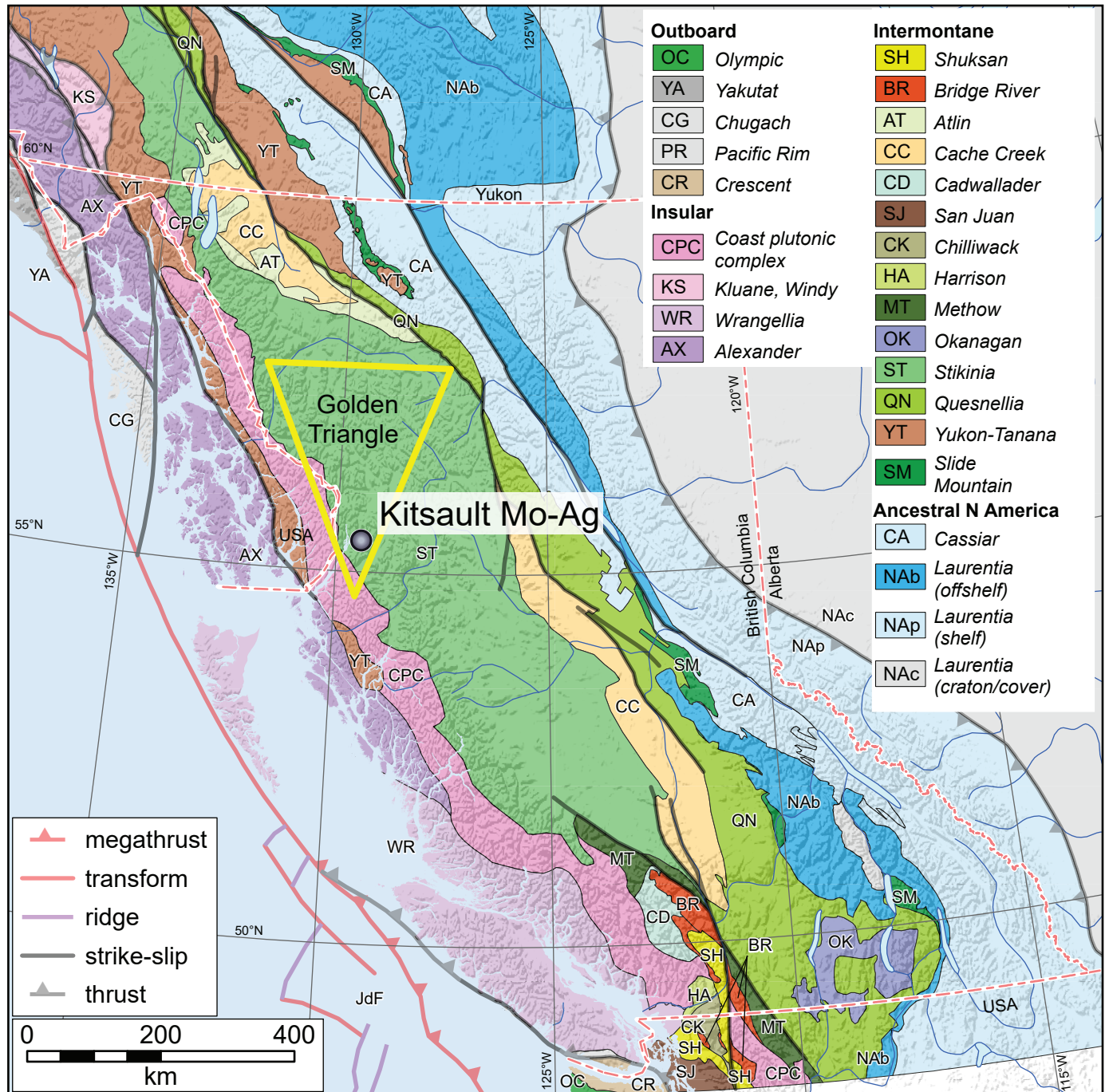


Fig. 1. Location of Kitsault Mo-Ag porphyry mine and the Golden Triangle. Terranes after Colpron (2020).

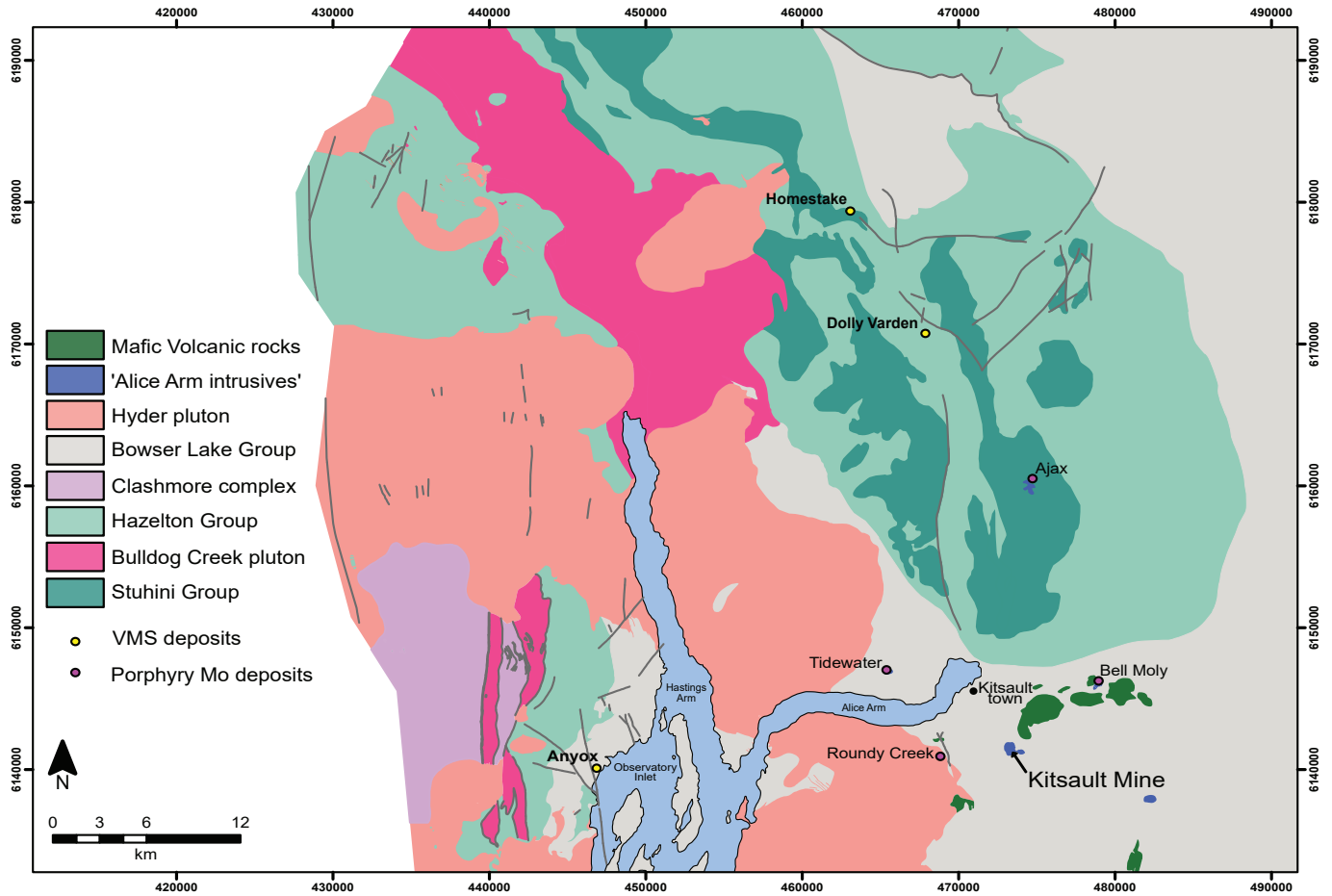


Fig. 2. Regional geology of the Kitsault Mo-Ag mine with selected porphyry Mo, and volcanogenic massive sulphide deposits. NAD83, UTM zone 9. Modified after Colpron and Nelson (2011).

In the Kitsault area (Fig. 2), stratified units include the Bowser Lake Group (Upper Jurassic), which consists of interbedded greywacke and argillite with minor limestone and conglomerate (Steinger, 1985). A suite of Coast Plutonic complex granodiorite to quartz monzonite stocks, commonly referred to as the 'Alice Arm intrusives', were emplaced between 55 and 50 Ma (Carter, 1981). Some of these stocks host Mo, including Kitsault, Roundy Creek, Bell Moly, Tidewater, and Ajax (Fig. 2). Post-mineralization, a swarm of 36 to 34 Ma, northeast-striking, lamprophyre dikes intruded the Bowser Lake Group and Alice Arm intrusives. The youngest igneous rocks in the area are 1.60 to 0.62 Ma plateau-type basaltic flows and related vesicular dikes (Steinger, 1985).

3. Kitsault Mo-Ag deposit

The Kitsault Mo-Ag mine is a low-F porphyry Mo deposit 6 km southeast of the town of Kitsault (Fig. 2). The mine site is approximately 600 m above sea level in an area of significant relief. Molybdenum mineralization is manifested as disseminations, quartz vein stockworks, and sheeted vein arrays that define a cylindrical mineralized body (Figs. 3, 4).

This body has an internal barren core, 100-150 m wide on its east, west, and north sides, and at least 300 m wide on its south side. For this study, we logged and sampled 15 drill holes (A-A', B-B'; Figs. 3, 5). These holes were drilled post-mining by Avanti Mining Ltd in 2008 and 2011 and intersect the Lime Creek intrusive complex and sedimentary rocks of the Bowser Lake Group (Figs. 3, 5). We collected 158 samples for further petrographic and geochemical study.

Surrounding the Lime Creek intrusive complex, the Bowser Lake Group consists of variably hornfelsed interbedded argillite and greywacke with lesser conglomerate and limestone (Figs. 3, 6a). Steinger (1985) determined that the argillite and greywacke consist of variable proportions of plagioclase, quartz, chert, sericite, and chlorite. The sedimentary rocks have been thermally altered up to 750 m from the contact with the Lime Creek intrusive complex (Fig. 3). The hornfels is zoned from a weakly developed albite-epidote outer zone, to a medial moderately developed biotite zone, to an inner zone that has more intensely developed biotite (Fig. 6a). In the biotite hornfels zones, calcareous horizons have been altered to skarn consisting of epidote, carbonate, and garnet.

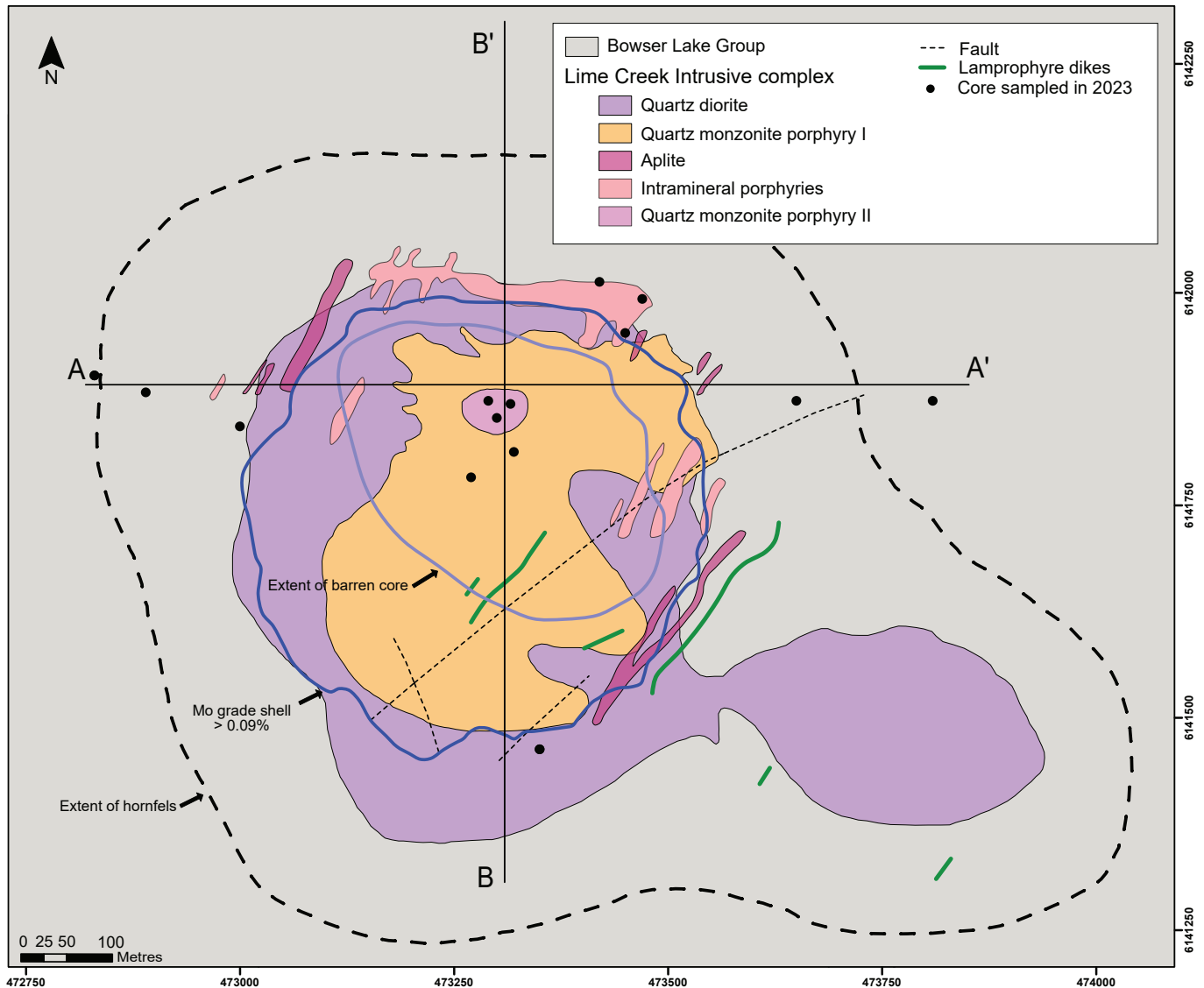


Fig. 3. Relationships of phases in the Lime Creek intrusive complex, Mo grade shell, and extent of the barren core. See Figure 5 for cross sections A-A' and B-B'. NAD83, UTM zone 9. Modified after Fulton (2014).

3.1. Lime Creek intrusive complex

In this study, the intrusive rocks have been named according to the most recent technical reports (Barresi, 2011; Fulton, 2014). The intrusive complex largely consists of equigranular to variably porphyritic granitic rocks consisting of feldspar, quartz, and biotite. Three major phases have been delineated, including quartz diorite, quartz monzonite porphyry I, and quartz monzonite porphyry II (Figs. 3, 5, 6).

Quartz diorite is the oldest phase. It can be distinguished based on its darker appearance, equigranular texture, and presence of minor amphibole (Figs. 6b, d). Quartz diorite encircles quartz monzonite porphyry I and is the unit most observed in contact with the surrounding hornfelsed argillite and greywacke of the Bowser Lake Group (Figs. 3, 5). Quartz monzonite porphyry I crosscuts quartz diorite, forming an embedded ~500 m-wide plug (Figs. 3, 5). The plug has steeply

outward-dipping contacts with the enclosing quartz diorite. The contacts are locally obscured by hydrothermal alteration, but where visible are sharp (Fig. 6d). Both quartz diorite and quartz monzonite porphyry I host Mo mineralization and are crosscut by many of the vein stages, showing no changes in Mo grade at or across the contacts (Fig. 3). Quartz monzonite porphyry II apparently postdates most of the economic Mo mineralization but is crosscut by quartz-carbonate veins (Fig. 7g). This unit has a more conspicuous porphyritic appearance than quartz diorite and quartz monzonite porphyry I (Fig. 6) and can also be distinguished by the presence of feldspar rafts and a greater abundance of quartz phenocrysts (Fig. 6e). This unit forms an elliptical plug roughly coincident with the barren core of the deposit (Figs. 3-5).

A variety of dikes have been observed within and surrounding the Lime Creek intrusive complex. Sets of well-mineralized



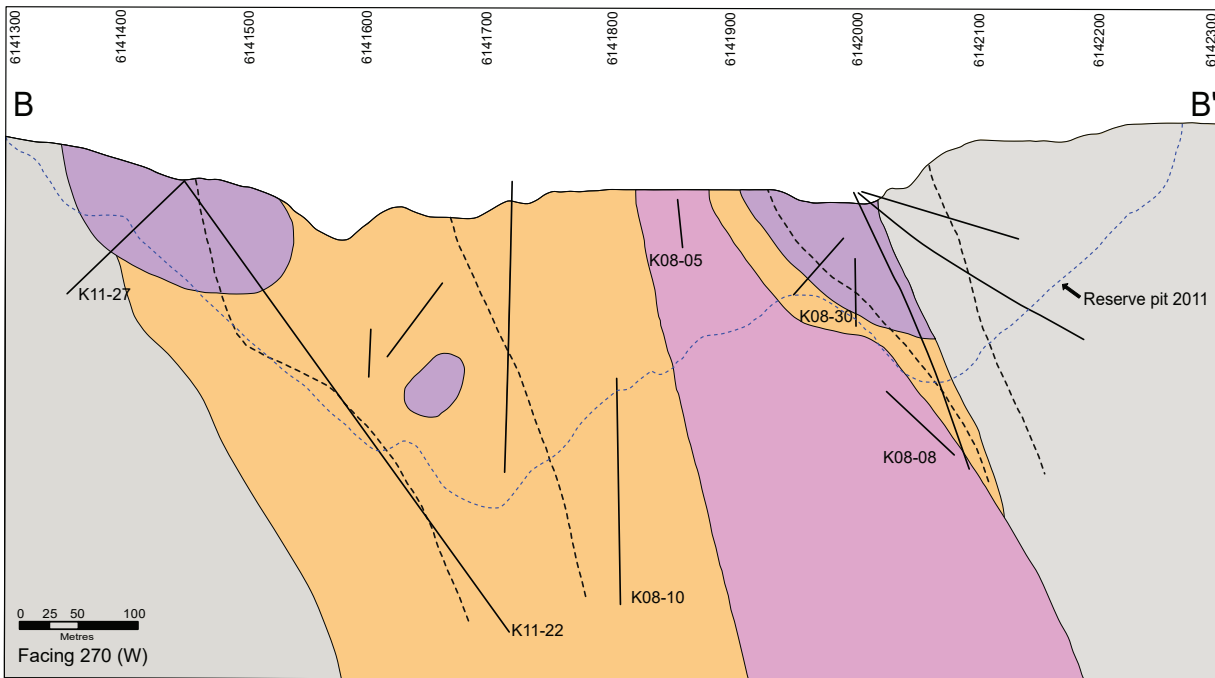
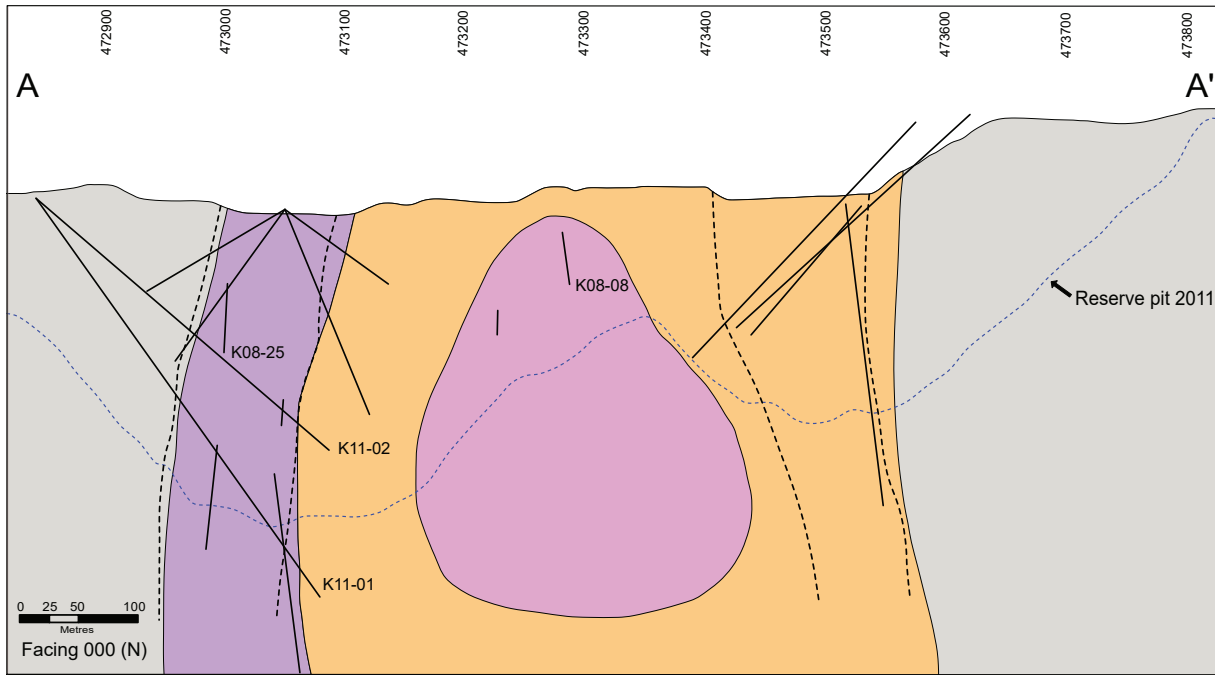
Fig. 4. Aerial photograph taken from a drone in 2023. The image shows the Kitsault Mo-Ag mine and an outline of the barren core depicted in Figure 3. View to the west.

aplite dikes crosscut the quartz diorite and quartz monzonite porphyry I but are absent in the quartz monzonite porphyry II (Figs. 3, 7g). Based on observations made during drill core logging, these dikes are the only unit to contain molybdenite disseminations and are spatially coincident with abundant quartz-molybdenite veins (Carter, 1981; Fulton, 2014). These north-striking dikes have been mapped along strike for 15-75 m (Fulton, 2014), and have been observed in drill core to have apparent widths of 0.5-15 cm. These dikes can cluster, forming sheeted zones with a cumulative width of 10 m or more (Fulton, 2014).

The aplite dikes locally have a sucrose texture, but they also present as pegmatitic pods of K-feldspar and quartz (Fig. 7e). Elsewhere, layers of quartz are apparently semi-parallel, wavy, heterogranular, and monomineralic (cf. Müller et al., 2023) and are interlayered with aplite (Figs. 7c-f). Some quartz layers have a more irregular form showing diffuse margins (Figs. 7a, c).

Near some of the quartz layers, irregular shaped cavities have formed that are lined with inward projecting crystals of quartz (Fig. 7f). These features are the oldest observed segregations of quartz observed at Kitsault and are crosscut by every quartz-bearing vein stage.

A separate set of dikes has been referred to as “Intramineral dikes” by Steininger (1985) and Fulton (2014). The affinity of the “Intramineral dikes” is not well known; they have been hypothesized to be related to quartz monzonite porphyry II on the basis of texture, chemistry, and spatial relationships (Steininger, 1985). Our preliminary observations suggest that they have been subjected to more intense hydrothermal alteration and veining than the quartz monzonite porphyry II and can be distinguished by the presence of amphibole and less biotite (Figs. 6f, 7g). The youngest intrusive phase observed at Kitsault during this study consists of northeasterly striking, 0.5 to 10 m-wide biotite- and hornblende-phyric lamprophyre



- Bowser Lake Group
- Quartz diorite
- Quartz monzonite porphyry I
- Quartz monzonite porphyry II
- Drill traces
- Fault

Fig. 5. Cross sections of the Kitsault mine; see Figure 3 for locations. Labeled drill traces represent holes sampled in 2023. The trace of the 2011 reserve pit indicates previously economic Mo grade. The quartz monzonite porphyry II is spatially coincident with the barren core of the deposit. The aplite, intramineral porphyries, and lamprophyre dikes, which are all narrow, apparently sporadic, and difficult to trace between drill holes are not shown. The aplite dikes and intramineral porphyries mainly occur within quartz diorite and quartz monzonite porphyry I, with narrow branches observed crosscutting the Bowser Lake Group sedimentary rocks. The lamprophyre dikes crosscut every phase of the Lime Creek intrusive complex and the Bowser Lake Group. NAD83, UTM zone 9.

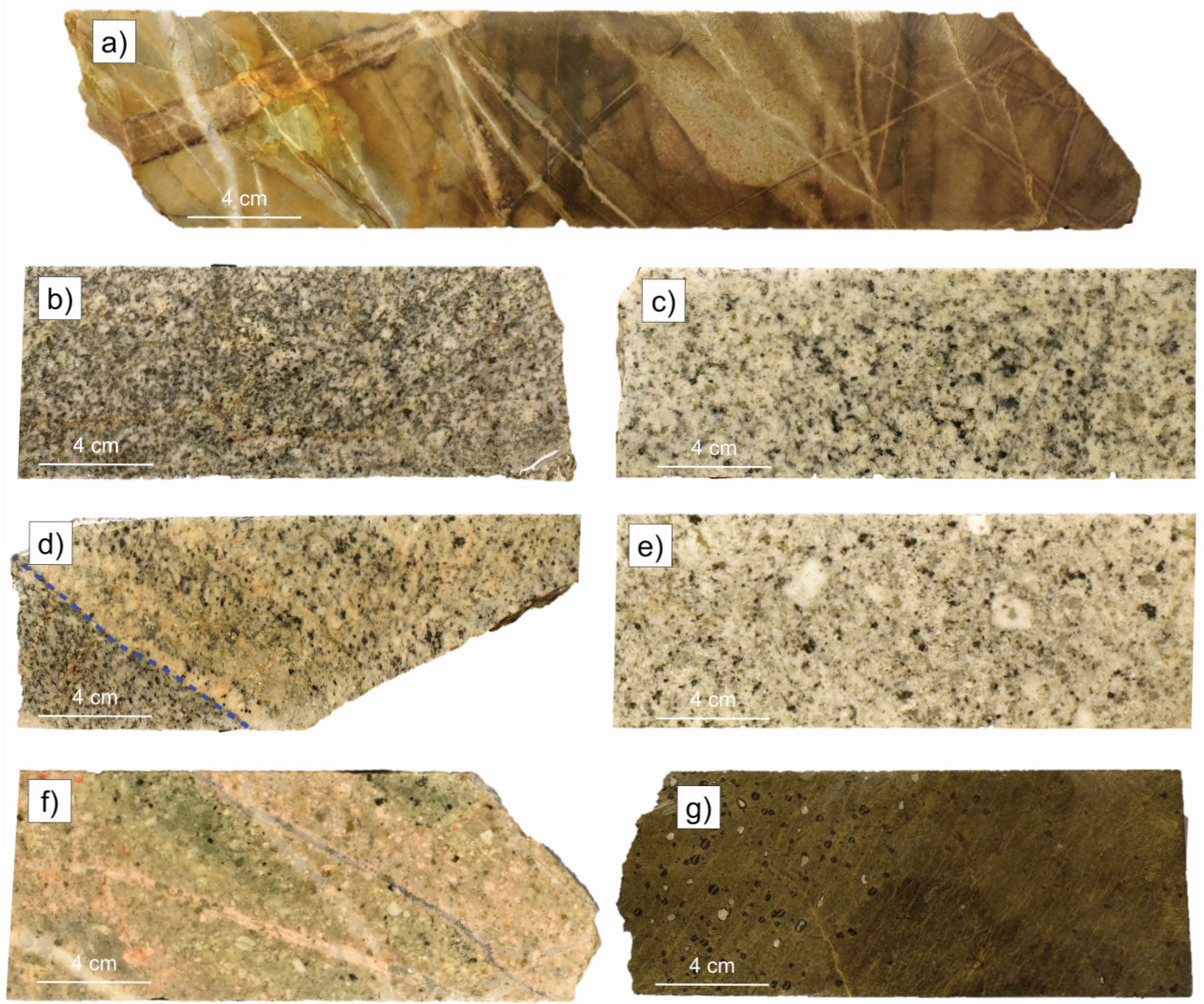


Fig. 6. Representative drill core photographs of the main rock types found at the Kitsault Mo-Ag deposit. **a)** Biotite hornfels greywacke containing fine-grained, disseminated pyrite and numerous quartz veins. **b)** Quartz diorite. **c)** Quartz monzonite porphyry I. **d)** Contact between quartz monzonite porphyry I and quartz diorite (the blue dashed line delineates the contact). **e)** Quartz monzonite porphyry II. **f)** Intramineral porphyry. **g)** Lamprophyre.

dikes (Figs. 3, 6g). These dikes crosscut every phase of the Lime Creek intrusive complex and the surrounding Bowser Lake Group sedimentary rocks (Fig. 3). The lamprophyres do not contain any molybdenite mineralization. They are crosscut by rare calcite veins (Steinger, 1985).

3.2. Veins

We observed four distinct hydrothermal vein stages. The oldest observed vein stage is quartz-molybdenite±pyrite veinlets, veins and stockworks that are well developed within and surrounding the aplite dikes (Figs. 7a-c), but rare or absent in the quartz monzonite porphyry II (Fig. 7g). Some of the quartz-molybdenite veins appear to originate internally to the aplite dikes, and can present subparallel or oblique, and

in some cases are truncated at the dike margins (Figs. 7a-c). Many of these veins have K-feldspar±biotite halos, making up a significant amount of the potassic alteration observed in this study (Fig. 7h). Subparallel, 3-20 cm-wide, sheeted 'ribbon' quartz veins containing epitaxial bands of fine-grained molybdenite occur within the quartz diorite and quartz monzonite porphyry I (Fig. 8a), but do not occur within the aplite.

Pyrite veins and veinlets with subordinate molybdenite and quartz occur mostly within the hornfelsed argillite and greywacke (Fig. 8b). These structures locally have pyrite-sericite-quartz halos and have not been observed in direct relationship with the above quartz veins. The youngest vein stage observed in this study consist of quartz-carbonate

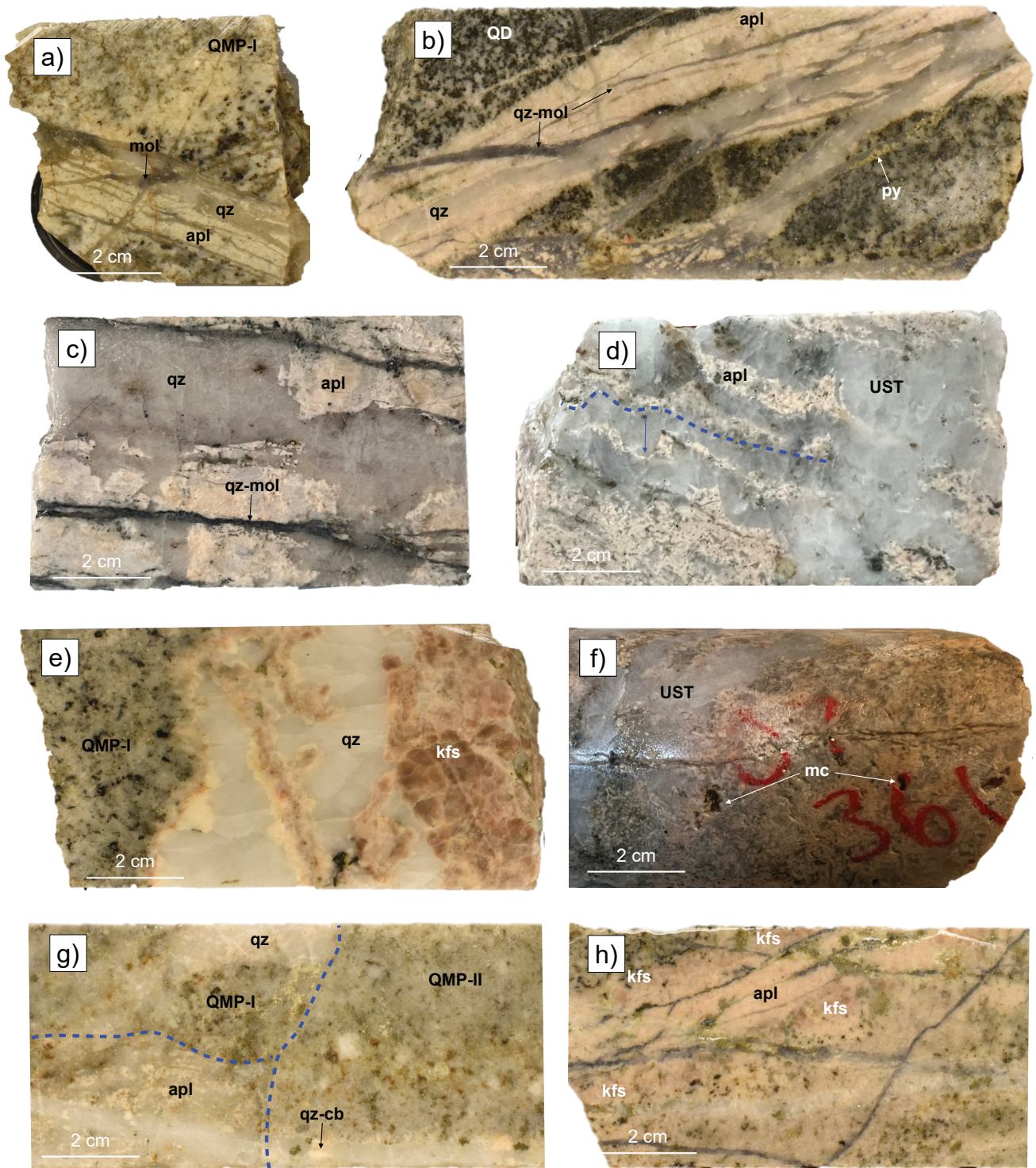


Fig. 7. Drill core photographs of aplite dikes and disequilibrium textures at the Kitsault Mo-Ag deposit. **a)** 2 cm-wide dike of interfingered aplite and quartz in quartz monzonite porphyry I, indicating mingling of magmatic silicate liquids and hydrothermal fluids. **b)** 4 cm-wide mineralized aplite dike with early quartz layers with diffuse margins, and quartz-molybdenite veins (with pyrite) locally internal to the aplite body and at low angles to the dike walls. **c)** Aplite dike with early quartz crosscut by quartz-molybdenite veins. **d)** Sequence of unidirectional solidification textures (UST; blue arrow marking c-axis) in an aplite dike, indicating rapid pressure fluctuations during dike emplacement. **e)** Pegmatite with K-feldspar and quartz. **f)** Mirolitic cavities on the backside of the sample in Figure 7d showing a close spatial relationship between mirolitic cavities and USTs. **g)** Three-way contact between aplite, QMP-I, and QMP-II (blue dashes). The QMP-II truncates the aplite and most quartz veins. A quartz-carbonate vein crosscuts aplite and QMP-II. **h)** Aplite dike with intensely developed K-feldspar alteration. Abbreviations: apl – aplite, kfs – K-feldspar, mc – mirolitic cavity, mol – molybdenite, py – pyrite, QD – quartz diorite, QMP-I – quartz monzonite porphyry I, QMP-II – quartz monzonite porphyry II, qz – quartz, qz-cb – quartz-carbonate vein, qz-mol – quartz-molybdenite vein, UST – unidirectional solidification textures.

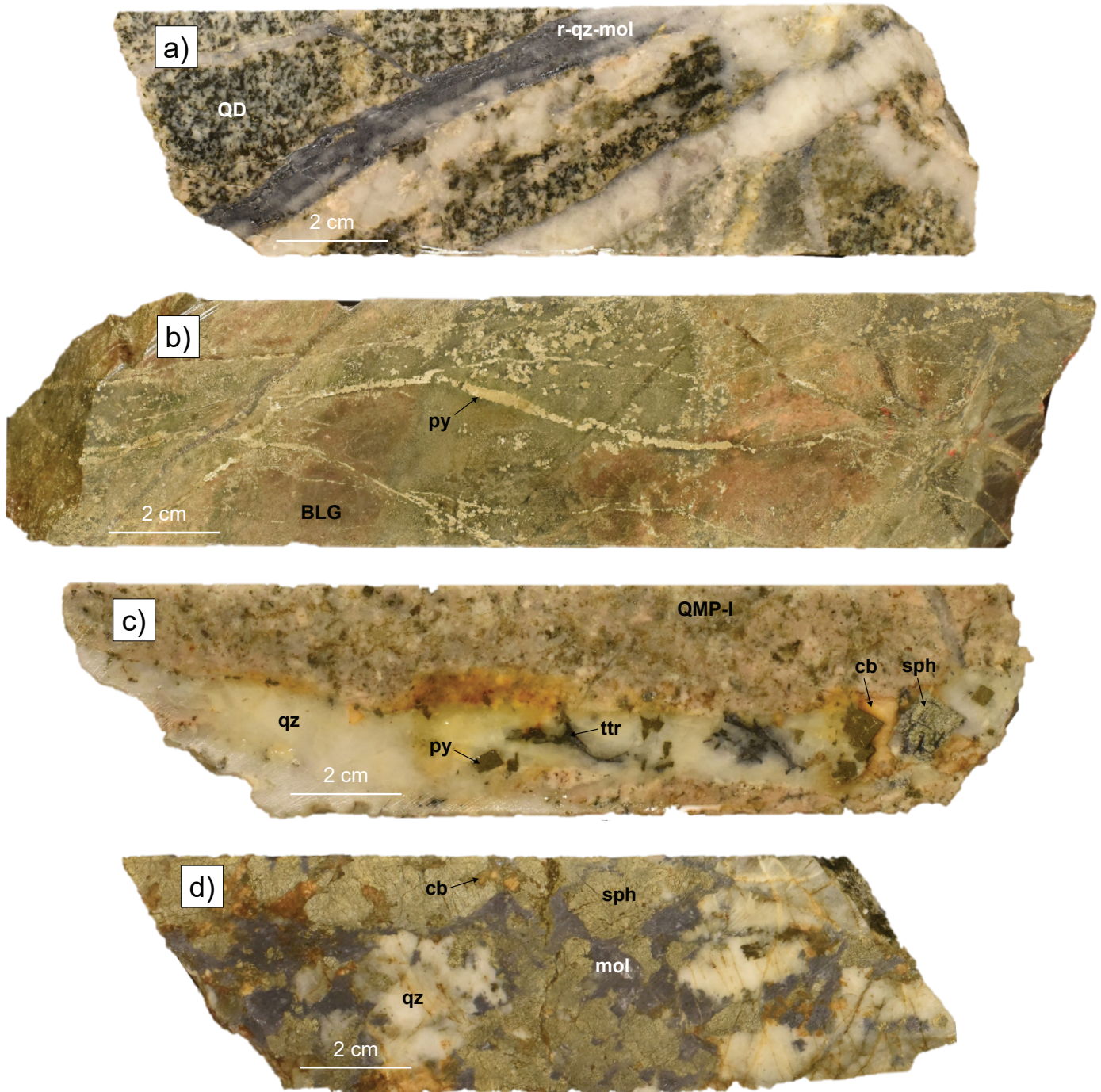


Fig. 8. Drill core photographs of vein stages at the Kitsault Mo-Ag deposit. **a)** Ribbon quartz-molybdenite vein crosscutting quartz diorite. These veins are typically >1.5 cm-wide and contain multiple epitaxial bands of molybdenite alternating with quartz. **b)** Bowser Lake Group sedimentary rock crosscut by pyrite veins and veinlets. **c)** 2 cm-wide polymetallic quartz-carbonate vein that is predominantly quartz with subordinate carbonate, sphalerite, pyrite and tetrahedrite. **d)** >8 cm-wide polymetallic quartz-carbonate vein that is predominantly sphalerite, quartz, and molybdenite with subordinate carbonate and pyrite. Abbreviations: BLG – Bowser Lake Group, cb – carbonate, mol – molybdenite, QD – quartz diorite, r-qz-mol – ribbon quartz-molybdenite vein, sph – sphalerite, ttr – tetrahedrite.

with variable amounts of sphalerite, galena, chalcopyrite, molybdenite and Pb-Bi sulphosalts (Figs. 8c, d). These veins are best developed on the south side of the deposit and crosscut every unit except for the lamprophyre dikes.

4. Discussion

4.1. Magmatic to hydrothermal transition

Unidirectional solidification textures (USTs) can act as useful pathfinders to mineralization in porphyry deposits (Shannon et al., 1982; Lowenstern and Sinclair, 1996; Bain et al., 2022; Müller et al., 2023). Rather than being considered veins, they are layers of hydrothermal or magmatic crystals (typically quartz) with a common growth direction (hence unidirectional), perpendicular to lithological interfaces. These quartz layers crystallize from an exsolved, magmatic fluid/melt that accumulated at the top or margins of shallow intrusions (Lowenstern and Sinclair, 1996; Seo et al., 2021). The fluid/melt act as a medium for rapid diffusion and transport of silica from the crystallizing magma to the growing quartz layers (Müller et al., 2023), and formation of successive quartz UST layers may result from cyclical fluctuations in the P-T-X conditions of this fluid/melt. A mechanism to reduce pressure rapidly is by hydraulic fracturing of the wall-rock (e.g., Candela, 1989), which allows fluid escape through accommodating structures, and then portions of the underlying melt quench against the quartz layer as aplite. These escape structures then heal due to mineral precipitation resulting in renewal of hydrostatic pressure build up, and quartz then nucleates on the newly formed aplite and grows toward the volatile-rich, over-pressured environment. Hydrostatic pressure continues to build until the process is repeated. This is the first study to document similar structures at Kitsault (Fig. 7d). These interpreted USTs are similar to textures observed at the Henderson Mo mine (Shannon et al., 1982). Further petrographic work is required to confirm what other minerals are present (e.g., molybdenite or other sulphides and oxides) and determine intricate growth sequences. The formation of USTs is the first stage of melt segregation from a crystal mush that sequesters metals from silica melts leading to the subsequent precipitation of the metals, which is consistent with the abundant early quartz-molybdenite veins that crosscut the aplite dikes at Kitsault (Figs. 7b, c).

Unidirectional solidification textures are only one type of disequilibrium texture associated with the magmatic to hydrothermal transition that can occur in porphyry deposits. At Kitsault, USTs occur together with pegmatite segregations (Fig. 7e) and cavities (Fig. 7d), that are interpreted here to be miarolitic cavities due to their irregular shape, inward-projecting crystals and close spatial relationship with USTs (e.g., Candela, 1997). Miarolitic cavities are formed by bubble growth during magma ascent and are locked in place by the rapid quenching of the melt due to decompression (Candela, 1997); they are direct evidence for volatile phase saturation and exsolution. Pegmatites in the aplite dikes are composed of coarse K-feldspar and quartz crystals (Fig. 7e) and indicate that the melt was subjected to undercooling (e.g., London, 1992;

London and Morgan, 2012). Together, these features indicate melt immiscibility, volatile exsolution and enrichment at the apex and margins of the aplite dikes.

4.2. Fluid transport in crystal mush dikes

There are no observed magmatic-hydrothermal features in the early Lime Creek intrusives (quartz diorite, quartz monzonite porphyry I, quartz monzonite porphyry II) to suggest exsolution of mineralizing fluids (e.g., miarolitic cavities, USTs, internally derived veins), and there are no abrupt changes in vein abundance at intrusive contacts. These intrusives are crosscut by quartz-molybdenite veins and other mineralization (Figs. 7a, c), but the source of the fluids is likely from elsewhere. Therefore, these intrusions are interpreted as a passive host to mineralization at Kitsault.

Multiple generations of aplite dikes occur throughout the Kitsault deposit. They typically crosscut the quartz diorite and quartz monzonite porphyry I, but have an unclear relationship with the intramineral porphyry dikes (Fig. 7g). The aplite dikes are truncated by the quartz monzonite porphyry II (Fig. 7g). The aplite dikes contain magmatic to hydrothermal transition textures (e.g., USTs, pegmatite segregations, miarolitic cavities; cf. ‘vein dikes’ from Henderson Mo deposit; Shannon et al., 1982; Kirkham and Sinclair, 1988), as well as disseminated molybdenite mineralization indicating that they formed contemporaneous with early- to syn-mineralization. Based on field observations, the potassic alteration and quartz-molybdenite veining at Kitsault is well developed and typically intense surrounding the aplite dikes, suggesting that they contributed significantly to hydrothermal alteration and substantive hypogene mineralization. The presence of interfingering aplite and quartz segregations that appear to pinch and swell within the aplite dikes (cf. ‘parting veins’, which are quartz veins that contain numerous septa or partings of aplite; Kirkham and Sinclair, 1988; Figs. 7a, b), as well as early internal, continuous and irregular quartz veins that are subparallel and locally bound by the aplite margins suggests there is a hydrothermal component (Figs. 7a, b); whereas aplite is generally considered to be of entirely magmatic origin. These textures together suggest that the aplitic melts functioned as a magmatic crystal mush framework producing fluid exsolution (e.g., evidenced by the miarolitic cavities). This interconnected permeable framework may have acted as a conduit for the upward migration of pressurized mineralizing fluids from an underlying parent magma (e.g., Carter et al., 2021).

5. Conclusions

The Lime Creek intrusive Complex, which hosts the Kitsault Mo-Ag porphyry deposit, intruded the Bowser Lake Group sedimentary rocks during the Paleogene, and exhibits a variety of magmatic-hydrothermal disequilibrium textures that provide insights into the mechanisms that formed the deposit. Upward emplacement of quartz diorite to quartz monzonite magmas formed numerous generations of porphyry stocks and aplite dikes, which have complex relationships with mineralization.

Fluid/melt flow and crystallization within the aplite dikes during periods of pressure change and undercooling likely formed layers of USTs, and resultant fluid exsolution formed miarolitic cavities. The aplite structures acted as an important pathway for at least some of the fluid-saturated magmas and ore fluids at Kitsault to migrate through the deposit. Further work is required to identify other mechanisms that focused Mo-rich ore fluids. Some of the porphyry-style mineralization was focused as narrow zones around the aplite dikes, which was largely disrupted by a late mineralization quartz monzonite stock lacking mineralized aplite (quartz monzonite porphyry II).

Acknowledgments

We thank Shane Uren and New Moly LLC for logistical support and providing access to the Kitsault mine and data. A special thanks to Chris Grant and Jocelyn White from Wildwood Engineering & Environmental Ltd. for managing the camp and providing guidance. Thanks to Eric Franz and Jenna Keen for providing access to their drone photos. Constructive reviews and comments by JoAnne Nelson and Tony Barresi helped improve the paper.

References cited

- Bain, W.M., Lecumberri-Sanchez, P., Marsh, E.E., and Steele-MacInnis, M., 2022. Fluids and melts at the magmatic-hydrothermal transition, recorded by unidirectional solidification textures at Saginaw Hill, Arizona, USA. *Economic Geology*, 117, 1543-1571.
<<https://doi.org/10.5382/econgeo.4952>>
- Barresi, T., 2011. Geological mapping, rock sampling, and data compilation on the Kitsault Property. Assessment Report, 75 p. Available from <http://sedar.com/>
- Brown, E.H., 2020. Magma loading in the southern Coast Plutonic complex, British Columbia and Washington. *Lithosphere*, article 8856566.
<<https://doi.org/10.2113/2020/8856566>>
- Bysouth, G.D., and Wong, G.Y., 1995. The Endako molybdenum mine, central British Columbia: An update. In: Schroeter, T.G., (Ed.), *Porphyry Deposits of the Northwestern Cordillera of North America*. Canadian Institute of Mining, Metallurgy, and Petroleum Special Volume 46, pp. 697-703.
- Candela, P.A., 1989. Felsic magmas, volatiles, and metallogenesis. In: Whitney, J.A., and Naldrett, A.J., (Eds.), *Ore Deposits Associated with Magmas*. *Reviews in Economic Geology* 4, pp. 223-233.
- Candela, P.A., 1997. A review of shallow, ore-related granites: textures, volatiles, and ore metals. *Journal of Petrology*, 38, 1619-1633.
- Carr, J.M., 1966. Geology of the Endako area, British Columbia. BC Department of Mines and Petroleum Resources, Annual Report, 1965, pp. 114-135.
- Carten, R.B., White, W.H., and Stein, H.J., 1993. High-grade granite-related molybdenum systems: Classification and origin. In: Kirkham, R.V., Sinclair, W.D., Thorpe, R.I., and Duke, J.M., (Eds.), *Mineral Deposits Modelling*. Geological Association of Canada Special Paper 40, pp. 521-554.
- Carter, N.C., 1981. Porphyry copper and molybdenum deposits, west central British Columbia. Canada Ministry of Energy, Mines and Petroleum Resources, British Columbia Geological Survey Bulletin 64, 150 p.
- Carter, L.C., Williamson, B.J., Tapster, S.R., Costa, C., Grime, G.W., and Rollinson, G.K., 2021. Crystal mush dykes as conduits for mineralising fluids in the Yerington porphyry copper district, Nevada. *Communications Earth & Environment*, 2, article 59.
<<https://doi.org/10.1038/s43247-021-00128-4>>
- Clarke, G., Northcote, B., Corcoran, N.L., Pothorin, C., Heidarian, H., and Hancock, K., 2024. Exploration and Mining in British Columbia, 2023: A summary. In: *Provincial Overview of Exploration and Mining in British Columbia, 2023*. British Columbia Ministry of Energy, Mines and Low Carbon Innovation, British Columbia Geological Survey Information Circular 2024-01, pp. 1-53.
- Colpron, M., 2020. Yukon terranes-A digital atlas of terranes for the northern Cordillera. Yukon Geological Survey.
<<https://data.geology.gov.yk.ca/Compilation/2#InfoTab>>
- Colpron, M., and Nelson, J.L., 2011. A digital atlas of terranes for the Northern Cordillera; British Columbia Ministry of Energy and Mines, British Columbia GeoFile 2011-11.
- Fulton, S., 2014. Kitsault molybdenum project British Columbia, Canada. NI 43-101 Technical Report, 327 p. Available from <http://sedar.com/>
- Gehrels, G., Rusmore, M., Woodsworth, G., Crawford, M., Andronicos, C., Hollister, L., Patchett, J., Ducea, M., Butler, R., Klepeis, K., Davidson, C., Friedman, R., Haggart, J., Mahoney, B., Crawford, W., Pearson, D., and Girardi, J., 2009. U-Th-Pb geochronology of the Coast Mountains batholith in north-coastal British Columbia: Constraints on age and tectonic evolution. *Geological Society of America Bulletin* 121, pp. 1341-1361.
<<https://doi.org/10.1130/B26404.1>>
- George, S.W.M., Nelson, J.L., Alberts, D., Greig, C.J., and Gehrels, G.E., 2021. Triassic-Jurassic accretionary history and tectonic origin of Stikinia from U-Pb geochronology and Lu-Hf isotope analysis, British Columbia. *Tectonics*, 40, article e2020TC006505.
<<https://doi.org/10.1029/2020TC006505>>
- John, D.A., and Taylor, R.D., 2016. By-products of porphyry copper and molybdenum deposits. *Reviews in Economic Geology*, 18, 137-164.
- Kirkham, R.V., and Sinclair, W.D., 1988. Comb quartz layers in felsic intrusions and their relationship to the origin of porphyry deposits. In: Taylor R.P., and Strong, D.F., (Eds.), *Recent Advances in the Geology of Granite-related Mineral Deposits*. Canadian Institute of Mining Metallurgy Special Volume 39, pp. 50-71.
- London, D., 1992. The application of experimental petrology to the genesis and crystallisation of granitic pegmatites. *Canadian Mineralogist*, 30, 499-540.
- London, D., and Morgan, G.B., 2012. The pegmatite puzzle. *Elements*, 8, 263-268.
<<https://doi.org/10.2113/gselements.8.4.263>>
- Lowenstern, J.B., and Sinclair, W.D., 1996. Exsolved magmatic fluid and its role in the formation of comb-layered quartz at the Cretaceous Logtung W-Mo deposit, Yukon Territory, Canada. *Trans Royal Society of Edinburgh*, 87, 291-303.
- Müller, A., Kirwin, D., and Seltmann, R., 2023. Textural characterization of unidirectional solidification textures related to Cu-Au deposits and their implication for metallogenesis and exploration. *Mineralium Deposita*, 58, 1211-1235.
<<https://doi.org/10.1007/s00126-023-01175-x>>
- Natural Resources Canada, 2022. The Canadian critical minerals strategy. 52 p.
<<https://www.canada.ca/en/campaign/critical-minerals-in-canada/canadian-critical-minerals-strategy.html>> (date accessed November 26, 2023).
- Nelson, J., 2017. Composite pericratonic basement of west-central Stikinia and its influence on Jurassic magma conduits: Examples from the Terrace-Ecstall and Anyox areas. In: *Geological Fieldwork 2016*, British Columbia Ministry of Energy and Mines, British Columbia Geological Survey Paper 2017-1, pp. 61-82.
- Nelson, J.L., and van Straaten, B.I., 2020. Recurrent syn- to post-subduction mineralization along deep crustal corridors in the Iskut-

- Stewart-Kitsault region of western Stikinia, northwestern British Columbia. In: Sharman, E.R., Lang, J.R., and Chapman, J.B., (Eds.), *Porphyry Deposits of the Northwestern Cordillera of North America: A 25-Year Update*. CIM Special Volume 57, pp. 149-211.
- Nelson, J.L., van Straaten, B.I., and Friedman, R., 2022. Latest Triassic-Early Jurassic Stikine-Yukon-Tanana terrane collision and the onset of accretion in the Canadian Cordillera: Insights from Hazelton Group detrital zircon provenance and arc-back-arc configuration. *Geosphere*, 18, 670-696.
<<https://doi.org/10.1130/GES02444.1>>
- Selby, D., and Creaser, R.A., 2001. Re-Os geochronology and systematics in molybdenite from the Endako porphyry molybdenum deposit, British Columbia, Canada. *Economic Geology*, 96, 197-204.
- Selby, D., Nesbitt, B.E., Muehlenbachs, K., and Prochaska, W., 2000. Hydrothermal alteration and fluid chemistry of the Endako porphyry molybdenum deposit, British Columbia. *Economic Geology*, 95, 183-202.
- Seo J.H., Kim, Y., Lee, T., and Guillong, M., 2021. Periodically released magmatic fluids create a texture of unidirectional solidification (UST) in ore-forming granite: a fluid and melt inclusion study of W-Mo forming Sannae-Eonyang Granite, Korea. *Minerals*, 11, article 888.
<<https://doi.org/10.3390/min11080888>>
- Shannon, J.R., Walker, B.M., Carten, R.B., and Geraghty, E.P., 1982. Unidirectional solidification textures and their significance in determining relative ages of intrusions at the Henderson Mine, Colorado. *Geology*, 10, 293-297.
- Sinclair, W.D., 2007. Porphyry deposits. In: Goodfellow, W.D., (Ed.), *Mineral deposits of Canada*. Geological Association of Canada Special Publication 5, pp. 223-243.
- Steininger, R.C., 1985. Geology of the Kitsault molybdenum deposit, British Columbia. *Economic Geology*, 80, 57-71.
- Villeneuve, M.E., Whalen, J.B., Anderson, R.G., and Struik, L.C., 2001. The Endako batholith: Episodic plutonism culminating with formation of the Endako porphyry molybdenum deposit, north-central British Columbia. *Economic Geology*, 96, 171-196.
- Whalen, J.B., Anderson, R.G., Struik, L.C., and Villeneuve, M.E., 2001. Geochemistry and Nd isotopes of the Francois Lake plutonic suite, Endako batholith: Host and progenitor to the Endako molybdenum camp, central British Columbia. *Canadian Journal of Earth Sciences*, 38, 603-618.



Sulphide mineralization at the E&L magmatic Ni-Cu-PGE deposit: Textural evidence for contamination, vapour saturation, fluid immiscibility, and metal remobilization

Matthew J. Brzozowski^{1, a}, and Katya Zaborniak¹

¹ British Columbia Geological Survey, Ministry of Energy, Mines and Low Carbon Innovation, Victoria, BC, V8W 9N3

^a corresponding author: Matthew.Brzozowski@gov.bc.ca

Recommended citation: Brzozowski, M.J., and Zaborniak, K., 2024. Sulphide mineralization at the E&L magmatic Ni-Cu-PGE deposit: Textural evidence for contamination, vapour saturation, fluid immiscibility, and metal remobilization. In: *Geological Fieldwork 2023*, British Columbia Ministry of Energy, Mines and Low Carbon Innovation, British Columbia Geological Survey Paper 2024-01, pp. 65-78.

Abstract

The E&L magmatic Ni-Cu-PGE sulphide deposit is hosted by a small (~150 m wide near surface) stock with an apparent conduit geometry comprising varitextured gabbroic to wehrlitic rocks that crosscut the Nickel mountain gabbro and Middle Jurassic sedimentary rocks of the Hazelton Group. Sulphide mineralization occurs as disseminated, blebby, net-textured, and (semi-)massive sulphides. Several lines of textural evidence suggest that assimilation of sedimentary rocks likely played a role in the sulphide saturation history of the E&L magma including: 1) mixtures of gabbroic rock and sedimentary rock in which the two have diffuse boundaries; 2) an association of carbonate with sulphides; and 3) an association of sulphides with felsic patches in mafic rock. Considering that the sedimentary country rocks also contain sulphides, direct addition of S, either via bulk or selective assimilation, also likely played a role. Compound structures, which comprise segregated sulphide blebs with rims of fine-grained hydrous silicates (interpreted as former vapour bubbles), are common in the E&L deposit and imply that: 1) the E&L magma was volatile rich; 2) the magmas were emplaced at shallow crustal levels to permit volatile exsolution; and 3) sulphide liquid was transported upwards through the intrusive plumbing system. The inferred volatility of the E&L magmas is consistent with the common occurrence of orbicular textures in the gabbros. We interpret these orbicules to represent saturation of the E&L magma in H₂O and exsolution of a hydrous fluid phase, with the orbicules representing the melt and the interstitial material representing the immiscible fluid. After crystallization of the stock and generation of the primary sulphide mineralization, it is likely that metals were remobilized by the circulation of hydrothermal fluids. This inference is supported by: 1) the pervasive alteration of the rocks; 2) the replacement of chalcopyrite by pyrite; 3) the replacement of olivine ± pyroxene by an assemblage of hydrous silicates and sulphides; 4) the replacement of magnetite in magnetite-ulvöspinel-ilmenite intergrowths by an assemblage of hydrous silicates and sulphides; 5) the occurrence of sulphides in late-stage veins that crosscut the host rocks; and 6) the replacement of sulphides by magnetite (i.e., S loss).

Keywords: E&L deposit, Ni-Cu-PGE, magmatic sulphide, metal remobilization, mineral textures

1. Introduction

Nickel, Cu, Co, and the platinum-group elements (PGE) are considered critical metals because they are essential components of the batteries, electronics, and alloys that are needed for the transition to low-carbon emission economies. Intracontinental mafic-ultramafic intrusion-hosted magmatic sulphide deposits are the main global hosts of Ni and PGE resources (Mudd and Jowitt, 2014, 2022; Mudd et al., 2018) and are also significant hosts of Cu and Co. Although convergent-margin mafic-ultramafic intrusions are known to contain significant concentrations of PGE in Alaskan-type deposits (e.g., Tulameen, Nixon et al., 2018; Polaris, Milidragovic et al., 2021, 2023), they have generally not been considered good targets for other critical metals like Ni. Yet, several arc-related, mafic-ultramafic-hosted deposits exist globally that are base-metal enriched, including Giant Mascot and Turnagain in British Columbia (Scheel, 2004; Jackson-Brown et al., 2014; Manor et al., 2014, 2016), the Huangshan camp (Gao et al., 2013; Mao et al., 2015; Wang et al., 2021), Halatumiao (Sun et al., 2021), and Taoke (Zhang et al., 2021) in China,

Aguablanca in Spain (Pina et al., 2010), Duke Island in Alaska (Thakurta et al., 2008; Stifter et al., 2016), Ferguson Lake in Nunavut (Acosta-Góngora et al., 2018), and Portneuf-Mauricie in Quebec (Sappin et al., 2009). Although the fundamental mechanisms by which arc-related magmatic sulphide deposits form are the same as in intracontinental settings (i.e., mantle partial melting, sulphide saturation, enrichment of sulphide liquid in metal by sulphide liquid-silicate melt interaction, and concentration of sulphide liquid; Naldrett, 2010), several aspects of their genesis remain poorly constrained, including mantle source composition, sulphide saturation and metal enrichment mechanisms, and the nature of the critical mineral hosts (e.g., sulphide, chromite, platinum-group minerals, and alloys). These ambiguities reflect that, relative to deposits in intracontinental settings (e.g., Noril'sk, Naldrett, 1992; Duluth, Lee and Ripley, 1995; Jinchuan, Li et al., 2005; Eagle, Ding et al., 2011; Voisey's Bay, Lightfoot et al., 2012; Marathon, Brzozowski et al., 2020), little research has been done on this subtype of the Ni-Cu-PGE sulphide system.

In British Columbia, Ni and the PGE are almost exclusively

hosted by mafic-ultramafic intrusions, many of which are Cu-bearing. Nickel-Cu-PGE deposits in British Columbia are principally hosted by Alaskan-type and other mafic-ultramafic intrusions in the Quesnel and Stikine terranes (Fig. 1; Nixon et al., 2020). These deposits exhibit a range of sulphide contents and host a variety of metals; some are endowed in the PGE, but have limited sulphide (e.g., Tulameen, Polaris), whereas others are endowed in base metals and are sulphide rich (e.g., Giant Mascot, Turnagain, E&L). The cause of this mineralogical and geochemical diversity remains poorly understood because

the mechanisms leading to the formation of many of these deposits have not been well studied. To address this deficiency and improve our understanding of convergent margin-related magmatic Ni-Cu-PGE sulphide deposits, we initiated a multi-year project of the E&L property in northwestern British Columbia (Fig. 1) in the traditional lands of the Tahltan First Nation. In collaboration with Garibaldi Resources Corp., the goals of this project are to: 1) determine the age of the E&L stock; 2) establish the magmatic source(s) of the E&L pluton; 3) assess the genetic relationship between the mineralized E&L

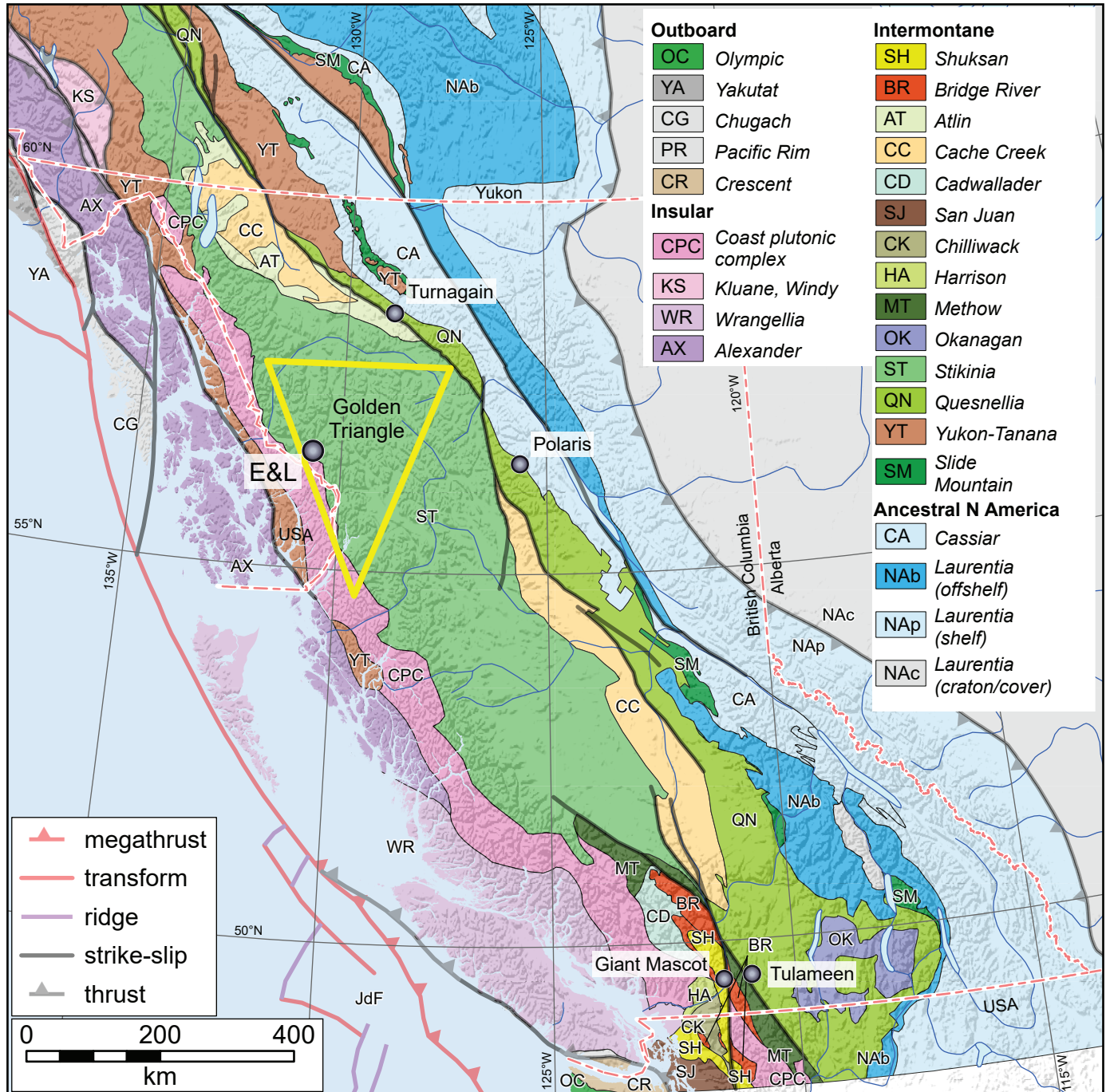


Fig. 1. Location of the E&L property in Stikine terrane. Terranes modified from Colpron (2020).

pluton and the barren country rocks of the Nickel mountain gabbro that it was emplaced into; 4) consider sulphide saturation and metal enrichment mechanisms and the possible role of Hazelton Group country rock assimilation; and 5) determine the hosts to the critical metals. In this initial report, we summarize the geometry of the E&L deposit based on drilling by Garibaldi Resources Corp., document the lithological, mineralogical, and textural variations observed throughout the E&L deposit based on examination of drill core samples, and provide preliminary interpretations into what these variations may indicate about the processes that generated the deposit.

2. Regional setting

The E&L property is in northern Stikinia, the northwest-trending terrane extending for about 1000 km along the length of the Canadian Cordillera and containing prominent Carboniferous to Middle Jurassic island arc-related volcano-sedimentary successions and allied intrusive rocks (Fig. 1; Nelson et al., 2013, 2022). The property is in the ‘Golden Triangle’, the popular name for a loosely defined area remarkably well-endowed with economic metals, with more than 150 deposits that have been mined since the end of the 19th

century, many proposed mines, numerous advanced exploration projects, and two current mines (Red Chris, Brucejack, Fig. 2; British Columbia Geological Survey, 2023). The main rock units in the region include the Stikine assemblage (lower Paleozoic), Stuhini Group (Upper Triassic), and the Hazelton Group (Upper Triassic to Middle Jurassic), and the alkalic to calc-alkaline intrusive rocks spatially and temporally related to these units. These units are covered by the Bowser Lake Group (Middle Jurassic) and cut by Cretaceous to Eocene rocks of the Coast Plutonic complex (Fig. 2).

3. Local geology

In the study area, the geology comprises mudstone, siltstone, and carbonate-rich rocks of the Spatsizi Formation (for Hazelton Group stratigraphy see Nelson et al., 2018) that were intruded by four 100-m wide plugs and one 800-m wide stock (Hancock, 1990), which Garibaldi Resources Corp. refer collectively to as the ‘Nickel mountain gabbro complex’. These plugs and stocks comprise equigranular Fe-Ti oxide-bearing gabbro and minor norite that intruded Hazelton Group volcano-sedimentary rocks at ca. 180 Ma (Fig. 3; Hancock, 1990; Chamberlain, unpublished zircon CA-TIMS U-Pb data,

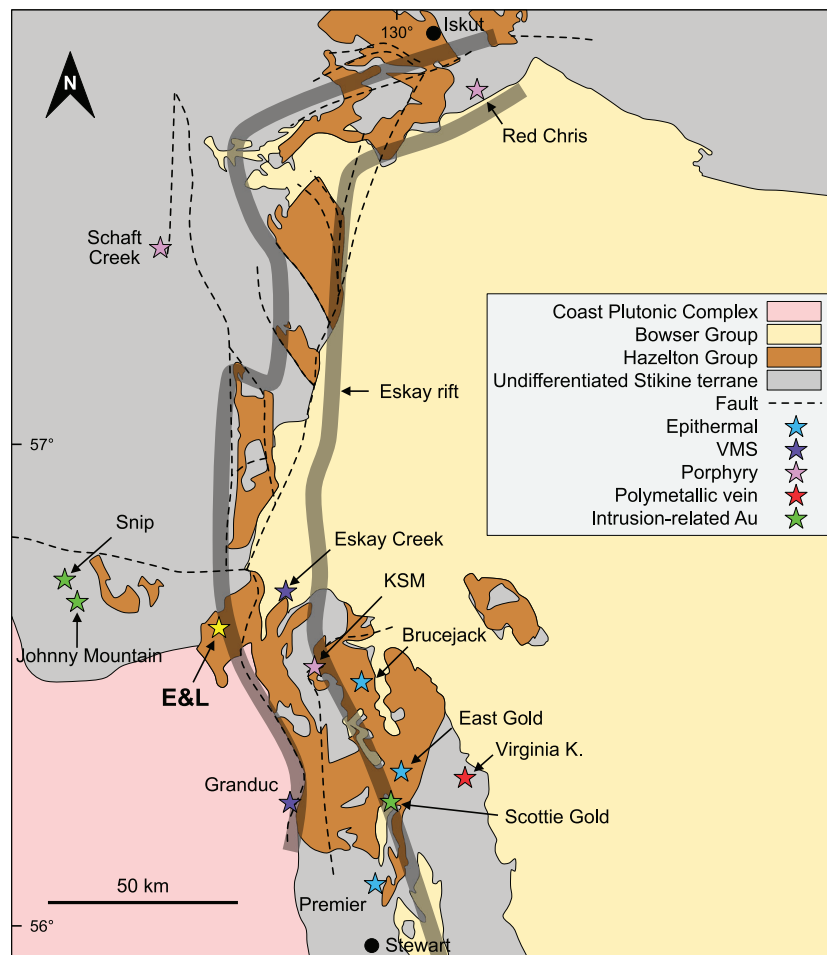


Fig. 2. Generalized geology of the Iskut River region showing the location of the E&L magmatic sulphide deposit, producing mines (Red Chris, Brucejack), and past-producing base metal deposits. Modified after Nelson et al. (2018). Outline of Eskay rift from Gagnon et al. (2012).

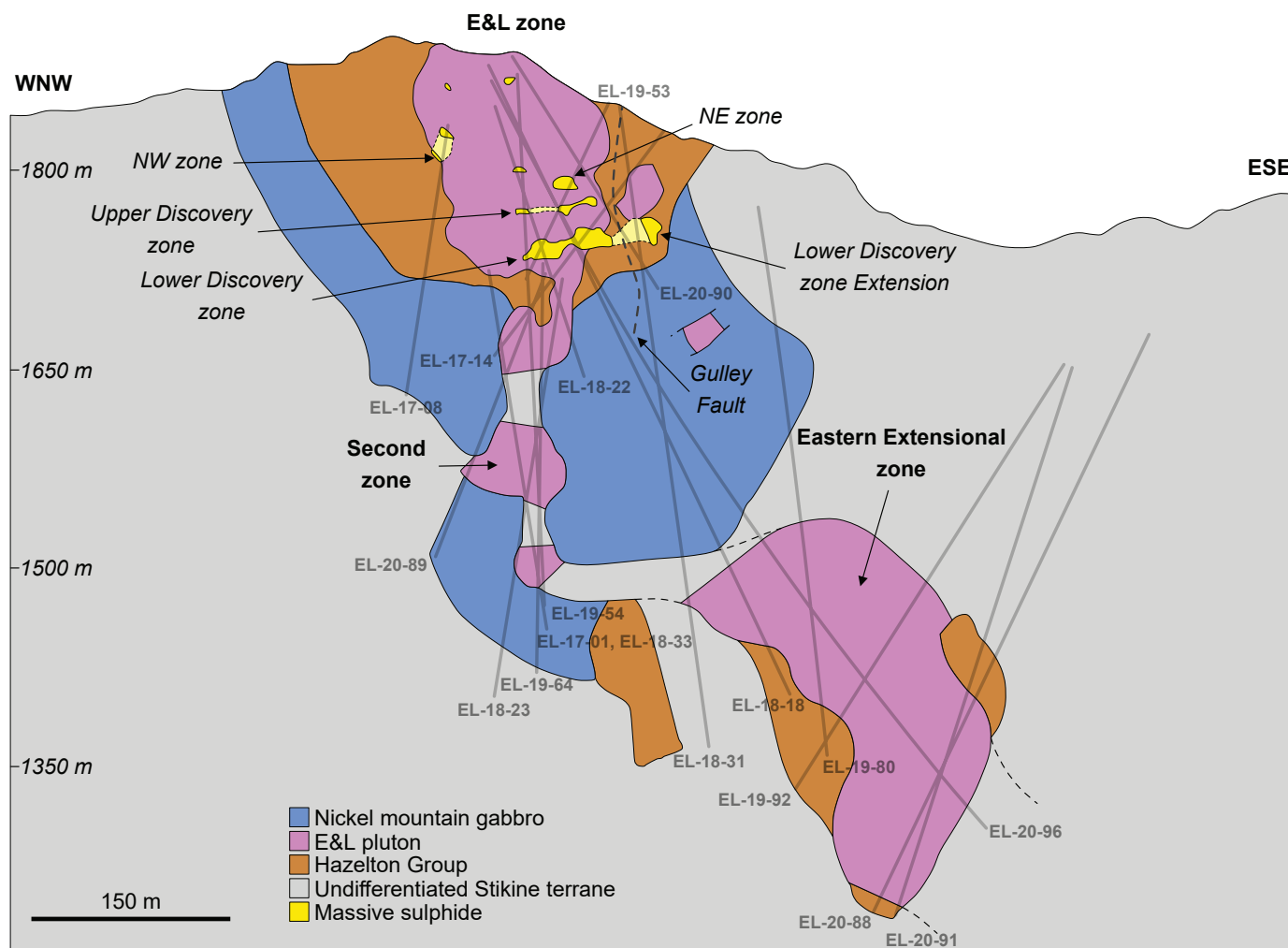


Fig. 3. Schematic cross-section of the E&L deposit illustrating the conduit-like geometry of the E&L pluton and its relationship to older gabbros and sedimentary rocks of the Hazelton Group, and the locations of massive sulphide orebodies. Modified after Hanson et al. (2022).

cited in Vandenberg, 2020). The E&L stock is a relatively small base- and precious-metal-mineralized deposit which, based on drilling data, appears to have a conduit geometry (~150 m wide near surface, ~250 m wide at depth) and to have intruded the Nickel mountain gabbro and sedimentary rocks (mudstones, siltstones, and carbonate-rich rocks) of the Spatsizi Formation (Fig. 3) on the southwestern flank of Nickel mountain. The stock outcrops at the top of Nickel mountain at ~1900 m asl and extends to a depth of at least 1200 m asl (Fig. 3). It comprises orbicular to varitextured Fe-Ti oxide-bearing olivine melagabbro, gabbronorite, and gabbro, with lesser wehrlite (Vandenberg, 2020). Rocks of the Nickel mountain gabbro and the E&L stock contain propylitic and potassic alteration assemblages and were metamorphosed to greenschist facies during regional ca. 110 Ma deformation (Alldrick et al., 1987; Hancock, 1990). The rocks lack macroscopic textural evidence for deformation. Of the gabbroic rocks in the area, only those of the E&L stock host significant magmatic Ni-Cu-PGE mineralization in the form of disseminated, net-textured, and semi-massive to massive pyrrhotite, pentlandite,

and chalcopyrite (Vandenberg, 2020). Based on whole-rock primitive mantle-normalized trace-element patterns, Nb-Ta depletion, and decoupled large ion lithophile and high field strength element signatures, Vandenberg (2020) suggested that the rocks of the Nickel mountain gabbro and E&L stock crystallized from subduction-derived magmas that originated from distinct mantle sources. For the E&L gabbros, Vandenberg (2020) suggested that the elevated forsterite contents of olivine (Fo_{78-84}) and low Ni-Co contents indicated they crystallized from a high-Mg parent magma, and that sulphide saturation likely occurred before olivine crystallization.

4. Deposit geology

Based on drilling data (Fig. 3), the E&L deposit appears to represent a conduit-type magmatic Ni-Cu-PGE sulphide system. The deposit has been informally subdivided by Garibaldi Resources Corp. into: 1) the E&L zone, which is exposed on Nickel mountain and extends to a depth of ~1700 m asl; 2) the Eastern Extensional zone, which extends to depths greater than at least 1500 m asl; and 3) the Second zone, which

connects these zones and has a thin (~50-100 m wide), pipe-like morphology (Fig. 3). Mineralization occurs within orbicular and taxitic gabbros of the E&L stock and comprises a textural spectrum of sulphides ranging from disseminated and blebby to net-textured to massive sulphide (pyrrhotite>chalcopyrite>pentlandite ±sphalerite, pyrite, violarite; Vandenberg, 2020). Disseminated and blebby sulphide mineralization contains 1-25 vol.% sulphide, with higher abundances in olivine-rich gabbros that have well-developed orbicules. Texturally, the sulphides may be interstitial to silicate and oxide minerals or occur as blebs. Net-textured sulphide (5-20 vol.%) represents a (semi-)continuous matrix of sulphide in a framework of olivine, clinopyroxene, and plagioclase. Semi-massive sulphide (20-90 vol.%) is at the boundaries of massive sulphide orebodies and commonly contains inclusions of recrystallized Hazelton Group country rock. Several massive sulphide (>90 vol.%) orebodies have been identified: Upper Discovery zone, Lower Discovery zone (largest), Northwest zone, and Northeast zone (Fig. 3). Many of the massive sulphide orebodies have been deformed, which may have remobilized some of the chalcopyrite. In terms of metal tenors, Cu, Pt, Pd, and Au concentrations are typically greatest at the tops of the massive sulphide orebodies, Rh concentrations are typically greatest in the central portion of the orebodies, and Ni concentrations are generally uniform (Lightfoot, pers. comm., 2023). Platinum-group minerals are uncommon, occurring primarily as tellurides (<1 vol.%; Vandenberg, 2020).

5. Sample descriptions

We collected five outcrop samples and 309 core samples from nine holes drilled by Garibaldi Resources Corp. between 2017 and 2020 at Nickel mountain. Representative samples were selected for thin section examination, and for future geochemical and isotopic analyses.

5.1. Hand samples

5.1.1. E&L stock

Variably mineralized samples of leucogabbro, melagabbro, olivine gabbro, varitextured gabbro, wehrlite, and mixtures of these rocks with sedimentary rock were collected from the E&L stock, including samples from the E&L zone (n=58), the Second zone (n=18), and the Eastern Extension zone (n=40). These samples largely consist of variable proportions of medium- to coarse-grained olivine, pyroxene, and plagioclase. Mineralization comprises disseminated (Fig. 4a), blebby (Fig. 4b), semi-massive, (Fig. 4c), and massive sulphide (Fig. 4d), mainly pyrrhotite, pentlandite, and chalcopyrite. Blebby sulphides are typically segregated into pyrrhotite-pentlandite-rich and chalcopyrite-rich portions, the latter with rims of fine-grained hydrous silicates (Fig. 4b). Some disseminated and blebby sulphides display rims of pyroxene (Fig. 4e). Many samples contain cm-scale orbicules with variable proportions of plagioclase, olivine, and clinopyroxene, an assemblage similar to the interstitial rock (Fig. 4f). Some of these orbicules exhibit crude zoning defined by modal

variations in the proportions of olivine+pyroxene versus plagioclase, with a mafic core and plagioclase-rich rim (Fig. 4f), and some have coarse centres surrounded by finer grained rims (Fig. 4f). A smaller variety of these orbicules is also common in many samples; these circular features also typically display a core of mafic minerals and a rim of plagioclase (Fig. 4g). The regions interstitial to the orbicules appear to be more mafic in composition and coarser grained; sulphides seem to largely be restricted to regions interstitial to the orbicules, but fine-grained sulphides also occur within them (Figs. 4f, g). Where orbicules touch one another, contacts are deformed, the finer grained cores are preserved, and the orbicules retain their individual identities rather than merging into a single body (Fig. 4g). Although most of the samples are mafic, comprising variably altered plagioclase, pyroxene, and olivine, a few samples contain felsic patches (Figs. 4c, h). The diffuse boundaries between Hazelton Group material and gabbro (Fig. 4i), and possibly these felsic patches, indicate interaction between mafic magma and sedimentary country rock. An additional 12 samples of what is potentially E&L gabbro were obtained from an exploratory hole drilled below glacial ice. These samples lack orbicules and significant sulphides, most of which are fine disseminations (Fig. 4j).

5.1.2. Nickel mountain gabbro and country rock

Samples from the Nickel mountain gabbro (n=80) include leucogabbro, melagabbro, and olivine gabbro. These gabbroic rocks are equigranular assemblages of variably altered plagioclase, pyroxene, olivine, and magnetite, with plagioclase-rich (Fig. 4k) and plagioclase-poor variants (Fig. 4l). In general, the subhedral-euhedral plagioclase ±magnetite and common interstitial pyroxene suggest that plagioclase and magnetite crystallized before pyroxene. Although not significantly mineralized, a few samples contain sparse fine-grained sulphide and, rarely, semi-massive sulphide (Fig. 4m). The most notable feature of the siltstone and mudstone samples from the Spatsizi Formation (n=42), is the presence of sulphides, typically pyrite (Figs. 4n, o).

5.2. Thin section descriptions

The gabbroic rocks of both the E&L stock and Nickel mountain gabbro consist mainly of olivine, pyroxene, and plagioclase that display an ophitic texture, with pyroxene interstitial to euhedral laths of plagioclase and rounded olivine crystals. The inferred order of crystallization is olivine, plagioclase, and pyroxene. All of the rocks are extremely altered, with primary silicates in some samples completely replaced by hydrous silicates. In general, olivine is the most intensely altered, commonly appearing as hydrous silicate aggregate pseudomorphs. Plagioclase and pyroxene are variably altered. The olivine has been serpentinized and replaced by sulphides, plagioclase has been sericitized and chloritized, and pyroxene was chloritized or uralitized and replaced by sulphides.

Mineralization in the E&L stock occurs as disseminated, blebby, net-textured, and semi-massive sulphides comprising

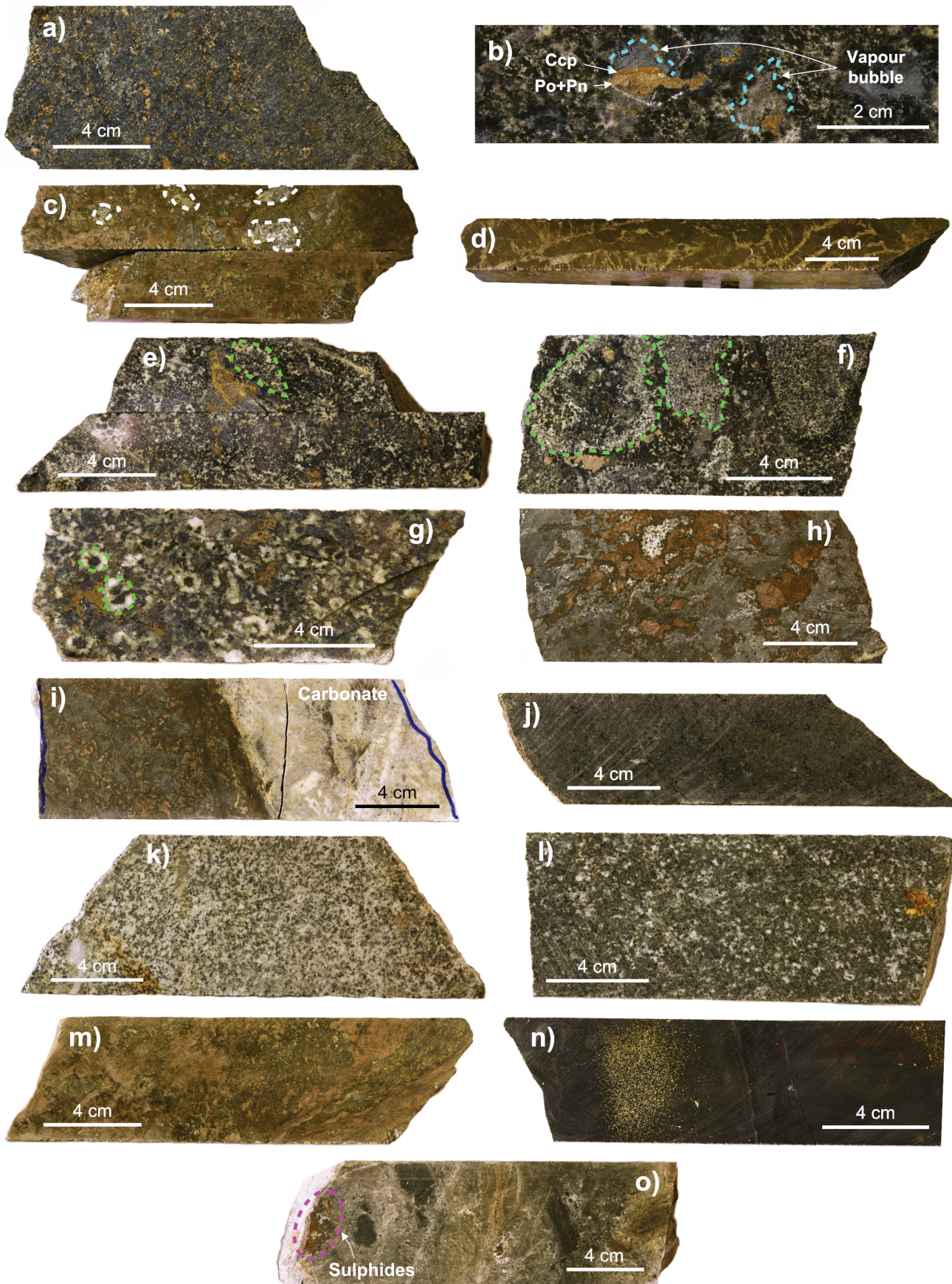


Fig. 4. See opposite page for caption.

Fig. 4. Continued. Images of representative drill core samples of (a-j) E&L gabbro and sulphide mineralization, (k-m) Nickel mountain gabbro, and (n-o) Hazelton Group (Spatsizi Formation) sedimentary rock. **a)** Disseminated sulphide mineralization in E&L gabbro. **b)** Blebby sulphide mineralization in E&L gabbro. Note the segregation of the sulphide bleb into Fe-rich and Cu-rich portions, the latter of which is surrounded by a fine-grained assemblage of hydrous minerals. **c)** Semi-massive sulphide mineralization with felsic patches. **d)** Massive sulphide mineralization showing loop texture (rounded aggregates of pyrrhotite surrounded by pentlandite and chalcopyrite). **e)** Blebby sulphide mineralization in E&L gabbro; the sulphide bleb is surrounded by pyroxene. **f)** Varitextured gabbro with well-defined orbicules (outlined by green dashed lines). The sulphides are largely interstitial to the orbicules. **g)** Varitextured gabbro with small-scale orbicular features; two are highlighted by green dashed lines. Sulphides are interstitial to the orbicular features. **h)** Semi-massive sulphide mineralization in rock comprising a mixture of mafic material with more silicic material. Sulphides are associated with the more felsic-rich domains. **i)** Disseminated sulphide mineralization in a sample of E&L gabbro in contact with sedimentary country rock. **j)** Disseminated sulphide mineralization in gabbroic rock from the exploratory drill hole under the glacier on top of Nickel mountain. **k)** Plagioclase-rich Nickel mountain gabbro. **l)** Plagioclase-poor Nickel mountain gabbro. **m)** Nickel mountain gabbro hosting semi-massive sulphide mineralization. **n)** Siltstone of the Spatsizi Formation containing fine-grained, disseminated pyrite. **o)** Mudstone of the Spatsizi Formation containing blebby sulphides (highlighted by purple dashed circle). The teal dashed lines delineate features interpreted as former vapour bubbles, the white dashed lines highlight felsic patches, and the green dashed lines are orbicules.

pyrrhotite, chalcopyrite, pentlandite, and pyrite; cubanite, violarite, and troilite are rare. Where pyrite is absent, the order of sulphide abundance is generally pyrrhotite > chalcopyrite \geq pentlandite (Fig. 5a). However, pyrite may make up a significant portion of the sulphide assemblage, with some samples containing predominantly pyrite (Fig. 5b). Given that pyrite is rarely a primary sulphide in magmatic deposits because sulphide liquids typically do not achieve high enough S/metal ratios (Naldrett et al., 1967; Kellerud et al., 1969; Craig, 1973; Piña et al., 2016), it is likely that pyrite is hydrothermal in origin, as described by Brzozowski et al. (2023) for the Current deposit in the Midcontinent Rift. The sulphide assemblage at E&L may, therefore, be broadly grouped into two categories: primary, lacking abundant pyrite, and secondary, with abundant pyrite. There appears to be no systematic variation in sulphide mineralogy across different parts of the deposit.

The primary sulphide assemblage comprises pyrrhotite, chalcopyrite, and pentlandite that exhibit sharp, rounded inter-grain boundaries (Fig. 5a), a mineralogical and textural assemblage typical of sulphides that crystallized from a sulphide liquid. Generally, pyrrhotite is the predominant sulphide, with chalcopyrite occurring along its periphery (although locally as streaks within pyrrhotite). Pentlandite occurs as aggregates near contacts between pyrrhotite and chalcopyrite, as grains within pyrrhotite (Fig. 5a), and locally as flames in pyrrhotite. The secondary sulphide assemblage comprises pyrite \pm pyrrhotite, chalcopyrite, and pentlandite. Pyrite typically occurs as porous aggregates of fine-grained crystals spatially associated with mineralogically variable assemblages of pyrrhotite-chalcopyrite-pentlandite (Fig. 5b) or as isolated clusters (Fig. 5c). Where spatially associated with other sulphides, pyrite typically appears to have replaced pyrrhotite (Fig. 5b).

Regardless of whether primary or secondary, the sulphides are almost always spatially associated with hydrous silicates reflecting the pervasive alteration of the rocks; in some assemblages, the hydrous silicates also protrude into the sulphides. Where sulphides are associated with what we interpret as vapour bubbles (e.g., Fig. 4b), the vapour bubble now comprises an assemblage of hydrous silicates (Fig. 5d). Although not as common, some sulphide assemblages may also

contain carbonate, either within the assemblage or along its periphery (Fig. 5e). Additionally, pyrrhotite in both assemblage types can exhibit undulose extinction in cross-polarized reflected light, with some pyrrhotite grains displaying distinct flaser texture (Fig. 5f) or 120° dihedral angles (Fig. 5g). In most samples, fine-grained specks of sulphide occur throughout the alteration assemblages. A specific example of this sulphide-alteration association are the intensively altered olivine grains that commonly contain variable amounts of fine-grained pyrrhotite (\pm chalcopyrite and pentlandite), with some of the olivine grains being almost completely pseudomorphed by sulphide (Fig. 5h). Although less common, an assemblage of hydrous silicates+chalcopyrite has also been observed as partial pseudomorphs of altered primary silicates (Fig. 5i). Similarly, where Fe-Ti oxide minerals (i.e., magnetite-ulvöspinel-ilmenite intergrowths) have been altered, the magnetite interstitial to relics of the lamellae has been replaced by hydrous silicates+sulphides (Fig. 5j). Although uncommon, some sulphides occur within veinlets (Fig. 5k). Similarly uncommon, some sulphide assemblages are rimmed by magnetite (Fig. 5l).

6. Discussion

6.1. Sulphide saturation via contamination?

Magmas emplaced at crustal levels are typically undersaturated in sulphide because the sulphur content at sulphide saturation increases as pressure decreases (Mavrogenes and O'Neill, 1999). The formation of magmatic sulphide deposits, therefore, requires some additional process(es) to cause the parental magmas to become saturated in sulphide and segregate a sulphide liquid, which then scavenges and concentrates base and precious metals. Achieving sulphide saturation is problematic in subduction zones because the magmas are oxidized and sulphur may be present as sulphate (SO_4^{2-}) rather than sulphide (S^{2-}) anions (Jugo, 2004, 2009), requiring reduction. Several processes have been proposed to assist magmas in becoming saturated in sulphide (e.g., Ripley and Li, 2013) including: 1) closed-system fractional crystallization; 2) magma mixing; 3) decrease in magma $f\text{O}_2$; and 4) addition of externally derived S and/or Si. Ripley and Li (2013) evaluated each of these processes and concluded that direct addition of externally derived S is the most viable for generating sufficient

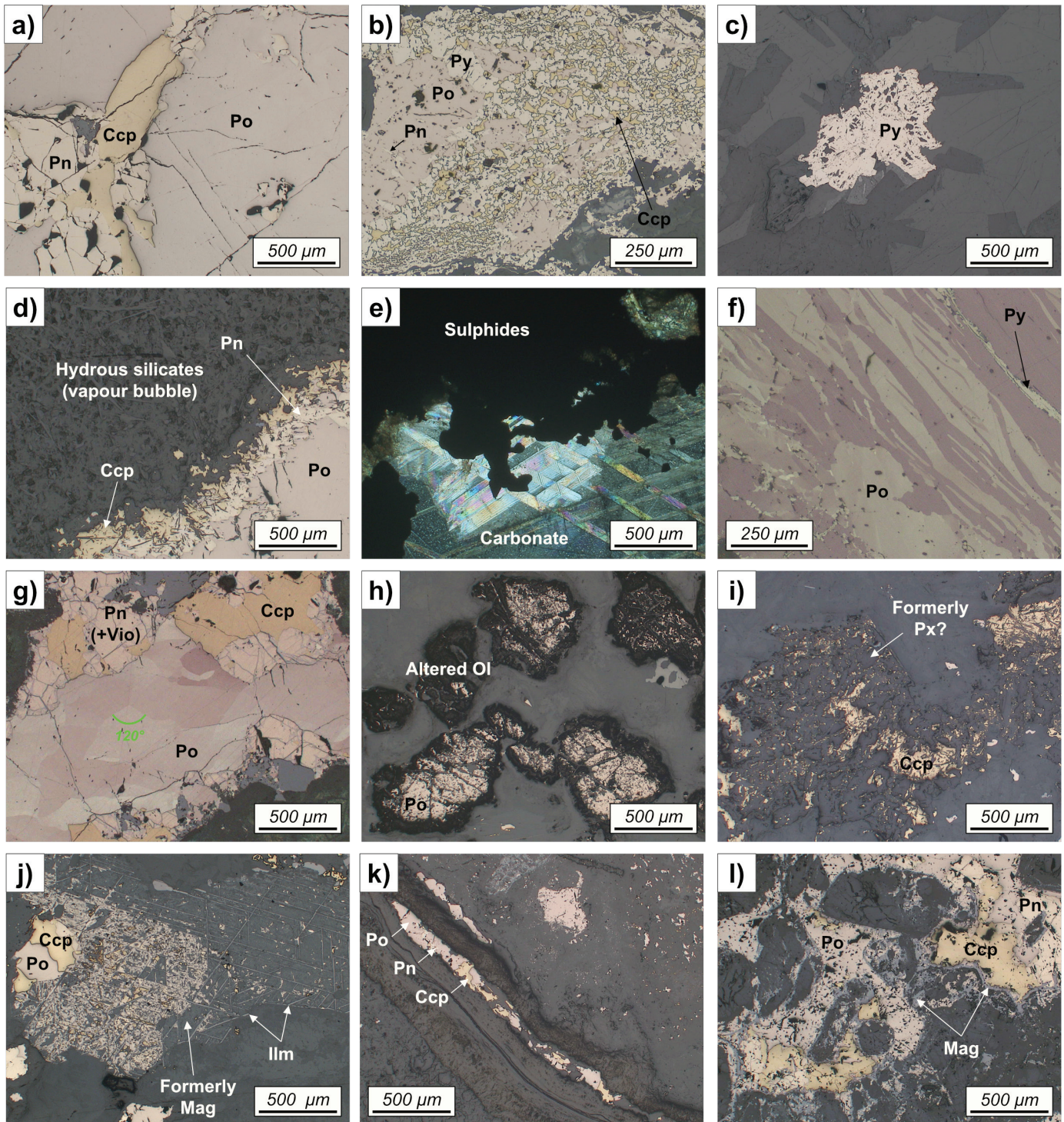


Fig. 5. Photomicrographs of representative sulphide textures in the E&L deposit; (a-d) and (h-l) are in reflected light, (e) is in cross-polarized transmitted light, and (f-g) are in cross-polarized reflected light. **a)** A magmatic sulphide assemblage comprising pyrrhotite-pentlandite-chalcopyrite. **b)** An altered sulphide assemblage comprising pyrrhotite-pentlandite-chalcopyrite-pyrite, with pyrite forming aggregates. **c)** An aggregate of pyrite grains isolated from other sulphides. **d)** A magmatic sulphide assemblage comprising pyrrhotite-pentlandite-chalcopyrite adjacent to a rounded hydrous silicate assemblage that is interpreted as a former vapour bubble. **e)** Carbonate and hydrous silicates adjacent to sulphides. **f)** Pyrrhotite with flaser texture. **g)** A magmatic assemblage of pyrrhotite-pentlandite-chalcopyrite in which the pyrrhotite occurs as an aggregate of grains that exhibit dihedral angles. **h)** Olivine that has been partially to completely replaced by hydrous silicates and pyrrhotite. **i)** Pyroxene(?) replaced by an assemblage of hydrous silicates and chalcopyrite. **j)** A grain of Fe-Ti oxide (magnetite+ilmenite) in which the magnetite has been replaced by an assemblage of hydrous silicates and sulphides. **k)** A late-stage vein containing pyrrhotite, pentlandite, and chalcopyrite. **l)** A magmatic sulphide assemblage of pyrrhotite, pentlandite, and chalcopyrite rimmed by magnetite.

Abbreviations: Po – pyrrhotite, Pn – pentlandite, Ccp – chalcopyrite, Py – pyrite, Vio – violarite, Ilm – ilmenite, Ol – olivine, Mag – magnetite.

sulphide liquid to form economic Ni-Cu-PGE deposits. Below we make a preliminary assessment of the saturation mechanisms that may have operated in the E&L deposit using textural observations.

Saturation of the E&L magma via closed-system fractional crystallization of the stock seems unlikely for two reasons. First, the geometry of the E&L deposit appears to define an open, conduit-like system, and so the cumulate rocks likely crystallized from multiple batches of magma rather than from a single, evolving magma. This interpretation is consistent with what appears to be two magma chambers in the E&L intrusive system that are interpreted to be connected by a pipe-like body (Fig. 3) similar to, for example, the Voisey's Bay (Evans-Lamswood et al., 2000; Ripley and Li, 2011), Noril'sk (Barnes et al., 2015), and Eagle (Ripley and Li, 2011) deposits. Furthermore, the elevated metal contents of the E&L deposit, and other volumetrically small sulphide deposits, require larger volumes of magma than represented by the stock itself (Campbell and Naldrett, 1979; Naldrett, 1989, 1992, 1999; Arndt et al., 2005). Second, sulphide saturation via crystallization generates small volumes of sulphide liquid late in the crystallization history of a magma (after up to 40% crystallization, Ripley and Li, 2013; Mungall, 2014). Such late saturation is inconsistent with the net-textured and (semi-) massive sulphide orebodies (Figs. 3, 4c, d, m) at E&L, which would have required relatively early saturation to prevent sulphide liquid from being completely trapped in the cumulate pile. The high volumes of sulphide at E&L are inconsistent with magma mixing, which generally produces only small amounts of sulphide (Ripley and Li, 2013), and textural evidence of mixing is lacking. Decreasing the fO_2 of a magma, although not necessarily important to the saturation history of intracratonic magmatic systems where fO_2 values are lower than fayalite-magnetite-quartz (FMQ) buffer (Mavrogenes and O'Neill, 1999; O'Neill and Mavrogenes, 2002), may be important to the saturation histories of arc-related magmas where both sulphide and sulphate can coexist (FMQ to FMQ+2; Jugo, 2009). Changes in magma fO_2 may be associated with changes in either H_2O or CO_2 (Lehmann et al., 2007; Ripley and Li, 2013). For example, one way that CO_2 is added to magmas is through assimilation of carbonate material, where the principal mechanism is carbonate dissociation via the simplified reaction: $CO_2 + 2FeO \rightleftharpoons CO + Fe_2O_3$ (Xue et al., 2023). Although the importance of changes to magma fO_2 on sulphide saturation at E&L cannot be currently assessed, textural evidence for mafic magma-carbonate interaction (Fig. 4i) suggests that carbonate-bearing material was likely assimilated by the magma and that contamination may have played a role in sulphide saturation. Although the carbonate that occurs interstitial to primary silicates and commonly with sulphides may be hydrothermal in origin, it is also possible that this carbonate crystallized from the magma as a result of assimilation of carbonate-rich country rock (Fig. 5e).

The simplest and most efficient way of triggering sulphide saturation in a magma is by the direct addition of sulphur,

either by bulk assimilation of S-rich country rocks or selective assimilation of country-rock sulphides (Barnes and Robertson, 2019), with the former also contributing SiO_2 , which serves to lower the sulphur content at sulphide saturation. Although the scale at which these processes operated at E&L is currently unknown, addition of S from country rocks is likely because: 1) the S-rich nature of the siltstones and mudstones of the Spatsizi Formation (Figs. 4n, o); 2) the occurrence of (semi-) massive sulphide orebodies near contacts with, and hosted in, sedimentary rocks of the Hazelton Group (Fig. 3); and 3) the close spatial association of semi-massive sulphides with felsic patches (Figs. 4c, h) that are consistent with localized silica addition.

6.2. Vapour-assisted transport of sulphide liquid?

Considering that assimilation of Hazelton Group sedimentary rocks may have contributed to the formation of sulphides, the occurrence of sulphides in shallow and deep portions of the E&L deposit (e.g., wehrlite from the Eastern Extensional zone; Fig. 4j), and the presence of Hazelton Group sedimentary rocks at depth (Fig. 3), some sulphide liquid may have been carried upwards through the intrusive plumbing system. Although upward transport of dense ($4\text{--}5\text{ g/cm}^3$; Mungall and Su, 2005), low viscosity ($0.01\text{--}0.1\text{ Pa}\cdot\text{s}$; Dobson et al., 2000) sulphide liquid is possible in mafic magmas, the notably lower density and fluidity of these magmas ($2.7\text{--}2.9\text{ g/cm}^3$, $1\text{--}100\text{ Pa}\cdot\text{s}$; Williams et al., 1998) generally hinders efficient upward transport of all but the finest dispersions of sulphide liquid (Lesher, 2019). Based on experimental observations (Mungall et al., 2015), natural observations (Barnes et al., 2019, 2023; Brzozowski et al., 2023), and numerical simulations (Yao and Mungall, 2020), it has been demonstrated that upward transport of sulphide liquid can be facilitated by vapour bubbles attached to sulphide droplets (i.e., compound droplets). These compound droplets, which have been identified in other magmatic sulphide systems globally, including Norilsk (Barnes et al., 2019, 2023) and Current (Brzozowski et al., 2023), generally comprise a sulphide assemblage that has segregated into an Fe-rich portion (pyrrhotite+pentlandite) and a Cu-rich portion (chalcopyrite ±cubanite), with the latter portion being rimmed by an assemblage of silicate minerals that is finer grained than the host rock. A texturally similar style of blebby sulphide is common at E&L (Figs. 4b, 5a, d), implying that: 1) the fertile E&L magma(s) contained sufficient volatiles to become saturated, potentially because of assimilation of sedimentary country rock (e.g., Iacono-Marziano et al., 2012, 2017); 2) the magma(s) were emplaced at relatively shallow depths (low confining pressures) where volatiles could exsolve; and 3) some amount of upward transport of sulphide liquid may have occurred. If our interpretation of vapour bubbles illustrated in Figure 4b is correct, it would imply significant tilting of the E&L deposit after it formed because the core was taken from a relatively steep drill hole and the bubbles indicate tops perpendicular to the long axis of the core.

6.3. Metal remobilization?

The rocks that host the E&L deposit are pervasively altered, indicating that fluids fluxed through the mineralizing system after it had solidified. Alongside the primary silicates that were replaced by hydrous silicates, the oxides and sulphides were also altered. Several lines of textural evidence indicate that this hydrothermal activity likely remobilized metals, an understanding of which is vital given that such remobilization can have beneficial (e.g., Roby zone of Lac des Iles; Watkinson and Dunning, 1979; Hinchey and Hattori, 2005) or detrimental effects on the economic value of deposits (Holwell et al., 2017). Several factors support metal remobilization in the E&L deposit. First, given that pyrrhotite appears to have been partially to completely replaced by pyrite (Fig. 5b), as is typical of sulphide assemblages containing pyrite in these mineralizing systems (Djon and Barnes, 2012; Duran et al., 2015; Holwell et al., 2017; Brzozowski et al., 2023), Fe must have been released to the fluid and remobilized because pyrrhotite has a higher Fe content than pyrite (~62 wt.% vs. 47 wt.%). Second, the partial to complete replacement of olivine and pyroxene by sulphides (Figs. 5h, i) is strong evidence for metal remobilization. Although the Fe in this secondary sulphide assemblage could have been sourced from the primary silicates, the fact that some of these assemblages also contain chalcopyrite (Figs. 5i) and pentlandite implies that at least some of the metals were provided by the fluid that interacted with olivine and pyroxene. Third, the replacement of magnetite interstitial to ilmenite lamellae with a hydrous silicate-sulphide assemblage (Fig. 5j) indicates that metals precipitated from a hydrothermal fluid. This is because oxy-exsolution of ilmenite is a post-cumulus process that occurs at temperatures below which sulphide liquids crystallize (Buddington and Lindsley, 1964; Brzozowski et al., 2021), indicating that any sulphides present in the replacement assemblage must be hydrothermal. Fourth, some sulphides are rimmed by magnetite (Fig. 5l), which indicates S loss. Given that magnetite is unable to contain all the Cu and Ni (as well as other metals) in chalcopyrite and pentlandite (ppm vs. wt.%), respectively, these metals must have been remobilized. Finally, the occurrence of chalcopyrite, pyrrhotite, and pentlandite in late-stage veins that crosscut the E&L host rocks (Fig. 5k) implies that at least Cu, Fe, Ni, and S were remobilized by hydrothermal fluids, with other mobile trace metals likely being remobilized as well.

Given that the E&L deposit was metamorphosed at greenschist facies and that deformation is locally recorded in the sulphides (Figs. 5f, g), it is possible that sulphides were mechanically remobilized. A single sample of semi-massive sulphide exhibits textural evidence of sulphide flow, and segregation of Fe-rich and Cu-rich sulphides (Fig. 4m), indicating that some degree of mechanical remobilization could have occurred. Additionally, Vandenburg (2020) reported folded loop textures, which indicate ductile deformation. Deformation of sulphides is most prominently recorded as undulose extinction of pyrrhotite (Figs. 5g, h) and, rarely, as pyrite aggregates with flow textures in pyrrhotite-pentlandite-chalcopyrite assemblages.

Nonetheless, sulphide grains overall retain magmatic textures and do not appear to be severely deformed (Fig. 5g), suggesting minimal deformation-induced remobilization.

Taken together, it is evident that metals were remobilized by hydrothermal fluids in the E&L deposit. However, the metals that were remobilized (apart from Fe-Ni-Cu), the extent of this remobilization, and the nature of the hydrothermal fluids that caused the remobilization (e.g., deuteritic vs. meteoric) remain unknown. These will be assessed in future research using bulk-rock geochemistry, in situ trace-element chemistry of sulphides, and Cu-Fe-O isotopes.

6.4. Origin of orbicular textures?

Gabbroic rocks of the E&L deposit exhibit conspicuous orbicular textures that are generally more plagioclase rich compared to the interstitial material (Figs. 4e-g). Orbicular textures have been described in a variety of rock types ranging from gabbros to granites and in a diversity of tectonic settings (Leveson, 1966). Nonetheless, the mechanism(s) by which orbicules form remains unresolved. Numerous models have been proposed, almost exclusively for those in granitic rocks, including: 1) fractional crystallization of small blebs of melt in a host magma; 2) nucleation on xenoliths; 3) mingling of compositionally distinct magmas; 4) metasomatism; and 5) liquid immiscibility (Moore and Lockwood, 1973; Sylvester, 2011; Smillie and Turnbull, 2014; Ballhaus et al., 2015; McCarthy et al., 2016; McCarthy and Müntener, 2017). Most of these models can be ruled out as having played a significant role in generating the orbicular textures at E&L. Fractional crystallization of small melt bodies can be ruled out because, although some orbicules exhibit mineralogical zonation, this is not pervasive even at the scale of a hand sample, and repetitive concentric zoning, which would be expected if each orbicule fractionally crystallized in a relatively closed system, is not observed nor was a more evolved mineral assemblage (e.g., alkali feldspar, quartz). Nucleation on xenoliths is untenable because the E&L orbicules lack xenolithic cores (Figs. 4e-g) and orbicular rocks are not restricted to the margins of the intrusion. Magma mingling can also be ruled out because the mineralogy of the orbicules at E&L is the same as that of the interstitial material, albeit the mineral abundances are different (Figs. 4e-g). Although formation of conduit-type Ni-Cu-PGE deposits generally requires input of multiple pulses of magma, these pulses are typically of similar chemical and physical composition (e.g., Shahabi Far et al., 2019), and thus will not possess sufficient contrast in physical properties (e.g., viscosity) to generate orbicules. Metasomatic reaction between magma and xenoliths can be ruled out because xenoliths of country rock material are rare at E&L and the cores of the orbicules are not xenoliths (Smillie and Turnbull, 2014).

Fluid-melt immiscibility is one of the only models of orbicule formation that has been applied to mafic-ultramafic rocks (Ballhaus et al., 2015). This model considers that all immiscible systems behave the same way and generate spheroidal textures upon exsolution, and that co-existing melts

and fluids at equilibrium are saturated in the same crystalline phases and phase compositions, and thus will crystallize to the same anhydrous minerals, but with variable proportions and grain size. Ballhaus et al. (2015) attributed the mineralogical variability to the wettability and degree of polymerization of different minerals, with neosilicates (e.g., olivine), chain silicates (e.g., pyroxene and amphibole), and oxides being transferred preferentially from melt to fluid, such that the fluid becomes more mafic, and grain size variability to faster growth rates in depolymerized fluids, such that the fluid becomes coarser grained than the melt.

The orbicules observed at E&L are similar to an immiscibility texture described by Ballhaus et al. (2015) who considered its formation to be a result of exsolution of limited amounts of water from melts during crystallization, with the two phases having a significant viscosity contrast. Accordingly, the orbicules represent the melt and the interstitial material represents the exsolved fluid (Ballhaus et al., 2015). Applied to the present example, the E&L orbicules should be relatively more felsic (e.g., contain more plagioclase) and finer grained, and the interstitial material should be relatively more mafic (e.g., contain more olivine and pyroxene) and coarser grained. This is what is observed (Figs. 4e-g). Additionally, because the orbicules that are in contact with one another along deformed boundaries retain their individual character rather than merging into a single entity (Figs. 4f, g) supports the interpretation that they represent melt rather than exsolved fluid (Ballhaus et al., 2015).

Although mineralogical and grain size zonation of orbicules, and distribution of sulphides was not described by Ballhaus et al. (2015), some E&L orbicules display a crude zonation and sulphides are generally concentrated in the interstitial material (Figs. 4e-g). If the orbicules represent melt, then the coarser grained mafic cores and finer grained felsic rims likely represent heterogeneous transfer of mafic minerals from melt to fluid (Ballhaus et al., 2015). This heterogeneous transfer may have occurred for two reasons. First, mafic minerals at the rims of orbicules would have been more easily wetted by the exsolved fluid than the minerals in the cores and thus would have been more readily transferred from melt to fluid. Second, the physical movement of coarser grained minerals in the cores would have been impeded by the crystal mush, preventing transfer. With respect to the sulphides, because they are generally concentrated in the interstitial material implies that sulphide liquid, which exsolved from the silicate melt, was preferentially transferred to the exsolved fluid, consistent with the low degree of polymerization of sulphide liquids. The occurrence of small volumes of sulphide within the cores of orbicules (Fig. 4f) may be attributed to the impeded movement of mafic minerals described above.

In summary, we conclude that the magmas from which the E&L deposit crystallized may have contained sufficient H₂O to become saturated and exsolve a hydrous fluid at depth. The lack of these orbicular textures in the barren Nickel mountain gabbro may indicate that the fertile magmas from which the

mineralized E&L stock crystallized were more hydrous. However, it remains unclear if such possible fluid-rich magmas played a role in generating the mineralization and in altering the host rocks (i.e., auto-hydrothermal alteration).

7. Conclusion

The mafic-ultramafic rocks of the E&L Ni-Cu-PGE sulphide deposit that intruded sedimentary rocks of the Spatsizi Formation and the Nickel mountain gabbro exhibit a variety of macro- and micro-scale textures that provide insights into potential mechanisms that may have formed and modified the deposit. The spatial association of carbonates with sulphides and the occurrence of sulphides in felsic patches in the mafic host rock suggest that assimilation of country rock material contributed to the sulphide saturation history of the E&L magma. The occurrence of compound droplets (sulphide+hydrous silicates/vapour bubbles) is inferred to represent vapour saturation in the magma, which likely assisted in the upward transport of sulphide liquid. The widespread mineralogical and textural evidence indicative of sulphide remobilization (pyrite after pyrrhotite, sulphides after olivine, pyroxene, and magnetite, sulphides in veins, magnetite after sulphides) indicates that metals were remobilized throughout the E&L deposit, although the extent of remobilization remains unclear. Although sulphides are deformed, they retain magmatic textures, suggesting minimal deformation-induced remobilization. The occurrence of orbicules in many of the E&L gabbros may indicate H₂O saturation of the magma and fluid immiscibility, with the orbicules representing the silicate melt and the interstitial material representing the exsolved hydrous fluid. Planned future work will use bulk-rock geochemistry, Sr-Nd-S-C-O ±Cu-Fe isotopes, and sulphide trace-element chemistry to more fully document the processes that formed and modified the E&L deposit.

Acknowledgments

We thank Garibaldi Resources Corp. for providing us information about the E&L deposit before fieldwork, for supporting our drill core sampling, and for logistical support. We also thank Graham Nixon and Rafael Bacha for constructive comments that strengthened the article.

References cited

- Acosta-Góngora, P., Pehrsson, S.J., Sandeman, H., Martel, E., and Peterson, T., 2018. The Ferguson Lake deposit: an example of Ni-Cu-Co-PGE mineralization emplaced in a back-arc basin setting? *Canadian Journal of Earth Sciences*, 55, 958-979.
- Alldrick D.J., Brown D.A., Harakal J.E., Mortensen J.K., and Armstrong R.L., 1987. Geochronology of the Stewart Mining Camp (104B/1). In: *Geological Fieldwork 1986*. British Columbia Ministry of Energy, Mines and Petroleum Resources, British Columbia Geological Survey Paper 1987-01, pp. 81-92.
- Arndt, N., Leshner, C.M., and Czamanske, G.K., 2005. Mantle-derived magmas and magmatic Ni-Cu-(PGE) deposits. In: Hedenquist, J.W., Thompson, J.F.H., Goldfarb, R.J., Richards, J.P., (Eds.), *Economic Geology, 100th Anniversary Volume*, pp. 5-24.
- Ballhaus, C., Fonseca, R.O.C., Münker, C., Kirchenbaur, M., and Zirner, A., 2015. Spheroidal textures in igneous rocks - Textural

- consequences of H₂O saturation in basaltic melts. *Geochimica et Cosmochimica Acta*, 167, 241-252.
- Barnes, S.J., and Robertson, J.C., 2019. Time scales and length scales in magma flow pathways and the origin of magmatic Ni-Cu-PGE ore deposits. *Geoscience Frontiers*, 10, 77-87.
- Barnes, S.J., Cruden, A.R., Arndt, N., and Saumur, B.M., 2015. The mineral system approach applied to magmatic Ni-Cu-PGE sulphide deposits. *Ore Geology Reviews*, 76, 296-316.
- Barnes, S.J., Le Vaillant, M., Godel, B., and Leshner, C.M., 2019. Droplets and bubbles: Solidification of sulphide-rich vapour-saturated orthocumulates in the Norilsk-Talnakh Ni-Cu-PGE Ore-bearing Intrusions. *Journal of Petrology*, 60, 269-300.
- Barnes, S.J., Yudovskaya, M.A., Iacono-Marziano, G., Vaillant, M.L., Schoneveld, L.E., and Cruden, A.R., 2023. Role of volatiles in intrusion emplacement and sulfide deposition in the supergiant Norilsk-Talnakh Ni-Cu-PGE ore deposits. *Geology*, 51, 1027-1032.
- British Columbia Geological Survey, 2023. The Golden Triangle of northwestern British Columbia. British Columbia Ministry of Energy, Mines and Petroleum Resources, British Columbia Geological Survey Information Circular 2023-05, 6 p.
- Brzozowski, M.J., Samson, I.M., Gagnon, J.E., Good, D.J., and Linnen, R.L., 2020. On the mechanisms for low-sulfide, high-platinum group element and high-sulfide, low-platinum group element mineralization in the Eastern gabbro, Coldwell Complex, Canada: Evidence from textural associations, S/Se values, and platinum group element concentrations of base metal sulfides. *Economic Geology*, 115, 355-384.
- Brzozowski, M.J., Samson, I.M., Gagnon, J.E., Linnen, R.L., and Good, D.J., 2021. Effects of fluid-induced oxidation on the composition of Fe-Ti oxides in the Eastern Gabbro, Coldwell Complex, Canada: implications for the application of Fe-Ti oxides to petrogenesis and mineral exploration. *Mineralium Deposita*, 56, 601-618.
- Brzozowski, M.J., Hollings, P., Heggie, G., MacTavish, A., Wilton, D., and Evans-Lamswood, D., 2023. Characterizing the supra- and subsolidus processes that generated the Current PGE-Cu-Ni deposit, Thunder Bay North Intrusive Complex, Canada: insights from trace elements and multiple S isotopes of sulfides. *Mineralium Deposita*, 58, 1559-1581.
- Buddington, A.F., and Lindsley, D.H., 1964. Iron-titanium oxide minerals and synthetic equivalents. *Journal of Petrology*, 5, 310-357.
- Campbell, I.H., and Naldrett, A.J., 1979. The influence of silicate: sulfide ratios on the geochemistry of magnetic sulfides. *Economic Geology*, 74, 1503-1506.
- Colpron, M., 2020. Yukon terranes-A digital atlas of terranes for the northern Cordillera. Yukon Geological Survey. <https://data.geology.gov.yk.ca/Compilation/2#InfoTab>
- Craig, J.R., 1973. Pyrite-pentlandite assemblages and other low temperature relations in the Fe-Ni-S system. *American Journal of Science*, 273-A, 496-510.
- Ding, X., Ripley, E.M., and Li, C., 2011. PGE geochemistry of the Eagle Ni-Cu-(PGE) deposit, Upper Michigan: constraints on ore genesis in a dynamic magma conduit. *Mineralium Deposita*, 47, 89-104.
- Djon, M.L.N., and Barnes, S.J., 2012. Changes in sulfides and platinum-group minerals with the degree of alteration in the Roby, Twilight, and High Grade Zones of the Lac des Iles Complex, Ontario, Canada. *Mineralium Deposita*, 47, 875-896.
- Dobson, D.P., Crichton, W.A., Vočadlo, L., Jones, A.P., Wang, Y., Uchida, T., Rivers, M., Sutton, S., and Brodtholt, J.P., 2000. In situ measurement of viscosity of liquids in the Fe-FeS system at high pressures and temperatures. *American Mineralogist*, 85, 1838-1842.
- Duran, C.J., Barnes, S.J., and Corkery, J.T., 2015. Chalcophile and platinum-group element distribution in pyrites from the sulfide-rich pods of the Lac des Iles Pd deposits, Western Ontario, Canada: Implications for post-cumulus re-equilibration of the ore and the use of pyrite compositions in exploration. *Journal of Geochemical Exploration*, 158, 223-242.
- Evans-Lamswood, D.M., Butt, D.P., Jackson, R.S., Lee, D.V., Muggridge, M.G., and Wheeler, R.I., 2000. Physical Controls Associated with the Distribution of Sulfides in the Voisey's Bay Ni-Cu-Co Deposit, Labrador. *Economic Geology*, 95, 22.
- Gagnon, J.-F., Barresi, T., Waldron, J.W.F., Nelson, J.L., Poulton, T.P., and Cordey, F., 2012. Stratigraphy of the upper Hazelton Group and the Jurassic evolution of the Stikine terrane, British Columbia. *Canadian Journal of Earth Sciences*, 49, 1027-1052.
- Gao, J.-F., Zhou, M.-F., Lightfoot, P.C., Wang, C.Y., Qi, L., and Sun, M., 2013. Sulfide Saturation and Magma Emplacement in the Formation of the Permian Huangshandong Ni-Cu Sulfide Deposit, Xinjiang, Northwestern China. *Economic Geology*, 108, 1833-1848.
- Hancock, K.D., 1990. Geology of Nickel Mountain and the E&L nickel-copper prospect (104B/10E). In: *Geological Fieldwork 1989*, British Columbia Ministry of Energy, Mines and Petroleum Resources, British Columbia Geological Survey Paper 1990-1, pp. 337-341.
- Hanson, J., Lightfoot, P.C., and Goldie, R., 2022. Nickel mountain and Casper exploration: 2022 corporate presentation. Garibaldi Resources Corp. <<https://garibaldiresources.com/site/assets/files/3966/ggi-investor-presentation-july-2022.pdf>>. Accessed November 17, 2023.
- Hinchey, J.G., and Hattori, K.H., 2005. Magmatic mineralization and hydrothermal enrichment of the High Grade Zone at the Lac des Iles palladium mine, northern Ontario, Canada. *Mineralium Deposita*, 40, 13-23.
- Holwell, D.A., Adeyemi, Z., Ward, L.A., Smith, D.J., Graham, S.D., McDonald, I., and Smith, J.W., 2017. Low temperature alteration of magmatic Ni-Cu-PGE sulfides as a source for hydrothermal Ni and PGE ores: A quantitative approach using automated mineralogy. *Ore Geology Reviews*, 91, 718-740.
- Iacono-Marziano, G., Marecal, V., Pirre, M., Gaillard, F., Arteta, J., Scaillet, B., and Arndt, N.T., 2012. Gas emissions due to magma-sediment interactions during flood magmatism at the Siberian Traps: Gas dispersion and environmental consequences. *Earth and Planetary Science Letters*, 357-358, 308-318.
- Iacono-Marziano, G., Ferraina, C., Gaillard, F., Di Carlo, I., and Arndt, N.T., 2017. Assimilation of sulfate and carbonaceous rocks: Experimental study, thermodynamic modeling and application to the Noril'sk-Talnakh region (Russia). *Ore Geology Reviews*, 90, 399-413.
- Jackson-Brown, S., Scoates, J.S., Nixon, G.T., and Ames, D.E., 2014. Mineralogy of sulphide, arsenide, and platinum group minerals from the DJ/DB Zone of the Turnagain Alaskan-type ultramafic intrusion, north-central British Columbia. In: *Geological Fieldwork 2013*, British Columbia Ministry of Energy and Mines, British Columbia Geological Survey Paper 2014-1, pp. 157-168.
- Jugo, P.J., 2004. An experimental study of the sulfur content in basaltic melts saturated with immiscible sulfide or sulfate liquids at 1300°C and 1.0 GPa. *Journal of Petrology*, 46, 783-798.
- Jugo, P.J., 2009. Sulfur content at sulfide saturation in oxidized magmas. *Geology*, 37, 415-418.
- Kellerud, G., Yund, R.A., and Moh, G.H., 1969. Phase relations in the Cu-Fe-S, Cu-Ni-S, and Fe-Ni-S systems. *Economic Geology Monograph*, 4, 323.
- Lee, I., and Ripley, E.M., 1995. Genesis of Cu-Ni sulfide mineralization in the South Kawishiwi intrusions, Spruce Road area, Duluth Complex, Minnesota. *The Canadian Mineralogist*, 33, 723-743.
- Lehmann, J., Arndt, N., Windley, B., Zhou, M.-F., Wang, C.Y., and Harris, C., 2007. Field Relationships and Geochemical Constraints on the Emplacement of the Jinchuan Intrusion and its Ni-Cu-PGE

- Sulfide Deposit, Gansu, China. *Economic Geology*, 102, 75-94.
- Leshner, C.M., 2019. Up, down, or sideways: emplacement of magmatic Fe-Ni-Cu-PGE sulfide melts in large igneous provinces. *Canadian Journal of Earth Sciences*, 56, 756-773.
- Leveson, D.J., 1966. Orbicular Rocks: A Review. *Geological Society of America Bulletin*, 77, 409-426.
- Li, X.H., Su, L., Chung, S.-L., Li, Z.X., Liu, Y., Song, B., and Liu, D.Y., 2005. Formation of the Jinchuan ultramafic intrusion and the world's third largest Ni-Cu sulfide deposit: Associated with the ~825 Ma south China mantle plume? *Geochemistry, Geophysics, Geosystems*, 6, 1-16.
- Lightfoot, P.C., Keays, R.R., Evans-Lamswood, D., and Wheeler, R., 2012. S saturation history of Nain Plutonic Suite mafic intrusions: origin of the Voisey's Bay Ni-Cu-Co sulfide deposit, Labrador, Canada. *Mineralium Deposita*, 47, 23-50.
- Manor, M.J., Scoates, J.S., Nixon, G.T., and Ames, D.E., 2014. Platinum-group mineralogy of the Giant Mascot Ni-Cu-PGE deposit, Hope, B.C. In: *Geological Fieldwork 2013*, British Columbia Ministry of Energy and Mines, British Columbia Geological Survey Paper 2014-1, pp. 141-156.
- Manor, M.J., Scoates, J.S., Nixon, G.T., and Ames, D.E., 2016. The Giant Mascot Ni-Cu-PGE deposit, British Columbia: Mineralized conduits in a convergent margin tectonic setting. *Economic Geology*, 111, 57-87.
- Mao, Y.-J., Qin, K.-Z., Li, C., and Tang, D.-M., 2015. A modified genetic model for the Huangshandong magmatic sulfide deposit in the Central Asian Orogenic Belt, Xinjiang, western China. *Mineralium Deposita*, 50, 65-82.
- Mavrogenes, J.A., and O'Neill, H.S.C., 1999. The relative effects of pressure, temperature and oxygen fugacity on the solubility of sulfide in mafic magmas. *Geochimica et Cosmochimica Acta*, 63, 1173-1180.
- McCarthy, A., and Müntener, O., 2017. Mineral growth in melt conduits as a mechanism for igneous layering in shallow arc plutons: mineral chemistry of Fisher Lake orbicules and comb layers (Sierra Nevada, USA). *Contributions to Mineralogy and Petrology*, 172, 55.
- McCarthy, A., Müntener, O., Bouvier, A.-S., and Baumgartner, L., 2016. Melt Extraction Zones in Shallow Arc Plutons: Insights from Fisher Lake Orbicules (Sierra Nevada, Western USA). *Journal of Petrology*, 57, 2011-2052.
- Milidragovic, D., Nixon, G.T., Scoates, J.S., Nott, J.A., and Spence, D.W., 2021. Redox-controlled chalcophile element geochemistry of the Polaris Alaskan-type mafic-ultramafic complex, British Columbia, Canada. *The Canadian Mineralogist*, 59, 1627-1660.
- Milidragovic, D., Nott, J.A., Spence, D.W., Schumann, D., Scoates, J.S., Nixon, G.T., and Stern, R.A., 2023. Sulfate recycling at subduction zones indicated by sulfur isotope systematics of Mesozoic ultramafic island arc cumulates in the North American Cordillera. *Earth and Planetary Science Letters*, 620, article 118337.
<<https://doi.org/10.1016/j.epsl.2023.118337>>
- Moore, J.G., and Lockwood, J.P., 1973. Origin of comb layering and orbicular structure, Sierra Nevada Batholith, California. *Geological Society of America Bulletin*, 84, 1-19.
- Mudd, G.M., and Jowitt, S.M., 2014. A detailed assessment of global nickel resource trends and endowments. *Economic Geology*, 109, 1813-1841.
- Mudd, G.M., and Jowitt, S.M., 2022. The new century for nickel resources, reserves, and mining: Reassessing the sustainability of the devil's metal. *Economic Geology*, 117, 1961-1983.
- Mudd, G.M., Jowitt, S.M., and Werner, T.T., 2018. Global platinum group element resources, reserves and mining - A critical assessment. *Science of The Total Environment*, 622-623, 614-625.
- Mungall, J.E., 2014. Geochemistry of magmatic ore deposits. In: *Treatise on Geochemistry*, Elsevier, pp. 195-218.
- Mungall, J., and Su, S., 2005. Interfacial tension between magmatic sulfide and silicate liquids: Constraints on kinetics of sulfide liquation and sulfide migration through silicate rocks. *Earth and Planetary Science Letters*, 234, 135-149.
- Mungall, J.E., Brennan, J.M., Godel, B., Barnes, S.J., and Gaillard, F., 2015. Transport of metals and sulphur in magmas by flotation of sulphide melt on vapour bubbles. *Nature Geoscience*, 8, 216-219.
- Naldrett, A.J., 1989. Introduction: Magmatic deposits associated with mafic rocks. In: Whitney, J. A., Naldrett, A.J., (Eds.), *Ore Deposition Associated with Magmas*. Society of Economic Geologists, 4, pp. 1-3.
- Naldrett, A.J., 1992. A model for the Ni-Cu-PGE ores of the Noril'sk region and its application to other areas of flood basalt. *Economic Geology*, 87, 1945-1962.
- Naldrett, A.J., 1999. World-class Ni-Cu-PGE deposits: key factors in their genesis. *Mineralium Deposita*, 34, 227-240.
- Naldrett, A.J., 2010. From the mantle to the bank: The life of a Ni-Cu-(PGE) sulfide deposit. *South African Journal of Geology*, 113, 1-32.
- Naldrett, A.J., Cragi, J.R., and Kellurud, G., 1967. The central portion of the Fe-Ni-S system and its bearing on pentlandite exsolution in iron-nickel sulfide ores. *Economic Geology*, 62, 826-847.
- Nelson, J.L., Diakow L., van Staal, C., and Chipley, D., 2013. Ordovician volcanogenic sulphides in the southern Alexander terrane, coastal NW British Columbia: geology, Pb isotopic signature, and a case for correlation with Appalachian and Scandinavian deposits. In: *Geological Fieldwork 2012*, British Columbia Ministry of Energy, Mines and Natural Gas, British Columbia Geological Survey Paper 2013-1, pp. 13-33.
- Nelson, J., Waldron, J., van Straaten, B., Zagorevski, A., and Rees, C., 2018. Revised stratigraphy of the Hazelton Group in the Iskut River region, northwestern British Columbia. In: *Geological Fieldwork 2017*. British Columbia Ministry of Energy, Mines and Petroleum Resources, British Columbia Geological Survey Paper 2018-01, pp. 15-38.
- Nelson, J.L., van Straaten, B., and Friedman R., 2022. Latest Triassic-Early Jurassic Stikine-Yukon-Tanana terrane collision and the onset of accretion in the Canadian Cordillera: Insights from Hazelton Group detrital zircon provenance and arc-back-arc configuration. *Geosphere*, 18, 670-696.
- Nixon, G.T., Manor, M.J., and Scoates, J.S., 2018. Cu-PGE Sulphide mineralization in the Tulameen Alaskan-type Intrusion: Analogue for Cu-PGE reefs in layered Intrusions? *British Columbia Ministry of Energy, Mines and Petroleum Resources, British Columbia Geological GeoFile 2018-02*.
- Nixon, G.T., Scheel, J.E., Scoates, J.S., Friedman, R.M., Wall, C.J., Gabites, J., and Jackson-Brown, S., 2020. Syn-accretionary multistage assembly of an Early Jurassic Alaskan-type intrusion in the Canadian Cordillera: U-Pb and ⁴⁰Ar/³⁹Ar geochronology of the Turnagain ultramafic-mafic intrusive complex, Yukon-Tanana terrane. *Canadian Journal of Earth Sciences*, 57, 575-600.
- O'Neill, H.S.C., and Mavrogenes, J.A., 2002. The Sulfide Capacity and the Sulfur Content at Sulfide Saturation of Silicate Melts at 1400°C and 1 bar. 43, 39.
- Piña, R., Romeo, I., Ortega, L., Lunar, R., Capote, R., Gervilla, F., Tejero, R., and Quesada, C., 2010. Origin and emplacement of the Aguablanca magmatic Ni-Cu-(PGE) sulfide deposit, SW Iberia: A multidisciplinary approach. *Geological Society of America Bulletin*, 122, 915-925.
- Piña, R., Gervilla, F., Barnes, S.-J., Oberthür, T., and Lunar, R., 2016. Platinum-group element concentrations in pyrite from the Main Sulfide Zone of the Great Dyke of Zimbabwe. *Mineralium Deposita*, 51, 853-872.
- Ripley, E., and Li, C., 2011. A review of conduit-related Ni-Cu-(PGE) sulfide mineralization at the Voisey's Bay Deposit, Labrador, and the Eagle Deposit, northern Michigan. *Reviews in Economic Geology*, 17, 181-197.

- Ripley, E.M., and Li, C., 2013. Sulfide saturation in mafic magmas: is external sulfur required for magmatic Ni-Cu-(PGE) ore genesis? *Economic Geology*, 108, 45-58.
- Sappin, A.-A., Constantin, M., Clark, T., and Van Breemen, O., 2009. Geochemistry, geochronology, and geodynamic setting of Ni-Cu±PGE mineral prospects hosted by mafic and ultramafic intrusions in the Portneuf-Mauricie Domain, Grenville Province, Quebec. *Canadian Journal of Earth Sciences*, 46, 331-353.
- Scheel, J.E., 2004. Age and origin of the Turnagain Alaskan-type intrusion and associated Ni-sulphide mineralization, north-central British Columbia, Canada. Unpublished MSc. thesis, University of Alberta, 201 p.
- Shahabi Far, M., Samson, I.M., Gagnon, J.E., Good, D.J., Linnen, R.L., and Ames, D., 2019. Evolution of a conduit system at the Marathon PGE-Cu deposit: Insights from silicate mineral Textures and Chemistry. *Journal of Petrology*, 60, 1-3.
- Smillie, R.W., and Turnbull, R.E., 2014. Field and petrographical insight into the formation of orbicular granitoids from the Bonney Pluton, southern Victoria Land, Antarctica. *Geological Magazine*, 151, 534-549.
- Stifter, E.C., Ripley, E.M., and Li, C., 2016. Os and S isotope studies of ultramafic rocks in the Duke Island Complex, Alaska: variable degrees of crustal contamination of magmas in an arc setting and implications for Ni-Cu-PGE sulfide mineralization. *Mineralium Deposita*, 51, 903-918.
- Sun, T., Tan, S.-C., Yang, S.-H., Hanski, E., Zhou, J.-X., Li, H.-T., Zhang, A.-P., Li, W.-T., and Zhou, Y.-G., 2021. Early Permian subduction-related Ni-Cu sulfide mineralization in the Central Asian Orogenic Belt: A case of the Halatumiao deposit. *Ore Geology Reviews*, 130, article 103974.
<<https://doi.org/10.1016/j.oregeorev.2020.103974>>
- Sylvester, A.G., 2011. The nature and polygenetic origin of orbicular granodiorite in the Lower Castle Creek pluton, northern Sierra Nevada batholith, California. *Geosphere*, 7, 1134-1142.
- Thakurta, J., Ripley, E.M., and Li, C., 2008. Geochemical constraints on the origin of sulfide mineralization in the Duke Island Complex, southeastern Alaska. *Geochemistry, Geophysics, Geosystems*, 9, 1-34.
- Vandenburg, E.D.J., 2020. The E&L magmatic Ni-Cu-(PGE) deposit, northwestern British Columbia: Preliminary sulfide petrology, platinum-group element mineralogy and lead isotope systematics. Unpublished B.Sc. thesis, The University of British Columbia, 194 p.
- Wang, S., Wu, C., Muhtar, M.N., Lei, R., and Brzozowski, M.J., 2021. Mobilization of ore-forming metals during post-magmatic hydrothermal overprinting of the Huangshandong Ni-Cu sulfide deposit, Eastern Tianshan, NW China. *Ore Geology Reviews*, 137, article 104315.
<<https://doi.org/10.1016/j.oregeorev.2021.104315>>
- Watkinson, D.H., and Dunning, G., 1979. Geology and platinum-group mineralization, Lac-des-Iles Complex, northwestern Ontario. *Canadian Mineralogist*, 17, 453-462.
- Williams, D.A., Kerr, R.C., and Leshner, C.M., 1998. Emplacement and erosion by Archean komatiite lava flows at Kambalda: Revisited. *Journal of Geophysical Research: Solid Earth*, 103, 27533-27549.
- Xue, S., Wang, Q., Wang, Y., Song, W., and Deng, J., 2023. The roles of various types of crustal contamination in the genesis of the Jinchuan magmatic Ni-Cu-PGE deposit: New mineralogical and C-Sr-Nd isotope constraints. *Economic Geology*.
<<https://doi.org/10.5382/econgeo.5017>>
- Yao, Z., and Mungall, J.E., 2020. Flotation mechanism of sulphide melt on vapour bubbles in partially molten magmatic systems. *Earth and Planetary Science Letters*, 542, article 116298.
<<https://doi.org/10.1016/j.epsl.2020.116298>>
- Zhang, A., Sun, T., Zhao, Z., Zhou, J., Li, W., Qi, Q., and Wei, X., 2021. Genesis of the Neoproterozoic subduction-related Taoke Ni-Cu-PGE sulphide deposit in the North China Craton: Constraints from Os-S isotopes and PGE geochemistry. *Geological Journal*, 56, 4888-4903.

Mineral potential modelling results for northwestern British Columbia, a comparison between past and current work at the British Columbia Geological Survey



Curran D. Wearmouth¹, Katie J. Peters², Thomas A. Czertowicz², and Evan A. Orovan¹

¹ British Columbia Geological Survey, Ministry of Energy, Mines and Low Carbon Innovation, Victoria, BC, V8W 9N3

² Kenex Pty Ltd., Wellington, New Zealand, 5013

^a corresponding author: Curran.Wearmouth@gov.bc.ca

Recommended citation: Wearmouth, C.D., Peters, K.J., Czertowicz, T.A., and Orovan, E.A., 2024. Mineral potential modelling results for northwestern British Columbia, a comparison between past and current work at the British Columbia Geological Survey. In: Geological Fieldwork 2023, British Columbia Ministry of Energy, Mines and Low Carbon Innovation, British Columbia Geological Survey Paper 2024-01, pp. 79-95.

Abstract

Nearly thirty years ago, the British Columbia Geological Survey (BCGS) initiated a project to assess the mineral potential of the entire province, the first assessment of its kind. This project combined data about known mineral occurrences and the geology of the province, and what was then understood about which rocks favour mineral deposition to develop a relative ranking of mineral potential for a broad range of deposit types. To aid in the search for the critical minerals needed for a low-carbon future, the BCGS has revitalized its mineral potential mapping efforts, taking advantage of about 30 years of new data, knowledge, advances in GIS applications, and computer power to enable statistical analysis of spatial data using weights of evidence modelling. A comparison of results between work done in the 1990s and the current modelling for a large region of northern British Columbia indicates that the new work largely corroborates the old. Both are of value for assisting land-use decisions and for mineral exploration. The 1990s work ranks certain areas as having a significantly higher relative prospectivity because the original work focused on deposit profiles that classified occurrences into about 120 deposit types for a wide range of metals whereas the new work adopted a mineral systems approach to examine critical mineral potential, considering only the porphyry, volcanogenic massive sulphide, and magmatic mafic-ultramafic systems. The recent work ranks some areas as having a significantly higher relative prospectivity mainly because it uses new data and knowledge accumulated in the last 30 years. The revitalized modelling is far less labour intensive than the work done in the 1990s. Automated manipulation of spatial data and statistical analysis will ease making updates and making future iterations more comprehensive by including other mineral systems.

Keywords: Mineral potential modelling, mineral potential map, land-use planning, mineral systems, statistical methods, geospatial data treatment, predictive maps, weights of evidence, data-driven modelling, porphyry deposits, volcanogenic massive sulphide deposits, magmatic mafic-ultramafic deposits

1. Introduction

Nearly 30 years ago, the British Columbia Geological Survey (BCGS) initiated a project to assess the mineral potential of the entire province in support of land-use decisions. Applying approaches developed by the United States Geological Survey (Brew, 1992; Singer, 1993) but modified for British Columbia, this work was the first state- or province-wide assessment of its kind. The project combined data about known mineral occurrences and the geology of the province, and what was then understood about which rocks favour mineral deposition to develop a relative ranking of mineral potential, with defined 'tracts' of lower to higher potential (Kilby, 1995, 1996, 2004). Prompted by the global search for the critical minerals needed for a low-carbon future, the BCGS started a program to inventory the critical minerals that are produced or could be produced in the province (Hickin et al., 2023) and renew mineral potential studies with a focus on these minerals. Since the original assessment was carried out, bedrock mapping

projects have increased our knowledge of the rocks underlying the province. Additionally, exploration techniques have improved, many new mineral occurrences have been discovered and the geologic processes leading to mineralization have been intensively investigated. Furthermore, exponential increases in computing power have led to significant advances in applying geographic information system (GIS) platforms and using computerized statistical methods to model mineral potential (Partington, 2010; Porwal and Kreuzer, 2010; Harris et al., 2015; Kreuzer et al., 2015; Ford et al., 2019; Yousefi et al., 2019, 2021; Ford, 2020; Lawley et al., 2021). These advances have been adopted by geoscientists in industry, government, and academia for appraising mineral potential (Knox-Robinson and Wyborn, 1997; Harris et al., 2015; Kreuzer et al., 2015; Lawley et al., 2021; Nykanen et al., 2023).

The rejuvenated modelling at the BCGS also applies these advances (for details see Wearmouth et al., in press). Like the original program of the 1990s, the new modelling will

assist land-use conversations between multiple parties with diverse interests. Also, the new work will be used to evaluate the provincial endowment of the critical minerals needed to support the low-carbon transition, grow the economy, diversify global supply chains, and continue as a preferred supplier for partner nations (Hickin et al., 2023). In this paper we describe the methods used in the work done in the 1990s and the work currently being done, then compare the results for a large area of northwest British Columbia, which includes the traditional lands of the Gitanyow, Kaska Dena, Kwadacha, Metlakatla, Nisga'a, Tahltan, Takla Lake, Taku River Tlingit, Tsay Keh Dene, and Tsetsaut Skii Km Lax Ha First Nations (Fig. 1).

2. Geologic context

The study area spans a large segment in the northwestern part of the Canadian Cordillera (Fig. 1). This 2000 km long northwest-trending accretionary orogen consists of several long, narrow, far-travelled terranes (in some cases, 1000s of km) that welded to the western margin of Ancestral North America in the last 180 million years (e.g., Nelson et al., 2013; Colpron and Nelson, 2021). The Cordillera records a history of supercontinent rifting and a succession of island arc volcanosedimentary and intrusive assemblages (terranes) developed outboard of Ancestral North America and accreted to each other and to the proto-continental margin with final amalgamation produced by collisions driven by the westward motion of the North American continental plate. The amalgamated Cordillera then became the site of Cretaceous and Cenozoic arc and post-arc magmatism. Terrane evolution continues today as the Juan de Fuca plate slides beneath Vancouver Island. As reviewed by Nelson et al. (2013), Hickin et al. (2017) and Colpron and Nelson (2021), the diverse tectonic processes, from supercontinent breakup through development of long-lived arc terranes, to terrane accretion and post-accretion magmatism, metamorphism, deformation, and sedimentation, have generated diverse mineral systems across the province.

West of Ancestral North America, Cordilleran terranes are commonly grouped into superterranes and terranes (Fig. 1). Ancestral North America (including Cassiar terrane) consists of predominantly sedimentary rocks that were deposited on cratonic basement during the Paleoproterozoic and Mesoproterozoic and during and after the Neoproterozoic to Cambrian breakup of the supercontinent Rodinia, which created the western margin of Laurentia, the nucleus of what is now North America. The Intermontane superterrane consists of a diverse group of Late Paleozoic to Mesozoic volcanosedimentary assemblages and kindred intrusive bodies that formed mainly in and adjacent to island arcs outboard of Ancestral North America in the proto-Pacific Ocean. The Insular superterrane consists of similar island arc terranes; the Intermontane-Insular terrane boundary lies within the syn- to post-accretionary Coast Plutonic complex, a linear arc-axial belt that extends the length of the Cordillera. The Outboard terranes are mostly late Mesozoic to Cenozoic forearc

siliciclastic assemblages, bounded to the west by the present-day Cascadia subduction zone and Queen Charlotte fault. Modern-day volcanic complexes related to Cascadia subduction are distributed along the length of the western Cordillera, and many of the terranes are partially covered by sedimentary rocks that were deposited during terrane accretion and collision, when older rocks were deformed, uplifted, eroded, and redeposited in newly created sedimentary basins. The variety of tectonic settings and paleogeographic environments recorded by these terranes and superterranes since the Mesoproterozoic generated conditions favourable for a variety of mineral systems.

Current exploration in the study area, which includes parts of the Northwest and North Central mining regions, focuses on a diverse suite of deposits (see summary in Clarke et al., 2024). The study area includes two active mines (Brucejack and Red Chris) and one mine (Premier Gold) is on track to have its first gold pour in 2024. All three are in the 'Golden Triangle', the popular name for a loosely defined area in the Northwest Region containing significant gold, silver, copper, and molybdenum deposits (British Columbia Geological Survey, 2023).

3. Mineral potential modelling methods in British Columbia, past and present

Depending on the purpose and the data available for a given area, different methods can be used to assess the prospectivity of an area of interest. These methods are commonly expressed in terms of being 'knowledge-driven' ('expert-driven') or 'data-driven' (e.g., Bonham-Carter, 1994, p. 269). However, these terms are pure end-members of a continuum and are unlikely to fully apply to any given case. For example, even though the early BCGS modelling relied heavily on geoscience experts to make key decisions, it was fundamentally based on mineral occurrence (MINFILE), bedrock geology, geochronologic, geochemical, aeromagnetic, and industry assessment report (ARIS) data and the knowledge gained from these data. Similarly, even though the current modelling uses computer algorithms instead of geoscience experts, human interventions and expert knowledge are still required at different stages. Furthermore, both the old and new modelling use similar data sources; although the new modelling accesses more up-to-date data, much of the data in both cases are not entirely 'raw' but based on human interpretations. For example, all geological maps are inherently interpretive and rock unit boundaries, or the existence, positioning, or relative age of faults are made by mappers. Or knowledge experts make decisions about what deposit type or mineral system a given mineral occurrence should be assigned to in the MINFILE or ARIS databases. The fundamental difference between knowledge-driven and data-driven modelling is in how weights are assigned to the data (Bonham-Carter, 1994, p. 269). In knowledge-driven methods, data are reviewed and subjectively weighted by experts, relying on their level of expertise and knowledge and are thus considered more subjective (Bonham-Carter, 1994). Examples of knowledge-driven techniques include index overlay

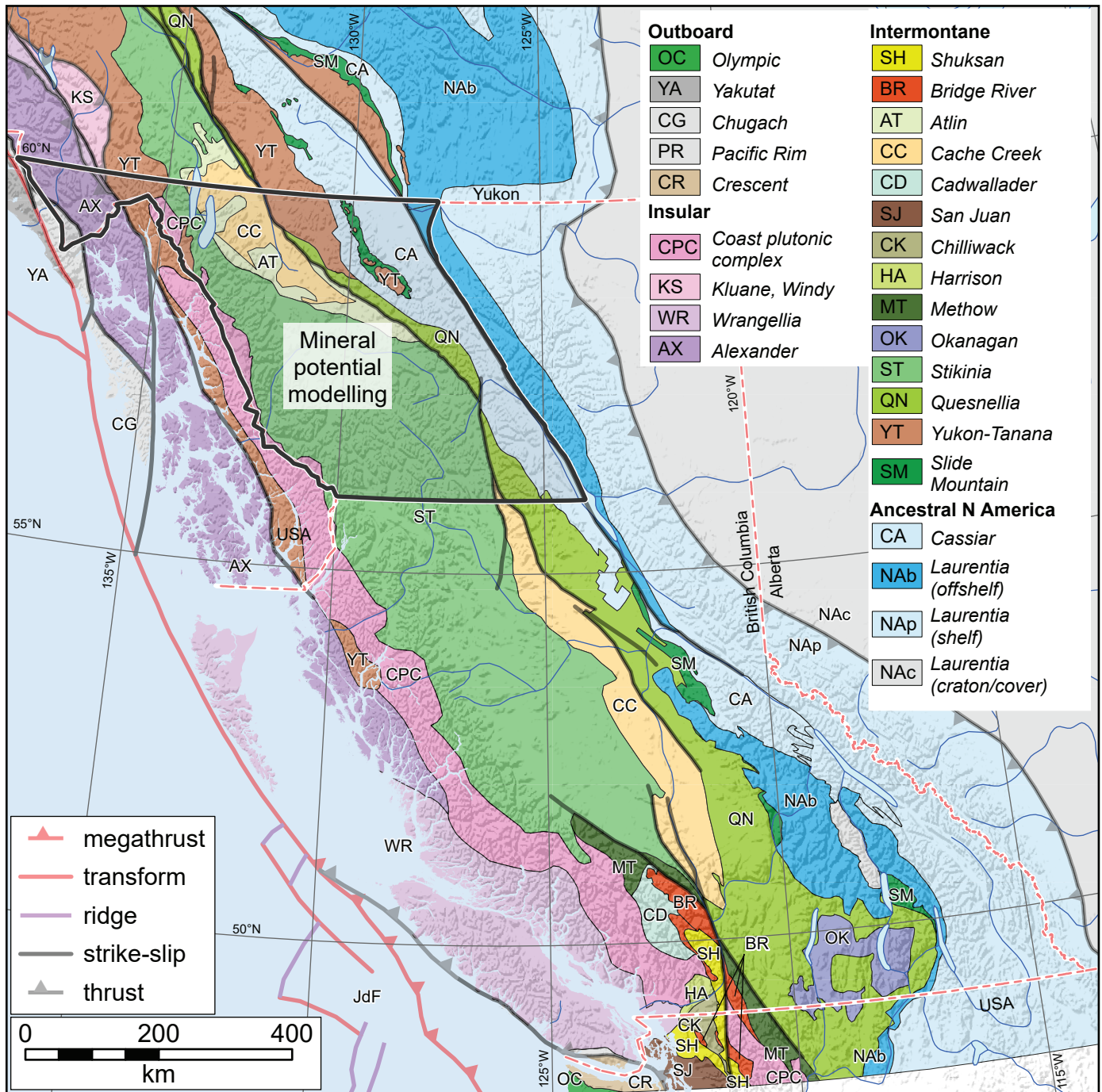


Fig. 1. Mineral potential modelling study area, 2023. Terranes after Colpron (2020).

(Yousefi and Carranza, 2016) and fuzzy logic (e.g., Porwal et al., 2003). In data-driven methods, computer algorithms seek statistical associations or patterns within data to determine relevance to known training data and are thus considered more objective. Examples of data-driven methods include weights of evidence (e.g., Bohnam-Carter et al., 1990), random forest (Ford, 2020), and neural networks (Singer and Koudu, 1999).

3.1. 1990s mineral potential project

The British Columbia Geological Survey has mapped and inventoried the mineral deposits of the province for more than 130 years (Sutherland Brown, 1998). The Mineral Potential project, later referred to as the Level 1 Mineral Resource Assessment (MacIntyre et al., 2004, 2009), was initiated in 1992 by the British Columbia Geological Survey to assist land-use decisions. The project objectives were to: 1) rank the land base of the province by its ability to support economic activity

through mineral exploration and extraction, 2) produce credible and understandable evaluations by all users; and 3) incorporate the expertise of the mining and exploration communities (Kilby, 2004). Level 2 mineral resource assessments were developed for smaller areas in northwest (MacIntyre and Kilby, 2009; MacIntyre et al., 2009) and coastal British Columbia (MacIntyre et al., 2003, 2004).

The 1990s work combined known mineral occurrences, what was then understood about which rocks favour mineral deposition, and the geology of a given area to develop a relative ranking of mineral potential (Kilby, 1995, 2004; MacIntyre and Kilby, 2009). Emphasizing the differences between deposit types, mineral potential assessments focused on deposit profiles that classified occurrences into about 120 deposit types based mainly on genetic models (see Lefebure and Jones, 2022). The profiles included descriptions of geological characteristics, mineral exploration techniques, resource data, age of mineralization, tectonic setting, and concepts about deposit origins. The approach used built on work by the United States Geological Survey (Brew, 1992; Singer, 1993) but modified for British Columbia (Kilby, 2004). Tracts of land of similar geological character were defined and experts from government, industry, and academia assessed all available data to determine probabilistic estimates for the expected number of undiscovered deposits. The ranking of the land base for metallic deposits was based on the gross in-place value of the commodities for both known and estimated undiscovered deposits. The dollar value of each tract was determined using expert input, commodity prices, and a Monte Carlo simulation to determine probable tonnage and grade information for each deposit type. Importantly, the dollar scores were intended as a ranking tool and not intended to imply a particular dollar value to the ground being ranked.

Mineral potential regions were defined and divided further into tracts, which contain similar geological characteristics, but separated from other tracts by faults or major contacts (Kilby, 2004). The final products included regional maps, showing the relative ranking of tracts based on metallic mineral potential. Additional attribute information such as tract area, number of mineral occurrences, value of known resources, value of past production, and value of exploration expenditures were provided. Mineral resource assessment data were also provided for each tract and included the number of potential new deposit discoveries by type, dollar value of commodities in potential discoveries, types of commodities expected to be discovered, and the relative ranking of a tract out of 794 tracts in the province (Fig. 2).

3.2. 2023 mineral potential modelling

To support current land-use decisions and to evaluate critical mineral opportunities, the Survey is now reviving provincial mineral potential assessment. Like the work done in the 1990s, the data used in the current work comes from MINFILE, BC Digital Geology, and geochemical databases curated by the British Columbia Geological Survey and integrated with

MapPlace, the BCGS open access geospatial web service (Cui et al., 2018). We also used regional-scale gravity (Natural Resources Canada, 2020a) and aeromagnetic data (Natural Resources Canada, 2020b).

The current work adopts mineral systems concepts that can be used to focus on specific commodities such as critical minerals in contrast to the 1990s work, which does not provide commodity-specific information. The current work also uses a data-driven weights of evidence approach.

3.2.1. Mineral systems

In contrast to the 1990s work, which emphasized the differences between deposits split into about 120 types (Lefebure and Jones, 2022), the current assessment adopts a mineral system approach, which emphasizes similarities between deposits and uses a large-scale view of all the factors that control generating and preserving deposits (e.g., Knox-Robinson and Wyborn, 1997; Hronsky and Groves, 2008; McCuaig et al., 2010; Ford et al., 2019; Groves et al., 2022). Originally proposed by Wyborn et al. (1994) and drawing on ideas from the petroleum industry (e.g., Magoon and Dow, 1994), the geological components that have been traditionally used to define a single mineral system include energy to drive the system, source of ligands, source of metals, transport pathways, traps, and outflow zones (Knox-Robinson and Wyborn, 1997). Adapting the traditional use, the mineral system concept we adopt uses source, transport, trap and direct detection of ore deposits as a proxy for the presence of a complete mineral system. The approach recognizes that the ore deposit, which is relatively small (<km in plan view), is the central feature of a larger system that may be detectable at a regional scale (>10 km in plan view). The mineral systems approach focuses on processes that are common across mineral systems, which enables the simultaneous assessment of many deposit types at a variety of scales (McCuaig et al., 2010). An economic deposit is unlikely if any one of source, transport, and trap are lacking; areas that bear evidence for all components will be evaluated as being favorable for mineralization. Being process-based, the mineral systems approach is neither restricted to a geological setting nor limited to a specific ore deposit type. To date, the new modelling has focused on the porphyry, volcanogenic massive sulphide, and magmatic mafic to ultramafic sulphide mineral systems.

3.2.2. Weights of evidence modelling

The current work uses weights of evidence modelling to rank the mineral potential of the study area (see Wearmouth et al., in press for details). Weights of evidence is a Bayesian statistical approach that allows the analysis and combination of various datasets to predict the location of the feature in question (Bonham-Carter, 1994). This technique calculates the relationship of the feature being tested for a given area and the number of training data points (sites of known mineralization; Tables 1-3) that fall within that area. The statistical spatial analysis allows for a non-biased assessment of a large

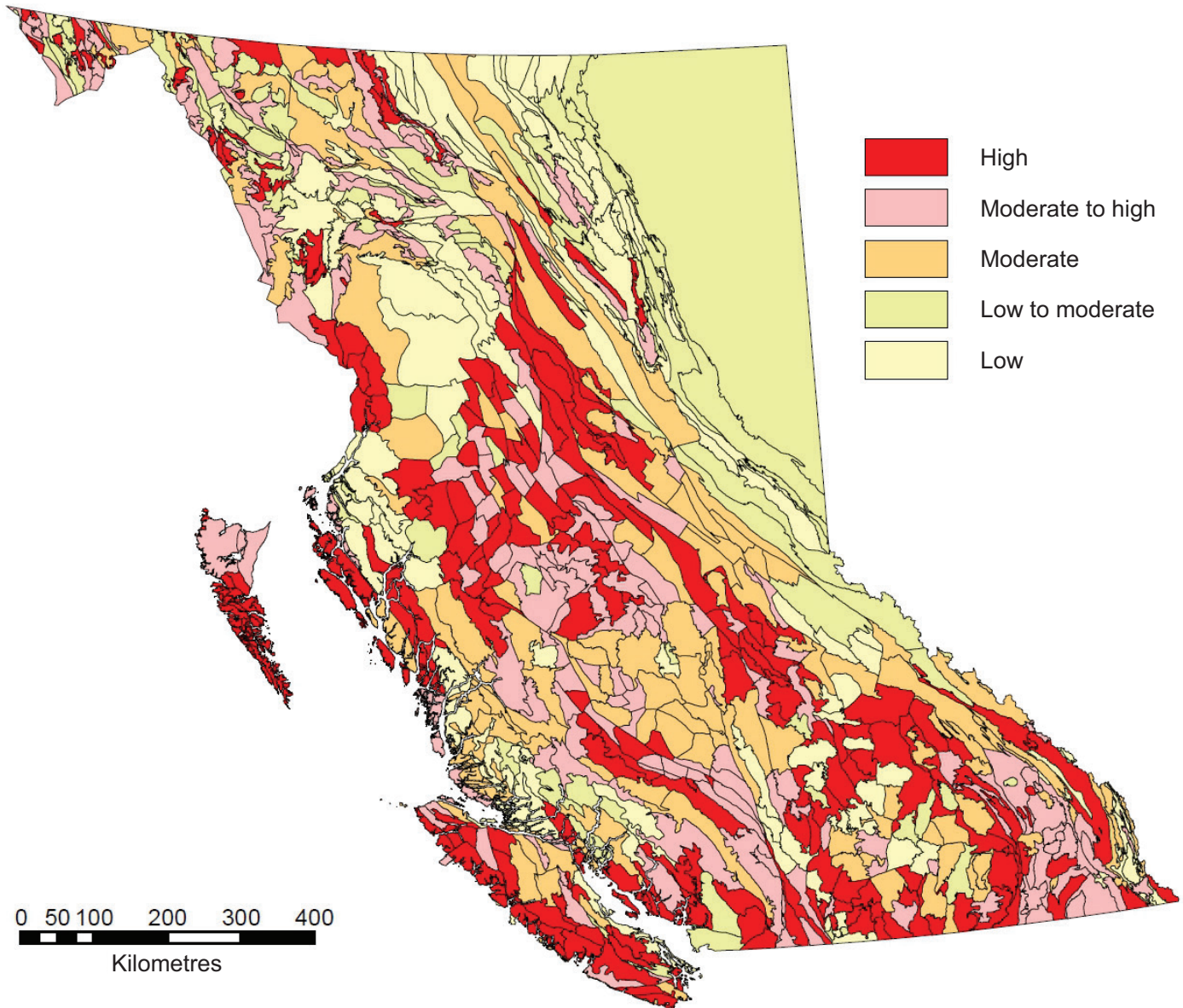


Fig. 2. Metallic mineral potential map for British Columbia based on the Mineral Potential project completed in 1997. Total number of tracts is 794. From MacIntyre (2004).

Table 1. Porphyry model training points.

Name	Status	Mineralization style	Belt	Terrane
Galore Creek	Developed prospect	Alkalic porphyry Cu-Au	Intermontane	Stikine
Kemess South	Past producer	Porphyry Cu +/- Mo +/- Au	Intermontane	Stikine
Schaft Creek	Developed prospect	Porphyry Cu +/- Mo +/- Au	Intermontane	Stikine
Saddle North	Prospect	Porphyry Cu +/- Mo +/- Au,	Intermontane	Stikine
KSM	Developed prospect	Porphyry Cu +/- Mo +/- Au	Intermontane	Stikine
Red Chris	Producer	Porphyry Cu +/- Mo +/- Au	Intermontane	Stikine
Thorn	Prospect	Subvolcanic Cu-Ag-Au	Insular	Stikine
Eaglehead	Developed prospect	Porphyry Cu +/- Mo +/- Au	Intermontane	Cache Creek
Bronson Slope	Developed prospect	Porphyry Cu +/- Mo +/- Au	Insular	Stikine
Gnat Pass	Developed prospect	Porphyry Cu +/- Mo +/- Au	Intermontane	Stikine
Hat	Prospect	Alkalic porphyry Cu-Au	Intermontane	Stikine
Ruby Creek	Developed prospect	Porphyry Mo (Low F- type)	Intermontane	Cache Creek

Table 2. Volcanogenic massive sulphide model training points.

Name	Status	Mineralization style	Belt	Terrane
Eskay Creek	Past producer	Noranda/Kuroko	Intermontane	Stikine
Dago	Past producer	Noranda/Kuroko	Intermontane	Stikine
Tulsequah Chief	Past producer	Noranda/Kuroko	Coast Plutonic	Nisling
Kutcho	Developed prospect	Noranda/Kuroko	Intermontane	Cache Creek
Granduc	Past producer	Besshi	Intermontane	Stikine
Rock and Roll	Developed prospect	Besshi	Intermontane	Stikine
Joss'alun	Prospect	Cyprus	Intermontane	Stikine
Windy Craggy	Developed prospect	Besshi	Insular	Alexander
Mount Henry	Prospect	None attributed	Insular	Alexander

Table 3. Magmatic mafic-ultramafic model training points.

Name	Status	Mineralization style	Belt	Terrane
E&L	Developed prospect	Tholeiitic intrusion-hosted	Intermontane	Stikine
Turnagain Nickel	Developed prospect	Alaskan-type	Intermontane	Quesnel
Orca	Showing	Alaskan-type	Intermontane	Cache Creek
Nixon	Showing	Alaskan-type	Intermontane	Quesnel
Mandible	Prospect	Alaskan-type	Intermontane	Cache Creek
Queen	Prospect	Alaskan-type	Intermontane	Quesnel
HC	Prospect	Alaskan-type	Intermontane	Quesnel
Anyox-Rodeo	Showing	Flood basalt-associated	Coast Plutonic	Nisling
Taurus	Showing	Alaskan-type	Intermontane	Quesnel
TNS12	Showing	Tholeiitic intrusion-hosted	Intermontane	Stikine

number of mappable proxies (e.g., distance to intrusive rock contacts, density of fault intersections, presence of anomalous geochemical stream-sediment sample, and occurrence of magnetic high anomalies) for ore-forming processes to determine their relevance to the mineral system (Bonham-Carter, 1994). We used the Arc-SDM extension for ArcGIS to carry out this analysis and the mineral potential modelling.

Using input parameters (area being examined, unit cell area, number of training points) a 'prior probability' was calculated for each mineral system. The prior probability represents the chance of randomly discovering a deposit in the study area before any additional evidence for mineralization is applied. The aim of weights of evidence modelling is to add evidence in support of hypotheses to increase or decrease the prior probability of each grid cell in the study area. The probability of finding a new occurrence after adding layers of evidence is referred to as the 'posterior probability'. Layers of evidence, or predictive maps, that reduce the search space while capturing the most training points will have the best spatial correlations and their combination will result in highest posterior probabilities when combined into the model (Bonham-Carter, 1994; Bonham-Carter et al., 1990). The spatial correlation, or the contrast value (C), of a mappable feature (e.g., distance to faults) was calculated by using the relationship between the area with the feature being tested and the number of training

data points that fall within that area compared with the number of points that fall in the remainder of the study area. The studentized contrast (StudC) value is also calculated during the weights of evidence process and indicates the uncertainty in the C value (Tables 4-6).

The predictive maps derived from the spatial correlation analysis are typically binary, distinguishing areas favourable or unfavourable for capturing training points (Figs. 3-5). These predictive maps were input into the final mineral potential model for each mineral system. The output of the mineral potential modelling is a grid that maps the geological potential for mineralization for each grid cell (Fig. 6). The output grid values range from 0 to 1 and map the posterior probability, which has either increased or decreased from the prior probability, depending on the combination of weighted predictive map variables. The final grid represents the relative prospectivity ranking of cells rather than an absolute measure of the probability of finding a deposit (Agterberg and Bonham-Carter, 1990; Bonham-Carter, 1994; Ford et al., 2019). This is because ore-forming geological processes are commonly interconnected and not strictly independent. Therefore, weights of evidence assumes conditional independence, which leads to posterior probabilities being overestimated in the final mineral potential model (Bonham-Carter, 1994; Bonham-Carter et al., 1990).

Table 4. Statistical spatial analysis results for predictive maps used in the porphyry model.

Mineral system component	Spatial variable	Variable ID	# TP	C	StudC
Source	Distance to 237-170 Ma rocks	200 m	11	3.7	3.6
	Distance to volcanic rocks	2350 m	11	3.0	2.9
Transport	Distance to contacts of intermediate and felsic intrusives (+ high total residual total field magnetic areas)	Class 9-10 (>160 nT/m), felsic intrusive, 1000 m	11	4.0	3.8
	Distance to all faults	850 m	10	3.0	3.8
Trap	Fault intersection density	Class 4-10 (moderate to high density)	12	2.7	2.6
Deposition	Ag stream anomalies	Ag > 0.33 ppm	11	2.0	1.9
	Au stream anomalies	Au > 0.01 ppm	12	1.9	1.8
	Cu stream anomalies	Cu > 106.05 ppm	10	1.9	2.5

Table 5. Statistical spatial analysis results for predictive maps used in the volcanogenic massive sulphide model.

Mineral system component	Spatial variable	Variable ID	# TP	C	StudC
Source	Distance to volcanic and volcanoclastic rocks (and metamorphic equivalents)	300 m	9	3.2	4.1
Transport	Distance to minor faults	3100 m	10	3.0	2.8
Trap	Fault intersection density	Class 5-10 (moderate to high density)	9	2.2	2.8
Deposition	Stream sediment Ag anomaly (mean, reclassified)	Class 10 (>0.27 ppm)	5	2.3	3.6
	Stream sediment Cu anomaly (mean of each catchment)	Class 8-10 (>50.4 ppm Cu)	10	3.1	2.9
	Rock chip Au anomaly	66.75 ppb Au, 2000 m buffer	3	2.2	1.9

Table 6. Statistical spatial analysis results for predictive maps used in the magmatic mafic-ultramafic model.

Mineral system component	Spatial variable	Variable ID	# TP	C	StudC
Source	Distance to ultramafic or mafic intrusives	300 m	6	5.0	6.1
Transport	Distance to minor faults	2700 m	7	2.8	2.6
Trap	Magnetics 1st vertical derivative	Class 8 – 10 (>0.0085 nT/m)	7	3.0	2.8
	Fault density	Class 7-10 (high density)	8	2.4	2.2
Deposition	Gravity isostatic residual	Class 7 – 10 (>9.50 mGal)	7	2.4	2.2
	Stream sediment Co anomaly	33.05 ppm	7	2.4	2.2

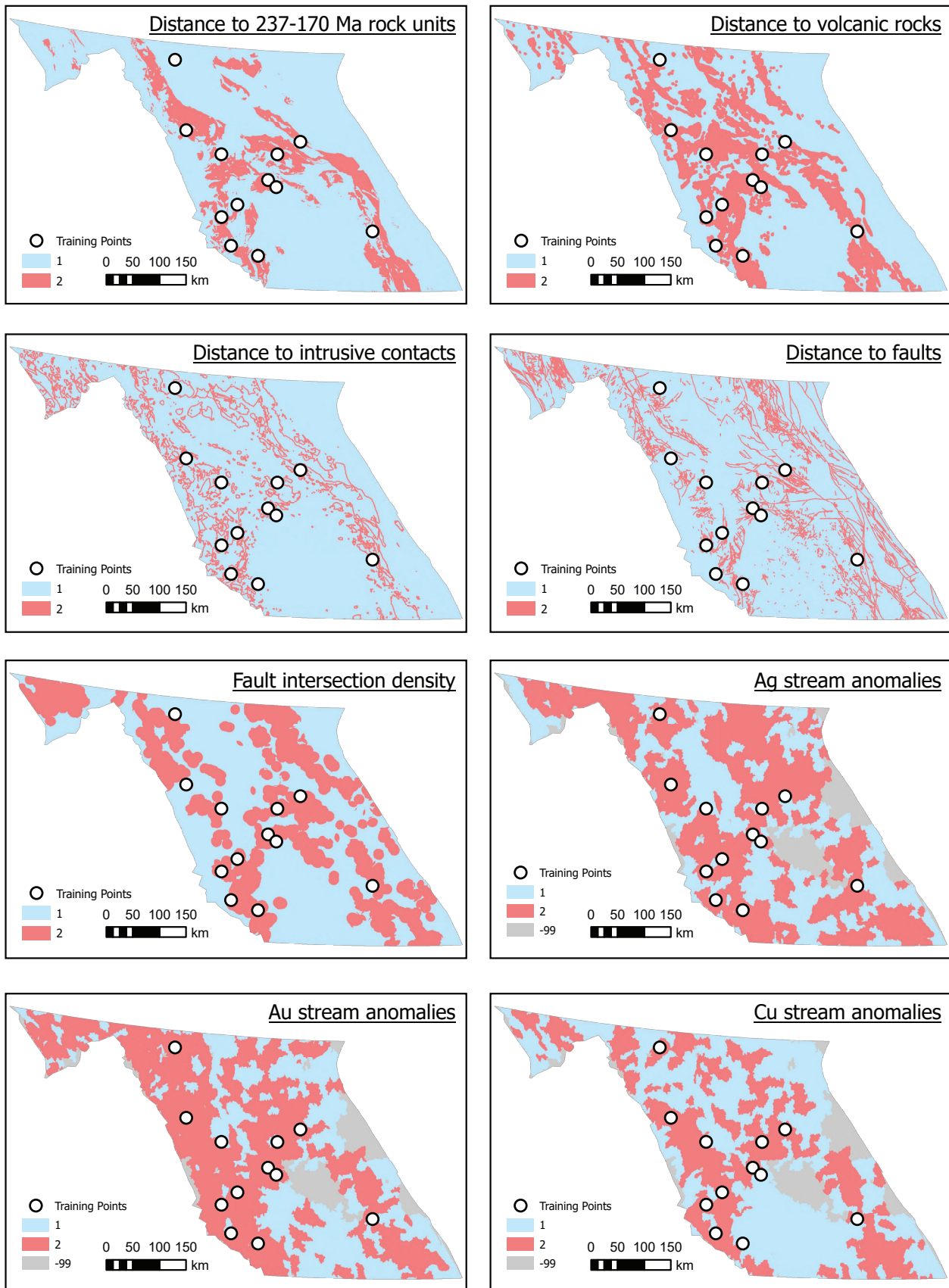


Fig. 3. Predictive maps used in the porphyry model. Red indicates areas that are favourable for capturing training data, blue are areas that are less favourable, and grey (-99 in the legend) areas indicate data gaps.

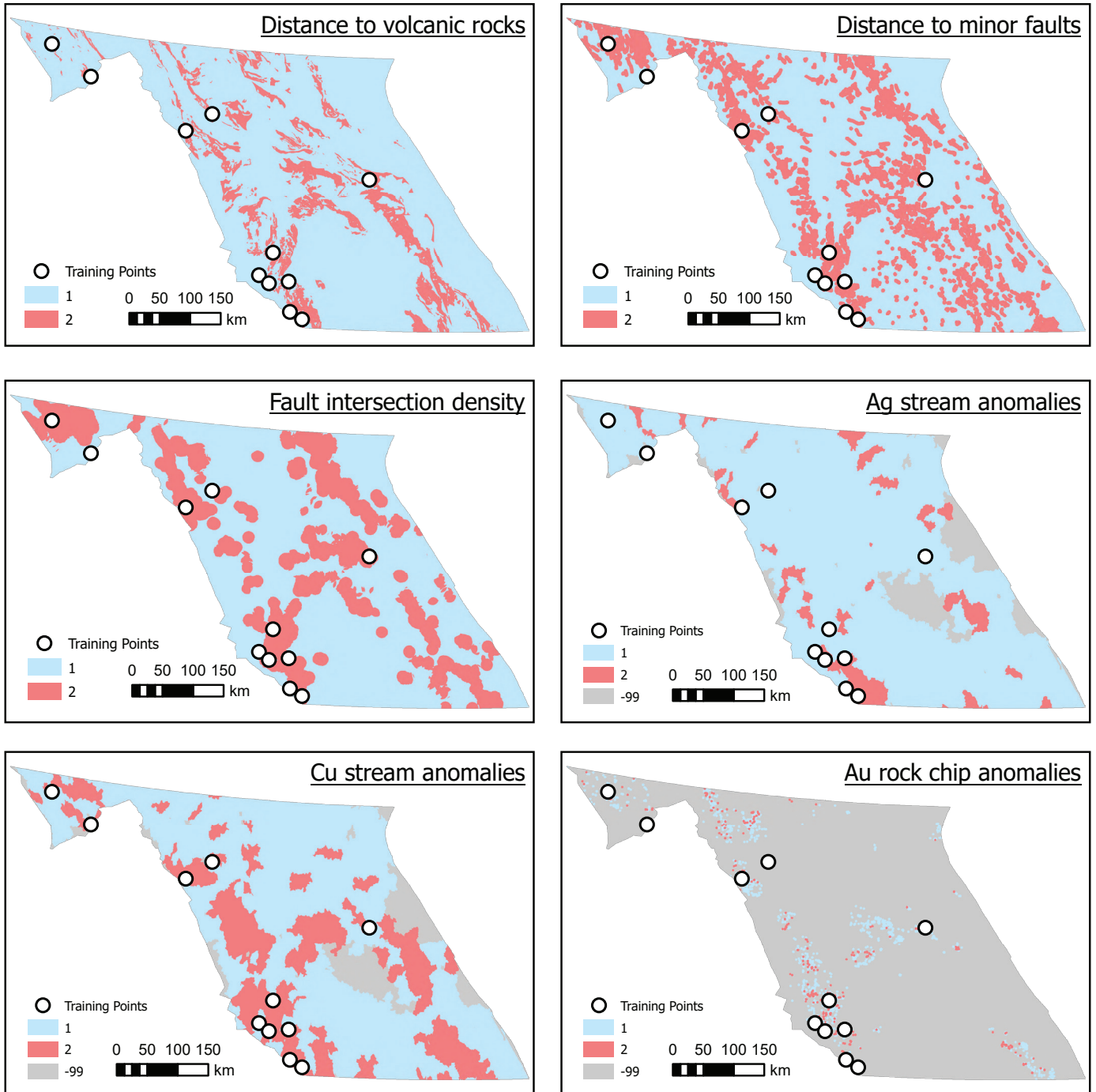


Fig. 4. Predictive maps used in the volcanogenic massive sulphide model. Red indicates areas that are favourable for capturing training data, blue are areas that are less favourable, and grey (-99 in the legend) areas indicate data gaps.

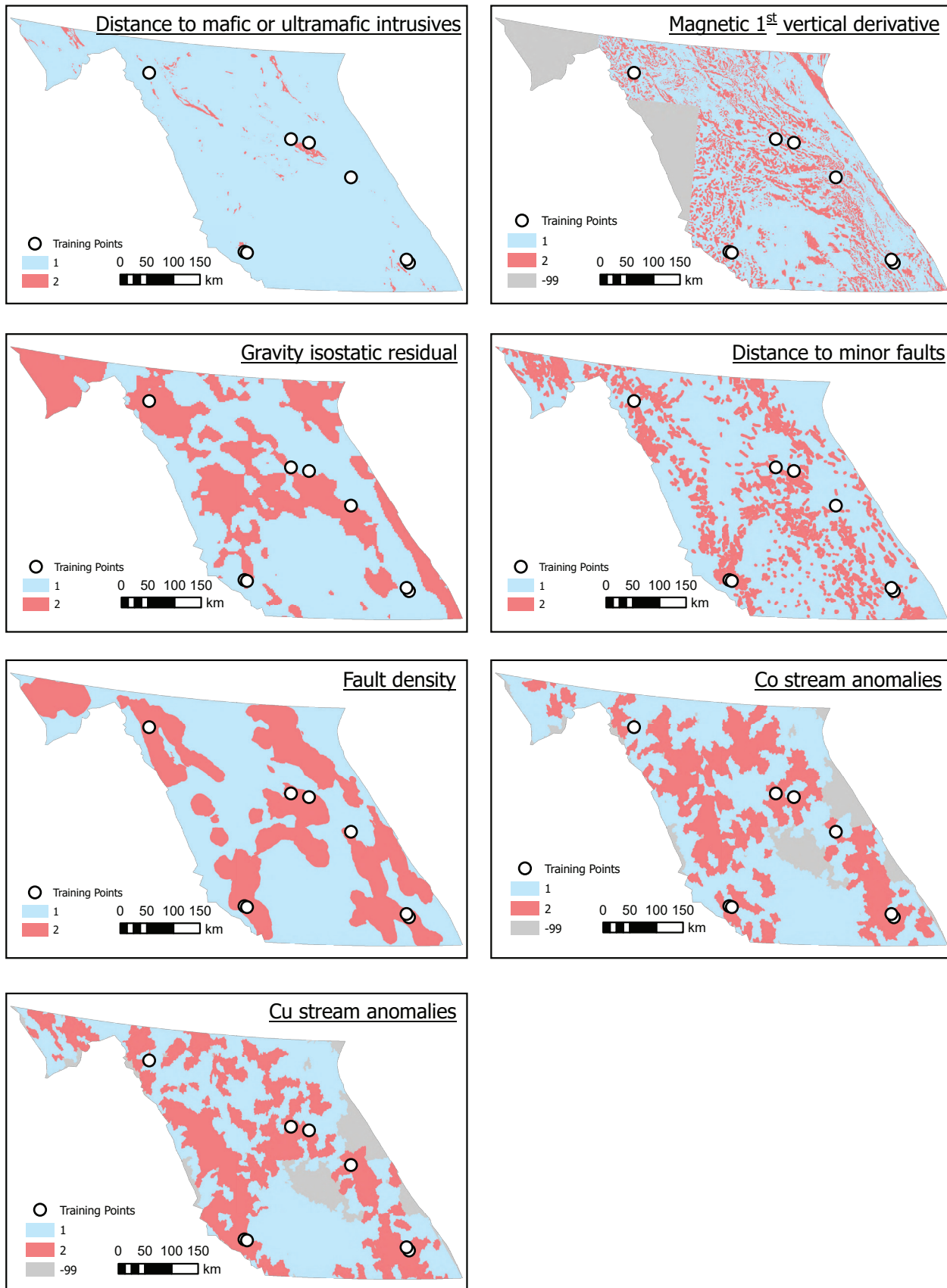


Fig. 5. Predictive maps used in the magmatic mafic to ultramafic model. Red (1 in the legend) indicates areas that are favourable at capturing training data, blue (2 in the legend) is less favourable, and grey (-99 in the legend) areas indicate data gaps.

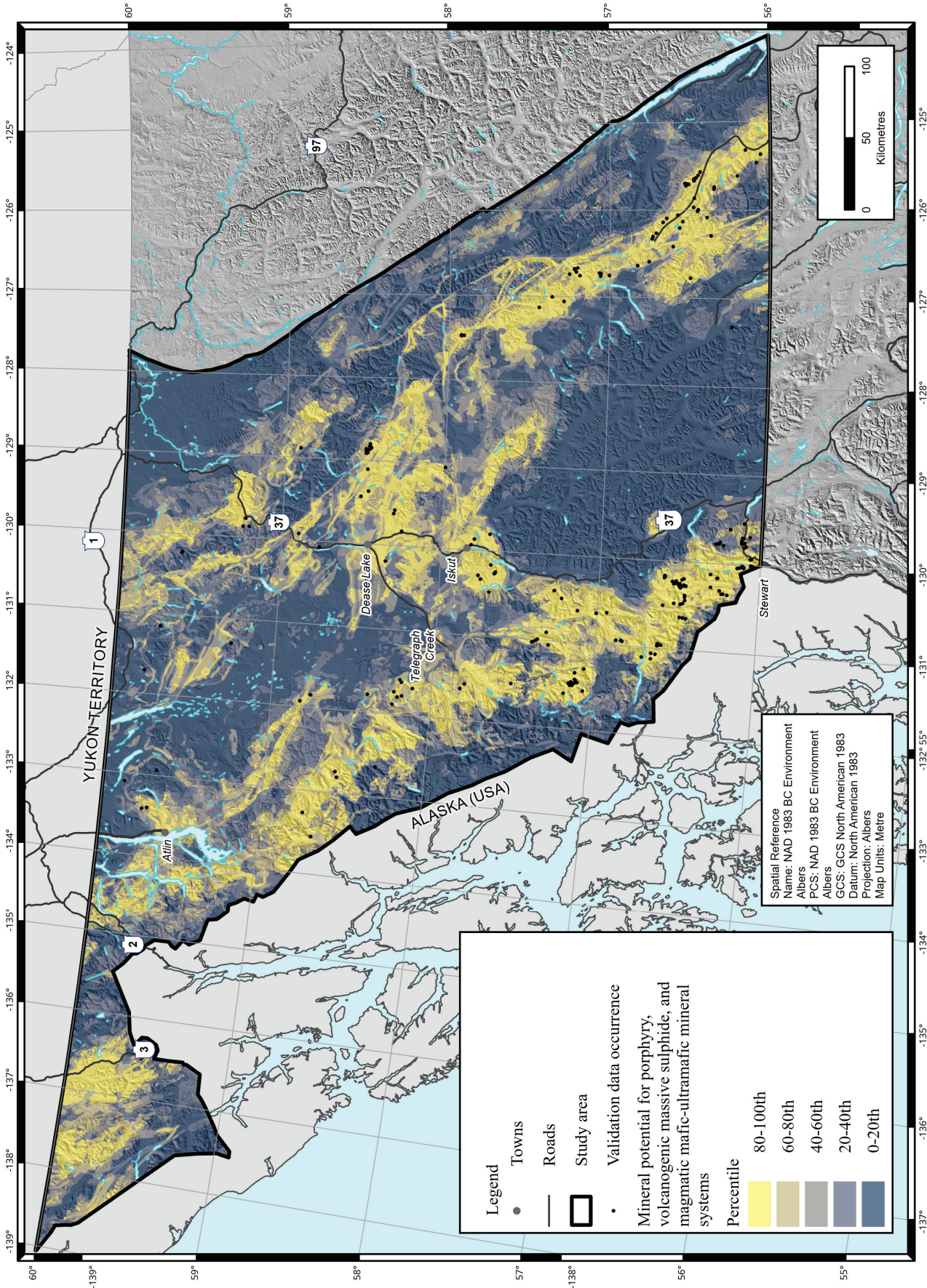


Fig. 6. Combined mineral potential map for porphyry, volcanic massive sulphide and magmatic mafic-ultramafic deposits from current modelling.

We used a subset of mineral occurrences not used as training points to validate the mineral potential model (Fig. 6). To ensure the validation data set was independent of the modelling process, it was excluded in the production of the final mineral potential map. We divided the final mineral potential maps into ten equal percentile divisions based on the posterior probability values (Table 7; Fig. 6). Of note, all three mineral systems capture approximately 70% of all the validation data in the 70th percentile or greater.

4. Comparing results from past and current modelling

To compare the results, the land-based rankings from Kilby (2004; Fig. 7) and the current work were converted to percentile or quantile values. These values were subtracted in a GIS to illustrate and quantify the difference of rankings for the same area. Areas with the highest percentile difference have the greatest difference in ranking; areas with the lowest percentile

difference indicate general agreement between the two results.

Five equal percentile divisions were used to compare the results from the past and current work (Fig. 8; Table 8).

For 33% of the study area the studies are in broad agreement (± 0 -20% percentile difference, Table 8). The area surrounding the Kerr deposit (Fig. 8, location C) is ranked as the 100th percentile by the current work and as the 99th percentile in the past work. Current work recognizes that all the statistically significant mappable features used to model porphyries capture the Kerr deposit. Historical work calculated that the tract containing the Kerr deposit has close to the highest dollar values in region, based on variables such as known resources and future undiscovered deposits. The area mainly underlain by Bowser basin rocks (Fig. 8, location D) also yielded close results, receiving a ranking in the <10th percentile in the current work and the 16th percentile in the past work. The 1990s work suggested that Bowser basin is devoid of metallic economic mineral deposits and predicted few to no future deposits to be

Table 7. Distribution of validation data for each mineral system within each tenth percentile division.

Hierarchy	Percentile	Porphyry	VMS	Mafic-ultramafic
Highest	90-100	62%	51%	51%
	80-90	13%	15%	16%
Moderate to high	70-80	4%	2%	7%
	60-70	11%	14%	4%
Moderate	50-60	1%	2%	6%
	40-50	0%	3%	0%
Moderate to low	30-40	2%	1%	5%
	20-30	1%	1%	8%
Lowest	10-20	5%	8%	3%
	0-10	2%	1%	1%

n = 121 n = 86 n = 106

Table 8. Percentile difference between the Level 1 Mineral Assessment of Kilby (2004) and current work. Negative percentile difference indicates Kilby (2004) provided a higher assessment than the current work for the same area. Positive values represent areas ranked higher in the current work than in Kilby (2004).

Percentile difference	Area (km ²)	Percentage of study area
+100-80	5,619	3%
+80-60	12,023	6%
+60-40	17,553	9%
+40-20	31,492	16%
(+/-) 20-0	63,688	33%
(-) 40-20	38,012	20%
(-) 60-40	15,005	8%
(-) 80-60	7,019	4%
(-) 100-80	3,295	2%

discovered within it. Current modelling suggests the Bowser basin contains few of the statistically significant mappable features used for any of the mineral systems modelled.

For 2% of the study area (Table 8; Fig. 8, highlighted in purple) the two studies yielded markedly different results. For example, in the general Atlin area (Fig. 8, location A) Kilby et al. (2004) assigned a relative ranking 80-100% higher than in the present work. This is primarily because Kilby et al. (2004) examined all metallic minerals and all deposit types whereas the current work focused only on the porphyry, volcanogenic massive sulphide, and magmatic mafic-ultramafic sulphide systems and did not model for placer gold. An area in the southeastern part of the study yielded similarly different results (Fig. 8, location E). This area was indicated to have a low relative prospectivity ranking (<12th percentile) in the current work but a high ranking (88th percentile) by Kilby et al. (2004). This difference may highlight gaps in fault data used in the present work.

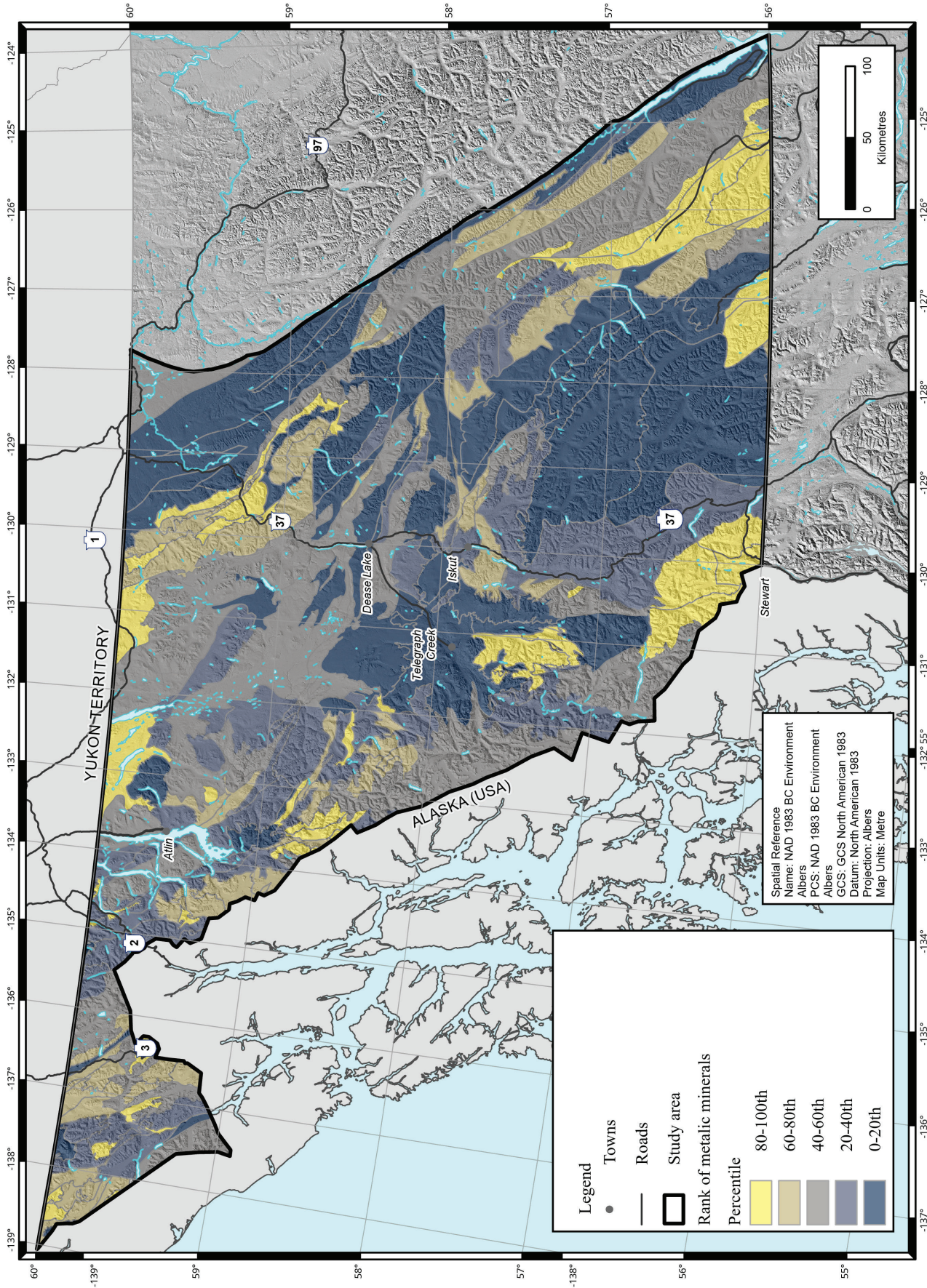


Fig. 7. Metallic mineral potential evaluation from 1990s (after Kilby, 2004).

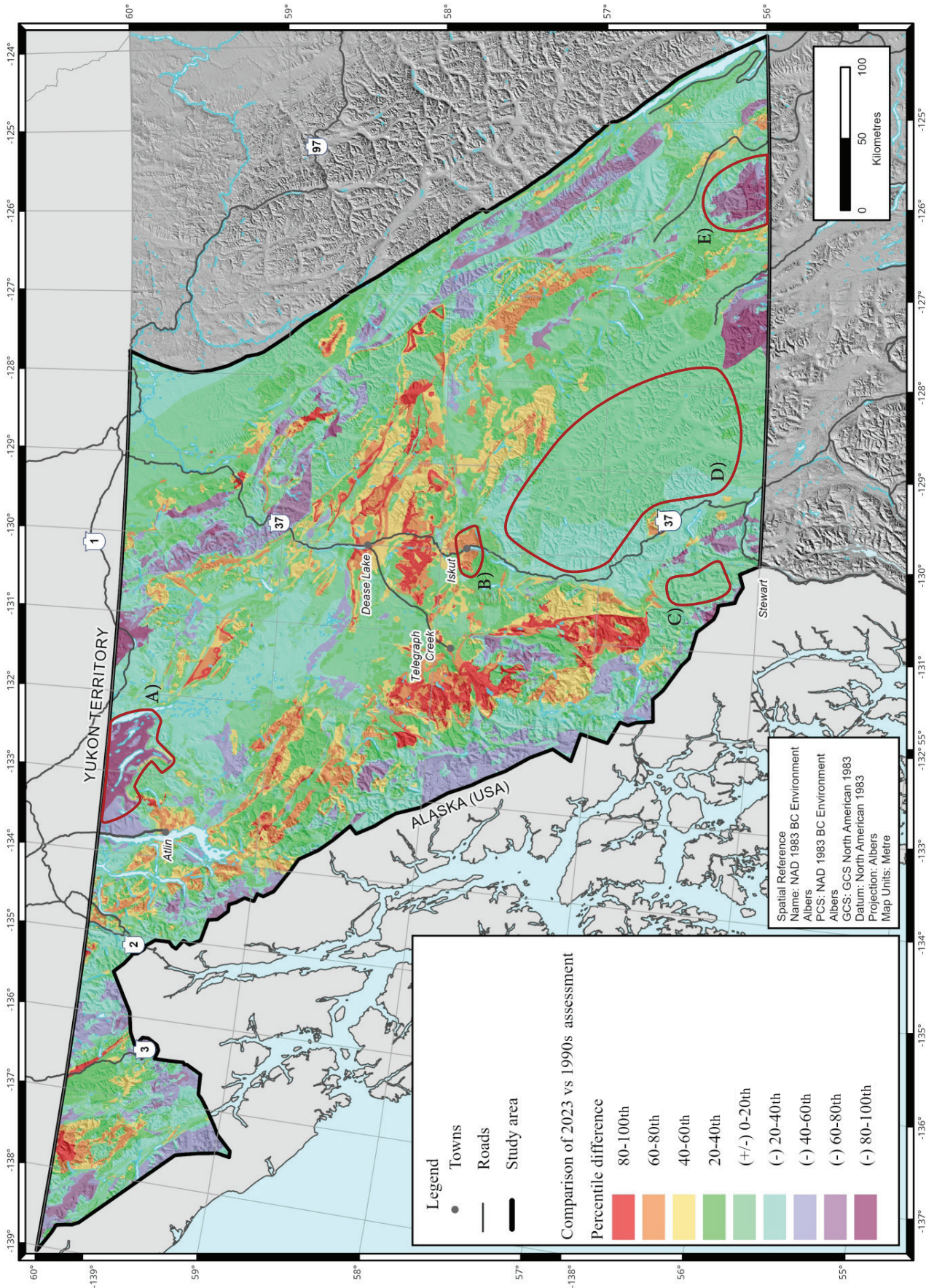


Fig. 8. Difference in relative prospectivity ranking between current and past modelling. Positive percentile differences indicate areas where the current work assigned greater relative prospectivity values than Kilby et al., 2004; greatest differences in red. Negative percentile differences indicate areas where Kilby (2004) assigned greater relative prospectivity values than the current work; greatest differences in purple. Areas of close similarity ($\pm 0-20\%$) are indicated in light green. Areas discussed in text: A- Atlin area, B- Iskut area, C- area surrounding Kerr deposit, D- Bowser basin, E- Oslinka River area.

For 3% of the study area (Table 8; Fig. 8, highlighted in red), the current work ranked relative prospectivity significantly higher than Kilby et al. (2004), likely because the current work has the advantage of new data. For example, the Iskut area (Fig. 8, location B) has seen significant mapping and exploration work in the last ten years and includes the Saddle North deposit, originally discovered as a soil geochemistry anomaly between 2013-14 (Flynn, 2020).

In general, the mineral potential maps produced by the current modelling resolve prospectivity at a finer scale compared to the broader 'tract' areas of historical results. Current modelling was completed on 50 m² grid. As a result, the study area consisted of 77,523,332 cells, each being tested for the absence or presence of a predictive map and given a relative ranking. The tract approach by Kilby (2004) was completed on a much broader scale with an average tract area of 1000 km².

5. Conclusion

Both the work done in the 1990s and the current work are of value for modelling mineral potential in support of land-use decisions, and the new work largely corroborates the old. In large part, differences arise because the recent work has the benefit of about 30 more years of data, the knowledge derived from these data, and the knowledge derived from investigations into the processes that generate deposits. The original work focused on deposit profiles that classified occurrences into about 120 deposit types for a wide range of metals. In contrast, the new work adopted a mineral systems approach to examine critical mineral potential, considering only the porphyry, volcanogenic massive sulphide, and magmatic mafic-ultramafic systems. Future iterations that include other mineral systems will make updates of new modelling more comprehensive.

Mineral potential evaluations have uncertainties related to data availability, data quality, the level of relationship between mineral occurrences and the input data, the estimation method, and the deposit model. Because of these uncertainties neither the past nor present mineral potential assessments can be used to indicate the size or economics of a potential mineral deposit and cannot be used to make valuations on any resource. Any approach to modelling is limited by available data, and results represent a time-specific evaluation (Ford et al., 2019). Because of advances in GIS applications and computer power, statistical analysis of spatial data in the new modelling is far less labour intensive than the 1990s work, can be readily updated, and is more easily reproducible. As more data and knowledge become available, past evaluations may be updated to keep understanding the mineral potential of the study area current.

Acknowledgments

We thank Paulina Marczak for GIS support. Ken Ford, Adrian Hickin, and an anonymous reviewer provided constructive comments to an early draft.

References cited

- Agterberg, F.P., and Bonham-Carter, G.F., (Eds.), 1990. Statistical applications in the earth sciences. Geological Survey of Canada Paper 89-09, 588 p.
<<http://doi.org/10.4095/128125>>
- Bonham-Carter, G.F., Agterberg, F.P., and Wright, D.F., 1990. Weights of evidence modelling: a new approach to mapping mineral potential. In: Agterberg F.P., and Bonham-Carter G.F., (Eds.), Statistical Applications in the Earth Sciences. Geological Survey of Canada, Paper 89-09, pp. 171-183.
- Bonham-Carter, G.F., 1994. Geographic information systems for geoscientists: modelling with GIS, Pergamon, 398 p.
<<https://doi.org/10.1016/C2013-0-03864-9>>
- Brew, D.A., 1992. Decision points and strategies in quantitative probabilistic assessment of undiscovered mineral resources. US Geological Survey, Open File 92-308, 23 p.
<<https://doi.org/10.3133/ofr92307>>
- British Columbia Geological Survey, 2023. The Golden Triangle of northwestern British Columbia. British Columbia Ministry of Energy, Mines and Petroleum Resources, British Columbia Geological Survey Information Circular 2023-05, 6 p. (brochure)
- Clarke, G., Northcote, B., Corcoran, N.L., Pothorin, C., Heidarian, H., and Hancock, K., 2024. Exploration and Mining in British Columbia, 2023: A summary. In: Provincial overview of exploration and mining in British Columbia, 2023. British Columbia Ministry of Energy, Mines and Low Carbon Innovation, British Columbia Geological Survey Information Circular 2024-01, pp. 1-53.
- Colpron, M., 2020. Yukon terranes-A digital atlas of terranes for the northern Cordillera. Yukon Geological Survey.
<<https://data.geology.gov.yk.ca/Compilation/2#InfoTab>>
- Colpron, M., and Nelson, J., 2021. Northern Cordillera: Canada and Alaska. In: Elias, S., and Alderton, D., (Eds.), Encyclopedia of Geology, Second Edition. Academic Press, pp. 93-106.
- Cui, Y., Hickin, A.S., Schiarizza, P., Miller, D., Nixon, G.T., Nelson, J.L., and Ferri, F., 2018. Methods to update the digital geology of British Columbia and synopses of recently integrated mapping programs. In: Geological Fieldwork 2017, British Columbia Ministry of Energy, Mines and Petroleum Resources, British Columbia Geological Survey Paper 2018-1, pp. 197-215.
- Flynn, R., 2020. NI-43-101 Technical report on the Saddle North Copper-Gold Project, Tatogga Property.
<<https://www.sedar.com>>
- Ford, A., 2020. Practical implementation of random forest-based mineral potential mapping for porphyry Cu-Au mineralization in the Eastern Lachlan Orogen, NSW, Australia. Natural Resources Research, 29, 267-283.
<<https://doi.org/10.1007/s11053-019-09598-y>>
- Ford, A., Miller, J.M., and Mol, A.G., 2015. A comparative analysis of weights of evidence, evidential belief functions, and fuzzy logic for mineral potential mapping using incomplete data at the scale of investigation. Natural Resources Research, 25, 19-3.
<<https://doi.org/10.1007/s11053-015-9263-2>>
- Ford, A., Peters, K.J., Partington, G.A., Blevin, P.L., Downes, P.M., Fitzherbert, J.A., and Greenfield, J.E., 2019. Translating expressions of intrusion-related mineral systems into mappable spatial proxies for mineral potential mapping: Case studies from the Southern New England Orogen, Australia. Ore Geology Reviews, 111, article 102943.
<<https://doi.org/10.1016/j.oregeorev.2019.102943>>
- Groves, D.L., Santosh, M., Müller, D., Zhang, L., Deng, J., Yang, L., and Wang, Q., 2022. Mineral systems: Their advantages in terms of developing holistic genetic models and for target generation in global mineral exploration. Geosystems and Geoenvironment, 1, article 100001.
<<https://doi.org/10.1016/j.geogeo.2021.09.001>>

- Harmel, R.D., Cooper R.J., Slade R.M., Haney R.L., and Arnold, J.G., 2006. Cumulative uncertainty in measured streamflow and water quality data for small watersheds. *Transactions of the American Society of Agricultural and Biological Engineers*, 49, 689-701.
- Harris, J.R., Grunsky, E., Behnia, P., and Corrigan, D., 2015. Data- and knowledge-driven mineral prospectivity maps for Canada's North. *Ore Geology Reviews*, 71, 788-803.
<<https://doi.org/10.1016/j.oregeorev.2015.01.004>>
- Hickin, A.S., Ward, B.C., Plouffe, A., and Nelson, J., 2017. Introduction to the geology, physiography, and glacial history of the Canadian Cordillera in British Columbia and Yukon. In: Ferbey, T., Plouffe, A., and Hickin, A.S., (Eds.), *Indicator Minerals in Till and Stream Sediments of the Canadian Cordillera*. Geological Association of Canada Special Paper Volume 50, and Mineralogical Association of Canada Topics in Mineral Sciences Volume 47, pp. 1-25.
- Hickin, A.S., Orovan, E., Brzozowski, M., McLaren, K., Shaw, K., and Van der Vlugt, J., 2023. Critical minerals in British Columbia: An atlas of occurrences and producing mines in 2023. British Columbia Ministry of Energy, Mines and Low Carbon Innovation, British Columbia Geological Survey Open File, 2023-02, 102 p.
- Hronsky, J.M.A., and Groves, D.I., 2008. The science of targeting: definition, strategies, targeting and performance measurement. *Australian Journal of Earth Science*, 55, 3-12.
<<https://doi.org/10.1080/08120090701581356>>
- Kilby, W.E., 1995. Mineral potential project-overview. In: *Geological Fieldwork 1994*, British Columbia Ministry of Energy, Mines and Petroleum Resources, British Columbia Geological Survey, Paper 1995-1, pp. 411-416.
- Kilby, W.E., 1996. Mineral potential assessment projects-An update. In: *Geological Fieldwork 1995*, British Columbia Ministry of Energy, Mines and Petroleum Resources, British Columbia Geological Survey, Paper 1996-1, pp. 301-308.
- Kilby, W.E., 2004. The British Columbia mineral potential project 1992-1997 - methodology and results. Ministry of Energy and Mines, British Columbia Geological Survey, GeoFile 2004-2, 324 p.
- Knox-Robinson, C.M., and Wyborn, L.A.I., 1997. Towards a holistic exploration strategy: Using Geographic Information Systems as a tool to enhance exploration. *Australian Journal of Earth Sciences*, 44, 453-463.
<<https://doi.org/10.1080/08120099708728326>>
- Kreuzer, O.P., Miller, A.V.M., Peters, K.J., Payne, C., Wildman, C., Partington, G.A., Puccioni, E., McMahon, M.E., and Etheridge, M.A., 2015. Comparing prospectivity modelling results and past exploration data: A case study of porphyry Cu-Au mineral systems in the Macquarie Arc, Lachlan Fold Belt, New South Wales. *Ore Geology Reviews*, 71, 516-544.
<<https://doi.org/10.1016/j.oregeorev.2014.09.001>>
- Lawley, C.J.M., Tschirhart, V., Smith, J.W., Pehrsson, S.J., Schetselaar, E.M., Schaeffer, A.J., Houlé, M.G., and Eglington, B.M., 2021. Prospectivity modelling of Canadian magmatic Ni (\pm Cu \pm Co \pm PGE) sulphide mineral systems. *Ore Geology Reviews*, 132.
<<https://doi.org/10.1016/j.oregeorev.2021.103985>>
- Lefebvre, D.V., and Jones, L.D., (compilers) 2022. British Columbia Geological Survey mineral deposit profiles, 1995 to 2012; updated with new profiles for VMS, porphyry, and mafic-ultramafic deposits. British Columbia Ministry of Energy, Mines and Low Carbon Innovation, British Columbia Geological Survey GeoFile 2020-11, 652 p.
- MacIntyre, D.G., Massey, N.W.D., and Kilby, W.E., 2003. The B.C. mineral potential project-new level 2 mineral resource assessment methodology and results. In: *Geological Fieldwork 2003*, British Columbia Ministry of Energy and Mines, Paper 2004-1, pp. 125-140.
- MacIntyre, D.G., Massey, N.W.D., and Kilby, W.E., 2004. Level 2 mineral resource assessment, Coastal British Columbia-methodology and results. British Columbia Ministry of Energy and Mines, British Columbia Geological Survey, GeoFile, 2004-08, 38 p.
- MacIntyre, D.G., Kilby, W.E., Aspinall, C., Duncan, R., Hancock, K., Mihalynuk, M., O'Donnell, M., Panteleyev, A., Simandl, G., and Wojdak, P., 2009. Summary report-Atlin-Taku mineral resource assessment, British Columbia Geological Survey Ministry of Energy, Mines and Petroleum Resources GeoFile 2009-05, 11 p.
- MacIntyre, D.G., and Kilby, W.E., 2009. Atlin-Taku mineral resource assessment, northwestern British Columbia (Parts of NTS 104F, J, K, L, M, N): Methodology and results. In: *Geological Fieldwork 2008*, British Columbia Ministry of Energy, Mines and Petroleum Resources, British Columbia Geological Survey Paper 2009-01, pp. 45-53.
- Magoon, L.B., and Dow, W.G., 1994. The petroleum system. In: Magoon, L.B., and Dow, W.G., (Eds.), *The Petroleum System: From Source to Trap*. American Association of Petroleum Geologists Memoir, 60, pp. 2-24.
- McCuaig, T.C., Beresford, S., and Hronsky, J., 2010. Translating the mineral systems approach into an effective exploration targeting system. *Ore Geology Reviews*, 38, pp. 128-138.
<<https://doi.org/10.1016/j.oregeorev.2010.05.008>>
- Natural Resources Canada, 2020a. Canada-gravity compilation. <<https://open.canada.ca/data/en/dataset/5a4e46fe-3e52-57ce-9335-832b5e79fecc>> Last accessed December 16, 2023.
- Natural Resources Canada, 2020b. Canada-aeromagnetic survey data compilation. <<https://open.canada.ca/data/en/dataset/752fe3fc-d871-5ae1-9bd9-2b6f65880a8d>> Last accessed December 16, 2023.
- Nelson, J.L., Colpron, M., and Israel, S., 2013. The Cordillera of British Columbia, Yukon and Alaska: tectonics and metallogeny. In: Colpron, M., Bissig, T., Rusk, B.G., and Thompson, F.H., (Eds.), *Tectonics, Metallogeny, and Discovery: The North American Cordillera and Similar Accretionary Settings*. Society of Economic Geologists Special Publication 17, pp. 53-109.
- Nykänen, V., Törmänen, T., and Niiranen, T., 2023. Cobalt prospectivity using a conceptual fuzzy logic overlay method enhanced with the mineral systems approach. *Natural Resources Research*, 32, pp. 2387-2416.
<<https://doi.org/10.1007/s11053-023-10255-8%3e>>
- Partington, G., 2010. Developing models using GIS to assess geological and economic risk: an example from VMS copper gold mineral exploration in Oman. *Ore Geology Reviews*, 38-3, 197-207.
<<https://doi.org/10.1016/j.oregeorev.2010.02.002>>
- Porwal, A., Carranza, E.J.M., and Hale, M., 2003. Knowledge driven and data-driven fuzzy models for predictive mineral potential mapping. *Natural Resources Research*, 12, 1-25.
<<https://doi.org/10.1023/A:1022693220894>>
- Porwal, K., and Kreuzer, O., 2010. Introduction to the special issue: mineral prospectivity analysis and quantitative resource estimation. *Ore Geology Reviews*, 38-3, 121-127.
- Singer, D.A., 1993. Basic concepts in three-part quantitative assessments of undiscovered mineral resources. *Natural Resources Research*, 2, 69-81.
<<https://doi.org/10.1007/BF02272804>>
- Singer, D.A., and Kouda, R., 1999. A comparison of the weights-of-evidence method and probabilistic neural networks. *Natural Resources Research*, 8, 4, 287-298.
<<https://doi.org/10.1023/A:1021606417010>>
- Sutherland Brown, A., 1998. British Columbia's Geological Surveys: A century of science and dedication. Pacific Section Geological Association of Canada, 157 p.
- Wearmouth, C.D., Czertowicz, T.A., Peters, K.J., and Orovan, E.A., 2024. Renewed mineral potential modelling at the British

- Columbia Geological Survey, with an application to porphyry, volcanogenic massive sulphide, and magmatic mafic to ultramafic mineral systems in northwestern British Columbia. British Columbia Ministry of Energy, Mines and Low Carbon Innovation, British Columbia Geological Survey Paper, in press.
- Wyborn, L.A.I., Heinrich, C.A., and Jaques, A.L., 1994. Australian Proterozoic mineral systems: essential ingredients and mappable criteria. In: Proceedings Australian institute of mining and metallurgy annual conference, Melbourne, pp. 109-115.
- Yousefi, M., and Carranza, E.J.M., 2016. Data-driven index overlay and boolean logic mineral prospectivity modeling in greenfields exploration. *Natural Resources Research*, 25, pp. 3-18.
<<https://doi.org/10.1007/s11053-014-9261-9>>
- Yousefi, M., Kreuzer, O.P., Nykänen, V., and Hronsky, J.M.A., 2019. Exploration information systems-a proposal for the future use of GIS in mineral exploration targeting. *Ore Geology Reviews*, 111, 103005, 14 p.
<<https://doi.org/10.1016/j.oregeorev.2019.103005>>
- Yousefi, M., Carranza, E.J.M., Kreuzer, O.P., Nykänen, V., Hronsky, J.M.A., and Mihalasky, M.J., 2021. Data analysis methods for prospectivity modelling as applied to mineral exploration targeting: state-of-the-art and outlook. *Journal of Geochemical Exploration*, 229, article 106839.
<<https://doi.org/10.1016/j.gexplo.2021.106839>>

Geochemical signals of carbonatite-related critical metals in provincial stream sediments



Alexei S. Rukhlov^{1,a}, Yao Cui¹, Quinn Cunningham¹, Gabe Fortin¹, and Cameron Anderson¹

¹ British Columbia Geological Survey, Ministry of Energy, Mines and Low Carbon Innovation, Victoria, BC, V8W 9N3

^a corresponding author: Alexei.Rukhlov@gov.bc.ca

Recommended citation: Rukhlov, A.S., Cui, Y., Cunningham, Q., Fortin, G., and Anderson, C., 2024. Geochemical signals of carbonatite-related critical metals in provincial stream sediments. In: *Geological Fieldwork 2023*, British Columbia Ministry of Energy, Mines and Low Carbon Innovation, British Columbia Geological Survey Paper 2024-01, pp. 97-122.

Abstract

Consisting of at least 30% primary carbonate minerals, carbonatites are rare igneous rocks that have become increasingly important exploration targets, because they are major sources of Nb, rare earth elements (REE), and other critical minerals. Demand for these minerals has rapidly increased as the world transitions to low-carbon technologies. The British Columbia alkaline province, which defines a long (at least 1000 km), narrow (ca. 200 km) orogen-parallel belt along the western flank of Ancestral North America, contains numerous carbonatites and related silica-undersaturated and alkaline silicate rocks that host REE and rare-metal resources. Using multi-element stream-sediment geochemical data collected as part of the Regional Geochemical Survey (RGS) program since 1976, we define a multivariate 'critical mineral index' to assess prospectivity for carbonatite-hosted critical metals. Based on discriminant analysis of a training sub-set of the data downstream of known carbonatite occurrences (n=26), our carbonatite index, which is validated by a test sub-set of the data (n=27), highlights numerous areas prospective for REE in the alkaline province. Stream-sediment data showing carbonatite index scores greater than the 93rd percentile (n=50) reveal maximum contrast of REE, Nb, Ta, Ti, Zr, Hf, Th, U, P, K and other carbonatite indicators relative to the median (background) concentrations in stream sediments of the study area. Estimated predicted geochemical resources (in tonnes of metal per 1 m depth), based on productivities of metals in the stream basins, suggest significant potential for REE and other carbonatite-hosted critical metals. Based on data from known carbonatites, we propose a refined prospectivity approach to assess the critical metals potential of underexplored regions that includes detailed stream-sediment, panned heavy mineral concentrate, and soil lithochemical surveys and high-resolution airborne radiometric and magnetic data.

Keywords: Carbonatite, alkaline rocks, regional geochemical survey (RGS), stream sediments, heavy mineral concentrate (HMC), drainage geochemistry, critical minerals, rare earth elements (REE), rare metals, niobium, tantalum, Blue River, Upper Fir, Aley, multivariate statistics, discriminant analysis, carbonatite index, predicted geochemical resources

1. Introduction

Reconnaissance geochemical surveys have a long history of supporting mineral exploration in underexplored regions of British Columbia. Regional sampling of stream sediments and waters has been carried out by mining companies since 1950s and was later adopted by the Geological Survey of Canada, the British Columbia Geological Survey, and Geoscience BC as part of the Regional Geochemical Survey (RGS) programs (Lett and Rukhlov, 2017). Interpretation of these data has led to the discovery of precious and base metal deposits such as the Highland Valley Copper mine and the Galore Creek proposed mine (e.g., Brummer et al., 1987).

Consisting of at least 30% primary carbonate minerals, carbonatites are rare igneous rocks that have become increasingly important exploration targets, because they are major sources of Nb, rare earth elements (REE), and other critical minerals needed as the world transitions to low-carbon technologies (Hickin et al., 2024). Although lithochemistry of panned heavy mineral concentrate (HMC) and indicator minerals of stream sediments have become established techniques for rare-metal and REE prospecting (e.g., Rukhlov and Gorham, 2007;

Gorham, 2008; Gorham et al., 2009; Simandl et al., 2017) the application of regional geochemical surveys to carbonatite-hosted minerals has not been evaluated.

The British Columbia alkaline province, which defines a long (at least 1000 km), narrow (ca. 200 km) orogen-parallel belt along the western flank of Ancestral North America, contains numerous carbonatites and related silica-undersaturated and alkaline silicate rocks (Fig. 1). Some of these rocks host REE (e.g., Wicheeda; Dalsin et al., 2015; Trofanenko et al., 2016) and Ta-Nb (e.g., Aley; Mäder, 1987; Chakhmouradian et al., 2015; and Upper Fir; Rukhlov et al., 2018). This study evaluates multi-element stream-sediment geochemical data collected as part of the RGS program in the Omineca and Foreland morphotectonic belts for prospectivity indicators of carbonatite-hosted critical metals. We also consider examples of detailed surveys near known carbonatite occurrences in the Blue River area and at the Aley deposit (Fig. 2) to discuss applications of panned heavy-mineral concentrate and soil lithochemistry, high-resolution airborne radiometrics and magnetics, and productivities of carbonatite indicators in stream basins. Using these data, we define a multivariate 'critical mineral index' that can be used to

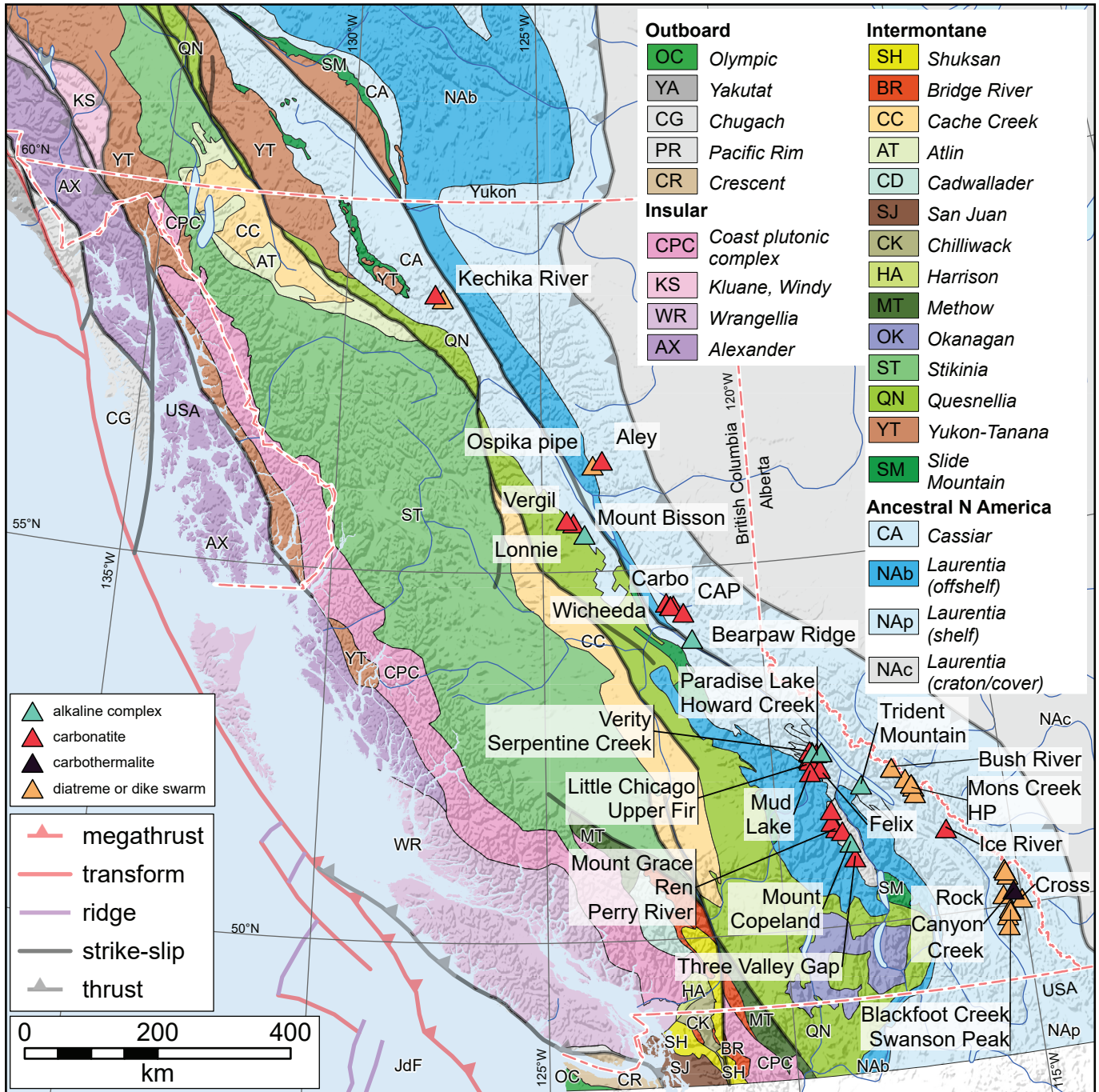


Fig. 1. Carbonatite and related-rock occurrences along the British Columbia alkaline province (after Höy, 1988; Parrish and Scammell, 1988; Pell, 1994; Millonig and Groat, 2013; Rukhlov et al., 2018). Terranes after Colpron (2020).

highlight prospective areas in the alkaline province and regions elsewhere that warrant prospecting for carbonatite-hosted commodities.

2. British Columbia carbonatites and related rocks

In the Canadian Cordillera, carbonatite and related ultramafic, silica-undersaturated and alkaline silicate bodies were emplaced episodically at ca. 810-700 Ma (Mount Copeland, Perry River, Ren), 500-400 Ma (Blackfoot Creek,

Bush River, Felix, HP, Kechika River, Little Chicago, Mons Creek, Swanson Peak), and 360-320 Ma (Aley, Howard Creek, Ice River, Lonnie, Mount Grace, Mud Lake, Ospika, Paradise Lake, Serpentine Creek, Three Valley Gap, Upper Fir, Trident Mountain, Vergil, Verity, Wicheeda); the Cross kimberlite is 245 Ma. Collectively, these rocks form part of the British Columbia alkaline province (Fig. 1; Höy, 1988; Parrish and Scammell, 1988; Pell and Höy, 1989; Pell, 1994; Rukhlov and Bell, 2010; Millonig et al., 2012; Millonig and Groat, 2013;

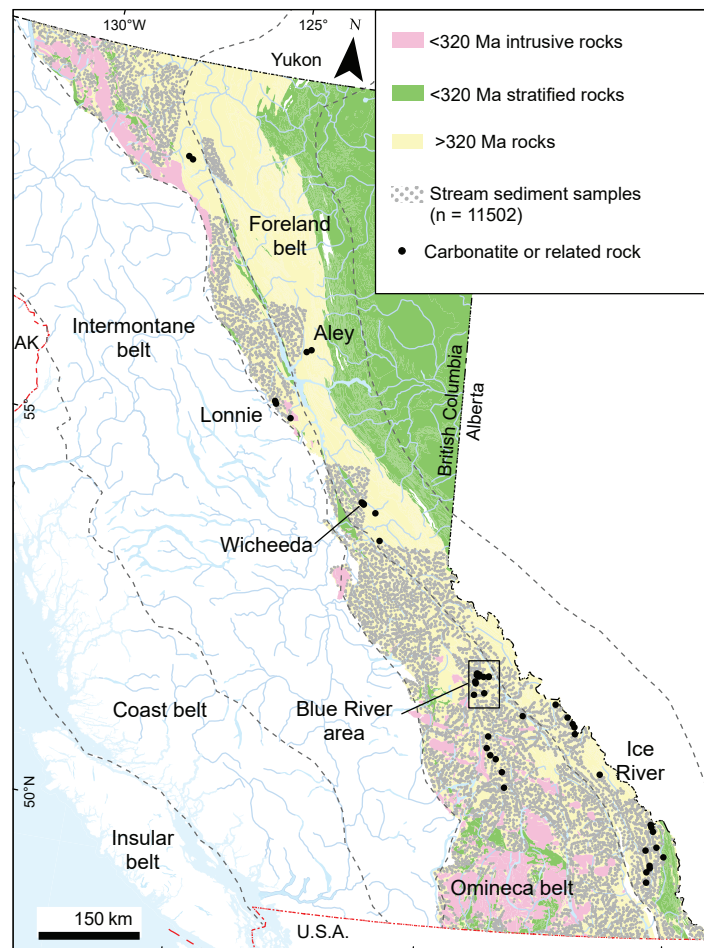


Fig. 2. Selected stream sediment samples in the study area (after Han and Rukhlov, 2017, 2020b). Carbonatite and related-rock occurrences after Höy (1988), Parrish and Scammell (1988), Pell (1994), Millonig and Groat (2013), and Rukhlov et al. (2018). Morphotectonic boundaries after Gabrielse et al. (1991). Geology from BC Digital Geology version 2021-12-19 (Cui et al., 2017).

Chakhmouradian et al., 2015; Mitchell et al., 2017; Rukhlov et al., 2018; McLeish and Johnston, 2019; McLeish et al., 2020; Burgess et al., 2023). The Neoproterozoic and early Paleozoic pulses of carbonatite and alkaline magmatism mark protracted breakup of the supercontinent Rodinia and subsequent passive margin development on the western flank of Laurentia (Li et al., 2008; Bond and Kominz, 1984; Ross, 1991; Colpron et al., 2002). The late Paleozoic carbonatite and alkaline complexes, which host Nb-Ta deposits (e.g., Upper Fir in the Blue River area and Aley) and REE deposits (e.g., Wicheeda), were injected near the continental margin while subduction was taking place to the west (Nelson et al., 2013).

Hosted by the parautochthonous rocks of the Omineca and Foreland belts (Fig. 2), carbonatites and related rocks range from intrusive complexes with a paucity of carbonatites (e.g., Trident Mountain, Mount Copeland) to carbonatite complexes with a paucity of silicate rocks (e.g., Aley, Blue River, Frenchman Cap). Both the carbonatites and host rocks experienced multiple episodes of deformation and metamorphism during Mesozoic and Cenozoic accretionary tectonics while outboard terranes welded to each other and to Laurentia (Scammell, 1987, 1993;

Scammell and Brown, 1990; Pell, 1994; Millonig et al., 2013). Intrusive complexes made up of mainly silica-undersaturated and alkaline silicate rocks, such as the Ice River complex, form small (up to 29 km² at surface), compositionally zoned bodies that are circular to elongate to amoeboid in plan view (Dawson, 1886; Currie, 1975; Peterson and Currie, 1994). Associated ultramafic lamprophyres and REE-Sr-rich carbothermalite dikes are common, with the latter consisting of Mn-calcite, barytocalcite, and zeolite with minor strontianite, Nb-ilmenite, and REE-F-carbonates (Mumford, 2009; Brown, 2013). Carbonatites lacking associated contemporaneous silicate rocks typically form regional swarms of individual occurrences across areas of 1000 km² (e.g., Blue River; Pell, 1994; Mitchell et al., 2017; Rukhlov et al., 2018; Çimen et al., 2019).

3. Blue River area

In the Blue River area (Fig. 3), at least 18 carbonatite and two alkaline, silica-undersaturated-rock bodies are exposed, including at the Upper Fir deposit, one of the largest and best studied Nb-Ta occurrences in the Canadian Cordillera (Chudy, 2013; Rukhlov et al., 2018). Both Cambrian and late

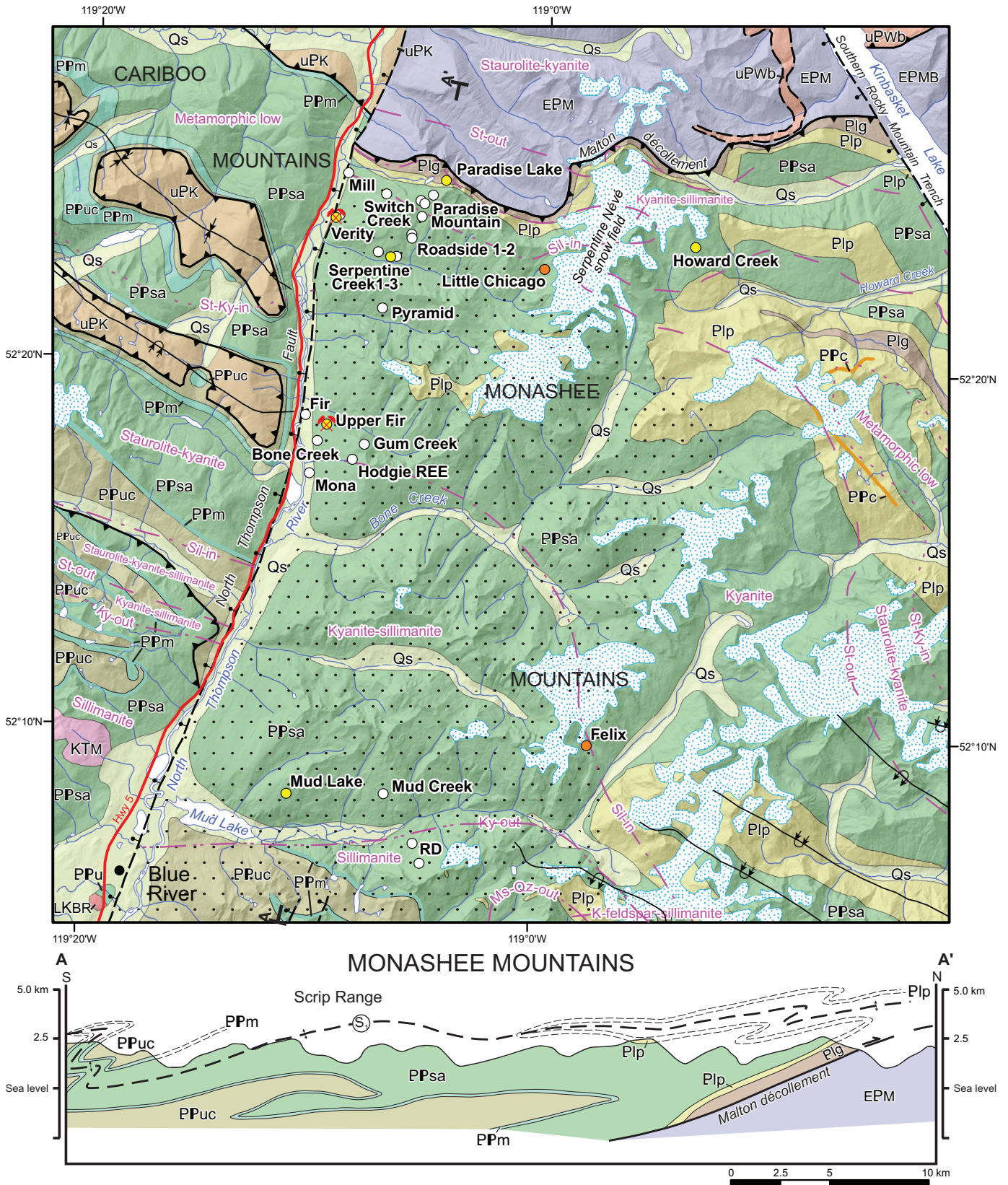


Fig. 3. Carbonatite and related-rock occurrences of the Blue River area (after Pell, 1994; Rukhlov and Bell, 2010; Millonig et al., 2012, 2013; Millonig and Groat, 2013; Rukhlov et al., 2018). Geology and metamorphic isograds after Campbell (1968), Simony et al. (1980), Raeside and Simony (1983), Pell and Simony (1987), McDonough and Murphy (1990), McDonough et al. (1991a, b, 1992), Digel et al. (1998), and Murphy (2007).

UNCONSOLIDATED DEPOSITS

Quaternary

Qs Undifferentiated sand, silt, clay, gravel, till, and colluvium

INTRUSIVE ROCKS

Cretaceous to(?) Paleogene

Murtle pluton

KTM Quartz monzonite and muscovite-biotite granite

Late Cretaceous

Blue River pluton

LKBR Weakly foliated muscovite ±biotite granite

METAMORPHIC ROCKS

Neoproterozoic

Windermere Supergroup

Kaza Group

uPK Undivided psammite, grit, pelitic schist, phyllite, slate, marble

-  Thrust fault
-  Normal fault
-  Fault
-  Upright syncline
-  Overtured syncline
-  Overtured anticline
-  Hinge surface S₁
-  Line of cross section (N-S)

Undivided basal Windermere Supergroup

uPWb Grit, conglomerate or diamictite, psammite, mylonitic quartzite at base, pelitic phyllite or schist, marble and calc-silicate rocks

Proterozoic and(?) Paleozoic

PPu Undivided metamorphic rocks of unknown, probably Proterozoic and possibly Paleozoic age

Upper division of Horsethief Creek Group (equivalent units of Mica Creek succession)

Upper clastic unit

PPuc Quartzofeldspathic psammite and grit, pelitic schist, minor amphibolite

Marble unit

PPm Marble, calcareous pelite, semipelite, schist, discontinuous interbedded pelite, psammite, grit, quartzite, sandy marble

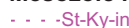
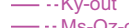
Conglomerate in **PPsa** (Cariboos) and

Plp (Monashees) units

PPc Conglomerate with clasts of marble, calc-silicate rock, quartzite and granite

REGIONAL METAMORPHISM

Mesozoic isograds

-  - - - -St-Ky-in Stauroilite and kyanite in
-  — — — —St-out Stauroilite out
-  — — — —Sil-in Sillimanite in
-  — — — —Ky-out Kyanite out
-  — · · — —Ms-Qz-out Muscovite and quartz out

Paleocene overprint

 Pod sillimanite

Semipelite-amphibolite unit

PPsa Quartzose and quartzofeldspathic psammite, grit, pelitic schist, concordant and discordant amphibolite, minor marble, locally marble at base

Proterozoic

Lower division of Horsethief Creek Group (equivalent units of Mica Creek succession)

Lower pelite unit

Plp Pelitic schist, minor quartzofeldspathic psammite, concordant and discordant amphibolite

Lower grit unit

Plg Quartzofeldspathic psammite and grit, minor pelitic schist and amphibolite, locally prominent diamictite-bearing, conglomeratic horizon at base

Paleoproterozoic

Malton gneiss complex

EPM Undivided foliated granitic augen orthogneiss, mafic orthogneiss, paragneiss

Mount Blackman gneiss

EPMB Amphibolitic mafic gneiss, granitic gneiss

Carbonatite and related-rock occurrence

-  Unknown age
-  ca. 360-330 Ma
-  ca. 500 Ma
-  Nb-Ta deposit

Fig. 3. Continued. Legend.

Paleozoic carbonatites made up of dolomite and calcite are hosted by metamorphosed Neoproterozoic pelitic, arenaceous, and amphibolitic rocks of the Mica Creek assemblage. Metamorphosed to amphibolite grade during Mesozoic to Cenozoic orogeny, the carbonatites form isoclinally folded, sill-like tabular bodies up to 72 m thick and display diverse fabrics, including coarse-grained, granoblastic to fine-grained, foliated, and porphyroclastic varieties. They contain 10-15 vol.% fluorapatite, 5-10 vol.% amphiboles, and variable amounts of olivine, chondrodite, clinopyroxene, phlogopite, magnetite, ilmenite, pyrrhotite, pyrite, pyrochlore supergroup, ferrocolumbite, fersmite, nyoboaeschnite, zircon, baddeleyite, zirconolite, and monazite (Rukhlov et al., 2018). The Upper Fir carbonatite contains an NI 43-101-compliant resource of 48.4 million tonnes (Indicated) grading 1610 ppm Nb₂O₅ and 197 ppm Ta₂O₅ plus 5.4 million tonnes (Inferred) averaging 1760 ppm Nb₂O₅ and 191 ppm Ta₂O₅ (Kulla and Hardy, 2015). Pyrochlore and ferrocolumbite are the main hosts of Nb and Ta (Chudy, 2013; Rukhlov et al., 2018). Molybdenite occurs in some carbonatites and related rocks, including alkali-rich metasomatic rocks such as fenites and glimmerites at Fir, Perry River, Mount Grace, Wicheeda, and the Mount Copeland past producer (Currie, 1976; White, 1982; Höy, 1988; Trofanenko et al., 2016; Rukhlov et al., 2018).

4. Rock, soil, and drainage lithogeochemical data from the Blue River area

In addition to distinct physical and mineralogical characteristics, carbonatites are readily distinguished from sedimentary carbonate rocks (Table 1) by their extremely high concentrations (up to 1000 times the average upper continental crust) of REE, rare metals, F, P, Sr, Ba, Th, U, and other elements (Fig. 4). Data from both provincial, reconnaissance-scale drainage surveys and detailed lithogeochemical drainage and soil surveys in the Blue River area (Table 2) highlight the geochemical response from known carbonatite and related rock occurrences (Figs. 5-7). Ratios of the maximum concentrations per element show enrichment of soil samples (residual anomaly) in Ba, Mo, and Th, and the <0.18 mm fraction of stream-sediment samples in Yb and Lu relative to carbonatites (primary anomaly; Table 3). In contrast, panned stream-sediment (<2 mm fraction) heavy mineral concentrate (HMC) samples show up to 192 times enrichment of all carbonatite indicator elements, except Sr, relative to carbonatites, soils, and the <0.18 mm fraction of stream-sediment samples. Panned stream-sediment HMC samples enhance the contrast of carbonatite indicators such as Ta (Fig. 6) and thus are the preferred medium for drainage surveys targeting critical metals (Rukhlov et al., 2020a).

Table 1. Provincial lithogeochemical data from carbonatites and carbonate sedimentary rocks.

Element	Unit	Sedimentary carbonate rocks				Carbonatites			
		Count	Minimum	Maximum	Mean	Count	Minimum	Maximum	Mean
SiO ₂	wt%	32	0.27	67.44	15.62	600	0.09	35.72	5.33
TiO ₂	wt%	34	<0.02	1.42	0.15	594	<0.01	5.96	0.19
Al ₂ O ₃	wt%	34	0.06	10.03	1.97	600	<0.01	12.64	0.68
Fe ₂ O ₃ (T)	wt%	35	0.06	9.00	1.37	600	0.51	83.28	8.56
MnO	wt%	35	<0.01	0.35	0.07	599	0.15	4.11	0.69
MgO	wt%	35	0.15	20.80	4.17	600	0.26	26.02	12.63
CaO	wt%	35	7.77	60.60	40.80	600	3.66	54.50	31.44
Na ₂ O	wt%	35	<0.01	1.82	0.23	600	<0.01	6.84	0.43
K ₂ O	wt%	35	<0.01	1.65	0.38	600	<0.01	4.79	0.38
P ₂ O ₅	wt%	35	<0.01	0.18	0.07	600	<0.01	14.87	3.15
LOI	wt%	31	9.10	44.30	34.91	598	2.30	43.90	34.92
C(T)	wt%	25	2.03	12.26	9.67	516	0.01	12.90	10.35
S(T)	wt%	27	<0.01	0.48	0.06	515	<0.01	3.97	0.30
F	wt%	1	na	na	0.01	14	<0.01	1.45	0.27
Ag	ppm	22	0.03	0.40	0.09	197	<0.1	5.7	0.54
As	ppm	28	<0.5	17	2.2	192	<0.5	77	3.0
Au	ppb	20	<2	8	1.2	110	<0.5	426	6.7
Ba	ppm	29	<5	2379	275	610	15.1	288595	1825
Be	ppm	15	0.06	1.0	0.67	512	<1	11	0.91
Bi	ppm	16	<0.02	0.2	0.09	192	<0.1	3.1	0.24
Br	ppm	4	<0.5	<1	na	1	na	na	2.8
Cd	ppm	21	<0.2	6.9	0.46	110	<0.1	1.5	0.33
Ce	ppm	28	0.8	51	14.7	611	7.1	53200	1169
Co	ppm	30	<1	50	5.1	586	<1	73	15.5
Cr	ppm	30	3.4	506	38.0	556	<0.1	2230	60.8
Cs	ppm	28	<0.5	2.0	0.48	535	<0.1	114	1.73
Cu	ppm	22	0.4	26	6.1	584	<0.1	308	11.3
Dy	ppm	17	0.28	3.3	1.32	606	0.37	106	11.2
Er	ppm	17	0.15	1.9	0.76	606	0.15	17.8	3.54
Eu	ppm	28	0.04	1.1	0.34	607	0.2	179	10.4
Ga	ppm	17	0.1	8.4	2.91	596	<0.5	126	6.1
Gd	ppm	17	0.36	3.5	1.46	604	0.53	404	25.2
Ge	ppm	2	<0.1	0.4	0.23	81	<1	14	2.1
Hf	ppm	28	0.03	4.4	0.93	584	<0.1	53	1.96
Hg	ppb	15	<10	20	7	110	<10	110	8
Ho	ppm	17	<0.1	0.63	0.260	606	0.06	10.8	1.60
In	ppm	2	<0.02	<0.04	na	81	<0.2	<0.3	na
La	ppm	30	<0.5	24	7.4	611	3.2	40500	734
Lu	ppm	28	0.017	0.3	0.097	607	0.03	2.0	0.326
Mo	ppm	29	0.04	3.0	0.470	478	<0.1	125	3.24
Nb	ppm	27	0.12	22	5.25	609	2.8	6532	576
Nd	ppm	28	1.21	23	7.17	610	3.7	11900	347
Ni	ppm	30	0.98	209	15.9	536	<0.1	1237	38.1
Pb	ppm	23	0.54	19	6.56	586	0.5	643	16.2
Pr	ppm	17	0.23	5.94	2.205	606	0.86	4300	90.0
Rb	ppm	28	0.2	59	12.3	594	<0.1	327	12.7
Sb	ppm	28	<0.1	1.1	0.14	191	<0.1	4.7	0.10
Sc	ppm	27	0.20	26	3.84	207	0.24	62	16.7
Se	ppm	19	0.01	0.5	0.23	110	<0.5	7.3	0.56
Sm	ppm	28	0.23	4.2	1.40	607	0.68	947	42.0
Sn	ppm	17	<0.02	2	0.74	344	<1	25	1.6
Sr	ppm	30	47	3882	914	611	360	>50000	4401
Ta	ppm	28	<0.1	1.4	0.24	599	<0.01	646	101
Tb	ppm	28	0.046	0.64	0.176	607	0.07	36.3	2.77
Th	ppm	30	0.06	7.1	1.64	611	<0.1	>10000	71.6
Tl	ppm	15	0.05	1.3	0.16	197	<0.1	1.3	0.10
Tm	ppm	17	0.02	0.31	0.117	606	0.03	2.17	0.433
U	ppm	28	0.2	2.6	0.79	609	<0.1	379	40.0
V	ppm	23	1	139	26.7	585	<5	2713	49.6
W	ppm	28	0.2	1.4	0.34	350	<0.1	22.5	0.89
Y	ppm	28	1.5	22.3	8.43	611	1.7	323	43.0
Yb	ppm	28	<0.2	1.86	0.636	607	0.19	14.1	2.44
Zn	ppm	29	<1	173	24.4	307	2	1949	77.3
Zr	ppm	28	1	173	38.8	610	<0.1	2978	104.8

Data from Chakhmouradian et al. (2015), Chudy (2013), Dalsin et al. (2015), Gorham (2008), Han et al. (2016), Han and Rukhlov (2020a), Locock (1994), Mäder (1987), Mumford (2009), Rukhlov and Gorham (2007), Simandl et al. (2013), Trofanenko (2014), Trofanenko et al. (2016), and Ya'acoby (2014). **na** - not analyzed.

Table 3. Blue River area relative enrichment of selected carbonatite indicator elements in different sample media.

Element	$\frac{S}{P}$	$\frac{Db}{P}$	$\frac{Db}{S}$	$\frac{Dc}{P}$	$\frac{Dc}{S}$	$\frac{Dc}{Db}$
Sr	0.4	0.02	0.04	0.4	1.1	24
Ba	1.4	0.2	0.2	3.7	2.6	17
Mo	4.0	0.2	0.05	35	8.7	192
Nb	0.8	na	na	2.6	3.1	na
Ta	0.6	0.02	0.03	3.8	6.1	190
La	0.7	0.3	0.4	8.1	11	27
Ce	0.6	0.4	0.7	11.8	19	28
Eu	1.1	0.4	0.4	9.2	8.7	25
Yb	0.8	2.0	2.6	48	63	24
Lu	0.8	2.0	2.5	48	62	24
Y	1.1	na	na	48	43	na
Th	2.8	0.9	0.3	23	8.4	25
U	0.6	0.1	0.2	6.2	11	65

Enrichment factors calculated as ratios of maximum element concentrations in different sample media (Table 2). **Db** – the <0.18 mm sieved fraction of bulk stream sediment (RGS sample medium), **Dc** – panned heavy mineral concentrate (HMC) of the <2 mm sieved fraction of stream sediment, **P** – rock (carbonatite), and **S** – soil. Values >1 indicate enrichment of the numerator medium relative to the denominator and vice versa. **na** - not analyzed.

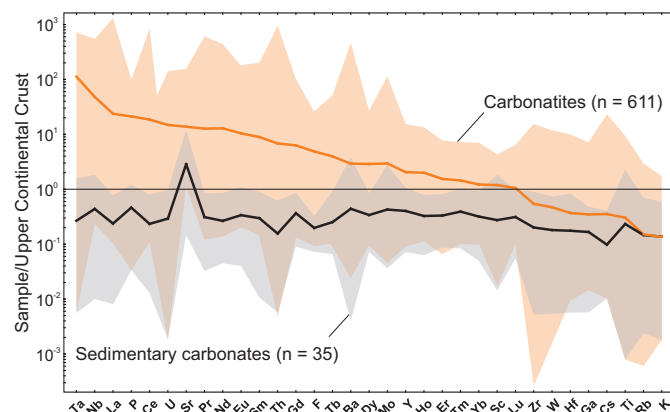


Fig. 4. Compositional ranges and mean compositions (solid lines) of carbonatites and sedimentary carbonate rocks in British Columbia, normalized to the upper continental crust of Rudnick and Gao (2005). Data from Mäder (1987), Locock (1994), Rukhlov and Gorham (2007), Gorham (2008), Mumford (2009), Chudy (2013), Simandl et al. (2013), Trofanenko (2014), Ya'acoby (2014), Chakhmouradian et al. (2015), Dalsin et al. (2015), Han et al. (2016), Trofanenko et al. (2016), and Han and Rukhlov (2020a).

5. Regional geochemical survey data

Collected as part of the Regional Geochemical Survey (RGS) program since 1976, the data for this study (Table 4) include the multi-element determinations for a total of 11502 stream-sediment (<0.18 mm fraction) and water samples at an average sampling density of about 1 site per 10 km² (Han and Rukhlov,

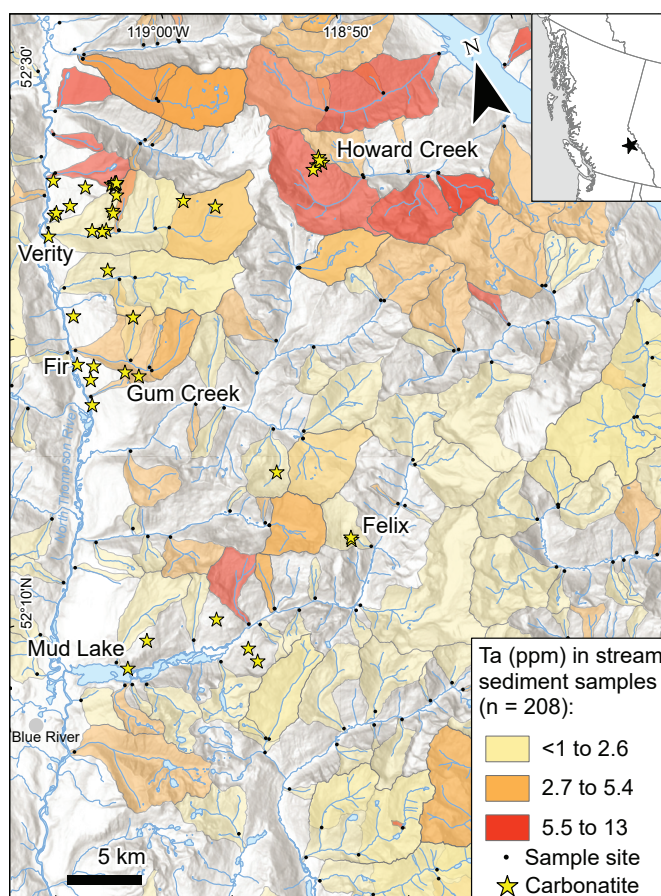


Fig. 5. Blue River area, tantalum-themed catchment basins of regional geochemical survey stream-sediment samples (<0.18 mm fraction; after Han and Rukhlov, 2017, 2020a). Carbonatite occurrences after Rukhlov and Gorham (2007), Gorham (2008), Gorham et al., 2009, 2011a, 2011b, 2013), Millonig and Groat (2013), and Rukhlov et al. (2018).

2017; 2020b; Lett and Rukhlov, 2017). Considering the emplacement ages of carbonatites and related rocks (>320 Ma), the selected stream sediment samples have catchment basins (Cui et al., 2009) that are underlain by the >320 Ma rocks in the study area (Fig. 2). The determinations by aqua-regia digestion with atomic absorption spectrometry (AAS) or a combination of inductively coupled plasma atomic emission spectroscopy (ICP-AES) and inductively coupled plasma mass spectrometry (ICP-MS) are underestimated for elements hosted by silicate and oxide minerals because of only partial dissolution in HCl-HNO₃ acid mixtures. In contrast, instrumental neutron activation analysis (INAA) provides total determinations. Elevated concentrations of carbonatite indicator elements such as La (Fig. 8), Ta (Fig. 9), U (Fig. 10), and P (Fig. 11) in the stream sediments reflect local background variations, including at known carbonatite and related rock occurrences.

6. Discriminant analysis method

Below we evaluate the multi-element drainage geochemical data to identify the carbonatite signature (Fig. 12). To construct

Table 4. Regional geochemical survey (RGS) lithochemical data from stream-sediment samples.

Variable	Method	Unit	Count	<MDL ¹	Mean	Minimum	Median	Percentiles			Maximum	Skewness	DPA ²
								87th	93rd	98th			
Area³		km ²	11502		9.9	0.008	5.5	18	28	54	193	4	
Ag	AAS, ICP-MS	ppb	11073	0.13	122	<2	57	184	278	587	>100000	87	
Al	ICP-AES	wt%	11002	0.00	1.2	0.02	1.07	1.75	2.03	2.53	5.86	1	
As	AAS, ICP-MS	ppm	11467	0.68	9.2	<0.1	4.5	14	21	42	5370	68	
Au	ICP-MS	ppb	11263	11	14	<0.2	1.2	7.6	13	47	40630.4	78	
Ba	ICP-MS	ppm	11002	0.00	136	2.2	72	230	361	856	2769	5	
Ba	INAA	ppm	10104	0.48	835	<50	603	1200	1500	3400	37000	11	Y
Bi	AAS, ICP-MS	ppm	11117	0.97	0.29	<0.02	0.19	0.40	0.51	1.0	125	61	
Ca	ICP-AES	wt%	11002	0.01	2.5	<0.02	0.62	5.87	10.22	18.79	40.00	3	Y
Cd	AAS, ICP-MS	ppm	11298	2.0	0.53	<0.01	0.13	0.5	0.93	3	644.53	83	
Ce	INAA	ppm	10107	0.33	129	<3	100	210	270	430	1450	4	Y
Co	ICP-MS	ppm	11002	0.00	12	0.3	11	18	22	31	173	5	
Co	INAA	ppm	10107	5.4	15	<1	14	24	29	41	217	4	
Cr	ICP-MS	ppm	11002	0.00	27	0.7	21	43	55	90	1051	12	
Cr	INAA	ppm	10107	0.63	115	<5	81	170	230	390	8750	19	
Cs	INAA	ppm	10106	2.6	3.8	<0.5	3.1	6.0	7.6	12	67	5	
Cu	AAS, ICP-MS	ppm	11497	0.00	27	0.71	22	44	54	81	1200	14	
Eu	INAA	ppm	1851	5.0	2.0	<0.2	1.8	3.2	4.0	5.7	20	3	
F	ISE	ppm	4259	0.00	485	50	430	750	890	1189	2040	1	
Fe	ICP-AES	wt%	11002	0.00	2.4	0.04	2.25	3.51	3.95	4.75	26.0	2	Y
Fe	INAA	wt%	10107	0.12	3.6	<0.2	3.5	5.1	5.8	7.3	26.3	1	
Ga	ICP-MS	ppm	11002	0.08	3.5	<0.2	3.3	5.4	6.3	8.2	17	1	
Hf	INAA	ppm	10107	2.3	9.5	<1	8	15	20	31	308	8	
Hg	AAS, ICP-MS	ppb	11000	5.8	40	<5	26	66	92	166	4480	29	
K	ICP-AES	wt%	11002	0.32	0.13	<0.01	0.07	0.25	0.36	0.64	1.46	3	Y
La	ICP-MS	ppm	11002	0.06	20	<0.5	16	29	37	62	1146	19	
La	INAA	ppm	10107	0.48	71	<2	55	119	150	242	1160	5	Y
Li	ICP-MS	ppm	5743	0.00	21	0.5	18	38	46	60	131	1	
Lu	INAA	ppm	10107	28	0.48	<0.05	0.40	0.87	1.1	1.7	21	9	
Mg	ICP-AES	wt%	11002	0.00	0.96	0.03	0.64	1.48	2.18	4.96	21.79	5	Y
Mn	AAS, ICP-AES	ppm	11497	0.00	522	15	402	770	984	1765	>30000	21	Y
Mo	ICP-MS	ppm	11002	0.00	1.1	0.02	0.53	1.6	2.7	6.6	113	17	Y
Na	ICP-AES	wt%	11002	5.4	0.012	<0.001	0.006	0.022	0.032	0.06	1.76	30	
Na	INAA	wt%	10102	1.2	1.1	<0.1	1.0	1.9	2.2	2.7	10.3	1	
Nb	ICP-MS	ppm	5743	3.5	0.51	<0.02	0.27	1.1	1.4	2.3	8.3	4	
Nd	INAA	ppm	1462	0.21	70	<5	59	120	140	207	638	3	
Ni	ICP-MS	ppm	11002	0.00	33	0.3	25	49	62	112	2369	22	Y
P	ICP-AES	wt%	11002	0.00	0.09	0.007	0.074	0.129	0.157	0.234	1.064	8	Y
Pb	AAS, ICP-MS	ppm	11497	0.00	17	0.57	10	21	27	47	>20000	98	Y
Rb	INAA	ppm	10107	0.86	87	<5	84	121	140	170	400	1	
S	ICP-AES	wt%	11002	20	0.059	<0.01	0.03	0.10	0.14	0.31	6.77	21	
Sb	ICP-MS	ppm	11002	3.3	0.39	<0.02	0.15	0.58	0.98	2.3	297	81	
Sb	INAA	ppm	10106	25	0.88	<0.1	0.4	1.4	2.2	4.9	566	82	
Sc	ICP-MS	ppm	11002	0.00	2.6	0.1	2.3	4.0	5.0	7.4	20	2	
Sc	INAA	ppm	10107	0.04	12	<0.5	11	17	20	26	107	2	Y
Se	ICP-MS	ppm	11002	7.0	0.70	<0.1	0.4	1.2	1.7	3.2	58	19	
Sm	INAA	ppm	10107	0.19	10	<0.1	8.2	16	21	34	165	5	Y
Sr	ICP-MS	ppm	11002	0.00	66	0.3	31	127	199	357	1978	7	Y
Ta	INAA	ppm	10107	13	1.7	<0.5	1.5	2.8	3.4	5.7	70	12	
Tb	INAA	ppm	10107	14	1.3	<0.5	1.1	2.1	2.7	4.2	25	6	
Te	ICP-MS	ppm	11002	59	0.02	<0.01	<0.01	0.04	0.05	0.09	10	92	
Th	ICP-MS	ppm	11002	0.16	5.4	<0.1	4.4	9.5	12	16	363	28	
Th	INAA	ppm	10107	0.12	19	<0.2	14	30	41	75	488	7	Y
Ti	ICP-AES	wt%	11002	0.63	0.051	<0.001	0.029	0.112	0.144	0.216	0.990	4	Y
Tl	ICP-MS	ppm	11002	9.7	0.12	<0.02	0.08	0.23	0.31	0.46	3.3	7	
U	ICP-MS	ppm	11002	0.06	2.7	<0.1	1.3	4.1	6.8	15	244	18	
U	INAA	ppm	10105	0.25	6.7	<0.2	4.7	11	15	26	228	10	Y
V	AAS, ICP-MS	ppm	11199	0.32	30	<1	24	53	67	97	500	3	Y
W	ICP-MS	ppm	11002	58	0.49	<0.05	<0.05	0.5	1.2	4.3	101	22	
W	INAA	ppm	10106	78	1.7	<1	<1	3	4	9	1950	92	
Y	ICP-MS	ppm	5743	0.00	9.6	0.27	7.4	13	17	31	647	23	
Yb	INAA	ppm	10107	32	2.8	<0.2	3.0	5.0	6.3	9.5	59	3	
Zn	AAS, ICP-MS	ppm	11497	0.00	99	2.8	59	102	140	360	88000	89	Y
Zr	ICP-MS	ppm	5743	1.9	1.6	<0.1	1.2	2.9	3.7	5.7	103	25	
Zr	INAA	ppm	7035	28	394	<200	330	640	830	1400	15000	10	

¹ Percentage of values less than the minimum detection limit (MDL).

² Variables having value of 'Y' (shaded rows) used in discriminant projection analysis (DPA).

³ Area of catchment basin in square kilometres.

Analytical method abbreviations: **AAS** – aqua regia digestion and atomic absorption spectrometry, **ICP-AES** – aqua regia digestion and inductively coupled plasma atomic emission spectroscopy, **ICP-MS** – aqua regia digestion and inductively coupled plasma mass spectrometry, **INAA** – instrumental neutron activation analysis, **ISE** – Na₂CO₃+KNO₃ fusion followed by H₂O leach and ion selective electrode. Data from Han and Rukhlov (2017; 2020b).

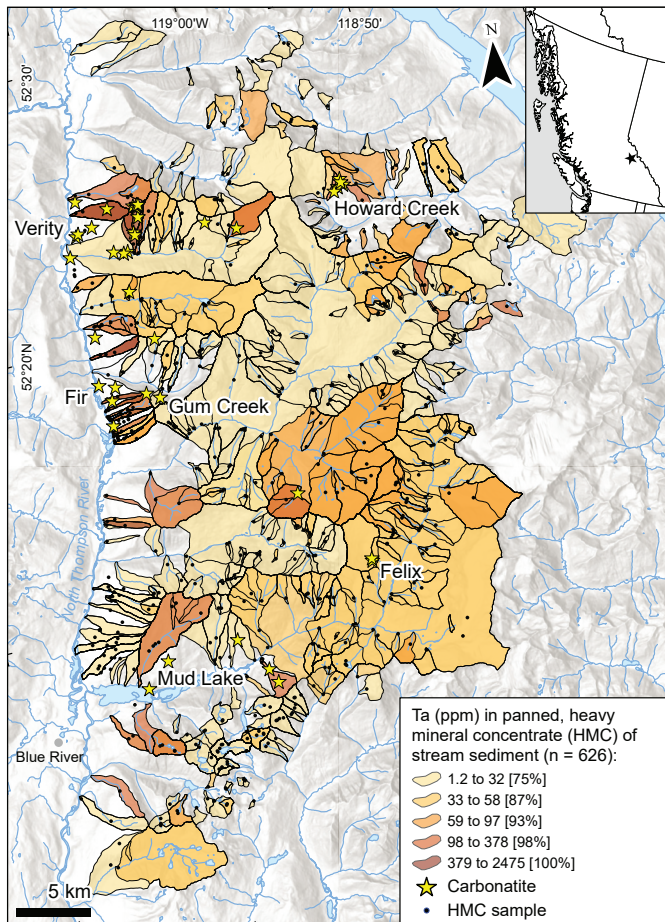


Fig. 6. Blue River area, tantalum-themed, percentile-ranked catchment basins of panned, stream-sediment (<2 mm fraction), heavy mineral concentrate (HMC) samples. Data and carbonatite occurrences from Dahrouge and Reeder (2001), Reeder and Dahrouge (2002), Smith and Dahrouge (2003), Dahrouge and Wolbaum (2004), Rukhlov and Gorham (2007), Gorham (2008), Gorham et al. (2009, 2011a, 2011b, 2013).

the best criteria for discriminating between carbonatite and other signals using multi-element stream-sediment data, we performed a discriminant projection analysis (DPA) on a sub-set of stream-sediment data taken from the regional geochemical survey area (Fig. 13) in ioGAS™ software. DPA is a supervised multivariate statistical technique that determines an optimum projection of multivariate data into a lower dimensional (e.g., bivariate) space to achieve the best separation between user-defined groups (Flury, 1997). The DPA uses an a priori knowledge of the group memberships to define discriminant parameters (DP1, DP2, DPn) that maximize the ratio of the within-groups sum of squares (W) to between-groups sum of squares (B) matrices (W/B). The between-groups matrix is effectively the covariance of the group means and the within-groups matrix is the weighted covariance matrix for the groups. Our group 1 includes stream-sediment data that are downstream of known carbonatite or related rock occurrences (n=53); group 2 consists of stream sediments derived mainly from carbonate sedimentary rocks (n=90); and group 3 is a random

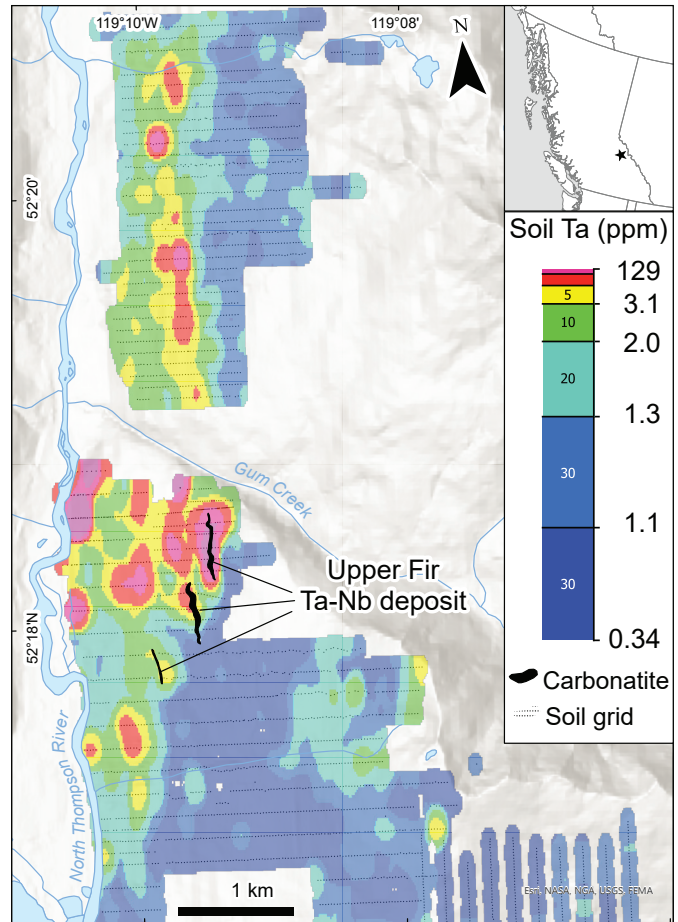


Fig. 7. Blue River area, percentile-gridded, Ta concentrations (ppm) in soil samples (after Reeder and Dahrouge, 2002; Smith and Dahrouge, 2003; Dahrouge and Wolbaum, 2004; Rukhlov and Gorham, 2007; Gorham, 2008; Gorham et al., 2009, 2011a, 2011b). Upper Fir carbonatite-hosted Ta-Nb deposit footprint after Kraft (2011) and Gorham et al. (2013).

20% sub-sample of all stream-sediment data in the study area (n=1943; Fig. 13). A ranked element contrast (REC) plot for the average Group 1 stream sediment relative to the median stream sediment in the study area (Fig. 14a) reveals maximum contrast of the carbonatite and related-rock association (Th-K-REE-W-U-Ti-Ta-Hf-Mo-P-Sr). In contrast, the average of a random sub-set of stream sediment samples (Group 3) shows maximum contrast of precious and base metals, along with other pathfinders of hydrothermal ore deposits (Fig. 14b); the ranked element contrast profile for group 2 is similar to that of group 3. Based on the ranked element contrast associations, we selected 20 elements that have <1% of values below the minimum detection limit for the discriminant projection analysis (Table 4). We performed the discriminant projection analysis on a random 50% training sub-set of the group 1 to 3 data (Fig. 12). The constructed discriminant parameters (DP1 and DP2) are linear combinations of the log₁₀-transformed element concentrations that optimally separate the data of groups 1 to 3 (Table 5) as summarized in Equations 1 and 2.

$$DP1 = 0.5125 \cdot Ba - 0.1132 \cdot Ca + 0.019 \cdot K - 0.3508 \cdot Mg - 0.7108 \cdot Mn - 0.7341 \cdot Mo - 0.8466 \cdot Ni - 0.8647 \cdot P + 0.8483 \cdot Pb + 1.108 \cdot Sc - 0.8055 \cdot Sm - 0.1415 \cdot Sr - 2.78 \cdot Th - 0.1456 \cdot Ti + 0.2234 \cdot U - 0.2579 \cdot V + 0.9749 \cdot Zn - 2.181 \cdot La + 2.225 \cdot Fe + 1.957 \cdot Ce + 0.038113$$

(Eqn. 1)

$$DP2 = 1.008 \cdot Ba - 0.6432 \cdot Ca - 0.834 \cdot K + 2.034 \cdot Mg - 0.1111 \cdot Mn - 0.2682 \cdot Mo - 0.5129 \cdot Ni - 0.2222 \cdot P + 0.3704 \cdot Pb + 0.01757 \cdot Sc - 0.02553 \cdot Sm - 0.7922 \cdot Sr - 1.464 \cdot Th + 1.035 \cdot Ti + 2.46 \cdot U - 0.8935 \cdot V + 0.2481 \cdot Zn + 0.2286 \cdot La + 0.5293 \cdot Fe - 0.7624 \cdot Ce + 1.6581$$

(Eqn. 2)

Calculated contours of constant Mahalanobis distance at $\chi^2 = 0.975$, using robust multivariate estimation (Campbell, 1980), outline most of the data in each group (Fig. 15a). Projecting a random 50% test sub-set of the group 1 to 3 data, which were not used in the discriminant projection analysis, into the DP1 versus DP2 space validates separation of most of the data in each group (Fig. 15c). The DP1 contributes 73% in discriminating the stream-sediment data downstream of known carbonatites and other stream-sediment data, with the calculated Pearson correlation coefficients of the DP1 variables showing significant contributions of Th, La, Sm, Ce, U, K, P, and Ti (Table 5).

We then used the training sub-set of the group 1 to 3 data to construct the DP1 versus DP2 discrimination diagram with a boundary separating most of the data from stream sediments downstream of known carbonatite or related-rock occurrences and other stream-sediment data (combined groups 2 and 3) using the Auto-Domain Classification Diagram tool in ioGAS™, based on the lowest Mahalanobis distance (Fig. 15b). The final discrimination diagram DP1 versus DP2 with the statistically defined boundary separating carbonatite or related rock sources and other rock sources is validated by the test sub-set of the stream-sediment data (Fig. 15d).

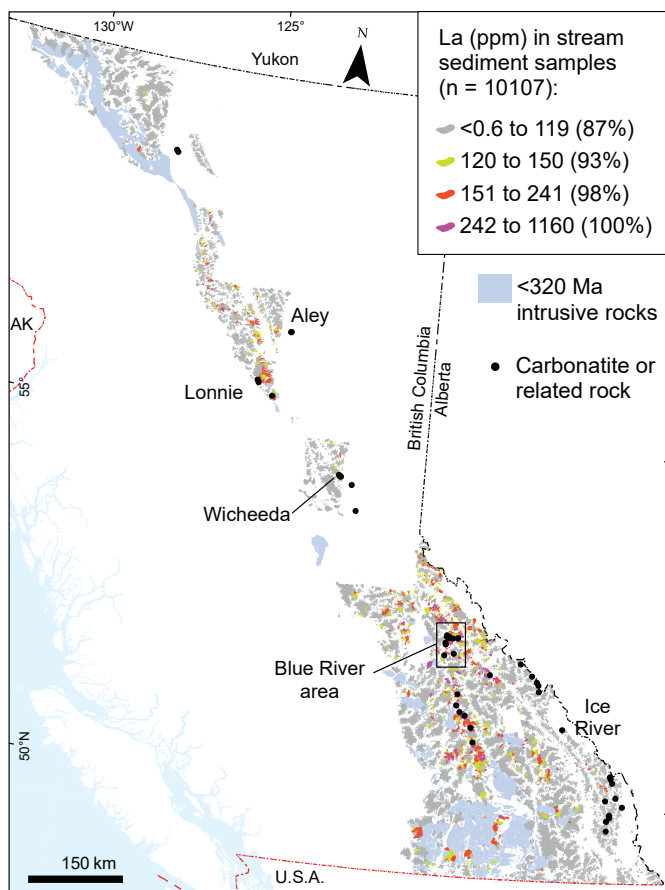


Fig. 8. Regional geochemical survey area, lanthanum-themed, percentile-ranked catchment basins of stream-sediment samples (<0.18 mm fraction; after Han and Rukhlov, 2017, 2020b). Carbonatite and related-rock occurrences after Höy (1988), Parrish and Scammell (1988), Pell (1994), Millonig and Groat (2013), and Rukhlov et al. (2018). The post-320 Ma intrusive rocks from BC Digital Geology version 2021-12-19 (Cui et al., 2017).

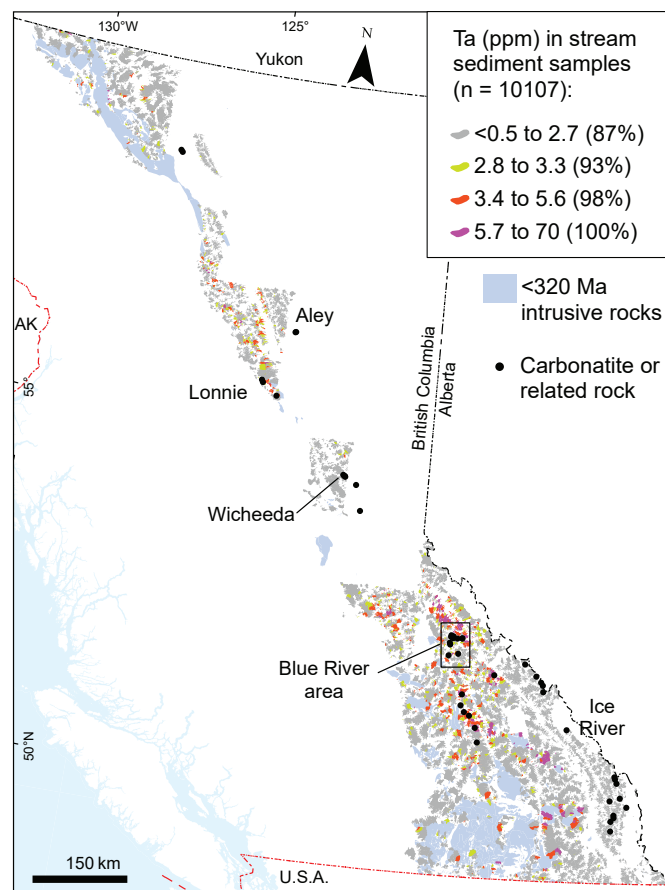


Fig. 9. Regional geochemical survey area, tantalum-themed, percentile-ranked catchment basins of stream-sediment samples (<0.18 mm fraction; after Han and Rukhlov, 2017, 2020b). Carbonatite and related-rock occurrences after Höy (1988), Parrish and Scammell (1988), Pell (1994), Millonig and Groat (2013), and Rukhlov et al. (2018). The post-320 Ma intrusive rocks from BC Digital Geology version 2021-12-19 (Cui et al., 2017).

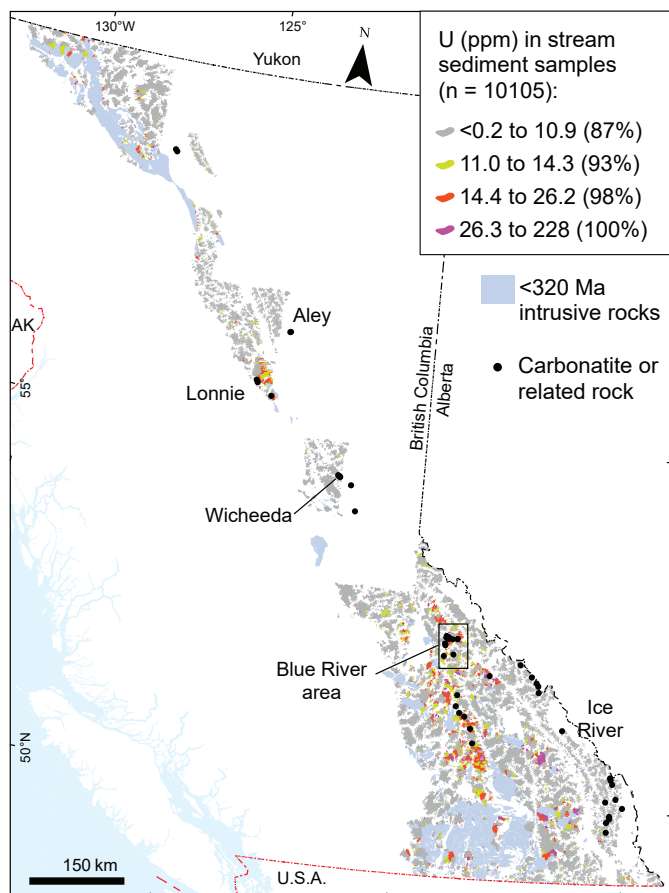


Fig. 10. Regional geochemical survey area, uranium-themed, percentile-ranked catchment basins of stream-sediment samples (<0.18 mm fraction; after Han and Rukhlov, 2017, 2020b). Carbonatite and related-rock occurrences after Höy (1988), Parrish and Scammell (1988), Pell (1994), Millonig and Groat (2013), and Rukhlov et al. (2018). The post-320 Ma intrusive rocks from BC Digital Geology version 2021-12-19 (Cui et al., 2017).

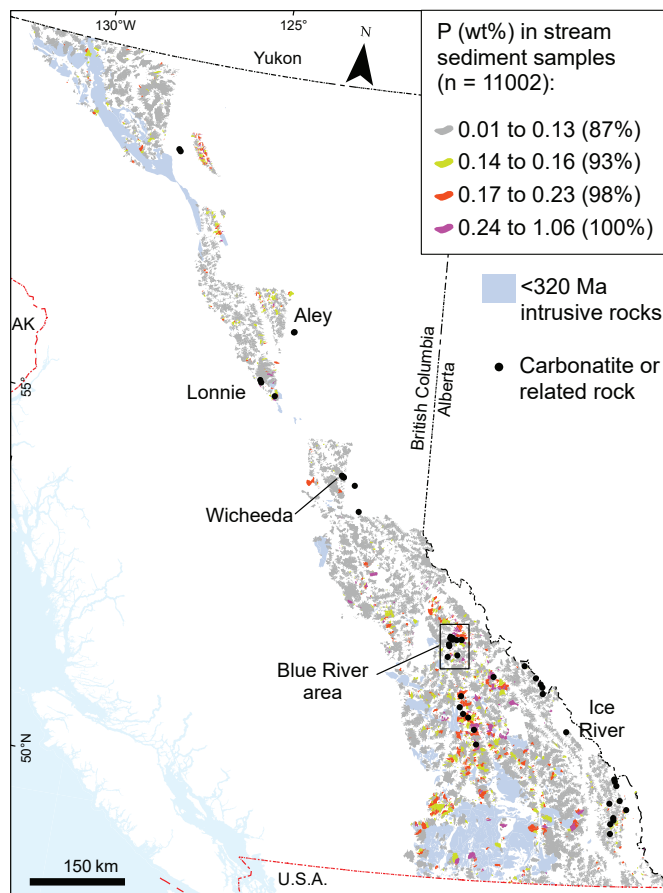


Fig. 11. Regional geochemical survey area, phosphorous-themed, percentile-ranked catchment basins of stream-sediment samples (<0.18 mm fraction; after Han and Rukhlov, 2017, 2020b). Carbonatite and related-rock occurrences after Höy (1988), Parrish and Scammell (1988), Pell (1994), Millonig and Groat (2013), and Rukhlov et al. (2018). The post-320 Ma intrusive rocks from BC Digital Geology version 2021-12-19 (Cui et al., 2017).

7. Discriminant analysis results

7.1. A 'carbonatite index'

Applied to all the regional geochemical survey stream-sediment data in the study area, the DP1 versus DP2 discrimination diagram identified a total of 721 stream sediment samples (6.3% of all the data) showing a multivariate carbonatite or related rock signal (Fig. 16). Herein we refer to this signal, which is recast as the DP1 value multiplied by minus one, as the 'carbonatite index'. The percentile-ranked index highlights prospective stream basins for carbonatite- and related rock-hosted critical metals (Fig. 17). Stream-sediment data showing carbonatite index scores greater than the 93rd percentile ($n=50$) reveal elevated concentrations of carbonatite indicator elements such as REE, Nb, Ta, Ti, Zr, Hf, Th, U, P, K, and Na, along with indicators of other mineralization-types (e.g., granitoid-related rare metals, precious and base metals), relative to the median (background) concentrations in stream sediments of the study area (Table 6). These geochemical anomalies conspicuously follow a trend of known carbonatite

occurrences in the Blue River and Frenchman Cap areas, extending it both to the northwest and southeast (Fig. 18).

7.2. Measure of geochemical anomaly

The quantity of metal above background (or predicted geochemical resources) based on productivity of an element in a dispersion stream is a parametric and thus an objective measure of a geochemical anomaly, which is the basis of evaluating prospective areas (Rukhlov et al., 2020a, b). The productivity of an element in an ideal dispersion stream, P_x (in $m^2\%$) is given in Equation 3.

$$P_x = (1/k) \cdot S_x \cdot (C_x - C_b) \quad (\text{Eqn. 3})$$

where

$k < > 1$ is the local proportionality coefficient between the productivity of an element in the dispersion stream and productivity of an element in the secondary or residual dispersion halo (soil anomaly), which depends on hydrography and individual properties of elements resulting in their supergene enrichment or leaching.

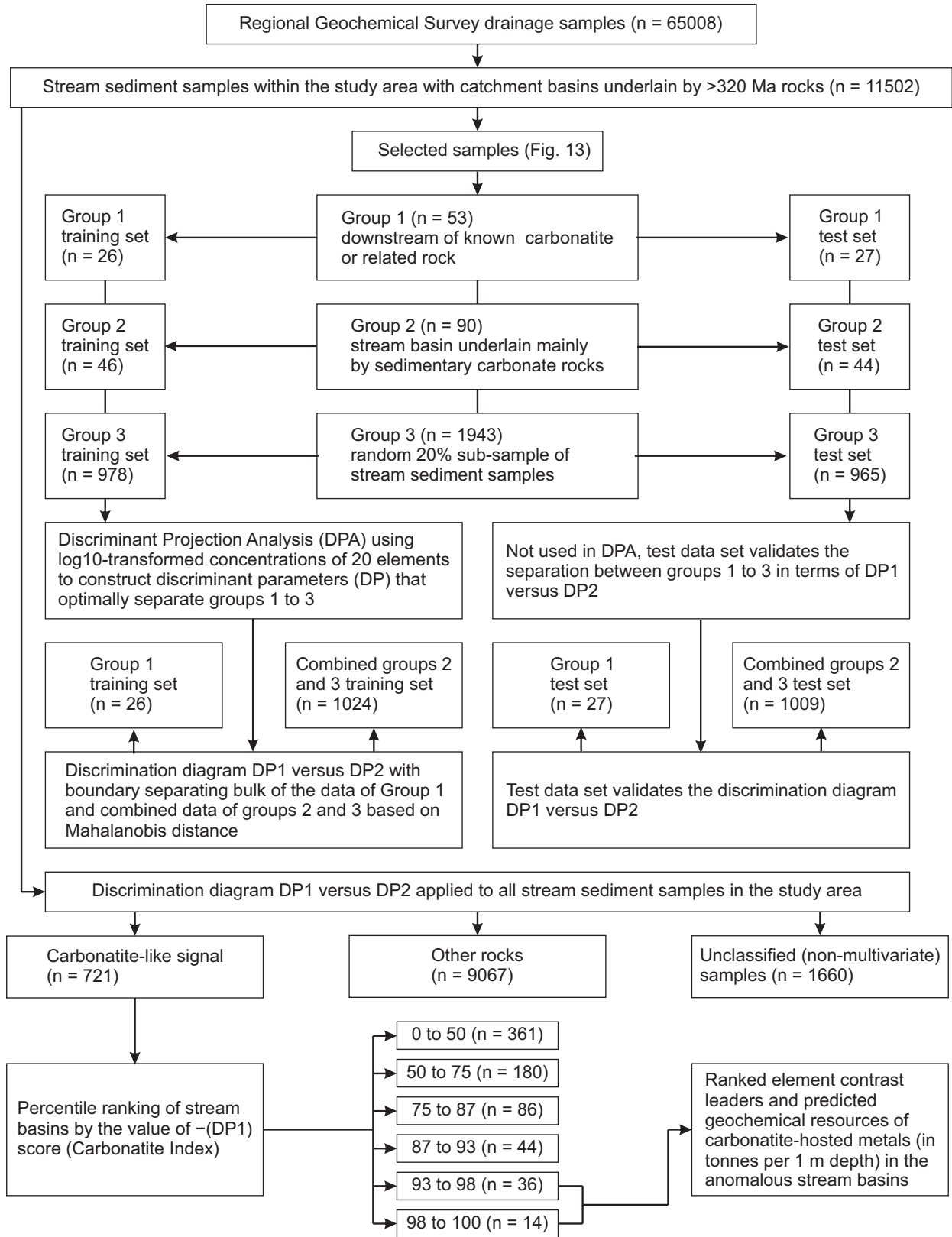


Fig. 12. Workflow used in this study.

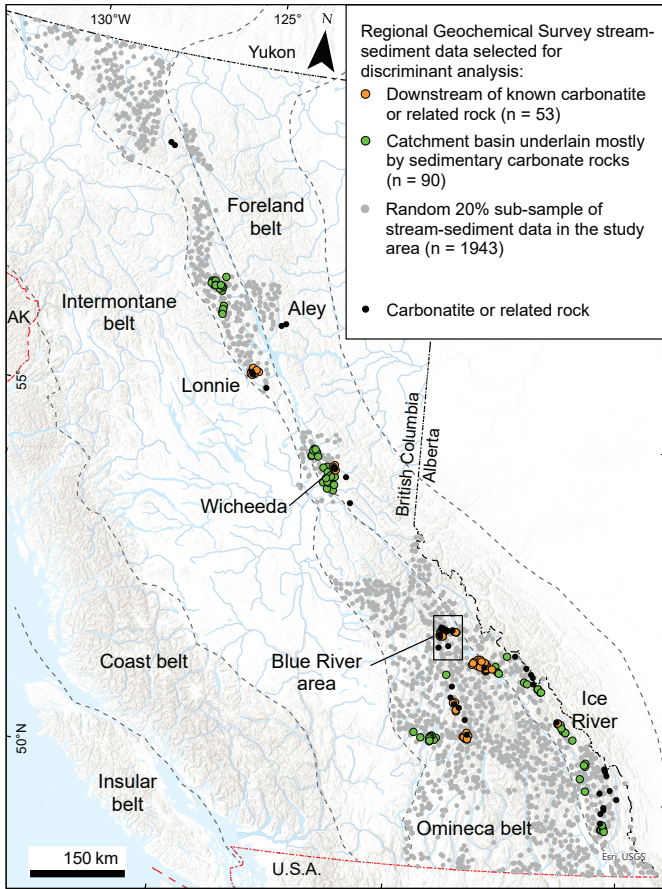


Fig. 13. Selected stream-sediment data from regional geochemical survey area used in training and validating discriminant analysis (after Han and Rukhlov, 2017, 2020b). Carbonatite and related-rock occurrences after Høy (1988), Parrish and Scammell (1988), Pell (1994), Millionig and Groat (2013), and Rukhlov et al. (2018). Morphotectonic boundaries after Gabrielse et al. (1991).

Table 5. Coefficients for discriminant parameters.

Variable	DP1		DP2	
	Projection ¹	Correlation ²	Projection ¹	Correlation ²
log (Ba ppm)	0.5125122	-0.023	1.0080582	0.369
log (Ca wt%)	-0.1132357	0.213	-0.6432403	-0.602
log (K wt%)	0.0190009	-0.458	-0.8340383	0.250
log (Mg wt%)	-0.3508289	0.167	2.0342928	-0.024
log (Mn ppm)	-0.7107679	0.159	-0.1111433	0.119
log (Mo ppm)	-0.7341133	-0.104	-0.2681685	0.191
log (Ni ppm)	-0.8465542	0.004	-0.5128953	0.209
log (P wt%)	-0.8646799	-0.434	-0.2221829	0.034
log (Pb ppm)	0.8482791	0.251	0.3704230	0.073
log (Sc ppm)	1.1082783	-0.233	0.0175719	0.362
log (Sm ppm)	-0.8054578	-0.722	-0.0255307	0.228
log (Sr ppm)	-0.1415442	0.113	-0.7922373	-0.636
log (Th ppm)	-2.7800825	-0.792	-1.4640319	0.140
log (Ti wt%)	-0.1456117	-0.383	1.0353020	0.505
log (U ppm)	0.2233847	-0.648	2.4597713	0.497
log (V ppm)	-0.2578595	-0.102	-0.8935080	0.217
log (Zn ppm)	0.9749035	0.171	0.2481454	0.192
log (La ppm)	-2.1814112	-0.740	0.2285954	0.156
log (Fe wt%)	2.2246271	-0.027	0.5292998	0.188
log (Ce ppm)	1.9567853	-0.718	-0.7624135	0.128
Constant	0.0381130		1.6581413	
Eigenvalue ³	0.286 (73%)		0.103 (27%)	

¹ Scaled eigenvectors or projection coefficients.

² Pearson correlation coefficients between the input data and the projected data indicating contributions of each element in discriminating between groups of samples.

³ Relative significance of discriminant parameter in terms of eigenvalues of the within-groups sum of squares to between-groups sum of squares ratio matrix and their percentage values (in parentheses).

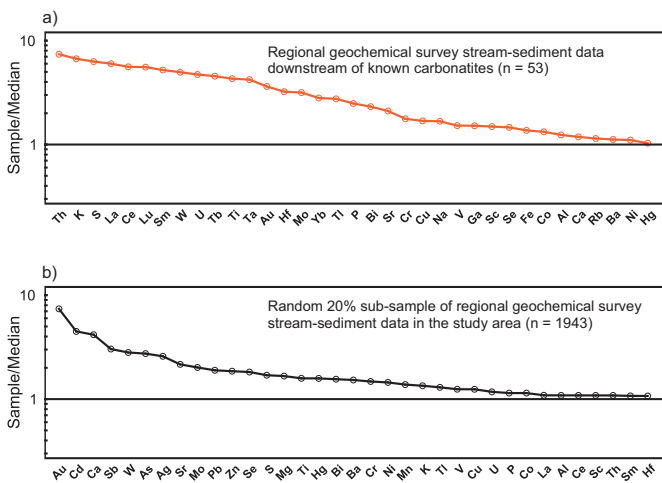


Fig. 14. Ranked element contrast plots relative to the median regional geochemical survey stream-sediment data (Table 4; after Han and Rukhlov, 2017, 2020b). **a)** The average stream-sediment data downstream of known carbonatite or related-rock occurrences. **b)** The average random 20% sub-sample of stream-sediment data.

S_x is the catchment area of stream basin at the sampling site (in m^2).

C_x is the concentration of an element in the stream sediment sample (in wt.%).

C_b is the background concentration of an element (in wt.%).

We estimate local background as the geometric mean or median concentration of an element in stream sediment samples ($n=20$ to 170) that are close to a geochemical anomaly. Downstream of a metal source (secondary dispersion halo), P_x is constant in an ideal dispersion stream, which may not be true for the second- or higher-order drainages (Rukhlov et al., 2020b).

Assuming $k=1$, the quantity of metal above background or predicted geochemical resources of an element in the stream basin, q (in tonnes per 1 m depth), is calculated as

$$q = H \cdot P_x / 40 = P_x / 40 \quad (\text{Eqn. 4})$$

where

$H=1$ is the calculation depth (in m).

P_x is the productivity of an element in dispersion stream (in $m^2\%$). The denominator ‘40’ converts $m^2\%$ into tonnes. We set the calculation depth, which refers to a probable depth of a mineralized zone, to a constant value of 1 m to simplify

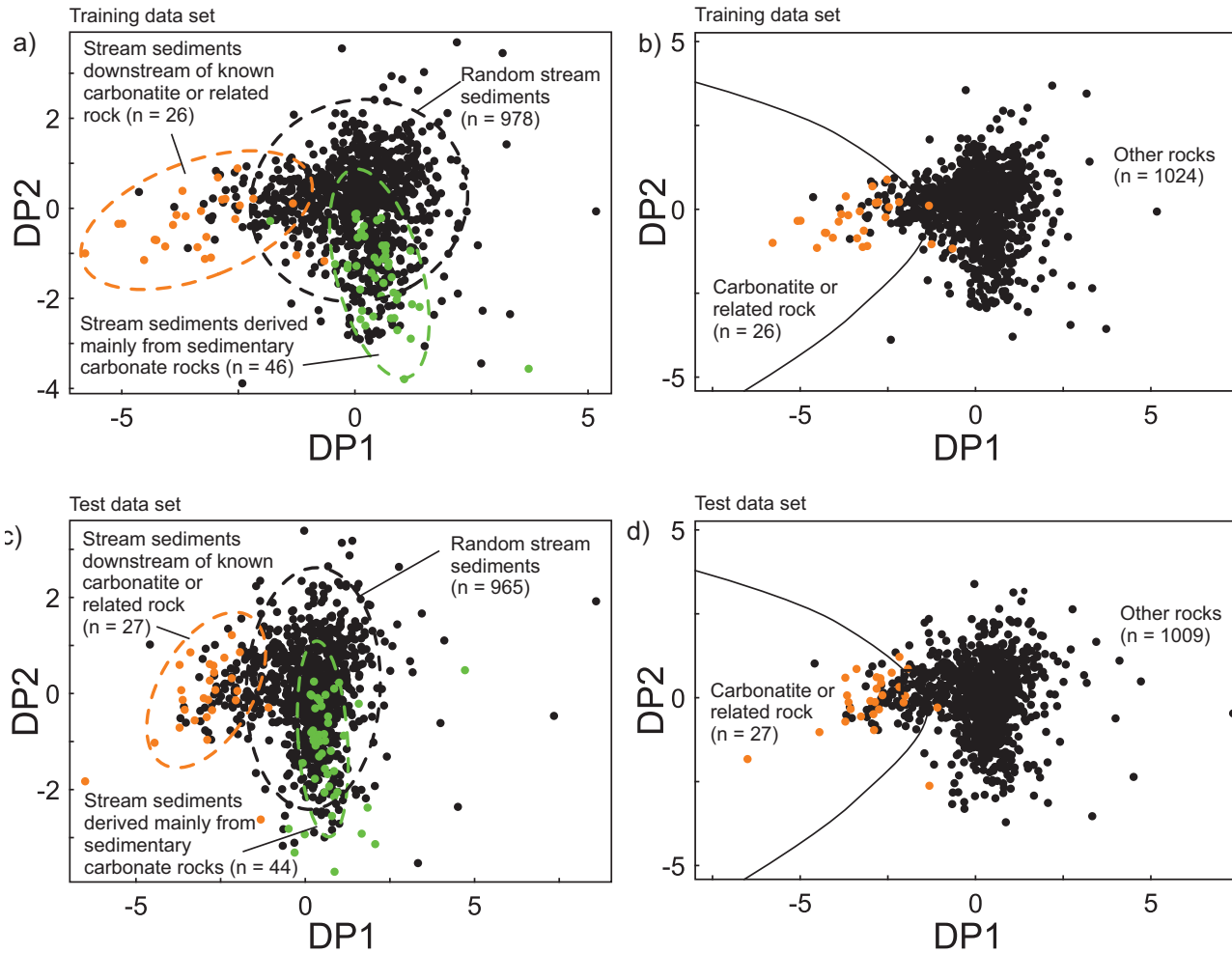


Fig. 15. Discrimination diagram DP1 versus DP2 for regional geochemical survey stream-sediment data. The discriminant-parameter (DP) variables are log₁₀-equivalents of element concentrations in parts per million (ppm) for all elements, except Ca, K, Mg, P, Ti, and Fe which are in weight per cent (wt.%; Table 5). **a)** DP1 versus DP2 for the training data set. **b)** DP1 versus DP2 for the training data set. **c)** DP1 versus DP2 for the test data set (not used in the discriminant analysis). **d)** DP1 versus DP2 for the test data set (not used in the discriminant analysis).

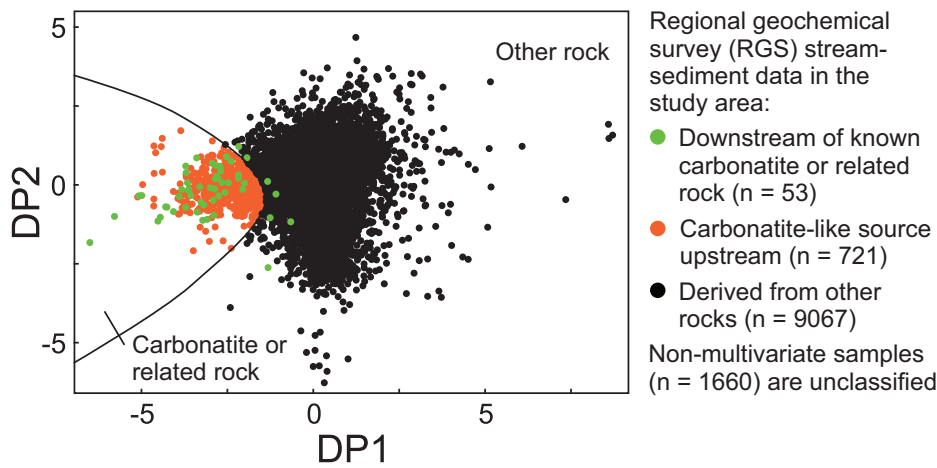


Fig. 16. Discrimination diagram DP1 versus DP2 for all regional geochemical survey stream-sediment data in the study area (after Han and Rukhlov, 2017, 2020b), showing boundary between carbonatite or related-rock sources and other rock sources in the upstream basins. Stream-sediment data downstream of known carbonatite and related-rock occurrences shown separately (green symbols).

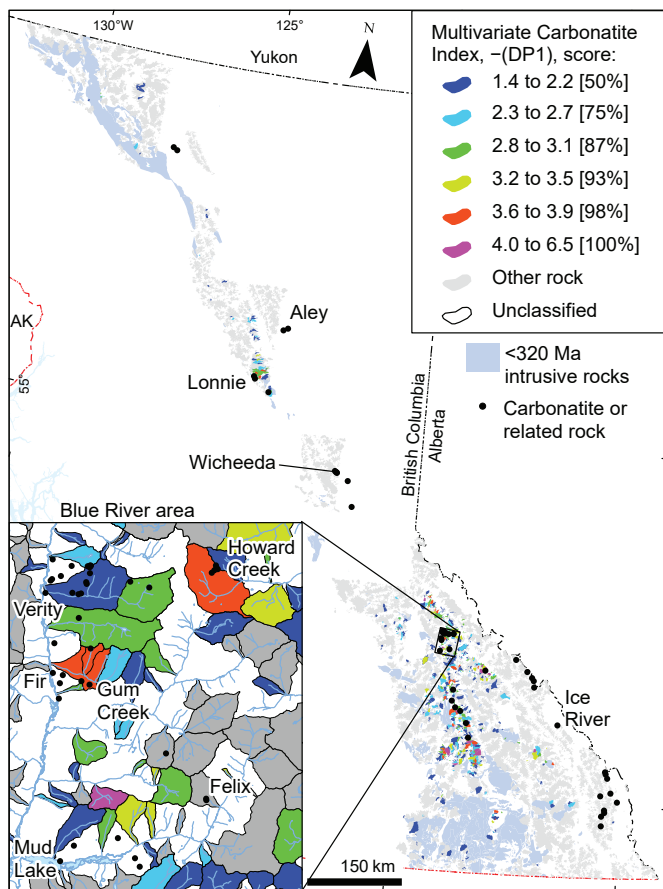


Fig. 17. Carbonatite index-themed, percentile-ranked catchment basins of regional geochemical survey stream-sediment samples (<0.18 mm fraction; after Han and Rukhlov, 2017, 2020b). Carbonatite and related-rock occurrences after Höy (1988), Parrish and Scammell (1988), Pell (1994), Millonig and Groat (2013), and Rukhlov et al. (2018). The post-320 Ma intrusive rocks from BC Digital Geology version 2021-12-19 (Cui et al., 2017).

equation 4 for a regional evaluation of geochemical anomalies (see Rukhlov et al., 2020a, b for details about predicted geochemical resources). The estimated predicted geochemical resources (in tonnes of metal per 1 m depth) suggest significant potential for REE and other carbonatite-hosted critical metals in the identified stream basins (Table 6).

7.3. Application to Aley carbonatite complex

Here we use an example of detailed stream-sediment litho-geochemical data downstream of the Aley carbonatite (Mackay and Simandl, 2014) to evaluate the mechanical dispersion of carbonatite indicators and ultimately the utility of the estimated predicted geochemical resources assuming an ideal dispersion (Table 6). Hosted by siliciclastic and carbonate rocks of the Kechika Group (Cambrian to Ordovician), the Aley carbonatite complex (ca. 370 Ma; Fig. 19) contains an NI 43-101-compliant resource of 286 million tonnes (Measured+Indicated) grading 0.37% Nb₂O₅ plus 144 million tonnes (Inferred) grading 0.32% Nb₂O₅ (Jones et al., 2017), making it the largest Nb deposit of the Cordilleran alkaline

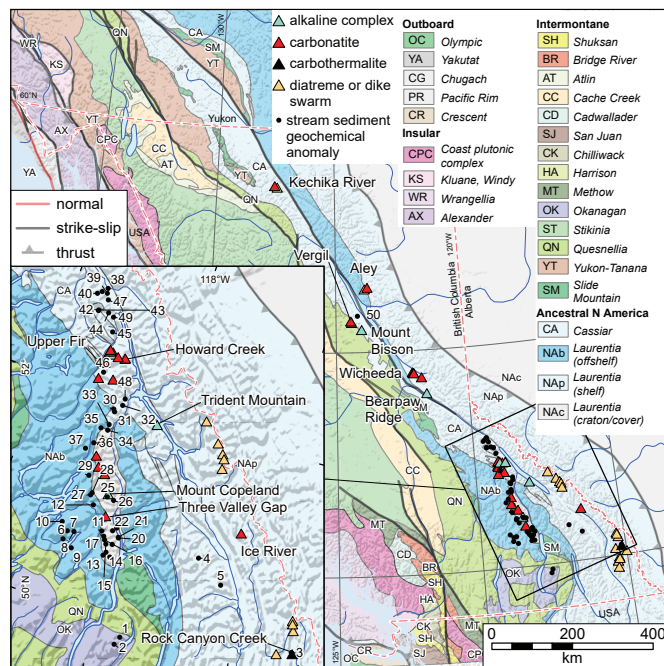


Fig. 18. Stream-sediment geochemical anomalies showing carbonatite index score greater than the 93rd percentile (see Table 6 for locations and other details). Carbonatite and related-rock occurrences after Höy (1988), Parrish and Scammell (1988), Pell (1994), Millonig and Groat (2013), Rukhlov et al. (2018). Terranes after Colpron (2020).

province (Pride, 1983; Mäder, 1987; McLeish, 2013; Chakhmouradian et al., 2015; McLeish and Johnston, 2019; McLeish et al., 2020). Based on determinations using a portable X-ray fluorescence analyzer (Mackay and Simandl, 2014), concentrations of carbonatite indicator elements such as Nb, La, Y, and Sr in the 0.125 to 0.250 mm fraction of stream sediment decrease exponentially downstream of the carbonatite (Fig. 20). Calculated using equation 3 above, productivities of Nb and Y obey an ideal dispersion law (i.e. $P_x \approx \text{constant}$ downstream of the anomaly) even in the second- and higher-order drainage system (Fig. 19). In contrast, productivity of La decreases and productivity of Sr increases downstream of the Aley carbonatite (Fig. 20). The main hosts of Nb and Y at Aley are the pyrochlore supergroup, ferrocolumbite, and other Nb-minerals, including euxenite (Chakhmouradian et al., 2015). These minerals are more resistant relative to monazite and REE \pm F-carbonate minerals, which are the main hosts of REE at Aley (Mäder, 1987; Mackay and Simandl, 2014; Simandl et al., 2017). The increasing productivity of Sr (Fig. 20d) probably reflects contribution from the carbonate country rocks of the Kechika and Road River groups and the Skoki Formation downstream of the Aley carbonatite complex (Fig. 19). More detailed surveys are needed to evaluate dispersion of critical metals downstream of other known carbonatite and related-rock occurrences, but the data from Aley indicate that resistant critical minerals generally obey an ideal dispersion law even in the high-order streams, thereby validating the estimated predicted geochemical resources (Table 6).

Table 6. Regional geochemical survey stream-sediment data showing carbonatite index scores >93rd percentile and predicted geochemical resources (g) of carbonatite-hosted metals (in tonnes per 1 m depth) in stream basins.

N ¹	RGS sample	X ²	Y ²	S ³	CI ⁴	Ranked element contrast leaders ⁵	Predicted geochemical resources (in tonnes per 1 m depth) ⁶														Predominant host rock		
							Nb	Ta	La	Ce	Nd	Sm	Eu	Tb	Yb	Lu	Y	Sc	Mo	Th		U	
1	082F775336	-117.623	49.883	25	3.7	W-41, Nb-14, Au-12, U-11, Th-9, Mo-8, La-7, (Ce, Cd)-5, (Sm, Se, Na, Ti, Ti)-3, (K, Te)-2	0	16	13709	19844	na	551	na	16	0	0	0	0	0	158	4897	983	metamorphic rocks (Harper Ranch assemblage; Carboniferous to Permian)
2	082F775345	-117.670	49.804	3	3.7	Nb-17, Mo-9, K-8, Th-6, (P, La, Ti, Ti)-5, Ce-4, (Y, Hf, Te, W, Sm, U, Cd)-3, (Zr, Ba, V)-2	2.5	0	1019	1528	na	48	na	0.51	0	0	119	0	27	324	na	metamorphic rocks (Harper Ranch assemblage; Carboniferous to Permian)	
3	082J901240	-115.162	50.223	2	3.5	Ca-21, Au-14, (Ba, Mo)-13, Sb-11, Mg-10, La-9, (Te, Cd)-8, Ti-7, (Sb, Sr, W)-6, Th-5	2.6	0	936	1749	na	66	na	3.5	0	2.3	86	0	37	185	2.2	limestone, slate, siltstone, argillite (Banff and Exshaw formations; Mississippian)	
4	082K775330	-116.879	50.820	19	4.6	Bi-147, Th-82, U-48, Ta-47, Te-29, La-23, Nb-22, W-19, (Hf, V, Zr, Tb)-6, Ce-5, (Fe, Na, Y)-3	280	3257	24198	16529	na	712	na	219	0	0	682	0	17	22111	10485	coarse siliceous rocks (Horsethief Creek Group; Neoproterozoic)	
5	082K777088	-116.445	50.639	13	3.6	W-158, Nb-22, U-17, Ta-11, Th-9, La-7, U*-6, Mo-5, F*-4, (Ce, P, Y, Na)-3, (Bi, Rb, Cs)-2	192	502	3531	4663	na	55	na	3.3	0	0	447	0	67	1785	1916	quartzite, quartz arenite (Purcell Supergroup, Mount Nelson and Dutch Creek formations; Mesoproterozoic)	
6	082L763159	-118.876	50.589	15	3.7	Th-13, Ce-8, (Sm, Hf, Zr, Lu, La, Tb)-6, U-5, (W, Na)-4, (Cr, Ti)-3, (Ta, K, Se, P, S, Yb)-2	na	54	7931	19105	na	1261	na	144	37	59	na	218	0	4979	553	limestone, marble, calcareous sedimentary rocks (Shuswap assemblage; Proterozoic to Paleozoic)	
7	082L763165	-118.855	50.674	23	3.6	(Au, Th)-11, Lu-8, Sm-7, (Ce, La, W)-6, (Tb, Hf, U, Na)-5, (Zr, Ti)-4, (Cr, K, Yb, Sc, Ta)-3	na	125	14252	23051	na	2071	na	205	289	139	na	771	0	6184	757	limestone, marble, calcareous sedimentary rocks (Shuswap assemblage; Proterozoic to Paleozoic)	
8	082L763168	-118.759	50.688	69	5.0	Au-56, W-54, Th-23, Lu-19, Sm-13, La-12, (U, Tb)-11, (Ce, Hf)-9, Zr-8, (Na, Yb)-4, (Ta, Cr)-3	na	562	96127	106998	na	14985	na	1690	1202	1185	na	1743	0	47411	7265	limestone, marble, calcareous sedimentary rocks (Shuswap assemblage; Proterozoic to Paleozoic)	
9	082L763198	-118.717	50.535	20	5.1	Au-50, Th-25, Lu-22, La-17, (Sm, Ce)-15, U-14, Tb-12, (Hf, Zr)-11, W-7, Na-6, Cr-5, Yb-4	na	135	38930	58564	na	4990	na	529	439	381	na	583	0	15229	2753	quartzite, quartz arenite (Shuswap assemblage; Proterozoic to Paleozoic)	
10	082L765210	-118.973	50.742	14	3.8	Th-9, Zr-8, (Hf, Ce, La, Sm)-6, Lu-5, (U, Tb, Na)-4, (K, Ti, Cr)-3, (Na, P, Ba, Yb, Se, Ti)-2	na	0	6794	11991	na	941	na	86	34	34	na	52	0	2663	384	metamorphic rocks (Shuswap assemblage; Proterozoic to Paleozoic)	
11	082L765223	-118.372	50.778	46	3.6	W-34, Th-10, (Zr, Ce, La)-8, Sm-7, (Hf, Lu, Na)-6, (U, Tb, Ti, K)-5, (Cr, Yb)-3, (Sc, P, Ti)-2	na	129	30216	49718	na	3647	na	229	228	114	na	1197	25	9061	976	limestone, marble, calcareous sedimentary rocks (Shuswap assemblage; Proterozoic to Paleozoic)	

¹ Anomaly number as shown in Fig. 18.² Longitude (X) and latitude (Y) coordinates (in decimal degrees) of regional geochemical survey (RGS) stream sediment sample.³ Area of catchment basin (in km²).⁴ Carbonatite index (CI) score values; CI = -DPI (Table 5).⁵ Ranked element contrast (REC) leaders are sorted (maximum to minimum) element concentrations normalized to the median values of regional geochemical survey stream-sediment data (Table 4). REC leaders reveal associations of elements showing the maximum contrast to background and the magnitude of the contrast (geochemical anomaly), which identify mineralization in the stream basin.⁶ Anomalies 1 to 37 and 50 lack Nd and Eu determinations; anomalies 6 to 50 lack Nb and Y determinations. F* and U* are fluorine and uranium determinations in stream water. na = not analyzed.⁷ Predicted geochemical resources in the stream basin (in tonnes of metal per 1 m depth); see text for details.

Table 6. Continued.

N ¹	RGS sample	X ²	Y ²	S ³	Cl ⁴	Ranked element contrast leaders ⁵	Predicted geochemical resources (in tonnes per 1 m depth) ⁶														Predominant host rock	
							Nb	Ta	La	Ce	Nd	Sm	Eu	Tb	Yb	Lu	Y	Sc	Mo	Th		U
12	082L765268	-118.616	50.985	3	3.9	(Th, W)-12, Lu-10, (U)*, La, Ce)-8, Sm-7, (U, Tb)-6, Yb-5, (Hf, F*, Zr)-4, (Ta, W, Na, Ti)-3	na	20	2006	3606	na	236	na	26	68	24	na	57	0	841	115	coarse siliceous rocks (Horseshoe Creek Group; Neoproterozoic)
13	082L769008	-118.239	50.566	9	3.6	(K, Th)-10, (W, Lu)-9, (Na, Ce)-7, (Ti, La, Tb, Zr, Sm, U, Ti)-6, Hf-5, Cr-4, (Yb, Sc, P)-3, Ga-2	na	27	4072	6882	na	538	na	76	87	50	na	155	8.0	1600	282	quartzite, quartz arenite (Monashee complex; Proterozoic to Early Paleozoic)
14	082L769010	-118.210	50.602	16	3.5	W-18, Th-8, Lu-7, (Ce, U, Tb, Sm, La)-5, (Yb, Au, K, Zr)-4, (Na, Ti, Hf)-3, (Ti, P, Cr, Na)-2	na	21	4561	8113	na	649	na	101	282	52	na	121	0	2198	394	quartzite, quartz arenite (Monashee complex; Proterozoic to early Paleozoic)
15	082L769070	-118.252	50.674	7	4.4	(Lu, Th)-16, W-14, U-12, Tb-11, Sm-10, (Ce, La)-9, Yb-7, Au-6, (K, Zr)-5, (Hf, Na)-4, Ti-3	na	9.3	6323	10626	na	934	na	153	263	91	na	35	0	2871	726	quartzite, quartz arenite (Monashee complex; Proterozoic to early Paleozoic)
16	082L769071	-118.290	50.707	3	4.4	Lu-24, Th-22, U-16, Tb-15, (La, Sm, Ce)-13, Yb-10, Zr-7, (W, Hf)-6, K-5, (Cr, Ti)-4, Na-3	na	12	4920	7943	na	690	na	111	209	71	na	64	0	2103	540	quartzite, quartz arenite (Monashee complex; Proterozoic to early Paleozoic)
17	082L769075	-118.319	50.738	4	3.9	W-23, Th-17, Tb-12, (Lu, U)-11, Sm-10, (La, Ce)-9, Ti-7, (Zr, Yb)-6, Hf-5, (Au, Rb, Ba)-4	na	30	3495	5656	na	581	na	99	122	33	na	82	7.3	1788	379	quartzite, quartz arenite (Monashee complex; Proterozoic to early Paleozoic)
18	082L769153	-118.135	50.570	7	3.9	W-30, Lu-17, Yb-12, (Th, U)-11, Tb-9, (U, Ce)-8, (Sm, Na, La)-7, (Zr, Hf)-5, (Ti, K, P)-3	na	5.5	3583	7419	na	530	na	113	488	89	na	153	0	1539	376	orthogneiss (Paleoproterozoic)
19	082L769158	-118.160	50.690	5	3.7	(Th, Lu)-13, W-12, (Tb, Ce)-9, (Sm, La)-8, U-7, (Yb, Au)-6, Hf-5, (Zr, K, Na)-4, (Cr, Ti, Ti)-2	na	2.7	3294	6338	na	524	na	80	155	47	na	36	0	1497	198	paragneiss (Paleoproterozoic)
20	082L769159	-118.102	50.766	57	4.6	W-19, Th-15, Lu-13, Sm-9, (Tb, Ce, La)-8, U-7, Yb-6, Hf-5, Zr-4, (Na, Ba, Rb, Au)-2	na	61	37810	66635	na	7103	na	857	1569	542	na	0	0	21751	2447	quartzite, quartz arenite (Monashee complex; Proterozoic to early Paleozoic)
21	082L769160	-118.110	50.771	37	4.6	Th-20, Lu-16, (Tb, W)-14, Sm-12, U-10, (La, Ce)-9, Yb-7, (Zr, S)-5, Hf-4, (Na, K, As)-3	na	143	34167	52331	na	6785	na	1096	1404	477	na	0	0	20635	2963	Paragneiss (Paleoproterozoic)
22	082L769169	-118.220	50.813	10	4.6	Lu-21, Th-20, (La, Sm)-13, (Ce, Hf, Tb)-12, (U, K)-11, Zr-10, Yb-7, Ti-6, Ti-5, Cr-4, (Na, Se)-3	na	0	13707	22151	na	1944	na	241	372	174	na	171	8.7	5251	933	quartzite, quartz arenite (Monashee complex; Proterozoic to early Paleozoic)
23	082L769171	-118.174	50.851	34	3.5	Th-6, (Zr, Hf)-5, (Lu, Sm, Tb, Ce)-4, (U, La, K, Na)-3, (W, Ti, P, Yb, Ta)-2	na	46	1126	1048	na	653	na	70	0	26	na	0	0	2303	83	calc-silicate metamorphic rocks (Monashee complex; Proterozoic to early Paleozoic)
24	082L769172	-118.174	50.851	34	3.6	W-27, Th-6, (Zr, Hf)-5, (Ce, Lu, Sm)-4, (La, Tb, U, Na)-3, (K, Yb, P, Ti)-2	na	28	1985	7064	na	464	na	27	0	17	na	0	0	2157	0	calc-silicate metamorphic rocks (Monashee complex; Proterozoic to early Paleozoic)
25	082M763128	-118.457	51.098	4	3.6	Mo-159, Na-11, W-8, (K, Ti)-7, (La, F*, Au, U, Zr)-6, (Hf, Ta, Ce, Sr, Tb)-4, (P, Ga, Ti)-3	na	44	1083	1748	na	38	na	6.5	20	4.0	na	0	837	48	65	calc-silicate metamorphic rocks (Monashee complex; Proterozoic to early Paleozoic)

Table 6. Continued.

N ¹	RGS sample	X ²	Y ²	S ³	CI ⁴	Ranked element contrast leaders ⁵	Predicted geochemical resources (in tonnes per 1 m depth) ⁶														Predominant host rock
							Nb	Ta	La	Ce	Nd	Sm	Eu	Tb	Tb	Yb	Lu	Y	Sc	Mo	
26	082M763135	-118.351	51.086	41	3.9	W-45, Mo-18, Zr-11, Hf-8, (Na, Th, La, Ce)-6, (Ta, U)-5, (Lu, F*, Sm, K, Ti, Tb)-4, Sr-3	531	19006	32392	na	1504	na	147	405	111	na	0	861	4263	983	calcareous metamorphic rocks (Monashee complex; Proterozoic to early Paleozoic)
27	082M767025	-118.703	51.065	4	4.6	Th-15, La-12, Ce-9, Sm-7, (Hf, P)-6, (Tb, Zr)-5, (U, Ti)-4, (Na, K)-3, (Cr, W, Ca, Ga, Ba, Ta)-2	1.3	4724	5753	na	351	na	31	0	0	na	0	0	1616	80	coarse siliciclastic rocks (Horseshief Creek Group; Neoproterozoic)
28	082M767028	-118.692	51.089	14	3.9	Th-9, W-8, (La, Na)-7, Ce-6, Sm-5, (Au, Ti, Zr)-4, (Tb, Hf, K, S, U)-3, (P, Sc, Sr, Mo)-2	na	9233	12010	na	671	na	49	0	0	na	120	0	3079	54	calcareous metamorphic rocks (Monashee complex; Proterozoic to early Paleozoic)
29	082M769045	-118.823	51.234	59	3.5	W-24, Na-9, (Th, Sm, Tb)-5, (K, Zr, Ti, La, Ce)-4, (Hf, Ta, U, Lu)-3, (Cr, P, Ti, Yb, Mo, Au)-2	150	12964	20801	na	3031	na	339	0	67	na	201	0	5753	223	calcareous metamorphic rocks (Monashee complex; Proterozoic to early Paleozoic)
30	082M775247	-118.797	51.898	22	3.6	W-198, Na-12, (Lu, Th)-10, (Tb, Ce)-9, Sm-8, (La, U)-7, (Ta, Yb)-5, (Bi, Au, Cr, Ti, Zr)-4	282	13883	32403	na	2392	na	376	485	172	na	386	0	5005	1093	limestone, marble, calcareous sedimentary rocks (Horseshief Creek Group; Neoproterozoic)
31	082M775249	-118.772	51.876	30	3.7	Lu-13, Th-12, Tb-10, (Sm, Ce)-9, (W, La)-8, (Na, U)-7, (Zr, Yb)-5, Hf-4, (Ti, Ta, K)-3, Cr-2	146	21534	49050	na	4092	na	603	832	318	na	414	0	9598	1542	limestone, marble, calcareous sedimentary rocks (Horseshief Creek Group; Neoproterozoic)
32	082M775264	-118.687	51.958	8	3.7	Th-9, (Tb, Sm, W)-8, (Zr, Lu)-7, (Na, U, La)-6, (Ce, Hf)-5, (Ta, Yb, K, Ti)-4, (Cr, Au, Sc, P)-2	78	3439	4349	na	845	na	125	162	34	na	161	0	1619	304	limestone, marble, calcareous sedimentary rocks (Horseshief Creek Group; Neoproterozoic)
33	082M775405	-118.786	51.746	4	3.7	W-12, (Th, Na)-8, Au-6, (Sm, Tb)-5, (La, Ti, Ce)-4, (K, Ta, U, Mo)-3, (Cr, Hf, Zr, Sc, P)-2	15	917	1358	na	167	na	20	0	0	na	28	6.4	590	19	limestone, marble, calcareous sedimentary rocks (Horseshief Creek Group; Neoproterozoic)
34	082M775408	-118.779	51.692	15	3.8	Th-8, (Na, La, Zr, Sm)-6, (Hf, Ce, Tb, K)-5, (Ti, U, Cr, Lu)-4, Ta-3, (Yb, P, W, Ti, Sc)-2	85	7017	9210	na	915	na	87	73	22	na	109	0	2632	293	limestone, marble, calcareous sedimentary rocks (Horseshief Creek Group; Neoproterozoic)
35	082M775413	-118.887	51.692	20	3.8	Au-14, Th-10, Zr-8, (Sm, Hf, Tb, Lu)-7, (La, Na, Ce)-6, (W, U)-5, (K, Yb)-4, Ti-3, (Cr, Ta)-2	26	10734	14754	na	1855	na	210	294	83	na	308	0	4952	540	limestone, marble, calcareous sedimentary rocks (Horseshief Creek Group; Neoproterozoic)
36	082M775470	-118.916	51.538	5	4.1	W-15, Th-12, (La, Ce, Sm)-8, Tb-7, Lu-6, (Ti, U)-5, (Na, K, Ta)-4, (Cr, Hf, Zr, Yb, Au)-3	31	3671	6367	na	501	na	57	35	19	na	35	0	1406	129	coarse siliciclastic rocks (Horseshief Creek Group; Neoproterozoic)
37	082M775479	-119.007	51.463	18	3.8	(Th, Lu)-8, W-7, (Sm, Tb)-6, (La, Ce, Zr, Hf)-5, (U, Na)-4, (Yb, S, Cr)-3, (Ti, K, Ta)-2	na	7286	11239	na	1152	na	149	220	92	na	43	0	3205	352	coarse siliciclastic rocks (Horseshief Creek Group; Neoproterozoic)
38	083D051004	-119.499	52.949	0.3	3.5	S-17, Th-6, (La, K)-5, (Ta, Hf, Sm, Ce, Eu)-4, (Cu, U, Lu, Ti)-3, (Yb, Na, Ti, P, Bi, Tb, Te)-2	1.2	61	68	0	6.4	1.9	0	0.21	0.07	na	na	0.08	21	2.7	dolomitic carbonate rocks (Rocky Mountain assemblage; middle Cambrian)
39	083D051005	-119.484	52.904	7	3.6	Th-8, Ta-7, (La, Ce, K, Sm)-6, (Lu, Yb, U)-5, (Hf, Nd, Tb)-4, (Ti, P, Eu, Ti, W, F*, Na, Sc)-3	89	2892	5332	2006	352	32	26	135	17	na	195	4.2	973	184	mudstone, siltstone, shale (Kaza Group, lower division; Neoproterozoic)

Table 6. Continued.

N ¹ RGS sample	X ²	Y ²	S ³	Cl ⁴	Ranked element contrast leaders ⁵	Predicted geochemical resources (in tonnes per 1 m depth) ⁶														Predominant host rock		
						Nb	Ta	La	Ce	Nd	Sm	Eu	Tb	Yb	Lu	Y	Sc	Mo	Th		U	
40	083D051070	-119.630	52.872	16	4.4	Ti-34, (Hf, Th)-13, (Ce, La, K, Sm)-10, (Au, U)-9, S-8, Tb-7, (Nd, Eu)-6, (Ta, Cu, Lu, Yb)-5	na	136	14860	27435	10643	2083	276	211	280	35	na	59	26	5211	1261	mudstone, siltstone, shale (Kaza Group, lower division; Neoproterozoic)
41	083D051077	-119.569	52.903	3	3.5	Th-10, (La, Ce)-8, (Lu, Yb, Sm, K)-7, (Tb, Ta)-6, (U, Nd)-5, (Eu, Te, Ti, Hf, Ti)-4, (Sc, Fe)-3	na	24	1631	2936	1132	215	23	25	97	13	na	130	0	561	80	coarse siliclastic rocks (Kaza Group; Neoproterozoic)
42	083D051144	-119.525	52.723	2	3.8	K-10, (La, Ti, Ta, Th)-5, (Sm, Ce, Eu, P, Ti)-4, (Tb, Na, U, Cu, Yb, Mo)-3, (Hf, Ba, Cr, Nd)-2	na	13	510	399	43	40	14	4.9	5.1	0.43	na	8.5	3.4	74	13	mudstone, siltstone, shale (Horsechief Creek Group, lower pelite unit; Neoproterozoic)
43	083D051145	-119.522	52.729	4	3.7	Au-35, Th-6, La-5, (Ce, Sm, K, Ta)-4, (Tb, Eu, U, Ti, Hf, Ti, W)-3, (Lu, Yb, Se, Nd, Te, Na)-2	na	17	1163	1183	196	99	21	11	1.0	na	na	0	2.9	267	39	mudstone, siltstone, shale (Kaza Group, lower division; Neoproterozoic)
44	083D051157	-119.363	52.735	6	3.7	Th-8, (K, La)-7, (Sm, Ce, Ta)-6, U-5, (Tb, Ti, Lu, Yb, Hf, Eu)-4, (Ti, Te, Sc, Na, Co, Nd)-3	na	54	2928	3646	563	364	36	32	72	9.9	na	183	0	960	155	mudstone, siltstone, shale (Kaza Group, lower division; Neoproterozoic)
45	083D051371	-119.206	52.579	2	3.7	Th-7, (La, Ce)-6, (Sm, U)-5, (K, Tb, Hf)-4, (Nd, Ti, Eu, Ta, Ti, Lu)-3, (Bi, F*, Yb, Te, Na, Fe)-2	na	0	790	1392	455	108	6.2	11	0	0	na	0	0	266	63	mudstone, siltstone, shale (Kaza Group, lower division; Neoproterozoic)
46	083D051424	-119.131	52.193	8	3.9	K-12, (La, Th)-8, (Ti, Ce)-7, Sm-6, (Tb, U)-5, (Yb, Lu, Ti, Hf, Na, Te, Mo, Eu)-4, (S, Cr)-3	na	6.0	5528	6940	1248	476	58	33	85	9.2	na	15	12	1180	187	metamorphic rocks (Mica Creek succession; Neoproterozoic)
47	083D052034	-119.436	52.848	22	3.5	Th-10, (Ce, La, Bi)-8, Sm-7, (U, K, Nd, Tb)-6, (Ta, Lu)-5, (Hf, S, Yb, Eu)-4, (W, Ti, Ti, Sc)-3	na	181	13570	28871	12285	1996	161	193	285	50	na	580	0	4870	949	quartzite, quartz arenite (Neoproterozoic)
48	083D052128	-118.683	52.022	2	3.9	Th-12, Ce-10, (La, Sm)-9, (Na, Tb, Nd, Hf)-7, (U, Lu)-6, (K, Eu, Yb)-5, Ti-4, W-3, (P, Se)-2	na	0	2225	4410	1718	307	29	29	53	7.7	na	45	0	692	101	metamorphic rocks (Mica Creek succession; Neoproterozoic)
49	083D053028	-119.270	52.712	15	3.5	Th-11, Ce-10, (La, Sm)-9, U-7, (Ta, Nd, Tb, K, W)-6, (Hf, Lu, Yb)-5, (Eu, Ti)-4, (Ti, Sc, Fe)-3	na	185	12849	25279	9914	1718	145	139	271	38	na	572	0	4202	763	mudstone, siltstone, shale (Kaza Group, lower division; Neoproterozoic)
50	093N831597	-124.151	55.812	13	3.8	P-13, Th-9, (Lu, Ce)-6, (Sm, Au, La, U, Na)-5, (Zr, Tb)-4, (Hf, K)-3, (Ti, Te, Tl, Ta, Yb, Cr)-2	na	20	3805	6842	na	624	na	52	33	50	na	0	0	1911	118	argillite, greywacke, wacke, conglomerate (Ingenika Group, Swannell Formation; Neoproterozoic)

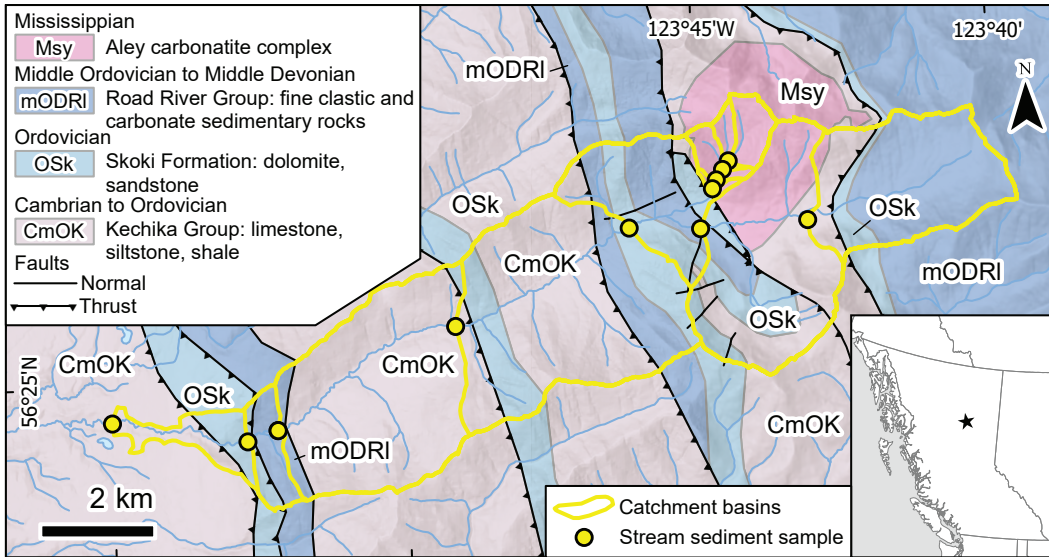


Fig. 19. Sampling sites and catchment basins at Aley carbonatite complex. Sampling sites after Mackay and Simandl (2014). Geology after Pride (1983), Mäder (1987), McLeish (2013), and BC Digital Geology version 2021-12-19 (Cui et al., 2017).

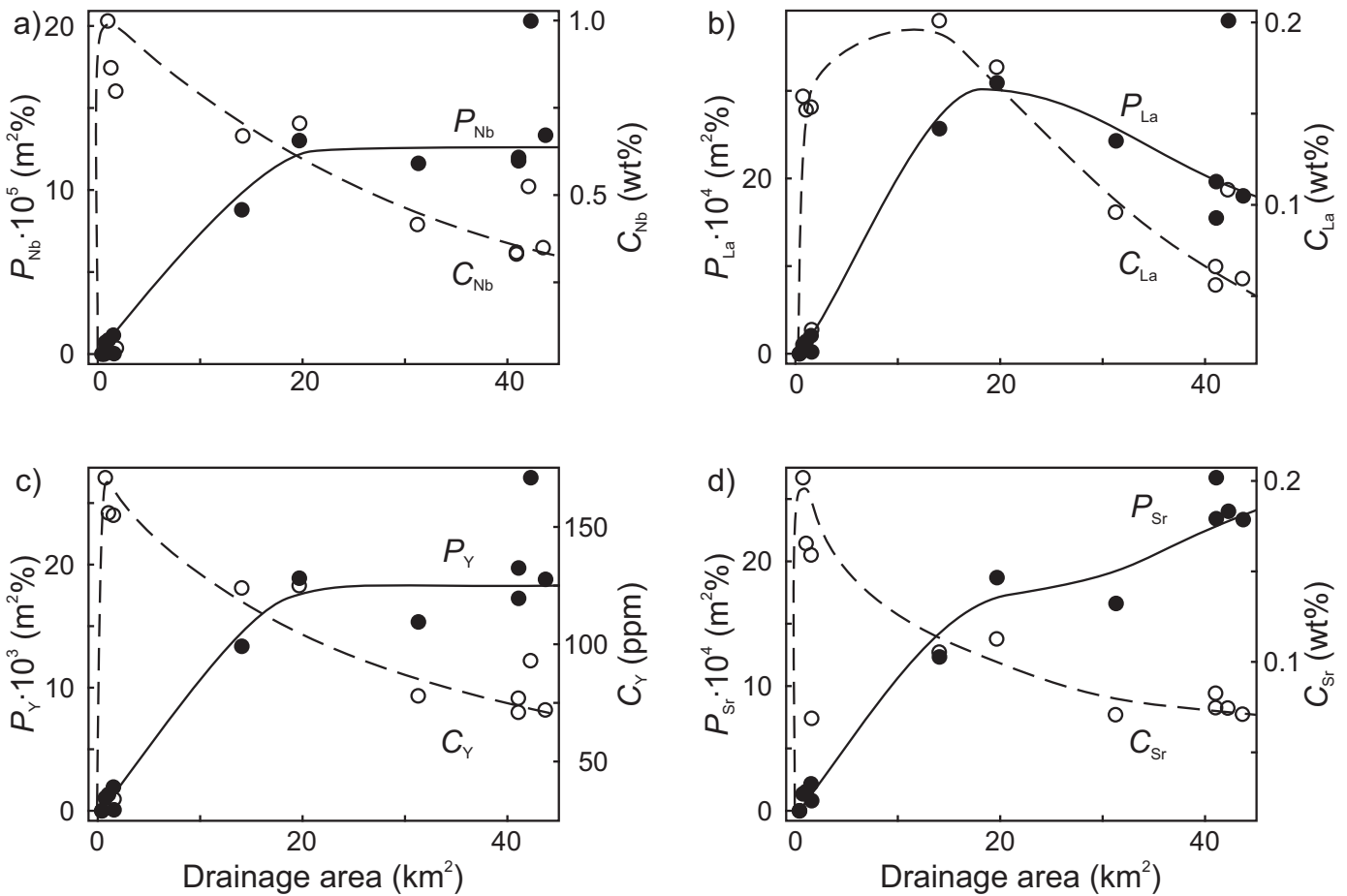


Fig. 20. Aley carbonatite complex, drainage area (km²) versus concentration, C_x (wt.% or ppm; open symbols; model dashed line), and productivity, P_x (m²%; solid symbols, model solid line), of selected elements for the 0.125 to 0.250 mm fraction of stream-sediment samples. Original concentrations from Mackay and Simandl (2014). **a)** Drainage area (km²) versus C_{Nb} (wt.%) and $P_{Nb} \cdot 10^5$ (m²%). **b)** Drainage area (km²) versus C_{La} (wt.%) and $P_{La} \cdot 10^4$ (m²%). **c)** Drainage area (km²) versus C_Y (ppm) and $P_Y \cdot 10^3$ (m²%). **d)** Drainage area (km²) versus C_{Sr} (wt.%) and $P_{Sr} \cdot 10^4$ (m²%).

8. Discussion

Based on data from known carbonatites, an integrated approach to assess the critical metals potential of underexplored regions might combine detailed stream-sediment sampling and application of the critical mineral index as defined herein, high-resolution airborne radiometric and magnetic data, and panned heavy mineral concentrate and soil lithochemical surveys.

8.1. Geophysical response from carbonatites of the Blue River area

Both airborne radiometric and magnetic surveys are effective prospecting tools for carbonatite-hosted critical minerals (e.g., Simandl and Paradis, 2018), many of which contain U and Th and are associated with abundant magnetic minerals such as magnetite or pyrrhotite and K-rich metasomatic rocks such as glimmerites (carbonate-amphibole-phlogopite rocks). High-resolution, airborne gamma-ray uranium (Fig. 21) and total magnetic intensity (Fig. 22) highs highlight numerous known carbonatite occurrences in the Blue River area, which illustrate the effectiveness of geophysics for critical minerals prospecting, especially in vegetated, low-elevation areas (Gorham, 2008; Shives, 2009). However, difficulty in maintaining constant ground clearance in rugged terrain results in gamma counts and total magnetic intensities that reflect topography, with generally stronger responses from ridges and peaks relative to low-elevation areas (Gorham, 2008).

8.2. Stream-sediment, panned heavy mineral concentrate and soil lithochemical surveys

Concentrations of carbonatite indicator elements such as Ba, Mo, Nb, Ta, REE, Th, and U in stream-sediment heavy mineral concentrate (HMC) samples are up to two orders of magnitude higher relative to those in carbonatites and soil samples, and

up to 192 times higher relative to the bulk stream-sediment <0.18 mm fraction (Table 3). Recovered by panning in the field or by laboratory techniques (Lett and Rukhlov, 2017), HMC lithochemistry enhances the contrast of stream-sediment anomalies compared to the conventional, bulk <0.18 mm fraction used in the RGS drainage programs (Rukhlov et al., 2020a, b). Panned, stream-sediment HMC samples in the Blue River area (n=626), containing 1.2 to 2475 ppm Ta determined by lithium-fusion ICP-MS (Fig. 6), highlight the known carbonatites in the area, including at the Upper Fir and Verity Ta-Nb deposits (Dahrouge and Reeder, 2001; Reeder and Dahrouge, 2002; Smith and Dahrouge, 2003; Dahrouge and Wolbaum, 2004; Rukhlov and Gorham, 2007; Gorham, 2008; Gorham et al., 2009, 2011a, 2011b). In contrast, the RGS stream-sediment data in the area (n=208) show only <1 to 13 ppm Ta by INAA (Fig. 5). In addition, HMC are routinely evaluated for indicator minerals (e.g., Tyson, 2009; Mackay and Simandl, 2014; Mao et al., 2016; Simandl et al., 2017).

As follow-ups to regional stream-sediment and airborne geophysical surveys, grid soil lithochemical surveys (Fig. 7), coupled with ground (in situ) gamma-ray and magnetic surveys, effectively delineate secondary (residual) dispersion haloes of carbonatite-related critical metals (Reeder and Dahrouge, 2002; Smith and Dahrouge, 2003; Dahrouge and Wolbaum, 2004; Rukhlov and Gorham, 2007; Gorham, 2008; Gorham et al., 2009, 2011a, 2011b).

9. Conclusion

Carbonatites and related rocks have a very distinct geochemical signature, characterized by extreme concentrations of critical metals such as REE, Nb, Ta and other elements. Because most carbonatites in British Columbia form small sills and dikes, the task of detecting their signal using the

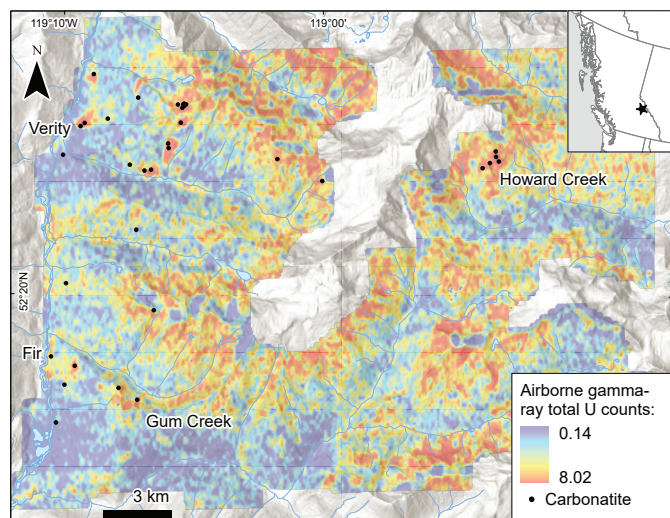


Fig. 21. Blue River area gridded airborne gamma-ray uranium response (total counts). After Gorham (2008) and Shives (2009). Grid cell size is 40 m. Carbonatite occurrences after Rukhlov and Gorham (2007), Gorham (2008), Gorham et al., 2009, 2011a, 2011b, 2013), Millonig and Groat (2013), and Rukhlov et al. (2018).

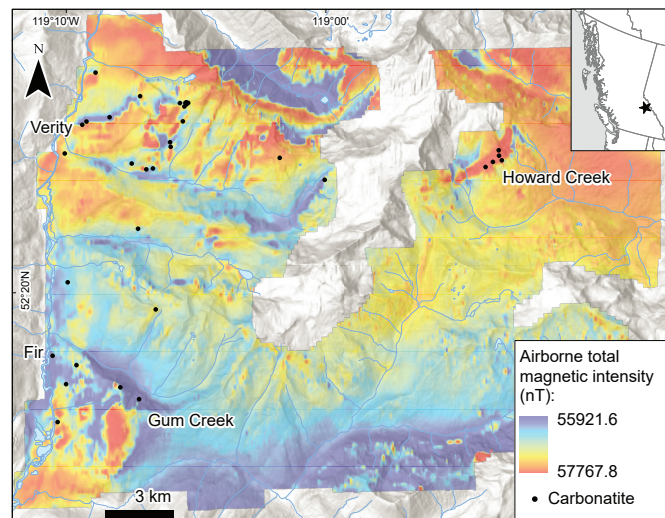


Fig. 22. Blue River area gridded airborne total magnetic intensity response (nT). After Gorham (2008) and Shives (2009). Grid cell size is 40 m. Carbonatite occurrences after Rukhlov and Gorham (2007), Gorham (2008), Gorham et al., 2009, 2011a, 2011b, 2013), Millonig and Groat (2013), and Rukhlov et al. (2018).

multi-element regional geochemical survey stream data with sample catchment areas of up to 193 km² (average 10 km²) is akin to looking for a needle in a haystack. Univariate data reflect background variations, including at known carbonatite and related-rock occurrences. In contrast, our multivariate carbonatite index identifies numerous stream basins that are prospective for carbonatite-related critical minerals. The top 50 anomalies (>93rd percentile) show maximum contrast of carbonatite indicator elements relative to the background in the study area. Estimated predicted geochemical resources suggest significant potential for REE and other carbonatite-related critical metals. We propose a refined prospectivity approach to assess the critical metals potential of underexplored regions that includes stream-sediment, panned heavy mineral concentrate lithochemical and indicator mineral surveys, coupled with high-resolution airborne radiometrics and magnetics, followed up by soil lithochemical and in situ (ground) radiometric and magnetic surveys.

Acknowledgments

We thank Purple Rock Inc. for capturing digital data from the provincial ARIS and Kaitlyn McLaren (British Columbia Geological Survey) for GIS support and data management. We also thank Christopher H. Gammons (Montana Tech of The University of Montana), Kathryn E. Watts (United States Geological Survey), and Lawrence B. Aspler (British Columbia Geological Survey) for thorough reviews and comments.

References cited

- Bond, G.C., and Kominz, M.A., 1984. Construction of tectonic subsidence curves for the early Paleozoic miogeocline, Southern Canadian Rocky Mountains: Implications for subsidence mechanisms, age of breakup and crustal thinning: *Geological Society of America Bulletin*, 95, 155-173.
- Burgess, S.D., Heaman, L.M., and Bowring, S.A., 2023. High-precision ID-TIMS U-Pb geochronology of perovskite (CaTiO₃) from the Ice River Complex, Southeastern British Columbia. *Chemical Geology*, 616, article 121187. <<https://doi.org/10.1016/j.chemgeo.2022.121187>>
- Brown, J.A., 2013. Waterloo Resources Ltd. 2012 field activities at the Ice River property, Waterloo Prospect area. British Columbia Ministry of Energy, Mines and Natural Gas, British Columbia Geological Survey, Assessment Report 33565, 39 p.
- Brummer, J.J., Gleeson, C.F., and Hansuld, J.A., 1987. A historical perspective of exploration geochemistry in Canada. *Journal of Geochemical Exploration*, 28, 1-39.
- Campbell, N.A., 1980. Robust procedures in multivariate analysis. I: Robust covariance estimation. *Journal of the Royal Statistical Society, Series C: Applied Statistics*, 29, 231-237.
- Campbell, R.B., 1968. Geology, Canoe River, British Columbia. Geological Survey of Canada, Preliminary Map 15-1967, 1:253,400 scale.
- Chakhmouradian, A.R., Reguir, E.P., Kressall, R.D., Crozier, J., Pisiak, L.K., Sidhu, R., and Yang, P., 2015. Carbonatite-hosted niobium deposit at Aley, northern British Columbia (Canada): Mineralogy, geochemistry and petrogenesis. *Ore Geology Reviews*, 64, 642-666.
- Chudy, T.C., 2013. The petrogenesis of the Ta-bearing Fir carbonatite system, east-central British Columbia, Canada. Unpublished Ph.D. thesis, University of British Columbia, Canada, 316 p.
- Çimen, O., Kuebler, C., Simonetti, S.S., Corcoran, L., Mitchell, R.H., and Simonetti, A., 2019. Combined boron, radiogenic (Nd, Pb, Sr), stable (C, O) isotopic and geochemical investigations of carbonatites from the Blue River Region, British Columbia (Canada): Implications for mantle sources and recycling of crustal carbon. *Chemical Geology*, 529, article 119240. <<https://doi.org/10.1016/j.chemgeo.2019.07.015>>
- Colpron, M., 2020. Yukon terranes - A digital atlas of terranes for the northern Cordillera. Yukon Geological Survey. <<https://data.geology.gov.yk.ca/Compilation/2#InfoTab>>
- Colpron, M., Logan, J., and Mortensen, J.K., 2002. U-Pb age constraint for late Neoproterozoic rifting and initiation of the lower Paleozoic passive margin of western Laurentia. *Canadian Journal of Earth Sciences*, 39, 133-143.
- Cui, Y., Eckstrand, H., and Lett, R.E., 2009. Regional geochemical survey: delineation of catchment basins for sample sites in British Columbia. In: *Geological Fieldwork 2008*, Ministry of Energy, Mines and Petroleum Resources, British Columbia Geological Survey Paper 2009-01, pp. 231-238.
- Cui, Y., Miller, D., Schiarizza, P., and Diakow, L.J., 2017. British Columbia digital geology. British Columbia Ministry of Energy, Mines and Petroleum Resources, British Columbia Geological Survey Open File 2017-8, 9p. Data version 2021-12-19.
- Currie, K.L. 1975. The geology and petrology of the Ice River Alkaline Complex, British Columbia. Geological Survey of Canada, Bulletin 245, 68 p.
- Currie, K.L., 1976. The alkaline rocks of Canada. Geological Survey of Canada, Bulletin 239, 228 p.
- Dahrouge, J. and Reeder, J., 2001. Commerce Resources Corp. 2001 geologic mapping, sampling and geophysical surveys on the Mara property, north of Blue River, British Columbia. British Columbia Ministry of Energy and Mines, British Columbia Geological Survey, Assessment Report 26733, 19 p.
- Dahrouge, J. and Wolbaum, R., 2004. Commerce Resources Corp. 2003 exploration at the Blue River property, north of Blue River, British Columbia. British Columbia Ministry of Energy and Mines, British Columbia Geological Survey, Assessment Report 27412, 16 p.
- Dalsin, M.L., Groat, L.A., Creighton, S., and Evans, R.J., 2015. The mineralogy and geochemistry of the Wicheeda Carbonatite Complex, British Columbia, Canada. *Ore Geology Reviews*, 64, 523-542.
- Dawson, G.M. 1886. Geological and Natural History Survey of Canada, Annual Report 1, 122B-124B.
- Digel, S.G., Ghent, E.D., Carr, S.D., and Simony, P.S., 1998. Early Cretaceous kyanite-sillimanite metamorphism and Paleocene sillimanite overprint near Mount Cheadle, southeastern British Columbia: geometry, geochronology, and metamorphic implications. *Canadian Journal of Earth Sciences*, 35, 1070-1087.
- Flury, B., 1997. A first course in multivariate statistics. New York, Springer-Verlag, 715 p.
- Gabrielse, H., Monger, J.W.H., Wheeler, J.O., and Yorath, C.J., 1991. Morphogeological belts, tectonic assemblages, and terranes. In: Gabrielse, H. and Yorath, C.J., (Eds.), *Geology of the Cordilleran Orogen in Canada*. Geological Survey of Canada, *Geology of Canada*, vol. 4, pp. 15-59 (also *Geological Society of America, The Geology of North America*, v. G-2).
- Gorham, J., 2008. Commerce Resources Corp. 2007 diamond drilling and exploration at the Blue River Property, north of Blue River, British Columbia. British Columbia Ministry of Energy, Mines and Natural Gas, British Columbia Geological Survey, Assessment Report 30011, 48 p.
- Gorham, J., Ulry, B., and Brown, J., 2009. Commerce Resources Corp. 2008 diamond drilling and exploration at the Blue River property, north of Blue River, British Columbia. British Columbia Ministry of Energy, Mines and Petroleum Resources, British Columbia Geological Survey, Assessment Report 31174, 149 p.

- Gorham, J., Ulry, B., and Brown, J., 2011a. Commerce Resources Corp. 2010 diamond drilling and exploration at the Blue River Property, north of Blue River, British Columbia. British Columbia Ministry of Energy and Mines, British Columbia Geological Survey, Assessment Report 32424, 55 p.
- Gorham, J., Ulry, B., Brown, J., and Carter, M., 2011b. Commerce Resources Corp. 2009 diamond drilling and exploration at the Blue River property, north of Blue River, British Columbia. British Columbia Ministry of Energy and Mines, British Columbia Geological Survey, Assessment Report 31948, 62 p.
- Gorham, J., Ulry, B., and Brown, J., 2013. Commerce Resources Corp. 2012 exploration at the Blue River Property, north of Blue River, British Columbia. British Columbia Ministry of Energy, Mines and Natural Gas, British Columbia Geological Survey, Assessment Report 33906, 37 p.
- Han, T. and Rukhlov, A.S., 2017. Regional Geochemical Survey (RGS) data update and release using the newly developed RGS database. British Columbia Ministry of Energy, Mines and Petroleum Resources, British Columbia Geological Survey GeoFile 2017-11, 7 p.
- Han, T. and Rukhlov, A.S. 2020a. Update of rock geochemical database at the British Columbia Geological Survey. British Columbia Ministry of Energy, Mines and Petroleum Resources, British Columbia Geological Survey GeoFile 2020-02, 4 p.
- Han, T. and Rukhlov, A.S. 2020b. Update of the provincial Regional Geochemical Survey (RGS) database at the British Columbia Geological Survey. British Columbia Ministry of Energy, Mines and Petroleum Resources, British Columbia Geological Survey GeoFile 2020-08, 3 p.
- Han, T., Rukhlov, A.S., Naziri, M., and Moy, A., 2016. New British Columbia litho-geochemical database: Development and preliminary data release. British Columbia Ministry of Energy and Mines, British Columbia Geological Survey GeoFile 2016-4, 6 p.
- Hickin, A.S., Ootes, L., Brzozowski, M.J., Northcote, B., Rukhlov, A.S., Bain, W.M., and Orován, E.A., 2024. Critical minerals and mineral systems in British Columbia. In: Geological Fieldwork 2023, Ministry of Energy, Mines and Low Carbon Innovation, British Columbia Geological Survey Paper 2024-01, pp. 13-51.
- Höy, T., 1988. Geology of the Cottonbelt lead-zinc-magnetite layer, carbonatites and alkaline rocks in the Mount Grace area, Frenchman Cap dome, southeastern British Columbia. British Columbia Ministry of Energy, Mines and Petroleum Resources, British Columbia Geological Survey, Bulletin 80, 99 p.
- Jones, S., Merriam, K., Yelland, G., Rotzinger, R., and Simpson, R.G., 2017. Technical report on mineral reserves at the Aley project, British Columbia, Canada. NI 43-101 Technical Report, 293 p.
<<https://www.sedarplus.ca/csa-party/records/document.html?id=505ac95c2aec63a87de95b61ab789d033eb8a64a937cf34a97506960da658bbb>>
- Kraft, J.L., 2011. Structural geology of the Upper Fir carbonatite deposit, Blue River, British Columbia: Report and addendum for Dahrouge Geological Consulting Ltd. and Commerce Resources Corp. In: Gorham, J., Ulry, B., and Brown, J. (compilers), Commerce Resources Corp. 2010 Diamond Drilling and Exploration at the Blue River Property, British Columbia Ministry of Energy, Mines and Lands, British Columbia Geological Survey, Assessment Report 32424, pp. 3225-3258.
- Kulla, G., and Hardy, J., 2015. Commerce Resources Corp. Blue River tantalum–niobium project, British Columbia, Canada, project update report. NI 43-101 Technical Report, 138 p.
<<https://www.sedarplus.ca/csa-party/records/document.html?id=7f946b8c242fc385f6d2b9dcee4b25648a80c7bb0fb1f6b09dc8d9105a8f213>>
- Lett, R., and Rukhlov, A.S., 2017. A review of analytical methods for regional geochemical survey (RGS) programs in the Canadian Cordillera. In: Ferbey, T., Plouffe, A., and Hickin, A.S., (Eds.), Indicator Minerals in Till and Stream Sediments of the Canadian Cordillera. Geological Association of Canada Special Paper Volume 50, and Mineralogical Association of Canada Topics in Mineral Sciences Volume 47, pp. 53-108.
- Li, Z.-X., Bogdanova, S.V., Collins, A.S., Davidson, A., De Waele, B., Ernst, R.E., Fitzsimons, I.C.W., Fuck, R.A., Gladkochub, D.P., Jacobs, J., Karlstrom, K.E., Lu, S., Natapov, L.M., Pease, V., Pisarevsky, S.A., Thrane, K., and Vernikovsky, V., 2008. Assembly, configuration, and break-up history of Rodinia: A synthesis. *Precambrian Research*, 160, pp. 179-210.
- Locock, A.J., 1994. Aspects of the geochemistry and mineralogy of the Ice River alkaline intrusive complex, Yoho National Park, British Columbia. Unpublished M.Sc. thesis, University of Alberta, Canada, 163 p.
- Mackay, D.A.R., and Simandl, G.J., 2014. Portable X-ray fluorescence to optimize stream sediment chemistry and indicator mineral surveys, case 1: Carbonatite-hosted Nb deposits, Aley carbonatite, British Columbia, Canada. In: Geological Fieldwork 2013, British Columbia Ministry of Energy and Mines, British Columbia Geological Survey Paper 2014-1, pp. 183-194.
- Mao, M., Rukhlov, A.S., Rowins, S.M., Spence, J., and Coogan, L.A., 2016. Apatite trace element compositions: A robust new tool for mineral exploration. *Economic Geology*, 111, 1187-1222.
- Mäder, U.K., 1987. The Aley carbonatite complex, northern Rocky Mountains, British Columbia (94B/5). In: Geological Fieldwork 1986, British Columbia Ministry of Energy, Mines and Petroleum Resources, British Columbia Geological Survey Paper 1987-1, pp. 283-288.
- McDonough, M.R. and Murphy, D.C., 1990. Geology, Valemount (830/14) map area, British Columbia. Geological Survey of Canada, Open File 2259, 1:50,000 scale.
- McDonough, M.R., Morrison, M.L., Currie, L.D., Walker, R.T., Pell, J., and Murphy, D.C., 1991a. Canoe Mountain, British Columbia; Geological Survey of Canada, Open File 2511, 1:50,000 scale.
- McDonough, M.R., Simony, P.S., Morrison, M.L., Oke, C., Sevigny, J.H., Robbins, D.B., Seigel, S.G., and Grasby, S.E., 1991b. Howard Creek, British Columbia; Geological Survey of Canada, Open File 2411, 1:50,000 scale.
- McDonough, M.R., Simony, P.S., Sevigny, J.H., Robbins, D.B., Raeside, R., Doucet, P., Pell, J., and Dechesne, R.G., 1992. Geology of Nagle Creek and Blue River, British Columbia (83d/2 and 83d/3). Geological Survey of Canada, Open File 2512, 1:50,000 scale.
- McLeish, D.F., 2013. Structure, stratigraphy, and U-Pb zircon-titanite geochronology of the Aley carbonatite complex, Northeast British Columbia: Evidence for Antler-aged orogenesis in the foreland belt of the Canadian Cordillera. Unpublished M.Sc. thesis, University of Victoria, 131 p.
- McLeish, D.F. and Johnston, S.T., 2019. The Upper Devonian Aley carbonatite, NE British Columbia: a product of Antler orogenesis in the western Foreland Belt of the Canadian Cordillera. *Journal of the Geological Society of London*, 176, 620-628.
- McLeish, D., Johnston, S., Friedman, R., and Mortensen, J., 2020. Stratigraphy and U-Pb zircon-titanite geochronology of the Aley carbonatite complex, northeastern British Columbia: evidence for Antler-aged orogenesis in the Foreland belt of the Canadian Cordillera. *Geoscience Canada*, 47, 171-186.
- Millonig, L.J., Gerdes, A., and Groat, L.A., 2012. U-Th-Pb geochronology of meta-carbonatites and meta-alkaline rocks in the southern Canadian Cordillera: a geodynamic perspective. *Lithos*, 152, 202-217.
- Millonig, L.J., and Groat, L.A., 2013. Carbonatites in western North America—occurrences and metallogeny. In: Colpron, M., Bissig, T., Rusk, B.G., and Thompson, F.H., (Eds.), *Tectonics, Metallogeny, and Discovery: The North American Cordillera and Similar Accretionary Settings*. Society of Economic Geologists, Special Publication 17, pp. 245-264.

- Millonig, L.J., Gerdes, A., and Groat, L.A., 2013. The effect of amphibolite facies metamorphism on the U-Th-Pb geochronology of accessory minerals from meta-carbonatites and associated meta-alkaline rocks. *Chemical Geology*, 353, 199-209.
- Mitchell, R., Chudy, T., McFarlane, C.R.M., and Wu, F.-Y., 2017. Trace element and isotopic composition of apatite in carbonatites from the Blue River area (British Columbia, Canada) and mineralogy of associated silicate rocks. *Lithos*, 286-287, 75-91.
- Mumford, T., 2009. Dykes of the Moose Creek Valley, Ice River alkaline complex, southeastern BC. Unpublished M.Sc. thesis, The University of New Brunswick, Canada, 230 p.
- Murphy, D.C., compiler, 2007. Geology, Canoe River, British Columbia-Alberta. Geological Survey of Canada, Map 2110A, 1:250,000 scale.
- Nelson, J.L., Colpron, M., and Israel, S., 2013. The Cordillera of British Columbia, Yukon and Alaska: tectonics and metallogeny. In: Colpron, M., Bissig, T., Rusk, B.G., and Thompson, F.H., (Eds.), *Tectonics, Metallogeny, and Discovery: The North American Cordillera and Similar Accretionary Settings*. Society of Economic Geologists, Inc. Special Publication 17, pp. 53-109.
- Parrish, R.R. and Scammell, R.J., 1988. The age of the Mount Copeland syenite gneiss and its metamorphic zircons, Monashee complex, southeastern British Columbia. In: *Radiogenic Age and Isotopic Studies: Report 2*, Geological Survey of Canada, Paper 88-2, pp. 21-28.
- Pell, J., 1994. Carbonatites, nepheline syenites, kimberlites and related rocks in B.C. British Columbia Ministry of Energy, Mines and Petroleum Resources, British Columbia Geological Survey, Bulletin 88, 136 p.
- Pell, J. and Höy, T., 1989. Carbonatites in a continental margin environment-the Canadian Cordillera. In: Bell, K. (Ed.), *Carbonatites: Genesis and Evolution*. Unwin Hyman, London, United Kingdom, pp. 200-220.
- Pell, J. and Simony, P.S., 1987. New correlations of Hadrynian strata, south-central British Columbia. *Canadian Journal of Earth Sciences*, 24, 302-313.
- Peterson, T.D., and Currie, K.L. 1994. The Ice River Complex, British Columbia. In: *Current Research, Part A*. Geological Survey of Canada, Paper 1994-A, pp. 185-192.
- Pride, K.R., 1983. Geological Survey on the Aley Claims. British Columbia Ministry of Energy, Mines, and Petroleum Resources, Assessment Report 12018, 16 p.
- Raeseide, R.P. and Simony, P.S., 1983. Stratigraphy and deformational history of the Scrip Nappe, Monashee Mountains, British Columbia. *Canadian Journal of Earth Sciences*, 20, 639-650.
- Reeder, J. and Dahrouge, J., 2002. Commerce Resources Corp. 2001 geologic mapping, sampling, and geophysical surveys on the Fir property, north of Blue River, British Columbia. British Columbia Ministry of Energy and Mines, British Columbia Geological Survey, Assessment Report 26781, 13 p.
- Ross, G.M., 1991. Tectonic setting of the Windermere Supergroup revisited. *Geology*, 19, 1125-1128.
- Rudnick, R.L., and Gao, S., 2005. Composition of the continental crust. In: Heinrich, D.H., Rudnick, R.L., and Turekian, K.K., (Eds.), *The Crust, Treatise on Geochemistry, Volume 3*, Elsevier, Amsterdam, pp. 1-64.
- Rukhlov, A.S. and Bell, K., 2010. Geochronology of carbonatites from the Canadian and Baltic Shields, and the Canadian Cordillera: clues to mantle evolution. *Mineralogy and Petrology*, 98, 11-54.
- Rukhlov, A.S., and Gorham, J., 2007. Commerce Resources Corp. 2006 diamond drilling and exploration at the Blue River Property, north of Blue River, British Columbia. British Columbia Ministry of Energy, Mines and Petroleum Resources, British Columbia Geological Survey, Assessment Report 29024, 41 p.
- Rukhlov, A.S., Chudy, T.C., Arnold, H., and Miller, D., 2018. Field trip guidebook to the Upper Fir carbonatite-hosted Ta-Nb deposit, Blue River area, east-central British Columbia. British Columbia Ministry of Energy, Mines and Petroleum Resources, Geological Survey GeoFile 2018-6, 67 p.
- Rukhlov, A.S., Fortin, G., Kaplenkov, G.N., Lett, R.E., Lai, V. W.-M., and Weis, D., 2020a. Multi-media geochemical and Pb isotopic evaluation of modern drainages on Vancouver Island. In: *Geological Fieldwork 2019*, British Columbia Ministry of Energy, Mines and Petroleum Resources, British Columbia Geological Survey Paper 2020-01, pp. 133-167.
- Rukhlov, A.S., Fortin, G., Kaplenkov, G.N., Lett, R.E., Lai, V. W.-M., and Weis, D., 2020b. Catching the tail of a golden dragon plus 60 elements in British Columbia. British Columbia Ministry of Energy, Mines and Petroleum Resources, British Columbia Geological Survey GeoFile 2020-04 (poster).
- Scammell, R.J., 1987. Stratigraphy, structure and metamorphism of the north flank of the Monashee complex, southeastern British Columbia: a record of Proterozoic extension and Phanerozoic crustal thickening. Unpublished M.Sc. thesis, Carleton University, Ottawa, Canada, 205 p.
- Scammell, R.J., 1993. Mid-Cretaceous to Tertiary thermotectonic history of former mid-crustal rocks, southern Omineca belt, Canadian Cordillera. Unpublished Ph.D. thesis, Queens University, Kingston, Ontario, 576 p.
- Scammell, R.J. and Brown, R.L., 1990. Cover gneisses of the Monashee terrane: a record of synsedimentary rifting in the North American Cordillera. *Canadian Journal of Earth Sciences*, 27, 712-726.
- Shives, R.B.K., 2009. 2007 Helicopter borne magnetic gradiometer and gamma ray spectrometer survey, Blue River Area, British Columbia, Canada. In: Gorham, J., Ulry, B., and Brown, J., (compilers), Commerce Resources Corp. 2008 diamond drilling and exploration at the Blue River property, north of Blue River, British Columbia. Appendix 17. British Columbia Ministry of Energy, Mines and Petroleum Resources, British Columbia Geological Survey, Assessment Report 31174D, pp. 19-142.
- Simandl, G.J. and Paradis, S., 2018. Carbonatites: related ore deposits, resources, footprint, and exploration methods. *Applied Earth Science (Transactions of the Institutions of Mining and Metallurgy)*, 127, 123-152.
- Simandl, G.J., Mackay, D.A.R., Ma, X., Luck, P., Gravel, J., and Akam, C., 2017. The direct indicator mineral concept and QEMSCAN® applied to exploration for carbonatite and carbonatite-related ore deposits. In: Ferbey, T., Plouffe, A. and Hickin, A.S., (Eds.), *Indicator Minerals in Till and Stream Sediments of the Canadian Cordillera*. Geological Association of Canada Special Paper Volume 50 and Mineralogical Association of Canada Topics in Mineral Sciences Volume 47, pp. 175-190.
- Simandl, G.J., Reid, H.M., and Ferri, F., 2013. Geological setting of the Lonnie niobium deposit, British Columbia, Canada. In: *Geological Fieldwork 2012*, British Columbia Ministry of Energy, Mines and Natural Gas, British Columbia Geological Survey Paper 2013-1, pp. 127-138.
- Simony, P.S., Ghent, E.D., Craw, D., and Mitchell, W., 1980. Structural and metamorphic evolution of the northeast flank of the Shuswap complex, southern Canoe River area, British Columbia. In: Crittenden, M.D., Coney, P.J., and Davis, G.H. (Eds.), *Cordilleran Metamorphic Core Complexes*. Geological Society of America Memoir 153, pp. 445-461.
- Smith, M. and Dahrouge, J., 2003. Commerce Resources Corp. 2002 diamond drilling and exploration on the Blue River property, north of Blue River, British Columbia. British Columbia Ministry of Energy and Mines, British Columbia Geological Survey, Assessment Report 27131, 31 p.
- Trofanenko, J., 2014. The nature and origin of the REE mineralization in the Wicheeda Carbonatite, British Columbia, Canada. Unpublished M.Sc. thesis, McGill University, Canada, 173 p.

- Trofanenko, J., Williams-Jones, A.E., Simandl, G.J., and Migdisov, A.A., 2016. The nature and origin of the REE mineralization in the Wicheeda carbonatite, British Columbia, Canada. *Economic Geology*, 111, 199-223.
- Tyson, R., 2009. Mineralogy of the 2008 stream sediment survey. In: Gorham, J., Ulry, B., and Brown, J., (compilers), Commerce Resources Corp. 2008 diamond drilling and exploration at the Blue River property, north of Blue River, British Columbia. Appendix 19. British Columbia Ministry of Energy, Mines and Petroleum Resources, British Columbia Geological Survey, Assessment Report 31174D, pp. 172-257.
- White, G.P.E., 1982. Notes on carbonatites in central British Columbia. In: *Geological Fieldwork 1981*. British Columbia Ministry of Energy, Mines and Petroleum Resources, British Columbia Geological Survey, Paper 1982-1, pp. 68-69.
- Ya'acoby, A., 2014. The petrology and petrogenesis of the Ren carbonatite sill and fenites, southeastern British Columbia, Canada. Unpublished M.Sc. thesis, The University of British Columbia, Canada, 463 p.

British Columbia Geological Survey rock geochemical and geochronological data products: Examples of utility



Luke Ootes^{1, a}, Alexei S. Rukhlov¹, and Tian Han¹

¹ British Columbia Geological Survey, Ministry of Energy, Mines and Low Carbon Innovation, Victoria, BC, V8W 9N3

^a corresponding author: Luke.Ootes@gov.bc.ca

Recommended citation: Ootes, L., Rukhlov, A.S., and Han, T., 2024. British Columbia Geological Survey rock geochemical and geochronological data products: Examples of utility. In: *Geological Fieldwork 2023*, British Columbia Ministry of Energy, Mines and Low Carbon Innovation, British Columbia Geological Survey Paper 2024-01, pp. 123-129.

Abstract

The British Columbia Geological Survey compiles, manages, and releases geochronology and geochemistry data updates. More than 8000 geochronological results from British Columbia are available from a data release in 2004 and an update in 2020, and this paper highlights one of the ways these datasets can be used to highlight episodes in the evolution of the Cordilleran orogen. Rock geochemical results are available from >12,000 samples across British Columbia and this paper also illustrates how these data can be used. Most of the data from Triassic to Early Jurassic intrusions overlap the field of rock compositions (Sr/Y vs. Sr/MnO) that are prospective for porphyry Cu, skarn, or epithermal mineralization. A plot of Cu concentrations from ~10,000 samples highlights elevated concentrations in western and eastern Stikine terrane and Quesnel terrane, areas with known porphyry Cu-Mo-Au deposits.

Keywords: BCGS data products, geochronology, geochemistry, data utility

1. Introduction

High-quality geochemical and geochronological data are fundamental to characterizing and understanding the geology and metallogeny of any region. In part because of continuous advances in analytical capabilities, the volume of rock geochemical and geochronological data has increased dramatically in recent years. The British Columbia Geological Survey (BCGS) provides systematic and consistent management of these data, which have been derived from province-wide collections. Current data compilations include previously published publicly available data and new data generated by ongoing projects (e.g., Han et al., 2019, 2020; Van der Vlugt et al., 2022; van Straaten et al., 2022). Data management includes compilation, metadata retrieval and verification, standardization and quality control, data query and extraction, and generation and release of data products. This paper highlights some general applications of the rock geochemical and geochronological data products from the British Columbia Geological Survey, showing a few of many potential applications of the data.

2. Rock geochemical and geochronological data products

The data products that the BCGS releases to the public are generated using data models (Figs. 1, 2) that define the structure of the database, specifying how data are organized and defined. Invisible in the data products, the models are the basis for capturing metadata using in-house dictionary guides; they work in the background to produce the simplified data products that the Survey releases (e.g., Han et al., 2020; Fig. 3). The geochemical and geochronological data products

have a common sample code attribute that can be used to link both datasets and can be spatially enabled in GIS software and as a relational database where complex queries can be performed. The metadata structure has been designed to align with the international open data standards for geochemical data (van Straaten et al., 2022) and are identical to those in the BC Digital Geology (Cui et al., 2017). The most recent dataset of geochemical data (Han and Rukhlov, 2024) is populated with ~500,000 analytical values and metadata from 12,413 samples that were collected between 1973 and 2023. Han et al. (2020) updated Breitsprecher and Mortensen (2004) and the geochronological dataset now contains age determinations from 8292 samples that were collected between 1960 and 2020.

3. Application of the geochronological dataset

Geochronology refers to the age of rocks and minerals using the decay of radiogenic isotopes to measure time. Different mineral and isotope systematics have different temperatures at which the decay from parent to daughter isotopes becomes a closed system, or when the 'geological time clock' starts ticking. Because these 'closure' temperatures range from >900°C to <100°C, an array of isotopic systems is available to track episodes in the history of a rock. For example: 1) U-Pb zircon, monazite, and titanite can establish the crystallization age of igneous rocks, the provenance and age estimate of sedimentary rocks, and cooling age of high-grade metamorphic rocks; 2) Ar-Ar sanidine, hornblende, muscovite, and biotite geochronology can provide crystallization ages of fresh volcanic rocks, or mid-temperature (300 to 600°C) cooling ages of metamorphic or altered rocks; and 3) fission track or U-Th/He zircon and

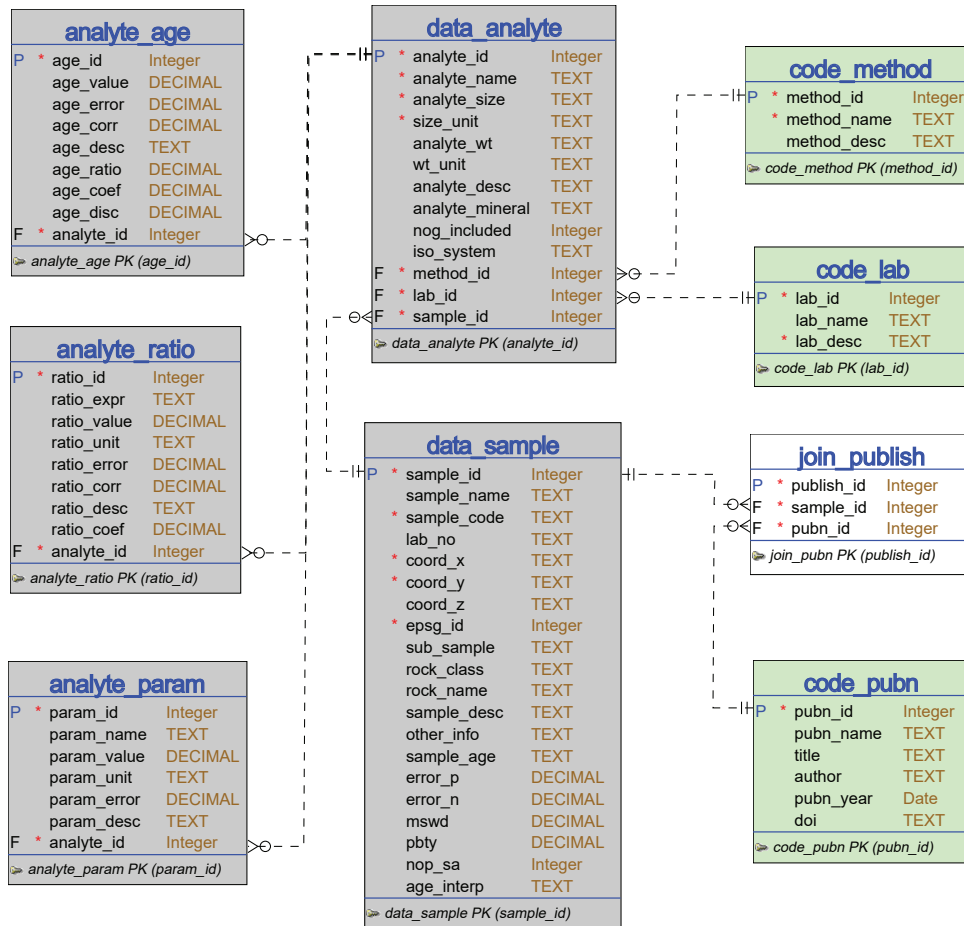


Fig. 1. Logical data model for the geochronological database. This data model is guided by an in-house data dictionary and used to produce simplified data products for release to the public (e.g., Han et al., 2020).

apatite data provide low-temperature results (<150°C), which can inform the time and pace of unroofing episodes.

The map of geochronological ages from across British Columbia (Fig. 3) was derived from 7759 age determinations from Breitsprecher and Mortensen (2004), which included results from a wide variety of isotopic systematics, including largely outdated methods (e.g., K/Ar), and 533 new results from data that were published between 2004 and 2020 (Han et al., 2020) and includes U-Pb, Ar-Ar, and Re-Os isotopic results. The age distribution of U-Pb and Ar-Ar results are plotted as Kernel density estimations (KDE; Figs. 4, 5; Vermeesch, 2018). Because U-Pb results are high-temperature (>600°C), these data record igneous crystallization or metamorphic resetting ages. The data show a background of continuous U-Pb results since ca. 400 Ma that is punctuated by peaks close to the Devonian-Carboniferous boundary, two peaks during the Jurassic, a subordinate Late Cretaceous peak (Fig. 4a), and a significant Paleocene to Eocene peak, specifically between the Thanetian to Lutetian (60-50 Ma; Figs. 4a, b). The Re-Os data mark the timing of molybdenite mineralization, typically from porphyry deposits, which formed in the Late Triassic to Early Jurassic, Early Cretaceous, and Eocene (Fig. 4a). The Ar-Ar data also show subordinate Late Jurassic and Late Cretaceous

peaks, with the most significant between the Thanetian to Lutetian (Figs. 4c, d). The ‘other’ data show a similar pattern to the Ar-Ar data, with an additional peak in the Late Miocene to Pleistocene (Figs. 4e, f). Part of Cordilleran orogen of British Columbia is underlain by terranes with Late Triassic volcanic successions that are predominantly mafic (Quesnellia, Stikinia, Wrangellia). These terranes are not well-represented in the data set, in general because not many of these rocks contain zircon for U-Pb dating, and the rocks may have undergone post-emplacement metamorphism so that lower temperature techniques (Ar-Ar, fission track) record more recent overprints (Fig. 4). All of the data (Fig. 4) highlight a Paleocene to Eocene (Thanetian to Lutetian; 60-50 Ma) thermo-magmatic episode across the province, representing a significant tectonic event that affected the entire Cordilleran orogen.

Comparing the pre-2004 and the post-2004 U-Pb data (Fig. 5) highlights shifting research focus. The first observation is that there are no Precambrian dates for rocks in the post-2004 data compilation. Precambrian basement occurs within some of the metamorphic core complexes, and the Purcell Supergroup (Mesoproterozoic) is a sedimentary succession with predominantly mafic igneous rocks. This lack of new Precambrian results in the post-2004 compilation indicates

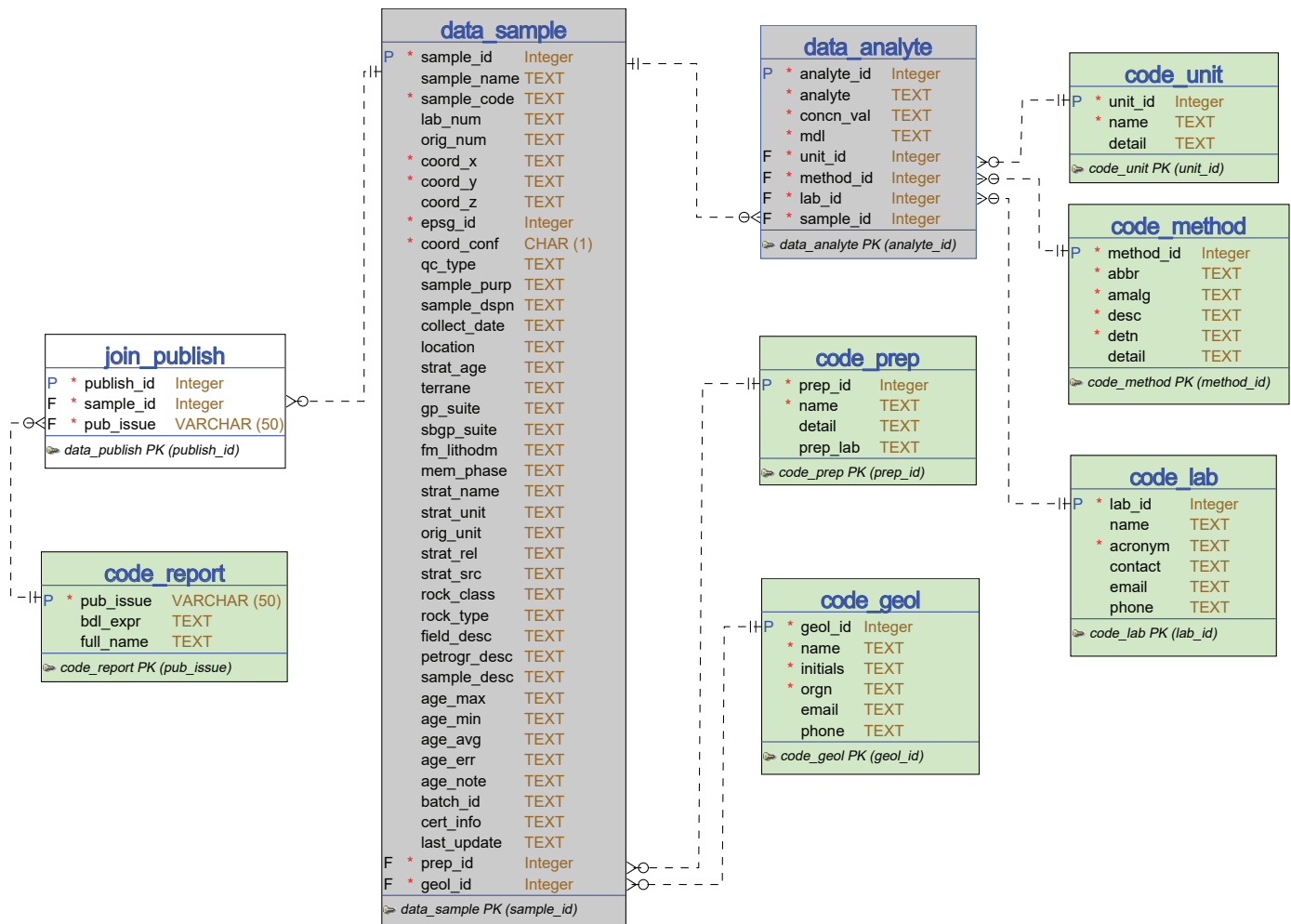


Fig. 2. Logical data model for the rock geochemical database. This data model is guided by an in-house data dictionary and used to produce simplified data products for release to the public (e.g., Van der Vlugt et al., 2022).

a shift away from research on these types of rocks and these geographic areas within British Columbia. The second is that the abundance of U-Pb results has shifted from predominantly Late Cretaceous-Paleocene/Eocene results toward Late Triassic-Early Jurassic. We speculate that this change may reflect a shift of research focus towards mineralized and barren plutons in porphyry environments (Quesnellia and Stikinia) in the last 20 years. This shift may also relate to advances in mineral separation and analytical techniques. For example, during the early to mid-2000s, laser ablation inductively coupled plasma mass spectrometry (LA-ICP-MS) became a mainstream geochronological tool, and this method is less expensive (both in cost and labour) than dating rocks by isotope dilution thermal ionization mass spectrometry (ID-TIMS).

4. Application of the rock geochemical dataset

British Columbia Geological Survey collects and maintains provincial lithochemical data from rocks, modern drainages, glacial sediments, and coal ash (Han et al., 2019). Modern whole-rock analysis determines up to 60 elements using partial (hot acid mixtures) or total (fusion at 1000°C)

digestions and a combination of high-precision inductively coupled plasma atomic emission spectroscopy (ICP-AES) and inductively coupled plasma mass spectrometry (ICP-MS). Non-destructive techniques such as instrumental neutron activation analysis (INAA) and X-ray fluorescence, and other methods (e.g., determination of Fe^{2+} concentration by digesting a sample in a hot, concentrated $\text{HF-H}_2\text{SO}_4$ mixture, followed by KMnO_4 titration of the H_3BO_3 -neutralized solution; determination of F concentration using a Na_2CO_3 - KNO_3 flux, followed by H_2O leaching of the fused sample and measuring fluoride ion concentration in the supernatant solution by ion selective electrode) extend the range of analytes and limits of detection. These determinations establish metal contents in altered and mineralized samples, whereas data on fresh igneous rocks help better understand the magmatic and geochemical evolution of the province and evaluate its large mineral endowment.

Data from fresh plutonic rocks that range from Mesoproterozoic to Neogene ($n=943$) overlap fields of barren, mixed-signal, and prospective rocks on a Sr/Y vs. Sr/MnO prospectivity diagram (Fig. 6; Ahmed et al., 2019). Data from the Cretaceous intrusions define the largest range of Sr/Y ratios,

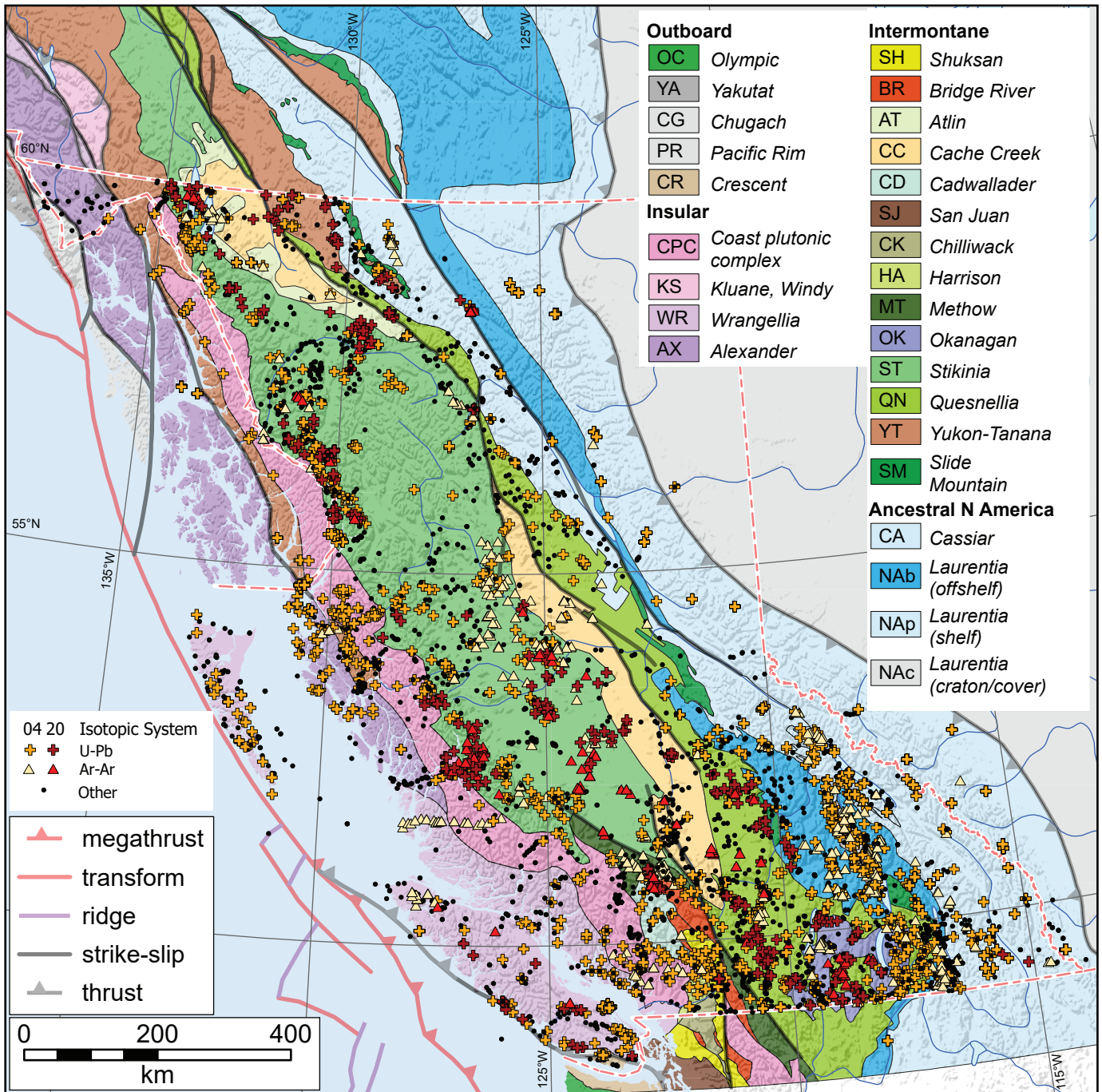


Fig. 3. Distribution of the geochronological samples in Han et al. (2020); '04' refers to 2004 compilation, '20' refers to 2020 compilation. Terranes modified from Colpron (2020).

and most of the data from Paleozoic and Jurassic plutons fall within the fields of barren and mixed-signal rocks. In contrast, most of data from the Triassic to Early Jurassic intrusions overlap the field of rock compositions that are prospective for porphyry Cu, skarn or epithermal mineralization. Elevated Cu

concentrations (Fig. 7) highlight both the western and eastern flanks of Stikine terrane and the porphyry Cu-Mo-Au camps along the Quesnel terrane, as well as accreted crust of southern British Columbia.

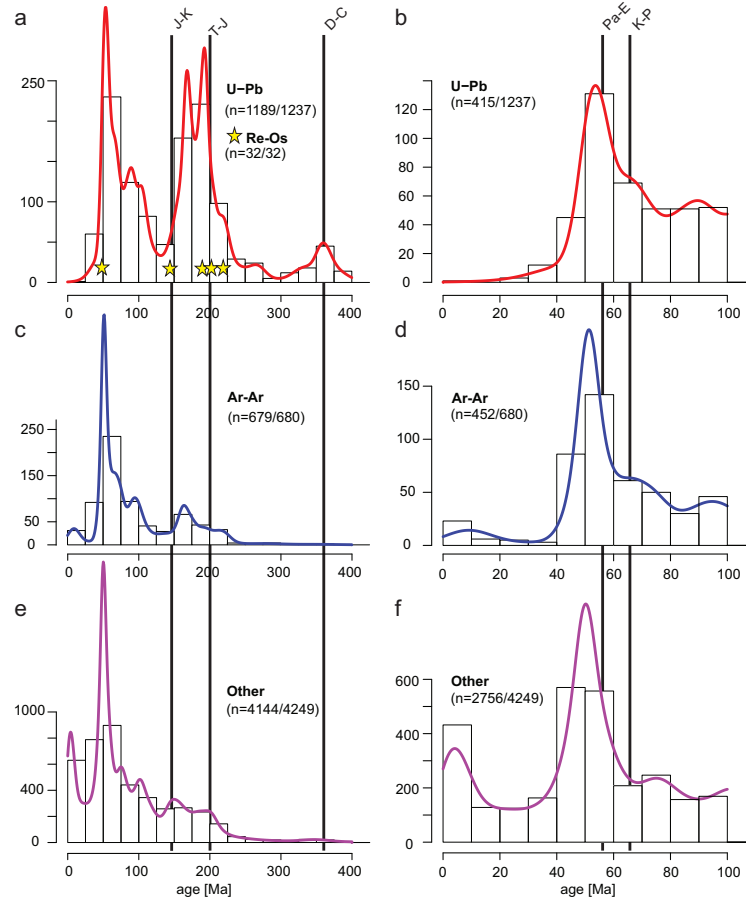


Fig. 4. Kernel density estimation (KDE; Vermeesch, 2018) plots of **a)** U-Pb and Re-Os results, **b)** U-Pb results, **c-d)** Ar-Ar results, and **e-f)** ‘other’ results. ‘Other’ refers to all isotope systematics that are not U-Pb or Ar-Ar results. Results within the data products that are listed as ‘Detrital’ are not plotted. Histogram bin widths are 25 Ma in a, c, e and 10 Ma in b, d, f. n=number used in plot/number available in dataset. Vertical black lines are stratigraphic time boundaries (Cohen et al., 2013): D-C=Devonian–Carboniferous; T-J=Jurassic–Triassic; J-K=Jurassic–Cretaceous; K-P=Cretaceous–Paleogene; Pa-E=Paleocene–Eocene.

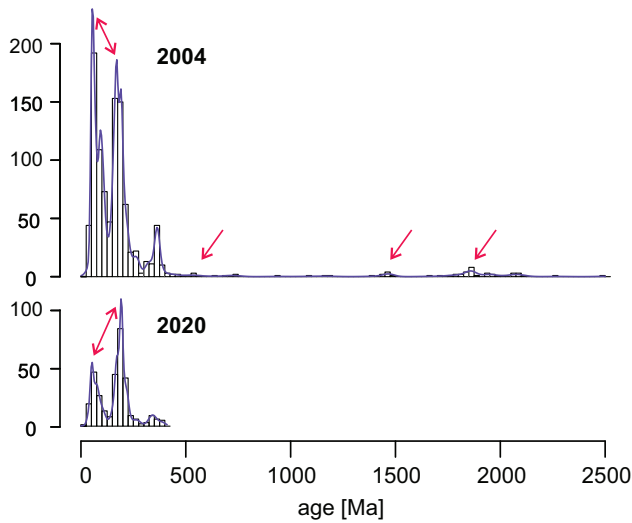


Fig. 5. Kernel density estimation (KDE) plots comparing U-Pb results from pre-2004 (Breitsprecher and Mortensen, 2004) and post-2004 to 2020 (Han et al., 2020). Red arrows point to Precambrian results in the pre-2004 data and the relative difference in the KDE peaks between the pre-2004 and post-2004 results.

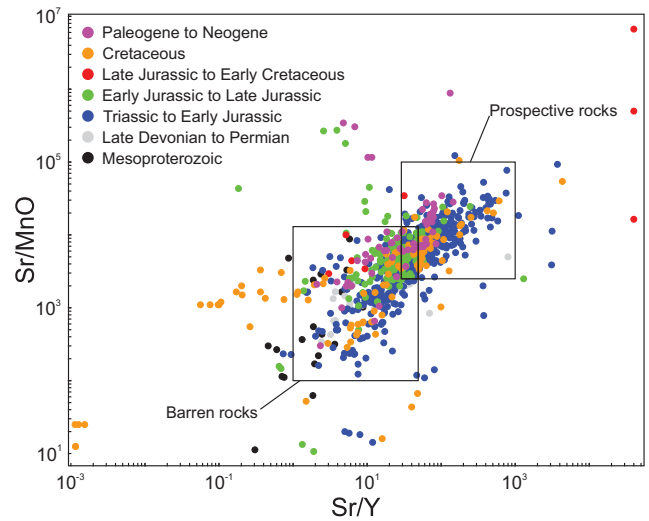


Fig. 6. Porphyry prospectivity diagram Sr/Y vs. Sr/MnO for plutonic rocks in British Columbia. Data from Han and Rukhlov (2024). Fields of prospective rocks for porphyry Cu, skarn or epithermal mineralization and barren rocks after Ahmed et al. (2019).

- ICS International Chronostratigraphic Chart. Episodes, 36, 199-204 (updated version September, 2023).
<<https://stratigraphy.org/ICSchart/ChronostratChart2023-09.pdf>>
- Colpron, M., 2020. Yukon terranes-A digital atlas of terranes for the northern Cordillera. Yukon Geological Survey.
<<https://data.geology.gov.yk.ca/Compilation/2#InfoTab>>
- Cui, Y., Miller, D., Schiarizza, P., and Diakow, L.J., 2017. British Columbia digital geology. British Columbia Ministry of Energy, Mines and Petroleum Resources, British Columbia Geological Survey Open File 2017-8, 9 p.
- Han, T., and Rukhlov, A.S., 2020. Update of the provincial Regional Geochemical Survey (RGS) database at the British Columbia Geological Survey. British Columbia Ministry of Energy, Mines and Petroleum Resources, British Columbia Geological Survey GeoFile 2020-08, 3 p.
- Han, T., and Rukhlov, A.S., 2024. Update of rock geochemical database at the British Columbia Geological Survey. British Columbia Ministry of Energy, Mines and Low Carbon Innovation, British Columbia Geological Survey GeoFile, in press.
- Han, T., Rukhlov, A.S., Riddell, J.M., and Ferbey, T., 2019. A skeleton data model for geochemical databases at the British Columbia Geological Survey. British Columbia Ministry of Energy, Mines and Petroleum Resources, British Columbia Geological Survey Paper 2019-01, pp. 125-135.
- Han, T., Ootes, L., and Yun, K., 2020. The British Columbia Geological Survey geochronologic database: Preliminary release of ages. British Columbia Ministry of Energy, Mines and Low Carbon Innovation, British Columbia Geological Survey GeoFile 2020-10, 4 p.
- Van der Vlugt, J., Rukhlov, A.S., and van Straaten, B.I., 2022. Lithochemical reanalysis of British Columbia Geological Survey archived rock samples from northwestern British Columbia. British Columbia Ministry of Energy, Mines and Low Carbon Innovation, British Columbia Geological Survey GeoFile 2022-14, 15 p.
- van Straaten, B.I., Logan, J.M., Hunter, R.C., Nelson, J.L., and Miller, E.A., 2022. Igneous lithochemical data for the Dease Lake, Kitsault River, Galore Creek, Telegraph Creek, Foremore, and other areas in northwestern British Columbia. British Columbia Ministry of Energy, Mines and Low Carbon Innovation, British Columbia Geological Survey GeoFile 2022-12, 14 p.
- Vermeesch, P., 2018. IsoplotR: A free and open toolbox for geochronology. *Geoscience Frontiers*, 9, 1479-1493.
<<https://doi.org/10.1016/j.gsf.2018.04.001>>

Preliminary results from revision mapping of the Gladys Lake area, near Atlin, northwest British Columbia



Mitchell G. Mihalynuk^{1, a}, Alex Zagorevski², Roddy Campbell¹, Abeer Hajiegeh², and Aeron Vaillancourt²

¹ British Columbia Geological Survey, Ministry of Energy, Mines and Low Carbon Innovation, Victoria, BC, V8W 9N3

² Geological Survey of Canada, Ottawa, ON, K1A 0E8

^a corresponding author: Mitch.Mihalynuk@gov.bc.ca

Recommended citation: Mihalynuk, M.G., Zagorevski, A., Campbell, R., Hajiegeh, A., and Vaillancourt, A., 2024. Preliminary results from revision mapping of the Gladys Lake area, near Atlin, northwest British Columbia. In: Geological Fieldwork 2023, British Columbia Ministry of Energy, Mines and Low Carbon Innovation, British Columbia Geological Survey Paper 2024-01, pp. 131-148.

Abstract

Geological mapping and sampling immediately south of the Yukon border, in the Gladys Lake area near Atlin, updates mapping of 1950s vintage that predates concepts derived from plate tectonics. Much of the area is underlain by deformed chert, primitive arc basalt, and slivers of mantle peridotite; all are extensively intruded by Jurassic and Cretaceous plutons. This study further documents the newly defined ophiolitic Atlin terrane, its obduction onto the Cache Creek terrane, and overlap of chert and siliciclastic deposits. Oceanic crustal sections in the map area record evidence of having formed during ocean floor detachment. Mineralized hemipelagic strata deposited atop mantle peridotite exposed by seafloor detachment contain Ag, Zn, Pb, Cu sulphides. These strata may be distal precipitates of hydrothermal plumes from ultramafic-associated seabed massive sulphide fields formed atop exposed, cooling mantle. Atlin terrane detachments have been identified along strike of the map area for more than 400 km, representing a significant untested mineral exploration opportunity.

Keywords: Atlin terrane, Cache Creek terrane, ophiolite, harzburgite, seafloor detachment, ultramafic associated massive sulphide, battery metals, molybdenite, Three Sisters suite, Surprise Lake suite, Gladys Lake, Fourth of July Creek, placer gold

1. Introduction

Western North America consists of crustal blocks (terrane) that originated along and outboard (west) of the Ancestral North America (Fig. 1). Accretion and translation of these crustal blocks along the margin since the Jurassic has resulted in formation of the mountainous Cordillera. Tectonic setting, paleo-environment, and subsequent geologic events that shaped these terranes are primary determinants of the types of mineral deposits contained within them and likelihood of their preservation. Correct terrane definition is, therefore, a critical first step in mineral potential evaluation and exploration strategy in the Cordillera. Recent re-evaluation of the formerly undifferentiated Cache Creek terrane in the Atlin area of northwest British Columbia (Zagorevski et al., 2015, 2016, 2021) revealed that it is composite, and comprises two separate terranes. Ophiolitic rocks that were previously included in Cache Creek terrane are now included in Atlin terrane (Figs. 2-4). A classic ophiolite section represents ocean crust from its mantle peridotite underpinnings, through ultramafic cumulate, gabbro, sheeted dikes, pillow basalt and pelagic sediment blanket (Anonymous, 1972; herein referred to as 'Penrose-style'). However, well-developed sheeted dike complexes or extensive sections of pillow basalts, the distinctive magmatic components at the subseafloor to seafloor interface of a normal spreading ridge, are missing in ophiolite sections preserved near Atlin. Instead, the Atlin ophiolites are

like those formed by asymmetric slow spreading systems that lead to detachment faulting and development of oceanic core complexes (Escartin et al., 2017, and citations therein), with basalt and sediments deposited directly atop mantle.

Tracking the Atlin terrane through areas last systematically mapped in the 1950s (Aitken, 1959), before plate tectonics was recognized and the tectonic significance of ophiolites and subduction melanges was realized, is a challenge. Such areas include a ~85 km long and ~30 km wide, mostly forested transect between Taku and Teslin lakes, bordered to the north by Yukon (NTS sheets 104N/14, 15, 16; ~2400 km²; Fig. 3). This report presents preliminary findings from the first of two planned field seasons of geological mapping and sampling along the transect, in the traditional territories of the Taku River Tlingit First Nation, Carcross/Tagish First Nation, and Teslin Tlingit Council. This mapping is part of the joint Federal-Provincial project begun in 2023 in the Gladys Lake area (NTS 104N/15, and adjacent 14E, 16W; Fig. 3). In this area, rocks of the Atlin and Cache Creek terranes are extensively intruded by Jurassic and Cretaceous plutons, which host the past producing polymetallic Atlin-Ruffner mine (MINFILE 104N 011) and the Adanac molybdenum deposit (MINFILE 104N 052) immediately south of the transect area. Herein we describe the regional geological setting of previously unrecognized mineralization in fine-grained rocks deposited above Atlin terrane mantle peridotite. Such mineralization may

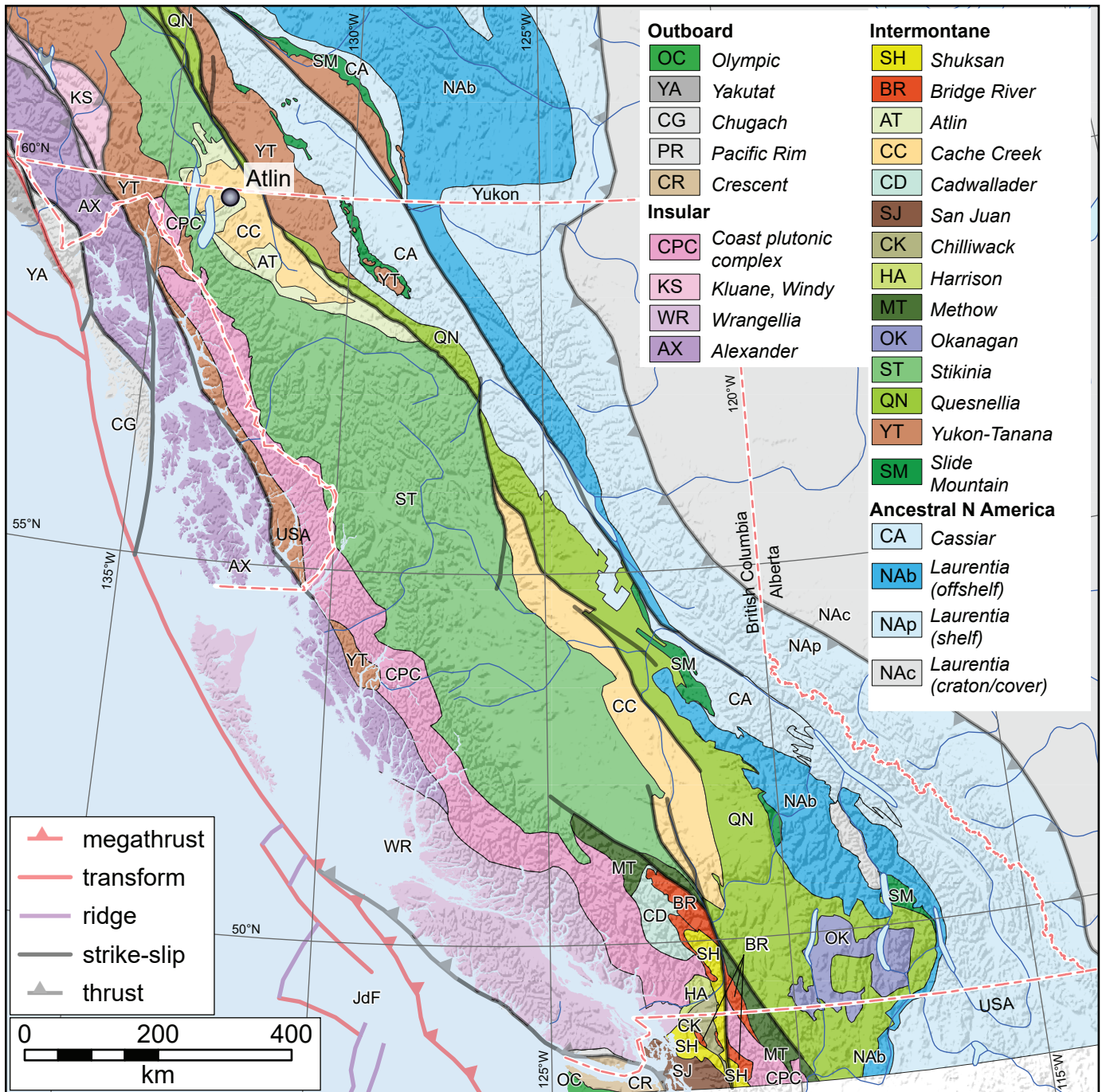


Fig. 1. Location of Gladys Lake-Atlin study area. Terranes after Colpron (2020) and Zagorevski et al. (2021).

represent an example of distal ultramafic-associated massive sulphide (UAMS) accumulations in submarine hydrothermal vent fields at sea-floor detachment faults.

2. Physiography and access

Our mapping crosses Atlin Lake and the paved Atlin Road, which follows the east shore, linking the Alaska Highway with the community of Atlin. A well-maintained gravel road extends from Atlin Road up Fourth of July Creek to MacDonald lakes (Fig. 2). Access to the areas farther northeast is limited

to mineral exploration and placer mining roads that reach to Marble Dome area, south of Gladys Lake. However, lack of road maintenance has rendered portions of the road unpassable by 4x4 pickup east of Consolation Creek (Fig. 3), limiting access to the 30 km-long Gladys Lake which would otherwise provide boat-based access across the east-central part of the transect. Boat access to the south-central part of the transect area can be gained from the northern tip of the 25-km long Surprise Lake, which is reached by gravel road from Atlin.

Much of the area is covered by well-drained glacial outflow

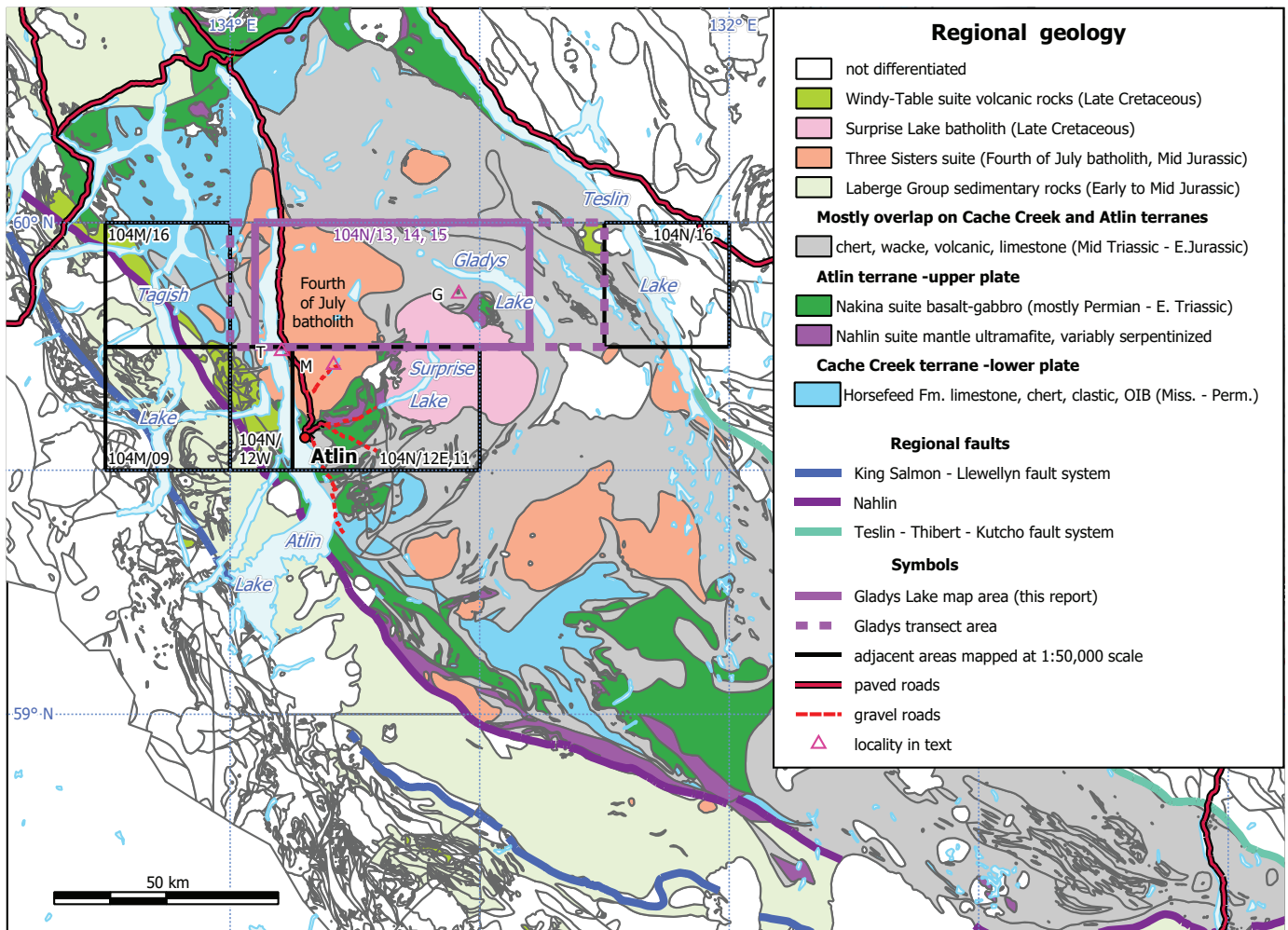


Fig. 2. Generalized geologic setting of the northern Cache Creek and Atlin terranes. Locality symbols: G, Gladys Lake property porphyry; M, McDonald lakes; T, Telegraph Bay.

terraces and open pine forest that can be crossed by long single, or multi-day foot traverses. However, the most efficient mode of travel is by helicopter based in Atlin. Most other areas are covered by extensive forest and brushy swamps requiring foot traverses between sparse helicopter landing sites. Less than 15% of the area is above tree line and many of the alpine areas marked on NTS topographic maps are extensively overgrown by dwarf birch and willow.

Due to its location on the lee side of the Coast Mountains, the Gladys Lake area is part of an orographic dry belt that receives only moderate winter snow and lacks glaciers. The highest points are Mount Carter (1784 m), Mount Hitchcock (1792 m), the northeast ridge (2049 m) of Mount Barham and an unnamed peak south of Marble Dome (2008 m).

3. Previous work

Systematic geologic surveys of the area began around 1900 (Gwillim, 1901). Quadrangle mapping in the 1950s by Aitken (1959) covered the area at 1:250,000 scale as part of the Atlin map (NTS 104N). More detailed surveys at 1:50,000 scale envelop the transect area in British Columbia, except south of

Gladys Lake (Fig. 2). From west to east, they are: Mihalynuk et al. (2018, 2022, Turtle Lake); Mihalynuk et al. (1990, Fantail Lake east); Mihalynuk and Smith (1992a, b, Mihalynuk et al., 1999, Atlin west); Bloodgood et al. (1989, Atlin east and Surprise Lake west); Mihalynuk et al. (2001, Dawson Peaks east). In many areas, but particularly near Atlin, these maps have benefitted from detailed industry mapping on, and around, mineral claims recorded in Assessment Reports and in Minister of Mines Annual reports (Annual Report to the Minister, 1874-2005).

Discovery of placer gold east of Atlin in 1898 (Robertson, 1899) drove mineral exploration in the area, especially for bedrock gold sources. To date, no economic bedrock gold resource found has sustained production. Most lode discoveries have been identified beneath known placer pay gravels, in varied bedrock, but mainly altered ultramafic or quartz-veined argillaceous rocks (e.g. Mihalynuk et al., 2017). Placer mineralogy also indicates multiple gold sources (Sack et al., 2004; Barkov et al., 2008; Mihalynuk et al., 2011), although the Surprise Lake batholith (Windy Table suite) may be the progenitor of most placer gold in the Atlin area (Zagorevski et al., 2017).

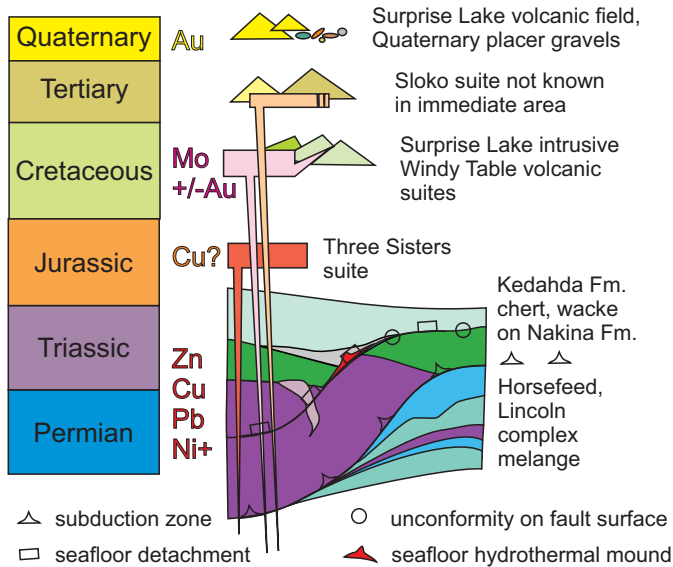


Fig. 4. Cartoon of tectonostratigraphic and metallogenic relations in the Gladys Lake area. Unit colours as in Figure 3.

4. Local geology

The map area is principally underlain by three layered successions (Figs. 3, 4). The oldest succession consists of Carboniferous to Late Permian marine strata of Cache Creek terrane. The terrane was formerly presumed to include widespread ribbon chert and minor Triassic limestone that are now largely included in ‘probable overlap’ units (see below). Middle Permian to Middle Triassic ophiolitic units (mantle peridotite and ultramafic cumulates of the Nahlin suite, and gabbro, diabase, and basalt of the Nakina suite) previously considered basement to Cache Creek terrane, were recognized by Zagorevski et al. (2021) as part of Atlin terrane. Probable Middle Triassic to Early Jurassic overlap units consist of chert (Kedahda Formation), siliciclastic rocks (Farnsworth wacke) and minor limestone. The siliciclastic rocks contain detritus from older units, as well as coarse pyroxene-phyric (\pm hornblende) pyroclastic rocks inferred to be sourced from volcanic arc rocks in Stikine and/or Quesnel terranes. These three successions are extensively cut by the Fourth of July batholith (Middle Jurassic; Mihalynuk et al., 2004, 2018 and citations therein) and rocks of the Surprise Lake batholith (Late Cretaceous; Zagorevski et al., 2017 and citations therein) which underlie most of the western and south-central parts of the area mapped in 2023.

Local units include a swarm of feldspar porphyritic dikes and stocks that cut deformed rocks of the Fourth of July batholith and thermally metamorphosed ribbon chert along Atlin Lake at Telegraph Bay and epiclastic strata and flow-banded rhyolite that are tentatively correlated with the Windy Table suite (Mihalynuk et al., 1999; Late Cretaceous, ca. 83 Ma; Zagorevski et al., 2017). Cinder cones and discontinuous ash layers of the Surprise Lake volcanic field are preserved at the headwater of Volcanic Creek. They are inferred to be post glacial.

4.1. Quaternary deposits

4.1.1. Surprise Lake volcanic field

The Surprise Lake volcanic field includes two ~150-200 m wide, partially eroded, nested scoria cones in the upper Volcanic Creek drainage (Fig. 3). It is considered part of the Northern Cordilleran Volcanic Province, which extends from northern British Columbia into Yukon (Edwards et al., 2003). Scoria consists of black to red (oxidized) poorly consolidated to unconsolidated lapilli-to ash-sized pyroclasts, and rare bomb-sized blocks. A 1 m to 10 m-thick grey basaltic flow at least 2 km long is recorded near the modern Volcanic Creek channel, enclosed within red-weathering tephra (Edwards et al., 1996). Olivine phenocrysts and xenocrysts can be found within the dense flows and clasts. Major element geochemical analyses of these volcanic rocks show them to be trachybasalt (Edwards and Bye, 2003).

The age of the Volcanic Creek centre remains uncertain. Preservation of the semi-consolidated cinder cones on a glacial valley bottom suggests that they were constructed following the exposure of the valley after the last regional glacial maximum (ca. 10,000 BCE; Clague, 1992). Drilling through the base of the Volcanic Creek flows intersected weathered bedrock below 1.5 to 4 m of reddish to light-toned partially oxidised gravels with boulder and pebble sized clasts including basalt and cinder fragments (Mioduszewska, 1980; Hainsworth, 1997). This gravel unit has produced placer gold (MINFILE 104N 024) and is similar to the ‘Miocene gravel’ which is considered the source of much historic gold production such as in the Ruby Creek drainage, immediately south of the study area (Fig. 3, inset). In Ruby Creek, lava flows covering placer gravels are dated at 0.54 ± 0.02 Ma (whole rock K-Ar cooling age; Hunt and Roddick, 1992), and most likely predate the Volcanic Creek field.

4.1.2. Miocene-Early Quaternary gravels

Most of the economic placer gold gravels in the Atlin area were deposited prior to Late Wisconsin continental glaciation (e.g., Aitken, 1959; Proudlock and Proudlock, 1976; Levson, 1992), which reached its northwestern limit about 23-24 ka BP and was in full recession by 14 ka BP (Dyke et al., 2002). Late Wisconsin glaciation was responsible for extensive glacial erosion and the blanketing of large parts of the map area with till deposits (e.g., Tallman, 1975), and other glaciogenic sediments locally more than 45 m thick (Aitken, 1959), and up to elevations of 1500 m (Tallman, 1975).

Most of the productive placer paleochannels contain weakly consolidated, ochre-stained gravels resting on bedrock. These gravels are commonly cobble to pebble clast supported, and directly overlie bedrock (e.g., Levson, 1992; Levson, and Blyth, 1993). They are locally referred to as ‘Miocene gravel’ or pre-glacial ‘yellow gravel’ (e.g., Black, 1953) and are blanketed by extensive grey-weathering glacial till deposits (Aitken, 1959).

The age of productive placer gravels is constrained in the Ruby Creek drainage where they are overlain by the late Pleistocene (ca. 0.5 Ma) Ruby Creek volcanic flows (see above).

Local basalt clasts, potential pillow lavas, and other primary volcanic products within the upper auriferous placer gravels (Levson and Blyth, 1993) suggest that volcanism was broadly contemporaneous with placer gravel sedimentation. Levson and Blyth (2001) obtained a radiocarbon date of >41,180 BP from charcoal in one part of the upper placer gravels in Ruby Creek.

Preservation of placer deposits is in part related to paleogeography, where valleys that were oblique to Wisconsinan ice flow were not eroded, especially those protected by thick glacial deposits or Quaternary volcanic flows (Levson and Blyth, 1993; 2001). Previous placer exploration and production work has focused on the creeks between Atlin and the southern end of Surprise Lake (e.g., Proudlock and Proudlock, 1976; Levson, 1992), but placer deposits are found in most drainages underlain by the Surprise Lake batholith (Sack and Mihalynuk, 2004) suggesting a genetic relationship. As early as the mid-1900s it was widely held that the possibility of discovering pre-glacial placer gravels, other than continuations of known deposits, was slight (Black, 1953). However, recent shoreline erosion at the northern end of Surprise Lake has exposed a 2-3 m section of semi-lithified, oxidised, red weathering gravel with several pebble to cobble, clast supported layers, overlain by grey-weathering till. There are no recorded placer showings (in MINFILE) or past exploration work (in ARIS) at the site, and the gravels remain untested.

4.2. Late Cretaceous magmatic rocks

Late Cretaceous igneous rocks in the area include the Surprise Lake plutonic suite (Woodsworth et al., 1992) and volcanic and minor coeval intrusive rocks of the Windy Table suite (Mihalynuk et al., 1999).

4.2.1. Surprise Lake plutonic suite

The Surprise Lake batholith is extensively exposed southwest of Gladys Lake and underlies approximately 10% of the map area. White-weathering monzogranite typical of the suite can be distinguished by intensely smoky quartz (grey-brown to almost black), low mafic content (represented by biotite, ~5%), minor muscovite, chalky plagioclase, and generally non-magnetic character; interstitial fluorite is local. Roof rocks and miarolitic cavities (Aitken, 1959), as well as syn-magmatic high-level hydrothermal vein complexes (Ballantyne and Littlejohn, 1982) are commonly preserved. This suggests that the batholith was emplaced at shallow depth and has experienced limited unroofing.

The plutonic suite is texturally variable with gradational to sharp contacts between different textural phases (Aitken, 1959). Most textural variation can be assigned to one of three phases: 1) medium- to coarse-grained weakly porphyritic to equigranular hypidiomorphic monzogranite (volumetrically predominant); 2) potassium feldspar megacrystic monzogranite with 5 to 40%, 2-3 cm phenocrysts; and 3) texturally variable, fine- to medium-grained aplitic to porphyritic. The suite includes nested intrusions such as the Mount Leonard stock,

containing the Ruby Creek Mo deposit (Fig. 2; Ballantyne and Littlejohn, 1982; Smith and Arehart, 2009) and satellite intrusions such as the Gladys Lake body ('G' on Fig. 3). The Mount Leonard stock preserves successive intrusions with an early coarse equigranular phase, cut by the megacrystic and porphyritic phases, followed by post-silicification (post-mineralisation?) finer grained aplitic phases (Smith, 2009; Smith and Arehart, 2009).

Parts of the Gladys Lake body are porphyritic with a fine-grained matrix cut by multiple generations of quartz veins. Veining can be intense, forming quartz domains across tens of square m. In many areas, early generations of mm-scale, contorted, verticulate, quartz vein arrays within a porphyritic aplite are crosscut by later 'planar' cm-scale quartz veins (\pm disseminated white mica). These early veins were likely emplaced during incomplete crystallization of a fluid-rich magma and are like 'brain rock' or unidirectional solidification texture (Fig. 5; Shannon et al., 1982; Müller et al., 2023).



Fig. 5. Dark grey verticulate quartz veins ('brain rock') and smoky, almost black, quartz eyes in a fine-grained, aplitic matrix is the high-level, porphyritic part of the Gladys Lake body (Surprise Lake intrusive suite). Traces of molybdenite have been found in some of these veins.

Magnetic susceptibility of Surprise Lake batholith rocks is low (0.01 to 0.07×10^{-3} SI (Campbell et al., 2024) consistent with their regional aeromagnetic signature (Lowe and Anderson, 2002). Exceptions include a series of northwest-trending magnetic structures (Lowe and Anderson, 2002) spatially coincident with magnetite-sphalerite vein occurrences of uncertain age (which appear to crosscut fluorite veins; Ballantyne and Littlejohn, 1982), and phases associated with molybdenum mineralization at the Mount Leonard Stock (1 to 1.58×10^{-3} SI), and at the north end of Surprise Lake (1.5 to 2.5×10^{-3} SI).

Geochemical analyses of the Surprise Lake plutonic suite indicate a highly fractionated, alkalic and peraluminous character (Zagorevski et al., 2017) with strong Cs, Rb, Pb, Th, and U enrichments. The suite plots in ‘within plate granite’ (Pearce et al., 1984), and anorogenic granite fields (A-type granite; Loiselle and Wones, 1979; Collins et al., 1982; Whalen et al., 1987). U-Pb crystallization ages from the Surprise Lake plutonic suite indicate emplacement between 83 to 78 Ma (Mihalynuk et al., 1992; Smith and Arehart, 2009; Zagorevski et al., 2017). Re/Os age determinations from molybdenite yield significantly younger ages, to ca. 70 Ma (Smith and Arehart, 2009).

4.2.2. Windy Table suite

Rocks tentatively correlated with the Windy Table suite include andesitic to rhyolitic volcanic and hypabyssal units underlying only the southwest-most corner of the 2023 study area (Figs. 2, 3) where they were identified by Aitken (1959) as “Undifferentiated, mainly volcanic rocks of uncertain, possibly several, ages.” They are an extension of volcanic strata more recently mapped to the south and west (Mihalynuk et al., 1992, 2022; Zagorevski et al., 2017). Four map units are identified in the southwest part of the map area: andesitic hypabyssal intrusions that cut lithologically similar lapilli tuff; augite-pyritic tuffite, and rare flow-banded rhyolite.

4.2.2.1. Andesitic hypabyssal intrusions and tuff

Grey-green homogeneous porphyritic lapilli to block tuff contains fine- to medium-grained hornblende (15%) and tabular feldspar (15%). It is cut by similar and presumably comagmatic hypabyssal intrusions rocks that are cut by compositionally similar, but finer grained and dark grey-green dikes.

4.2.2.2. Augite porphyry

Dark green augite porphyritic lapilli tuff and well-bedded, possibly waterlain and reworked ash tuff is found on both sides of Atlin Lake near the southern margin of the map area. Augite is medium to coarse-grained (20-25%) in an aphanitic, dark green groundmass (Fig. 6). This unit is visually similar to the Stuhini Group (Late Triassic) augite porphyry unit found in adjacent map areas and in epiclastic layers and clasts in the Farnsworth formation (see below). Samples of the epiclastic unit were collected for detrital zircon extraction to help evaluate the possibility of a Late Triassic correlation.



Fig. 6. Augite porphyry at Telegraph Bay mapped as Windy Table suite (Cretaceous) but could be correlative with similar but older units in adjacent Stikine terrane (Triassic?).

4.2.2.3. Rhyolite

Yellow to rust, flow-banded rocks of presumed rhyodacite composition form a single set of shoreline outcrops at the southern edge of the map area. They are cut by the andesitic hypabyssal intrusions. Similar aphyric, flow-banded rhyolite west of Atlin Lake contains zircons that yielded a U-Pb age of 85.0 ± 1.6 Ma (Zagorevski et al., 2017).

4.2.3. Three Sisters suite, including Fourth of July batholith (~166-174 Ma)

The Three Sisters plutonic suite (Woodsworth et al., 1992) intrudes the Cache Creek and Atlin terranes in northern British Columbia and southern Yukon (Mihalynuk et al., 2004). In the Atlin area, this suite is represented by the Fourth of July batholith, which underlies most of the western half of the study area. Aitken (1959) broadly distinguished the Black Mountain and Fourth of July Creek phases in the Fourth of July batholith. Remapping of the Fourth of July batholith indicates that it can be regionally subdivided based on mineralogic and magnetic properties into a predominantly K-feldspar porphyritic monzogranite, equigranular magnetic and non-magnetic granodiorite, and quartz diorite generally restricted to near the

margins of the batholith. Late aplite and lamprophyre dikes are locally common.

A characteristic feature of all but the most leucocratic phases of the Three Sisters suite intrusions near Atlin is pyroxene-cored hornblende crystals (Aitken, 1959; Mihalynuk et al., 1999, 2018). Petrographic analysis (Fig. 7) shows that transformation of clinopyroxene to more hydrous hornblende and biotite, results in excess titanium and growth of rutile (TiO_2). Also attributed to this hydration is the local introduction of chalcopyrite seen intergrown with hornblende (Fig. 8).

Three Sisters suite intrusions locally display igneous foliation but generally lack tectonic fabrics. Regional relationships suggest that the Three Sisters suite postdates much of the

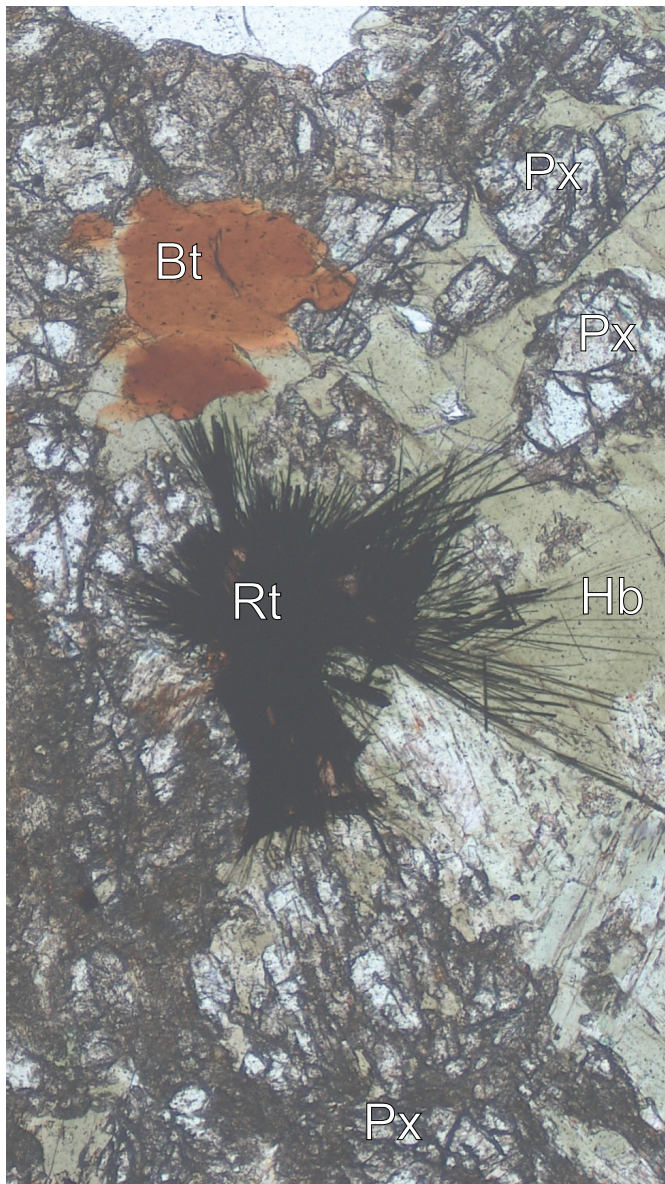


Fig. 7. Paragenetic sequence typical of the Fourth of July intrusions in plane polarized light: titanite (Px) replaced by hornblende (Hb), followed by biotite (Bt). Excess titanium from breakdown of titanite results in formation of rutile (Rt) sprays. Long dimension of photomicrograph represents 1.9 mm (Sample RCA23-08-16).

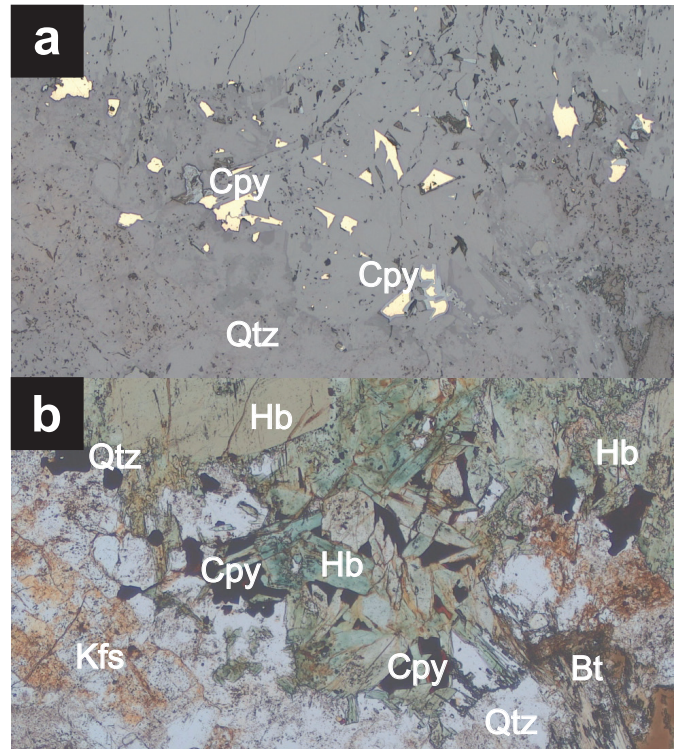


Fig. 8. A rare example of hypogene copper mineralization in a Fourth of July intrusion (marginal phase) is shown in **a**) reflected and **b**) plane polarized light. Chalcopyrite (Cpy) is interstitial to bladed hornblende (Hb), probably introduced with fluid causing hydration of pyroxene and replacement by hornblende and biotite (Bt). Orthoclase (Kfs) is hematite stained (red dusting). Long dimension of photomicrograph represents 1.9 mm (sample RCA23-23-01, see Figure 3 for location).

deformation in the area (e.g., Mihalynuk et al., 2004). This is supported by our mapping where foliated and folded Cache Creek and Atlin terrane rocks are intruded by the Fourth of July batholith. The Three Sisters suite yields Middle Jurassic crystallization ages in the Atlin region (ca. 174-172 Ma; summarized in Mihalynuk et al., 2004).

4.2.4. Como Lake phase

The Como Lake phase is widely distributed in the southwestern part of the study area. It is characterized by abundant, pink orthoclase megacrystic monzogranite (Fig. 9). Orthoclase megacrysts typically comprise 25% of the unit (10-40%) and locally display growth zones outlined by concentrations of fine biotite, hornblende, and/or quartz. Interstitial medium to coarse K-feldspar occurs with quartz (average ~30%), plagioclase (average ~30%), hornblende and biotite (5-10% combined mafic minerals, 1:3 to 3:1 ratios). Trace titanite and fine-grained dusting of magnetite are typical. The Como Lake phase commonly contains rounded enclaves (<0.1 up to 1 m) comprising up to 1% to rarely 3% of the outcrop. These generally have sharp boundaries and lack any clear reaction rims suggesting that they represent cogenetic magmas. Generally, enclaves appear to be more mafic, or at least finer grained with more evenly distributed mafic minerals than the much coarser

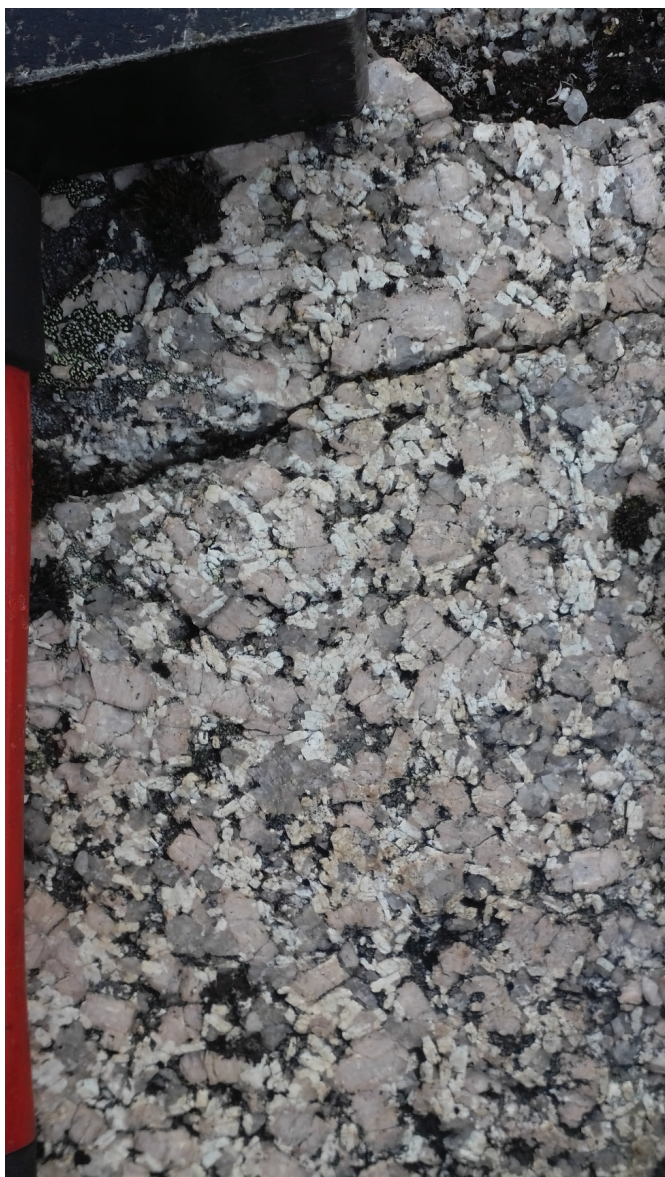


Fig. 9. Typical appearance of the K-feldspar megacrystic Como phase of the Fourth of July batholith (hammer for scale).

host phase. However, many enclaves lack appreciable quartz, suggesting more monzodioritic compositions. Some enclaves are characterized by sparse orthoclase megacrysts suggesting that they are cognate magmas.

The Como Lake phase is well-exposed in accessible roadcuts east of Como Lake (17 km south of the study area, near Atlin). These exposures are representative of this phase and would make a suitable type locality.

4.2.5. Mount Hitchcock phase

The Mount Hitchcock phase is texturally variable with gradational to sharp contacts of constituent rock types, mostly grey to beige, fine- to medium-grained diorite to quartz diorite and tonalite. Aitken (1959) referred to these rocks as the 'Black Mountain body'. Because the intrusion at Black Mountain

contains screens of country rock including chert, peridotite, and basalt, we consider it part of the marginal phase of the Fourth of July batholith (see below). Mount Hitchcock and its slopes expose rocks typical of the phase and, easily accessed along Atlin Road, would be good type localities.

Mafic minerals include brown biotite and medium- to coarse-grained green-black sparse pyroxene, or pyroxene-cored hornblende. Biotite may in part be secondary. Trace titanite is common. Plagioclase can form zoned laths with quartz which selectively replaces some zones. In part due to magnetite intergrowths in hornblende, the Mount Hitchcock phase is moderately to strongly magnetic.

4.2.6. Equigranular granodiorite

The equigranular granodiorite phase is medium- to coarse-grained and locally weakly porphyritic. It is generally tawny to grey weathering and is commonly cut by fine-grained 1 to 15 cm- thick pink granite and aplite dikes. Typical composition is 20-30% zoned K-feldspar, 25-30% interstitial quartz, 40-50% plagioclase, 10% mafic minerals with hornblende subequal to three times as abundant as biotite. Both hornblende and biotite display some degree of chloritization. The equigranular phase is well-exposed along the western shore of Atlin Lake, south of Hitchcock Creek, a good type locality.

4.2.7. Marginal phases

Marginal phases of the Fourth of July batholith are compositionally diverse. They include white to dark grey weathering, generally medium- to coarse-grained diorite to tonalite, and locally dark grey-green pyroxenite. Mafic minerals (15-30%) are typically clinopyroxene (probably titanite based on distinctive pleochroism) rimmed by amphibole, and biotite (although generally minor, biotite may locally be four times more abundant than hornblende). Mafic minerals commonly show some degree of alteration to chlorite and epidote. Outermost marginal phases are generally non-magnetic with magnetism increasing toward the core of the batholith.

Marginal phase mafic end member compositions are represented by pyroxenite that forms the lowest exposures west of southern Steamboat Mountain. Heterogeneity is well demonstrated east of Telegraph Bay where nonmagnetic, medium- to coarse-grained, diorite and tonalite grade into more homogeneous magnetic diorite. Intrusive contacts between country rocks and the marginal phase are exposed southwest of Black Mountain (on the mountain slopes, along the lakeshore, and along Atlin Road), which would be a suitable type locality.

4.2.8. Lamprophyre dikes

Lamprophyre dikes, decimetres to a few metres wide, are common in the western Gladys Lake area. Contact relations with the Three Sisters suite intrusive rocks west of Atlin Lake suggest that at least some lamprophyre dikes are late comagmatic phases, confirmed by cooling ages of 165.9 ± 1.1 Ma and 174 ± 2.7 Ma (Mihalynuk et al., 2018). These

ages overlap the range of cooling ages from dikes near Atlin Lake that are reported by Harris et al. (2003) as 165.3 ± 1.6 Ma and 161.8 ± 1.6 Ma (see discussion in Mihalynuk et al., 2018).

4.3. Middle Triassic to Lower Jurassic overlap units

4.3.1. Kedahda Formation

The Kedahda Formation is widespread within the Gladys Lake transect where it comprises chert, argillite, and wacke. Common rusty appearance on weathered surfaces is due to widespread pyrite that constitutes up to several percent, especially near intrusions. Chert displays a broad variation in colour (black, grey, green, beige, white, yellow, rust), bed thickness and continuity, and proportion of interbedded siliciclastic rocks. Chert beds are commonly parallel-sided and discontinuous, but range through lozenge shaped to bulbous. Chert can be massive to thinly (2-5 cm) bedded 'ribbon' chert. Argillite interbeds vary from a mere partings to being the predominant lithology in outcrop. Radiolaria are commonly conspicuous and are locally visible to the unaided eye. Preservation of radiolaria varies over short distances. They can be abundant in one bed and completely absent in an adjacent bed or portions of the same bed.

Previous workers have attempted to subdivide the Kedahda Formation based on the proportion of chert and argillite. In the Gladys Lake transect, areas such as Davenport Creek are underlain mostly by argillite with minor chert and wacke, whereas parts of Mount Boofus are almost entirely chert. Argillite is typically black, rusty weathering, pyritic and graphitic. Strain is commonly partitioned into the argillite, and it is almost everywhere finely cleaved, recessive, and is under-represented by bedrock exposures. As a result, it has been included with the Kedahda chert unit (Fig. 3). Nearly parallel bedding and cleavage and isoclinal fold hinges show that these rocks are at least locally intensely folded.

Chert and siliciclastic rocks in the Atlin area have been traditionally included in the Kedahda Formation (Watson and Mathews, 1944; Gabrielse, 1969; Monger, 1975). Prior to the development of radiolaria biochronology, the age of the Kedahda Formation was considered to be mainly Paleozoic on the basis of apparent intercalation with limestone beds and limestone pods containing Paleozoic fusulinids (Monger, 1975). Although Paleozoic radiolaria have been recovered from some chert localities, most radiolaria in the Kedahda Formation chert yield Middle Triassic to Early Jurassic ages (Cordey et al., 1991; Mihalynuk et al., 2003; Cordey, 2020). Fetid limestone beds intercalated with chert and argillite have yielded Late Triassic conodonts (Cordey et al., 1991). The preponderance of Mesozoic fossils and apparent unconformable relationship with the Paleozoic rocks led Zagorevski et al. (2021) to revise the age of the Kedahda Formation to Middle Triassic to Early Jurassic. Paleozoic chert localities are associated with the Atlin terrane ophiolites or Horsefeed formation limestone of the Cache Creek terrane.

4.3.2. Farnsworth wacke (new informal unit)

Wacke and pebble to cobble conglomerate are widespread in the Gladys Lake area but are subordinate to chert and argillite. These are herein included in the Farnsworth wacke (new informal unit) named for exposures underlying Mount Farnsworth, about 30 km south of the Gladys Lake map area. The Farnsworth wacke is generally resistant and is exposed in many upland areas where it is intercalated with and surrounded by chert. The distribution shown on Figure 3 is the minimum extent of this unit as it likely underlies parts of low-lying areas. Lack of magnetic contrast between this unit and chert or argillite as well as isoclinal folding makes projection of this unit under the extensive glacial sediments difficult.

The Farnsworth wacke weathers orange, green, grey, and rusty and commonly is emerald to dull blue-green on fresh surfaces. It is almost always pyritic and locally calcareous. Fine- to medium-grained feldspathic wacke is the most common rock type with common coarse sandstone to granule conglomerate interbeds.

Locally, feldspar rich beds are intercalated with beds that are relatively quartz rich, containing 30-50% quartz grains that are whitish and subrounded to subangular. Lithic grains include angular to subangular (10-15%) grey, tawny and black chert (Fig. 10) and black cherty argillite, up to 5% rusty lithic fragments, 10-20% plagioclase porphyry with

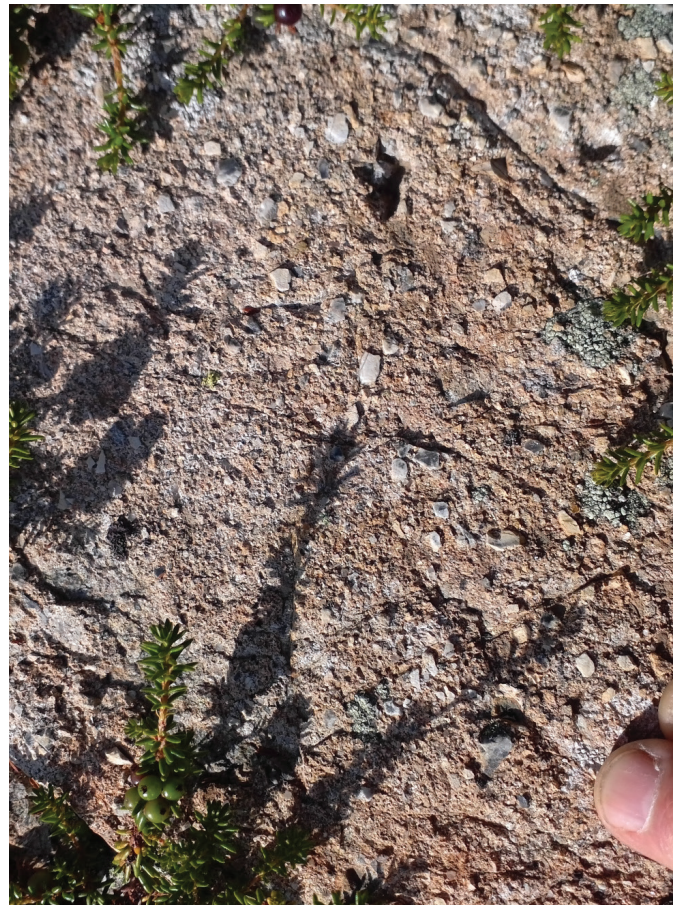


Fig. 10. Resistant chert clasts in conglomerate of the Farnsworth wacke unit.

varied composition and texture, commonly with equant laths in a dark grey matrix. Chert clasts contain both recrystallized and pristine radiolaria (Fig. 11). Feldspar porphyry clasts are locally abundant, with less common pyroxene and hornblende porphyritic clasts (Fig. 11). Mineral grains include feldspar, monocrystalline quartz grains (including subidiomorphic, embayed, rectangular beta quartz), pyroxene, hornblende, titanite, and biotite. Detrital grains of secondary epidote and pumpellyite are relatively common.

Farnsworth wacke and conglomerate represent rapid deposition of immature sediment probably generated during

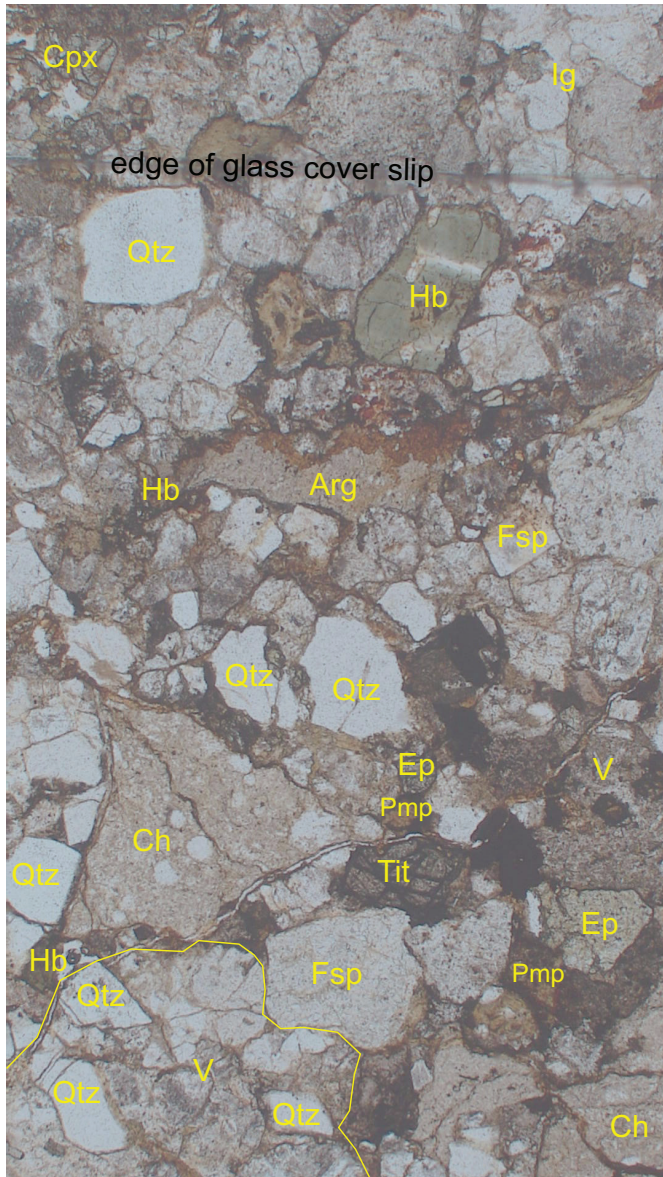


Fig. 11. Photomicrograph of Farnsworth wacke in plane polarized light. Hornblende (Hb), feldspar (Fsp), and quartz shards (Qtz) occur in clasts of felsic tuff (V, e.g., yellow outline), or occur as mineral grains, as does clinopyroxene (Cpx), titanite (Tit), and secondary minerals of (Ep) and ?pumpellyite (Pmp). Lithic grains also include holocrystalline granitoid (Ig), argillite (Arg), and chert (Ch, some with round radiolaria). Height of photo represents ~3.8 mm; sample MMI23-15-12.

unusual storm or tectonic events and carried into an otherwise quiescent environment. Some beds appear to be mass flow deposits with both sharpstone conglomerate and soft-sediment deformed chert and argillite. One of these beds contains a large raft of crinoidal packstone that probably slumped from a highland of Paleozoic rocks.

Farnsworth wacke and ribbon chert locally rest on mantle ultramafite, gabbro and basaltic rocks of the Nakina suite in the southern map area, near Marble Dome and Mount Barham (Fig. 3).

4.4. Middle Permian to Middle Triassic ophiolitic rocks of Atlin terrane

Atlin terrane is bounded to the east by the Cretaceous Teslin-Thibert-Kutcho fault system, and to the west and south, predominantly by the King Salmon and Nahlin Faults, with some outliers occurring elsewhere (Fig. 2), including in the Gladys Lake area (Fig. 3). In the study area, Atlin terrane ophiolites are subdivided into the Nahlin and Nakina suites, and slivers of ophiolite are contained in the newly defined Lincoln complex.

4.4.1. Nahlin Suite

The Nahlin suite is named after extensive exposures on Nahlin Mountain (~120 km to the south; Terry, 1977; McGoldrick et al., 2018; Zagorevski et al., 2021). It is exposed throughout the Atlin terrane and is generally interpreted as the mantle section of an ophiolite, although it locally includes minor ultramafic cumulates (Ash, 1994, 2004; Zagorevski et al., 2021). The Nahlin suite is characterized by voluminous harzburgite, dunite, sparse orthopyroxenite, rare lherzolite and rare clinopyroxenite. Harzburgite typically appears knobby on account of resistant, 1-2 cm orthopyroxene pseudomorphs (10-40%) in an olivine pseudomorph groundmass. Dunite lacks the knobby weathering surface and tends to weather a lighter, dun to olive. It is locally characterized by whisps of chromite.

Harzburgite is commonly interlayered with dunite and orthopyroxenite and deformed at high temperatures, as indicated by elongated orthopyroxene porphyroclasts and annealed olivine. Dunite and orthopyroxenite commonly form discordant dikes, channels, and pods. Nahlin suite peridotites are variably altered and range regionally from fresh (few percent serpentine), to serpentinite and/or listwanite (e.g., Terry, 1977; McGoldrick et al., 2018; Zagorevski et al., 2021). Orthopyroxenite may display chocolate tablet-like surfaces where host peridotite was serpentinized leading to volume gain in the host, and extension of the orthopyroxenite.

In some localities, especially near the contact with the Nakina suite and in the Lincoln complex (see below), Nahlin suite harzburgite displays a strong, macroscopically continuous foliation. This foliation is likely inherited from foliated serpentinite that was subsequently contact metamorphosed, obscuring primary textural relationships. Such contact metamorphism is common in the study area due to extensive intrusion by the Three Sisters (Middle Jurassic) and Surprise Lake (Late Cretaceous) suites.

4.4.2. Nakina suite

The Nakina suite is named after exposures of mafic volcanic and hypabyssal rocks in the Nakina area (~90 km to the south). The Nakina suite is spatially associated with the Nahlin suite and ranges from medium-grained gabbro to very fine-grained, flinty, flow-banded to foliated basalt. Nakina suite fine-grained gabbros appear to be intrusive into peridotites of the Nahlin suite, where they form dikes and pods with chilled margins in the peridotite, although some contacts appear to be tectonic. The transition from the Nahlin suite to the Nakina suite is characterized by intrusive and structural interleaving of the gabbro/basalt and peridotite. The main exposures of the Nakina suite occur in the Mount Barham area and on Marble Dome. In these areas, the Nakina suite consists of massive to almost flow-banded basalts and minor fine-grained gabbro. Clear contact relationships in the basalt/gabbro unit are rare but suggest that these are predominantly hypabyssal intrusions with very few true extrusive equivalents. Primary volcanic textures were not observed, except at rare exposures east of Mount Barham, where screens of pillow basalt are exposed on steep slopes (Fig. 12).

In the Mount Barham area, Nakina suite mafic hypabyssal bodies also intrude chert, suggesting that the chert is part of the ophiolite cover deposited synchronous with extension. Similar relationships were observed to the south of the study area, where Nakina suite gabbro and basalt intrude into Late Permian radiolarian chert (Zagorevski et al., 2021).

4.4.3. Lincoln complex

Northeast of Marble Dome, peridotite, gabbro, basalt, chert, limestone and fine-grained siliciclastic rocks are interleaved on a decameter scale. In this area, competent gabbro and peridotite are structurally juxtaposed with recrystallized marble and polydeformed siliciclastic rocks and chert, in part comprising a mixed siliceous and amphibolite mylonite. Overall, the interleaving of the disparate rock types suggests juxtaposition in a tectonic melange-like zone. Excellent exposures of these

rocks occur to the east of Lincoln Lake and Lincoln Creek and these rocks are herein referred to as the Lincoln complex.

4.4.4. Relationships between Atlin terrane units

Primary relationships between Nahlin and Nakina suites are preserved in the Mount Barham area. Emplacement of the fine-grained Nakina suite sills into peridotites suggests that peridotite was exhumed to shallow depth, cooled, and serpentinized before gabbro was chilled against it. The very thin crustal section overlying the peridotite, including presence of chert within a few 100 m of the contact (Fig. 3 inset; Fig. 12), suggests that Penrose-style ophiolite stratigraphy was not developed. Rather, this ophiolite appears to have formed by tectonically accommodated extension in an ocean core complex where mantle was exhumed to just below the sea floor along an extensional detachment (e.g., Ildefonse et al., 2007). Similar relationships are present throughout the Atlin terrane, including north of the study area along the Alaska highway, where Bogatu et al. (2023) constrained the detachment to 249 to 245 Ma.

Zagorevski et al. (2021) interpreted that the Atlin terrane was obducted onto the Cache Creek terrane carbonate platform (exposed immediately west of the study area) in the Middle to Late Triassic. The contact between Paleozoic limestones and Atlin terrane ophiolites is generally poorly exposed or has not been previously investigated in detail. South of the study area, coherent crust to mantle ophiolite seems to transition to the Lincoln complex across a valley with no exposure. In this context, the Lincoln complex may represent a tectonic melange formed during emplacement of the ophiolite onto the Paleozoic carbonate platform, resulting in juxtaposition and interleaving of crust and mantle rock along the interface. Future discovery of high-pressure mineral assemblages would support this interpretation.

5. Mineral occurrences

Well-known mineralized systems within or immediately

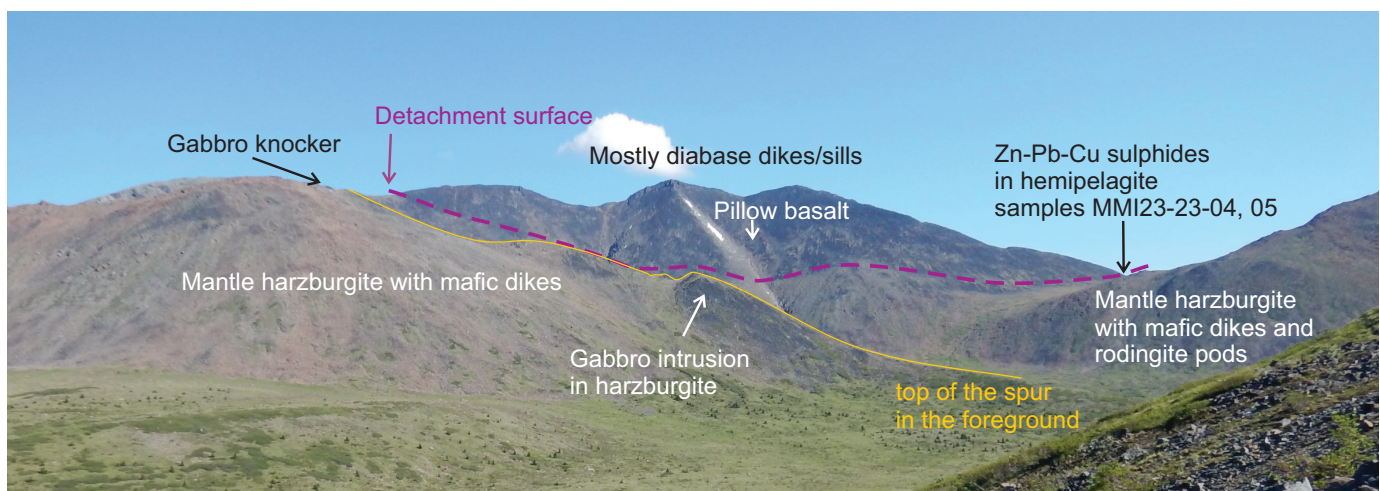


Fig. 12. View of the detachment surface near Mount Barham (dashed purple line). The mineralized (see below) hemipelagite sample collection site at the detachment is shown. This site was probably at a breakaway, where mantle was exposed on the seafloor.

adjacent the study area include porphyry and skarn mineralization related to the Surprise Lake plutonic suite evolved granite (Late Cretaceous), and polymetallic veins associated with the Three Sisters plutonic suite (Middle Jurassic) and related lamprophyre dikes. Identified here for the first time is mineralization at a preserved intraoceanic detachment within the Atlin terrane, perhaps a distal equivalent of modern ultramafic associated massive sulphide deposits forming today in analogous extensional seafloor settings.

5.1. Porphyries related to evolved granites

The Surprise Lake batholith and surrounding contact aureole contain several molybdenum and granophile mineral occurrences (Mo, \pm W, Sn, Au; e.g., Aitken, 1959; Ballantyne and Littlejohn, 1982; Ray et al., 2000; Smith and Arehart, 2009; Zagorevski et al., 2017). Currently, the most significant known mineralization is contained within the Ruby Creek deposit (formerly named Adanac), immediately south of the study area (Fig. 3, inset). It contains Measured and Indicated resources of 369,398,000 tonnes grading 0.053% Mo (Ristorcelli et al., 2022; MINFILE 104N 052). Molybdenite mineralization occurs in extensively quartz veined zones along with introduction of potassium as indicated by intergrowth of muscovite with molybdenite (Fig. 13). In addition to this synmagmatic-hydrothermal mineralization in the Mount Leonard stock, potential has also been identified in post-intrusion hydrothermal systems related to a continued enhanced heat flow generated by radioactive decay of elements concentrated in the highly evolved granite (e.g., Ballantyne and Littlejohn, 1982). Such late mineralizing systems include argillic alteration locally observed north of Zenazie Creek and around fracture zones near Mount Weir (~15 km south of Lincoln Lake) together with magnetite-sphalerite veins (Ballantyne and Littlejohn, 1982).

Farther to northeast, the Gladys Lake stock and ring dike complex (G on Figs. 2, 3) display many of the characteristics of the Mount Leonard stock. This includes polyphase pegmatitic to aplitic intrusions and extensive quartz veining, and limited molybdenite mineralization (Pinsent, 2005).

5.2. Skarn sulphide mineralization

The most extensive zone of skarn mineralization known in the Gladys Lake area is the Sunrise occurrence (MINFILE 104N 012; locality S on Fig. 3). There, magnetite-sphalerite-galenachalcocopyrite lenses tens of metres long and metres in thickness formed near the intrusive contact of the Surprise Lake batholith and Paleozoic Cache Creek terrane marble. Indications of mineralization extend along a 500 m strike length of the contact zone (Devine, 2020).

5.3. Lode gold veins

Most of the historic lode gold exploration in the Atlin district was focused on listwanite alteration (quartz-carbonate-chromite mica) of mafic and ultramafic rocks. Evaluation of mineral grains (especially thorite) intergrown with gold recovered from

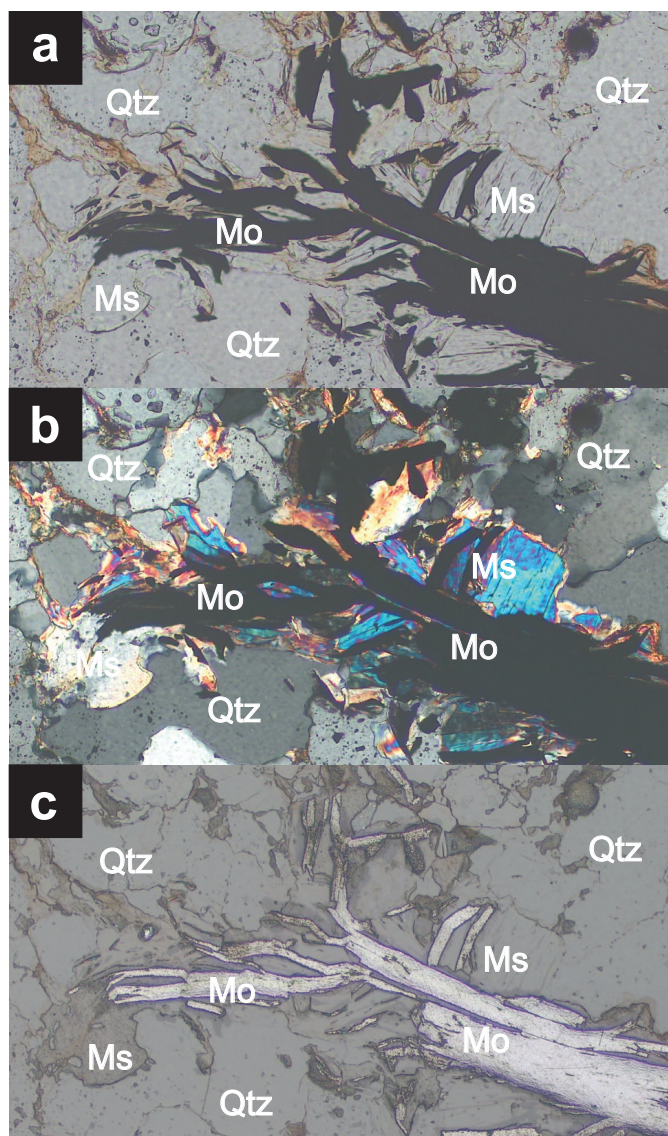


Fig. 13. Representative molybdenite mineralization in intensely quartz veined zone (Qtz) from a surface exposure of the Ruby Creek deposit. In all instances molybdenite (Mo) is mantled by muscovite (Ms). Plane polarized (a), cross polarized (b) and reflected light (c) views in photomicrographs with long dimensions representing ~1 mm (Sample 23ZE1475b1, location in Table 1 and on Figure 3).

placer operations south of the Surprise Lake batholith suggests a genetic relationship with the highly evolved, U-Th rich phases of the batholith (Sack and Mihalynuk, 2004). Coarse gold is demonstrably intergrown with chert-argillite in bedrock below producing placer gravels (Mihalynuk et al., 2017), suggesting that listwanite is not the singular major source of lode gold. Most of the placer gold mining has taken place on the south margin of the Surprise Lake batholith, with lesser placer operations in the Gladys Lake area. Considering that the Surprise Lake batholith intrudes the same rock types along its south and northern contacts, there may be similar lode gold potential in the Gladys Lake area, especially near known placer deposits.

No anomalous gold values were recovered from the Surprise Lake batholith-related samples. All of the anomalous gold analyses (and As \pm Au, Pb and Cu) were from the Three Sisters suite (Table 1), which is not known for Au potential. More focused mapping and sampling is required to assess the lode gold potential of the Gladys Lake area.

5.4. Ultramafic-associated massive sulphide (UAMS)

Ultramafic-associated massive sulphide (UAMS) deposits are polymetallic (Cu-Zn-Pb-Ni-Co) sulphide accumulations on or adjacent to sea floor detachment faults (Mihalynuk et al., 2019). The most extensively explored modern UAMS near the Mid Atlantic Ridge comprise some of the highest grade Cu-Zn deposits globally with combined Cu+Zn grades averaging 20% (Cherkashev et al., 2013). Typically, UAMS have low preservation potential because they must survive oxidizing bottom waters (e.g. Murton et al., 2019) and subduction or obduction to become part of an accretionary orogen. Atlin terrane preserves a rare example of a fossil intraoceanic detachment zone on land that can be traced along strike for hundreds of km (Fig. 2; Zagorevski et al., 2015, 2016, 2021; Corriveau, 2018; Bogatu et al., 2023). As such, it has potential for UAMS mineralization.

In the Mount Barham area, fine-grained, metalliferous sedimentary rocks are exposed in low, rubbly outcrops across an area of about 10 m² separated by ~300 m from outcrops of peridotite and ~40 m from outcrops of basalt (including hypabyssal gabbro). Contacts between the three units are covered, but projection of the detachment surface places it immediately below the metalliferous sedimentary rocks (Fig. 12) which display significant Au-Zn-Pb \pm Cu enrichment (Table 1). In outcrop, chalcopyrite and galena are visible as fine disseminations, whisps, and blebs elongated up to about 2 cm along bedding and 0.5 cm across. Sphalerite is not easily distinguished from the rock matrix but in polished section is widely disseminated and contains inclusions of chalcopyrite (Fig. 14).

It is possible that mineralization is related to the nearby Surprise Lake suite intrusions (see Fig. 3). However, comparison between the Ruby Creek deposit and mineralization near Mount Barham (red text versus grey highlight of Table 1) show significant differences in almost all elements (notably Nb, Mn, Sb, Ge, and Pd). Iron contents are 17.2% and 9.5% with corresponding S of 0.4 and 0.2%, indicating that most Fe is contained in oxides (see Fig. 14). Overall, together with the trace element profile, this may be an indicator of distal UAMS mineralization in the Atlin terrane.

6. Summary

Framework geological mapping and sampling in the Gladys Lake area revises the mapping of Aitken (1959) that predates plate tectonics and widespread recognition of ophiolitic sequences (Dilek, 2003). It builds upon the work of Zagorevski et al. (2021) who clarified relationships between the underlying terranes, separating upper plate Atlin terrane from lower plate

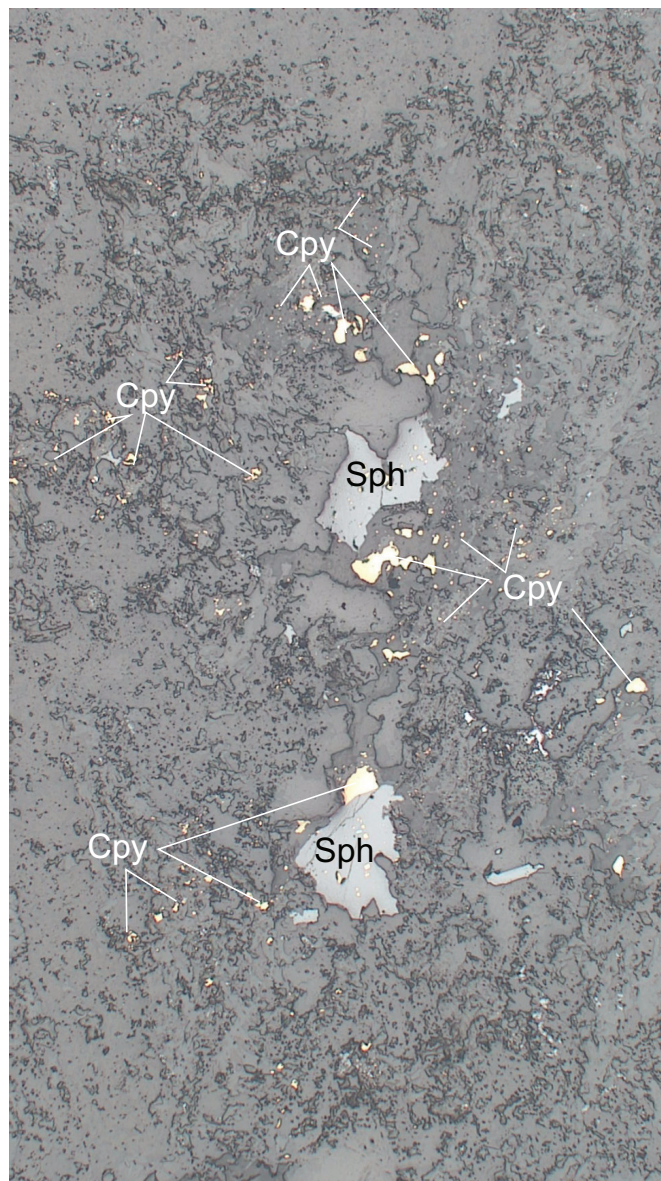


Fig. 14. Sphalerite (Sph) with inclusions of chalcopyrite and abundant scattered chalcopyrite (Cpy) in the matrix of fine-grained sedimentary rocks resting atop an interpreted mantle extensional fault in the Mount Barham area. Galena is present outside of the field of view. Chemical analysis of this sample returned 0.08% Cu, 0.4% Zn, 0.7% Pb, and 31 g/t Ag. Long dimension of photomicrograph represents 3.8 mm (Sample MMI23-23-05, location in Table 1 and on Figure 3).

Cache Creek terrane. That work also documented widespread ocean floor extension in the upper plate and deposition of overlap successions. During mapping, mineralization in fine-grained strata was discovered above one of the detachment surfaces exposed near Mount Barham. Analyses confirmed that it is strongly elevated in numerous metals, particularly Ag, Zn, and Pb. The preferred working hypothesis is that the mineralized rocks are distal precipitates of hydrothermal plumes at ultramafic-associated massive sulphide fields. Given that these extensional ocean crustal sections have been identified for more than 400 km along strike, and that modern

Table 1. Geochemical analyses of selected samples from the Gladys Lake area. See Campbell et al. (2024) for full suite of samples, descriptions, and all elements analyzed.

Statnum	Unit and rock type	Latitude	Longitude	Mo	Cu	Pb	Zn	Ag	Ni	Co	Mn	Fe	As	U	Au
		ppm	ppm	ppm	ppm	ppm	ppm	ppb	ppm	ppm	ppm	%	ppm	ppm	ppb
23ZE1298XY	LKS quartz eye porphyry	59.71175	-133.403944	253.5	7.8	4.8	11.4	28	1.6	0.8	158.0	0.9	1.0	22.9	0.2
23ZE1475b1	LKSg quartz veined granite	59.75268	-133.318717	>2000	5.9	8.9	10.5	32.9	3.0	0.5	97.0	0.9	4.2	18.2	73.6
MM123-07-19	MJTgd quartz eye porphyry dike MJTgd	59.92192	-133.802976	5.1	8.7	18.2	27.1	80	9.1	6.7	629.0	2.1	488.8	9.0	235.1
MM123-08-15	biotite>hornblende quartz diorite MJTgd	59.87746	-133.343889	3.3	45.7	0.9	43.4	57	19.8	13.2	258.0	2.4	1.5	2.6	1.7
MM123-08-25	fine- to medium-grained tonalite MJTgd	59.87638	-133.362252	2.2	102.1	146.2	1356.9	2823	1.6	1.0	64.0	2.7	3.1	14.6	0.5
MM123-12-32	clay altered cut by dikes & veins MJTgd	59.79794	-133.575532	7.4	293.4	285.8	497.3	9491	11.5	5.9	205.0	5.2	1177.4	12.7	79
MM123-12-32	clay altered cut by dikes & veins MJTgd	59.79794	-133.575532	6.4	274.4	265.7	476.0	9189	11.1	5.9	198.0	5.1	1123.3	12.4	74.2
MM123-20-02	80cm banded vein in quartz diorite	59.75044	-133.804428	4.6	28.5	8.8	17.8	199	16.9	7.8	311.0	1.7	2764.4	0.3	110.7
MM123-23-04	PTN distal exhalite?	59.75239	-133.317854	0.3	115.0	>10000	5994.2	41656	32.2	14.1	>10000	17.2	89.4	0.2	0.5
MM123-23-05	PTN distal exhalite?	59.75242	-133.317981	2.0	814.8	7283.9	4494.3	31354	32.5	27.0	6719.0	9.5	180.2	0.2	<0.2
MM123-23-08	PTN sulfide-rich pod in foliated gabbro	59.75295	-133.324153	0.7	164.7	16.5	52.3	346	27.1	23.9	277.0	3.4	0.6	<0.1	1.6
RCA23-12-20	MJTgd quartz-flooded breccia	59.79802	-133.575732	44.6	1162.4	3850.9	647.9	19668	12.4	3.7	59.0	2.7	>10000	0.7	198.7
Statnum	Unit and rock type	Th	Cd	Sb	Bi	V	Cr	Mg	Al	Sc	Ga	Cs	Nb	Re	Pd
		ppm	ppm	ppm	ppm	ppm	ppm	%	%	ppm	ppm	ppm	ppm	ppb	ppb
23ZE1298XY	LKS quartz eye porphyry	36.1	0.09	0.47	0.19	4	6.4	0.09	0.41	1	2.6	1.15	9.26	2	<10
23ZE1475b1	LKSg quartz veined granite	27	0.78	0.41	759.77	<1	15	0.02	0.77	0.9	4	4.55	20.72	26	<10
MM123-07-19	MJTgd quartz eye porphyry dike MJTgd	15.5	0.03	5.49	0.06	11	11.7	0.35	0.41	3.5	0.9	4.72	0.03	<1	<10
MM123-08-15	biotite>hornblende quartz diorite MJTgd	7.9	0.05	0.28	0.44	118	87.1	1.06	0.93	3.9	3.8	4.23	0.45	<1	<10
MM123-08-25	fine- to medium-grained tonalite MJTgd	30.2	0.75	0.22	5.17	3	7.5	0.02	0.49	0.9	3.2	5.29	1.2	<1	<10
MM123-12-32	clay altered cut by dikes & veins MJTgd	7.5	8.99	21.31	8.37	44	10.4	0.13	1.7	6.3	7.3	3.02	<0.02	<1	<10
MM123-12-32	clay altered cut by dikes & veins MJTgd	7.2	8.42	19.38	8.31	44	8	0.12	1.77	6.2	7.2	3	<0.02	<1	<10
MM123-20-02	80cm banded vein in quartz diorite	0.5	0.03	28.53	0.32	18	20.6	1.2	0.28	6.2	0.8	1.34	<0.02	<1	<10
MM123-23-04	PTN distal exhalite?	0.2	52.81	28.91	0.73	261	64.3	2.2	5.7	21.6	31.4	7.27	<0.02	<1	29
MM123-23-05	PTN distal exhalite?	0.1	71.75	16.37	0.66	208	61	2.16	4.23	18	21.8	8.64	<0.02	<1	*
MM123-23-08	PTN sulfide-rich pod in foliated gabbro	<0.1	0.26	0.12	3.43	92	51.2	1.08	3.06	7	10	4.5	<0.02	<1	<10
RCA23-12-20	MJTgd quartz-flooded breccia	2	11.58	86.83	23.79	11	24.6	0.02	0.22	3.2	2.1	1.6	0.02	<1	<10

fields can develop grades that average 20% combined Cu+Zn, Atlin terrane extensional structures represent a significant untested mineral exploration opportunity. More complete inventory of extensional structures, paleogeographic analyses, and relations to adjacent arc terranes, Stikinia and Quesnellia, will be considerations during framework mapping planned for 2024.

Acknowledgments

Joseph English, and JoAnne Nelson reviewed and improved earlier versions of this paper. Fieldwork benefited from the enthusiastic and capable assistance of Taku River Tlingit First Nation Land Guardians, Emma Law and Izaiah Carlick. Evan Orovan helped with interpretation of unidirectional solidification textures in samples of Surprise Lake porphyry. The pilots and staff at Discovery Helicopters, Atlin, transported us safely to and from remote corners of the field area.

References cited

- Aitken, J.D., 1959. Atlin map-area, British Columbia. Geological Survey of Canada, Memoir 307, 89 p.
<<https://doi.org/10.4095/100528>>
Annual Report to the Minister (1874-2005).
<<https://www2.gov.bc.ca/gov/content/industry/mineral-exploration-mining/british-columbia-geological-survey/publications/annual-report-to-the-minister>> (accessed December 2023).
- Anonymous, 1972. Penrose field conference on ophiolites. *Geotimes*, 17, 22-24.
- Anderson, J.H., 1970. A geobotanical study in the Atlin region in northwestern British Columbia and south-central Yukon Territory. Unpublished Ph.D. thesis, Michigan State University, Lansing, Michigan, 380 p.
- Ash, C.H., 1994. Origin and tectonics setting of ophiolitic (NTS 104N). British Columbia Ministry of Energy, Mines and Petroleum Resources, British Columbia Geological Survey, Bulletin 94, 54 p.
- Ash, C.H., 2004. Geology of the Atlin area, Northwestern British Columbia. British Columbia Ministry of Energy and Mines, British Columbia Geological Survey, Geoscience Map 2004-4, 1:25,000 scale.
- Ballantyne, S.B., and Littlejohn, A.L., 1982. Uranium mineralization and lithogeochemistry of the Surprise Lake batholith, Atlin, British Columbia. In: Maurice Y.T., (Ed.), Uranium in Granites. Geological Survey of Canada, Paper 81-23, pp. 145-155.
- Barkov, A.Y., Martin, R.F., Fleet, M.E., Nixon, G.T., and Levson, V.M., 2008. New data on associations of platinum-group minerals in placer deposits of British Columbia, Canada. *Mineralogy and Petrology*, 92, 9-29.
- Black, J.M., 1953. Report on the Atlin placer camp. British Columbia Department of Mines, British Columbia Geological Survey, Miscellaneous Report 1953-01, 71 p.
- Bloodgood, A., Rees, C.J., and Lefebvre, D.V., 1989. The geology of the Atlin area (NTS 104N/11W, 12E). Open File 1989-15, 1:50,000 scale.
- Bogatu, A., Bédard, J.H., Labrousse, L., Zagorevski, A., and Tremblay, A., 2023. An oceanic core complex preserved in the Squanga Lake ophiolite, northern Atlin terrane, Yukon. *Lithos*, 454-455, article 107269.
<<https://doi.org/10.1016/j.lithos.2023.107269>>
- Campbell, R.W., Mihalynuk, M.G., and Zagorevski, A., 2024. Geochemical and magnetic susceptibility of samples collected from the Gladys Lake area, near Atlin, northwest British Columbia (NTS 104N/11, 13, 14, and 15). British Columbia Ministry of Energy, Mines and Low Carbon Innovation, British Columbia Geological Survey GeoFile, in press.
- Cherkashev, G.A., Ivanov, V.N., Bel' Tenev, V.I., Lazareva, L.I., Rozhdstvenskaya, I.I., Samovarov, M.L., Poroshina, I.M., Sergeev, M.B., Stepanova, T.V., Dobretsova, I.G., and Kuznetsov, V.Y., 2013. Massive sulfide ores of the northern equatorial Mid-Atlantic Ridge. *Oceanology*, 53, 607-619.
- Clague, J.J., 1992. Quaternary glaciation and sedimentation. In: Gabrielse, H., and Yorath, C.J., (Eds.), *Geology of the Cordilleran Orogen in Canada*. Geological Survey of Canada, *Geology of Canada*, pp. 419-434.
- Collins, W.J., Beams, S.D., White, A.J.R., and Chappell, B.W., 1982. Nature and origin of A-type granites with particular reference to southeastern Australia. *Contributions to Mineralogy and Petrology*, 80, 189-200.
- Colpron, M., 2020. Yukon terranes-A digital atlas of terranes for the northern Cordillera. Yukon Geological Survey.
<<https://data.geology.gov.yk.ca/Compilation/2#InfoTab>> (accessed November 2023).
- Cordey, F., 2020. Timing of Cache Creek Ocean closure: insights from new Jurassic radiolarian ages in British Columbia and Yukon and their significance for Canadian Cordillera tectonics. *Canadian Journal of Earth Sciences*, 57, 1167-1179.
- Cordey, F., Gordey, S.P., and Orchard, M.J., 1991. New biostratigraphic data for the northern Cache Creek Terrane, Teslin map area, southern Yukon. In: *Current Research, Part E; Geological Survey of Canada, Paper 91-1E*, pp. 67-76.
- Corriveau, A.S., 2018. Caractérisation pétrologique et géochimique des roches mantelliques du terrane de Cache Creek Nord, Cordillère nord-américaine. Unpublished M.Sc. thesis, Université du Québec/Institut national de la recherche scientifique, Québec, Québec, 211 p.
- Devine, F.A.M., 2020. Report on the 2019 Exploration Program on the Sunrise Property, Atlin area, British Columbia, Canada. British Columbia Ministry of Energy, Mines and Low Carbon Innovation, Assessment Report 38901, 33 p.
- Dilek, Y., 2003. Ophiolite concept and its evolution. In: Dilek, Y. and Newcomb, S. (Eds.), *Ophiolite Concept and Evolution of Geological Thought*. Geological Society of America, Special Paper 373, pp. 1-16.
<<https://doi.org/10.1130/0-8137-2373-6.1>>
- Dyke, A.S., Andrews, J.T., Clark, P.U., England, J.H., Miller, G.H., Shaw, J., and Veillette, J.J., 2002. The Laurentide and Innuitian ice sheets during the Last Glacial Maximum. *Quaternary Science Reviews*, 21, 9-31.
<[https://doi.org/10.1016/S0277-3791\(01\)00095-6](https://doi.org/10.1016/S0277-3791(01)00095-6)>
- Edwards, B.R., and Bye, A., 2003. Preliminary results of field mapping, GIS spatial analysis, and major-element geochemistry, Ruby Mountain volcano, Atlin volcanic district, northwestern British Columbia. In: *Geological Survey of Canada, Current Research 2003-A10*, 9 p.
<<https://doi.org/10.4095/214027>>
- Edwards, B.R., Hamilton, T.S., Nicholls, J., Stout, M.Z., Russell, J.K., and Simpson, K., 1996. Late Tertiary to Quaternary volcanism in the Atlin area, northwestern British Columbia. In: *Current Research, Part A, Geological Survey of Canada Paper 96-A*, pp. 29-36.
- Edwards, B.R., Russell, J.K., Anderson, R.G., and Harder, M., 2003. Overview of Neogene to Recent volcanism in the Atlin volcanic district, Northern Cordilleran volcanic province, northwestern British Columbia. In: *Geological Survey of Canada, Current Research 2003-A8*, 6 p.
<<https://doi.org/10.4095/214025>>
- English, J.M., Mihalynuk, M.G., and Johnston, S.T., 2010. Geochemistry of the northern Cache Creek Terrane and implications for accretionary processes in the Canadian Cordillera. *Canadian Journal of Earth Sciences*, 47, 13-34.
<<https://doi.org/10.1139/E09-066>>

- Escartin, J., Mevel, C., Petersen, S., Bonnemains, D., Cannat, M., Andreani, M., Augustin, N., Bézou, A., Chavagnac, V., Choi, Y., and Godard, M., 2017. Tectonic structure, evolution, and the nature of oceanic core complexes and their detachment fault zones (13°20' N and 13°30' N, Mid Atlantic Ridge). *Geochemistry, Geophysics, Geosystems*, 18, 1451-1482.
- Gabrielse, H., 1969. Geology of Jennings River map-area, British Columbia (104-O). Geological Survey of Canada, Paper 68-55, 37 p.
<<https://doi.org/10.4095/102349>>
- Gwillim, J.C., 1901. Atlin mining district. Geological Survey of Canada, Annual Report 1899, Volume 12, 48 p.
<<https://doi.org/10.4095/294883>>
- Hainsworth, W.G., 1997. Assessment report of drilling on the rain group (rainbow, rain, ransom & rain again claims) Volcanic Creek area. British Columbia Ministry of Energy, Mines and Low Carbon Innovation, Assessment Report 25228, 22 p.
<<https://apps.nrs.gov.bc.ca/pub/aris/Detail/25228>> (accessed October 2023).
- Harris, M.J., Symons, D.T., Blackburn, W.H., Hart, C.J., and Villeneuve, M., 2003. Travels of the Cache Creek Terrane: a paleomagnetic, geobarometric and ⁴⁰Ar/³⁹Ar study of the Jurassic Fourth of July Batholith, Canadian Cordillera. *Tectonophysics*, 362, 137-159.
- Hunt, P.A., and Roddick, J.C., 1992. A compilation of K-Ar and ⁴⁰Ar-³⁹Ar ages: Report 22. In: Geological Survey of Canada, Radiogenic Age and Isotopic Studies: Report 6, Paper 92-2, pp. 179-226.
- Ildefonse, B., Blackman, D.K., John, B.E., Ohara, Y., Miller, D.J., MacLeod, C.J., Abe, N., Abratis, M., Andal, E.S., Andreani, S., Beard, J.S., Brunelli, D., Charney, A.B., Christie, D.M., Delacour, A.G., Delius, H., Drouin, M., Einaudi, F., and Zhao, X., 2007. Oceanic core complexes and crustal accretion at slow-spreading ridges. *Geology*, 35, 623-626.
<<https://doi.org/10.1130/G23531A.1>>
- Levson, V.M., 1992. Quaternary Geology of the Atlin area (104N/11W, 12E). In: Geological Fieldwork 1991, British Columbia Ministry of Energy, Mines and Petroleum Resources, British Columbia Geological Survey Paper 1992-01, pp. 375-392.
- Levson, V.M., and Blyth, H., 1993. Applications of Quaternary geology to placer deposit investigations in glaciated areas; a case study, Atlin, British Columbia. *Quaternary International*, 20, 93-105.
<[https://doi.org/10.1016/1040-6182\(93\)90039-1](https://doi.org/10.1016/1040-6182(93)90039-1)>
- Levson, V.M., and Blyth, H., 2001. Formation and preservation of a Tertiary to Pleistocene fluvial gold placer in northwest British Columbia. *Quaternary International*, 82, 33-50.
<[https://doi.org/10.1016/S1040-6182\(01\)00007-6](https://doi.org/10.1016/S1040-6182(01)00007-6)>
- Loiselle, M.C., and Wones, D.R., 1979. Characteristics and origin of anorogenic granites. *Geological Society of America, Abstracts with Programs*, 11, 468.
- Lowe, C., and Anderson, R.G., 2002. Preliminary interpretations of new aeromagnetic data for the Atlin map area, British Columbia. In: Geological Survey of Canada, Current Research 2002-A17, 11 p.
<<https://doi.org/10.4095/213081>>
- McGoldrick, S., Canil, D., and Zagorevski, A., 2018. Contrasting thermal and melting histories for segments of mantle lithosphere in the Nahlin Ophiolite, British Columbia, Canada. *Contributions to Mineralogy and Petrology*, 173, 1-25.
<<https://doi.org/10.1007/s00410-018-1450-9>>
- Mihalynuk, M.G., 2019. Reconnaissance mapping in the Lardeau Group, southeastern British Columbia, with implications for Outokumpu-style deposits and high-technology battery metals, Ni and Co. British Columbia Ministry of Energy, Mines and Petroleum Resources, British Columbia Geological Survey GeoFile 2019-13 (poster).
- Mihalynuk, M.G., and Smith, M.T., 1992a. Geology and geochemistry of the Atlin (west) map area (104N/12W). British Columbia Ministry of Energy, Mines and Petroleum Resources, British Columbia Geological Survey, Open File 1992-08, 1:50,000 scale.
- Mihalynuk, M.G., and Smith, M.T., 1992b. Highlights of 1991 Mapping in the Atlin-West Map Area. In: Geological Fieldwork 1991, British Columbia Ministry of Energy, Mines and Petroleum Resources, British Columbia Geological Survey, Paper 1992-01, 221-228.
- Mihalynuk, M.G., Mountjoy, K.J., Currie, L.D., Lofthouse, D.L., and Winder, N., 1990. Geology and geochemistry of the Edgar Lake and Fantail Lake map areas. British Columbia Ministry of Energy, Mines, and Petroleum Resources, British Columbia Geological Survey Open File 1990-04, 1:50,000 scale.
- Mihalynuk, M.G., Smith, M.T., Gabites, J.E., Runkle, D., and Lefebure, D., 1992. Age of emplacement and basement character of the Cache Creek Terrane as constrained by new isotopic and geochemical data. *Canadian Journal of Earth Sciences*, 29, 2463-2477.
<<https://doi.org/10.1139/e92-193>>
- Mihalynuk, M.G., Mountjoy, K.J., Smith, M.T., Currie, L.D., Gabites, J.E., Tipper, H.W., Orchard, M.J., Poulton, T.P., and Cordey, F., 1999. Geology and mineral resources of the Tagish Lake area (NTS 104M/ 8,9,10E, 15 and 104N/ 12W), northwestern British Columbia. British Columbia Ministry of Energy and Mines, British Columbia Geological Survey Bulletin 105, 217 p.
- Mihalynuk, M.G., Nelson, J.L., Friedman, R.M., Gleeson, T.P., and Roots, C.F., 2001. Geology of Gladys River (NTS 104N/16). British Columbia Ministry of Energy and Mines, British Columbia Geological Survey Open File 2001-04, 1:50,000 scale.
- Mihalynuk, M.G., Johnston, S.T., English, J.M., Cordey, F., Villeneuve, M.J., Rui, L., and Orchard, M.J., 2003. Atlin TGI Part II: Regional geology and mineralization of the Nakina area (NTS 104N/2W and 3). In: Geological Fieldwork 2002, British Columbia Ministry of Energy and Mines, British Columbia Geological Survey Paper 2003-01, pp. 9-37.
- Mihalynuk, M.G., Erdmer, P., Ghent, E.D., Cordey, F., Archibald, D.A., Friedman, R.M., and Johannson, G.G., 2004. Coherent French Range blueschist; subduction to exhumation in <2.5 m.y.. *Geological Society of America Bulletin*, 116, 910-922.
<<https://doi.org/10.1130/B25393.1>>
- Mihalynuk, M.G., Ambrose, T.K., Devine, F.A.M., and Johnston, S.T., 2011. Atlin placer gold nuggets containing mineral and rock matter: implications for lode gold exploration. In: Geological Fieldwork 2010, British Columbia Ministry of Forests, Mines and Lands, British Columbia Geological Survey Paper 2011-01, pp. 65-72.
- Mihalynuk, M.G., Zagorevski, A., Devine, F.A.M., and Humphrey, E., 2017. A new lode gold discovery at Otter Creek: Another source for the Atlin placers. In: Geological Fieldwork 2016, British Columbia Ministry of Energy and Mines, British Columbia Geological Survey Paper 2017-01, 179-193.
- Mihalynuk, M.G., Zagorevski, A., Milidragovic, D., Tsekhmistrenko, M., Friedman, R.M., Joyce, N., Camacho, A., and Golding, M., 2018. Geologic and geochronologic update of the Turtle Lake area, NTS 104M/16, northwest British Columbia. In: Geological Fieldwork 2017, British Columbia Ministry of Energy, Mines and Petroleum Resources, British Columbia Geological Survey, Paper 2018-01, 83-128.
- Mihalynuk, M.G., Milidragovic, D., Tsekhmistrenko, M., and Zagorevski, A., 2022. Turtle Lake area geology (NTS 104M/16). British Columbia Ministry of Energy, Mines and Low Carbon Innovation, British Columbia Geological Survey, Open File 2022-02, Geological Survey of Canada, Open File 8757, 1:50,000 scale.
- Mioduszewska, B.M., 1980. Drilling report on the VOL claim Atlin M.D., for Comino Ltd. British Columbia Ministry of Energy,

- Mines and Low Carbon Innovation, Assessment Report 8048, 17 p. <<https://apps.nrs.gov.bc.ca/pub/aris/Report/08048.pdf/>>
- Monger, J., 1975. Upper Paleozoic rocks of the Atlin Terrane, northwestern British Columbia and south-central Yukon. Geological Survey of Canada Paper 74-47, 63 p.
- Müller, A., Kirwin, D., and Seltmann, R., 2023. Textural characterization of unidirectional solidification textures related to Cu-Au deposits and their implication for metallogenesis and exploration. *Mineralium Deposita*, 58, 1211-1235. <<https://doi.org/10.1007/s00126-023-01175-x>>
- Murton, B.J., Lehrmann, B., Dutrieux, A.M., Martins, S., de la Iglesia, A.G., Stobbs, I.J., Barriga, F.J., Bialas, J., Dannowski, A., Vardy, M.E., and North, L.J., 2019. Geological fate of seafloor massive sulphides at the TAG hydrothermal field (Mid-Atlantic Ridge). *Ore Geology Reviews*, 107, 903-925.
- Pearce, J.A., Harris, N.B.W., and Tindle, A.G., 1984. Trace element discrimination diagrams for the tectonic interpretation of granitic rocks. *Journal of Petrology*, 25, 956-983. <<https://doi.org/10.1093/petrology/25.4.956>>
- Pinsent, R.H., 2005. Geological report on the Gladys Lake molybdenum property Atlin area. British Columbia Ministry of Energy, Mines and Low Carbon Innovation, Assessment Report 28276, 37 p. <<https://apps.nrs.gov.bc.ca/pub/aris/Report/28276.pdf/>> (accessed October 2023).
- Proudlock, P.J., and Proudlock, W.M., 1976. Stratigraphy of the placers in the Atlin placer mining camp. British Columbia, British Columbia Ministry of Energy and Mines, Miscellaneous Report, 71 p. <[BCGS_MR1976-01.pdf](https://www2.gov.bc.ca/gov/content/mines/BCGS_MR1976-01.pdf) (gov.bc.ca)> (accessed October 2023)
- Ray, G.E., Webster, I.C.L., Ballantyne, S.B., and Kilby, C.E., 2000. The geochemistry of three tin-bearing skarns and their related plutonic rocks, Atlin, northern British Columbia. *Economic Geology*, 95, 1349-1365. <<https://doi.org/10.2113/gsecongeo.95.6.1349>>
- Ristorcelli, S., Ronning, P., Bakker, F., and Eggert, J., 2022. Ruby Creek Project, northern British Columbia, Canada. Stuhini Exploration Ltd., 43-101 Technical Report, 148 p. <https://www.stuhini.com/s/43-101_Ruby_Creek_Resource_v21.pdf>
- Robertson, W.F., 1899. Cassiar district. In: Annual report of the Minister of Mines, 1898, Province of British Columbia, pp. 985-991.
- Sack, P.J., and Mihalynuk, M.G., 2004. Proximal gold-cassiterite nuggets and composition of the Feather Creek placer gravels: clues to a lode source near Atlin, B.C. In: Geological Fieldwork 2003, British Columbia Ministry of Energy, Mines and Petroleum Resources, British Columbia Geological Survey Paper 2004-01, pp. 147-161.
- Shannon, J.R., Walker, B.M., Carten, R.B., and Geraghty, E.P., 1982. Unidirectional solidification textures and their significance in determining relative ages of intrusions at the Henderson Mine, Colorado. *Geology*, 10, 293-297. <[https://doi.org/10.1130/0091-7613\(1982\)10<293:USTATS>2.0.CO;2](https://doi.org/10.1130/0091-7613(1982)10<293:USTATS>2.0.CO;2)>
- Smith, J.L., 2009. A Study of the Adanac porphyry molybdenum deposit and surrounding placer gold mineralization in northwest British Columbia with a comparison to porphyry molybdenum deposits in the North American Cordillera and igneous geochemistry of the Western United States. Unpublished M.Sc. thesis, University of Nevada, Reno, Nevada, 198 p.
- Smith, J.L., and Arehart, G.B., 2009. Isotopic Investigation of the Adanac Porphyry Molybdenum Deposit in Northwestern British Columbia (NTS 104N/11): Final Project Report. In: Geoscience BC Summary of Activities 2009, Geoscience BC, Report 2010-1, pp. 115-126.
- Tallman, A.M., 1975. The Glacial and periglacial geomorphology of the Fourth of July Creek Valley, Atlin region, Cassiar district, northwestern British Columbia. Unpublished Ph.D. thesis, Michigan State, Michigan, 204 p.
- Terry, J., 1977. Geology of the Nahlin ultramafic body, Atlin and Tulsequah map-areas, northwestern British Columbia. In: Report of Activities, Part A, Geological Survey of Canada Paper 77-1A, pp. 263-266. <<https://doi.org/10.4095/102697>>
- Watson, K.D., and Mathews, W.H., 1944. The Tuya-Teslin area, northern British Columbia. British Columbia Department of Mines, Bulletin 17, 11 p.
- Whalen, J.B., Currie, K.L., and Chappell, B.W., 1987. A-type granites: geochemical characteristics, discrimination and petrogenesis. *Contributions to Mineralogy and Petrology*, 95, 407-419. <<https://doi.org/10.1007/BF00402202>>
- Woodsworth, G.J., Anderson, R.G., Armstrong, R.L., Struik, L.C., and van der Heyden, P., 1992. Plutonic regimes. In: Gabrielse, H. and Yorath, C.J., (Eds.), *Geology of the Cordilleran Orogen in Canada, Geology of North America, Volume G-2*, pp. 493-531. <<https://doi.org/10.1130/DNAG-GNA-G2.491>>
- Zagorevski, A., Corriveau, A.S., McGoldrick, S., Bédard, J.H., Canil, D., Golding, M.L., Joyce, N., and Mihalynuk, M.G., 2015. Geological framework of ancient oceanic crust in northwestern British Columbia and southwestern Yukon, GEM 2 Cordillera, Geological Survey of Canada, Open File 7957, 12 p. <<https://doi.org/10.4095/297273>>
- Zagorevski, A., Mihalynuk, M.G., McGoldrick, S., Bédard, J.H., Golding, M., Joyce, N.L., Lawley, C., Canil, D., Corriveau, A.S., Bogatu, A., and Tremblay, A., 2016. Geological framework of ancient oceanic crust in northwestern British Columbia and southwestern Yukon, GEM 2 Cordillera, Geological Survey of Canada, Open File 8140, 15 p. <<https://doi.org/10.4095/299196>>
- Zagorevski, A., Mihalynuk, M.G., Joyce, N.J., and Anderson, R.G., 2017. Late Cretaceous magmatism in the Atlin-Tagish area, northern British Columbia (104M, 104N). In: Geological Fieldwork 2016, British Columbia Ministry of Energy and Mines, British Columbia Geological Survey, Paper 2017-01, pp. 133-152.
- Zagorevski, A., van Staal, C.R., Bédard, J.H., Bogatu, A., Canil, D., Coleman, M., Golding, M., Joyce, N.L., Lawley, C., McGoldrick, S., Mihalynuk, M.G., Milidragovic, D., Parsons, A., and Schiarizza, P., 2021. Overview of Cordilleran oceanic terranes and their significance for the tectonic evolution of the northern Cordillera. In: Ryan, J.J. and Zagorevski, A., (Eds.), *Northern Cordillera geology: a synthesis of research from the Geo-mapping for Energy and Minerals program*, British Columbia and Yukon. Geological Survey of Canada, Bulletin 610, 21-65. <<https://doi.org/10.4095/326053>>

Upper Hazelton Group stratigraphy along the Stikine arch, northwestern British Columbia



Bram I. van Straaten^{1, a}

¹ British Columbia Geological Survey, Ministry of Energy, Mines and Low Carbon Innovation, Victoria, BC, V8W 9N3

^a corresponding author: Bram.vanStraaten@gov.bc.ca

Recommended citation: van Straaten, B.I., 2024. Upper Hazelton Group stratigraphy along the Stikine arch, northwestern British Columbia. In: *Geological Fieldwork 2023*, British Columbia Ministry of Energy, Mines and Low Carbon Innovation, British Columbia Geological Survey Paper 2024-01, pp. 149-177.

Abstract

This paper presents new stratigraphic studies of the upper Hazelton Group (late Early to Middle Jurassic) along the Stikine arch, part of the Stikine terrane in northwestern British Columbia. Detailed maps, composite stratigraphic sections, lithological descriptions, contact relationships, and preliminary geochronological data are presented for four areas along the Stikine arch (Stikine batholith, Mount Blair, Spatsizi, and Yehiniko Lake areas), and compared to recent studies in the Dease Lake area.

The upper Hazelton Group unconformably overlies Late Triassic volcano-plutonic centres of the Stuhini arc. The unconformity spans at least 30 m.y. and indicates a prolonged period of uplift and erosion of the Stuhini arc that followed cessation of subduction and termination of arc activity in the latest Triassic. Thick (1-5 km) successions of upper Hazelton Group rocks extend for at least ~275 km along the Stikine arch. We apply uniform stratigraphic nomenclature to these rock units, which include basal sedimentary rocks of the Spatsizi Formation, and overlying volcanic rocks of the Horn Mountain Formation. Volcano-sedimentary units are lithologically similar along the entire length of the belt, and typically include basal granitoid clast-bearing conglomerates, overlain by marine siliciclastic sedimentary rocks that grade upward into subaqueous green mafic fragmental volcanic to reworked volcanic rocks. Thick overlying successions of maroon to grey, mafic to intermediate flows and fragmental volcanic rocks are found in all study areas and indicate the formation of subaerial volcanic centres. Preserved parts of the uppermost succession include subaerial felsic volcanic rocks, locally overlain by mafic volcanic rocks. The thickest successions are in the centre of the belt (>4.8 km), with thinner successions in the west and east (>0.7-1 km). The onset of sedimentary deposition atop the basal unconformity is constrained by late Pliensbachian to early Toarcian fossils, with the start of voluminous volcanism constrained by modern high-precision U-Pb zircon geochronology to ca. 185 Ma (latest Pliensbachian) in the southwest, ca. 175 Ma (latest Toarcian) in the centre, and before ca. 172 Ma (Aalenian) in the east. The general pattern is permissive of an eastward younging trend in the onset of upper Hazelton Group deposition atop the Stuhini arc. Horn Mountain volcanism in the southwest continued until at least the end of the Toarcian, but a lack of modern age dates and faulted or eroded top contacts preclude a confident interpretation. The end of Horn Mountain volcanism in the centre of the belt is well-constrained at ca. 171 Ma (latest Aalenian). Upper Hazelton Group volcanism occurred during accretion of the Quesnel, Cache Creek, and Stikine terranes to Ancestral North America, and was probably generated by re-melting of subduction-modified lithosphere during accretion.

The upper Hazelton Group is overlain by the Bowser Lake Group, where marine siliciclastic sedimentary rocks in the western and central parts of the Stikine arch (early Bajocian and younger) give way eastward to interstratified subaerial mafic volcanic and siliciclastic rocks of the newly defined Mount Blair Formation (ca. 171 Ma and younger). These successions represent the oldest preserved Bowser Lake Group and mark the onset of deposition of erosional products from the Stikinia-Cache Creek tectonic welt.

Keywords: Stratigraphy, upper Hazelton Group, Bowser Lake Group, Spatsizi Formation, Horn Mountain Formation, Mount Blair Formation, Stikine plutonic suite, Stuhini Group, Triassic, Jurassic, Stikinia, Stikine arch, Stuhini arc, Stikine batholith area, Mount Blair area, Spatsizi area, Yehiniko Lake area

1. Introduction

This paper focuses on arc-like volcanic successions in the upper Hazelton Group along the Stikine arch (Stikine terrane), in northwestern British Columbia on the traditional lands of the Tahltan First Nation (Fig. 1). Within Stikine terrane, upper Hazelton Group successions have previously been described as predominantly sedimentary (Gagnon et al., 2012). However, recent studies suggest that significant arc-like volcanic rocks are in the Dease Lake area of the Stikine arch (Fig. 2; van Straaten et al., 2022b, and references therein). Presented herein are stratigraphic studies of the upper Hazelton Group from four additional locations along the Stikine arch (Figs. 1, 2) that were carried out during a total of three weeks of fieldwork

between 2016 and 2019. The field studies and preliminary geochronology data show that thick (1-4 km) arc-like volcanic successions extend for at least ~275 km along the Stikine arch. The latest Pliensbachian to Aalenian (ca. 185-171 Ma) mafic to intermediate, and rare felsic volcanic rocks show remarkably similar rock types and facies along the entire Stikine arch. We interpret these successions to have formed during collision of Stikinia and intervening Intermontane terranes with Ancestral North America.

2. Geological setting

The Stikine arch is in the multi-episodic Stikine island arc terrane (Stikinia), in which volcano-sedimentary rocks of the

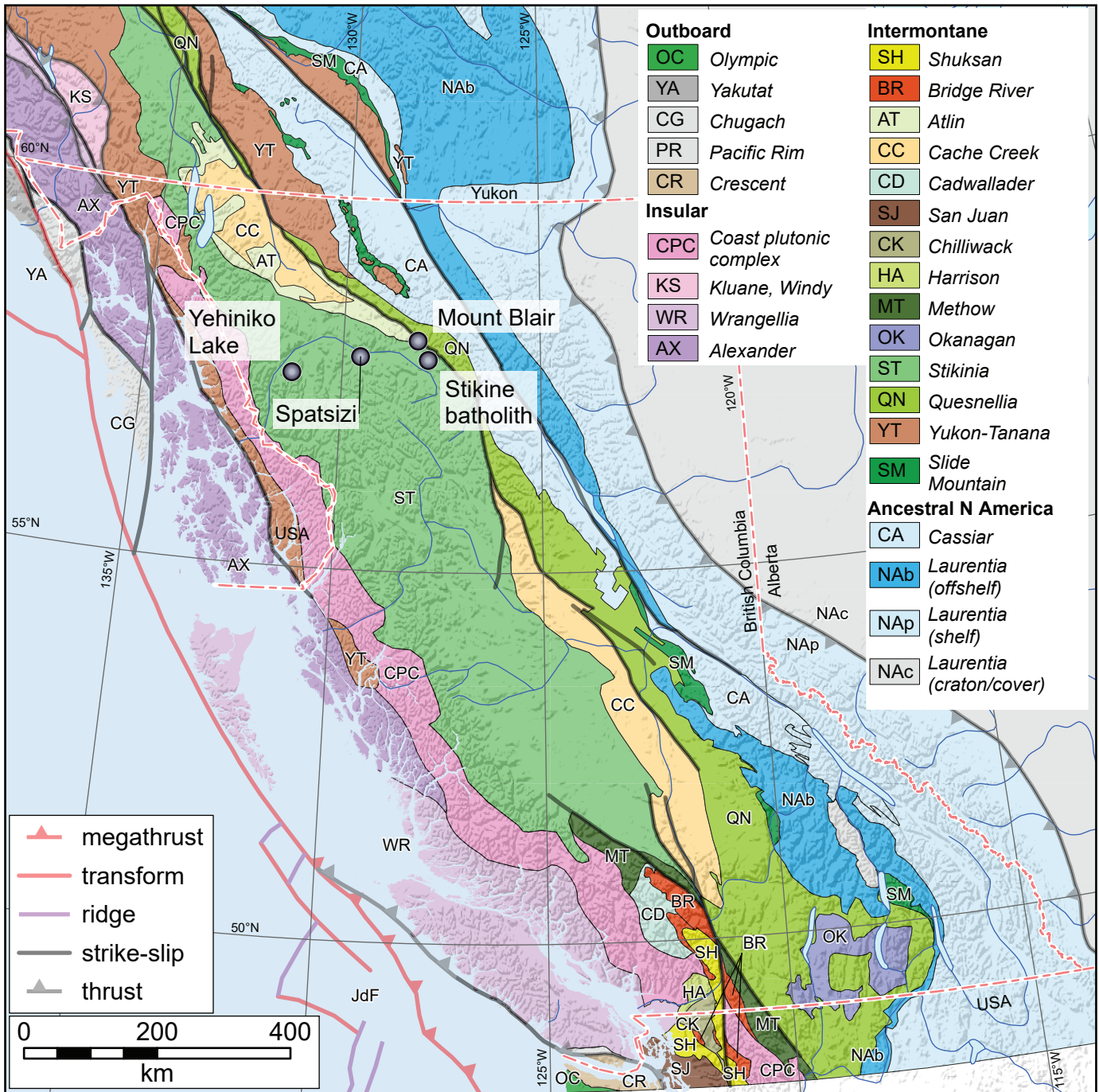


Fig. 1. Location of Stikine batholith, Mount Blair, Dease Lake, Spatsizi, and Yehiniko Lake areas in Stikine terrane. Terranes modified from Colpron (2020).

Stikine assemblage (Devonian to Permian) are overlain by the Stuhini Group (Upper Triassic) and the Hazelton Group (uppermost Triassic to Middle Jurassic). These successions are bounded by regional unconformities that mark significant deformation including: 1) poorly characterized Permo-Triassic deformation that affects Paleozoic rocks (Logan and Koyanagi, 1994); 2) latest Triassic deformation that affects Stuhini Group and older strata throughout northwestern British Columbia, and has been attributed to collision between the

Yukon-Tanana and Stikine terranes (Nelson et al., 2022); and 3) a Middle to early Late Jurassic fold-and-thrust belt along the northeastern margin of Stikinia, formed due to accretion of Stikinia and intervening Intermontane terranes to Ancestral North America (Mihalynuk et al., 1994; Nelson et al., 2013; van Straaten et al., 2022b). Accretion of Stikinia to inboard terranes and the Ancestral North American margin is recorded by deposition of Bowser Lake Group siliciclastic rocks (Middle Jurassic to mid-Cretaceous) in a foreland basin atop

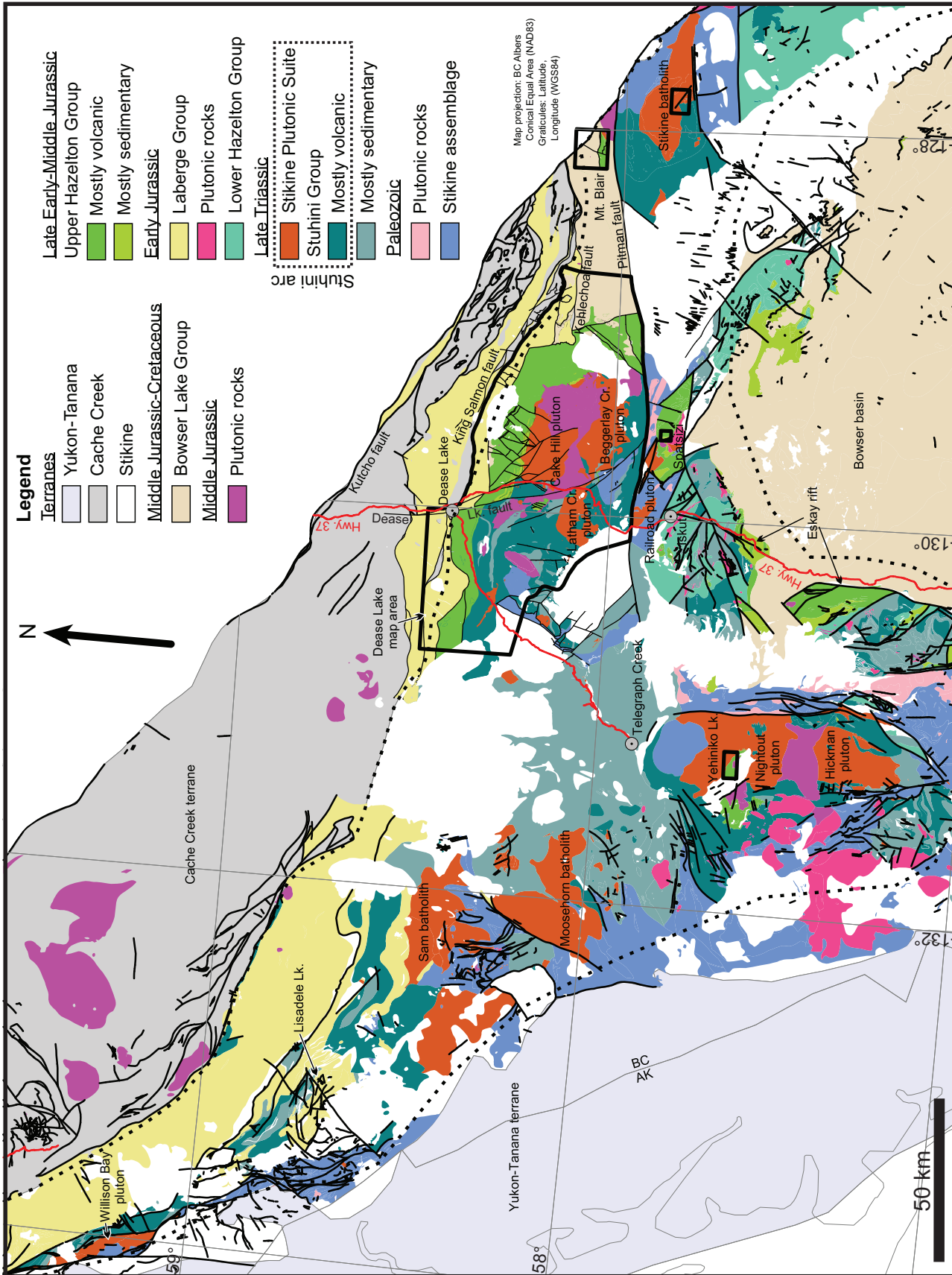


Fig. 2. Geological map of northwestern British Columbia, showing four study areas discussed herein, and outline of Dease Lake area map by van Straaten et al. (2020b). The map shows Paleozoic to Jurassic units of Stikinia, and Whitehorse trough overlap assemblage and post-accretionary plutons (latest Triassic to Middle Jurassic) in Cache Creek terrane. Younger units, and units on other terranes, are omitted. Modified from Cui et al. (2017).

Stikinia (Evenchick et al., 2007). Bowser Lake Group and older rocks are deformed by Cretaceous Skeena fold-and-thrust belt deformation linked to continued convergence between accreted terranes and Ancestral North America (Evenchick et al., 2007). The Stikine arch is a loosely defined area that exposes Triassic and older rocks of Stikinia between the Coast Plutonic complex, Cache Creek terrane, and the northern margin of the contiguous Bowser basin (e.g., Souther, 1971). It is characterized by Stikine plutonic suite intrusions (Late Triassic) and older rocks that were topographically elevated in the Early Jurassic (Gabrielse, 1998).

The main axis of Late Triassic magmatism in Stikinia (hereafter referred to as the Stuhini arc) is defined by thick accumulations of predominantly mafic volcanic strata assigned to the Lewes River Group in Yukon, Stuhini Group in northwestern and central British Columbia, and Takla Group in north-central British Columbia. These strata are accompanied by ca. 229–216 Ma Stikine plutonic suite intrusions. These volcanic and intrusive rocks extend for at least ~1300 km along the eastern margin and northern part of Stikinia and have been interpreted to have formed as an east-facing arc (Nelson and van Straaten, 2020; van Straaten et al., 2023).

Stuhini arc activity terminated in latest Triassic by a collision between northern Stikinia and the Yukon-Tanana terrane. This collision is expressed by: 1) the latest dated Stuhini arc magmatism at ca. 216 Ma (van Straaten et al., 2022b); 2) latest Triassic shortening of the Stuhini Group and older strata throughout northwestern British Columbia (Henderson et al., 1992; Rhys, 1993; Brown et al., 1996; Nelson et al., 2018); 3) a regional-scale unconformity between the Stuhini and Hazelton groups (Nelson et al., 2018; Nelson et al., 2022); 4) a ca. 9–12 m.y. magmatic gap south of the Stikine arch in the Kitsault, Stewart to Iskut corridor (ca. 216 to 207–204 Ma; Hollis and Bailey, 2013; Miller et al., 2023; Campbell, 2021); 5) an at least 30 m.y. magmatic gap along the Stikine arch (ca. 216 to 185–175 Ma; Brown et al., 1996; van Straaten et al., 2022b); 6) crustal thickening and burial of Yukon-Tanana terrane to amphibolite facies in southern Yukon, and coincident ca. 205–194 Ma mid- to lower-crustal magmatism along the Yukon-Tanana-Stikinia suture in southern Yukon (Colpron et al., 2022); and 7) deposition of siliciclastic sedimentary strata of the Laberge Group (Early Jurassic) in the syn-collisional Whitehorse trough (Colpron et al., 2015, 2022; van Drecht et al., 2022).

Within the Kitsault, Stewart to Iskut corridor, the Stuhini Group is overlain by intermediate and rare felsic volcanic rocks of the lower Hazelton Group (Rhaetian to Pliensbachian; Nelson et al., 2018). The Tatogga and Texas Creek plutonic suites (latest Triassic to Early Jurassic) are coeval and comagmatic with the lower Hazelton Group and are responsible for the formation of numerous porphyry Cu-Au and epithermal Au-Ag deposits (Nelson and van Straaten, 2020).

The upper Hazelton Group in the Kitsault, Stewart to Iskut corridor comprises sedimentary rocks of the Spatsizi and Quock formations (Gagnon et al., 2012), local bimodal volcanic and

sedimentary rocks of the Iskut River Formation within the Eskay rift (Nelson et al., 2018), and minor volcanic rocks of the Eddontenajon formation (Nelson et al., 2018), Mount Dilworth Formation (Alldrick, 1993), and Kitsault unit (Miller et al., 2023). Recent studies in the Dease Lake area of the Stikine arch have identified thick successions of arc-like volcanic rocks of the Horn Mountain Formation (van Straaten et al., 2022b, and references therein). Similar rocks elsewhere along the Stikine arch are the subject of this study.

3. Field results

Below I describe volcano-sedimentary successions in the upper Hazelton Group from four areas along the Stikine arch: Stikine batholith, Mount Blair, Spatsizi, and Yehiniko Lake (Fig. 2). All areas expose Spatsizi Formation sedimentary rocks and/or Horn Mountain Formation volcanic rocks, both part of the upper Hazelton Group (van Straaten et al., 2022b).

3.1. Stikine batholith area

The Stikine batholith area is approximately 145 km southeast of Dease Lake (Fig. 2). Regional 1:250,000-scale mapping identified an approximately 400 km² plutonic body cutting volcanic rocks of the Stuhini Group (Gabrielse et al., 1977; Cui et al., 2017), and a granitoid clast-bearing conglomerate of unknown age that locally rests unconformably above the plutonic rocks (Anderson, 1984). The plutonic body was named the Stikine batholith by Anderson (1984) and interpreted as Late Triassic based on ca. 222–213 K-Ar hornblende cooling ages, ca. 215–204 Ma K-Ar biotite cooling ages (Wanless et al., 1979; Hunt and Roddick, 1987), and lithological similarities to better constrained Late Triassic plutons elsewhere along the Stikine arch (Anderson, 1984).

New mapping in the south-central portion of the Stikine batholith (Fig. 3) indicates that the area is cut by a northwest-trending fault, marked by an at least 200 m-wide foliated zone. Fabrics dip steeply towards the southwest and rarely steeply to the northeast. This fault separates mafic volcanic rocks of the Stuhini Group (Upper Triassic) to the southwest from granitoids of the Stikine batholith (Late Triassic) to the northeast. The circular outlier of conglomerate and sandstone that rests above the Stikine batholith is assigned to the Spatsizi Formation, and mafic dikes that cut the conglomerate are inferred to be related to the Horn Mountain Formation.

3.1.1. Stuhini Group

The southern half of the map area exposes mafic volcanic rocks (unit uTrSvm) and minor intercalated sedimentary rocks (unit uTrSs) of the Stuhini Group (Upper Triassic; Fig. 3). In the west these strata dip moderately to steeply to the south-southeast to southwest. The mafic volcanic rocks are phyllitic adjacent to the northwest-trending fault, locally with the foliation wrapping around volcanic clasts or augite porphyroclasts.

3.1.2. Stikine plutonic suite

The Stikine plutonic suite is represented mainly by granitic rocks of the Stikine batholith (unit LTrSgg), but also includes plagioclase porphyritic hypabyssal intrusions of presumed Late Triassic age (unit LTrSh) that cut mafic volcanic rocks of the Stuhini Group in the western part of the map area (Fig. 3). The Stikine batholith is a porphyritic (rarely equigranular) monzogranite and locally displays a flow foliation. Tectonic foliation adjacent to the northwest-trending fault is defined by flattened quartz and mafic minerals, and local cm-wide planar bands of significantly reduced grain size (Fig. 4); subparallel tectonic fabrics are locally developed elsewhere in the batholith. A sample from a quartz and K-feldspar porphyritic monzogranite returned a CA-TIMS U-Pb zircon age of 218.89 ± 0.12 Ma (sample 17BvS-33-320; B. van Straaten and R. Friedman, unpublished data). The Late Triassic plutonic rocks of the Stikine batholith have been described to locally intrude the mafic volcanic rocks of the Stuhini Group (Anderson, 1984).



Fig. 4. Planar tectonic fabric defined by zones of significantly reduced grain size in monzogranite (unit LTrSgg) of the Stikine batholith.

3.1.3. Spatsizi Formation

A circular outlier of conglomerate and sandstone in the centre of the map area (unit ImJSsc, Figs. 3, 5, 6), about 375 m in diameter, is inferred to unconformably overlie the Stikine batholith. The unit is assigned to the Spatsizi Formation. Along the western margin of the outlier, a 2 m covered interval separates monzogranite from conglomerate and sandstone beds (Figs. 5, 7a, b) that dip 77° to 60° to the southeast. In the north, intact granitoid country rock transitions to highly fractured granitoid and then into polymictic cobble-boulder conglomerate. The sedimentary rocks are interpreted to post-date the granitoid, based on the presence of predominantly monzogranite clasts similar to the adjacent granitoid and a lack of evidence for a faulted or intrusive contact. The conglomerate contains subordinate angular to subangular, green mafic volcanic clasts, locally with lobate margins (Fig. 7c), suggesting

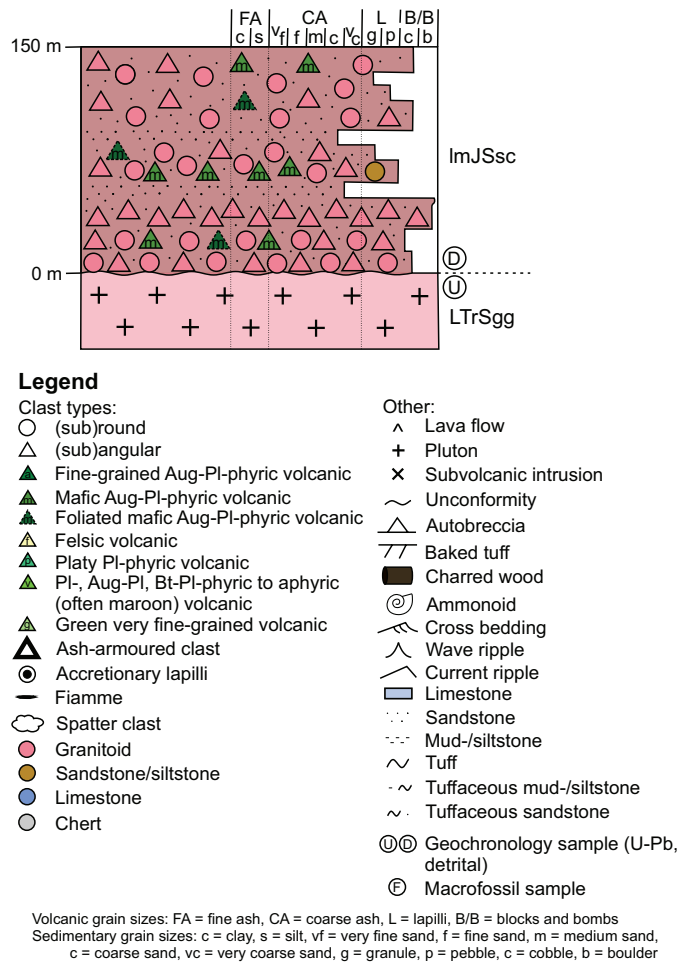


Fig. 5. Schematic stratigraphic section for the Stikine batholith area. See Figure 3 for location of stratigraphic section.

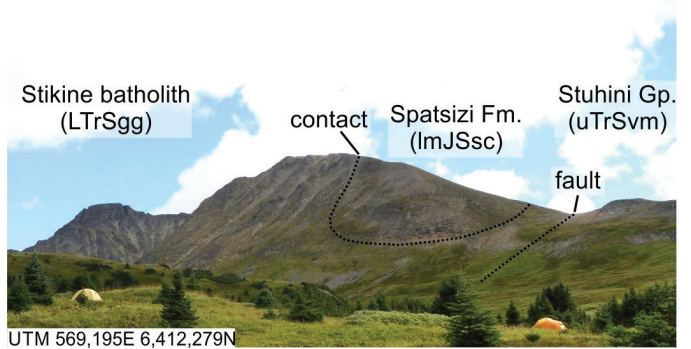


Fig. 6. Panoramic view of the Spatsizi Formation conglomerate and sandstone unit (ImJSsc) unconformably atop of monzogranite of the Stikine batholith (LTrSgg), faulted against Stuhini Group mafic volcanic rocks (unit uTrSvm). View towards the northeast. Stikine batholith area.

coeval volcanic activity. However, one 1.5 m angular clast is a plutonic rock cut by a green mafic dike, suggesting that at least some of the mafic clasts may have been derived from erosion of mafic dikes. Clasts appear largely locally derived, and the presence of minor phyllitic mafic volcanic and foliated

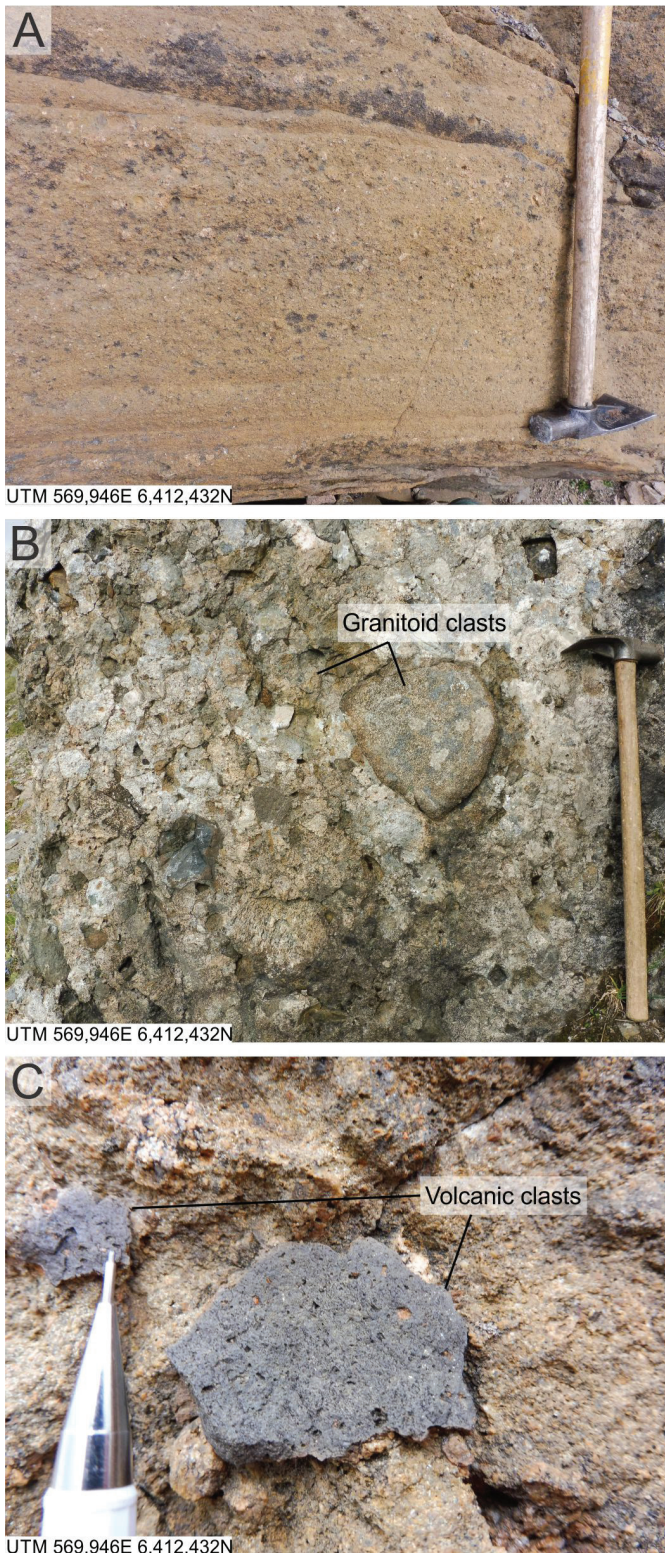


Fig. 7. Spatsizi Formation conglomerate and sandstone unit (1mJSSc). **a)** Stratified pebbly sandstone. **b)** Conglomerate with predominantly granitoid clasts. **c)** Mafic volcanic clasts with lobate margins in conglomerate. Stikine batholith area.

plutonic clasts suggests deformation pre-dates deposition of the conglomerate. A sandstone sample returned a ca. 215 Ma LA-ICP-MS U-Pb detrital zircon maximum depositional age (Fig. 3; sample 17BvS-33-317c; B. van Straaten and R. Friedman, unpublished data). Correlation with the Spatsizi Formation (Lower to Middle Jurassic, upper Hazelton Group) is based on a strong similarity to basal Spatsizi Formation granitoid clast-bearing conglomerate unconformably atop the Stikine plutonic suite in the Dease Lake map area (see van Straaten et al., 2022b).

3.1.4. Horn Mountain Formation dikes

Green augite-plagioclase-phyric mafic dikes (unit EMJhm, Fig. 3) locally cut the Spatsizi Formation. Potentially similar clinopyroxene-hornblende porphyry dikes crosscut the Stikine batholith (Anderson, 1984). Petrographic studies and litho-geochemical data show that they are similar to mafic subvolcanic feeders to the upper Hazelton Group in the Dease Lake map area (van Straaten et al., 2022a, b). The dikes are therefore inferred to be mafic subvolcanic intrusions related to the Horn Mountain Formation. Mafic dike clasts and mafic volcanic clasts in the Spatsizi Formation conglomerate (see above) are lithologically and geochemically similar to the mafic dikes and suggest that upper Hazelton Group mafic volcanism occurred before, during and after deposition of the conglomerate.

3.2. Mount Blair area

The Mount Blair area is 120 km east-southeast of Dease Lake, north of the Pitman fault and west of the terrane-bounding Kutcho fault (Fig. 2). The region was previously mapped at 1:250,000 scale by Gabrielse (1998; 2003), who distinguished a volcanic unit and a sedimentary unit both assigned to the Bowser Lake Group. A compositionally variable intrusive body in the southeastern part of the map area (Fig. 8) was previously mapped as syenite, monzonite, diorite, quartz monzonite, and granodiorite (Erdman, 1978; Gabrielse, 1998; Gabrielse, 2003). The intrusion was considered Middle to Late Jurassic based on a 162 ± 12 Ma K-Ar hornblende cooling age from a biotite-bearing hornblende diorite (Erdman, 1978; recalculated using IUGS decay constants by Breitsprecher and Mortensen, 2004).

Based on the current work and following nomenclature in van Straaten et al. (2022b), the volcano-sedimentary rocks in the southern part of the area are reassigned to the Spatsizi Formation and Horn Mountain Formation of the upper Hazelton Group (Lower to Middle Jurassic), and volcano-sedimentary rocks in the northern part of the map are assigned to the Mount Blair Formation (new formation, see below) of the Bowser Lake Group (Middle to Upper Jurassic). The northeastern granodioritic portion of the compositionally variable intrusive body is here interpreted as part of the Stikine plutonic suite (Late Triassic), the central part as intermediate subvolcanic intrusions that fed Horn Mountain Formation volcanic rocks (Early to Middle Jurassic) and the southeastern part as a younger dioritic pluton (Middle to Late Jurassic).

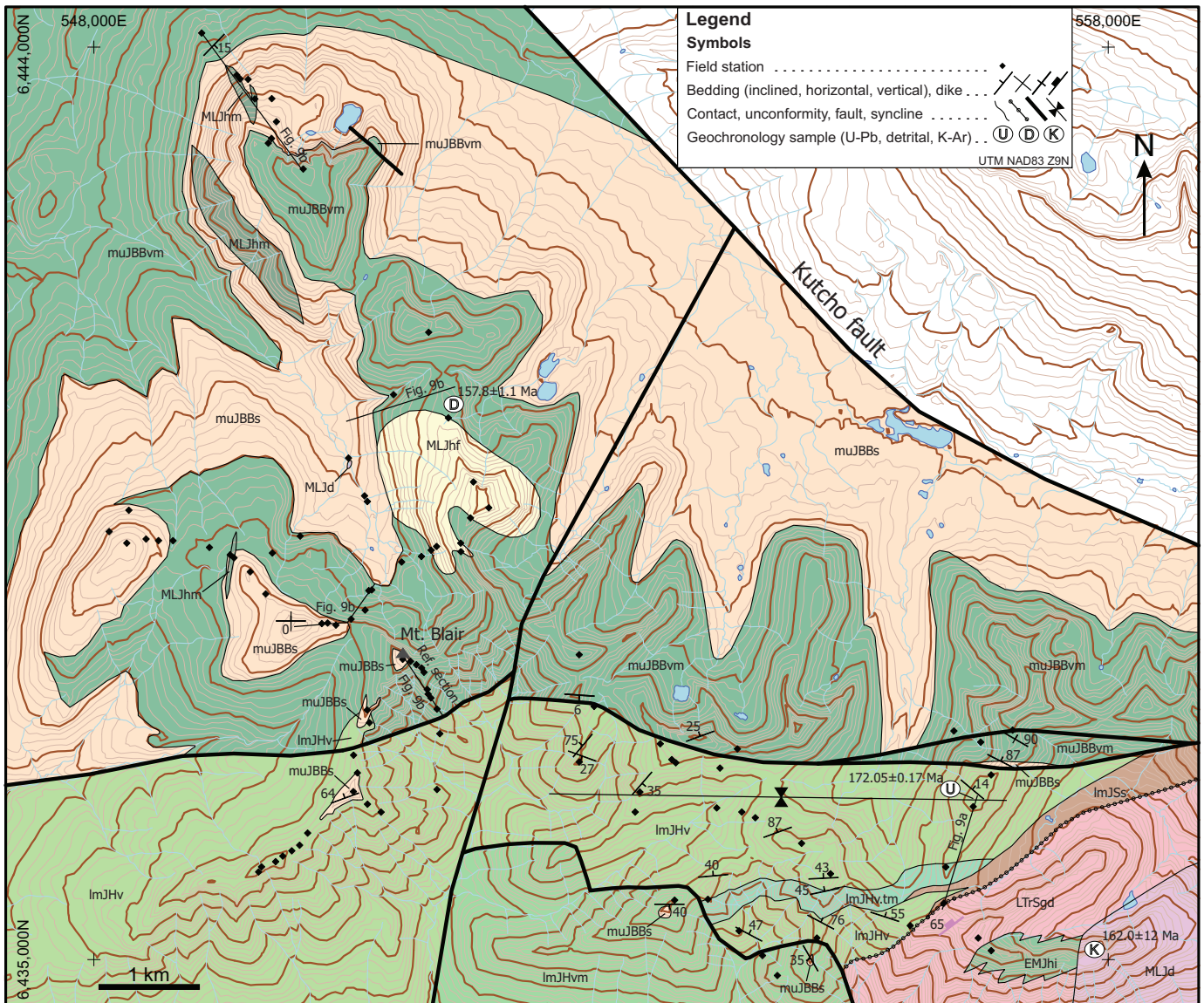


Fig. 8. Geological map of the Mount Blair area, incorporating data from Erdman (1978), Gabrielse (1998; 2003), Cui et al. (2017), and this study.

The revised geological map of the Mount Blair area (Fig. 8) shows the area is transected by several faults. The southern part of the map area exposes a subvertical west-striking fault that separates subhorizontal volcano-sedimentary rocks of the Bowser Lake Group (north) from sedimentary and volcanic rocks of the upper Hazelton Group (south). In the central part of the map area, this fault has a minor apparent dextral offset across a northerly-trending fault and continues east where it is inferred to bifurcate and enclose a lens of unusually steeply dipping Bowser Lake Group strata. The west-striking fault may represent a north-side-down normal fault, based on the steep to subvertical attitude and younger rocks on its northern side. It is similar in orientation and inferred kinematics to a west-southwest-trending normal fault in the southeastern portion of the Dease Lake map area (van Straaten et al., 2022b). In the southeast part of the map area is an inferred fault with a

moderate south-southwest dip. Hanging wall strata dip to the southwest and comprise mafic volcanic rocks of the Horn Mountain Formation (unit ImJHvm; see below) that are locally capped by sedimentary rocks of the Bowser Lake Group (Fig. 8). Footwall mafic to intermediate volcanic strata of the Horn Mountain Formation (unit ImJHv) are folded in a km-scale open syncline. Bedding attitudes in the southwestern fault block are subhorizontal in the north to unknown in the south.

3.2.1. Stikine plutonic suite

A biotite-bearing granodiorite pluton is exposed in the southeastern part of the Mount Blair area (unit LTrSgd, Fig. 8). It was previously interpreted as part of a compositionally variable Middle to Late Jurassic intrusive body, but is reassigned here to the Stikine plutonic suite (Late Triassic) based on unconformable relationships with overlying upper

MIDDLE TO LATE JURASSIC

MLJd Diorite, rare quartz monzodiorite and quartz monzonite; medium grained; biotite and/or hornblende; resistive; 162 ± 12 Ma K-Ar hornblende cooling age.

— — — — — intrusive contact — — — — —

Bowser Lake Group

Mount Blair Formation

MLJhf Felsic subvolcanic intrusions; yellow to orangey; aphanitic to plagioclase-phyric; often flow banded; rare marginal autobreccia; moderately resistant; interpreted as subvolcanic feeders to the Mount Blair Formation.

MLJhm Mafic subvolcanic dikes; intrusions contain 20-25% augite (0.2-2 mm) and 40-55% plagioclase (0.05-4 mm) phenocrysts; resistant; interpreted as subvolcanic feeders to the Mount Blair Formation.

muJBBs Siltstone, sandstone, and conglomerate; grey, yellowish grey, maroon, sea green; common very fine- to fine-grained sandstone, rare medium- to very coarse-grained sandstone with common black lustrous organic material; pebble to granule conglomerate contains chert and rare limestone clasts; very rare, laminated limestone bed near base; resistant knobably-weathering conglomerate beds form distinct bands in hillside; largely subaerial depositional environment.

muJBBvm Mafic flows and lapillistone; lesser mafic lapilli-tuff, tuff, tuff breccia and siltstone; rare reworked volcanic rocks; very rare limestone; orangey to medium grey, green, maroon; flows and clasts contain 15-25% augite (0.1-1 mm) and 15-55% plagioclase (0.1-0.2, rarely up to 1.5 mm) phenocrysts, and up to 5% amygdules (0.1-2 cm); locally minor felsic volcanic clasts; rare chert clasts; well-stratified; 5-40 m thick bedding parallel coherent intervals interpreted as flows based on common autobrecciated lower (rarely, upper) contact, and rare underlying brick red baked tuff; resistant flows form distinct bands in hillside; ca. 158 Ma U-Pb detrital zircon maximum depositional age; largely subaerial depositional environment.

LATE EARLY TO MIDDLE JURASSIC

Upper Hazelton Group

Horn Mountain Formation

EMJhi Horn Mountain intrusions: Intermediate subvolcanic intrusions; contain 20% plagioclase (1-4 mm) phenocrysts in an often pink-coloured aphanitic groundmass; resistive; interpreted as subvolcanic feeders to the Horn Mountain Formation.

ImJHvm Glacial Mountain unit: Lapilli-tuff; medium to light grey; contains predominantly medium-grey clasts with 25-30% plagioclase (1-5 mm) and 10% augite (0.5-1 mm) phenocrysts, subordinate lighter grey clasts with finer-grained plagioclase and augite phenocrysts, and pink fine-grained to aphanitic clasts; set in a matrix with abundant plagioclase crystals, lesser augite crystals, and fine ash; massive; resistive.

ImJHv.tm Cariboo unit: Intermediate coherent flows and/or subvolcanic intrusions, tuff breccia, rare crystal tuff and sandstone; coherent rocks and clasts contain 35% platy plagioclase (0.5-1.5 cm) phenocrysts; massive; resistive.

ImJHv Sister Mary unit: Mafic to intermediate lapilli-tuff, crystal tuff, tuff and lapillistone; lesser coherent flows and/or subvolcanic intrusions; rare felsic lapilli-tuff; very rare limestone; maroon, greenish grey, brick red; volcanic clasts are plagioclase-phyric, biotite-plagioclase-phyric, augite-plagioclase-phyric to aphyric; subordinate pink biotite-bearing possible (quartz) monzonite clasts, rare limestone clasts; coherent rocks are augite-plagioclase-phyric or biotite-plagioclase-phyric; unit includes subordinate fine-grained augite-plagioclase-phyric volcanic rocks (resembling unit muJBBvm); felsic lapilli-tuff contains plagioclase-phyric to aphyric volcanic clasts, and is locally welded; crudely stratified; resistive to moderately resistive; felsic volcanic rocks returned 172.05 ± 0.17 Ma U-Pb zircon age; predominantly subaerial depositional environment.

Spatsizi Formation

ImJSs Sandstone and basal conglomerate; dark brown to grey; basal pebble to cobble conglomerate with subround to subangular granitoid clasts set in a matrix with granule- to sand-sized granitoid-derived grains; conglomerate unconformably overlies granodiorite pluton; very fine- to fine-grained sandstone; stratified; recessive and poorly exposed.

— — — — — unconformity — — — — —

LATE TRIASSIC

Stikine Plutonic Suite

LTrSgd Granodiorite, rare quartz monzodiorite and quartz monzonite; medium grained, equigranular; biotite-bearing; moderately resistive.

Fig. 8. Continued. Legend.

Hazelton Group strata (Lower to Middle Jurassic) and lithological similarity to hornblende and/or biotite granodiorite and monzogranite of the Stikine plutonic suite elsewhere along the Stikine arch (e.g., Stikine batholith, unit LTrSgg, see Section 3.1.2.; Cake Hill pluton, unit LTrSgg, van Straaten et al., 2022b; Nightout pluton, unit LTrSgd, see Section 3.4.1.; Hickman pluton, Brown et al., 1996).

3.2.2. Spatsizi Formation

A sedimentary unit assigned to the Spatsizi Formation (Early to Middle Jurassic, unit ImJSs) unconformably overlies granodiorite of the Stikine plutonic suite in the southeast part of the map area (Figs. 8, 9a). The unconformity is exposed at 556,379E-6,435,556N (UTM NAD83 zone 9 north). As the

contact is approached, the plutonic rocks become increasingly more weathered and recessive. At the contact, the pluton is overlain by a thin (<5 m) conglomerate unit with granitoid clasts (Fig. 10), which grades up into recessive and poorly exposed sandstone. The section above the unconformity includes a 55 m-thick interval of fragmental volcanic rocks that we assign to the Horn Mountain Formation (Fig. 9a; unit ImJHv, see below), reflecting interfingering relationships between the two units.

3.2.3. Horn Mountain Formation

The upper Hazelton Group in the southern part of the Mount Blair area is represented mainly by volcanic rocks of the Horn Mountain Formation. Most rocks of the formation are assigned

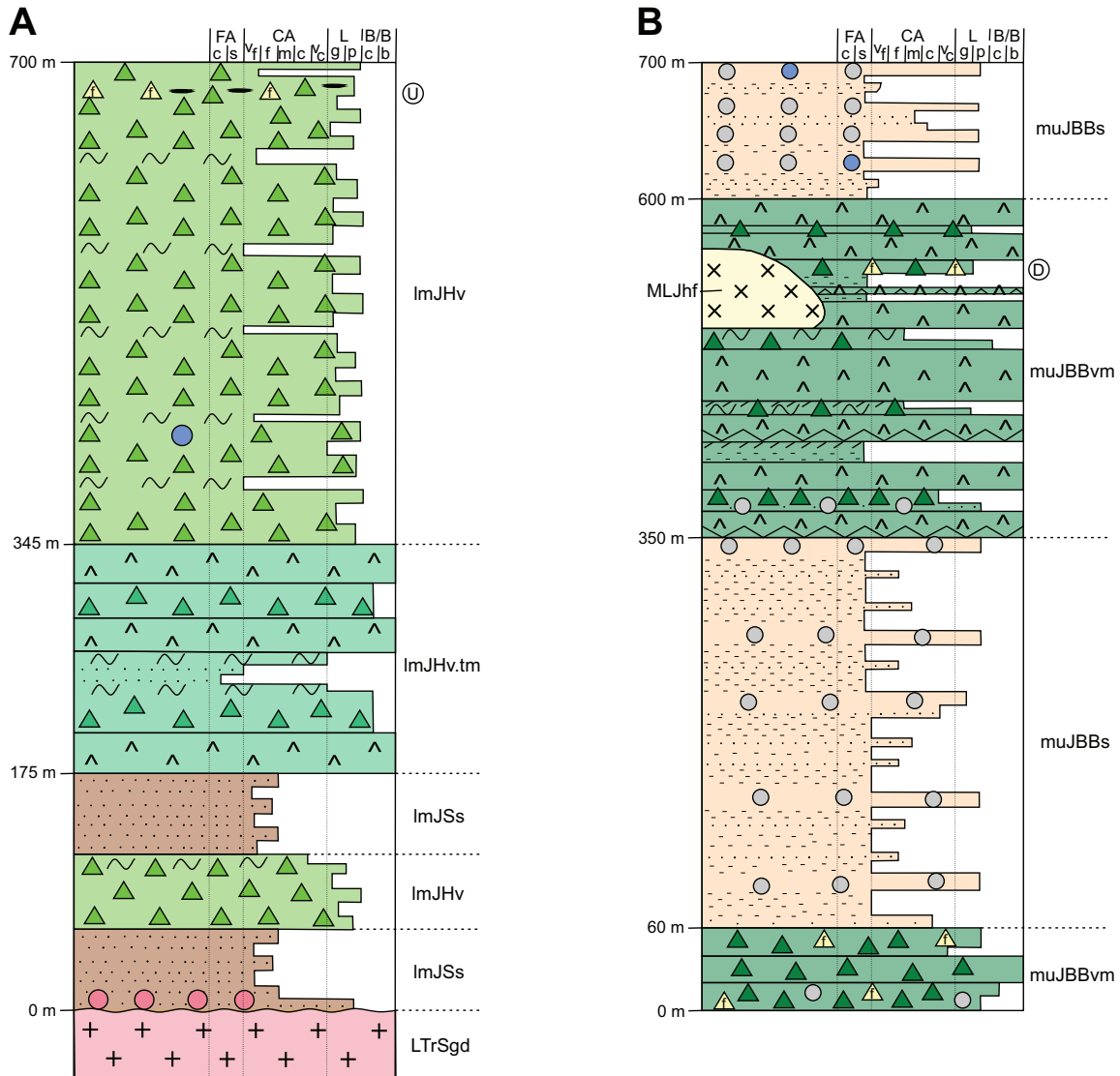


Fig. 9. Schematic stratigraphic sections for the Mount Blair area. **a)** Upper Hazelton Group. **b)** Bowser Lake Group composite stratigraphy based on sections exposed at four sites. See Figure 5 for legend, and Figure 8 for location of sections.

to unit ImJHv, which is well-represented by a section more than 350 m thick that unconformably overlies the granodiorite pluton (unit LTrSgd), and gradationally overlies and interfingers with sedimentary rocks of the Spatsizi Formation (see above). The unit comprises mafic to intermediate and rare felsic fragmental volcanic rocks (Fig. 11); subordinate mafic to intermediate coherent rocks may represent subvolcanic intrusions or flows. Volcanic clasts and coherent rocks are plagioclase-phyric, biotite-plagioclase-phyric, augite-plagioclase-phyric, and aphyric, with phenocryst-bearing clasts and units typically containing 0.5-5 mm plagioclase crystals. The upper portion of the succession (above unit ImJHv.tm, see below) is interpreted as largely primary volcanoclastic and subaerial based on the presence of welding textures (fiamme) observed at two locations, and the absence of substantially reworked volcanic rocks. The presence of limestone in one location may suggest local subaqueous deposition in a standing body of water. A

sample from a felsic lapilli tuff returned a 172.05 ± 0.17 Ma CA-TIMS U-Pb zircon age (Fig. 8; sample 19BvS-3-21, B. van Straaten and R. Friedman, unpublished data). Based on lithological, textural, mineralogical and compositional similarities we correlate unit ImJHv with the Sister Mary unit of the Horn Mountain Formation in the Dease Lake map area (van Straaten et al., 2022b) although, in the Mount Blair area, biotite phenocrysts are more common, the proportion of fragmental volcanic rocks is greater, and lava flows appear less numerous. Fine-grained coherent and very rare fragmental mafic volcanic rocks, texturally resembling mafic volcanic rocks in the Bowser Lake Group (unit muJBBvm, see below), occur locally within the Sister Mary unit. These rocks might be subvolcanic sills or intrusions related to the overlying Mount Blair Formation volcanic rocks (unit MLJhm, see below), represent unusual Horn Mountain Formation volcanic rocks, or perhaps reflect that the two units are partly coeval.



UTM 556,379E 6,435,556N

Fig. 10. Basal granitoid clast-bearing conglomerate of the Spatsizi Formation (unit lmJSs) unconformably above granodiorite (LTrSgd). Mount Blair area.

In the southeastern part of the map area, an approximately 170 m-thick volcanic unit with distinct cm-sized platy plagioclase phenocrysts (unit lmJHv.tm) is near the base of the Sister Mary unit (Figs. 8, 9a, 12). It is correlated with the Cariboo unit of the Horn Mountain Formation in the Dease Lake map area (van Straaten et al., 2022b).

The south-southwest-dipping fault panel in the south-central part of the map area contains grey weathering mafic lapilli-tuff with abundant plagioclase and lesser augite crystals (unit lmJHvm; Figs. 8, 13). These rocks are correlated with the Glacial Mountain unit of the Horn Mountain Formation in the Dease Lake map area (van Straaten et al., 2022b).

A plagioclase-phyric subvolcanic intrusion (unit EMJhi), commonly with a pinkish groundmass, and locally epidote-chlorite-sericite or silica altered, is inferred to cut granodiorite of the Stikine plutonic suite in the southeastern part of the map area. These rocks are lithologically similar to those of the Sister Mary unit, and likely represent subvolcanic feeders to the Horn Mountain Formation. We postulate that these rocks are similar to syenite, monzonite and feldspar porphyritic rocks described by Erdman (1978) and Gabrielse (1998; 2003).

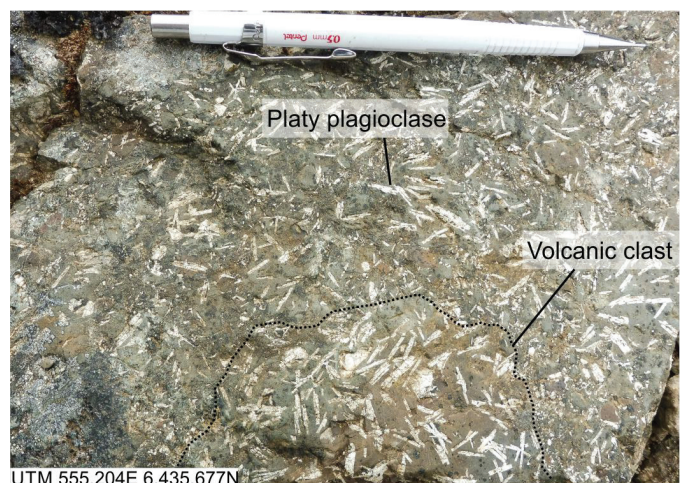
3.2.4. Mount Blair Formation (new formal unit)

The rocks on the north side of the prominent west-striking fault, making up the northern two-thirds of the map



UTM 554,106E 6,435,829N

Fig. 11. Horn Mountain Formation, Sister Mary mafic to intermediate volcanic unit (lmJHv). Lapilli-tuff with pinkish maroon to grey plagioclase-phyric volcanic clasts. Mount Blair area.



UTM 555,204E 6,435,677N

Fig. 12. Horn Mountain Formation, Cariboo intermediate volcanic unit (lmJHv.tm). Tuff breccia with platy plagioclase-phyric volcanic clasts. Mount Blair area.

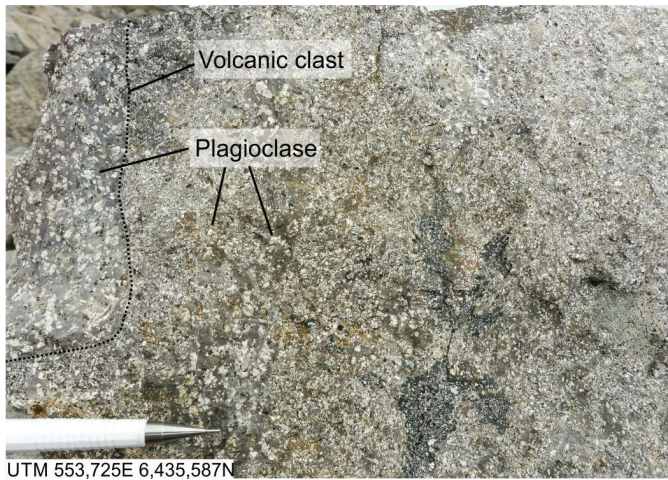


Fig. 13. Horn Mountain Formation, Glacial Mountain mafic volcanic unit (lmJHvm). Lapilli-tuff with abundant plagioclase crystals. Mount Blair area.

area (Fig. 8), comprise an at least 700 m-thick predominantly flat-lying succession of sedimentary rocks (unit muJBBS) and mafic volcanic rocks (unit muJBbvm) of the Bowser Lake Group. These rocks are defined herein as a new formation (Mount Blair Formation; Table 1), and correlate to rocks mapped as the informal ‘Mount Blair unit’ in the Dease Lake map area (van Straaten et al., 2022b). The formation comprises a mafic volcanic succession exposed near the lowest elevations of the map area, an overlying sedimentary succession that is succeeded by a second mafic volcanic succession, and an upper sedimentary succession exposed at the top of the highest ridges (Figs. 8, 9b, 14). Contacts between these alternating mafic volcanic and sedimentary successions are conformable.

The sedimentary unit (muJBBS) of the Mount Blair Formation comprises maroon to sea green siltstone, yellowish grey very fine- to fine-grained sandstone, and grey chert clast-bearing conglomerate (Fig. 9b). A largely subaerial setting is suggested by their intercalation with subaerial mafic volcanic rocks.

Table 1. Definition of the Mount Blair Formation. Coordinates in UTM NAD83 Zone 9 north.

Mount Blair Formation	
Category, rank	Lithostratigraphic unit with the rank of formation. Part of the Bowser Lake Group.
Name	Named for Mount Blair, a prominent peak at the top of a reference section.
Description of unit	Interbedded siltstone, sandstone, conglomerate, mafic flows, mafic fragmental volcanic rocks, rare felsic fragmental volcanic rocks (van Straaten and Bichlmaier, 2018; van Straaten et al., 2022b; this study). Siltstone is generally maroon to sea green. Conglomerate contains predominantly chert and lesser limestone granules to pebbles, and local cobbles. Mafic flows and volcanic clasts contain 10-25% augite (0.1-1 mm) and 15-55% plagioclase (0.1-0.2 mm) phenocrysts. Flows are 5-40 m thick, commonly have autobrecciated contacts, and are locally underlain by brick red baked tuff. Rare basal laminated limestone bed (<0.5 m thick). The presence of flows and common black organic material suggest a subaerial depositional environment. The succession is cut by mafic and felsic dikes and intrusions. The intrusions are likely coeval with the volcanic rocks based on similar texture and mineralogy. In regional studies, these intrusions could be included in the formation. The non-marine succession is lithologically distinct from mainly marine units in the Bowser Lake Group to the south (Evenchick and Thorkelson, 2005).
Geometry, thickness	The unit extends for at least ~70 km in a west to east trending belt between the McBride River, Pitman fault, Kutcho fault, and the King Salmon fault or Kehlechoa fault. The unit is at least 430 m thick east of the McBride River, and at least 700 m thick in the Mount Blair area (Fig. 9b).
Lower contact	Conformable and gradational contact above volcanic rocks of the Horn Mountain Formation (upper Hazelton Group). Lower boundary defined where sedimentary rocks are more abundant (>50%) than volcanic strata (type section: UTM 499,528 E-6,433,031N). The base of the reference section is a fault (UTM 551,426E-6,437,390N).
Upper contact	The top contact is not exposed. The top of the type section is at UTM 499,646E-6,432,733N. The top of the reference section is at the summit of Mount Blair (UTM 551,038E-6,437,997N).
Age	Middle Jurassic (Bajocian) to Upper Jurassic (Oxfordian), possibly younger. A high-precision CA-TIMS U-Pb zircon crystallization age on immediately underlying Horn Mountain Formation felsic volcanic rocks east of the McBride River constrains the onset of Bowser Lake Group sedimentation to 170.99 ± 0.13 Ma (van Straaten et al., 2022b), and shows that these units are the oldest known Bowser Lake Group strata in Stikinia.

Coordinates are in UTM NAD 83 zone 9 north.

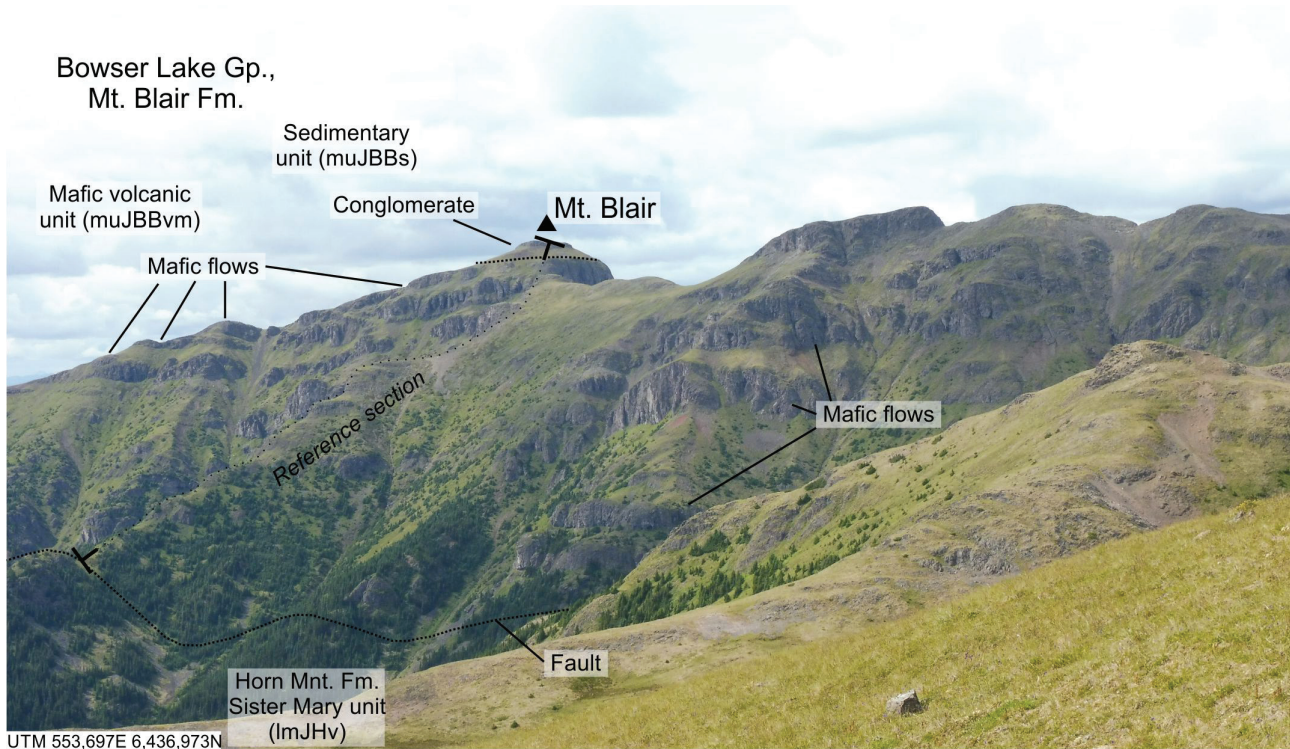


Fig. 14. Reference section, Mount Blair Formation (new unit), Bowser Lake Group. Resistant mafic flows and interbedded recessive fragmental volcanic rocks and siltstones (muJBBvm) overlain at the top of Mount Blair by recessive siltstone, sandstone, and resistant conglomerate (muJBBs). In the foreground a west-trending fault separates the Mount Blair Formation from volcanic rocks of the Horn Mountain Formation (unit ImJHv). View towards the northwest.

Lithologically similar sedimentary rocks of the Mount Blair Formation are in the Dease Lake map area, where intercalated mafic flows and adhesion warts provide evidence for a subaerial setting (van Straaten and Bichlmaier, 2018; van Straaten et al., 2022b). An outlier of the sedimentary unit in the southwestern part of the area gradationally overlies volcanic rocks of the Sister Mary unit (ImJHv). Here, a laminated limestone bed near the base of the unit likely represents short-lived subaqueous deposition following Horn Mountain volcanism, analogous to limestone observed at the same stratigraphic level in the Dease Lake map area (van Straaten and Bichlmaier, 2018). Small outliers of sedimentary rocks also occur in the southeast, at approximately 1700-1800 metres elevation, where the unit gradationally overlies volcanic rocks of the Glacial Mountain unit (ImJHvm).

The mafic volcanic unit of the Mount Blair Formation (muJBBvm) comprises interbedded mafic flows, mafic fragmental volcanic rocks, and siltstone. Flows commonly display autobrecciated margins and are locally underlain by brick red baked tuff (Fig. 15a). Mafic flows contain fine-grained augite and plagioclase phenocrysts (<1-1.5 mm; Fig. 15b), distinctly finer grained than volcanic rocks in the Horn Mountain Formation. Lapillistone is commonly well-sorted, clast-supported, and ash-poor, suggesting a probable origin as air fall deposits (Fig. 15c). A mafic lapillistone with subordinate felsic volcanic clasts yielded a 157.77 ± 1.1 Ma LA-ICP-MS U-Pb detrital zircon maximum depositional

age (Figs. 8, 9c; sample 18BvS-31-307, B. van Straaten and R. Friedman, unpublished data). The presence of mafic flows with autobrecciated margins, baked tuff, and air fall deposits suggests a predominantly subaerial setting.

In the eastern part of the map area, a fault block bounded by splays of the prominent west-trending fault contains steeply dipping sedimentary rocks overlain by mafic volcanic rocks of the Mount Blair Formation. The volcanic succession contains rare limestone beds, and a lapilli-tuff interbed similar to those within the Horn Mountain Formation (unit ImJHv). The presence of limestone (locally common near the base of the Mount Blair Formation) and volcanic rocks similar to those in the Horn Mountain Formation may suggest that the fault block represents part of a gradational contact between the Horn Mountain and Mount Blair formations. In the west-central part of the map area, immediately north of the major west-trending fault, volcanic rocks of the Horn Mountain Formation (unit ImJHv) appear to interfinger with Mount Blair Formation volcano-sedimentary rocks (Fig. 8).

Mafic subvolcanic dikes (unit MLJhm) are present throughout the area (Fig. 8). They are 3-300 metres wide and cut Mount Blair sedimentary and volcanic units. Some dikes are texturally similar to mafic flows within the Mount Blair Formation, others contain coarser grained (0.5-4 mm) augite and plagioclase phenocrysts.

A 1.5 km by 1.5 km body of felsic coherent rock (unit MLJhf) occurs within the mafic volcanic unit of the Mount

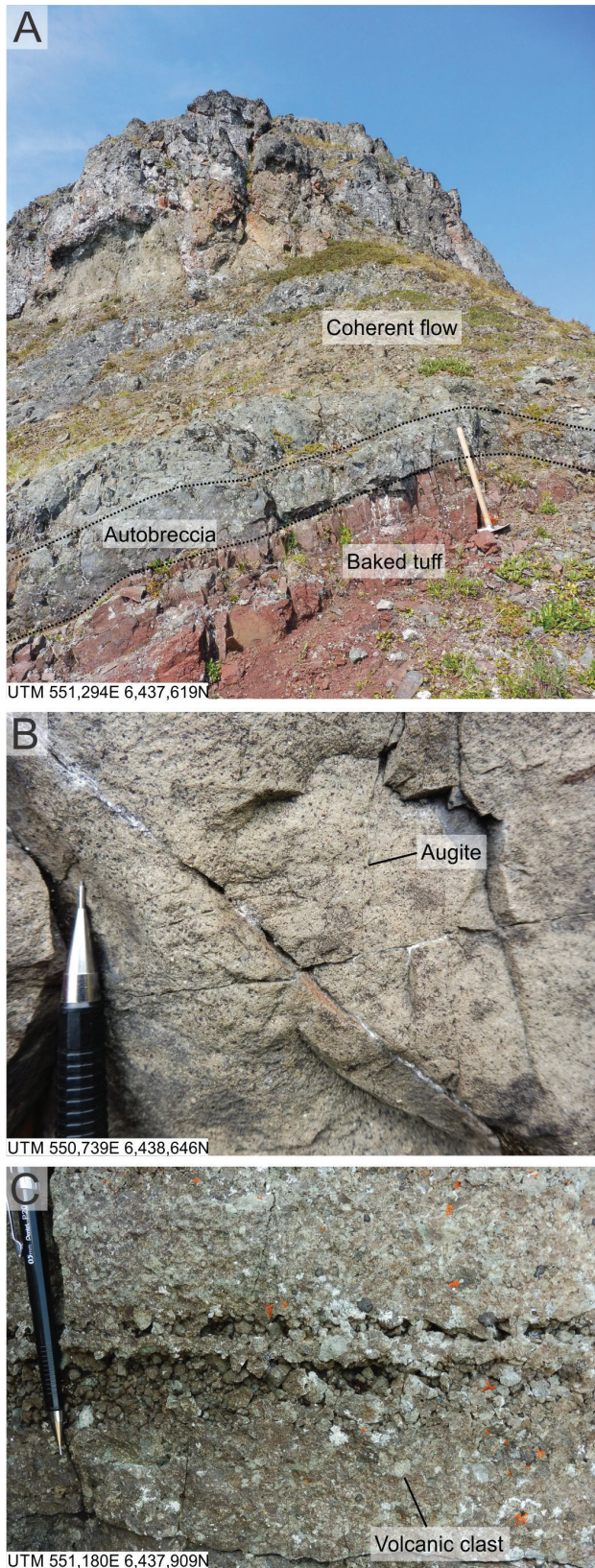


Fig. 15. Bowser Lake Group, Mount Blair Formation mafic volcanic unit (muJBBvm). **a)** Baked red tuff overlain by basal autobreccia grading upward into coherent mafic flow. **b)** Fine-grained augite-plagioclase-phyric mafic flow. **c)** Well-sorted, crudely stratified lapillistone. Mount Blair area.

Blair Formation in the central part of the map area (Fig. 8). The margins vary from sharp and intrusive (east) to autobrecciated (west), and the body is compositionally and texturally similar to felsic clasts in the adjacent mafic volcanic unit (Fig. 9b). These observations suggest it may be a felsic dome, and broadly coeval with Mount Blair volcanism. Metre-wide felsic dikes with a similar composition were locally observed in the map area.

3.2.5. Diorite intrusions (Middle-Late Jurassic)

A diorite body (Middle-Late Jurassic; unit MLJd) is inferred in the far southeast of the map area, following Erdman (1978), who reported a 162 ± 12 Ma K-Ar hornblende cooling age from a hornblende diorite. A vesicular microdioritic dike that cuts Late Triassic granodiorite 1.5 km to the west (Fig. 8) may be related. A very small hornblende diorite intrusion is also mapped about 1.8 km north of Mount Blair (Fig. 8), where it cuts and contact metamorphoses sedimentary rocks of the Mount Blair Formation. If all these intrusions are of the same generation, the K-Ar date and maximum depositional age for the Mount Blair volcanic rocks suggest a latest Jurassic age for their emplacement.

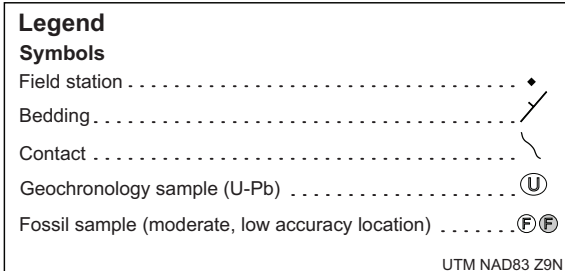
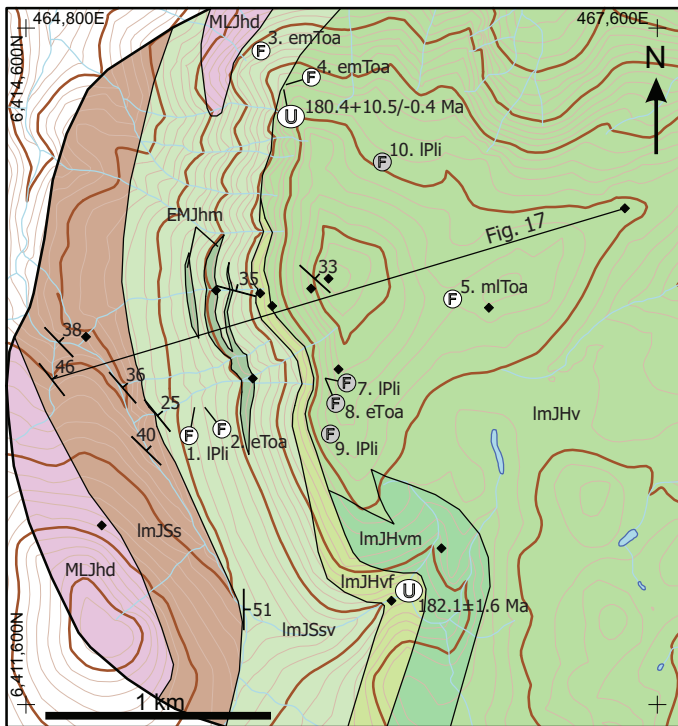
3.3. Spatsizi area

The Spatsizi area is 24 km east of the town of Iskut (Fig. 2). Geological mapping (Read and Psutka, 1990; Thorkelson, 1992; Evenchick and Thorkelson, 2005) and stratigraphic studies (Smith et al., 1984; Thomson et al., 1986; Pálffy et al., 2000) identified sedimentary strata of the Spatsizi Formation overlain by mafic, intermediate, and felsic volcanic rocks of the informal '(Mount) Brock volcanics'.

New mapping shows a right-way-up, moderately northeast dipping homocline (Fig. 16). The lower volcano-sedimentary succession is part of the Spatsizi Formation; the overlying volcanic rocks, originally assigned to the informal '(Mount) Brock volcanics' (Read and Psutka, 1990; Thorkelson, 1992; Evenchick and Thorkelson, 2005), are reassigned here to the Horn Mountain Formation based on similar lithology and late Early to Middle(?) Jurassic age.

3.3.1. Spatsizi Formation

The oldest map unit in the Spatsizi study area is a sedimentary unit (lmJSs) consisting of interbedded siltstone, feldspathic arenite, mudstone, siliceous mudstone, and minor limestone (Figs.16-18). The unit was previously referred to as part of the informal 'Spatsizi sediments' (Smith et al., 1984), later formally defined as the Spatsizi Group (Thomson et al., 1986), and subsequently demoted to Spatsizi Formation (within the Hazelton Group; Evenchick and Thorkelson, 2005). Common soft-sediment deformation structures, mud rip-up clasts, scours, current ripples, rare crossbedding, very rare oscillatory ripples, and ammonoids were observed, with ammonoids suggesting a marine setting. At the top of this unit is a conglomerate to breccia with limestone, mafic(?) volcanic and rare chert clasts (Fig. 17). Smith et al. (1984) and Read and



MIDDLE-LATE JURASSIC (?)

MLJhd **Microdiorite**; greenish grey; fine grained, equigranular; mafic-rich; Middle to Late Jurassic or possibly younger.

— — — — — intrusive contact

LATE EARLY TO MIDDLE JURASSIC

Upper Hazelton Group

Horn Mountain Formation (formerly 'Mount Brock volcanics')

EMJhm **Horn Mountain intrusions: Mafic subvolcanic intrusions**; grey; contain 50-60% plagioclase (2-4 mm) and 10-30% augite (0.5-3 mm) phenocrysts in an aphanitic groundmass; Interpreted as subvolcanic feeders to the Horn Mountain Formation.

ImJHv **Sister Mary unit: Mafic to intermediate flows, volcanic breccia, lapillistone, lapilli-tuff, and tuff**; maroon, green to greenish grey; flows contain 25-50% medium-grained (1-4 mm) to fine-grained (0.1-0.5 mm) plagioclase laths, 0-15% equant augite (0.3-2 mm) phenocrysts, and often vesicular bottom and top; fragmental rocks are predominantly clast-supported and contain maroon, red, green, and grey volcanic clasts that are non-vesicular to vesicular, plagioclase-phyric to aphyric to plagioclase-augite-phyric, and include irregular-shaped vesicular spatter clasts; interstratified flows (4-35 m thick) and fragmental volcanic rocks; rare Toarcian (and younger?) ammonoids, bivalves, brachiopods, and belemnites; predominantly subaerial depositional environment.

ImJHvm **Glacial Mountain unit: Mafic flows, volcanic breccia**; minor siltstone, mudstone, sandstone; flows and volcanic clasts are augite-plagioclase-phyric; laminated mudstone, siltstone, and fine-grained feldspathic wacke (locally fossiliferous) with common soft-sediment deformation structures are overlain by mafic volcanic breccia in mud matrix, which is in turn overlain by either mafic volcanic breccia with a crystal-rich clastic matrix or mafic coherent rocks; subaqueous depositional environment.

ImJHvf **Felsic lapillistone**, rare welded lapilli-tuff; greyish to greenish buff; contains cream white plagioclase-phyric felsic volcanic clasts, green fine-grained volcanic clasts, common equant plagioclase crystals, and rare charred wood fragments in a fine ash matrix; 182.1 ±1.6 and 180.4 +10.5/-0.4 Ma U-Pb zircon ages; predominantly subaerial depositional environment.

Spatsizi Formation

ImJSsv **Tuffaceous siltstone, tuff, tuffaceous sandstone, lapilli-tuff, lapillistone**; rare conglomerate, siltstone; maroon to green; volcanic rocks contain green fine-grained volcanic clasts, local ash-armoured volcanic clasts, and accretionary lapilli; very fine- to fine-grained, rare medium- to coarse-grained tuffaceous feldspathic wacke to rare tuffaceous feldspathic arenite, with common quartz grains and locally organic detritus; conglomerate contains predominantly chert pebbles, granules and rare cobbles; moderately stratified; rare lower Pliensbachian to middle Toarcian ammonoids; subaerial to submarine depositional environment.

ImJSs **Siltstone, feldspathic arenite, mudstone, siliceous mudstone, minor limestone**; rare conglomerate and breccia; very fine- to medium-grained, rare coarse-grained feldspathic arenite with 75-85% feldspar, 10-25% lithics (including hornblende) and 0-10% quartz grains; conglomerate contains rounded to subangular chert granules and pebbles; breccia contains angular to subrounded clasts (0.2-7 cm) of limestone, mafic(?) volcanic, and rare chert clasts; planar to wavy parallel laminated mudstone and siltstone; very thinly to very thickly bedded feldspathic arenite; common soft-sediment deformation structures, mud rip-up clasts, scours, current ripples, rare cross-bedding, and very rare oscillatory ripples; very rare ammonoids; marine depositional environment.

Fig. 16. Geological map of the Spatsizi area, incorporating data from Read and Psutka (1990), Evenchick and Thorkelson (2005), and this study. See Table 2 for fossil ages.

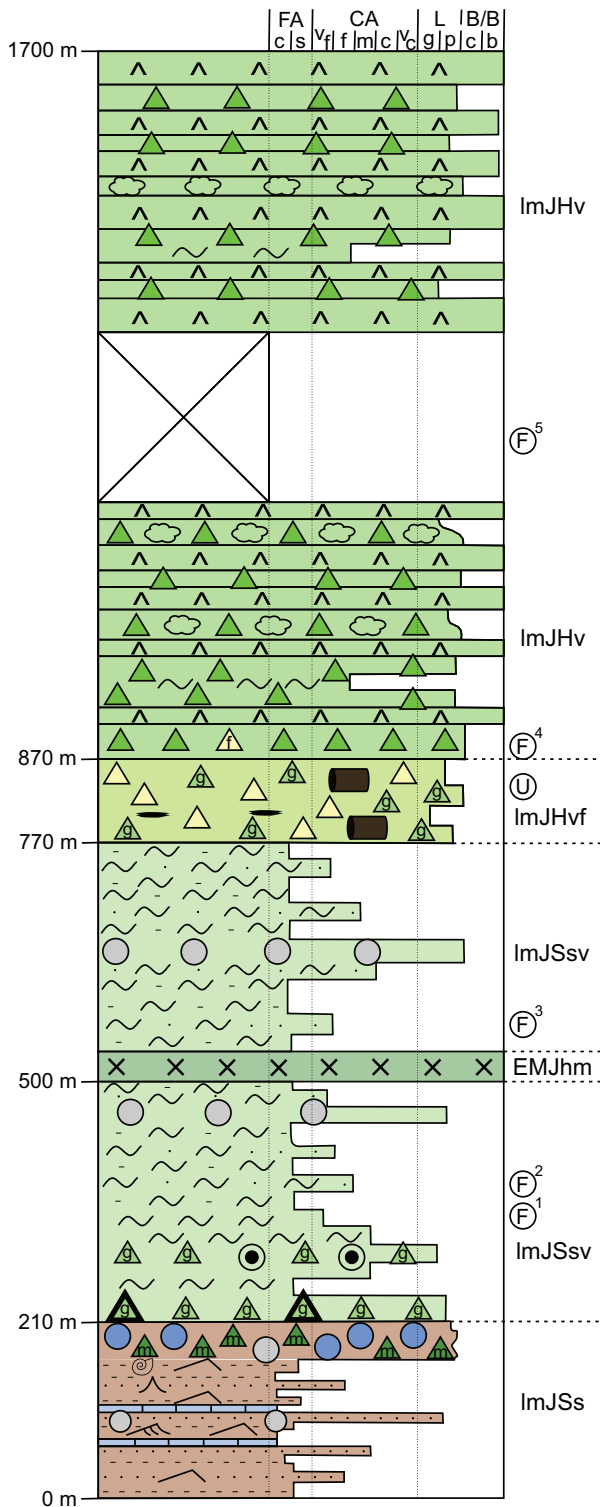


Fig. 17. Schematic stratigraphic section for the Spatsizi area. See Figure 5 for legend, Figure 16 for location of stratigraphic section, and Table 2 for fossil ages.



Fig. 18. Spatsizi Formation, sedimentary unit (ImJSs). Interstratified fine- to medium-grained feldspathic arenite, siltstone, and mudstone. Spatsizi area.

Psutka (1990) reported that the unit unconformably overlies diorite to monzodiorite of the Railroad pluton (Stikine plutonic suite, Late Triassic) along the valley bottom, however, we only encountered near-continuous outcrop of sedimentary rocks where plutonic rocks were mapped previously.

The sedimentary unit (ImJSs) is overlain by a tuffaceous sedimentary to volcanic unit (ImJSsv) that, following previous studies, is also included in the Spatsizi Formation (Figs. 16, 17). The base of the unit includes interbedded lapilli-tuff, lapillistone and tuff with common accretionary lapilli and ash-armoured volcanic clasts (Fig. 19), indicating subaerial deposition. Higher up in the section, the unit includes recessive maroon to green tuffaceous siltstone to fine tuff, tuffaceous sandstone to crystal tuff, rare chert-clast bearing conglomerate, and dark grey siltstone. Rare ammonoids suggest a late Pliensbachian to middle Toarcian age (Table 2) and, at least locally, a submarine setting for the middle and upper parts of the unit.

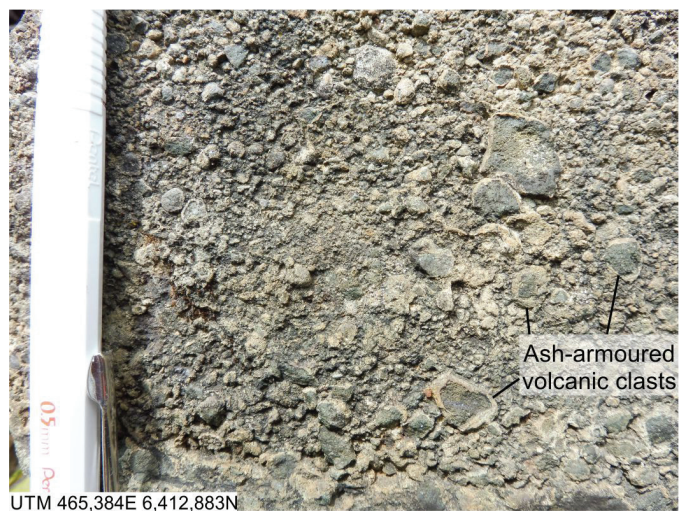


Fig. 19. Spatsizi Formation, tuffaceous sedimentary to volcanic unit (ImJSsv). Ash-armoured volcanic clasts in lapillistone. Spatsizi area.

Table 2. Compilation of fossil data for the Spatsizi area. Numbers 1-5 and 7-10 in first column correspond to fossil labels on Figures 16 and 17.

GSC no.	East- ing	North- ing	Loc. acc.	Unit	Age	Fossil description	Identified by	Source	Loc. source
1	C-103177	465548	6412919	lmJS	lPli	Ammonoid (<i>Lioceratoides propinquum</i> (Whiteaves, 1884), <i>Protoqrammoceras</i> sp.)	H.W. Tipper	1 (6)	6 ⁺
2	C-103182	465593	6412919	lmJS	eToa	Macrofossil	H.W. Tipper	1 (6)	6
3	C-087250	465843	6414499	lmJS	emToa	Ammonoid (<i>Dactyloceras</i> cf. <i>D. kanense</i> McLearn, <i>Dactyloceras</i> sp. indet., harpoceratinae gen. et sp. indet.)	G.K. Jakobs	2 (1,6)	6
4	C-090698	465953	6414349	lmJH	emToa (K-P)	Ammonoid (<i>Dactyloceras</i> cf. <i>D. kanense</i> McLearn, <i>Dactyloceras</i> cf. <i>D. commune</i> (Sowerby), harpoceratinae gen. et sp. indet.), Bivalve (<i>Weyla alata</i> (Buch), <i>Weyla</i> cf. <i>W. bodenbenderi</i> (Behrendsen), pectinid bivalves, bivalves), rhynchonellid brachiopods, terebratulid brachiopods	G.K. Jakobs	2 (1,4,6)	6
5	C-103428	466693	6413399	lmJH	mlToa	Ammonoid (<i>Polyplectus</i> sp. indet.), trigonid bivalves, bivalves	G.K. Jakobs	2 (1,6)	6
6	C-090732	469050	6413750	lmJH	Toa-?	True belemnite	H.W. Tipper	1 (6)	6*
7	C-103174	466125	6413050	lmJ	lPli (C)	Ammonoid (<i>Tiltoniceras propinquum</i> , <i>Protoqrammoceras</i> spp.)	P.L. Smith	5 (1)	5
8	C-103152, C-103153, C-103154, C-103188	466125	6413050	lmJS?	eToa (K)	Ammonoid (C-103152: <i>Dactyloceras</i> cf. <i>D. kanense</i> McLearn; C-103153: <i>Dactyloceras</i> cf. <i>D. simplex</i> Fucini, <i>Dactyloceras</i> cf. <i>D. kanense</i> McLearn; C-103154: <i>Dactyloceras</i> cf. <i>D. kanense</i> McLearn, harpoceratinae gen. et sp. indet.; C-103188: <i>Dactyloceras</i> cf. <i>D. kanense</i> McLearn)	G.K. Jakobs	2	2
9	C-103171, C-103173, C-103175, C-103179	466150	6412800	lmJ	lPli	Ammonoid (C-103171: <i>Lioceratoides propinquum</i> , ? <i>Protoqrammoceras paltum</i> ; C-103173: <i>Lioceratoides propinquum</i> , <i>Protoqrammoceras</i> sp.; C-103175: <i>Lioceratoides propinquum</i> , <i>Protoqrammoceras paltum</i> ; C-103179: <i>Protoqrammoceras paltum</i>)	H.W. Tipper	7	7
10	C-210959	466381	6414007	lmJS?	lPli (C)	Bivalve (<i>Posidonotis semiplicata</i>)	M. Aberhan	3	3

Coordinates in UTM NAD83 Zone 9 north.

Age: e, m, l = early, middle, late; Pli = Pliensbachian, Toa = Toarcian; C = Carlotense Zone (latest Pliensbachian), K = Kanense Zone (early Toarcian), P = Planulata Zone (early middle Toarcian).

Location accuracy (Loc. acc.): mod. = moderate - converted from tabulated coordinates in UTM NAD27 on map, and matching fossil location shown on 1:50,000 scale map (Read and Psutka, 1990); low - converted from latitude-longitude with poor or no accompanying location description.

Source, Location source (Loc. source): 1. Evenchick and Thorkelson (2005); 2. Jakobs (1997); 3. Aberhan and Pálffy (1996); 4. Jakobs et al. (1994); 5. Thomson and Smith (1992); 6. Read and Psutka (1990); 7. Tipper (1986); () = other source, often with superseded age determination; + = location slightly adjusted to correct elevation; * = location digitized from map.

3.3.2. Horn Mountain Formation

The Spatsizi Formation is conformably overlain by volcanic rocks of the Horn Mountain Formation, which is subdivided into three map units (Figs. 16, 17). At the base is a felsic volcanic unit (ImJHvf; Fig. 20) that includes welded lapilli-tuff indicating subaerial deposition. A sample of felsic volcanic breccia from the southern part of the map area, where the unit is about 150 m thick, returned a 182.1 ± 1.6 Ma LA-ICP-MS U-Pb zircon age (sample 16BvS-39-284, B. van Straaten and R. Friedman, unpublished data). The unit thins northward, becoming about 100 m thick in the centre of the map area, and ceasing to be a mappable unit farther north. It may, however, continue into the north part of the area and be represented by a 1.5 m thick felsic non-welded waterlain feldspar-phyric crystal tuff that returned a $180.4 +10.5/-0.4$ Ma U-Pb zircon age (Fig. 16; Pálffy et al., 2000).

In the southern part of the map area the felsic volcanic unit is overlain by a mafic volcanic unit (ImJHvm) of the Horn Mountain Formation (Fig. 16). Based on lithological similarity, we correlate it with the Glacial Mountain unit of the Horn Mountain Formation in the Dease Lake map area (van Straaten et al., 2022b). The presence of intercalated mudstone, siltstone and sandstone suggests transport and deposition by water such as in a subaqueous or fluvial setting.

Most of the Horn Mountain Formation in the Spatsizi area is composed of a mafic to intermediate volcanic unit (ImJHv; Figs. 16, 17), which overlies the felsic volcanic unit (ImJHvf), and overlies and interfingers with the mafic volcanic unit (ImJHvm). This unit comprises interbedded flows and fragmental volcanic rocks (Fig. 21a), locally with amoeboid vesicular spatter clasts (Fig. 21b). Based on lithological similarity, we correlate it with the Sister Mary unit of the Horn Mountain Formation in the Dease Lake map area (van Straaten et al., 2022b). Rare reports of ammonoids, bivalves, and brachiopods suggest a Toarcian age (Table 2). Vesicular flows and spatter clasts suggest a predominantly subaerial setting although rare marine macrofossils indicate periodic flooding by seawater.

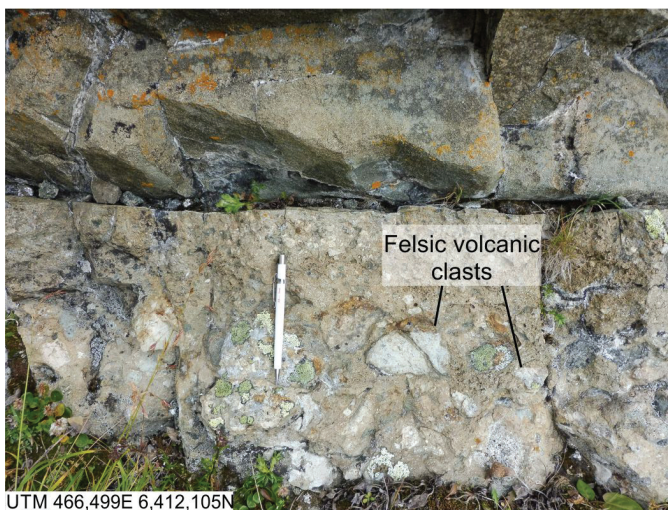


Fig. 20. Horn Mountain Formation, felsic volcanic unit (ImJHvf). Felsic volcanic breccia overlain by felsic crystal tuff. Spatsizi area.

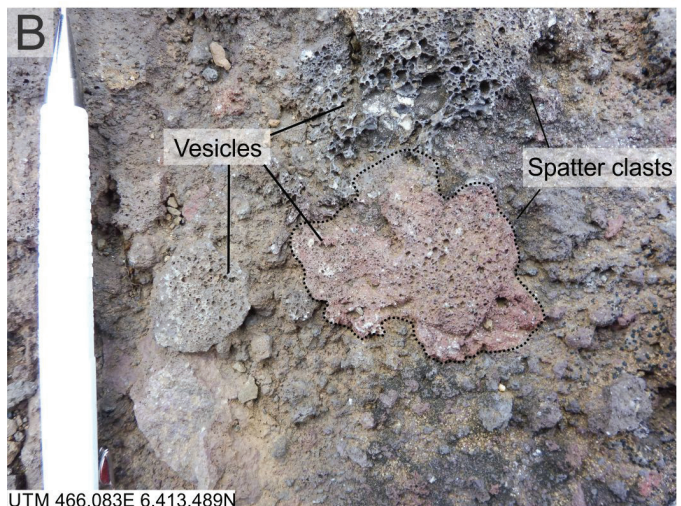
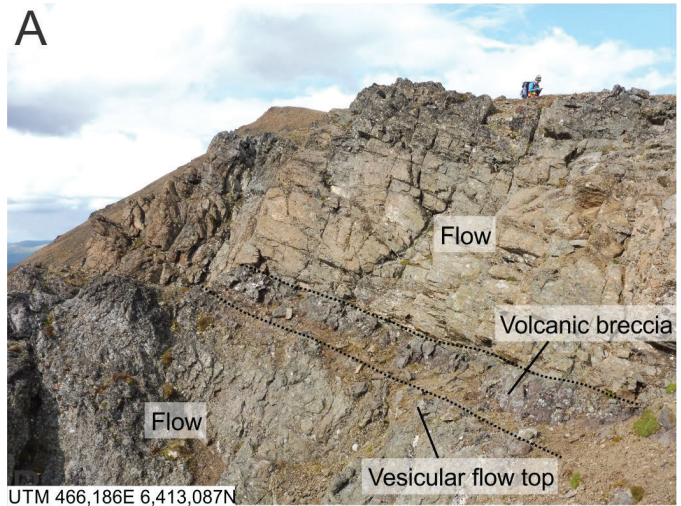


Fig. 21. Horn Mountain Formation, Sister Mary mafic to intermediate volcanic unit (ImJHv). **a)** At base, augite-plagioclase-phyric flow with highly vesicular top overlain by 1 m-thick bed of volcanic breccia with common spatter clasts, overlain by 4 m-thick augite-plagioclase-phyric flow. **b)** Lapillistone from 75 cm thick bed, with amoeboid, highly vesicular, brick red, maroon, and dark grey plagioclase-phyric spatter clasts. Spatsizi area.

Mafic subvolcanic sills and intrusions (unit EMJhm) cut the tuffaceous sedimentary and volcanic unit (ImJSSv) of the Spatsizi Formation (Fig. 16). Based on textural and compositional similarity they are interpreted as subvolcanic feeders to the Horn Mountain Formation.

3.3.3. Microdiorite (Middle-Late Jurassic)

A mafic-rich microdiorite (unit MLJhd) occurs in the southwest corner of the of the map area where it is inferred to cut sedimentary rocks of the Spatsizi Formation (Fig. 16). It is interpreted as Middle to Late Jurassic or possibly younger.

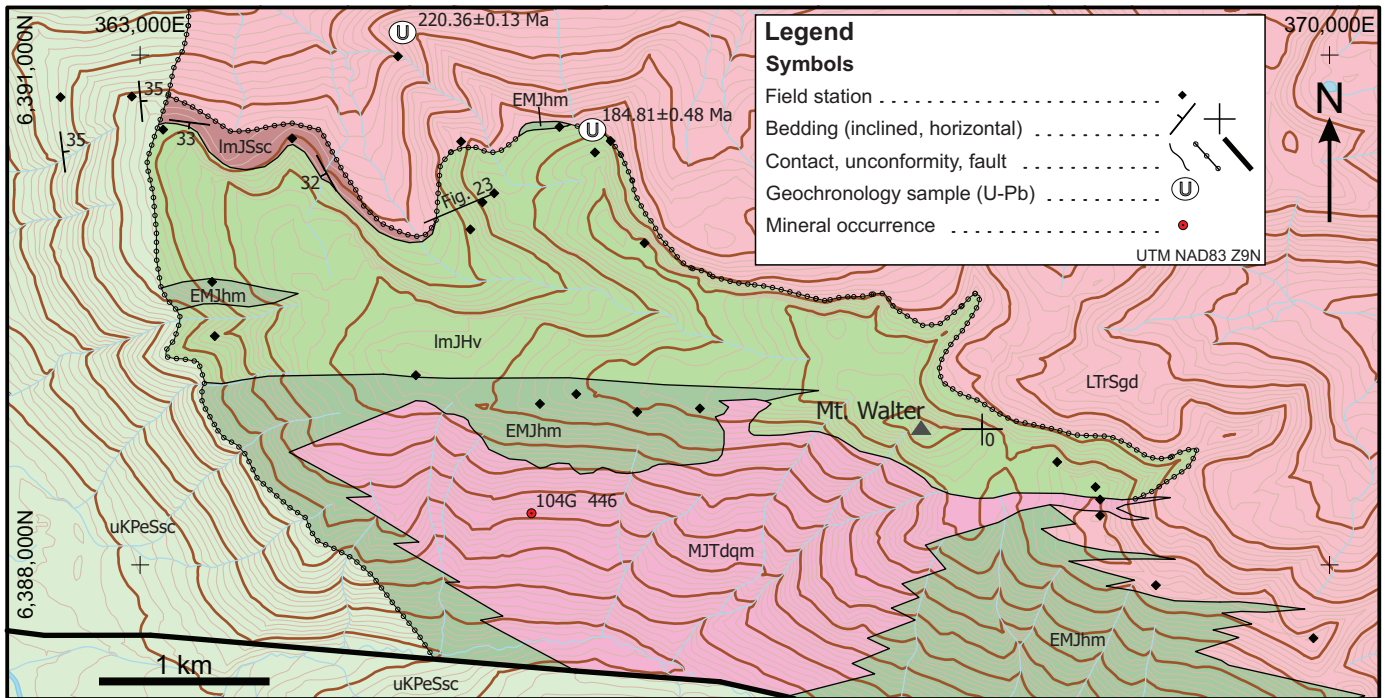
3.4. Yehiniko Lake area

The Yehiniko Lake area is 31 km south of Telegraph Creek (Fig. 2). The area was previously mapped at 1:250,000 scale by Souther (1972); the western portion was mapped at

1:50,000 scale by Brown et al. (1996). A revised geological map (Fig. 22) shows a granodiorite pluton (part of the Stikine plutonic suite, Late Triassic) unconformably overlain by subhorizontal sedimentary and volcanic rocks (Fig. 23). The sedimentary rocks are assigned to the Spatsizi Formation and the volcanic rocks, previously mapped as undivided Hazelton Group (Lower to Middle Jurassic; Brown et al., 1996), are assigned to the Horn Mountain Formation.

3.4.1. Nightout pluton (Stikine plutonic suite)

The northern part of the Yehiniko Lake map area is underlain by granodiorite (unit LTrSgd) of the Nightout pluton, which extends across 544 km² and was previously considered Middle to Late Triassic based on a number of K-Ar, Rb-Sr and U-Pb radiometric age determinations (Holbek, 1988; Brown et al., 1996; Logan et al., 2000; Breitsprecher and Mortensen, 2004). A sample of quartz porphyritic biotite-hornblende granodiorite



LATE CRETACEOUS TO PALEOCENE

Sustut Group

Brothers Peak Formation

uKPeSsc Conglomerate, lesser sandstone, siltstone, rare shale, felsic tuff, lapilli-tuff and flows, very rare basalt and andesite flows and breccia; brick red, brown, and grey; poorly indurated; 85.6 ± 6.0 Ma K-Ar biotite cooling age, rare Early Paleocene palynomorphs; terrestrial depositional environment.

unconformity

MIDDLE JURASSIC (?)

Three Sisters Plutonic Suite (?)

MJTdqm Quartz monzonite, feldspar porphyry intrusions; pink; fine- to coarse-grained, equigranular to feldspar porphyritic; biotite-hornblende, biotite; Middle Jurassic, or possibly younger.

intrusive contact

EARLY TO MIDDLE JURASSIC

Upper Hazelton Group

Horn Mountain Formation

EMJhm Horn Mountain intrusions: Mafic subvolcanic intrusions; dark grey; contain 25-35% plagioclase (0.5-4 mm) and 10-15% augite (0.5-1.5 mm) phenocrysts in a very fine-grained groundmass; interpreted as subvolcanic feeders to the Horn Mountain Formation.

ImJHv Sister Mary unit: Mafic to intermediate flows, lapillistone, tuff, volcanic breccia; rare felsic lapillistone; maroon to grey; flows contain 15-30% plagioclase (0.2-4 mm) and 10-15% augite (0.1-0.5 mm) phenocrysts; fragmental volcanic rocks contain augite-plagioclase-phyric, plagioclase-phyric and aphyric volcanic clasts; crudely stratified; 184.81 ± 0.48 Ma U-Pb zircon age from basal felsic volcanic rocks; subaerial depositional environment.

Spatsizi Formation

ImJSsc Sandstone and conglomerate; coarse- to very coarse-grained quartz-rich feldspathic arenite; conglomerate with granitoid granules and rare pebbles; unconformably overlies Nightout pluton; crudely stratified.

unconformity

LATE TRIASSIC

Stikine Plutonic Suite

Nightout pluton

LTrSgd Granodiorite; medium-grained, quartz to K-feldspar-quartz porphyritic; biotite-hornblende; moderately resistant; 220.36 ± 0.13 Ma U-Pb zircon age.

Fig. 22. Geological map of the Yehiniko Lake area, incorporating data from Souther (1972), Brown et al. (1966), Cui et al. (2017), and this study.

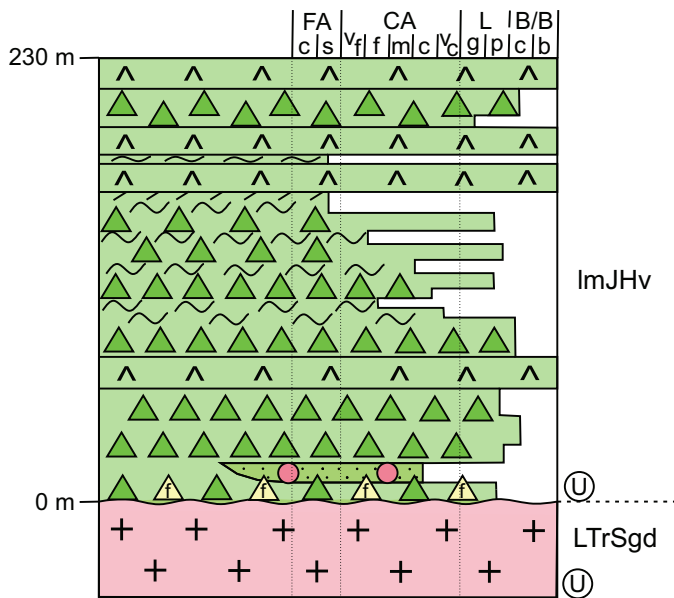


Fig. 23. Schematic stratigraphic section for the Yehiniko Lake area. See Figure 5 for legend, and Figure 22 for location.

from the northwestern part of the area (Fig. 22) returned a 220.36 ± 0.13 Ma CA-TIMS U-Pb zircon age (sample 18BvS-12-97; B. van Straaten and R. Friedman, unpublished data) confirming that it is Late Triassic and part of the Stikine plutonic suite.

3.4.2. Spatsizi and Horn Mountain formations

Within the study area, the Nightout pluton is unconformably overlain by flat-lying volcano-sedimentary rocks of the upper Hazelton Group. In the west, an eastward-thinning wedge of sandstone and conglomerate (unit ImJSsc) directly overlies the pluton. In the centre and east, a succession of maroon to grey volcanic rocks (unit ImJHv) directly overlies the pluton; in the west, the volcanic unit overlies the sandstone and conglomerate unit (Fig. 22). Based on similar lithology and age we assign the sedimentary rocks (ImJSsc) to the Spatsizi Formation, and the volcanic rocks (ImJHv) to the Horn Mountain Formation. The unconformity is well-exposed along the northern edge of the Mount Walter ridge system (Fig. 24) and was studied 2.4 km west-northwest of Mount Walter. Here, a 5-m covered interval separates granodiorite of the Nightout pluton from maroon to grey volcanic rocks. The lowest volcanic exposures comprise felsic lapillistone with aphyric volcanic, very fine-grained volcanic, and flow-banded volcanic clasts set in an ash matrix with common detrital quartz grains (2-3 mm). The felsic lapillistone returned a U-Pb CA-TIMS zircon age of 184.81 ± 0.48 Ma (sample 18BvS-12-99, B. van Straaten and R. Friedman, unpublished data), and constrains the onset of upper Hazelton Group volcanism in the area. The Early Jurassic age is based on five zircon grain analyses, and three older grains (ca. 224.1-219.4 Ma, B. van Straaten and R. Friedman, unpublished data) indicate that detrital material was derived from the subjacent Nightout pluton. At this locality, basal

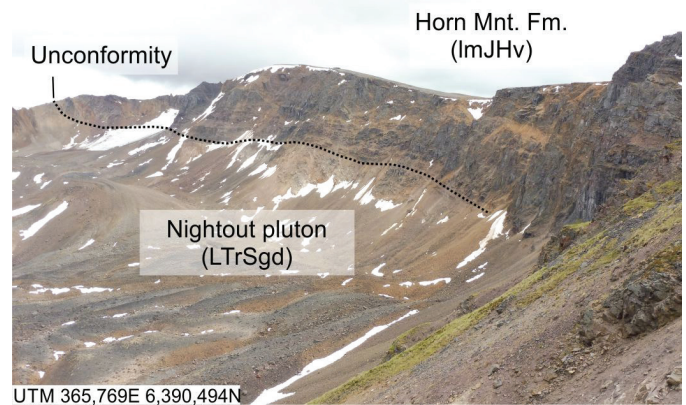


Fig. 24. Unconformity between flat-lying upper Hazelton Group volcanic rocks (Horn Mountain Formation, ImJHv) and subjacent Nightout pluton (LTrSgd) northeast of Yehiniko Lake. View towards the southeast.

volcanic rocks are locally interbedded with medium- to very coarse-grained quartz-rich feldspathic arenite and granular conglomerate (Fig. 25a). To the north of the map area, a relatively flat-topped plateau incised by creeks likely outlines the continuation of the subhorizontal erosional surface atop the Nightout pluton. It is similar in attitude to a largely flat-lying unconformity at the base of a larger outlier of Hazelton Group rocks to the west (Brown et al., 1996).

The volcanic unit (ImJHv) consists mainly of interbedded mafic to intermediate flows and fragmental volcanic rocks (Figs. 25b, 25c), which we assign to the Sister Mary unit of the Horn Mountain Formation (van Straaten et al., 2022b). Flows are generally 15 m thick, are locally underlain by red baked tuff, and locally grade upward into a vesicular flow top directly overlain by tuff breccia lacking interclast-matrix (interpreted as flow-marginal autobreccia; Fig. 25c). The succession is interpreted as subaerial.

Subvertical east-west trending mafic subvolcanic dikes and intrusions (unit EMJhm) cut broadly contemporaneous volcano-sedimentary rocks of the upper Hazelton Group and older rocks of the Nightout pluton (Fig. 22). The presence of different textural varieties of mafic subvolcanic intrusions, local sharp internal intrusive contacts, and rare screens of probable volcanic rocks, suggest the southern slopes of Mount Walter may represent an intrusive complex that fed Horn Mountain volcanism. This unit was mapped along the alpine ridges near Mount Walter; its presence on the lower southern slopes of Mount Walter is inferred based on regional mapping by Souther (1972).

3.4.3. Intrusions (Middle Jurassic)

A quartz monzonitic intrusive body was mapped by Souther (1972) in the southern part of the study area

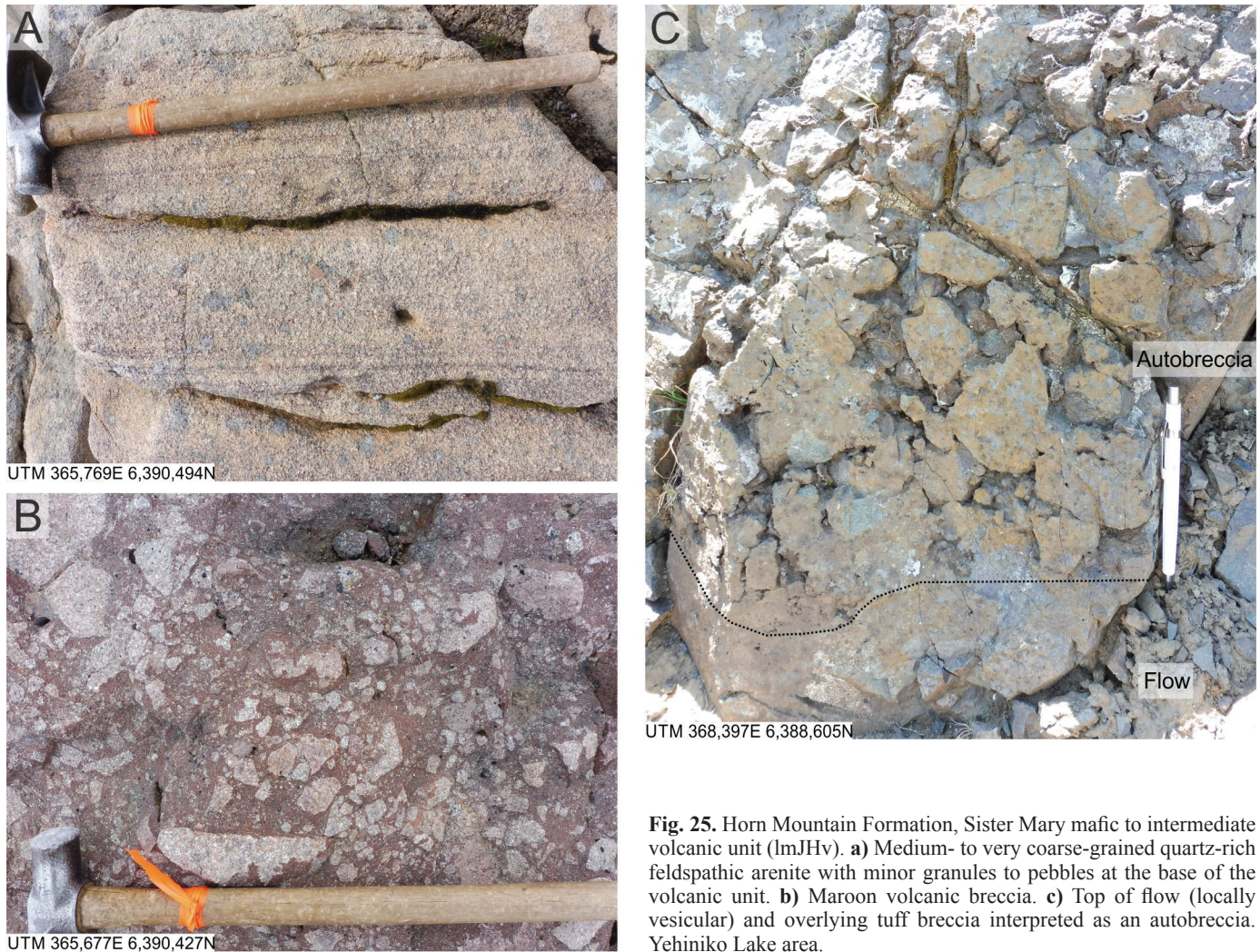


Fig. 25. Horn Mountain Formation, Sister Mary mafic to intermediate volcanic unit (ImJHv). **a)** Medium- to very coarse-grained quartz-rich feldspathic arenite with minor granules to pebbles at the base of the volcanic unit. **b)** Maroon volcanic breccia. **c)** Top of flow (locally vesicular) and overlying tuff breccia interpreted as an autobreccia. Yehiniko Lake area.

(Fig. 22; unit MJTdqm). The lithology, geometry, and age of this intrusion are poorly constrained. It is tentatively assigned to the Three Sisters plutonic suite (Middle Jurassic) based on lithological similarity to the nearby Yehiniko and Saffron plutons described by Brown et al. (1996). Pink feldspar to quartz-biotite-feldspar porphyritic dikes that cut Horn Mountain volcanic rocks throughout the study area are probably related. On the southern slopes of Mount Walter, the intrusive body and its wall rocks are commonly gossanous and host the Boomerang showing (MINFILE 104G 446).

3.4.4. Sustut Group

Exposures in the westernmost part of the study area include interbedded coarse- to very coarse-grained quartz-bearing feldspathic arenite, very fine- to medium-grained maroon to grey sandstone with minor pinkish (hematite-altered?) mica grains, and conglomerate with granitoid pebbles and granules. We tentatively correlate these with exposures of the Sustut Group described by Brown et al. (1996) in the valleys to the west and south of our study area, who assigned it an Upper

Cretaceous to Paleocene age based on an 85.6 ± 6.0 Ma K-Ar biotite cooling age and one Early Paleocene palynomorph collection.

4. Discussion

Below we discuss the spatial variation of upper Hazelton Group and coeval strata (Pliensbachian to Aalenian) and Bowser Lake Group (Bajocian and younger) atop the Stuhini arc.

4.1. Spatial variation of upper Hazelton Group and coeval strata (Pliensbachian to Aalenian) atop the Stuhini arc

This study shows that thick (1-4 km) upper Hazelton Group volcanic successions are present along most of the Stikine arch. The following considers the variation in thickness, depositional setting, preserved areal extent (Fig. 26), and age (Fig. 27) of upper Hazelton Group and broadly coeval strata. The successions unconformably overlie Late Triassic rocks of the Stuhini arc (see Section 2) separated by a ca. 30 m.y. hiatus, except in the Spatsizi area where the lower contact was

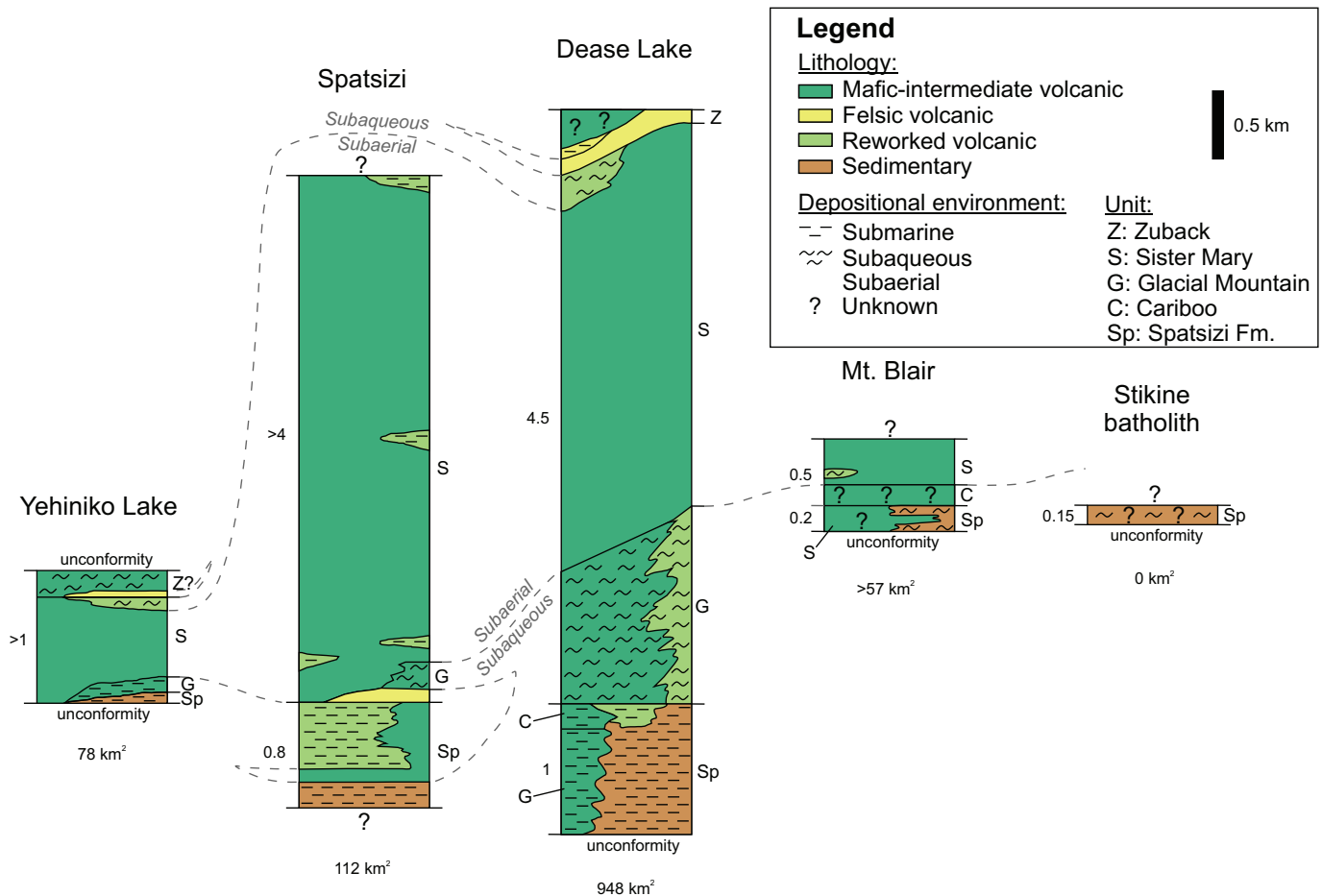


Fig. 26. Schematic representation of the variation in thickness, lithology, and depositional environment of upper Hazelton Group strata along the Stikine arch. Values at the bottom of each stratigraphic column represent the preserved areal extent of the Horn Mountain Formation in each area. Data from Read and Psutka (1990), Brown et al. (1996), Gabrielse (1998; 2003), Evenchick and Thorkelson (2005), Cui et al. (2017), van Straaten et al. (2022b), and this study.

not observed. Farther northwest along the Stikine arch, in the Sam batholith, Lisadele Lake, and Willison Bay areas (Fig. 2), broadly coeval sedimentary rocks of the Laberge Group (Lower Jurassic) unconformably overlie the Stuhini arc.

4.1.1. Stikine batholith and Mount Blair areas

The Stikine batholith and Mount Blair areas represent the easternmost occurrences of upper Hazelton Group strata documented in this study. In the Stikine batholith area, Spatsizi Formation granitoid clast-bearing conglomerate and sandstone unconformably overlie the Stikine batholith (Late Triassic). A sandstone sample returned a ca. 215 Ma U-Pb detrital zircon maximum depositional age, confirming derivation from Late Triassic plutonic rocks. Based on a similar lithology to elsewhere along the arch, the succession is likely late Pliensbachian to Toarcian. The unit contains mafic dike clasts, mafic volcanic clasts, and cross-cutting mafic dikes (all with similar lithology), suggesting mafic magmatism may have an overlapping, but broader, age range than the preserved sedimentary unit. Based on a similar lithology, composition,

and post-Late Triassic age, the mafic subvolcanic to volcanic activity is correlated with Horn Mountain volcanism (Early to Middle Jurassic). These observations suggest active Horn Mountain volcanism in the eastern part of the Stikine arch. The absence of volcanic rocks indicates that volcanism was relatively minor, and/or the volcanic strata have been eroded.

In the Mount Blair area, volcano-sedimentary rocks of the upper Hazelton Group unconformably overlie a granodiorite pluton with an inferred Late Triassic age. A section about 0.7 km thick is preserved in the eastern half of the study area, and felsic strata from near the top of the section returned a 172.05 ± 0.17 Ma CA-TIMS U-Pb zircon age. In the east, the upper part of the section is cut out by a fault. In the southeast and southwest, the contact between the Horn Mountain Formation and overlying Mount Blair Formation is conformable. The preserved areal extent of the Horn Mountain Formation is a minimum estimate because these strata likely extend west of the Tucho River. Poorly exposed basal conglomerate and sandstone of the Spatsizi Formation were likely transported and deposited by water and the depositional setting for the volcanic

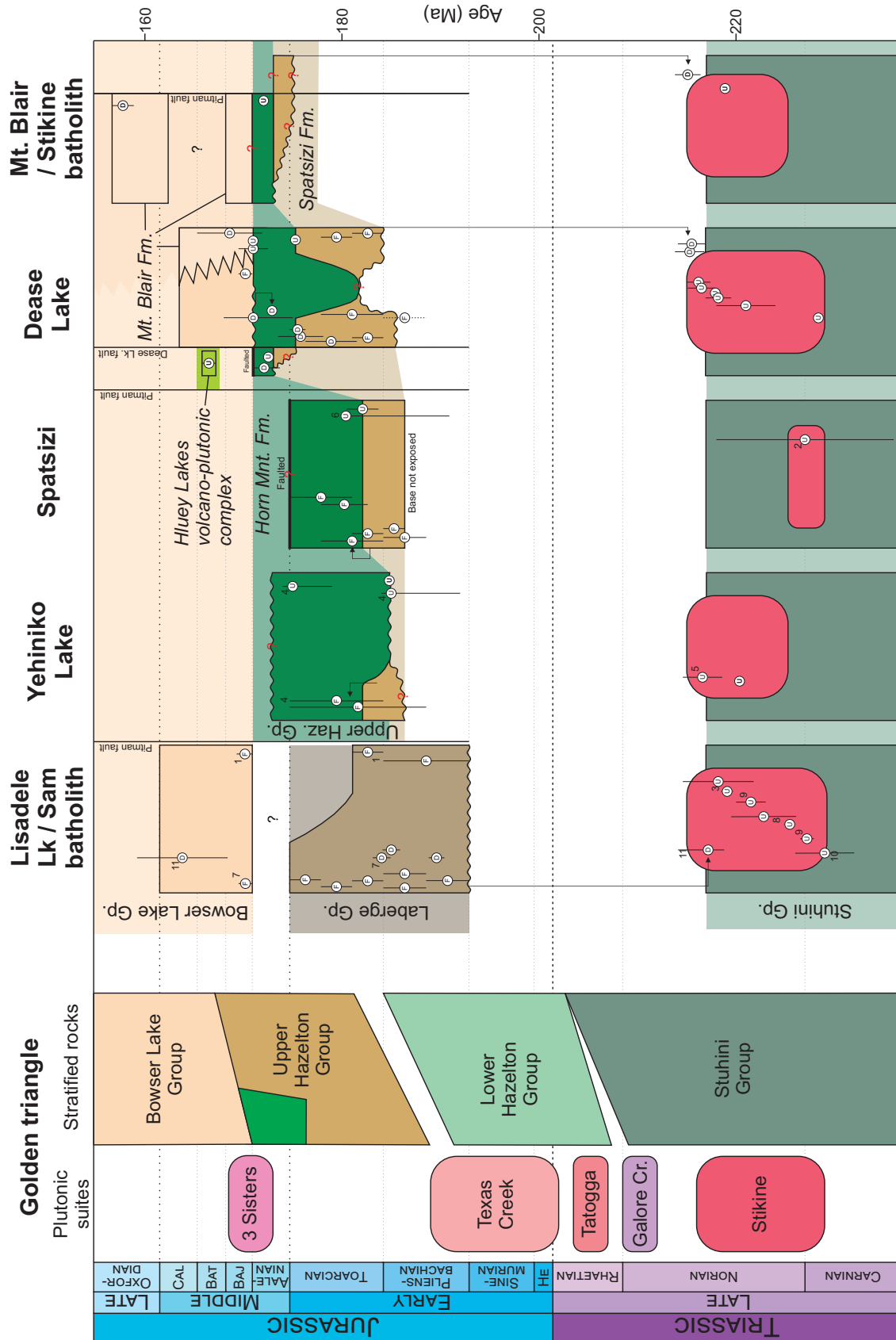


Fig. 27. Late Triassic to Jurassic stratigraphic framework for upper Hazelton Group and coeval strata atop the Stuhini arc in northwestern British Columbia. References for stratigraphic columns, fossil (F), U-Pb zircon (U) and U-Pb detrital zircon (D) ages: 1. Southern (1971), 2. Read and Psutka (1990), 3. Oliver and Gabites (1993), 4. Brown et al. (1966), 5. Logan et al. (2000), 6. Pálfi et al. (2000), 7. Shirmohammad et al. (2011), 8. Takaichi and Johnson (2012), 9. Takaichi (2013), 10. Mihalyuk et al. (2016), 11. Kellelt and Iraheta Muniz (2019). Stratigraphic column, fossil ages, and geochronological constraints for the Dease Lake area are from van Straaten et al. (2022b); fossil ages for the Spatsizi area are from Table 2; all other unlabelled geochronological ages are from this study. Red question marks denote poorly constrained age. The Golden triangle plutonic and stratigraphic framework is modified from Nelson et al. (2018) and Nelson and van Straaten (2020). Triassic and Jurassic time scale after Cohen et al. (2013). U-Pb detrital zircon maximum depositional ages for all samples were calculated by excluding individual grain ages with a probability of discordance <0.05, and using either the Youngest Statistical Population method of Coutts et al. (2019) or TuffZirc routine of Ludwig (2012), depending on which age is closest to the youngest graphical peak formed by three or more grains on an age-probability plot constructed using Isoplot (Ludwig, 2012).

rocks in the remainder of the lower half of the stratigraphic section is poorly constrained. The upper volcanic succession was largely deposited in a subaerial setting.

4.1.2. Dease Lake area

Along the Stikine arch, the thickest, most complete, and largest preserved areal extent of upper Hazelton Group strata are in the Dease Lake area (Fig. 26; van Straaten et al., 2022b). The best exposures are in a 70 km-long arcuate belt extending east to southeast from Highway 37 to the Pitman fault (Fig. 2). Here, a 5.5 km-thick volcano-sedimentary succession unconformably overlies the Cake Hill pluton (Late Triassic). In the west and east of the belt, basal strata are represented by sedimentary rocks of the Spatsizi Formation; in the centre of the belt, basal strata consist of Horn Mountain Formation volcanic rocks. The onset of deposition atop the basal upper Hazelton Group unconformity is constrained by late Pliensbachian(?) to early Toarcian fossils near the base of the Spatsizi Formation (Fig. 27; van Straaten et al., 2022b). The thickness variation within the Spatsizi Formation suggests that deposition was controlled by penecontemporaneous growth faults (van Straaten and Nelson, 2016; van Straaten and Gibson, 2017), where rapid basin deepening resulted in a change from subaerial erosion of granitoids and formation of grus, to granitoid clast-bearing conglomerates and fossiliferous sandstone deposited in a shallow-marine setting, to deeper marine interstratified argillite and siltstone (Henderson and Perry, 1981; van Straaten and Gibson, 2017). In the centre of the belt, subaqueous volcanic rocks of the Horn Mountain Formation rest directly on the basal upper Hazelton Group unconformity. They include mafic volcanic rocks of the Glacial Mountain unit overlain by distinct coarse platy plagioclase-phyric volcanic rocks of the Cariboo unit (lowermost unit of van Straaten and Gibson, 2017; van Straaten et al., 2022b). These volcanic rocks grade laterally into Spatsizi Formation sedimentary rocks containing late Pliensbachian(?) and early-middle Toarcian marine fossils, suggesting that the base of the Horn Mountain Formation is locally younger than ca. 175 Ma (Fig. 27; see below). This area may have been a topographic high or horst centred on the Cake Hill pluton (Late Triassic) during initial Spatsizi Formation sedimentation. In the west and east of the belt, sedimentary rocks of the Spatsizi Formation are overlain by volcanic rocks of the Horn Mountain Formation; in the centre of the belt, mafic volcanic rocks of the Glacial Mountain unit overlie coarse platy plagioclase-phyric volcanic rocks of the Cariboo unit. The age of this contact, which marks the onset of voluminous Horn Mountain volcanism, is well-constrained to ca. 175 Ma by a CA-TIMS U-Pb zircon age for basal felsic volcanic rocks and LA-ICP-MS U-Pb detrital zircon maximum depositional ages for immediately underlying sedimentary rocks of the Spatsizi Formation. The overlying Horn Mountain Formation is characterized by subaqueous mafic volcanic rocks of the Glacial Mountain unit, which transitions upward into maroon and grey subaerial mafic to intermediate volcanic rocks of the Sister Mary unit. In the west of the belt, a thick succession

of maroon subaerial volcanic rocks is overlain by reworked maroon epiclastic rocks (both of the Sister Mary unit), in turn overlain by subaerial felsic volcanic rocks with submarine strata locally reported near the top of the felsic unit (Zuback unit), and capped by mafic volcanic rocks with an unknown depositional setting (Zuback unit; Fig. 26). Here, the volcanic strata are unconformably overlain by marine sedimentary rocks of the Bowser Lake Group (van Straaten and Nelson, 2016; van Straaten and Gibson, 2017). Strong hydrothermal alteration along the Sister Mary-Zuback unit contact renders protolith identification locally challenging. In the east of the belt, maroon volcanic rocks of the Sister Mary unit are overlain by felsic volcanic rocks of the Zuback unit (Horn Mountain Formation, upper Hazelton Group), and interstratified sedimentary and volcanic rocks of the Mount Blair Formation (Bowser Lake Group; van Straaten and Bichlmaier, 2018; van Straaten et al., 2022b). The succession is conformable, and entirely subaerial. A high-precision CA-TIMS U-Pb zircon crystallization age on immediately underlying Horn Mountain Formation felsic volcanic rocks constrains the onset of Bowser Lake Group sedimentation to 170.99 ± 0.13 Ma. This age is based on the two youngest zircon grains, with three older antecrystic to xenocrystic grains showing 171.9, 172.1, and 173.7 Ma $^{206}\text{Pb}/^{238}\text{U}$ ages (B. van Straaten and R. Friedman, unpublished data), indicating significant inheritance. These observations suggest a nearly complete to completely preserved upper Hazelton Group stratigraphic section in this area.

From approximately 4 km east of Highway 37 to the Dease Lake fault, the Glacial Mountain unit shows a westward increase in the proportion of reworked volcanic strata. Here, the unit transitions from unconformably overlying the Cake Hill pluton (Late Triassic) to unconformably overlying the Stuhini Group (Upper Triassic; van Straaten et al., 2022b).

West of the Dease Lake fault, the upper Hazelton Group succession unconformably overlies the Stuhini Group (Upper Triassic) and is approximately 4 km thick. The succession has an approximately 30 km strike length, is poorly to moderately exposed, contains mainly reworked volcanic rocks, and returned a $172.1 \pm 1.6/-1.0$ Ma LA-ICP-MS U-Pb detrital zircon maximum depositional age. This unit conforms to a westward trend of increasing reworked volcanic strata described above. The top contact is the Kehlechoa fault. Farther west, a poorly to moderately exposed fault-bound succession of volcanic rocks (Glacial Mountain unit) with an approximately 10 km strike length may represent a separate Horn Mountain volcanic centre.

An outlier of upper Hazelton Group strata 27 km south of Dease Lake shows subaqueous sedimentary rocks of the Spatsizi Formation grading up into possibly subaerial volcanic rocks. Abrupt facies changes across north-trending faults may be related to syn-depositional faulting. The succession is 0.5 km thick, and the lower and upper contacts are not exposed. A 172.54 ± 0.11 Ma CA-TIMS U-Pb zircon age from the base of the volcanic rocks shows volcanism in this area started relatively late.

4.1.3. Spatsizi area

The Spatsizi area exposes the second largest preserved areal extent and second thickest succession of upper Hazelton Group along the Stikine arch. In the Spatsizi area, the base and top of the succession are not exposed. Here, volcano-sedimentary strata of the Spatsizi Formation are overlain by volcanic rocks of the Horn Mountain Formation. The Spatsizi Formation is at least 0.8 km thick (Figs. 17, 26) and contains late Pliensbachian, early Toarcian, and early-middle Toarcian fossils (Table 2). Latest Pliensbachian (Carlottense Zone) ammonoid collections with low accuracy locations (Table 2) were likely sampled from the Spatsizi Formation. A marine siliciclastic sedimentary unit (ImJSs) transitions upward into subaerial volcanic and subaqueous tuffaceous sedimentary rocks (unit ImJSsv; Fig. 26). Based on fossil evidence, volcanism within the Spatsizi Formation probably started in the latest Pliensbachian. The base of the overlying Horn Mountain Formation is constrained with a new 182.1 ± 1.6 Ma LA-ICP-MS U-Pb zircon age (Fig. 27), which matches an age with larger error reported by Pálffy et al. (2000). The Horn Mountain Formation comprises predominantly subaerial volcanic rocks (Evenchick and Thorkelson, 2005; this study) which we assign to the Sister Mary unit. The succession is at least 4 km thick (Read and Psutka, 1990), and contains rare early-middle Toarcian, middle-late Toarcian, Toarcian, probable Toarcian, and Early Jurassic fossils (Table 2; Read and Psutka, 1990; Evenchick and Thorkelson, 2005).

The volcanic unit has previously been interpreted as entirely Toarcian based on paleontological data and cross-cutting relationships with the McEwan Creek pluton (Evenchick and Thorkelson, 2005). However, the top of the volcanic unit is not exposed, and its uppermost strata in the north and east are bound by faults (Read and Psutka, 1990; Evenchick and Thorkelson, 2005). The paleontological evidence hinges on two localities near the top of the succession from which bivalves and belemnites with an Early Jurassic or probable Toarcian age were recovered (C-116297 and C-116299 in Read and Psutka, 1990; Evenchick and Thorkelson, 2005). To the immediate south of our study area the volcanic succession was described as being cut by leucogranite to quartz monzonite of the McEwan Creek pluton (Thorkelson, 1992; Evenchick and Thorkelson, 2005). A sample from the northwestern part of the pluton returned a 183.5 ± 0.5 Ma U-Pb zircon and 183.0 ± 0.5 Ma U-Pb titanite age (Evenchick and McNicoll, 1993). However, these ages were derived from one air abraded multi-grain zircon fraction and two unabraded multi-grain titanite fractions (Evenchick and McNicoll, 1993). As the pluton was mapped cutting the upper Hazelton Group volcano-sedimentary succession, the isotopic ages were proposed as a potential constraint for the Pliensbachian-Toarcian stage boundary (Evenchick and McNicoll, 1993; Pálffy, 1997). This interpretation is difficult to reconcile with the 182.1 ± 1.6 Ma LA-ICP-MS U-Pb zircon age (this study) for the base of the >4 km thick volcanic succession, a middle-late Toarcian fossil call for the volcanic strata (Table 2), the lack of detailed

presentation on crosscutting relationships between the pluton and the upper Hazelton Group volcano-sedimentary rocks, the several kilometre distance between the geochronological sample site and the location where the pluton is mapped in contact with upper Hazelton Group rocks, the use of a single air abraded zircon fraction for isotopic age determination, and the complexity and multi-episodic nature of many of the plutonic bodies along the Stikine arch (e.g., van Straaten et al., 2022b). Volcanism started significantly earlier in the Spatsizi area than in the nearby Dease Lake area, and, based on limited data, volcanic strata may be predominantly older than similar strata in the Dease Lake area (Fig. 27). Further geochronological and paleontological studies to constrain the age of the upper part of the succession are warranted.

4.1.4. Yehiniko Lake area

West of Yehiniko Lake, an outlier of relatively flat-lying Hazelton Group volcanic strata unconformably overlies the Stuhini Group (Brown et al., 1996). Individual stratigraphic sections show thicknesses ranging from 300 to 825 m, with a total thickness estimated at more than 1 km (Brown et al., 1996). In this outlier, the base is locally formed by a dacite flow or sill, locally overlain by a thin (<75 m) limy wacke unit with late Pliensbachian and Toarcian fossils; the sedimentary rocks are correlated here with the Spatsizi Formation. These units are overlain by andesitic breccias, flows and tuffs; these also form the base in the remainder of this outlier. An andesite flow breccia near the base of this unit returned a 185 ± 7 -1 Ma U-Pb zircon age (Brown et al., 1992), comparable to our more precise CA-TIMS U-Pb zircon age. The unit is lithologically similar to exposures near Yehiniko Lake described herein. The unit is interpreted as largely subaerial, except for rare thin marine volcanic rocks locally near the base, and we correlate it with the Sister Mary unit of the Horn Mountain Formation. Near the top of the andesitic unit are local epiclastic beds (Fig. 26), and they are locally overlain by a subaerial pink flow-banded rhyolite flow that returned a 175 ± 4 -1 Ma U-Pb zircon age (Brown et al., 1996). The age is based on a single strongly air abraded zircon fraction, all other unabraded fractions are discordant (interpreted to result from Pb loss; Brown et al., 1992). The felsic unit is in turn overlain by an up to 200 m thick unit of basalt flows and pillow basalt breccia, largely interpreted to be deposited subaqueously. The upper felsic and mafic units west of Yehiniko Lake are lithologically similar and have a similar stratigraphic position as felsic and overlying mafic volcanic rocks of the Zuback unit in the Dease Lake map area, albeit the former returned an older multi-grain U-Pb zircon age. Because inheritance is common in rhyolite of the upper Hazelton Group (e.g., Nelson et al., 2018; this study, see Section 4.1.2.), further geochronological analysis is warranted. The volcanic rocks are unconformably overlain by polymictic conglomerate and sandstone of unknown age, assigned by Brown et al. (1996) to the Sustut Group (Upper Cretaceous to Lower Paleocene). The unconformity is inferred to span >75 m.y. and may indicate a significant period of erosion; as a result, the upper Hazelton Group thickness estimate for this area is considered a minimum.

4.1.5. Lisadele Lake and Sam batholith areas

Several large Stikine plutonic suite (Late Triassic) intrusions mark the continuation of the Stuhini arc towards the northwest (Fig. 2). They include the Sam, Moosehorn, and other satellite stocks (Souther, 1971; Bradford and Brown, 1993) which returned ca. 229-217 Ma U-Pb zircon ages (Oliver and Gabites, 1993; Takaichi and Johnson, 2012; Takaichi, 2013; Zagorevski et al., 2015; Mihalynuk et al., 2016). Souther (1971) described at least 3.3 km of sedimentary rocks of the Takwahoni Formation (Lagerge Group) unconformably atop Late Triassic rocks, and reported Pliensbachian, early Toarcian, and middle Bajocian fossils. It should be noted that in 1980 the early Bajocian was formally changed to the Aalenian stage, and the middle Bajocian to early Bajocian. Detailed stratigraphic studies in the Lisadele Lake area show nearly 3 km of sedimentary strata unconformably overlying the Stuhini Group; the sedimentary rocks contain early Pliensbachian, late Pliensbachian, early, middle and late Toarcian, and early Bajocian fossils (Mihalynuk et al., 1995; Mihalynuk et al., 2004; Shirmohammad et al., 2011). The basal 150 m of the succession did not yield fossils, and its age is unconstrained. Previously the entire succession was assigned to the Takwahoni Formation (Lagerge Group). However, Shirmohammad et al. (2011) reassigned the uppermost chert-pebble conglomerate and immediately underlying 100 m of black mudstone (early Bajocian) to the Bowser Lake Group, a reassignment that is followed here for all other Bajocian strata in the region. U-Pb detrital zircon samples from the Lagerge Group (Shirmohammad et al., 2011; Kellett and Iraheta Muniz, 2019) yielded Late Triassic, and Pliensbachian to early Toarcian maximum depositional ages (Fig. 27), with Late Triassic peaks likely reflecting derivation from erosion of Stikine plutonic suite intrusions. A U-Pb detrital zircon sample from the overlying Bowser Lake Group (Kellett and Iraheta Muniz, 2019) shows a Callovian maximum depositional age (Fig. 27). Farther northwest, the Willison Bay pluton (Stikine plutonic suite, Late Triassic; Fig. 2) is unconformably overlain by conglomerate and sandstone (Mihalynuk, 1999), with a sandstone sample returning a Jurassic U-Pb detrital zircon maximum depositional age, suggesting correlation with the Lagerge Group (Zagorevski et al., 2015).

4.2. Spatial variation of Bowser Lake Group strata (Bajocian and younger) atop the Stuhini arc

In the Mount Blair and eastern Dease Lake map area, the Horn Mountain Formation (upper Hazelton Group) is conformably overlain by the newly defined Mount Blair Formation (Middle-Upper Jurassic, Bowser Lake Group). The Mount Blair Formation represents a unique subaerial unit of siltstone, sandstone, chert clast-bearing conglomerate, mafic flows, and mafic fragmental volcanic rocks. A precise 170.99 ± 0.13 Ma CA-TIMS U-Pb zircon age on immediately underlying volcanic rocks (van Straaten et al., 2022b) constrains the onset of deposition of erosional products from the Stikinia-Cache Creek tectonic welt. A thick succession of chert and limestone clast-bearing pebble to cobble conglomerate in the Dease Lake

map area is interpreted to have formed close to range-front faults along the building orogen. This coarse facies transitions southward to interbedded subaerial siltstone, sandstone, chert clast-bearing conglomerate and mafic volcanic rocks (van Straaten and Bichlmaier, 2018).

Bajocian and younger marine sedimentary rocks of the Bowser Lake Group are recorded in the centre and rarely east of the Dease Lake map area (van Straaten and Nelson, 2016; van Straaten and Bichlmaier, 2018; van Straaten et al., 2022b), and at Lisadele Lake (Shirmohammad et al., 2011). Together with the Mount Blair Formation, these occurrences represent the oldest documented rocks in the Bowser Lake Group. Farther south within the contiguous Bowser basin (Fig. 2), rocks at the base of the Bowser Lake Group get progressively younger from north to south. Basal strata in the northern part of the contiguous Bowser basin are Bathonian; in the centre and south they are Callovian to Oxfordian (Evenchick et al., 2010). Within the contiguous Bowser basin, the Bowser Lake Group (Middle Jurassic to Cretaceous) comprises a shallowing-upward succession deposited in submarine fan, submarine slope, shallow-marine shelf to deltaic environments (Evenchick and Thorkelson, 2005). The oldest (Bathonian) strata in the northern and northeastern part of the contiguous Bowser basin were deposited in submarine fan to submarine slope environments, followed by deposition in shallow-marine shelf and deltaic environments by the early Oxfordian (Evenchick and Thorkelson, 2005; Evenchick et al., 2010).

5. Conclusions

Stratigraphic studies presented here focus on Late Triassic to Jurassic strata in four study areas along the Stikine arch and compare them to well-studied successions in the Dease Lake area. The oldest units investigated in this study include Stuhini Group mafic volcanic rocks (Upper Triassic) cut by Stikine plutonic suite intrusions (Late Triassic). I provide two new ca. 220.36 ± 0.13 and 218.89 ± 0.12 Ma CA-TIMS U-Pb zircon ages for the Stikine plutonic suite, which conform to a previously established ca. 229-216 Ma age range. These units define major volcano-plutonic centres that make up the east-facing Stuhini arc.

Stuhini arc rocks are unconformably overlain by late Early to Middle Jurassic volcano-sedimentary strata of the upper Hazelton Group and coeval strata. The unconformity spans at least 30 m.y. and indicates a prolonged period of uplift and erosion of the Stuhini arc that followed cessation of subduction and termination of arc activity in the latest Triassic.

This study shows that thick (1-5 km) successions of upper Hazelton Group rocks extend for at least ~275 km along the Stikine arch. A uniform stratigraphic nomenclature for these successions includes basal sedimentary rocks of the Spatsizi Formation and overlying volcanic rocks of the Horn Mountain Formation. Volcano-sedimentary units are lithologically similar along the entire length of the belt, typically showing a transition from early submarine volcano-sedimentary facies to overlying subaerial volcanic facies. Where preserved,

uppermost volcanic facies range from subaqueous to subaerial. The thickest successions are in the Spatsizi and Dease Lake areas (>4.8 km), with thinner successions in the Yehiniko Lake and Mount Blair areas (>0.7-1 km). In the Yehiniko Lake and Dease Lake areas, the onset of sedimentary deposition atop the basal unconformity is constrained to late Pliensbachian to early Toarcian. New geochronological results show that Horn Mountain volcanism started ca. 185 Ma in the Yehiniko area, and the latest Pliensbachian to ca. 182 Ma in the Spatsizi area. Horn Mountain volcanism in the Yehiniko Lake and Spatsizi areas continued until at least the end of the Toarcian. Minor Horn Mountain volcanic activity in the Dease Lake area probably started as early as late Pliensbachian to middle Toarcian. However, voluminous and extensive volcanism occurred from ca. 175-171 Ma (Aalenian); this represents a significantly later onset of main-stage volcanism compared to the Yehiniko Lake and Spatsizi areas. Volcanic activity in the Dease Lake area is centred on a Late Triassic pluton, with primary volcanic strata giving way westward to reworked volcanic strata. In the Mount Blair area, volcanism may have started later than in the eastern Dease Lake area but shows similarities to exposures in the western Dease Lake area. The general pattern is permissive of an eastward younging trend in the onset of upper Hazelton Group deposition atop the Stuhini arc.

Horn Mountain volcanism does not record normal subduction-related arc magmatism, because it formed well after cessation of subduction in the latest Triassic. Instead, upper Hazelton Group volcanism occurred during accretion of the Quesnel, Cache Creek, and Stikine terranes to Ancestral North America, and was possibly generated by re-melting of subduction-modified lithosphere during accretion (van Straaten and Nelson, 2016). The upper Hazelton Group successions are coincident with major Late Triassic volcano-plutonic centres, suggesting that earlier arc magmatic reservoirs may have been tapped.

Farther northwest along the Stikine arch, the Stuhini arc is unconformably overlain by thick (~3 km) Pliensbachian to Toarcian marine siliciclastic rocks of the Laberge Group, part of the Whitehorse trough. It represents a syn-collisional depositional basin, formed as a result of collision between Stikinia and Yukon-Tanana (Colpron et al., 2022).

In the Lisadele Lake and parts of the Dease Lake area, upper Hazelton Group and coeval Laberge Group strata are overlain by marine siliciclastic rocks of the Bowser Lake Group. In the eastern part of the Dease Lake area and in the Mount Blair area, the upper Hazelton Group is conformably overlain by terrestrial siliciclastic and subaerial mafic volcanic rocks of the Mount Blair Formation (newly defined herein, part of the Bowser Lake Group). These successions represent the oldest preserved Bowser Lake Group and indicate the onset of deposition of erosional products from the Stikinia-Cache Creek tectonic welt.

Acknowledgments

Thanks to Carly Smythe, Rachel Gavin, Sadye Butler, Natasha Drage, Rebecca Hunter, and Meghan Holowath who assisted with fieldwork in 2016-19, Richard Friedman for providing preliminary geochronological data, Alexandra Pipe for expert figure drafting, and Lakelse Air and Tundra Helicopters for safe flying. A constructive review by Paul Schiarizza helped improve the paper.

References cited

- Aberhan, M., and Pálffy, J., 1996. A low oxygen tolerant East Pacific flat clam (*Posidonotis semiplicata*) from the Lower Jurassic of the Canadian Cordillera. *Canadian Journal of Earth Sciences*, 33, 993-1006.
<<https://doi.org/10.1139/e96-075>>
- Alldrick, D.J., 1993. Geology and metallogeny of the Stewart mining camp, northwestern British Columbia. British Columbia Ministry of Energy, Mines and Petroleum Resources, British Columbia Geological Survey, Bulletin 85, 105 p.
- Anderson, R.G., 1984. Late Triassic and Jurassic magmatism along the Stikine Arch and the geology of the Stikine batholith, north-central British Columbia. In: *Current Research, Part A, Geological Survey of Canada Paper 84-1A*, pp. 67-73.
- Bradford, J.A., and Brown, D.A., 1993. Geology, Mineral Occurrences and Geochemistry of the Bearskin and Tatsamenie Lakes Area, Northwestern B.C. British Columbia Ministry of Energy and Mines, British Columbia Geological Survey Open File 1993-01, 1:50,000 scale.
- Breitsprecher, K., and Mortensen, J.K., 2004. BC age 2004A-1: A database of isotopic age determinations for rock units from British Columbia. British Columbia Ministry of Energy, Mines and Petroleum Resources, British Columbia Geological Survey Open File 2004-03.
- Brown, D.A., Greig, C.J., Bevier, M.L., and McClelland, W.C., 1992. U-Pb zircon ages for the Hazelton Group and Cone Mountain and Limpoke plutonis, Telegraph Creek map area, northwestern British Columbia: age constraints on volcanism and deformation. In: *Radiogenic Age and Isotopic Studies: Report 6, Geological Survey of Canada, Paper 92-2*, pp. 153-162.
- Brown, D.A., Gunning, M.H., and Greig, C.J., 1996. The Stikine project: Geology of western Telegraph Creek map area, northwestern British Columbia. British Columbia Ministry of Employment and Investment, British Columbia Geological Survey Bulletin 95, 130 p.
- Campbell, M.E., 2021. The geology and geochemistry of the Sulphurets district porphyry Au-Cu-Mo deposits, British Columbia, Canada: Insights from a long-lived, gold-enriched porphyry district. Unpublished Ph.D. thesis, Oregon State University, 238 p.
- Cohen, K.M., Finney, S.C., Gibbard, P.L., and Fan, J.-X., 2013. The ICS International Chronostratigraphic Chart. *Episodes*, 36, 199-204 (updated version September, 2023).
<<https://stratigraphy.org/ICSchart/ChronostratChart2023-09.pdf>>
- Colpron, M., 2020. Yukon terranes-A digital atlas of terranes for the northern Cordillera. Yukon Geological Survey.
<<https://data.geology.gov.yk.ca/Compilation/2#InfoTab>>
- Colpron, M., Crowley, J.L., Gehrels, G., Long, D.G.F., Murphy, D.C., Beranek, L., and Bickerton, L., 2015. Birth of the northern Cordilleran orogen, as recorded by detrital zircons in Jurassic synorogenic strata and regional exhumation in Yukon. *Lithosphere*, 7, 541-562.
<<https://doi.org/10.1130/L451.1>>

- Colpron, M., Sack, P.J., Crowley, J.L., Beranek, L.P., and Allan, M.M., 2022. Late Triassic to Jurassic magmatic and tectonic evolution of the Intermontane terranes in Yukon, Northern Canadian Cordillera: Transition from arc to syn-collisional magmatism and post-collisional lithospheric delamination. *Tectonics*, 41, article e2021tc007060. <<https://doi.org/10.1029/2021TC007060>>
- Coutts, D.S., Matthews, W.A., and Hubbard, S.M., 2019. Assessment of widely used methods to derive depositional ages from detrital zircon populations. *Geoscience Frontiers*, 10, 1421-1435. <<https://doi.org/10.1016/j.gsf.2018.11.002>>
- Cui, Y., Hickin, A.S., Schiarizza, P., and Diakow, L.J., 2017. British Columbia digital geology. British Columbia Ministry of Energy, Mines and Petroleum Resources, British Columbia Geological Survey Open File 2017-08, 9 p.
- Erdman, L.R., 1978. Petrology, geochronology and geochemistry of Jurassic volcanic and granitic rocks of the Cry Lake and Spatsizi map sheets, north-central British Columbia. Unpublished B.Sc. thesis, The University of British Columbia, Vancouver, B.C., Canada, 63 p.
- Evenchick, C.A., and McNicoll, V.J., 1993. U-Pb age for the Jurassic McEwan Creek pluton, north-central British Columbia: regional setting and implications for the Toarcian stage boundary. In: Radiogenic age and isotopic studies: Report 7, Geological Survey of Canada Paper 93-2, pp. 91-97.
- Evenchick, C.A., and Thorkelson, D.J., 2005. Geology of the Spatsizi River map area, north-central British Columbia. Geological Survey of Canada Bulletin 577, 276 p.
- Evenchick, C.A., McMechan, M.E., McNicoll, V.J., and Carr, S.D., 2007. A synthesis of the Jurassic-Cretaceous tectonic evolution of the central and southeastern Canadian Cordillera: Exploring links across the orogen. In: Sears, J.W., Harms, T.A., and Evenchick, C.A., (Eds.), *Whence the Mountains? Inquiries into the Evolution of Orogenic Systems: A Volume in Honor of Raymond A. Price*. Geological Society of America Special Paper 433, 117-145.
- Evenchick, C.A., Poulton, T.P., and McNicoll, V.J., 2010. Nature and significance of the diachronous contact between the Hazelton and Bowser Lake groups (Jurassic), north-central British Columbia. *Bulletin of Canadian Petroleum Geology*, 58, 235-267. <<https://doi.org/10.2113/gscpgbull.58.3.235>>
- Gabrielse, H., 1998. Geology of Cry Lake and Dease Lake map areas, North-Central British Columbia. Geological Survey of Canada, Bulletin 504, 147 p.
- Gabrielse, H., 2003. Geology, Kechika River, British Columbia. Geological Survey of Canada, Open File 1633, 1:250,000 scale.
- Gabrielse, H., Doods, C.J., Mansy, J.L., and Eisenbacher, G.H., 1977. Geology of Toodogone and Ware map areas, British Columbia. Geological Survey of Canada, Open File 483, 1:250,000 scale.
- Gagnon, J.-F., Barresi, T., Waldron, J.W.F., Nelson, J.L., Poulton, T.P., and Cordey, F., 2012. Stratigraphy of the upper Hazelton Group and the Jurassic evolution of the Stikine terrane, British Columbia. *Canadian Journal of Earth Sciences*, 49, 1027-1052. <<https://doi.org/10.1139/e2012-042>>
- Henderson, C.M., and Perry, D.G., 1981. A Lower Jurassic heteroporid bryozoan and associated biota, Turnagain Lake, British Columbia. *Canadian Journal of Earth Sciences*, 18, 457-468. <<https://doi.org/10.1139/e81-040>>
- Henderson, J.R., Kirkham, R.V., Henderson, M.N., Payne, J.G., Wright, T.O., and Wright, R.L., 1992. Stratigraphy and structure of the Sulphurets area, British Columbia. In: *Current Research, Part A, Cordillera and Pacific Margin*, Geological Survey of Canada, Paper 92-1A, pp. 323-332.
- Holbek, P.M., 1988. Geology and mineralization of the Stikine assemblage, Mess Creek area, northwestern British Columbia. Unpublished M.Sc. thesis, University of British Columbia, 175 p. <<https://doi.org/10.14288/1.0052696>>
- Hollis, L., and Bailey, L., 2013. Assessment report on drilling, geological, geochemical and geophysical work conducted during 2012 at the GJ/Kinaskan copper-gold porphyry project. British Columbia Ministry of Energy and Mines, British Columbia Geological Survey Assessment Report 33815, 60 p.
- Hunt, P.A., and Roddick, J.C., 1987. A compilation of K-Ar ages, Report 17. In: *Radiogenic age and isotopic studies: Report 1*, Geological Survey of Canada Paper 87-2, pp. 143-210.
- Jakobs, G., 1997. Toarcian (Early Jurassic) ammonoids from western North America. Geological Survey of Canada Bulletin 428, 144 p.
- Jakobs, G.K., Smith, P.L., and Tipper, H.W., 1994. An ammonite zonation for the Toarcian (Lower Jurassic) of the North American Cordillera. *Canadian Journal of Earth Sciences*, 31, 919-942. <<https://doi.org/10.1139/e94-083>>
- Kellett, D.A., and Iraheta Muniz, P., 2019. Detrital U-Pb zircon and ⁴⁰Ar/³⁹Ar muscovite geochronology of the Whitehorse trough, and surrounding rocks, Yukon and British Columbia. Geological Survey of Canada, Open File 8565, 33 p.
- Logan, J.M., and Koyanagi, V.M., 1994. Geology and mineral deposits of the Galore Creek area. British Columbia Ministry of Energy, Mines and Petroleum Resources, British Columbia Geological Survey, Bulletin 92, 102 p.
- Logan, J.M., Drobe, J.R., and McClelland, W.C., 2000. Geology of the Forrest Kerr-Mess Creek area, northwestern British Columbia. British Columbia Ministry of Energy and Mines, British Columbia Geological Survey Bulletin 104, 132 p.
- Ludwig, K.R., 2012. *Isoplot 3.75. A geochronological toolkit for Microsoft Excel*. Berkley Geochronology Center, Special Publication 5, 75 p.
- Mihalynuk, M.G., 1999. Geology and mineral resources of the Tagish Lake Area, (NTS 104M/8, 9, 10E, 15 and 104N/12W), northwestern British Columbia. British Columbia Ministry of Energy and Mines, British Columbia Geological Survey Bulletin 105, 202 p.
- Mihalynuk, M.G., Nelson, J., and Diakow, L.J., 1994. Cache Creek terrane entrapment: Oroclinal paradox within the Canadian Cordillera. *Tectonics*, 13, 575-595. <<https://doi.org/10.1029/93TC03492>>
- Mihalynuk, M.G., Meldrum, D., Sears, S., and Johannson, G., 1995. Geology and mineralization of the Stuhini Creek area (104K/11). In: *Geological Fieldwork 1994*, British Columbia Ministry of Energy, Mines and Petroleum Resources, British Columbia Geological Survey Paper 1995-01, pp. 321-342.
- Mihalynuk, M.G., Erdmer, P., Ghent, E.D., Cordey, F., Archibald, D.A., Friedman, R.M., and Johannson, G.G., 2004. Coherent French Range blueschist: Subduction to exhumation in <2.5 m.y.? *Geological Society of America Bulletin*, 116, 910-922. <<https://doi.org/10.1130/B25393.1>>
- Mihalynuk, M.G., Zagorevski, A., Joyce, N.L., and Creaser, R.A., 2016. Age of magmatism and mineralization at the Star (Sheslay, Copper Creek) copper porphyry prospect: Inception of the Late Triassic mineralized arc. In: *Geological Fieldwork 2015*, British Columbia Ministry of Energy and Mines, British Columbia Geological Survey Paper 2016-1, pp. 65-75.
- Miller, E.A., van Straaten, B.I., and Hunter, R.C., 2023. Update on bedrock mapping in the Kitsault River area, northwestern British Columbia. Geological Fieldwork 2022, British Columbia Ministry of Energy, Mines and Low Carbon Innovation, British Columbia Geological Survey Paper 2023-01, pp. 23-32.
- Nelson, J.L., and van Straaten, B.I., 2020. Recurrent syn- to post-subduction mineralization along deep crustal corridors in the Iskut-Stewart-Kitsault region of western Stikinia, northwestern British Columbia. In: *Sharman, E. R., Lang, J. R., and Chapman, J.B., (Eds.), Porphyry Deposits of the Northwestern Cordillera of North America: A 25-Year Update*, CIM Special Volume 57, pp. 149-211.
- Nelson, J.L., Colpron, M., and Israel, S., 2013. The Cordillera of British Columbia, Yukon and Alaska: Tectonics and metallogeny.

- In: Colpron, M., Bissig, T., Rusk, B. G., and Thompson, J. (Eds.), *Tectonics, Metallogeny and Discovery: The North American Cordillera and Similar Accretionary Settings*, Society of Economic Geologists Special Publication 17, pp. 53-110.
- Nelson, J.L., Waldron, J., van Straaten, B.I., Zagorevski, A., and Rees, C., 2018. Revised stratigraphy and regional digital map representation of the Hazelton Group in the Iskut River region, northwestern British Columbia. In: *Geological Fieldwork 2017*, British Columbia Ministry of Energy, Mines and Petroleum Resources, British Columbia Geological Survey Paper 2018-1, pp. 15-38.
- Nelson, J.L., van Straaten, B., and Friedman, R., 2022. Latest Triassic-Early Jurassic Stikine-Yukon-Tanana terrane collision and the onset of accretion in the Canadian Cordillera: Insights from Hazelton Group detrital zircon provenance and arc-back-arc configuration. *Geosphere*, 18, 670-696. <<https://doi.org/10.1130/GES02444.1>>
- Oliver, J., and Gabites, J., 1993. Geochronology of rocks and polyphase deformation, Bearskin (Muddy) and Tatsamenie lakes district, northwestern British Columbia (104K/8, 1). In: *Geological Fieldwork 1992*, British Columbia Ministry of Energy, Mines and Petroleum Resources, British Columbia Geological Survey Paper 1993-1, pp. 177-188.
- Pálffy, J., 1997. Calibration of the Jurassic time scale. Unpublished Ph.D. thesis, University of British Columbia, 170 p. <<https://doi.org/10.14288/1.0052486>>
- Pálffy, J., Mortensen, J.K., Smith, P.L., Friedman, R.M., McNicoll, V., and Villeneuve, M., 2000. New U-Pb zircon ages integrated with ammonite biochronology from the Jurassic of the Canadian Cordillera. *Canadian Journal of Earth Sciences*, 37, 549-567. <<https://doi.org/10.1139/e99-115>>
- Read, P.B., and Psutka, J.F., 1990. Geology of Ealue Lake east-half (104H/13E) and Cullivan Creek (104H/14) map areas, British Columbia. Geological Survey of Canada, Open File 2241, 1:50,000 scale.
- Rhys, D.A., 1993. Geology of the Snip Mine, and its relationship to the magmatic and deformational history of the Johnny Mountain area, northwestern British Columbia. Unpublished M.Sc. thesis, The University of British Columbia, Vancouver, B.C., Canada. <<https://circle.ubc.ca/handle/2429/2173>> (accessed April 12, 2012).
- Shirmohammad, F., Smith, P.L., Anderson, R.G., and McNicoll, V.J., 2011. The Jurassic succession at Lisadele Lake (Tulsequah map area, British Columbia, Canada) and its bearing on the tectonic evolution of the Stikine terrane. *Volumina Jurassica*, 9, 43-60. <<https://doi.org/10.5604/17313708.1114171>>
- Smith, P.L., Thomson, R.C., and Tipper, H.W., 1984. Lower and Middle Jurassic sediments and volcanics of the Spatsizi area, British Columbia. In: *Current Research, Part A*, Geological Survey of Canada Paper 84-1A, pp. 117-120.
- Souther, J.G., 1971. Geology and mineral deposits of Tulsequah map area, British Columbia (104K). Geological Survey of Canada, Memoir 362, 84 p.
- Souther, J.G., 1972. Telegraph Creek map-area, British Columbia (104G). Geological Survey of Canada, Paper 71-44 and Map 11-1971, 36 p.
- Takaichi, M., 2013. Assessment Report on the 2012 Geological, Geochemical, and Geophysical Program at the Eagle Property, BC, Canada. British Columbia Ministry of Energy and Mines, British Columbia Geological Survey Assessment Report 34266, 22 p.
- Takaichi, M., and Johnson, C., 2012. Assessment Report on the 2011/2012 Geological, Geochemical, and Geophysical program at the Eagle Property, BC, Canada. British Columbia Ministry of Energy and Mines, British Columbia Geological Survey Assessment Report 33330, 27 p.
- Thomson, R.C., and Smith, P.L., 1992. Pliensbachian (Lower Jurassic) biostratigraphy and ammonite fauna of the Spatsizi area, north-central British Columbia. Geological Survey of Canada Bulletin 437, 87 p.
- Thomson, R.C., Smith, P.L., and Tipper, H.W., 1986. Lower to Middle Jurassic (Pliensbachian to Bajocian) stratigraphy of the northern Spatsizi area, north-central British Columbia. *Canadian Journal of Earth Sciences*, 23, 1963-1973. <<https://doi.org/10.1139/e86-182>>
- Thorkelson, D.J., 1992. Volcanic and tectonic evolution of the Hazelton group in Spatsizi River (104H) map-area, north-central British Columbia. Unpublished Ph.D. thesis, Carleton University, Ottawa, Ontario, Canada, 281 p.
- Tipper, H.W., 1986. Report on Pliensbachian fossils collected in the Spatsizi map area 104H collected between 1975 and 1985 and submitted for identification in November 1985. Geological Survey of Canada, Paleontological Report J19-1986-HWT.
- van Drecht, L.H., Beranek, L.P., Colpron, M., and Wiest, A.C., 2022. Development of the Whitehorse trough as a strike-slip basin during Early to Middle Jurassic arc-continent collision in the Canadian Cordillera. *Geosphere*, 18, 1538-1562. <<https://doi.org/10.1130/GES02510.1>>
- van Straaten, B.I., and Bichlmaier, S.J., 2018. Late Early to Middle Jurassic Hazelton Group volcanism and its tectonic setting, McBride River area, northwest British Columbia. In: *Geological Fieldwork 2017*, British Columbia Ministry of Energy and Mines, British Columbia Geological Survey Paper 2018-1, pp. 39-66.
- van Straaten, B.I., and Gibson, R., 2017. Late Early to Middle Jurassic Hazelton Group volcanism and mineral occurrences in the McBride-Tanzilla area, northwest British Columbia. In: *Geological Fieldwork 2016*, British Columbia Ministry of Energy Mines and Petroleum Resources, British Columbia Geological Survey Paper 2017-1, pp. 83-115.
- van Straaten, B.I., and Nelson, J.L., 2016. Syncollisional late Early to early Late Jurassic volcanism, plutonism, and porphyry-style alteration on the northeastern margin of Stikinia. In: *Geological Fieldwork 2015*, British Columbia Ministry of Energy and Mines, British Columbia Geological Survey Paper 2016-1, pp. 113-143.
- van Straaten, B.I., Logan, J.M., Hunter, R.C., Nelson, J.L., and Miller, E.A., 2022a. Igneous lithogeochemistry data for the Dease Lake, Kitsault River, Galore Creek, Telegraph Creek, Foremore, and other areas in northwestern British Columbia. British Columbia Ministry of Energy, Mines and Low Carbon Innovation, British Columbia Geological Survey GeoFile 2022-12, 14 p.
- van Straaten, B.I., Logan, J.M., Nelson, J.L., Moynihan, D.P., Diakow, L.J., Gibson, R., Bichlmaier, S.J., Wearmouth, C.D., Friedman, R.M., Golding, M.L., Miller, E.A., and Poulton, T.P., 2022b. Bedrock geology of the Dease Lake area. British Columbia Ministry of Energy, Mines and Low Carbon Innovation, British Columbia Geological Survey Geoscience Map 2022-01, 1:100,000 scale.
- van Straaten, B.I., Friedman, R.M., and Camacho, A., 2023. Stratigraphy of the Stuhini Group (Upper Triassic) in the Galore Creek area, northwestern British Columbia. In: *Geological Fieldwork 2022*, British Columbia Ministry of Energy, Mines and Low Carbon Innovation, British Columbia Geological Survey Paper 2023-01, pp. 33-49.
- Wanless, R.K., Stevens, R.D., Lachance, G.R., and DeLabio, R.N., 1979. Age determinations and geological studies: K-Ar isotopic ages, report 14. Geological Survey of Canada Paper 79-2, 67 p.
- Zagorevski, A., Mihalynuk, M.G., Joyce, N., Kellett, D.A., and Milidragovic, D., 2015. Characterization of volcanic and intrusive rocks across the British Columbia-Yukon border, GEM 2 Cordillera. Geological Survey of Canada, Open File 7956, 13 p.

British Columbia Geological Survey Publications 2023 including peer-reviewed external papers co-authored by BCGS staff

All BCGS publications are available for download, free of charge, from
www.BCGeologicalSurvey.ca

To receive notification of our latest releases email
Geological.Survey@gov.bc.ca



Papers

Paper 2023-01

Geological Fieldwork 2022. British Columbia Ministry of Energy, Mines and Low Carbon Innovation, British Columbia Geological Survey Paper 2023-01, 95 p.

Wildgust, N., Cui, Y., Clarke, G., and Hickin, A.S., 2023. British Columbia Geological Survey annual program review 2022-2023. In: Geological Fieldwork 2022, British Columbia Ministry of Energy, Mines and Low Carbon Innovation, British Columbia Geological Survey Paper 2023-01, pp. 1-11.

Ootes, L., 2023. Did epithermal mineralization in the northern Toodoggone region develop synchronously with large scale folding? In: Geological Fieldwork 2022, British Columbia Ministry of Energy, Mines and Low Carbon Innovation, British Columbia Geological Survey Paper 2023-01, pp. 13-21.

Miller, E.A., van Straaten, B.I., and Hunter, R.C., 2023. Update on bedrock mapping in the Kitsault River area, northwestern British Columbia. In: Geological Fieldwork 2022, British Columbia Ministry of Energy, Mines and Low Carbon Innovation, British Columbia Geological Survey Paper 2023-01, pp. 23-32.

van Straaten, B.I., Friedman, R.M., and Camacho, A., 2023. Stratigraphy of the Stuhini Group (Upper Triassic) in the Galore Creek area, northwestern British Columbia. In: Geological Fieldwork 2022, British Columbia Ministry of Energy, Mines and Low Carbon Innovation, British Columbia Geological Survey Paper 2023-01, pp. 33-49.

Johnston, R., Kennedy, L., and van Straaten, B.I., 2023. Preliminary observations of a high-strain zone along the western flank of the Galore Creek deposit area, northwestern British Columbia. In: Geological Fieldwork 2022, British Columbia Ministry of Energy, Mines and Low Carbon Innovation, British Columbia Geological Survey Paper 2023-01, pp. 51-63.

Schiarizza, P., and Friedman, R.M., 2023. U-Pb zircon dates for rhyolite and sandstone of Cadwallader terrane, lower Chilcotin River area, south-central British Columbia. In: Geological Fieldwork 2022, British Columbia Ministry of Energy, Mines and Low Carbon Innovation, British Columbia Geological Survey Paper 2023-01, pp. 65-84.

Rukhlov, A.S., Coats, B., Van der Vlugt, J., Beaupre-Olsen, I.J., and Zaborniak, K., 2023. British Columbia Geological Survey Sample Archive: An emerging resource for public geoscience. In: Geological Fieldwork 2022, British Columbia Ministry of Energy, Mines and Low Carbon Innovation, British Columbia Geological Survey Paper 2023-1, pp. 85-90.

Appendix: British Columbia Geological Survey Publications 2022, including peer-reviewed external papers co-authored by BCGS staff, pp. 91-95.

Open Files

OF 2023-01

Clarke, G., Northcote, B., Corcoran, N.L., Heidarian, H., and Hancock, K., 2023. Mines, mine development, selected proposed mines, and selected exploration projects in British Columbia, 2022. British Columbia Ministry of Energy, Mines and Low Carbon Innovation, British Columbia Geological Survey Open File 2023-01.

OF 2023-02

Hickin, A.S., Orovan, E.A., Brzozowski, M.J., McLaren, K., Shaw, K., and Van der Vlugt, J., 2023. Critical minerals in British Columbia: An atlas of occurrences and producing mines, 2023. British Columbia Ministry of Energy, Mines and Low Carbon Innovation, British Columbia Geological Survey Open File 2023-02, 102 p.

GeoFiles

GF 2023-01

Clarke, G., Northcote, B., Corcoran, N.L., Heidarian, H., and Hancock, K., 2023. Exploration and mining in British Columbia, 2022. British Columbia Ministry of Energy, Mines and Low Carbon Innovation, British Columbia Geological Survey GeoFile 2023-01 (poster).

GF 2023-02

Corcoran, N.L., 2023. Exploration and mining highlights, Northwest Region, 2022. British Columbia Ministry of Energy, Mines and Low Carbon Innovation, British Columbia Geological Survey GeoFile 2023-02 (poster).

GF 2023-03

Heidarian, H., 2023. Exploration and mining highlights, North Central and Northeast regions, 2022. British Columbia Ministry of Energy, Mines and Low Carbon Innovation, British Columbia Geological Survey GeoFile 2023-03 (poster).

GF 2023-04

Northcote, B., 2023. Exploration and mining highlights, Southwest and South Central regions, 2022. British Columbia Ministry of Energy, Mines and Low Carbon Innovation, British Columbia Geological Survey GeoFile 2023-04 (poster).

GF 2023-05

Hancock, K., 2023. Exploration and mining highlights, Southeast Region, 2022. British Columbia Ministry of Energy, Mines and Low Carbon Innovation, British Columbia Geological Survey GeoFile 2023-05 (poster).

GF 2023-06

Mihalynuk, M.G., Ootes, L., Drobe, J.R., Wall, C., and Friedman, R.M., 2023. Lardeau Group mapping update—implications for ultramafic-associated massive sulfide and critical metal exploration in southeast British Columbia. British Columbia Ministry of Energy, Mines and Low Carbon Innovation, British Columbia Geological Survey GeoFile 2023-06 (poster).

GF 2023-07

Elia, E.A., Ferbey, T., Ward, B.C., Shives, R.B.K., Best, M., and Martin-Burtart, N., 2023. Remotely piloted aircraft system (RPAS) for investigating surface sediments in the Interior Plateau of British Columbia: Methods, data, and products. British Columbia Ministry of Energy, Mines and Low Carbon Innovation, British Columbia Geological Survey GeoFile 2023-07, 22 p.

GF 2023-08

van Straaten, B.I., Logan, J.M., Nelson, J.L., Moynihan, D.P., Diakow, L.J., Gibson, R., Bichlmaier, S.J., Wearmouth, C.D., Friedman, R.M., Golding, M.L., Miller, E.A., and Poulton, T.P., 2023. Bedrock geology of the Dease Lake area: Supporting GIS, structural, magnetic susceptibility, and other digital data. British Columbia Ministry of Energy, Mines and Low Carbon Innovation, British Columbia Geological Survey GeoFile 2023-08, 5 p.

Information Circulars

IC 2023-01

Clarke, G., Northcote, B., Corcoran, N.L., Heidarian, H., and Hancock, K., 2023. Provincial Overview of Exploration and Mining in British Columbia, 2022. British Columbia Ministry of Energy, Mines and Low Carbon Innovation, British Columbia Geological Survey, Information Circular 2023-01, 142 p.

Clarke, G., Northcote, B., Corcoran, N.L., Heidarian, H., and Hancock, K., 2023. Exploration and Mining in British Columbia, 2022: A summary. In: Provincial Overview of Exploration and Mining in British Columbia, 2022. British Columbia Ministry of Energy, Mines and Low Carbon Innovation, British Columbia Geological Survey, Information Circular 2023-01, pp. 1-48.

Corcoran, N.L., 2023. Exploration and mining in the Northwest Region, British Columbia. In: Provincial Overview of Exploration and Mining in British Columbia, 2022. British Columbia Ministry of Energy, Mines and Low Carbon Innovation, British Columbia Geological Survey, Information Circular 2023-01, pp. 49-76.

Heidarian, H., 2023. Exploration and mining in the North Central and Northeast regions, British Columbia. In: Provincial Overview of Exploration and Mining in British Columbia, 2022. British Columbia Ministry of Energy, Mines and Low Carbon Innovation, British Columbia Geological Survey, Information Circular 2023-01, pp. 77-92.

Northcote, B., 2023. Exploration and mining in the South Central Region, British Columbia. In: Provincial Overview of Exploration and Mining in British Columbia, 2022. British Columbia Ministry of Energy, Mines and Low Carbon Innovation, British Columbia Geological Survey, Information Circular 2023-01, pp. 93-113.

Hancock, K., 2023. Exploration and mining in the Southeast Region, British Columbia. In: Provincial Overview of Exploration and Mining in British Columbia, 2022. British Columbia Ministry of Energy, Mines and Low Carbon Innovation, British Columbia Geological Survey, Information Circular 2023-01, pp. 115-128.

Northcote, B., 2023. Exploration and mining in the Southwest Region, British Columbia. In: Provincial Overview of Exploration and Mining in British Columbia, 2022. British Columbia Ministry of Energy, Mines and Low Carbon Innovation, British Columbia Geological Survey, Information Circular 2023-01, pp. 129-142.

IC 2023-02

British Columbia Geological Survey, 2023. British Columbia Geological Survey. British Columbia Ministry of Energy, Mines and Low Carbon Innovation, British Columbia Geological Survey Information Circular 2023-02, 14 p. (brochure)

IC 2023-03

British Columbia Geological Survey, 2023. Mineral Development Office. British Columbia Ministry of Energy, Mines and Low Carbon Innovation, British Columbia Geological Survey Information Circular 2023-03, 4 p. (brochure)

IC 2023-04

British Columbia Geological Survey, 2023. Online databases at the British Columbia Geological Survey. British Columbia Ministry of Energy, Mines and Low Carbon Innovation, British Columbia Geological Survey Information Circular 2023-04, 14 p. (brochure)

IC 2023-05

British Columbia Geological Survey, 2023. The Golden Triangle of northwestern British Columbia. British Columbia Ministry of Energy, Mines and Low Carbon Innovation, British Columbia Geological Survey Information Circular 2023-05, 6 p. (brochure)

IC 2023-07

British Columbia Geological Survey, 2023. Mineral potential modelling at the British Columbia Geological Survey: The next generation. British Columbia Ministry of Energy, Mines and Low Carbon Innovation, British Columbia Geological Survey Information Circular 2023-07, 7 p. (brochure)

External peer-reviewed journal and volume publications

Bai, S., Lei, R., Brzozowski, M.J., Hao, L., Zhang, K., and Wu, C., 2023. Constraints on the timing of magmatism and rare-metal mineralization in the Fangzheng Rb deposit, Altay, NW China: Implications for the spatiotemporal controls on rare-metal mineralization. *Ore Geology Reviews*, 157, article 105427.

<<https://doi.org/10.1016/j.oregeorev.2023.105427>>

Bain, W., Hollings, P., Djon, L.M., Brzozowski, M.J., Layton-Matthew, D., and Dobosz, A., 2023. The geology, geochemistry, and magmatic evolution of the Legris Lake mafic-ultramafic complex, Ontario, Canada. *Mineralium Deposita*.

<<https://doi.org/10.1007/s00126-023-01183-x>>

Brzozowski, M.J., Hollings, P., Heggie, G., MacTavish, A., Wilton, D., and Evans-Lamswood, D., 2023. Characterizing the supra- and subsolidus processes that generated the Current PGE-Cu-Ni deposit, Thunder Bay North Intrusive Complex, Canada: insights from trace elements and multiple S isotopes of sulfides. *Mineralium Deposita*.

<<https://doi.org/10.1007/s00126-023-01193-9>>

- Brzozowski, M.J., Hollings, P., Zhu, J., and Creaser, R.A., 2023. Osmium isotopes record a complex magmatic history during the early stages of formation of the North American Midcontinent Rift-Implications for rift initiation and platinum-group element mineralization. *Lithos*, 436-437, article 106966.
<<https://doi.org/10.1016/j.lithos.2022.106966>>
- Chen, J., Shao, Y., Xiong, Y., He, H., Brzozowski, M.J., Wen, C., Zhou, L., Lu, W., and Shi, J., 2023. Mechanisms of ore formation in Silurian (Caledonian) scheelite deposits of the Nanling Range, South China: a case study from the Pingtan W deposit. *Ore Geology Reviews*, 154, article 105347.
<<https://doi.org/10.1016/j.oregeorev.2023.105347>>
- Di, H., Shao, Y., Jiang, S., Brzozowski, M.J., Wang, Z., and Xiong, Y., 2023. Identifying superimposed W-Sn mineralization events using cassiterite microtextures, trace-element chemistry, and geochronology. *Ore Geology Reviews*, 153, article 105281.
<<https://doi.org/10.1016/j.oregeorev.2022.105281>>
- Hao, Y., Feng, Y., Liang, T., Brzozowski, M.J., Ju, M., Zhou, R., and Wang, Y., 2023. Quantitative evaluation of metamictisation of columbite-(Mn) from rare-element pegmatites using Raman spectroscopy. *Mineralogical Magazine*.
<<https://doi.org/10.1180/mgm.2023.18>>
- Hu, J., Zhang, Y., Jia, D., Muxworthy, A., Selby, D., Li, Y., Brzozowski, M.J., Wei, G., Cao, J., Yin, H., and Li, W., 2023. Combining paleomagnetic and Re-Os isotope data to date hydrocarbon generation and accumulation processes. *Journal of Geophysical Research: Solid Earth*, 128, article e2022JB025955.
<<https://doi.org/10.1029/2022JB025955>>
- Jones, G., Ootes, L., Luo, Y.A., Vezinet, A., Stern, R., Milidragovic, D., and Pearson, D.G., 2023. The relative roles of ancient and juvenile crust in building accretionary orogens-Minimal ancient crust involved in the magmatic evolution of a North American Cordillera accreted terrane indicated by igneous zircon Hf-O. *Lithos*, article 107213.
<<https://doi.org/10.1016/j.lithos.2023.107213>>
- Jun, M., Zhao, S., Brzozowski, M.J., Li, H., Wu, C., and Li, W., 2023. Geology, geochemistry and genesis of the world-class Shizhushan wollastonite deposit, Mengshan area, South China. *Ore Geology Reviews*, 158, article 105469.
<<https://doi.org/10.1016/j.oregeorev.2023.105469>>
- Liu, J., Yang, J., Cao, Y., Ding, T., Brzozowski, M.J., Zhang, H., Zheng, X., and Zhao, T., 2023. Indium mineralization and genesis of the Bainiuchang Ag-Sn polymetallic deposit in southeast Yunnan, China: Evidence from mineral chemistry and U-Pb geochronology. *Ore Geology Reviews*, 158, article 105531.
<<https://doi.org/10.1016/j.oregeorev.2023.105531>>
- Liu, Y., Zhao, Y., Xue, C., Wang, R., Chu, H., Zhao, X., Brzozowski, M.J., Seltmann, R., Chen, J., and Gao, J., 2023. Multiple stages of Au mobilization and in the Changshagou Au deposit, Eastern Tianshan, NW China: insights from mineral chemistry and fluid inclusions. *Journal of Asian Earth Sciences*, 255, article 105756.
<<https://doi.org/10.1016/j.jseaes.2023.105756>>
- Milidragovic, D., Nott, J.A., Spence, D.W., Schumann, D., Scoates, J.S., Nixon, G.T., and Stern, R.A., 2023. Sulfate recycling at subduction zones indicated by sulfur isotope systematics of Mesozoic ultramafic island arc cumulates in the North American Cordillera. *Earth and Planetary Science Letters*, 620, article 118337.
<<https://doi.org/10.1016/j.epsl.2023.118337>>
- Milidragovic, D., Ootes, L., Zagorevski, A., Cleven, N., Wall, C.J., and Luo, Y., 2023. Detrital geochronology of the Cunningham Lake formation: an overlap succession linking Cache Creek terrane to Stikinia at ~205 Ma. *Canadian Journal of Earth Sciences*, 60.
<<https://doi.org/10.1139/cjes-2023-0018>>
- Muhtar, M., Xiao, W., Brzozowski, M.J., Chen, S., Aibai, A., Wang, M., and Wu, C., 2023. Genetic link between orogenic Au and porphyry Cu (-Au) mineralization in the Dananhu Arc, NW China: Evidence from geochronology, geochemistry, and Sr-Nd-Hf isotopes of the Tudunbei Au deposit. *Journal of Geochemical Exploration*, 253, article 107280.
<<https://doi.org/10.1016/j.gexplo.2023.107280>>

Norris, J.R., Tosdal, R.M., Lipske, J., and Wilson, A.J., 2023. Late-stage low-temperature hydrothermal alteration overprint at the East zone in the Red Chris porphyry Cu-Au deposit, northwestern British Columbia, Canada. *Economic Geology*, 118, 391-409.

<<https://doi.org/10.5382/econgeo.4997>>

Rasmussen, K.L., Falck, H., Elongo, V., Reimink, J., Yan Luo, Y.D., Pearson, D.G., Ootes, L., Creaser, R.A., and Pilar Lecumberri-Sanchez, P., 2023. The source of tungsten-associated magmas in the northern Canadian Cordillera and implications for the basement. *Geology*, 51, 657-662.

<<https://doi.org/10.1130/G51042.1>>

Sun, X., Li, X., Lei, R., Brzozowski, M.J., Ma, H., Li, W., Xia, M., Yu, Y., and Wu, C., 2023. Paleoproterozoic crustal evolution of the Tarim Craton, NW China: Constraints from geochronology and geochemistry of orthogneisses and granitic veins in the Xingdi region of the Quruqtagh Block. *Precambrian Research*, 399, article 107247.

<<https://doi.org/10.1016/j.precamres.2023.107247>>

Wang, Y., Lai, J., Cao, Y., and Brzozowski, M.J., 2023. Compositional variations of magnetite in different sulfide ore types in the Jinchuan Ni-Cu-PGE sulfide deposit, NW China: insights into the mineralizing processes of conduit-type systems. *Chemical Geology*, 637, article 121679.

<<https://doi.org/10.1016/j.chemgeo.2023.121679>>

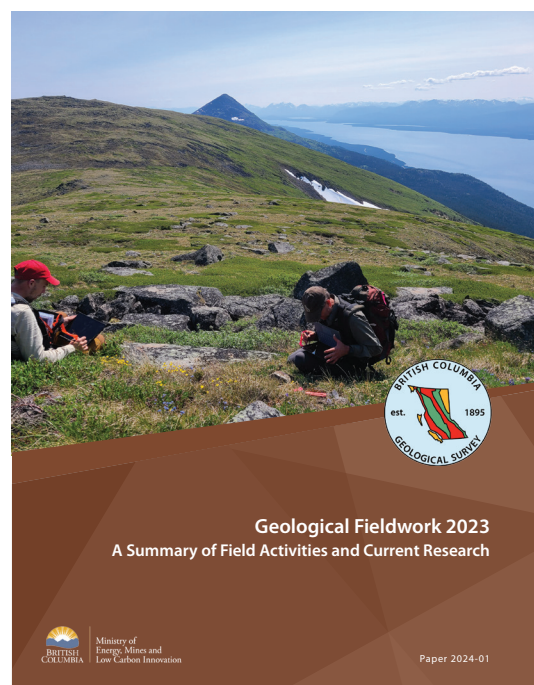
Wu, S., Lei, R., Brzozowski, M.J., Wang, W., Yuan, H., and Wu, C., 2023. Early Neoproterozoic magmatism in the Central Tianshan Block, China: Implications for its tectono-magmatic evolution and relationship to Rodinia. *Precambrian Research*, 397, article 107203.

<<https://doi.org/10.1016/j.precamres.2023.107203>>

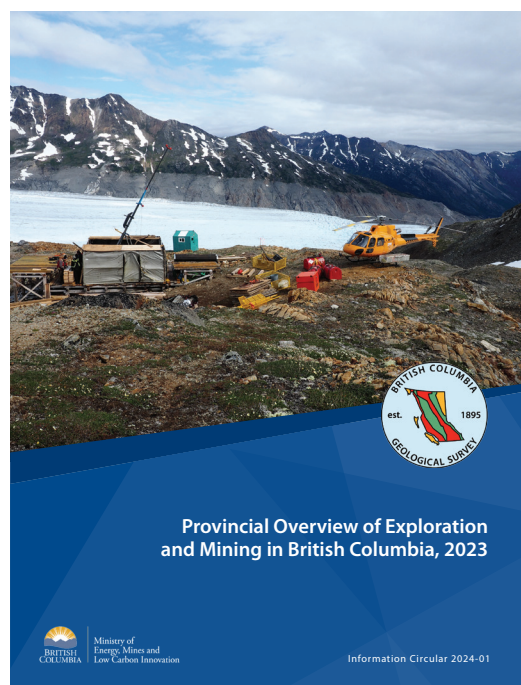
Ye, H., Wu, C., Brzozowski, M.J., Yang, T., Sun, X., Lei, R., and Li, W., 2023. Genesis of the Longwanggou iron deposit in the Yudongzi complex, South China: Implications for the redox state of seawater at the onset of the Great Oxidation Event. *Ore Geology Reviews*, 159, article 105562.

<<https://doi.org/10.1016/j.oregeorev.2023.105562>>

Each year, the British Columbia Geological Survey publishes *Geological Fieldwork*, a Summary of Fieldwork and Current Research (this volume), and the *Provincial Overview of Mining and Exploration in British Columbia*. All British Columbia Geological Survey publications can be downloaded, at no cost, from www.BCGeologicalSurvey.ca



Geological Fieldwork volume, British Columbia Geological Survey Paper 2024-01



Provincial Overview of Mining and Exploration in British Columbia volume, Information Circular 2024-01

